Energy and Environment Division

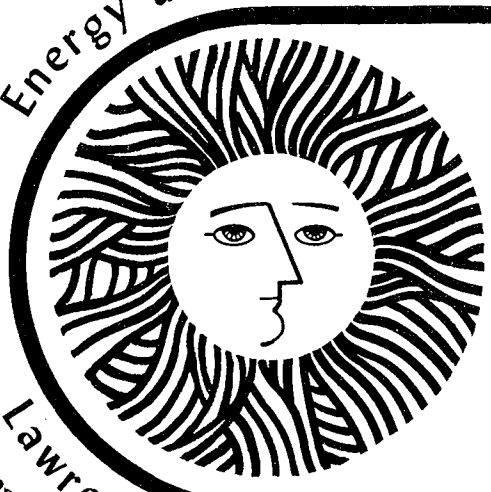

Telluric And D.C. Resistivity Techniques Applied To The Geophysical Investigation Of Basin And Range Geothermal Systems, Part II: A Numerical Model Study Of The Dipole-Dipole And Schlumberger Resistivity Methods

J.H. Beyer

(Ph.D. thesis)

June 1977

Lawrence Berkeley Laboratory University of California/Berkeley

Prepared for the U.S. Energy Research and Development Administration under Contract No. W-7405-ENG-48

TELLURIC AND D.C. RESISTIVITY TECHNIQUES APPLIED TO THE GEOPHYSICAL INVESTIGATION OF BASIN AND RANGE GEOTHERMAL SYSTEMS

PART II

A NUMERICAL MODEL STUDY OF THE DIPOLE-DIPOLE AND SCHLUMBERGER RESISTIVITY METHODS

J. H. Beyer

ABSTRACT

This paper is a two-dimensional numerical model study and comparison of the polar dipole-dipole and Schlumberger resistivity arrays. A catalog of dipole-dipole and Schlumberger apparent resistivity pseudo-sections is presented. It is concluded that: for the Schlumberger array, data can be accurately interpreted only if the resistivity structure is horizontally layered, and conductive bodies having a depth of burial greater than their width are not observed; for the dipole-dipole array, complex anomaly patterns unrelated in appearance to the causative structure result from simple models, hence, a familiarity with model results is essential to interpretation of these data.

PREFACE

Starting in the Summer of 1973, the Lawrence Berkeley Laboratory of the University of California has been involved in a geothermal assessment program with three main goals:

1) To evaluate, on the basis of detailed geological, geochemical and geophysical data, some geothermal systems in the mid Basin and Range geologic province.

2) To compare and evaluate geophysical techniques used in the exploration and delineation of geothermal reservoirs.

3) To develop new exploration techniques, and the instrumentation required, specifically for the deep penetration desired in geothermal investigations.

This report addresses various aspects of each of these points.

It is well documented that hot water geothermal reservoirs tend to have lower electrical resistivity than surrounding cold and/or dry rock by virtue of: (1) increased ion mobility, (2) more dissolved solids, and (3) increased permeability and porosity of the reservoir rocks as a result of convection of the geothermal fluids. Vapor dominated geothermal systems are resistive in the steam zone, but display anomalously conductive halos in intermediate temperature regions where there is condensation. Thus, one distinctive feature of geothermal reservoirs is that they may be electrically conductive targets which, to be of economic importance, may be a few cubic kilometers in size, but with a depth of burial of one or more kilometers.

When confronted with the problem of initial exploration of a several hundred square kilometer region in the vicinity of a hot spring, a rapid reconnaissance electrical method is important to locate areas of low resistivity for more intensive investigation. The E-field ratio telluric method described in Part I of this report appears to satisfy this need quite adequately.

Subsequent to the location of conductive anomalies by reconnaissance techniques an electrical method providing higher resolution and affording more quantitative interpretation capability is needed. For this purpose, and for correlation with and evaluation of other electrical exploration techniques, d.c. resistivity measurements using the polar dipole-dipole array were performed as a part of the LBL geothermal exploration program. A second resistivity electrode configuration, the Schlumberger method, has been widely used by other investigators. Part II of this report is a numerical model study and comparison of these two resistivity techniques.

An extensive program of geophysical exploration was undertaken by LBL in the vicinity of Leach Hot Springs in Grass Valley, Nevada. The detailed interpretation of E-field ratio telluric, dipole-dipole resistivity, and bipole-dipole resistivity mapping data is treated in Part III of this report, along with a description of the implementation of high-power d.c. resistivity exploration techniques. Several areas in Grass Valley emerge as being worthy of further investigation for their geothermal potential, and the interpretation process has provided a means of evaluating and comparing the exploration techniques.

ACKNOWLEDGEMENTS

The major portion of this work was supported by the U.S. Energy Research and Development Administration through the University of California - Lawrence Berkeley Laboratory. Some computer time was provided by the U.C. Berkeley Computer Center.

Special thanks are due Abhijit Dey for his helpfullness in the use of his computer code for calculation of the numerical models presented in this paper, and Art Paradis for his aid in developing the computer graphics code required to display the models.

TABLE OF CONTENTS

INTRODUCTION

D.C. resistivity exploration techniques, which generally employ two electrodes for the injection of electrical current and two electrodes for measuring the resultant potential difference, are dependent upon increasing the separation between the most distant electrodes for greater depth of penetration. To explore for potential geothermal reservoirs, which might lie at a depth of a kilometer or more, the maximum electrode separation can become very large. The situation is aggravated by the presence of conductive surface material, such as the alluvial fill in Basin and Range valleys, because the current tends to remain confined to this region rather than penetrating into more resistive bedrock. Maximum electrode separations in excess of 10 km may be required to obtain sufficient penetration.

As an alternative to spanning such distances with wire to inject current or to make measurements, as would be necessary for some commonly used resistivity methods such as Schlumberger, the dipole-dipole method employs an electrode array which consists of two relatively short-length dipoles--one for transmitting and the other for receiving. The distance between these is increased to give greater depth of penetration. This electrode configuration is shown in Figure II-1 at the top of the diagram. Also, the high data density obtained with this technique affords the possibility of detailed two-dimensional numerical modelling with high resolution of the resistivity structure. For these reasons the dipole-dipole method was used as part of the Lawrence Berkeley Laboratory geothermal exploration program in north central Nevada.

Other investigators have used the Schlumberger array for electrical

exploration of geothermal prospects. This electrode configuration is shown in Figure II-2 at the top of the diagram.

There was, and still is, considerable debate as to which method is "better." This report should help to answer that question. In it is presented a catalog of dipole-dipole and Schlumberger responses calculated for various two-dimensional resistivity structures. As is generally true for two time-honoured methods, each has its strong points and shortcomings, depending, in this case, upon the structure under investigation.

A third electrode array, variously called the bipole-dipole, dipole mapping, or roving dipole method has been widely used as an electrical reconnaissance method for geothermal investigations, and has been performed by Lawrence Berkeley Laboratory for comparison with other techniques. The dipole-dipole model data presented in this report has some applicability to the interpretation of bipole-dipole resistivity data.

MODEL STUDY OF THE DIPOLE-DIPOLE AND SCHLUMBERGER RESISTIVITY METHODS

This report is a numerical model study and comparison of two d.c. resistivity exploration techniques, the collinear or polar dipole-dipole method and the Schlumberger method, for two-dimensional resistivity structures. Such structures are of infinite extent in one lateral direction.

The computer code used to calculate the apparent resistivities for the models is described by Dey and Morrison (1976) and Dey (1976). It is a finite difference technique which calculates the potential distribution at grid nodal points due to point current sources at particular locations in a half-space consisting of arbitrarily shaped two-dimensional resistivity structures. Once the potentials have been calculated at unit intervals for sources at all interval locations it is quite inexpensive to calculate the apparent resistivities using geometric factors for more than one configuration of electrodes. The program requires about 16 CP seconds on a CDC 7600 computer to generate the dipole-dipole and Schlumberger apparent resistivity data for one model. Comparison with analytic solutions for some simple models indicates the numerical solutions have errors less than $\pm$ 5%.

As is shown in Figure II-1 the dipole-dipole method employs constant transmitter and receiver dipole lengths, a, with increased depth of penetration being achieved by increasing the separation between the transmitter and receiver dipoles at unit intervals of N times a, where N = 1, 2, 3, . . . The upper limit on N is determined by the maximum depth of interest or the separation at which the signal at the receiver is lost in the telluric or instrumental noise. Using the current, I, injected into the ground at the transmitter dipole, and the resulting

potential difference, ΔV, observed at the receiver dipole, an apparent resistivity, ρ_a , is calculated:

$$\rho_a = \pi a N (N+1)(N+2) \frac{\Delta V}{I} \quad . \qquad (II-1)$$

The apparent resistivity is defined as the resistivity of a homogeneous half-space required to produce the observed potential difference at the receiver electrodes for the known current injected at the transmitter electrodes and for the geometric configuration of the four electrodes.

As depicted in Figure II-1 the calculated values of ρ_a are conventionally plotted at the intersection of lines angling down at 45^o from the centers of transmitting and receiving dipoles to produce an apparent resistivity pseudo-section (Hallof, 1957; Marshal and Madden, 1959). The locations of point current sources and the positions at which the potential is calculated are the coordinates on the x-axis. In discussing the dipole-dipole pseudo-sections the term "transmitting dipole" is used to describe two adjacent current sources (of opposite polarity) and "receiving dipole" is used to describe two adjacent coordinates for which the potential difference is found. Due to reciprocity, however, it is irrelevant which dipole of a particular pair is considered to be the transmitter and which the receiver.

The Schlumberger resistivity array, shown in Figure II-2, employs four colinear electrodes, the outer two, located at A and B, normally forming the transmitter dipole used for current injection, and the inner two, located at M and N, being the receiver dipole used for a potential difference measurement. Once again reciprocity holds so that, disregarding the practical consideration of signal to noise ratios, the Schlumberger transmitting and receiving dipoles could be interchanged.

The receiver dipole is positioned in the central region of the transmitter array and its length is maintained at one-fifth or less of the transmitter length ($\overline{MN} \leq \overline{AB}/5$). When the Schlumberger array is used for soundings the receiver dipole is generally located at the center of the transmitter dipole and the length of the transmitter is increased to achieve greater penetration depth. The receiver dipole length, while remaining at less than one-fifth of the transmitter length, is increased when necessary to enhance the signal. The rule of thumb estimate of penetration depth, albeit a very inaccurate one, is one-half the transmitter length, AB/2.

Interpretation of Schlumberger sounding data is generally based upon one-dimensional, or horizontally layered models. As such, Schlumberger resistivity data is commonly plotted with log ρ_a along the ordinate and log AB/2 along the abscissa. The apparent resistivity, ρ_a , is determined by

$$\rho_a = \pi \left[\frac{(\overline{AB}\,2)^2}{MN} - \frac{\overline{MN}}{4} \right] \frac{\Delta V}{I} \quad . \qquad (II\text{-}2)$$

To present the Schlumberger data over two-dimensional structures a pseudo-section similar to that for dipole-dipole has been devised (See Figure II-2). In performing numerical modeling the minimum interval at which potentials were stored for apparent resistivity calculations was the dipole length used for the dipole-dipole method (the unit length shown for the models in Appendix II-A), so this length was used for the Schlumberger receiver electrode separation MN. The Schlumberger transmitter lengths were then 3, 5, 7, . . . , 17 units giving AB/2

separations of 1.5, 2.5, 3.5, . . ., 8.5, respectively. Thus, the center of each unit interval across the models is used as the mid-point of a Schlumberger sounding with each column of numbers representing, from top to bottom, an expansion of the AB/2 separation with MN remaining fixed at one unit.

For the AB/2 separation of 1.5, MN is one-third of AB which makes the array a Wenner configuration, but for larger values of AB/2 the array is a more legitimate Schlumberger configuration with MN less than 0.435 times AB/2 (Keller and Frischknecht, 1966).

Maximum electrode separation is an approximate criterion for depth of penetration, and is a gauge for difficulty of obtaining a field measurement. For these reasons the Schlumberger pseudo-sections have been designed for direct comparison with the dipole-dipole pseudo-sections such that apparent resistivity values at identical positions in the respective pseudo-sections are obtained with the outermost electrodes at the same locations. This means that the row for AB/2 = 1.5 in the Schlumberger pseudo-sections corresponds to the same maximum electrode separation (3 units) as N = 1 in the dipole-dipole pseudo-sections. Similarly, AB/2 = 2.5, 3.5, . . . , 8.5 correspond to N = 3, 5, . . ., 15, with maximum electrode separations of 5, 7, . . ., 17 units, respectively. The particular electrode configurations depicted in Figures II-1 and II-2 have the same maximum electrode separation of 7 units with the dipole-dipole array yielding an apparent resistivity of 47.9 at N = 5, and the Schlumberger array giving 41.2 at AB/2 = 3.5.

It must be stressed that the presentation of Schlumberger apparent resistivity data in a pseudo-section format does not imply that the data could (at reasonable expense) or should be obtained at such a high

density. The purpose of this study is to display the variations which would appear in Schlumberger data depending upon the location of a particular sounding with respect to two-dimensional inhomogenieties.

Appendix II-A (Figures II-A1 through II-A162) presents both dipole-dipole and Schlumberger pseudo-sections for two dimensional resistivity structures. The scale used for these models is the same in the horizontal and vertical directions, with the unit length being the dipole-dipole dipole length, which is the Schlumberger receiver dipole length. For the purpose of compution of potential distributions and apparent resistivities the models are not truncated at the right, left, or bottom as is suggested by the diagrams: the resistivity features which are shown at the right (x = +11), left (x = -11), and bottom (z = +6) edges of the models extend, respectively, horizontally to the right, horizontally to the left, and downward to "infinity". (See Dey and Morrison (1976) for a discussion of boundary conditions). The apparent resistivity values which appear along the right and left diagonal edges of the pseudo-sections employ transmitter or receiver electrodes located at x = +12 or -12.

At the right-hand side of each model diagram is the resistivity code. These model resistivities (ρ) and the apparent resistivity (ρ_a) values and contours in the pseudo-sections are expressed in the same units (e.g., ohm-meters or ohm-feet). The data in this model study can be scaled to any level by multiplying all model resistivities and all pseudo-section apparent resistivities by the same constant.

The resistivity pseudo-sections for both dipole-dipole and Schlumberger arrays have been computed for all models considered. All dipole-dipole plots have odd figure numbers, while Schlumberger plots

have even figure numbers; the two types of pseudo-sections for each model are mounted on successive pages for ease of comparison.

The apparent resistivity pseudo-sections are contoured at five roughly equal intervals per decade, at powers of 10 times 1.0, 1.5, 2.5, 4.0, and 6.5. Adjacent contour lines of this sequence reflect an increase in apparent resistivity of in the range of 150 - 167% (or conversely, a decrease of 60 - 67%). On some pseudo-sections additional contour lines have been added for resistivity values of 12, 80, 90, and 120 to enhance patterns or trends, and on a couple pseudo-sections contour lines have been deleted due to very abrupt apparent resistivity gradients.

In the ensuing discussion the term "anomaly amplitude" is used to describe the percent change in apparent resistivity with respect to the background resistivity, or for models including a layer of uniform thickness, with respect to the apparent resistivity found at the same N-spacing or AB/2 separation in a portion of the pseudo-section relatively unaffected by the inhomogeniety.

For purposes of discussing the model data it will be necessary to define a means of locating resistivity (ρ) zones in the models and apparent resistivity (ρ_a) values in the pseudo-sections. For both, the x-direction, positive to the right, will be that of the horizontal axes, which represent the surface of the earth. In the models the vertical axis will be the z-direction, positive downward. "Depth" in the pseudo-sections will be characterized by N for dipole-dipole and AB/2 for Schlumberger, as are labled along the left and right edges of the pseudo-sections. The statement that an anomaly lies "over" or is "centered on" the body indicates only that the most anomalous apparent resistivities at the smallest N or AB/2 separations lie at the same

x-coordinates as the body. As will become quite apparent in studying the pseudo-sections, the N or AB/2 separation at which an anomaly occurs does not bear a direct relationship to the depth of burial of an inhomogeneity.

To understand the dipole-dipole and Schlumberger responses to the various models discussed below, it is essential to bear in mind the transmitter and receiver locations used to obtain a particular apparent resistivity value (as shown in Figures II-1 and II-2). Anomalous apparent resistivities occur if the transmitter current flow in the vicinity of the receiver dipole is deviated from the path that it would take in a homogeneous earth, or if the receiver dipole is located on material having an anomalous resistivity.

Detailed Discussion of the Model Derived Data

The vertical contact.

Dipole-dipole response. The dipole-dipole pseudo-section for the semi-infinite vertical contact in Figure II-A1 bears little resemblence to the actual structure, which immediately demonstrates the importance of modeling in order to learn to recognize patterns for the interpretation of dipole-dipole data. The pseudo-section shows three distinct regions: the upper right-hand area which reflects the high resistivity side of the contact, the upper left-hand region which reflects the low resistivity side of the contact, and the area in between, for which $\rho_a = 18.1$. This pattern is characteristic of dipole-dipole pseudo-sections for structures having lateral resistivity contrasts which reach the surface. The effects are seen to propagate down-to-the-right or down-to-the-left diagonally through the pseudo-section from the surface location of the

contact. For any electrode configuration having parallel transmitting and receiving dipoles on opposite sides of a vertical contact, the apparent resistivity has a constant value given by:

$$\rho_a = \frac{2\rho_1\rho_2}{\rho_1 + \rho_2} \qquad \text{(II-3)}$$

where ρ_1 and ρ_2 are the two resistivities (Van Nostrand and Cook, 1966, p. 53-54; Furgerson, 1970, p. 41-47). With both transmitter and receiver dipoles on the same side of the contact all values of apparent resistivity will be close to the resistivity of the region over which they are located. A slight overshoot does occur for the values down-to-the-right from x = 0 to 2 as the N-spacing increases; the values rise above ρ_a = 100 in that region of the model. Similarly, down-to-the-left from x = -2 to -4 shows decreasing resistivity with greater N-spacing. The physical explanation of this is that if receiver electrodes are located at x = -1 and -2, as the transmitting dipole is moved to the left the amount of current at the receiver dipole will decrease as a result of being shielded by the ρ = 100 region immediately to the right of x = -1.

For the case of two vertical contacts with the intervening zone having lower resistivity than the regions on either side (Figure II-A3) the pseudo-section is quite complex; it must be understood in terms of the "interference" or "super-position" of two patterns like that shown in Figure II-A1. For N $\leq$ 5 the same effects are seen. For larger transmitter-receiver separations other patterns develop. For the two dipoles close to the respective contacts, but still within the conductive region, a false low of ρ_a = 3.2 is seen at x = -0.5, N = 7. When

the transmitting and receiving electrodes are spread further so that both are in the resistive material but straddling the conductive zone a region of $\rho_a \approx 37$ is obtained.

If the vertical extent of the two contacts is reduced to one unit (Figure II-A5), as would be expected, higher apparent resistivities are observed for stations with electrodes over the conductive region. The controlling factor seen in the pseudo-section is the location of the lateral resistivity contrasts, not the thickness of the conductive zone. For this reason, in interpreting a pseudo-section of field data which resembles Figure II-A5 it would be difficult to determine the thickness of the conductive layer, and if the survey were laterally confined to this layer, the true resistivity of the underlying material would also be difficult to ascertain. It should be noted that the region beneath the $\rho_a = 100$ contour in the center of the pseudo-section, for transmitter and receiver dipoles straddling the conductive zone, contains apparent resistivities over twice that of the resistive background.

Schlumberger response. The Schlumberger pseudo-section for the semi-infinite vertical contact in Figure II-A2 rather closely resembles the structure. Nearly vertical contours cluster in the vicinity of x = 0 to -1. To the left of this Schlumberger soundings suggest a slight increase in the resistivity; to the right, soundings suggest a resistive space with slightly decreasing resistivity as a function of depth. It is worth noting however, that if a sounding were made in the vicinity of x = 0 to -1, the interpretation would be a uniform half-space with $\rho = 53$, which could be quite misleading.

For two vertical contacts the structure is well simulated with vertical contours clustered at x = -5 and +4. If the thickness of the conductive central region is reduced to one unit (Figure II-A6) the data again suggests the model, however, a sounding centered at any location over the conductive area will not at any AB/2 separation yield apparent resistivities approaching the resistivity of the underlying material.

Buried faults or contacts.

Dipole-dipole and Schlumberger responses. Figures II-A7 and II-A8 show a buried vertical contact with the more conductive medium forming a one-half unit thick layer. The dipole-dipole pseudo-section reveals this structure if the pattern observed in Figure II-A1 is borne in mind. The Schlumberger pseudo-section more closely resembles the physical situation. However, it will be observed that a sounding to the left of the vertical contact, where the model is a two layer case, is less sensitive to the deeper resistive material than in the dipole-dipole situation, which at x = -6 to -7, N - 9 has already reached ρ_a = 81. At an equivalent location in the Schlumberger pseudo-section a value of only ρ_a = 42 is reached. The apparent resistivities at N = 1 for the dipole-dipole method are less, and therefore closer to the real case, than for the Schlumberger method at AB/2 = 1.5.

For the buried fault with limited vertical offset shown in Figures II-A9 and II-A10, both methods yield a discernable anomaly. For the Schlumberger method this occurs over the fault, whereas for dipole-dipole it is seen down-to-the-left and down-to-the-right from the surface projection of the fault. This is because it is for these locations in the pseudo-section that a transmitting or receiving dipole is located

close to the feature. The region between these diagonals in the pseudo-section is analogous to the ρ_a = 18 area in Figure II-A1. For a deeper fault with less throw (Figures II-A11 and II-A12) neither method produces a significant anomaly.

Figures II-A13 through II-A16 are for the faults shown in previous two models with the addition of narrow resistive regions extending upward along the planes of the faults. The geologic occurrence of such a structure might be the result of mineral deposition due to the flow of thermal fluids in a fault plane through alluvial material overlying a faulted basement. The dipole-dipole pseudo-section in both cases show slight perturbations for dipole locations at x = -1, 0 or x = 0, +1. Similarly, the Schlumberger data for appropriately located soundings reveal the feature. In real data for either method, however, these small anomalies would probably go unnoticed or would be attributed to other causes.

For a uniform layer over a vertical contact the anomaly is small if the layer is more conductive than the underlying material (Figures II-A17 and II-A18) because the current tends to stay confined to the layer. If, however, one of the materials is more conductive than the layer (Figures II-A19 and II-A20) substantial anomalies are observed with patterns similar to those for Figures II-A7 and II-A8. The dipole-dipole apparent resistivities more rapidly approach the deep model resistivities as a function of electrode separation than do the Schlumberger data.

For the gently dipping contact in Figure II-A21 the dipole-dipole pseudo-section shows the characteristic pattern for a lateral resistivity contrast which reaches the surface. Contour lines extend down-to-the-left and down-to-the-right from the surface expression of the contact at

x = 5.5. The contour pattern gives little indication of the dip of the contact. Rather, apparent resistivities for the two dipoles straddling the contact ($\rho_a \approx 50$) are markedly higher than those for the similar region in Figure II-A1, which can be calculated using equation (II-3). It is this block of apparent resistivities which indicate that the contact is either dipping (Figure II-A21) or of limited vertical extent (Figure II-A5).

The Schlumberger pseudo-section (Figure II-A22) shows greatly different resistivities for soundings made on opposite sides of the contact. Even at x = 4.5 the apparent resistivities for large AB/2 do not approach the resistivity of the underlying material.

For contacts or faults with resistive overburden material (Figures II-A23 through II-A26) the anomaly patterns are consistent with discussions given above, with the exception of the false low anomaly outlined by the ρ_a = 65 contour in Figure II-A24. This potentially misleading feature appears when one of the Schlumberger current electrodes is located over the conductive mass.

Surface layers with varying thickness.

Dipole-dipole and Schlumberger responses. Figures II-A27 through II-A34 demonstrate the effects that surface layers with moderate thickness variations can have upon dipole-dipole and Schlumberger data. In all cases the apparent resistivity pattern at small maximum electrode separations accurately reflects the physical situation. Observe the ρ_a = 15 and 25 contours for the models in which the layer is more conductive than the half-space, and the ρ_a = 15, 25, 40 and 65 contours for the cases in which the layer is more resistive than the

half-space. At greater separations, the dipole-dipole pseudo-sections display some potentially misleading characteristics: false anomalies suggest the presence of a conductive feature at the center of the models for the thinning conductive layer (Figure II-A27) and the thickening resistive layer (Figure II-A33), and the presence of a resistive feature at the center of the model for the thickening conductive layer (Figure II-A29). However, as will be seen later, these anomalies are not of the same shape as those which result from conductive or resistive bodies. It should be noted that, for the layer more resistive than the half-space, both the dipole-dipole and Schlumberger pseudo-sections show regions which have lower apparent resistivities than the ρ = 10 half-space.

The conductive body in a homogeneous half-space.

Figures II-A35 through II-A42 depict a series of conductive bodies with increasing depth extent. In every case the body has ρ = 1, is one unit wide, and is buried one unit in an otherwise homogeneous half-space with ρ = 100.

Dipole-dipole response. For the one-half unit thick body (Figure II-A35) the dipole-dipole pseudo-section shows a 44% anomaly centered on the body at x = 0, N = 4. The triangular or boomerang shaped low anomaly enclosed by the ρ_a = 65 contour is characteristic of a conductive body in a half-space when the dipole-dipole method is used. A physical explanation for this anomaly pattern in the pseudo-section is that the transmitting dipole source field or the receiver dipole potential field will be most greatly affected when one of these dipoles is in the immediate vicinity of the anomalous body. For example, for a transmitting dipole located at x = -1, -2 the apparent resistivity values obtained

when the receiving dipole is moved to the right of x = 0 yields the string of numbers down-to-the-right from x = -1.5. Similarly with a dipole located at x = 1, 2 when the other dipole is moved to the left of x = 0 the string of apparent resistivities down-to-the-left from x = 1.5 yields the low values shown in the pseudo-section. As the depth extent of the body is increased (Figures II-A37, II-A39, and II-A41) the triangular anomaly pattern remains unchanged with the apex located over the body at about x = 0 to -1, and with the lowest apparent resistivity being located at N = 4 or 5. As the depth extent of the body doubles from one to two to four units the anomaly increases from 54 to 64 to 74%. Also, the anomalous highs enclosed by the ρ_a = 120 contour become more pronounced. These features occur for dipole locations which also yield some of the lowest apparent resistivities in the pseudo-section. The difference is determined by whether or not the conductive body lies not only near, but between the transmitting and receiving dipoles, or whether it lies outside the two dipoles. For a receiver dipole centered at x = -1.5, and with the transmitter to the left, current from the source will be drawn through the area of the receiver electrodes into the conductive body thereby increasing the current flow in the vicinity of x = -1.5 and increasing the apparent resistivity calculated for a receiver at this location.

Notice that even for the smallest of these conductive bodies (Figure II-A35) the apparent resistivities are anomalously low for very large transmitter-receiver locations (N = 15) which straddle the inhomogeniety. This is an artifact of two-dimensional modeling of the dipole-dipole method: regardless of the distance from an infinitely long conductive body, the dipole current field will at some point become tangent to the

feature and will therefore be highly coupled, resulting in significant perturbation of the source field.

If the depth to the top of a tabular body is increased from one to two units (Figure II-A43) the anomaly is sharply reduced, however, at a very large separation there is a significant 69% anomaly which is centered over the body.

Figures II-A45 and II-A47 demonstrate the effects of increasing the lateral extent of a conductive body. If Figure II-A45 is compared with Figure II-A39 for a body with the same cross section area, it is seen that the amplitude of the dipole-dipole anomaly does not change. The anomaly pattern, however, as shown by the ρ_a = 40 contour, has become broader with limbs extending down-to-the-left and down-to-the-right from dipole locations over the body. With further increased width of the body (Figure II-A47) there is very high coupling with dipoles located over it, producing an anomaly of 71% or greater in the limbs extending down-to-the-right from x = 0 to 2 and down-to-the-left from x = 1 to 3.

If the resistivity of the conductive body is reduced to 10 while the background remains unchanged at ρ = 100, Figures II-A49, II-A51, and II-A53 show a significant decrease in dipole-dipole anomaly amplitude when compared with the previous cases for bodies with ρ = 1 (Figures II-A39, II-A45, and II-A47, respectively), because current flow through the inhomogeneity is greatly diminished.

Figures II-A55 and II-A57 show conductive bodies dipping to the right at 45° and 27°; they have the same maximum depth, minimum depth, and cross-section area as the vertical body shown in Figure II-A39. The dipole-dipole anomalies have approximately the same amplitude as that

for the vertical body, but the anomalous lows extend down-to-the-left from x = 1 to 3. Only the shallowest portions of the apparent resistivity lows at N = 3 and 4 lie over the body, which could be very misleading to the naive interpreter. The explanation for the anomaly skewing in the opposite direction from the dip of the body is that the greatest perturbation of the dipole field occurs when the body is roughly coincident with current lines from the source or transmitter. Thus, for transmitters located at x = 1 and 2, or x = 3 and 4, the dipole source field would be significantly affected as observed by receivers to the left. Conversely, and as reprocity dictates, if transmitters were located to the left of x = -2, the current flow would tend to be channelled through the body, greatly perturbing the potential field observed at x = 1 to 3.

Figures II-A59, II-A61, and II-A63 depict the responses due to massive conductive bodies with depths of burial of two, three and four units. These should be compared with Figure II-A43 for a tabular body with a depth of burial of two units. The dipole-dipole response is quite large in each case, but with an enormous dipole separation of N = 14 being required to reach the lowest apparent resistivities for a depth of burial of four units. However, significantly anomalous apparent resistivities are observed at shorter N-spacings. As can be seen from these as well as from previous models, if a conductive body is wide with respect to its depth of burial, the lowest apparent resistivities form a crescent shaped pattern, but as the depth to width ratio becomes larger, this pattern becomes more triangular or circular.

The ability, or lack of same, of the dipole-dipole method to resolve two vertical bodies as the distance between them is increased

from one, to two, to four units is demonstrated in Figures II-A65, II-A67, and II-A69. Only at a separation of four units are the two inhomogeneities clearly resolved. The anomaly pattern is the superposition of two patterns similar to that shown in Figure II-A39.

Schlumberger response. The pseudo-section for the small conductive body in Figure II-A36 shows a widely distributed anomaly of about 15 to 17%. The sounding located at x = -0.5 most clearly defines the location of the body. However, it is clear that an anomaly of this low magnitude, particularly if observed at several sounding locations, would probably not be interpreted as a small conductive body located beneath x = 0 to -1. As the depth extent of the body increases (Figures II-A38, II-A40, and II-A42) there is the development of anomalous low apparent resistivity "sidelobes" enclosed by the ρ_a = 80 contours. The reason that these pseudo-section features lie on either side of the location of the body is that the greatest perturbation of the source field is obtained when one of the transmitting electrodes is in the vicinity of the body. That is to say, when a transmitting electrode is at x = +1 and the second transmitting electrode is located a large distance to the left, the effect of the body is most significant. If Schlumberger soundings were made at only several locations along the profile line, it is doubtful that the existence of a body would be interpreted, certainly not a conductive body located at x = 0 to -1, at which location the sounding would yield a nearly constant apparent resistivity greater than 82.

If the depth to the top of a tabular body is increased from one to two units (Figure II-A44) the Schlumberger method reveals no anomaly for the sounding over the body and only a 23% anomaly seen off to the

sides beneath x = +5, and x = -5. If by chance one were to perform soundings at these two locations without a sounding located in between, the interpretation would clearly be that of a layered section with conductivity increasing at depth.

The response to increasing the body width from one unit (Figure II-A40) to two units (Figure II-A46) is quite dramatic. The anomaly amplitude increases from 17 to 43%, making it easily detectable for a sounding fortuitously located over the body. And with a width of four units (Figure II-A48) nearly a 70% anomaly is observed. The explanation for this is that for Schlumberger current electrodes located on opposite sides of a wide body, there is high coupling with the predominantly horizontal current flow. The result is a large perturbation of the potential field seen by receiver dipoles located over the body. However, the Schlumberger anomaly for a two unit wide, one unit thick body with ρ = 10, (Figure II-A52) is not greatly reduced from that for the body with ρ = 1 (Figure II-A46). The combined width and depth extent of the body are sufficient to alter significantly the transmitted current field, whereas for the thin, four unit wide body at ρ = 10 (Figure II-A54) the response is about half of that seen over the same body at ρ = 1 (Figure II-A48).

For dipping bodies (Figures II-A56 and II-A58) the Schlumberger pseudo-sections reveal that as the body becomes more nearly horizontal the anomaly for soundings centered over it increase from 18% for the vertical case (Figure II-A40) to 34% and 46% for the body dipping at 45° and 27°, respectively. As has been mentioned before, coupling of the Schlumberger source current with the body is responsible for this result.

For massive conductive bodies at large depths of burial (Figures II-A60, II-A62, and II-A64) the Schlumberger data demonstrate that the conductive body affects the apparent resistivities far beyond the edges of the calculated pseudo-section. For large transmitter lengths ($AB/2 \geqslant 5.5$) the body at a depth of two units produces a significant anomaly of at least 38% for soundings located over it. However, with the body three or four units deep the effect of having a current electrode over the body dominates, resulting in a diffuse anomaly pattern which would be interpreted as an extensive region in which the resistivity decreases as a function of depth.

As can be seen from Figures II-A66, II-A68, and II-A70, the Schlumberger method is exceptionally poor at resolving two tabular bodies. In all of these cases the anomaly pattern is that which would be produced by a single wide body having lower resistivity contrast with the background than the two bodies shown.

The resistive body.

Resistive bodies are very seldom sought as geophysical targets. Geothermal steam reservoirs are a notable exception, however, these are generally surrounded by anomalously conductive condensation zones. For this reason an extensive model study of buried resistive bodies will not be presented.

Dipole-dipole response. The pseudo-section in Figure II-A71 displays apparent resistivity highs extending down-to-the-left from x = -1 to 2, and down-to-the-right from x = -2 to 1. For transmitter dipoles located at these positions above the body the current will be forced to flow laterally to circumvent the resistive feature. The result is higher

potential differences measured at the receiver dipoles, and a higher calculated apparent resistivity. For widely spaced transmitter-receiver arrays straddling the body, current flow is shielded from the receiver dipoles to produce a region of apparent resistivities lower than the background resistivity. These values are seen centered on the body for N greater than 6.

Schlumberger response. The pseudo-section in Figure II-A72 reveals an anomaly with twice the amplitude than was observed for the identically shaped conductive body (Figure II-A40). The transmitted Schlumberger current, which tends to flow horizontally in the vicinity of the receiver dipole, is not greatly deviated by a thin vertical conductive body, whereas a vertical resistive body forces the current to flow around it. Conversely, a thin horizontal resistive body will produce a small anomaly for soundings centered above it.

Conductive bodies beneath an overburden layer.

Figures II-A73 through II-A100 demonstrate the effects that a conductive overburden layer has upon the anomaly patterns for some of the conductive bodies discussed above. For most of the models presented, the apparent resistivities for the simple two layer structure (the overburden layer and the ρ = 100 half-space), undisturbed by the inhomogeneity, can be seen along the left or right edges of the pseudo-sections down through N = 8 or AB/2 = 5.5. The anomaly amplitude will be based upon these undisturbed two layer values for the same N or AB/2 spacing as the apparent resistivity value being considered.

Dipole-dipole response. The models in Figures II-A73 and II-A75 have a one-half unit thick layer with ρ = 30 and 10, respectively,

above the conductive body in Figure II-A39. The closed contour apparent resistivity low no longer exists because it merges with low near surface apparent resistivities resulting from the conductive layer. However, if the apparent resistivities across any particular row in the pseudo-section (constant N-spacing) are scanned, it can be seen that a significant anomaly remains in the presence of the layer. For example, centered on the body at N = 4 there are anomalies of 50% and 33% for the layer resistivities of 30 and 10, respectively. As would be expected, at large transmitter-receiver separations the apparent resistivities approach those for the model without the overburden layer. If the resistivity of the body is increased to 10 with the ρ = 30 overburden (Figure II-A77) there is a 26% anomaly at N = 4, only slightly less than that without the layer (Figure II-49). With the ρ = 10 overburden (Figure II-A79) this is reduced to 16%.

If the depth extent of the body in the Figure II-A75 is increased (Figure II-A81) there is only a minor increase in anomaly amplitude. Whereas, if the depth of burial of the vertical body increased from one to two units (Figure II-A83) the anomaly is significantly reduced. On the other hand, if the overburden thickness is doubled (Figure II-A85) the anomaly amplitude is virtually unchanged, being 16% at N = 4, and 32% at N = 8 in both Figures II-A83 and II-A85. This is a rather interesting result. While the dipole-dipole method is very sensitive to the depth of burial of a conductive body, the thickness of a conductive overburden layer in the range of one-half to one dipole length has virtually no effect upon the anomaly amplitude.

The odd Figures II-A87 through II-A93 show the dipole-dipole pseudo-sections for the conductive bodies having two (Figure II-A51) and four (Figure II-A53) unit widths, with the addition of a one-half unit thick,

ρ = 30 or ρ = 10 overburden layer. In every case high amplitude anomalies similar to those discussed previously are observed. This is also true for the conductive layer above the dipping body (Figure II-A95) and the pair of vertical bodies (Figures II-A97 and II-A99). As was the case without the overburden, at four units separation there is reasonable resolution of the two bodies.

Schlumberger response. The Schlumberger method, which for practical purposes was unable to reveal a one unit wide conductive body at a depth of burial of one unit shows reduced detectability with the addition of a conductive overburden layer. In Figure II-A74 the anomalous effect of having a transmitter electrode located over the body dominates the response, producing slight apparent resistivity lows on either side of the inhomogeneity. The even Figures II-A76 through II-A86 show insignificant anomalies which would be interpreted in terms of a somewhat varied layered structure.

The effect of increasing the width of the body (even Figures II-A88 through II-A94) is once again to couple better with the transmitter current, resulting in higher amplitude anomalies. With a ρ = 30 overburden the two unit wide body yields a 23% anomaly at AB/2 = 3.5, and the thin four unit wide body shows a strikingly definitive anomaly at all large transmitter lengths. With the ρ = 10 overburden this wide body produces a 25% anomaly at AB/2 = 3.5 and 4.5. An anomaly pattern such as this could easily be confused with that produced by variations in the thickness or resistivity of the surface layer. This is also the case for the dipping body or pairs of bodies in Figures II-A96, II-A98, and II-A100.

Surface resistivity contrasts.

Figures II-A101 through II-A118 demonstrate the effects that small conductive or resistive inhomogeneities at the surface of the earth can have upon dipole-dipole and Schlumberger resistivity data. In all cases two bodies have been placed in the model to show the differing effects of electrode placement with respect to the position of the bodies. The upper halves of the pseudo-sections show the anomalies for each of the bodies relatively independently, and the bottom halves show the anomalous interference patterns which develop.

Dipole-dipole response. The model in Figure II-A101 contains two very conductive inhomogeneities at the surface. The body at z = -5 is located where transmitting and receiving electrodes are placed, while the body at x = +4.5 is straddled by transmitting and receiving dipoles. The upper half of the dipole-dipole pseudo-section shows very similar anomalies caused by these identical bodies. However, there are subtle differences as a result of electrode placement. The body on the left gives a slightly lower value of ρ_a = 9.9 while the body on the right yields ρ_a = 15. At N = 1 the body on the left produces two low apparent resistivity values at x = -4.5 and -5.5, outside of which are apparent resistivities of 111, higher than the background. The body on the right produces one low apparent resistivity value at x = 4.5 which is bounded by intermediate values of ρ_a = 69.7, beyond which are apparent resistivities of 111. This pattern at N = 1 propagates down through the pseudo-section. For dipoles centered at x = -4.5 and +3.5 a particularly anomalously high apparent resistivity at N = 7 is the result. For transmitter-receiver arrays straddling both bodies anomalous lows are observed in a triangular region extending downward from an apex

beneath x = 0 at N = 9. If the locations of the inhomogeneities remain the same, but the depth extent is reduced (Figure II-A103) the same effects are observed, but at lower amplitudes. If the resistivity contrast between bodies and background is reduced (Figure II-A105), the low apparent resistivities which were found beneath each body in the upper half of the pseudo-section (for transmitter-receiver arrays straddling a body) become insignificant. The only values affected are those for which an electrode is located in a body or a dipole straddles a body.

Figure II-A107 shows the effects of a pair of unconnected conductive bodies with the electrodes from one dipole placed in each, and a conductive body long enough for both electrodes to be placed within it. The dipole-dipole anomaly which results from the pair of bodies on the left is similar to the anomaly pattern which was seen for the body between two electrodes (the inhomogeneity on the right in Figures II-A101 and II-A103). The body on the right, in which both electrodes are placed, yields exceptionally low apparent resistivities for all values down-to-the-right and down-to-the-left from this dipole location. Reduction of the resistivity contrast with the background results in similar, lower amplitude anomalies, with one curious exception. For transmitter-receiver arrays straddling the right-hand body in Figure II-A107 (ρ = 1) the apparent resistivities are low, whereas for the same shaped body with ρ = 10 (Figure II-A109) these apparent resistivities are higher than background. At ρ = 10 the inhomogeneity attracts the dipole source current, resulting in increased near-surface current flow, hence, higher apparent resistivities. At ρ = 1 there appears to be a saturation effect.

Figure II-A111 displays the pseudo-section produced by bodies having a resistivity 100 times greater than the background. A very striking effect is seen: low apparent resistivity values occur beneath and spreading to the right and left from the locations of the resistive bodies. The reason for this is that for dipole-dipole arrays straddling a resistive body the transmitter current is partially blocked from reaching the receiver array. This lowers the voltage seen by the receiver dipole array and reduces the apparent resistivity calculated. The differences between this anomaly pattern and that for the conductive bodies in Figure II-A101 are subtle. For the body on the left in which an electrode is placed the values of apparent resistivity at N = 1 in the vicinity of the body are considerably greater than the background resistivity. This was not the case for the conductive body. For the resistive body on the right a very low value of apparent resistivity, ρ_a = 10.5, is found at N = 1 at the location of the body. This is similar to the low value of ρ_a = 15 at N = 1 and x = +4.5 found in the conductive cases. The difference between the two anomaly patterns is that the resistive body produces highs adjacent to the central low value, while the conductive body yields apparent resistivities lower than the half-space at these locations in the pseudo-section. For smaller resistive bodies having lower contrast with background (Figure II-A113) the apparent resistivity low beneath a body tends to disappear, leaving as the dominant effect apparent resistivity highs at locations for which a dipole straddles the resistive feature or an electrode is placed on it. These conclusions also apply to the resistive bodies in Figure II-A115. As can be seen in Figure II-A117, a relatively shallow depth of burial to the top of a resistive body results in substantially

increased apparent resistivities for transmitter-receiver arrays straddling the feature.

Schlumberger response. For the two conductive surface inhomogeneities in Figure II-A102 the Schlumberger pseudo-section displays two quite predictable effects. For a receiver dipole straddling a body or a receiver electrode located on a body the apparent resistivities for those soundings are noticeably reduced. Placing a transmitter electrode on or near a conductive body also reduces the apparent resistivity because current is conducted deeper into the half-space, reducing the potential difference observed at the receiver dipole. This effect becomes quite pronounced for both transmitter electrodes located in the vicinities of the conductive bodies, resulting in the anomalous low enclosed by the ρ_a = 65 contour. As the bodies are reduced in size (Figure II-A104) the only effect which remains important is that of having a conductive body within the span of a receiver dipole.

For the two unconnected conductive bodies and the single conductive body spanning a receiver dipole in Figures II-A108 and II-A110 the response is similar. The sounding at x = +4.5 is overwhelmed by the shunting effect of the conductive inhomogeneity.

For the resistive surface features in Figure II-A112 apparent resistivity highs are found for soundings having receiver dipoles on or straddling a body. Lows occur if a transmitter electrode is on the opposite side of a resistive body from the receiver dipole. For smaller, less resistive bodies at various locations with respect to electrodes (Figures II-A114 and II-A116) these effects diminish considerably. A shallow depth of burial significantly reduces the apparent resistivity high over a resistive body (Figure II-A118).

Dipole-dipole and Schlumberger pseudo-sections along a profile line at 45° to strike.

Figures II-A119 through II-A162 depict dipole-dipole and Schlumberger pseudo-sections for selected models discussed above, with the survey profile line at 45° to strike. This is accomplished numerically by performing a y-shift transformation of the potentials found at nodal points along the x-axis. The model shown in the bottom half of each figure is the cross-section of the structure in the profile line direction--a projection at 45° to strike. This portrayal of the models is useful in that it gives an accurate representation of the electrode locations with respect to lateral resistivity contrasts. However, it must be borne in mind that the actual cross-section (perpendicular to strike) would show all horizontal distances divided by $\sqrt{2}$.

A structure with the same model name as was used for the profile lines perpendicular to strike is similar to it, with the following modifications. Structures with a "B" designation after the model name are nearly identical to the corresponding 90° model. They are simply traversed at 45° to strike. (As a result of a constraint of four grid divisions per unit (dipole) length for the numerical calculations, the correspondence is not exact, e.g., bodies one unit wide at 90° to strike have been made 1.5, rather than 1.414, units wide in the 45° profile direction). The electrodes are no longer at the same locations with respect to lateral boundaries as was the case for the profiles perpendicular to strike. The "B" pseudo-section for a particular model can be compared with that at 90° to strike to estimate the anomaly variation which will occur if a known feature is traversed at an angle other than perpendicular to strike.

Structures with an "A" designation at the end of the model name have cross-sections in the 45^{o} profile direction which are identical to the 90^{o} cross-sections for the models described previously. This means that actually they are only $1/\sqrt{2}$ times as wide as the models shown perpendicular to strike. The electrode locations with respect to lateral resistivity contrasts are the same as in the perpendicular cases. The "A" pseudo-section for a particular model can be compared with the 90^{o} pseudo-section for the same model to estimate the anomaly variations which might occur in traversing a body of unknown strike direction.

A detailed discussion of the pseudo-sections at 45^{o} to strike is not warranted. None of the anomalies shows a radical departure from the patterns seen at 90^{o} to strike, and all the characteristics displayed have been pointed out or discussed previously. The interested reader can easily compare the details of these pseudo-sections.

A couple of general observations whould be made, however. For a survey line at 45^{o} to the strike of two-dimensional conductive bodies, there is better coupling between the transmitted current and the body than was the case at 90^{o}. This tends to produce higher amplitude anomalies. In addition, for the "B" models it takes a larger number of unit length dipoles to traverse a body at 45^{o} to strike, which results in a larger anomalous pattern in the pseudo-section. The "A" models, on the other hand, yield anomaly amplitudes and patterns quite similar to those at 90^{o} to strike. This indicates that the effect of reducing the true cross-section area of the body by $1/\sqrt{2}$ is approximately offset by the effect of the increased coupling at 45^{o} to strike.

Summary of Observations for the Dipole-Dipole Method

1) Contacts which reach the surface produce three zones of apparent resistivities in the pseudo-section depending upon whether the two dipoles straddle the contact or both lie on one side or the other. The method is quite insensitive to the dip angle of contacts greater than 30^{o}.

2) Buried faults are not easily located by the dipole-dipole method because across any row in a pseudo-section (constant N) there is only a gradual transition in the apparent resistivity.

3) A small surficial resistivity inhomogeneity with moderate contrast affects all apparent resistivities calculated for transmitter or receiver dipoles which straddle or are in contact with it. Hence, the effect is seen along diagonals in the pseudo-section, down-to-the-right and down-to-the-left from the inhomogeneity. As the size or contrast of such features becomes large, the apparent resistivity for electrode arrays straddling the inhomogeneity are also influenced, but this effect diminishes with increased transmitter-receiver separation.

4) Resistive bodies at the surface can produce anomalies very similar to those seen for conductive features, but they can be distinguished by subtle differences at N = 1. Both produce apparent resistivity lows for transmitter and receiver dipoles on opposite sides of inhomogeneity, however, this effect decreases sharply for a resistive body if it is buried.

5) A pair of near surface inhomogeneities can produce false closed contour apparent resistivity highs or lows located half-way between them at depth (large N) in a pseudo-section. The apparent resistivity can be

higher or lower than any actual resistivity in the model or structure. Often such anomalies can be recognized as occurring at the intersection of diagonal trends extending through the data. These anomalies are generally not the proper shape for structural features at depth, and yield more abrupt changes in apparent resistivity from one station to the next than would be observed for deep structures.

6) The method accurately represents small variations in surface layers for small separations, but at large N deceptive apparent resistivities can be produced. These anomalies are quite distinguishable, however, from those caused by simple buried bodies.

7) For a large conductive region at the surface surrounded by more resistive material, extraordinary apparent resistivity highs and lows are observed depending upon whether the two dipoles are located just beyond or just within the distant edges of the conductive zone. This means that, for example, if a sedimentary valley is only several dipole lengths wide the dipole-dipole method will be very insensitive to the depth to the resistive basement. Furthermore, if measurements are confined to the sedimentary basin, the resistivity of the underlying bedrock is very difficult to ascertain. For this purpose surveys should extend at least one full dipole length into bedrock at one, or preferably both, ends of the line.

8) Simple conductive bodies at a depth of one dipole length produce characteristic anomaly patterns which are crescent shaped lows if the body is wide and more triangular if it is narrow. In either case the apex is centered over the body at small N spacings.

9) For conductive bodies within one dipole length of the surface the most anomalous apparent resistivities at small dipole separations are

for one dipole approximately over the body. For deeper inhomogeneities anomalous values are observed for arrays more nearly straddling the feature.

10) There is a significant reduction in anomaly amplitude with increased depth of burial from one to two dipole lengths. Large conductive bodies at three or more dipole lengths can produce significant anomalies, but very large transmitter-receiver separations (N = 10-15) are required.

11) Dipping conductive bodies produce pseudo-section anomalies which dip in the oppostie direction with only the shallowest anomalous apparent resistivities lying over the top of the body.

12) A buried resistive body produces a crescent shaped apparent resistivity high with lows for large arrays straddling the body.

13) Increasing the conductive overburden thickness up to one dipole length does not significantly reduce the anomaly amplitude for dipole separations several times the overburden thickness.

Summary of Observations for the Schlumberger Method

1) Schlumberger soundings are relatively well behaved in the vicinity of vertical contacts, although anomalous apparent resistivities do occur when the transmitter array straddles a contact.

2) Over faulted layered structures soundings tend to reflect the structure directly beneath the center of the array.

3) Gradually varying surface layer thickness is accurately reflected in Schlumberger soundings.

4) Soundings over conductive material surrounded by a more resistive background will yield nearly constant apparent resistivities once the current electrodes have been expanded to the resistive material. This means that soundings made over sedimentary basins will not continue to

approach the bedrock resistivity once the transmitter electrodes have spanned the valley.

5) There are two quite different effects seen in Schlumberger data gathered in the presence of inhomogeneous bodies, depending upon whether it is a transmitter or receiver electrode in the vicinity of the body. This is a result of the different influence that an inhomogeneity will have upon the radial flow from a current electrode versus the horizontal flow in the vicinity of the receiver dipole at the surface in the center of the array.

6) A small surficial inhomogeneity with moderate contrast affects only the soundings for which a receiver dipole straddles or is in contact with it. If such a feature is large or has high contrast substantial anomalies will be observed at AB/2 separations for which a transmitter electrode is in the vicinity of the inhomogeneity.

7) Low apparent resistivities are observed for a transmitter electrode in the vicinity of a surficial or near surface conductive inhomogeneity. If the feature is resistive, apparent resistivities are high for transmitter electrode locations between it and the receiver dipole, and low for electrode locations beyond it.

8) A conductive body whose width is less than or equal to its depth of burial will not produce a significant Schlumberger anomaly for a sounding performed off to the side when a current electrode is located over the inhomogeneity.

9) A conductive body whose width is at least twice its depth of burial will yield a substantial anomaly for soundings located above it.

10) Soundings located over a buried resistive body will yield a significant anomaly if the inhomogeneity has considerable vertical extent,

but not if it is thin and horizontal.

11) Schlumberger detection of buried conductive bodies is severely hampered by the existence of a conductive overburden layer because the current tends to stay confined to this layer.

The Relationship Between Two-Dimensional Modeling and Three-Dimensional Structures

For small two-dimensional conductive bodies at shallow depths of burial, the dipole-dipole anomaly amplitude remains high for very large N-spacings if the dipoles are situated on opposite sides of the inhomogeneity. An explanation of this lies in the fact that a dipole current field will tend to couple with an infinitely long conductive feature, regardless of its distance away. On the other hand, three-dimensional conductive bodies with limited strike length will not couple well with a distant dipole source, so apparent resistivities will rapidly approach the resistivity of the background with increased N-spacing. This has been demonstrated by numerical modeling for three-dimensional bodies (Bakbak, 1977; Dey, 1977).

For a Schlumberger expansion perpendicular to and centered over a conductive inhomogeneity, the source current tends to flow perpendicular to the long axis of the body, so the degree of coupling, and therefore the anomaly amplitude, is not greatly influenced by its strike length. However, the Schlumberger anomalies observed for a current electrode in the vicinity of a conductive two-dimensional body should decrease significantly with the strike length of the inhomogeneity as the source current will be less widely dispersed into the background material.

CONCLUSIONS AND RECOMMENDATIONS

1) For a conductive layer over a more resistive half-space, the dipole-dipole method is more sensitive to the resistivity contrast than the Schlumberger method for equivalent maximum electrode separations. At short separations, the dipole-dipole apparent resistivities are lower than for Schlumberger, and at large separations they are higher. However, the Schlumberger method is quite responsive to deviations in predominantly layered structure beneath the center of the array, whereas the dipole-dipole response to faulted layers can be complex and does not occur abruptly in pseudo-section.

2) Anomalous bodies of any shape buried less than two dipole lengths can display a significant and distinctive dipole-dipole response. The Schlumberger method yields little correctly interpretable response to conductive bodies with a depth of burial greater than the body width.

3) Points (1) and (2) are consistent with the common usage of these two resistivity methods: the dipole-dipole method, with separations up to N = 4 or 5, predominantly being employed in mineral exploration, and the Schlumberger method being applied to soundings over flat lying structures such as sedimentary basins.

4) If in performing a Schlumberger sounding a current electrode comes into the vicinity of a surficial or buried resistivity inhomogeneity, apparent resistivity anomalies will be observed which, without a pseudo-section of data, may be indistinguishable from those produced by layered structure. A dipole-dipole array expansion (with one fixed transmitter location) should never be used as a means of resistivity depth sounding because the effects of near surface inhomogeneities will overwhelm those of most layered structures.

5) If the Schlumberger array is used for resistivity profiling, whereby the whole array is moved along a line with AB/2 kept constant, many types of inhomogeneity could cause a larger anomaly when a current electrode, rather than a receiver electrode, is located near the feature. This could be rather misleading because other inhomogeneities will produce a single broad anomaly.

6) In the presence of a conductive overburden layer the dipole-dipole method will reveal a conductive body buried in the underlying resistive half-space for N-spacings sufficiently large to yield apparent resistivities well above the resistivity of the overburden. For equivalent maximum electrode separations the Schlumberger method produces very poor response to conductive bodies buried beneath a conductive overburden because the current flow in the vicinity of the receiver dipole tends to be confined to the overburden layer. For conductive bodies buried more than half their width, larger anomalies are observed for a current electrode over the body than for the receiver dipole over the inhomogeneity. Thus, an anomaly is observed for soundings not centered over the body which would appear to be attributable to a conductive region at depth beneath the center of the array.

7) For resolving two buried conductive inhomogeneities, the dipole-dipole method is not particularly successful, and the Schlumberger method is quite useless.

8) The use of very large transmitter lengths to determine deep structures with the Schlumberger method is clearly appropriate only for layered situations. Very large dipole-dipole transmitter-receiver separations can afford some resolution of major lateral resistivity changes at depth, but the resultant anomalies may be difficult or

impossible to recognize as a result of complex patterns in the pseudo-section due to shallower inhomogeneities.

9) The Schlumberger sounding method as commonly practiced recognizes the reduction in resolution with increased depth of penetration: the transmitter length is increased logarithmically. Dipole-dipole data for separations greater than about N = 6 should follow the same principle: not every value deep in the pseudo-section need be obtained for the purposes of modeling and interpretation.

10) Surveys performed along profile lines at 45^{o} to strike yield anomaly patterns similar to those seen perpendicular to strike, except that anomalies are broader and have higher amplitude. Surveys might under some circumstances be deliberately run at an angle other than perpendicular to strike to enhance the anomaly of a buried target with considerable strike length.

11) The discrepancy between the anomalies observed for deep conductive two- and three-dimensional bodies is greater for the dipole-dipole than for the Schlumberger method. (However, the Schlumberger method does not reveal such features at all unless they are very wide.)

12) As applied to the deep probing and delineation of potential geothermal systems, the relative advantages and disadvantages of each method make the nature of the target the determining factor. For locating an extensive flat lying geothermal reservoir, as is found at Ahuachapán, El Salvador, the Schlumberger method is most useful in that it need be performed only at random locations. In an environment such as the Basin and Range valleys of Nevada, where the structure is complex and hydrothermal fluids may be brought closer to the surface via convection in narrow vertical zones, the dipole-dipole method shows

greater promise for analyzing the resistivity structure. A note of warning must be added, however. The dipole-dipole pseudo-section which results from the interference of the anomalies from two or more simple inhomogeneities can become very complex. This means that field data obtained over complex geological structure can be exceptionally difficult to interpret quantitatively, with accurate representations based upon two- or three-dimensional modeling.

APPLICABILITY OF THE DIPOLE-DIPOLE MODEL CATALOG TO THE INTERPRETATION OF BIPOLE-DIPOLE DATA

A d.c. resistivity technique which has been applied to geothermal reconnaissance of several hundred square kilometer areas is variously called the bipole-dipole, dipole mapping, or roving dipole method. A thorough treatment of the method is given by Keller, et al. (1975).

A large grounded transmitter bipole of 1.5 to 3.0 kilometers in length is used. It remains in one place long enough that considerable effort can be put into achieving low contact resistance with the earth for high current injection. The area of interest is then mapped at discrete points with potential difference measurements. At each receiver station two short orthogonal grounded dipoles of approximately 100 meters in length are laid out, and the voltage measured in the two directions. For consistency, directions parallel and perpendicular to the transmitting bipole are often used. The electrode configuration is shown in Figure II-3. For the geometric arrangement of the electrodes an apparent resistivity, ρ_a , is generally calculated to give the homogeneous half-space resistivity necessary to produce the observed total electric field amplitude, regardless of direction, at the receiver array as a result of the known transmitter current.

An analysis of this method with extensive numerical modeling of the response over two-dimensional models has been undertaken by Dey (1977a). As is done with field data, he presents contour maps of the apparent resistivity at the earth's surface based upon the values calculated for each station plotted at the receiver location. The dipole-dipole pseudo-section data shown in the odd numbered figures in Appendix II-A can, to a limited extent, be used as supplementary information.

For a bipole-dipole transmitter perpendicular to the strike of two-dimensional structures, and for the receiver array located along the axis of the transmitter, the only difference between this and the dipole-dipole method is that the transmitting and receiving dipoles are unequal in length. If there are near-surface resistivity contrasts in the immediate vicinity of the electrodes this can, of course, make an appreciable difference. However, for deeper structures the apparent resistivity is nearly the same, particularly as the separation between the transmitting and receiving arrays becomes large.

Thus, any dipole position on a dipole-dipole pseudo-section can be considered to be the fixed bipole-dipole transmitter location, and the apparent resistivities down-to-the-right or down-to-the-left are approximately the values which would be calculated for bipole-dipole receiver arrays at successive locations on the surface. The apparent resistivity value would be plotted at the receiver positions.

As an example, let us consider Figure II-A1 for the vertical contact. For a bipole-dipole transmitter perpendicular to strike and centered at, for instance, x = -6.5, a receiver array moving to the right would observe the apparent resistivities down-to-the-right from this location: declining until the contact had been crossed, and then constant at ρ_a = 18.1 for all locations on the resistive side (ρ = 100). The contact would be clearly delineated. However, with a conductive overburden layer this would not necessarily be the case. If in Figure II-A9 the transmitter were located at x = -6.5, receivers to the right would observe only a gradually increasing apparent resistivity.

For the conductive body in Figure II-A39 with a transmitter at x = 4.5 measurements to the left would show a sharp drop in apparent

resistivity for receivers over the body, and a slight low-anomaly further to the left. An abrupt drop, however, is also observed when crossing a contact if the transmitter is on the resistive side. (See Figure II-A1).

With the addition of a conductive overburden layer the body in Figure II-A75, for a transmitter at x = 5.5, would yield a low for receivers between x = -1 and -3, however, a similar anomaly is seen for the same transmitter location over the buried fault in Figure II-A9.

An endless number of comparisons could be made of the bipole-dipole responses for various transmitter locations. Some would fortuitously reveal structures of interest, others would not, or could even prove to be misleading. Ambiguity exists as to whether anomalies are caused by shallow or deep sources. The fundamental difficulty is the single transmitter location. In practice two or more transmitters are used for bipole-dipole surveys in an effort to resolve some of this ambiguity.

In any event, a complete analysis of the bipole-dipole method requires surface maps of apparent resistivity, not just values along a line perpendicular to strike. For these the reader is referred to the papers mentioned above by Keller, et al. (1975), and Dey (1977a).

REFERENCES

Bakbak, R., 1977, Three-dimensional numerical modelling in resistivity and IP prospecting: unpublished Ph.D. thesis, University of California, Berkeley.

Beyer, H., 1977a, Telluric and d.c. resistivity techniques applied to the geophysical investigation of Basin and Range geothermal systems, Part I: The E-field ratio telluric method, LBL-6325-1/3: Lawrence Berkeley Laboratory, University of California, Berkeley.

Beyer, H., 1977b, Telluric and d.c. resistivity techniques applied to the geophysical investigation of Basin and Range geothermal systems, Part III: The analysis of data from Grass Valley, Nevada, LBL-6325-3/3: Lawrence Berkeley Laboratory, University of California, Berkeley.

Dey, A., 1977a, An analysis of the bipole-dipole method of resistivity surveying, LBL-6332: Lawrence Berkeley Laboratory, University of California, Berkeley. Also, submitted for publication to Geothermics.

Dey, A., 1977b, Resistivity modeling for arbitrarily shaped three-dimensional structures, LBL-6347: Lawrence Berkeley Laboratory, University of California, Berkeley. Also, submitted for publication to Geophysics.

Dey, A., 1976, Resistivity modeling for arbitrarily shaped two-dimensional structures, Part II: User's guide to the FORTRAN algorithm RESIS2D, LBL-5283: Lawrence Berkeley Laboratory, University of California, Berkeley.

Dey, A., and Morrison, H.F., 1976, Resistivity modeling for arbitrarily shaped two-dimensional structures, Part I: Theoretical formulation, LBL-5223: Lawrence Berkeley Laboratory, University of California, Berkeley.

Furgerson, R.B., 1970, A controlled-source telluric current technique and its application to structural investigations: unpublished Masters degree thesis, Colorado School of Mines.

Hallof, P., 1957, On the interpretation of resistivity and induced polarization results: unpublished Ph.D. thesis, Massachusetts Institute of Technology, Cambridge.

Keller, G.V., and Frischknecht, F.C., 1966, Electrical methods in geophysical prospecting: Pergamon Press, New York.

Keller, G.V., Furgerson, R., Lee, C.Y., Harthill, N., and Jacobson, J.J., 1975, The dipole mapping method: Geophysics, v. 40, no. 3, p. 451-472.

Marshall, D.J., and Madden, T.R., 1959, Induced polarization, a study of its causes: Geophysics, v. 24, no. 4, p. 790-816.

Morrison, H.F., 1975, The up-down counter: a synchronous signal averager for earth resistivity measurements, in "The Study of Temporal Resistivity Variations on the San Andreas Fault": Technical progress report on U.S.G.S. grant #14-08-0001-G-124, period ending February 1, 1975; Engineering Geoscience, University of California, Berkeley.

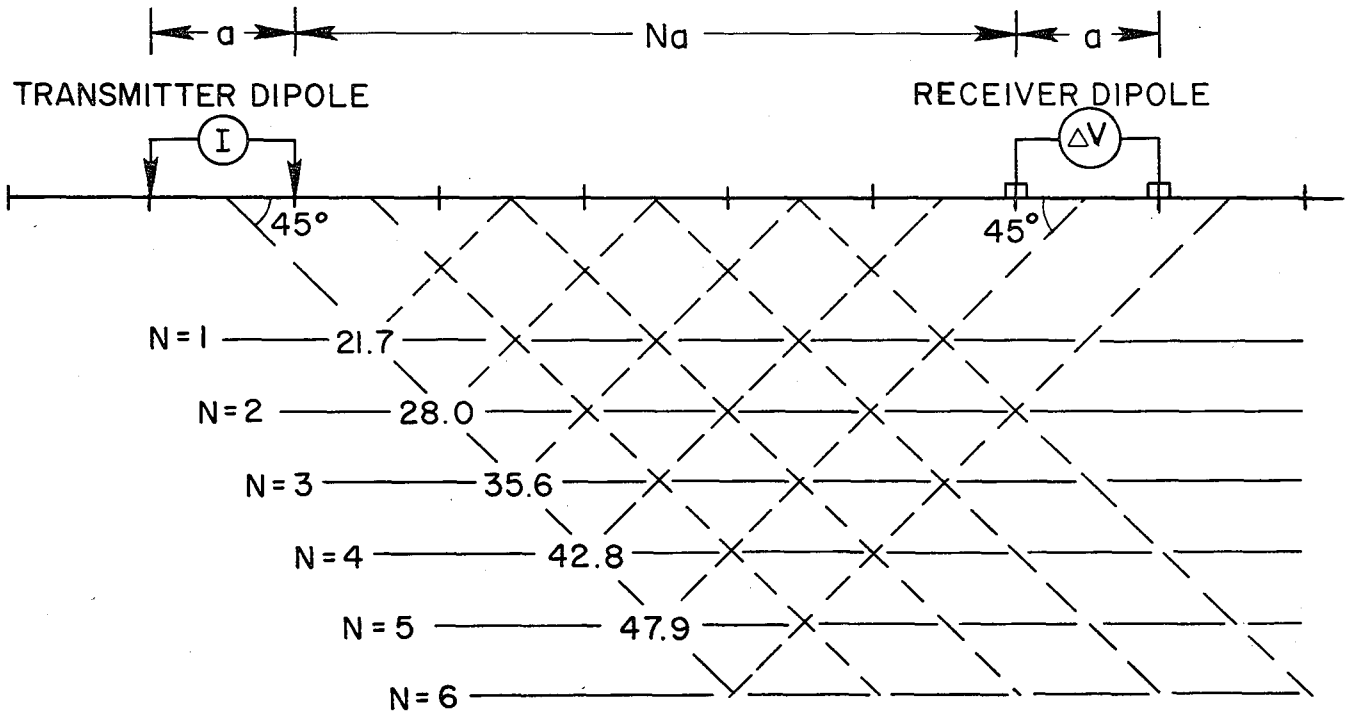

$\rho_a = k\frac{\Delta V}{I}$ WHERE GEOMETRIC FACTOR, $k = \pi a N(N+1)(N+2)$, AND $N = 1, 2, 3, \ldots$

XBL 774-8521

Figure II-1. The dipole-dipole electrode configuration and the construction of the apparent resistivity pseudo-section. The particular transmitter and receiver dipole locations shown are separated by (N =) 5 dipole lengths, and are used to calculate the apparent resistivity, ρ_a = 47.9.

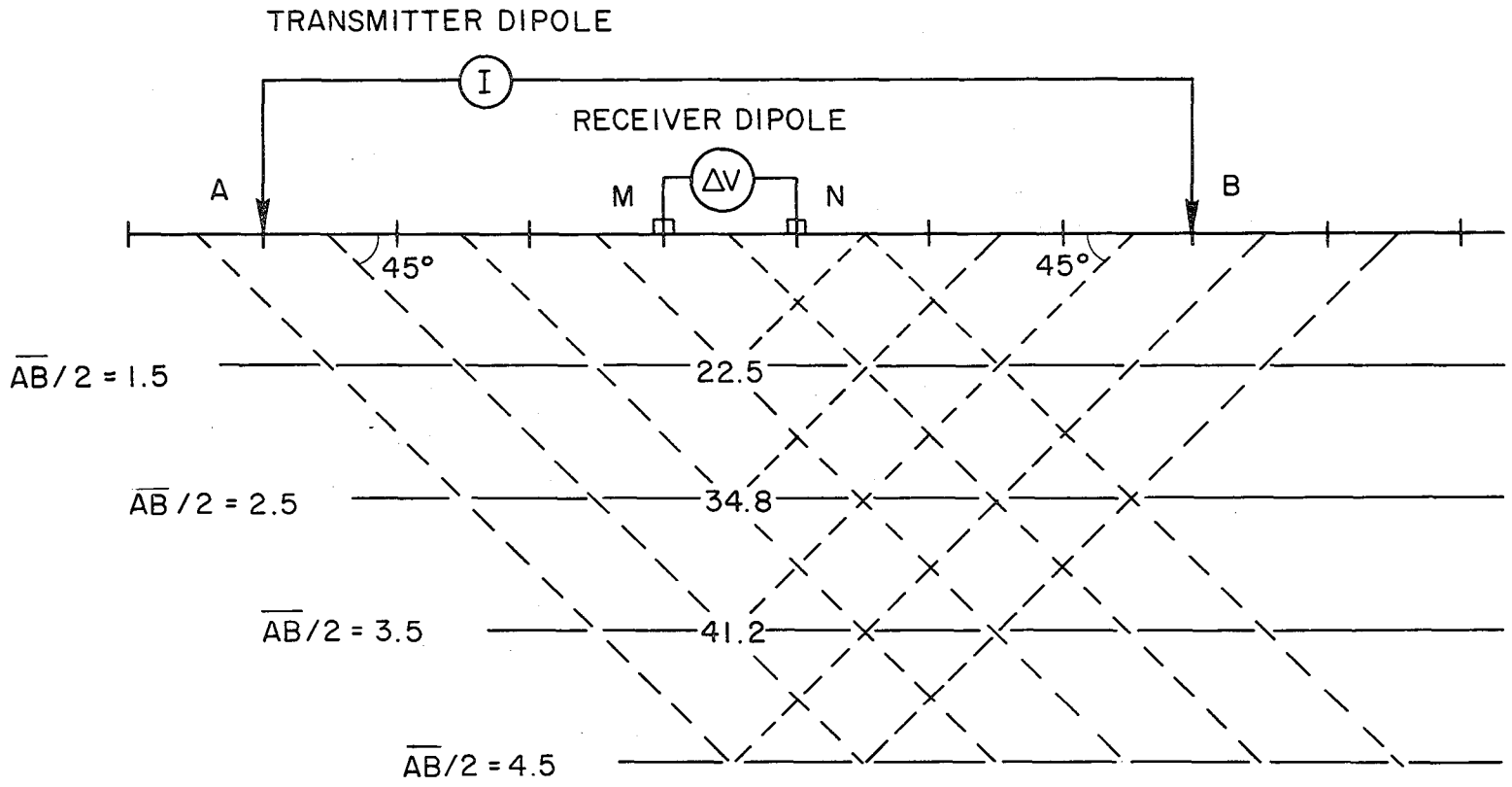

$$\rho_a = k\frac{\Delta V}{I} \quad \text{WHERE GEOMETRIC FACTOR, } k = \pi\left[\frac{(\overline{AB}/2)^2}{\overline{MN}} - \frac{\overline{MN}}{4}\right]$$

XBL 774-8522

Figure II-2. The Schlumberger electrode configuration and the construction of the apparent resistivity pseudo-section. The particular transmitter and receiver dipole locations shown are used to calculate the apparent resistivity, ρ_a = 41.2 at AB/2 = 3.5.

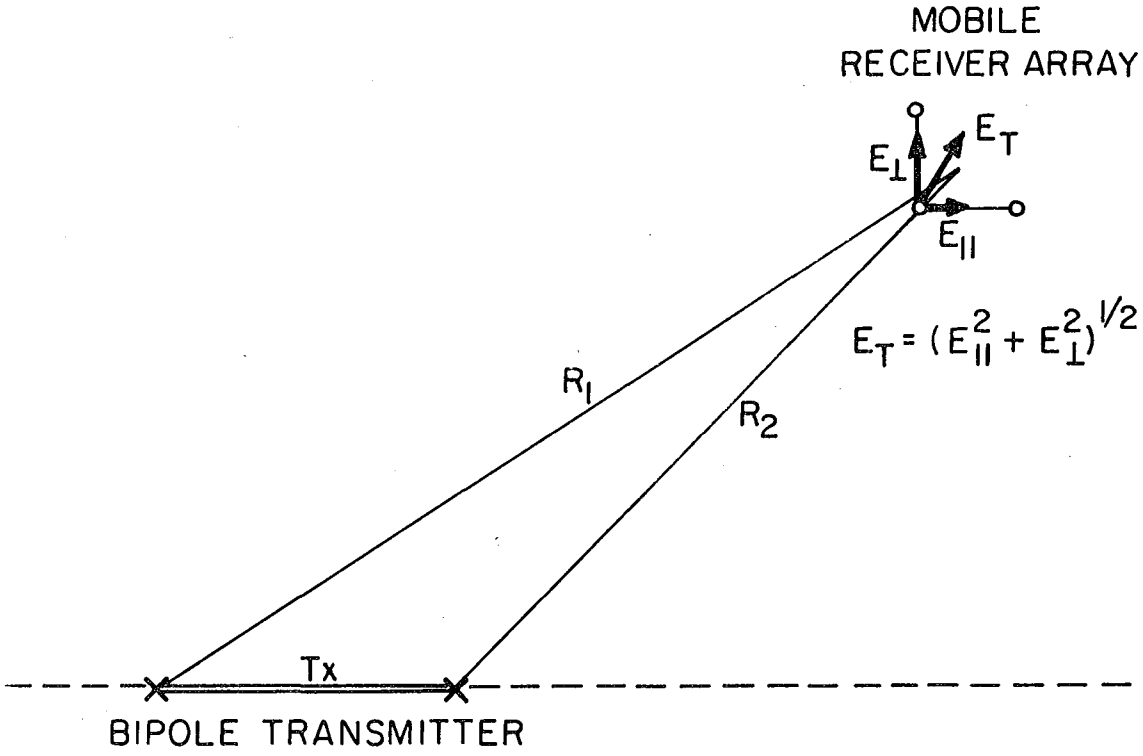

XBL 776-9368

Figure II-3. Plan view of the bipole-dipole resistivity array. Along the longitudinal axis of the transmitter bipole (dashed line) the apparent resistivities calculated for two-dimensional structures perpendicular to the transmitter are similar to those found by the dipole-dipole method.

APPENDIX II-A

Dipole-Dipole and Schlumberger Apparent Resistivity Pseudo-Sections for Two-Dimensional Models

MODEL--VERTICAL CONTACT
DIPOLE-DIPOLE APPARENT RESISTIVITY PSEUDO-SECTION
PROFILE LINE IS INCLINED AT 90.0 DEGREES TO STRIKE

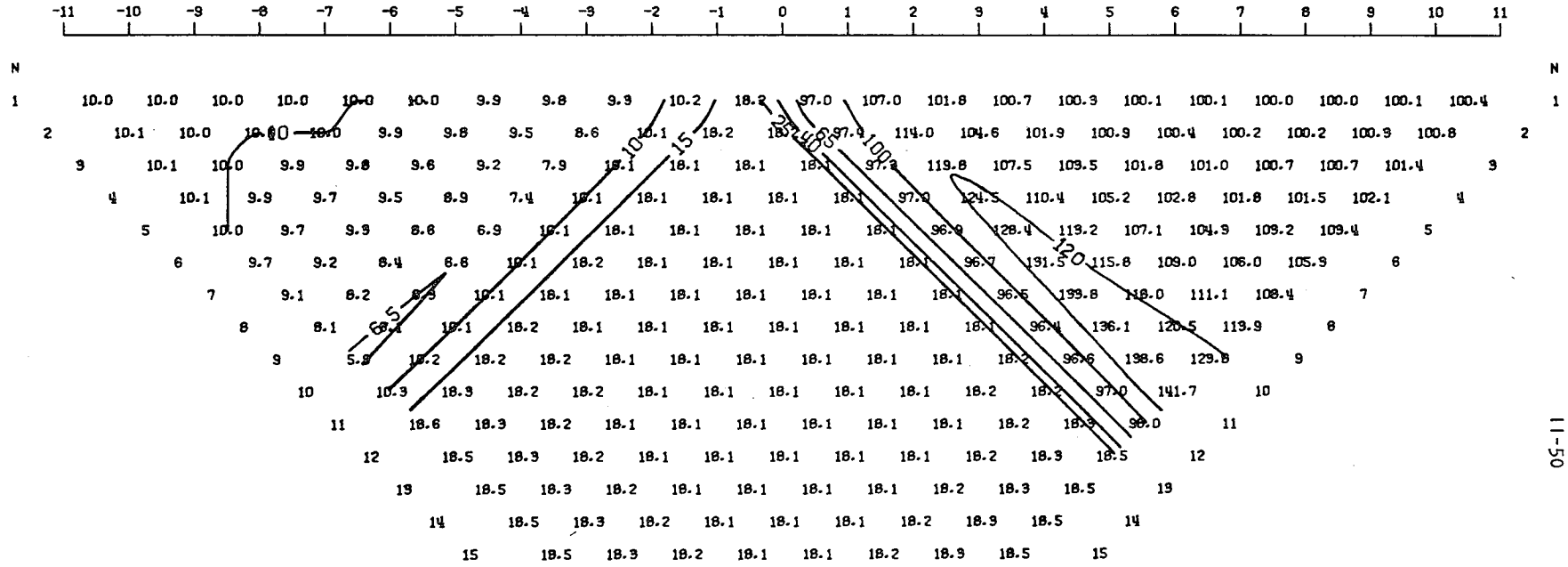

2-D RESISTIVITY MODEL -- VERTICAL CONTACT

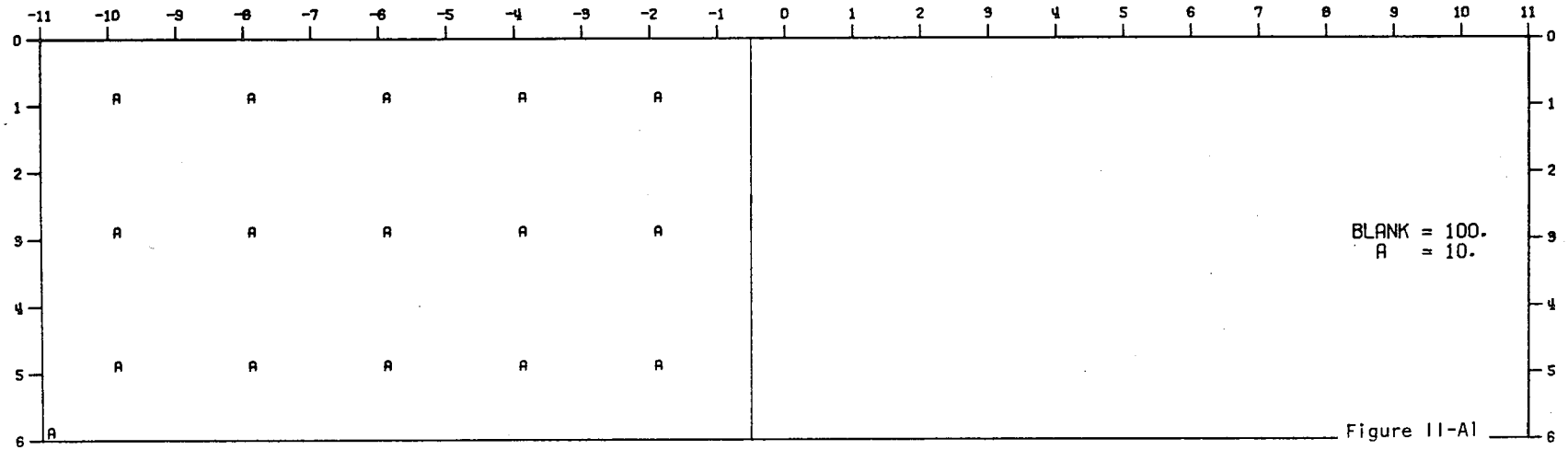

Figure II-A1

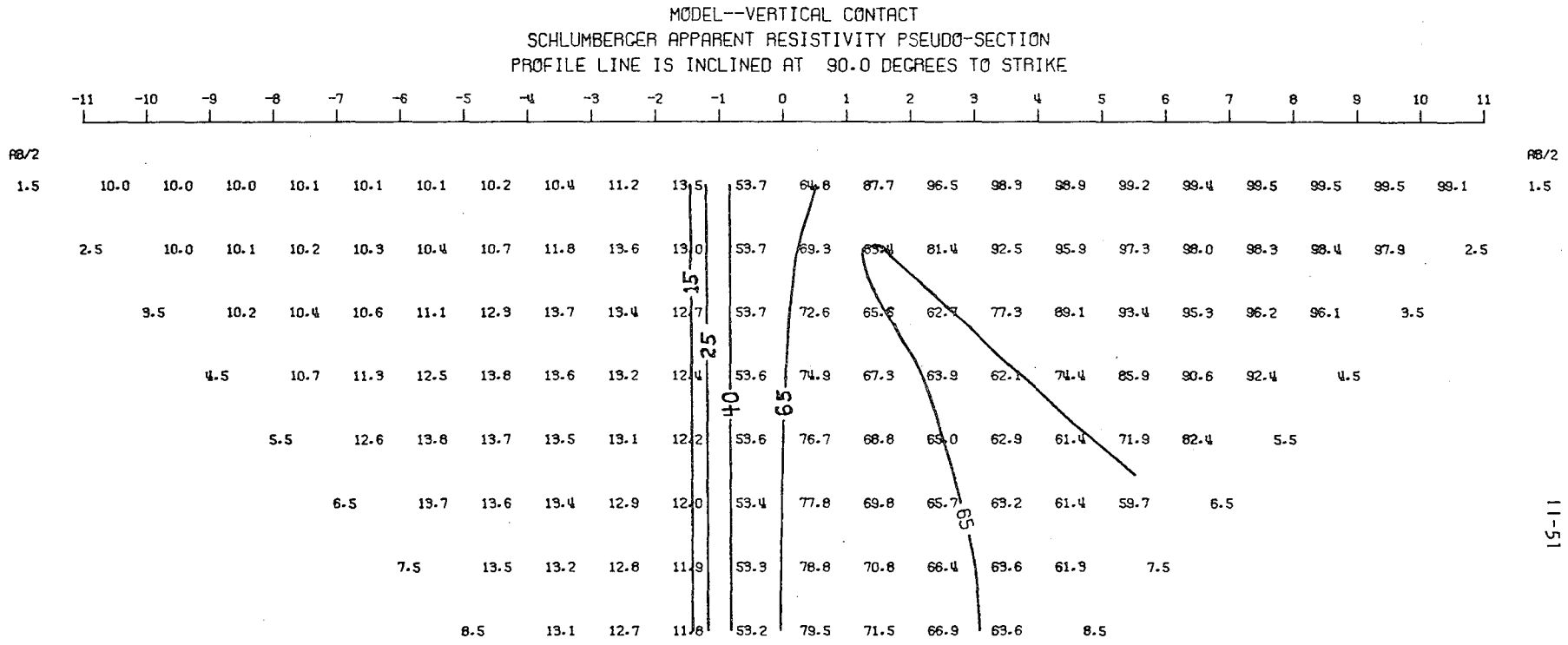
MODEL--VERTICAL CONTACT
SCHLUMBERGER APPARENT RESISTIVITY PSEUDO-SECTION
PROFILE LINE IS INCLINED AT 90.0 DEGREES TO STRIKE
AB/2
AB/2
15
25
40
65
65

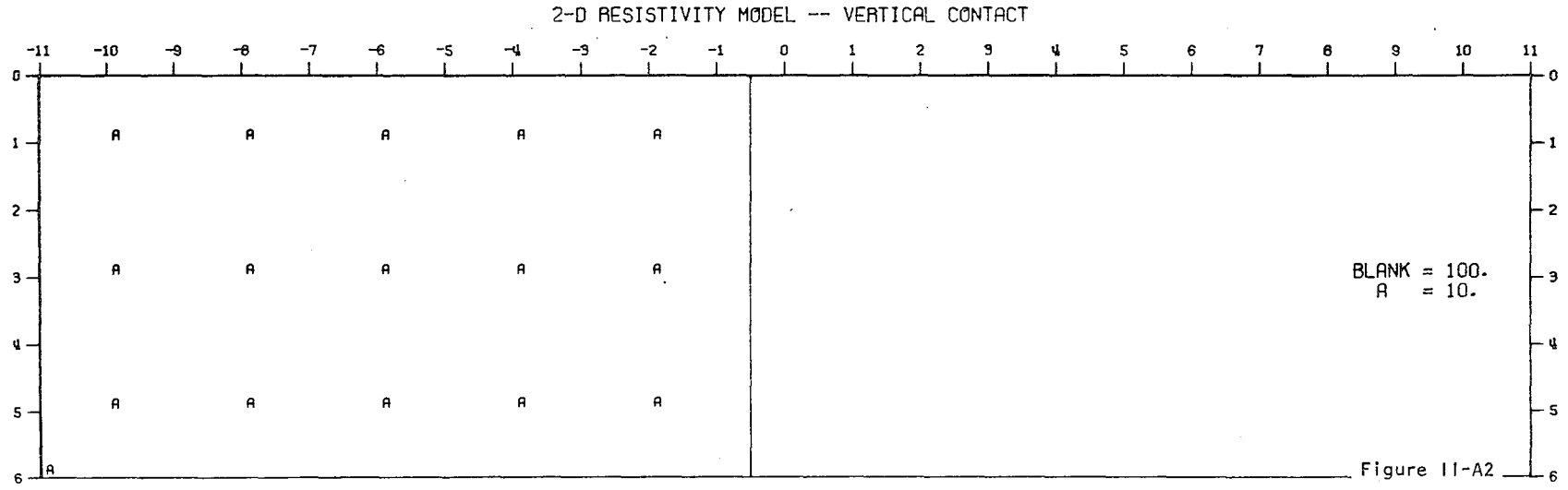
2-D RESISTIVITY MODEL -- VERTICAL CONTACT
BLANK = 100.
A = 10.

Figure II-A2

MODEL--TWO CONTACTS
DIPOLE-DIPOLE APPARENT RESISTIVITY PSEUDO-SECTION
PROFILE LINE IS INCLINED AT 90.0 DEGREES TO STRIKE

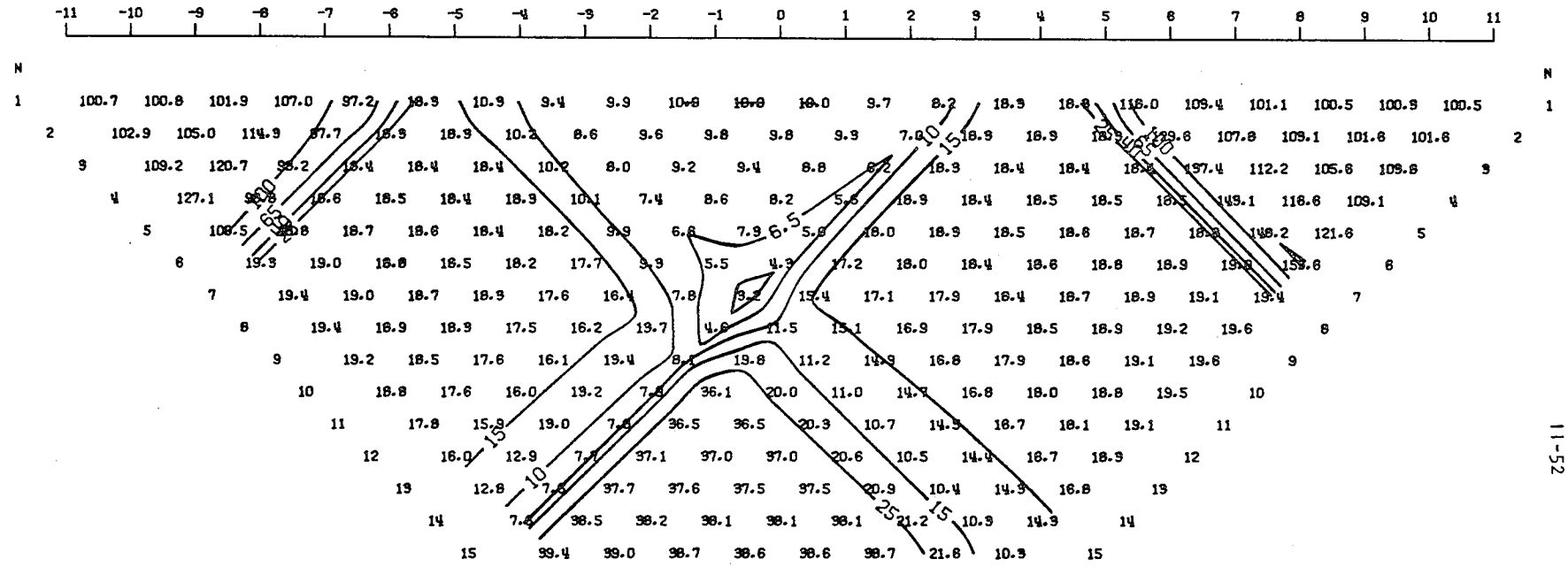

2-D RESISTIVITY MODEL -- TWO CONTACTS

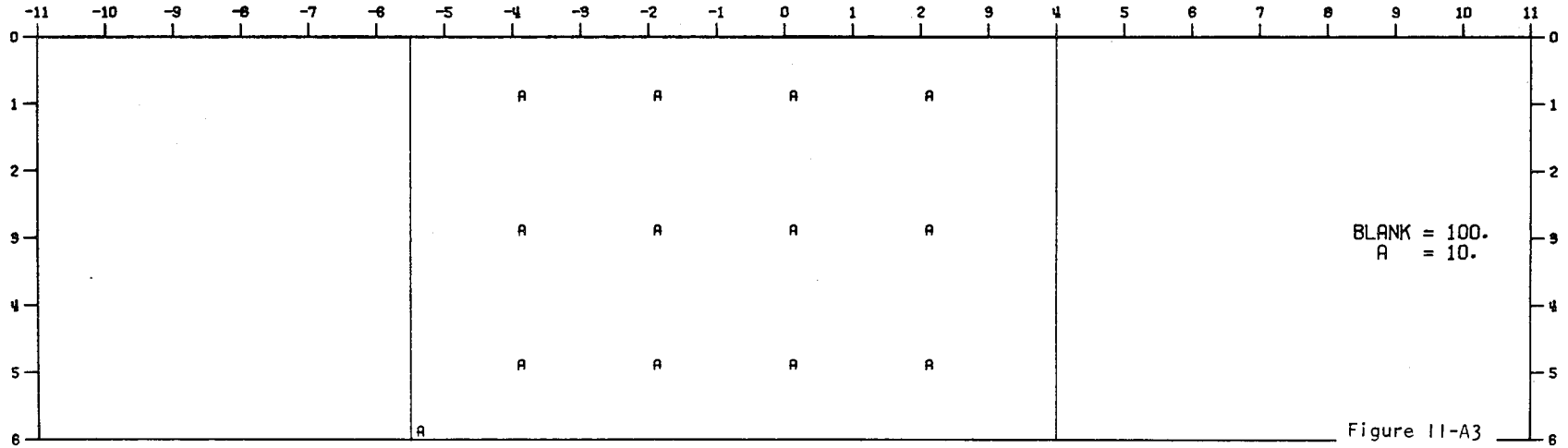

Figure II-A3

MODEL--TWO CONTACTS
SCHLUMBERGER APPARENT RESISTIVITY PSEUDO-SECTION
PROFILE LINE IS INCLINED AT 90.0 DEGREES TO STRIKE

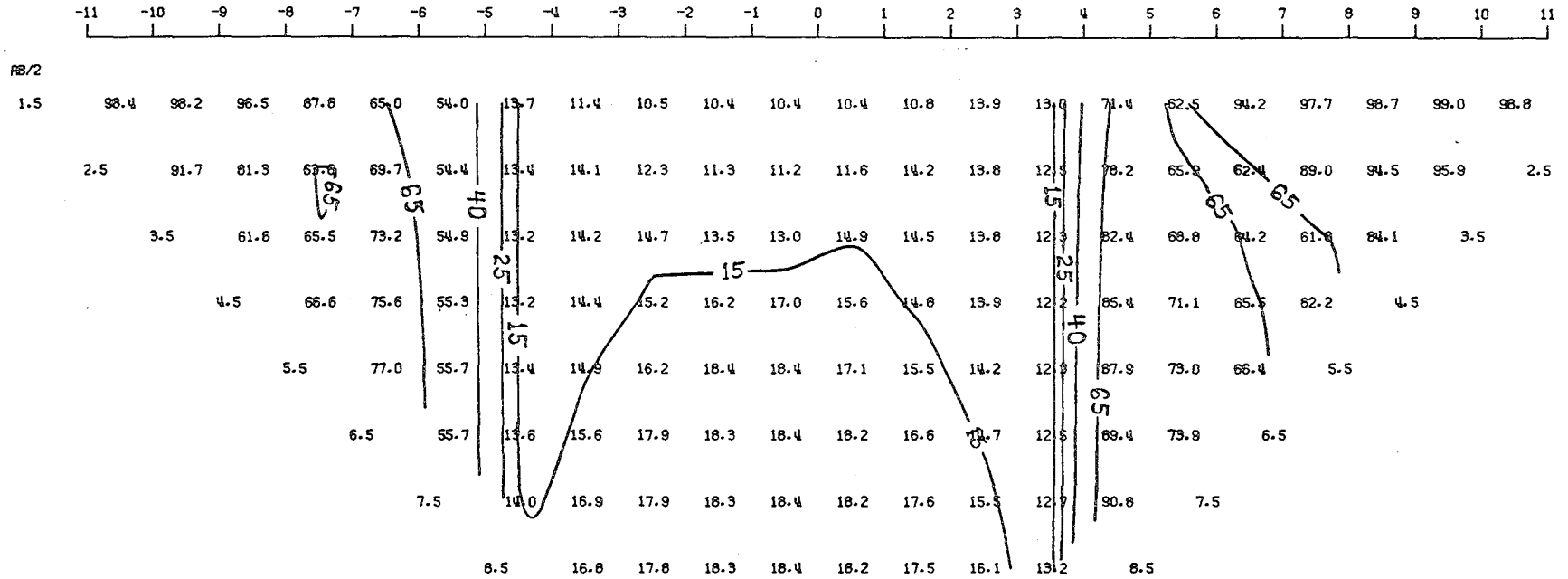

2-D RESISTIVITY MODEL -- TWO CONTACTS

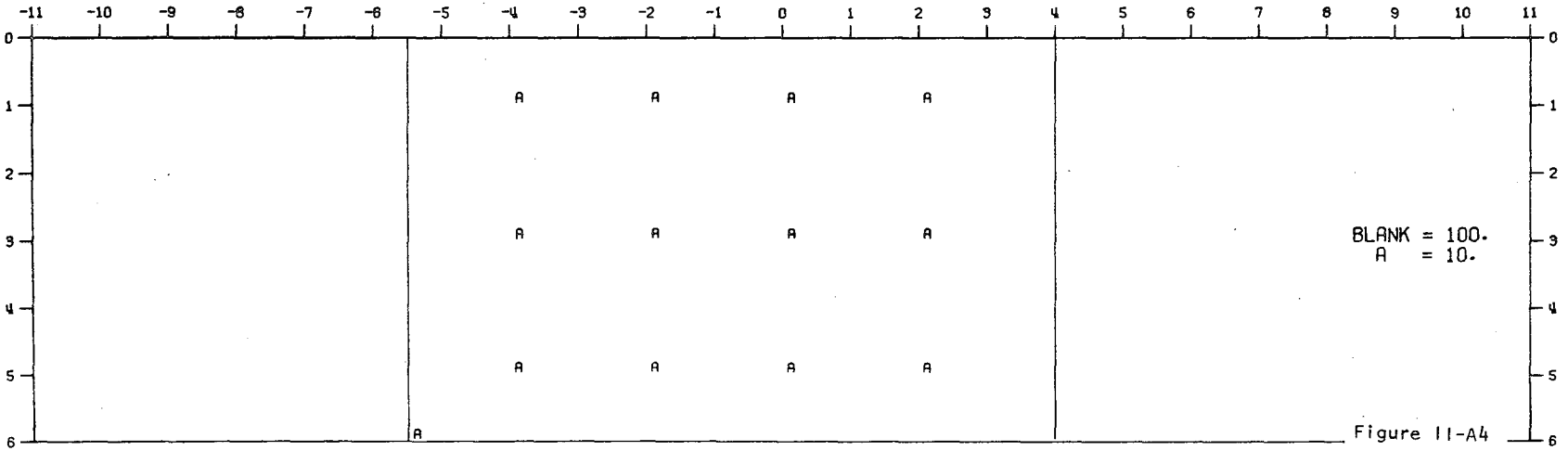

Figure II-A4

MODEL--SHALLOW VALLEY
DIPOLE-DIPOLE APPARENT RESISTIVITY PSEUDO-SECTION
PROFILE LINE IS INCLINED AT 90.0 DEGREES TO STRIKE

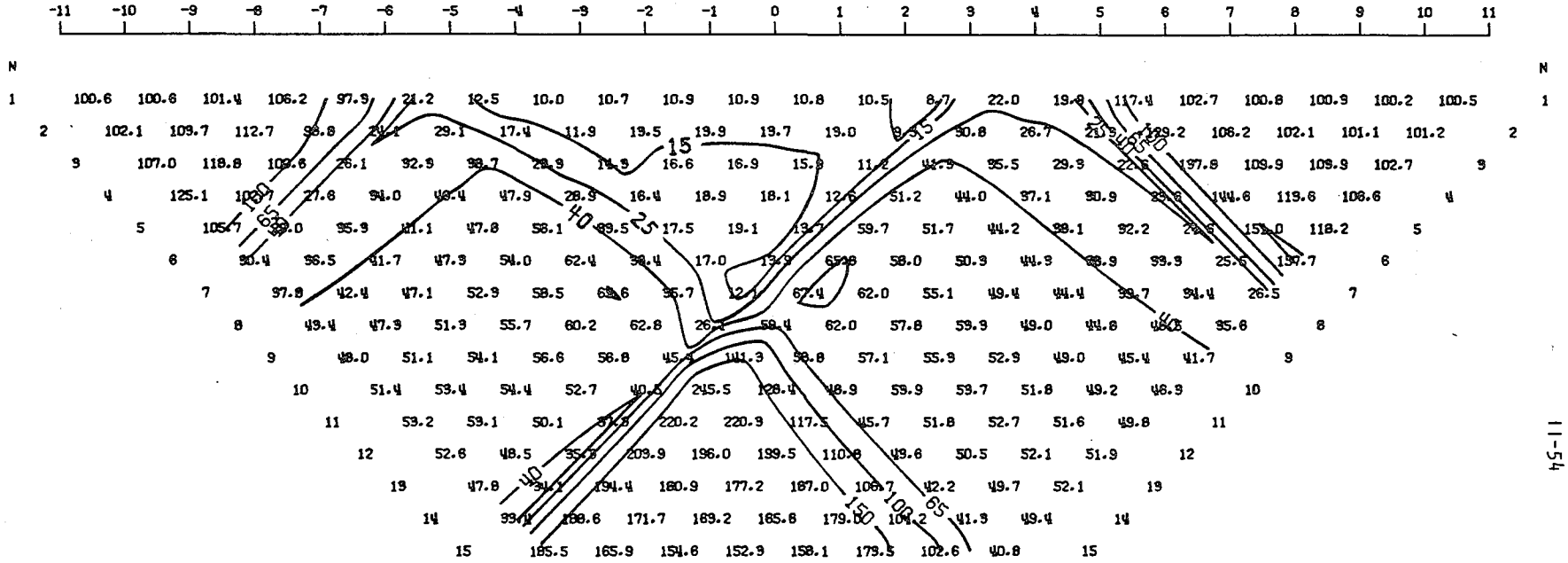

2-D RESISTIVITY MODEL -- SHALLOW VALLEY

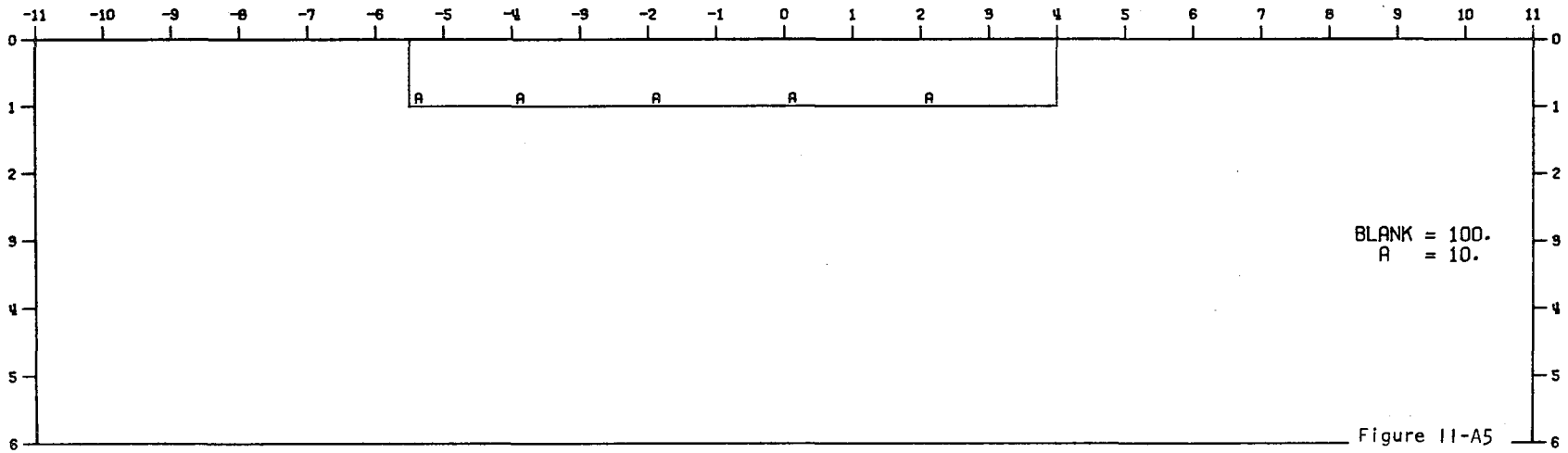

Figure II-A5

MODEL--SHALLOW VALLEY
SCHLUMBERGER APPARENT RESISTIVITY PSEUDO-SECTION
PROFILE LINE IS INCLINED AT 90.0 DEGREES TO STRIKE

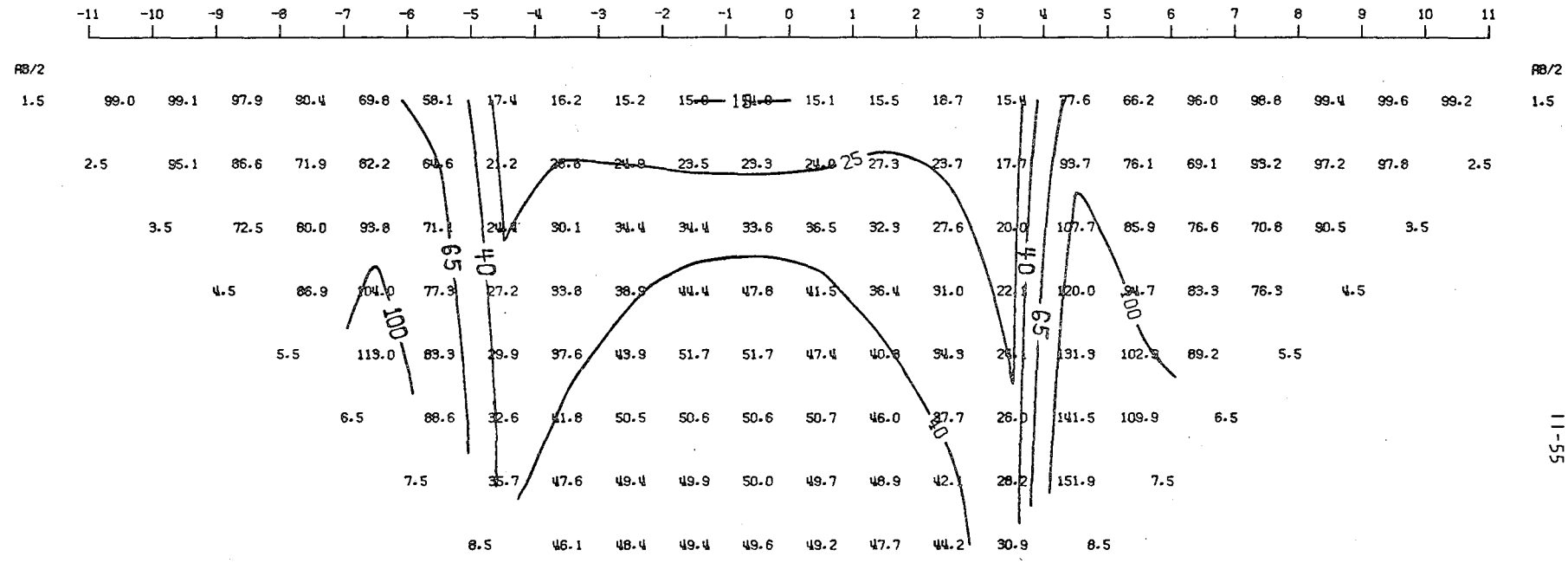

2-D RESISTIVITY MODEL -- SHALLOW VALLEY

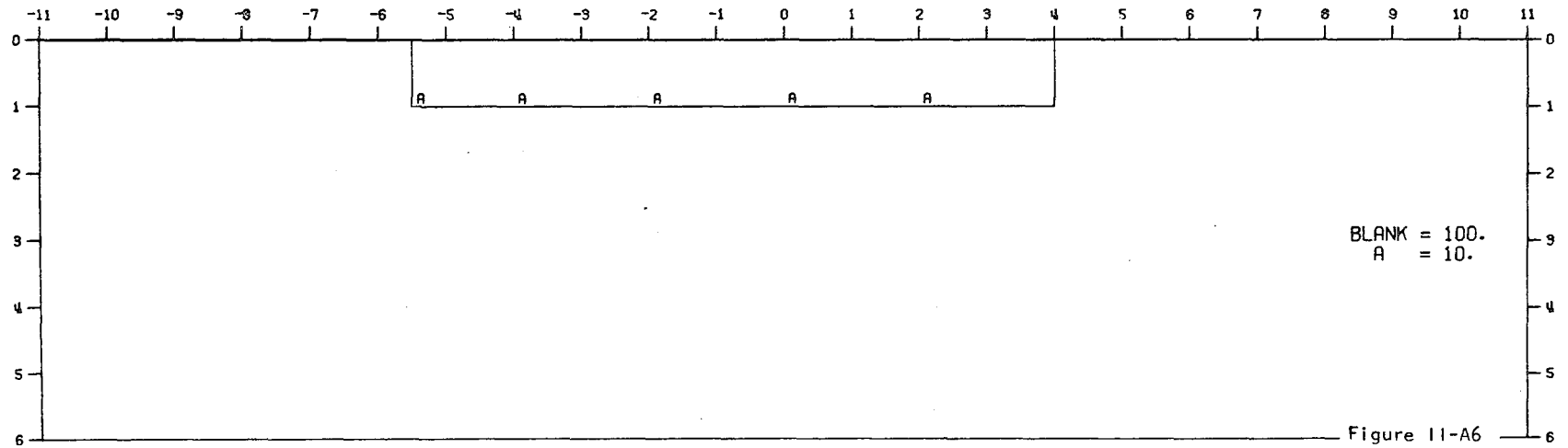

Figure 11-A6

MODEL-- BURIED VERTICAL CONTACT 1
DIPOLE-DIPOLE APPARENT RESISTIVITY PSEUDO-SECTION
PROFILE LINE IS INCLINED AT 90.0 DEGREES TO STRIKE

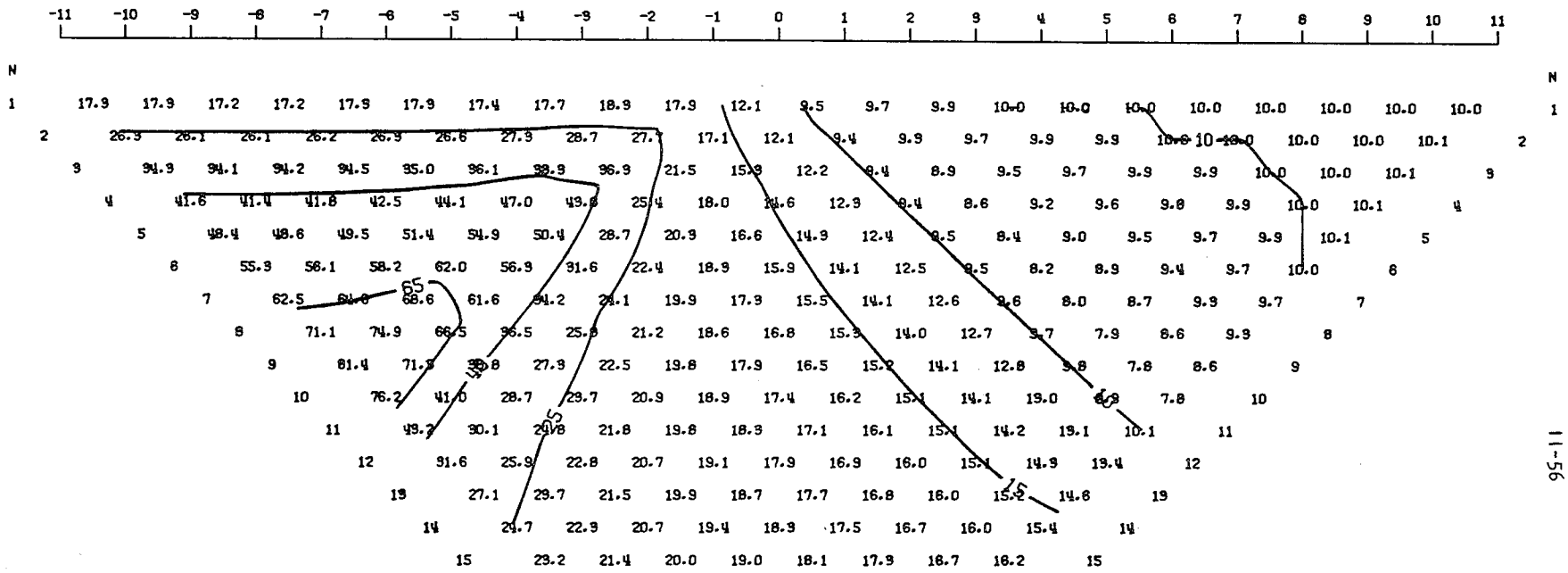

2-D RESISTIVITY MODEL -- BURIED VERTICAL CONTACT 1

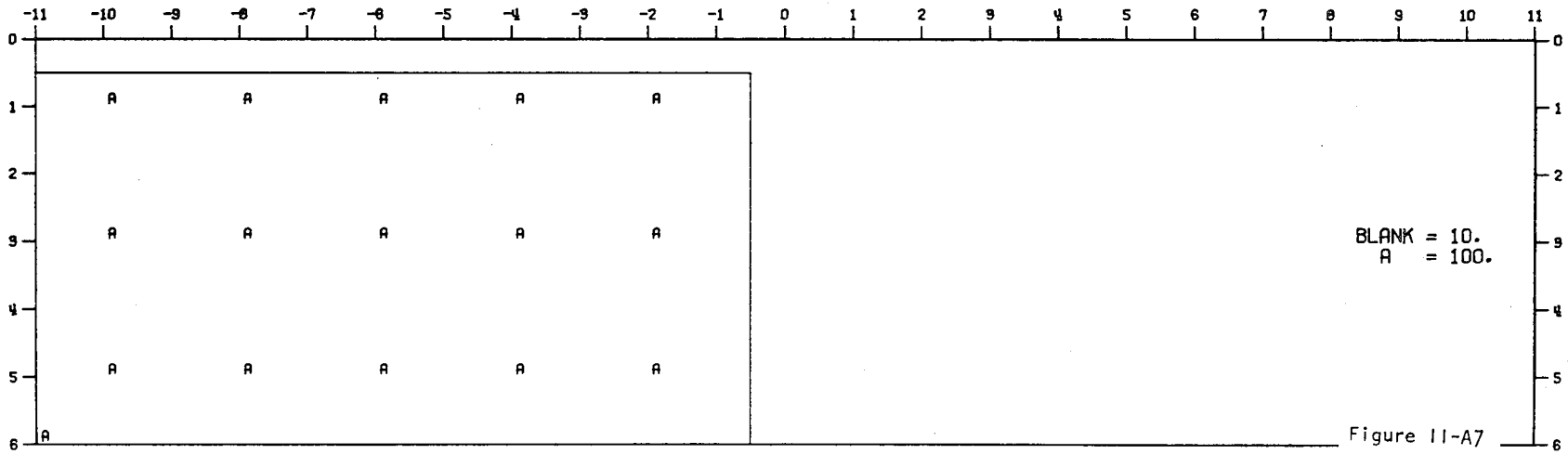

Figure II-A7

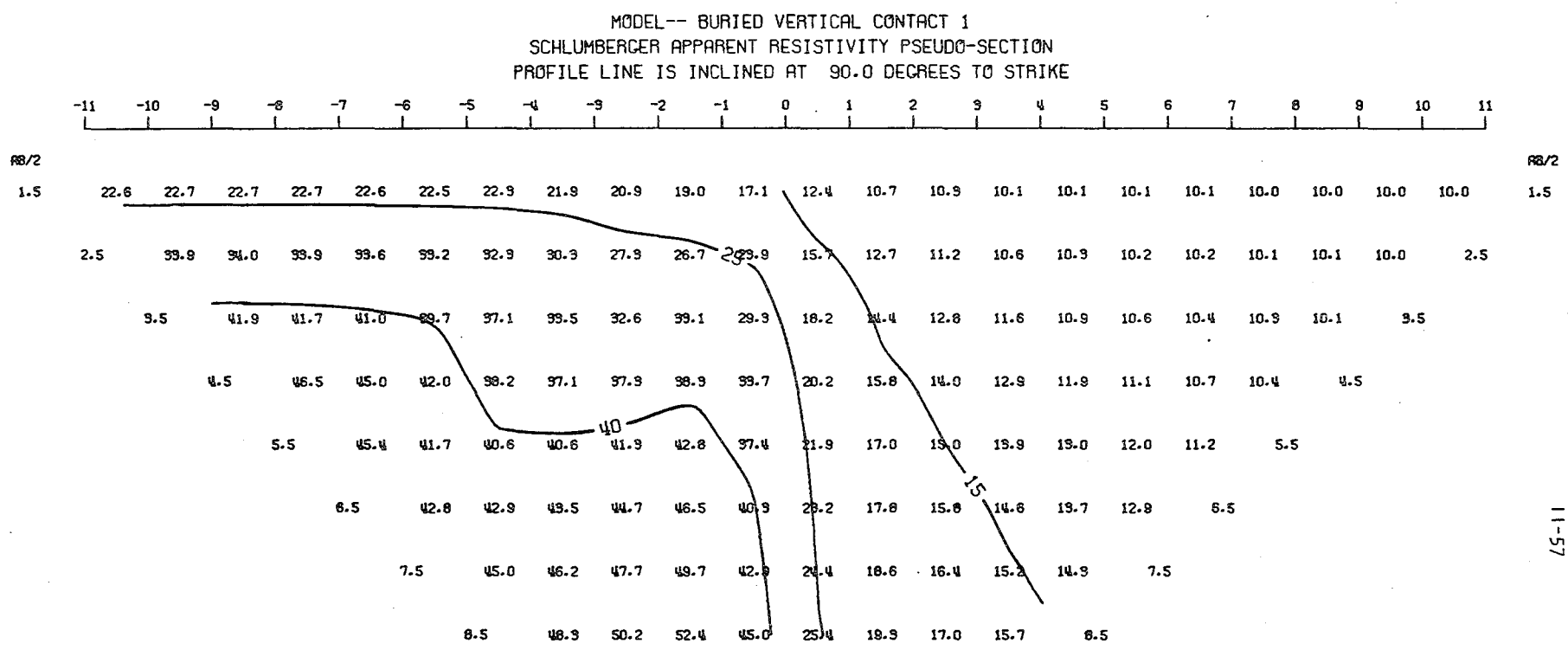
MODEL-- BURIED VERTICAL CONTACT 1
SCHLUMBERGER APPARENT RESISTIVITY PSEUDO-SECTION
PROFILE LINE IS INCLINED AT 90.0 DEGREES TO STRIKE
AB/2
40
15

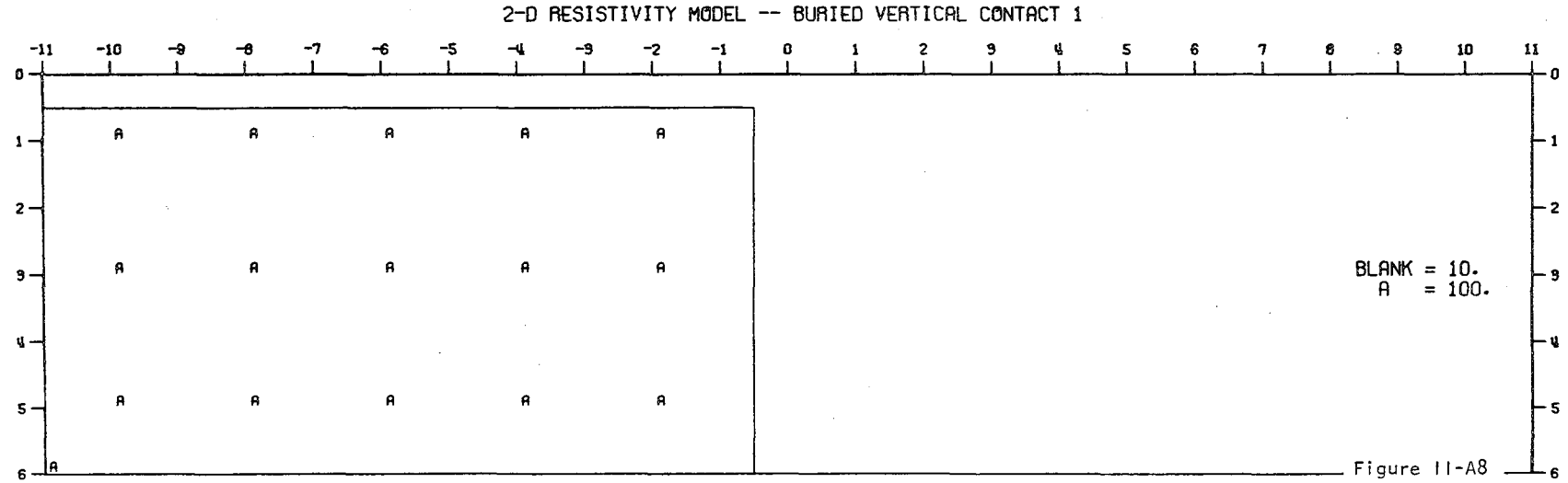
2-D RESISTIVITY MODEL -- BURIED VERTICAL CONTACT 1
BLANK = 10.
A = 100.

Figure II-A8

MODEL--FAULT 1
DIPOLE-DIPOLE APPARENT RESISTIVITY PSEUDO-SECTION
PROFILE LINE IS INCLINED AT 90.0 DEGREES TO STRIKE

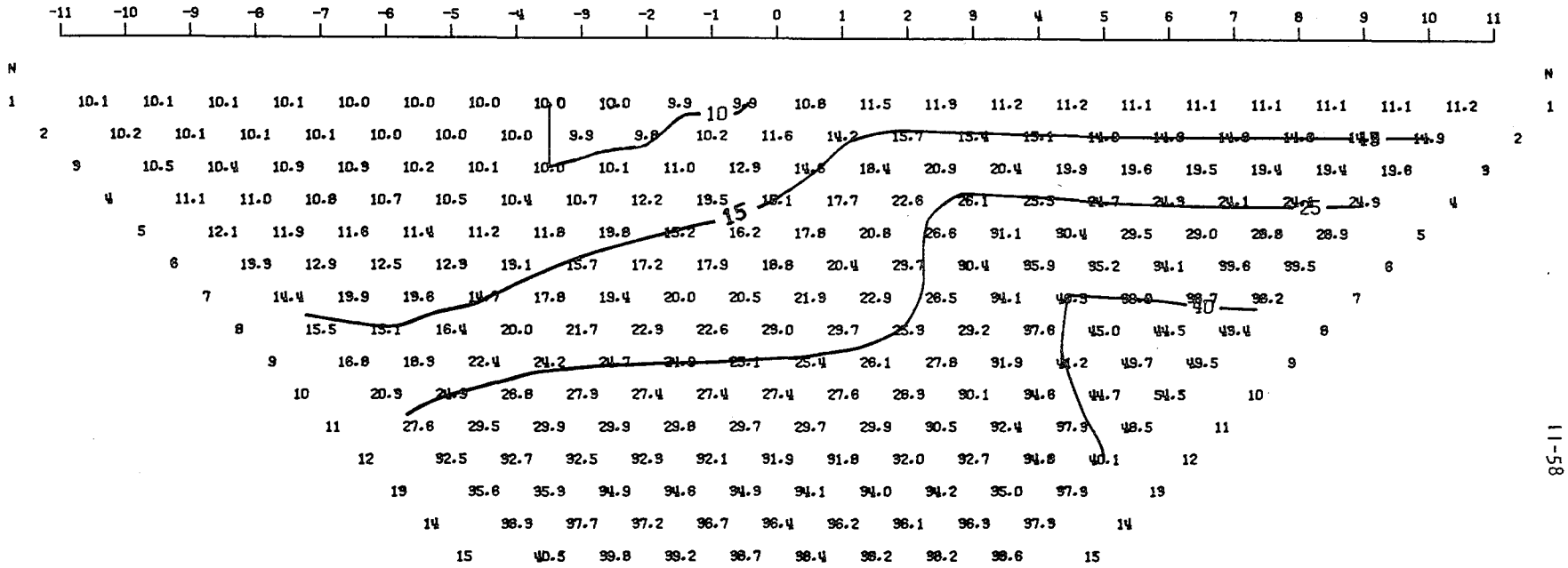

2-D RESISTIVITY MODEL -- FAULT 1

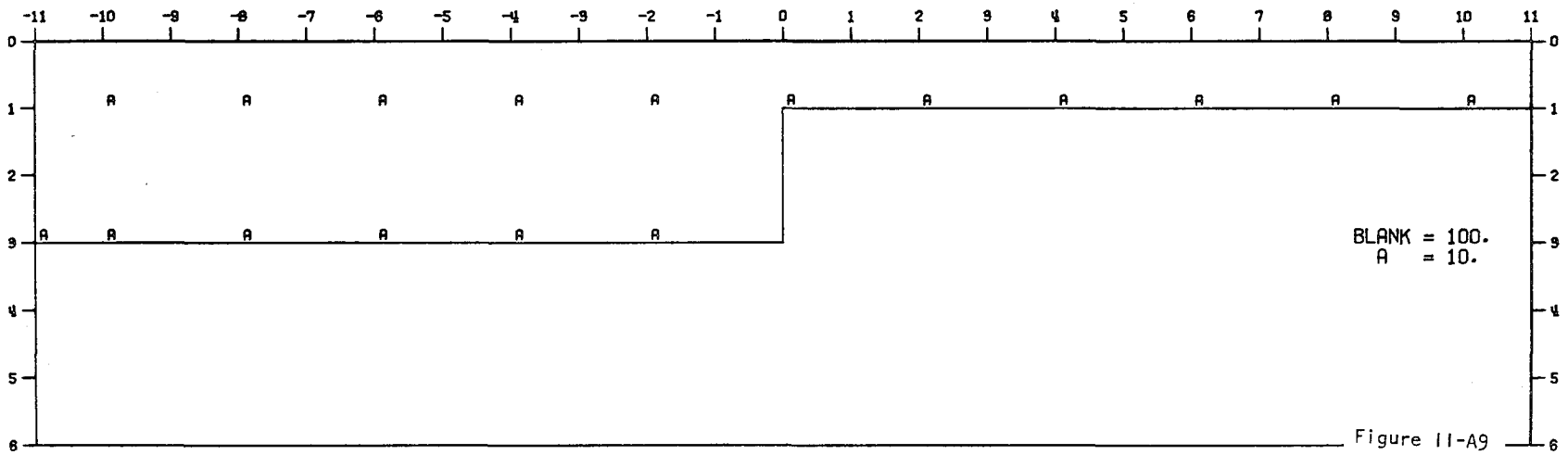

Figure II-A9

MODEL--FAULT 1
SCHLUMBERGER APPARENT RESISTIVITY PSEUDO-SECTION
PROFILE LINE IS INCLINED AT 90.0 DEGREES TO STRIKE

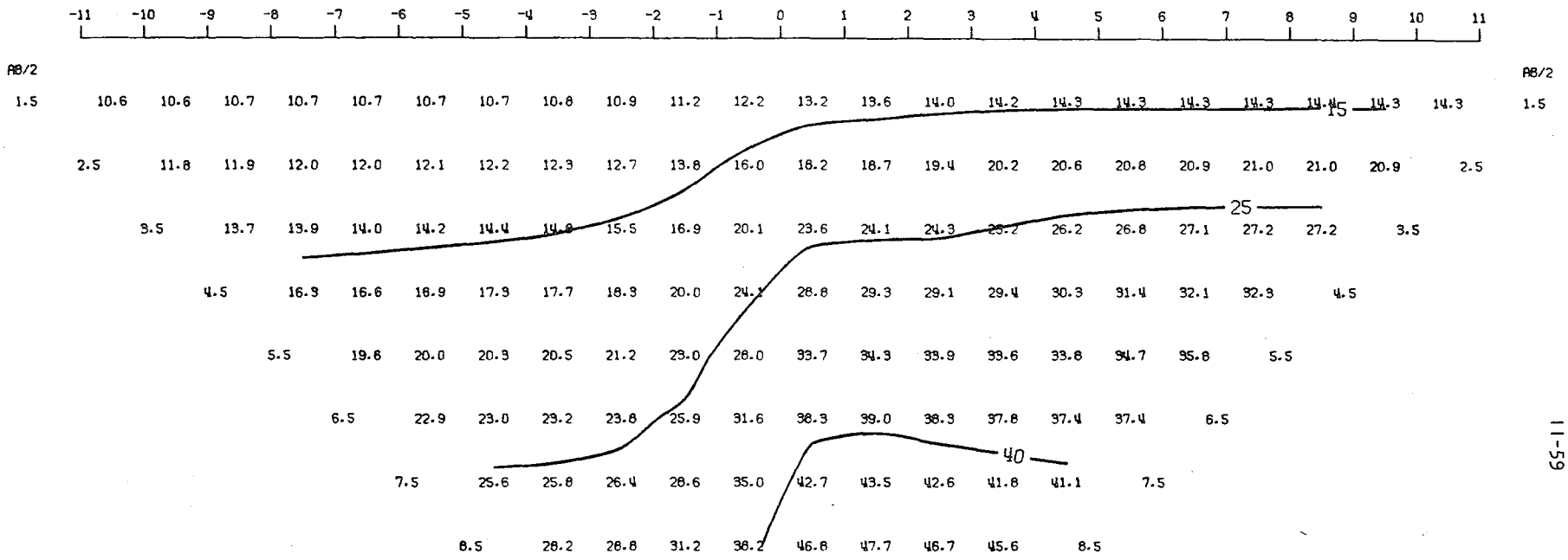

2-D RESISTIVITY MODEL -- FAULT 1

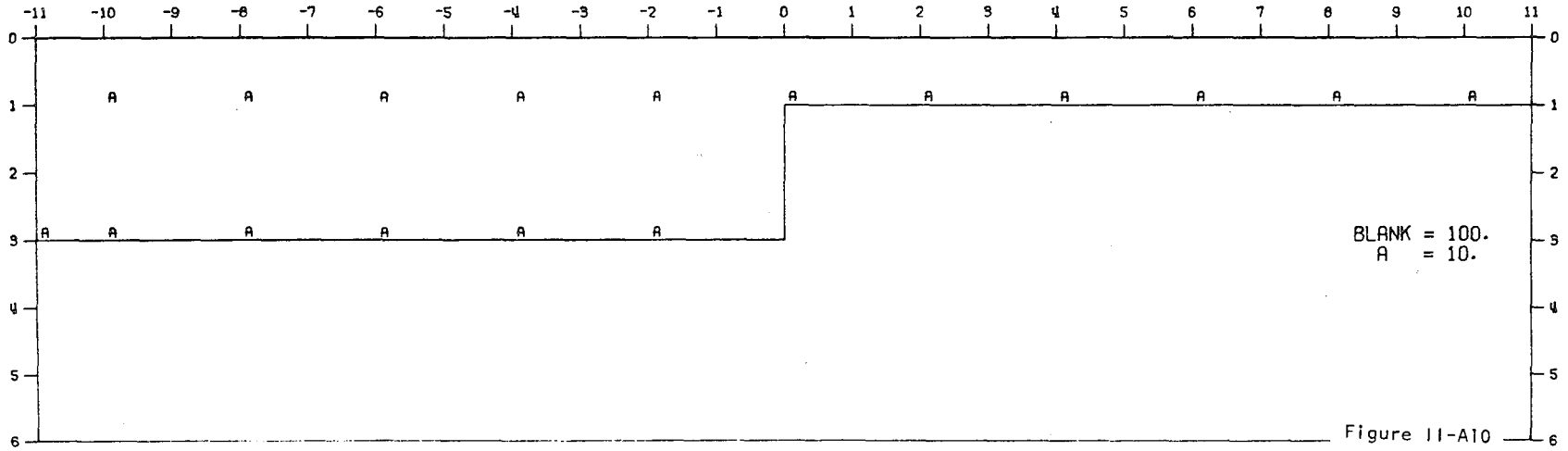

Figure II-A10

MODEL--FAULT 3
DIPOLE-DIPOLE APPARENT RESISTIVITY PSEUDO-SECTION
PROFILE LINE IS INCLINED AT 90.0 DEGREES TO STRIKE

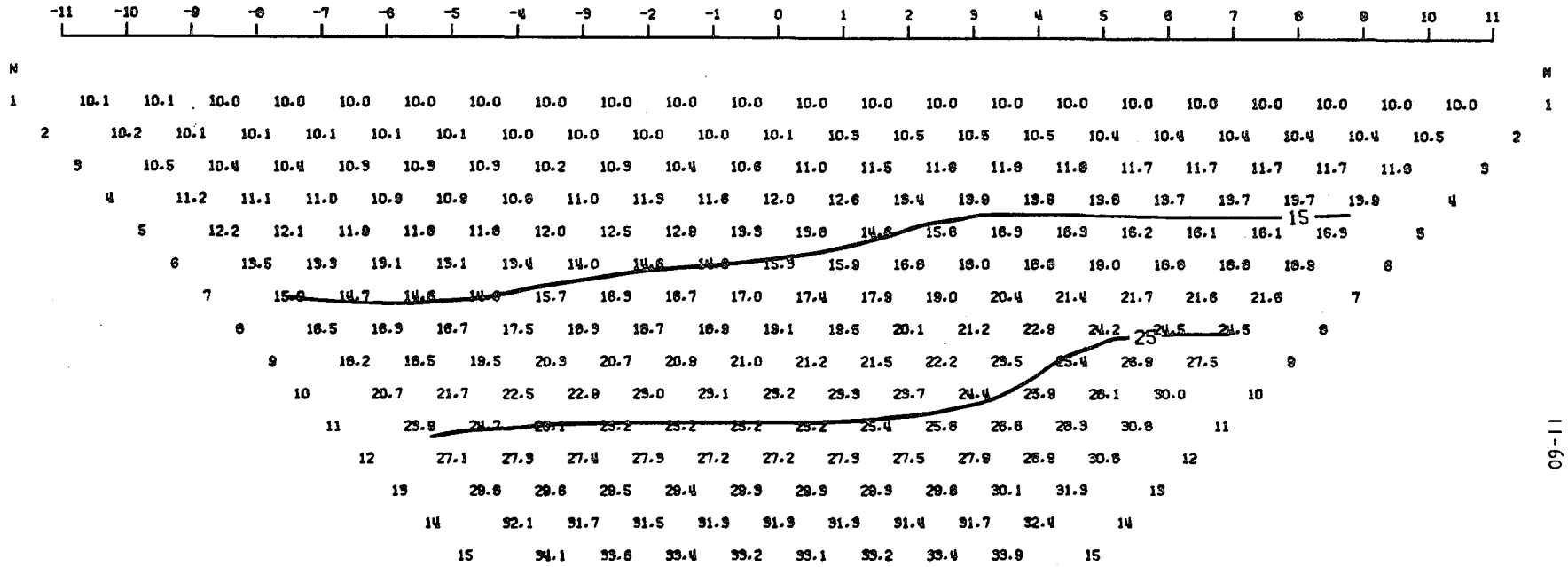

2-D RESISTIVITY MODEL -- FAULT 3

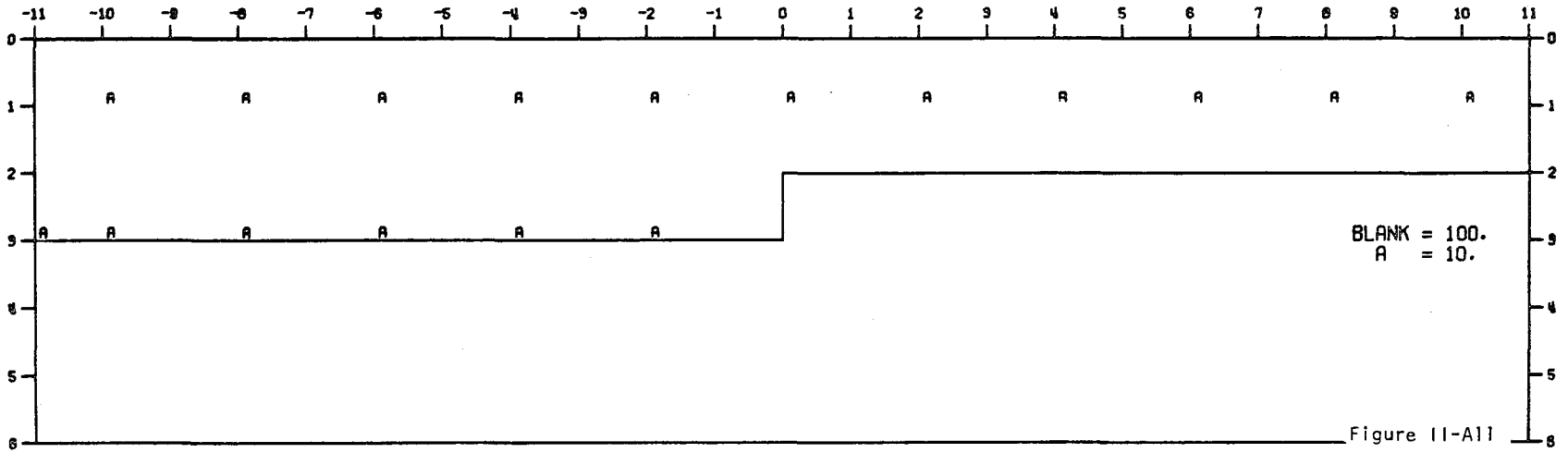

Figure II-A11

MODEL--FAULT 3
SCHLUMBERGER APPARENT RESISTIVITY PSEUDO-SECTION
PROFILE LINE IS INCLINED AT 90.0 DEGREES TO STRIKE

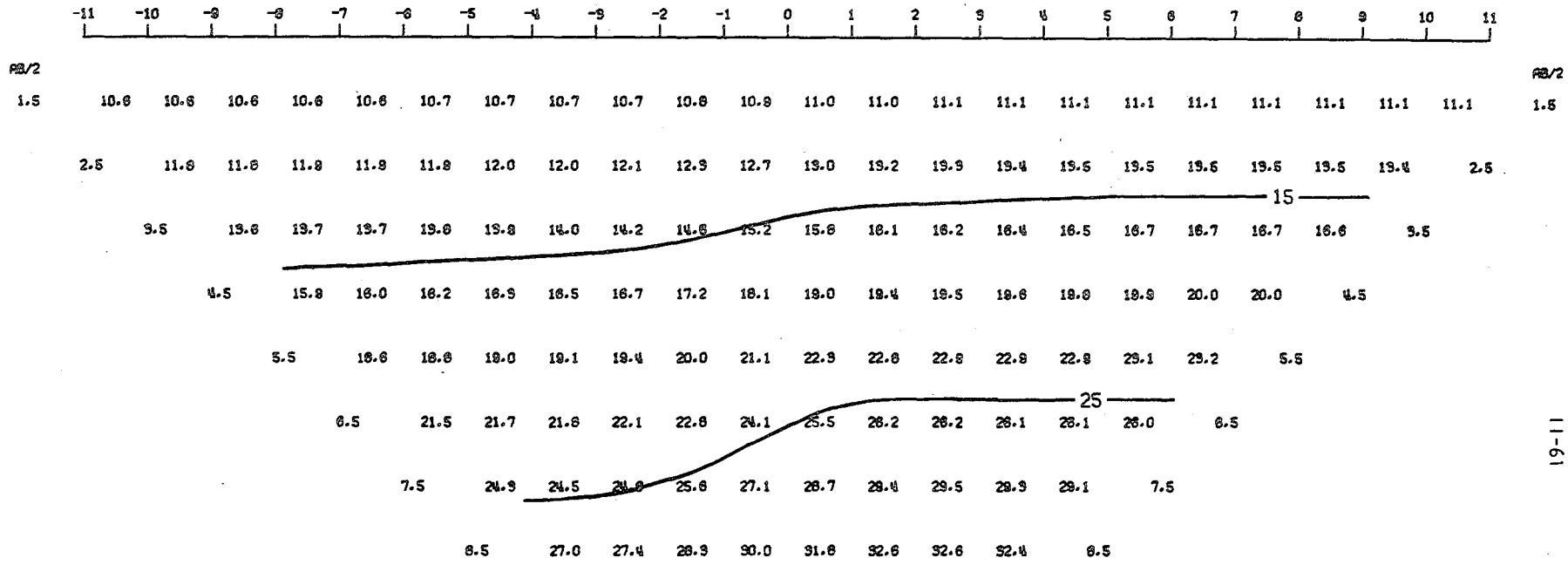

2-D RESISTIVITY MODEL -- FAULT 3

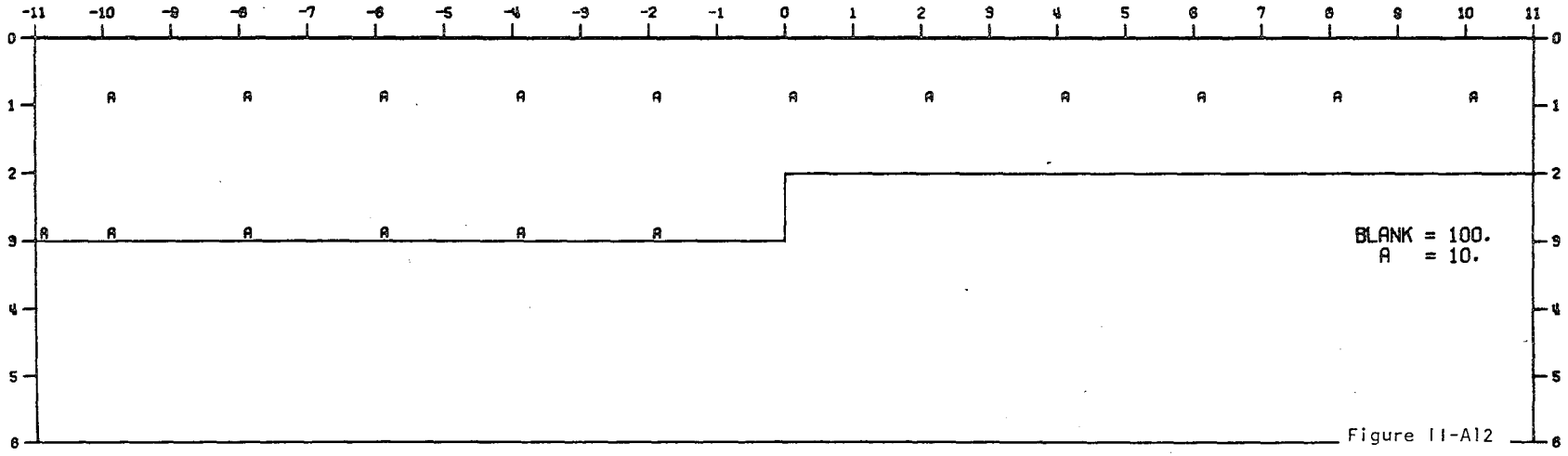

Figure II-A12

MODEL--FAULT W/ PROJECTION 1
DIPOLE-DIPOLE APPARENT RESISTIVITY PSEUDO-SECTION
PROFILE LINE IS INCLINED AT 90.0 DEGREES TO STRIKE

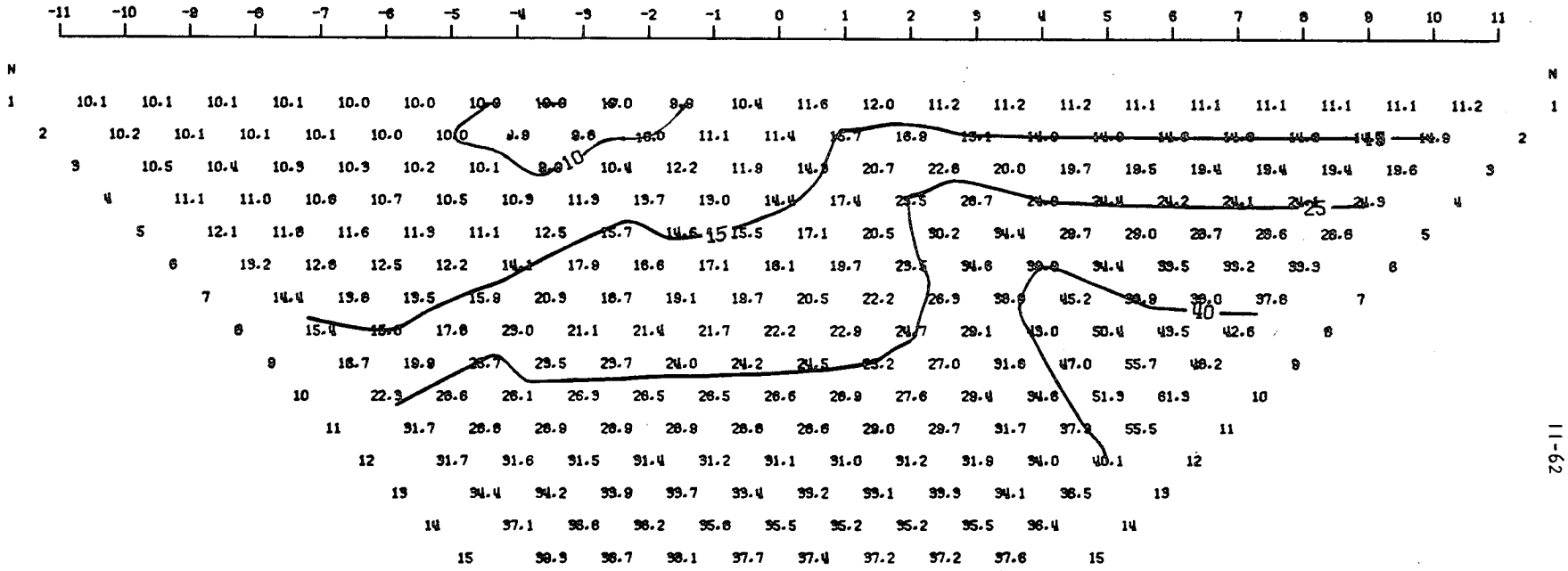

2-D RESISTIVITY MODEL -- FAULT W/ PROJECTION 1

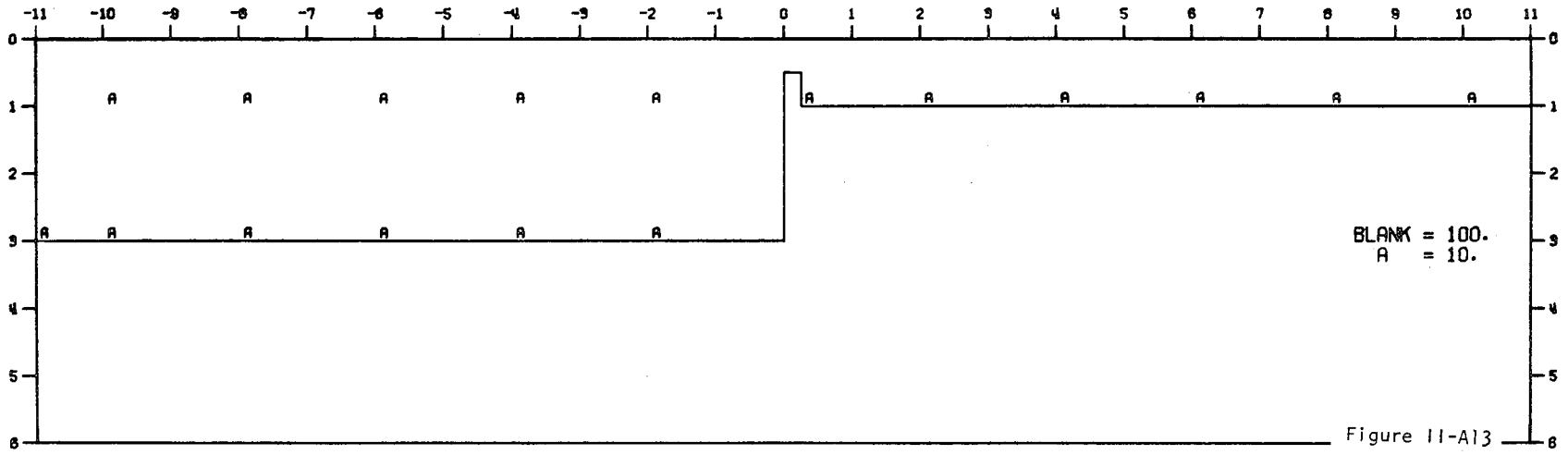

Figure II-A13

MODEL--FAULT W/ PROJECTION 1
SCHLUMBERGER APPARENT RESISTIVITY PSEUDO-SECTION
PROFILE LINE IS INCLINED AT 90.0 DEGREES TO STRIKE

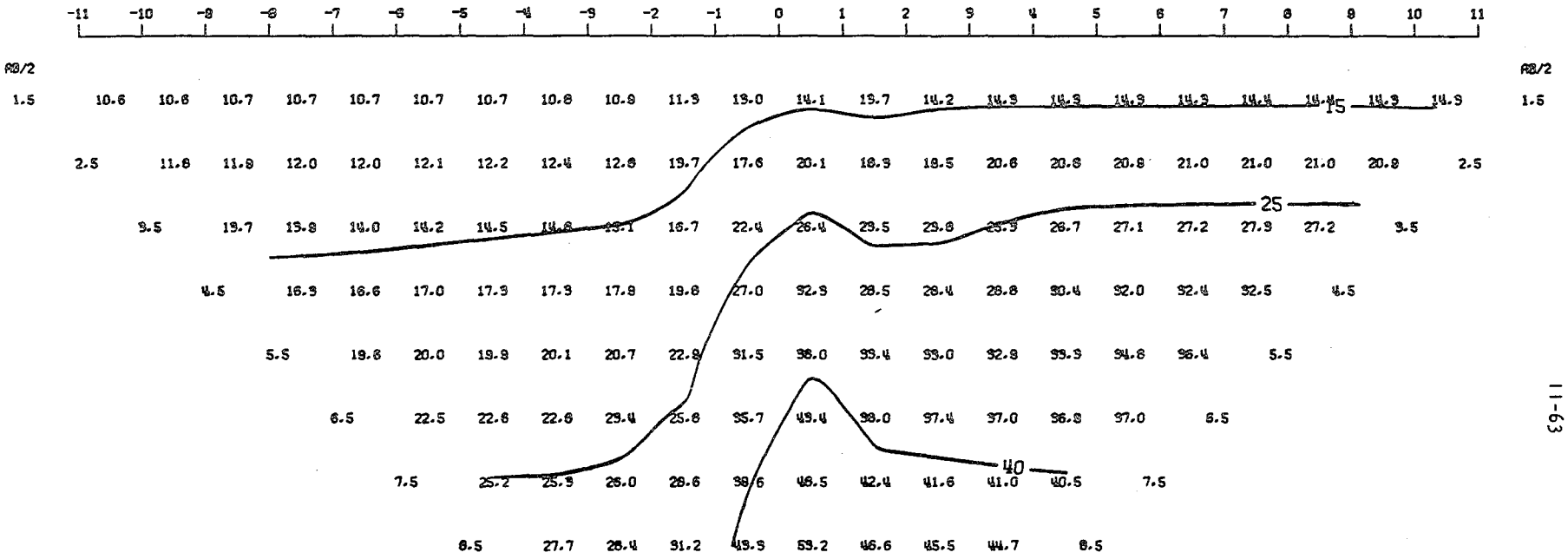

2-D RESISTIVITY MODEL -- FAULT W/ PROJECTION 1

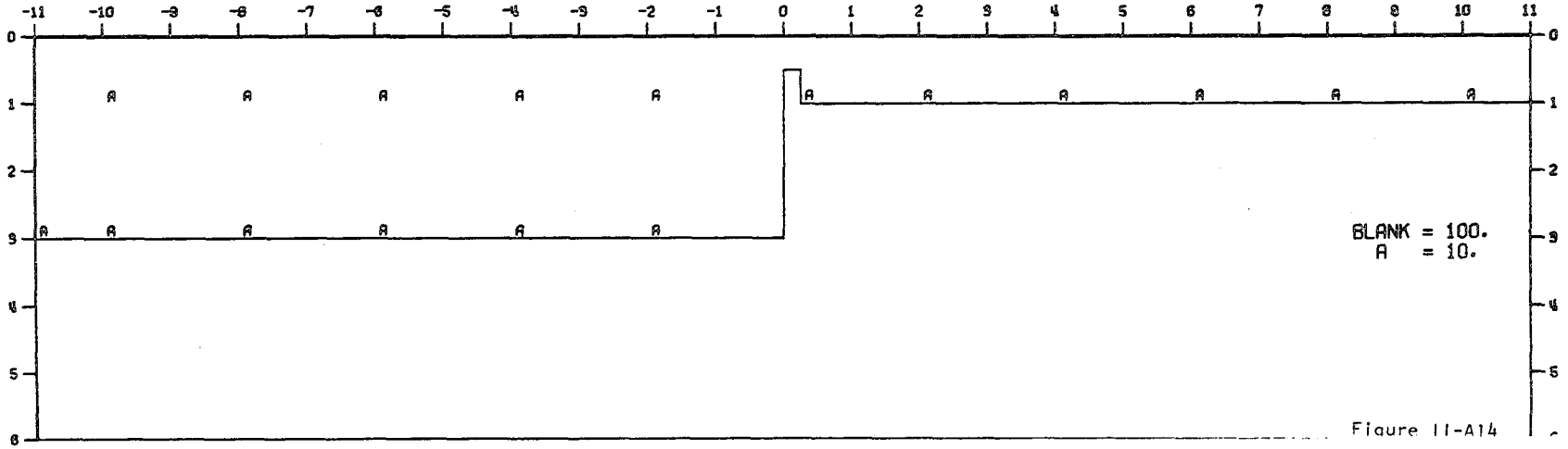

Figure II-A14

MODEL--FAULT W/ PROJECTION 2
DIPOLE-DIPOLE APPARENT RESISTIVITY PSEUDO-SECTION
PROFILE LINE IS INCLINED AT 90.0 DEGREES TO STRIKE

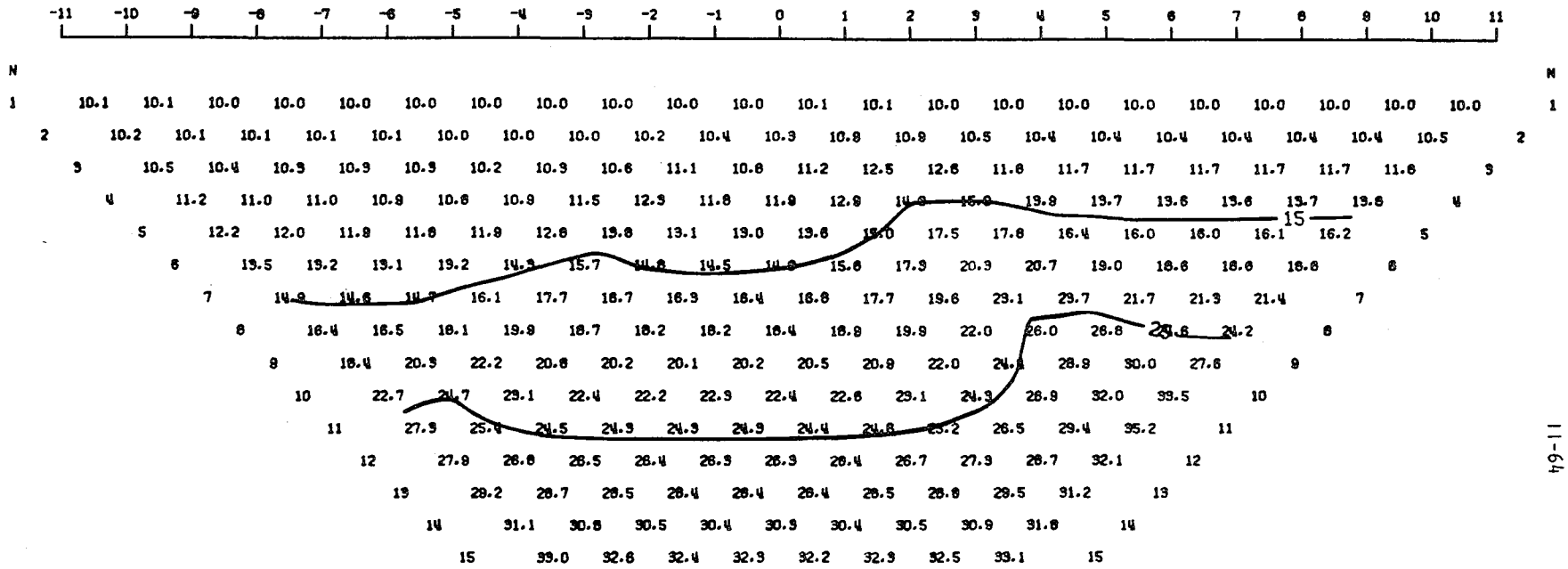

2-D RESISTIVITY MODEL -- FAULT W/ PROJECTION 2

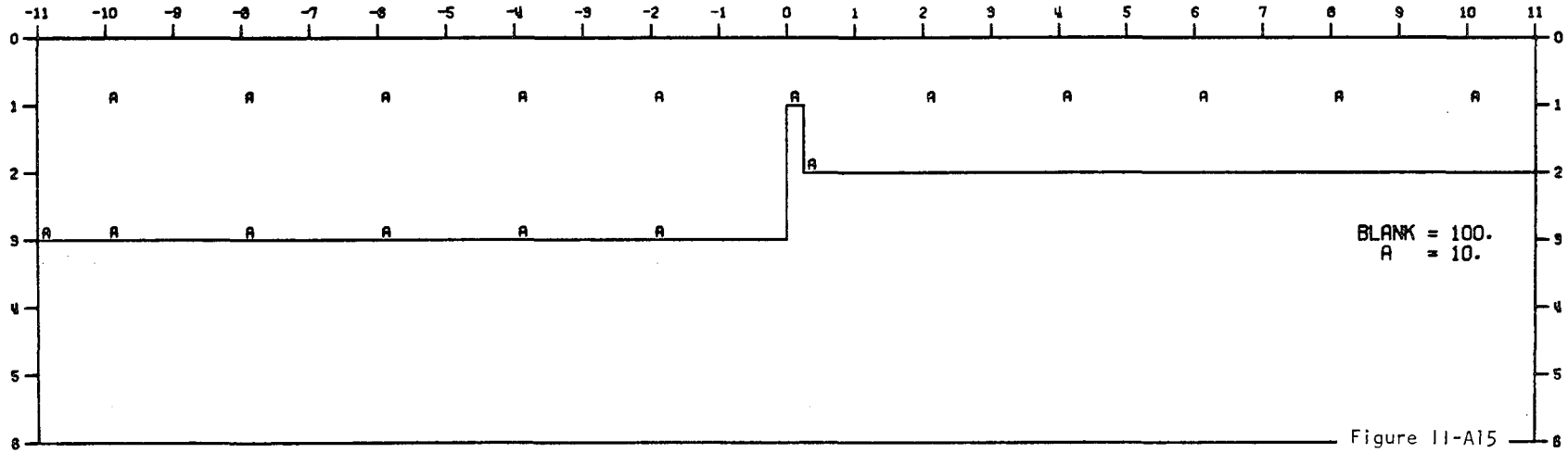

Figure 11-A15

MODEL--FAULT W/ PROJECTION 2
SCHLUMBERGER APPARENT RESISTIVITY PSEUDO-SECTION
PROFILE LINE IS INCLINED AT 90.0 DEGREES TO STRIKE

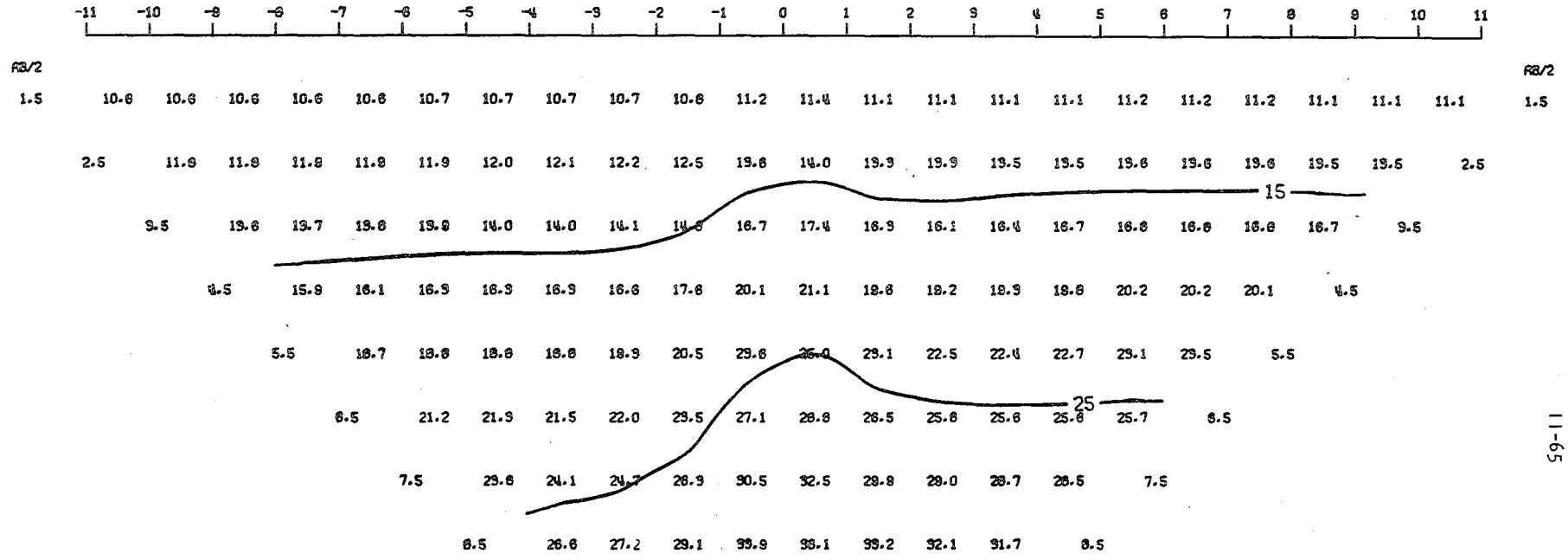

2-D RESISTIVITY MODEL -- FAULT W/ PROJECTION 2

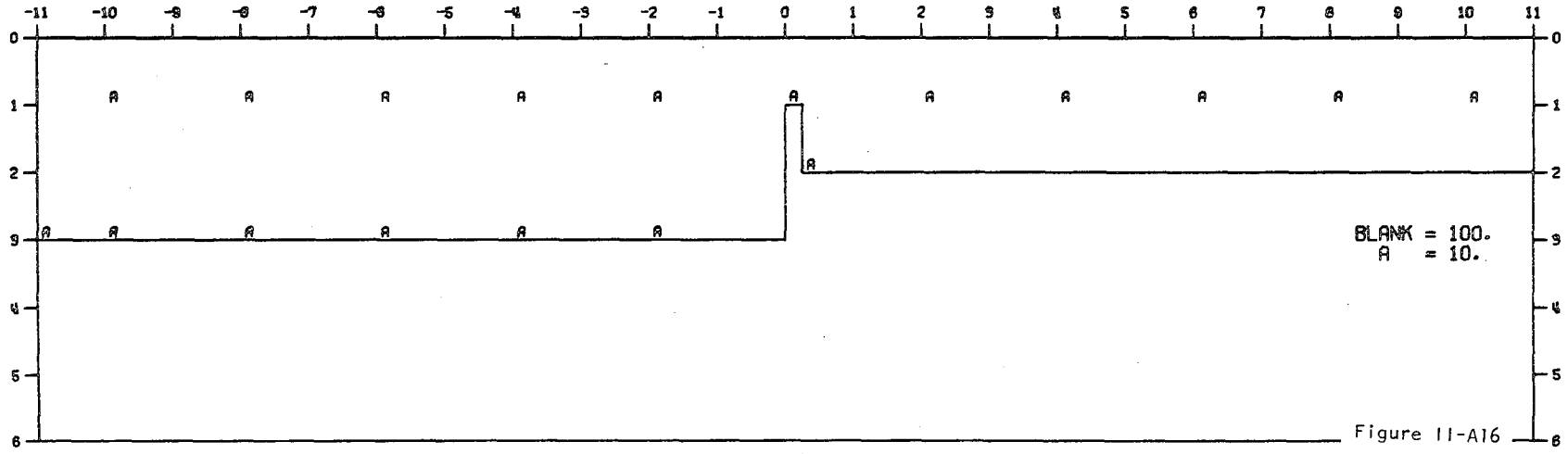

Figure 11-A16

MODEL-- BURIED VERTICAL CONTACT 2
DIPOLE-DIPOLE APPARENT RESISTIVITY PSEUDO-SECTION
PROFILE LINE IS INCLINED AT 90.0 DEGREES TO STRIKE

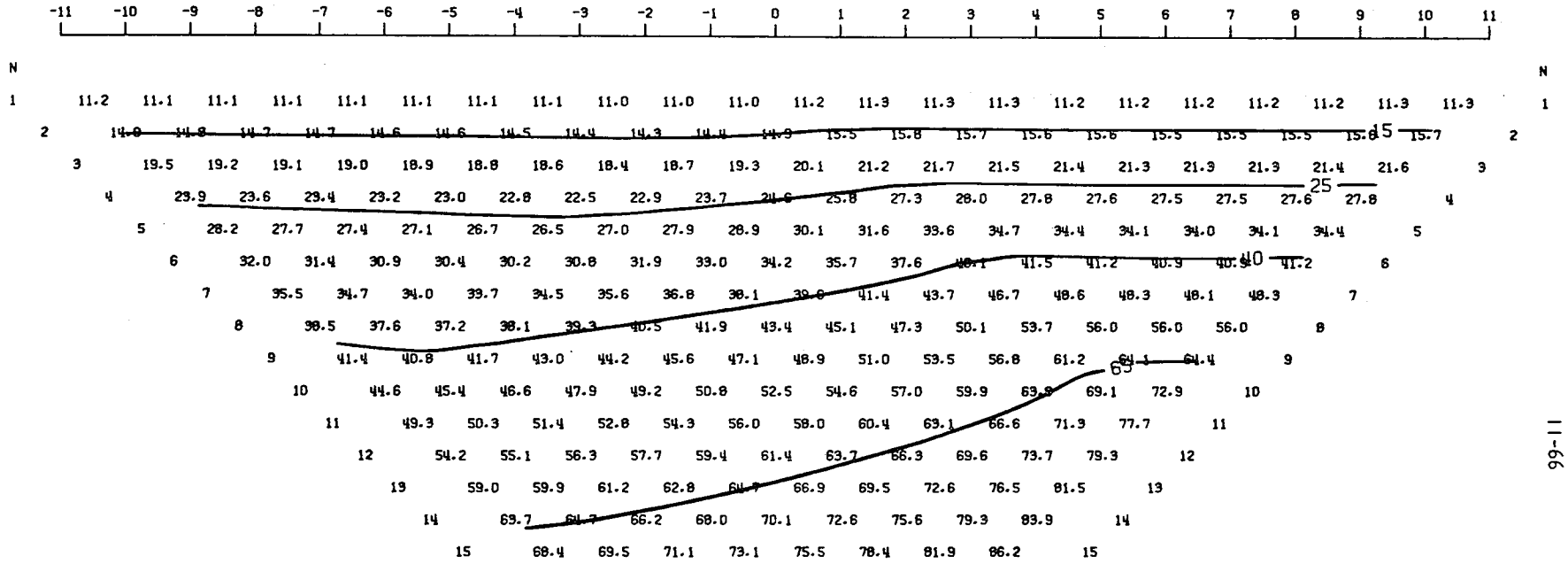

2-D RESISTIVITY MODEL -- BURIED VERTICAL CONTACT 2

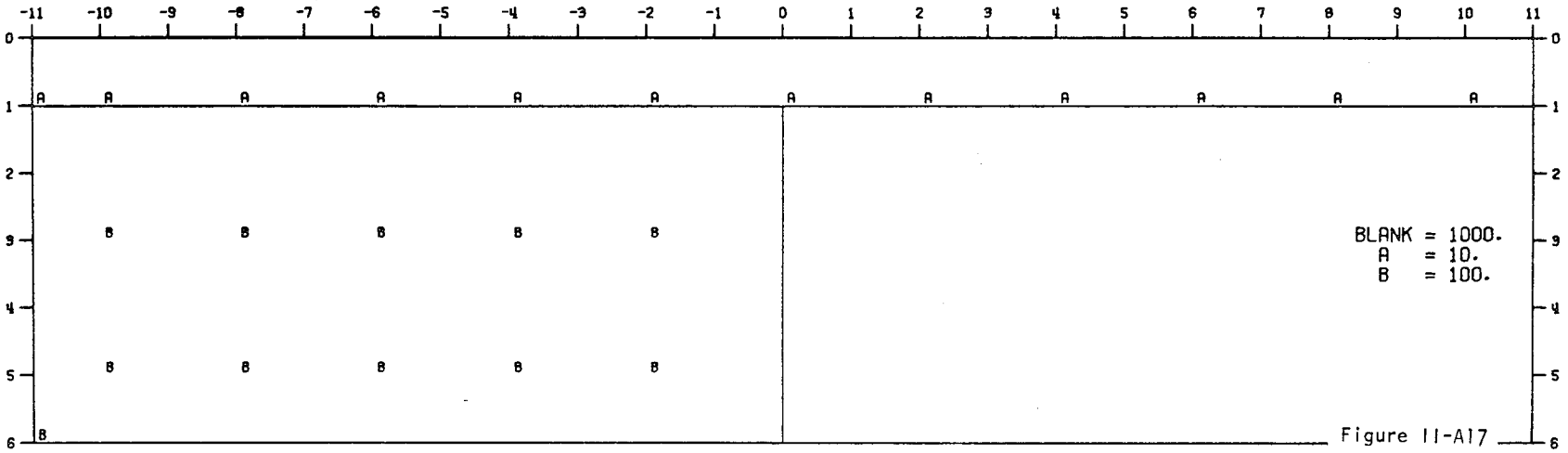

Figure II-A17

MODEL-- BURIED VERTICAL CONTACT 2
SCHLUMBERGER APPARENT RESISTIVITY PSEUDO-SECTION
PROFILE LINE IS INCLINED AT 90.0 DEGREES TO STRIKE

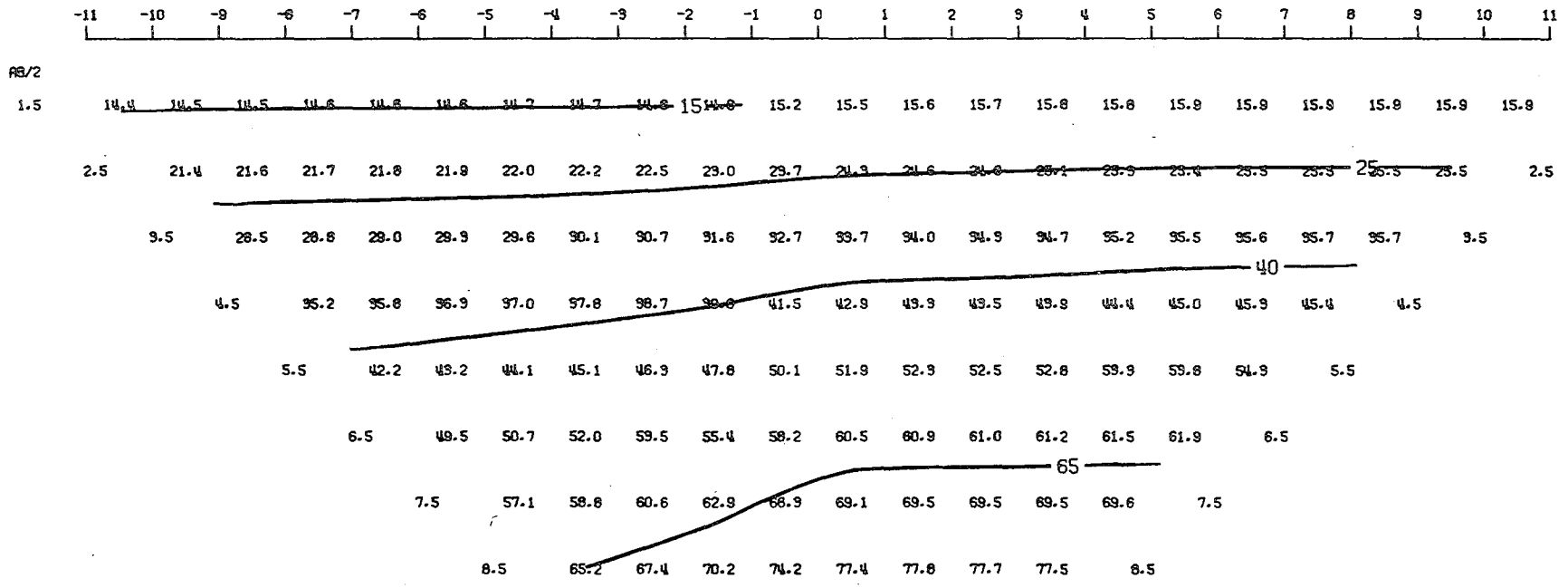

2-D RESISTIVITY MODEL -- BURIED VERTICAL CONTACT 2

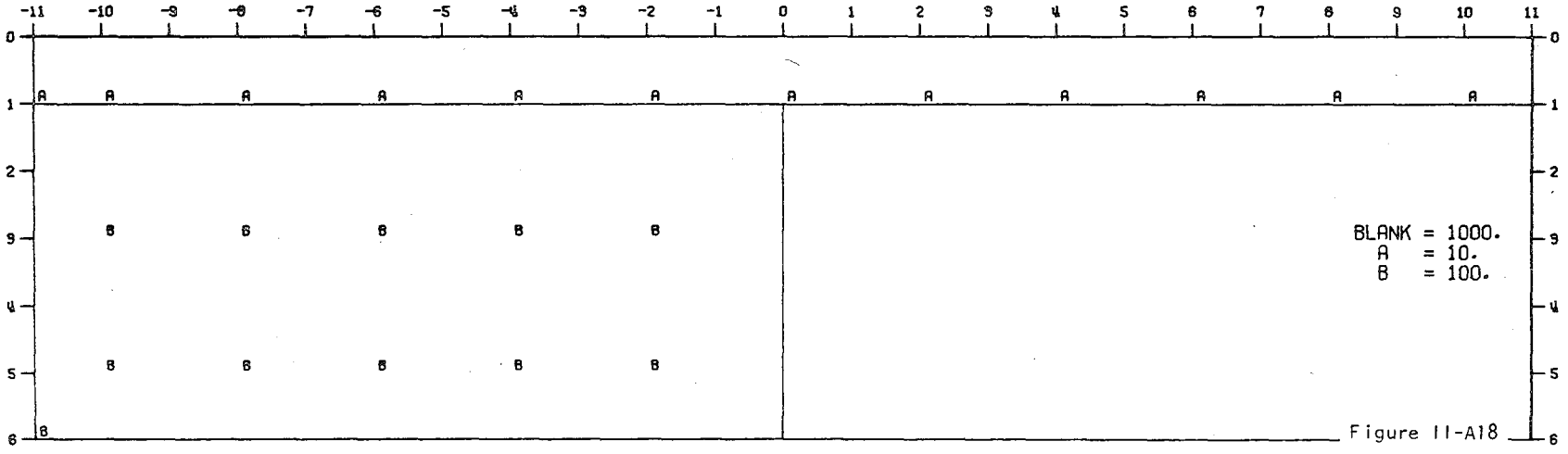

Figure II-A18

MODEL-- BURIED VERTICAL CONTACT 3
DIPOLE-DIPOLE APPARENT RESISTIVITY PSEUDO-SECTION
PROFILE LINE IS INCLINED AT 90.0 DEGREES TO STRIKE

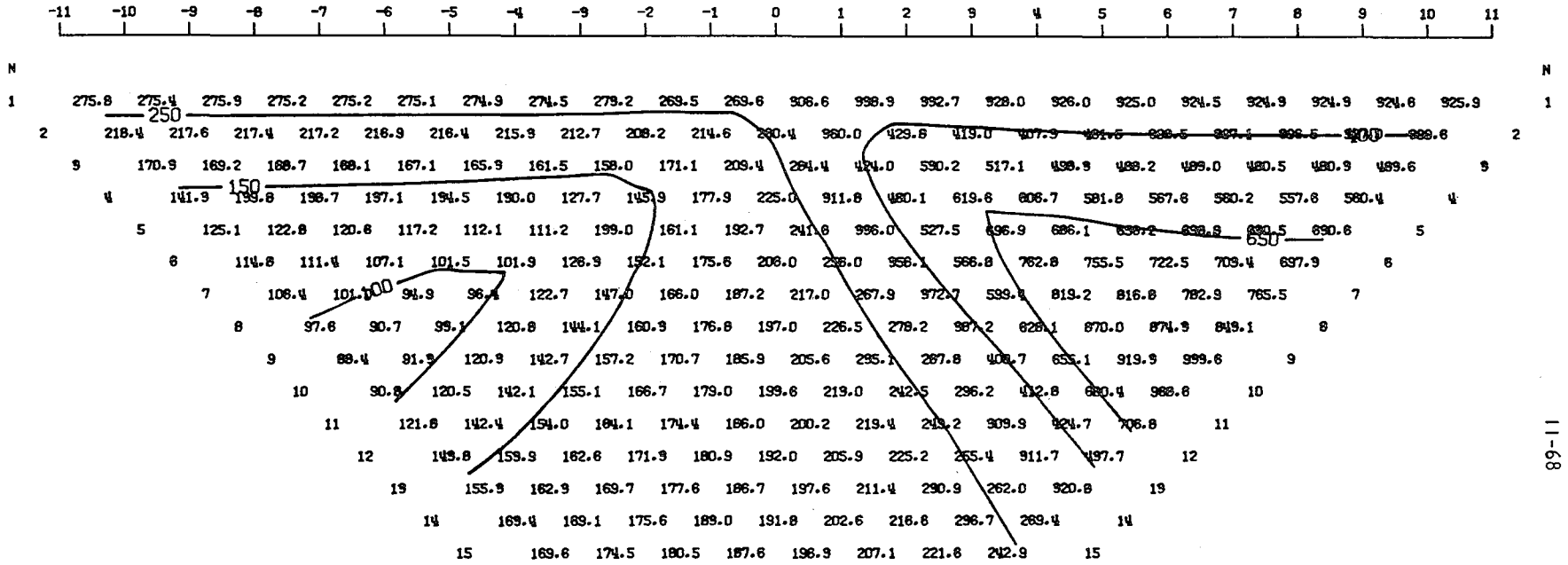

2-D RESISTIVITY MODEL -- BURIED VERTICAL CONTACT 3

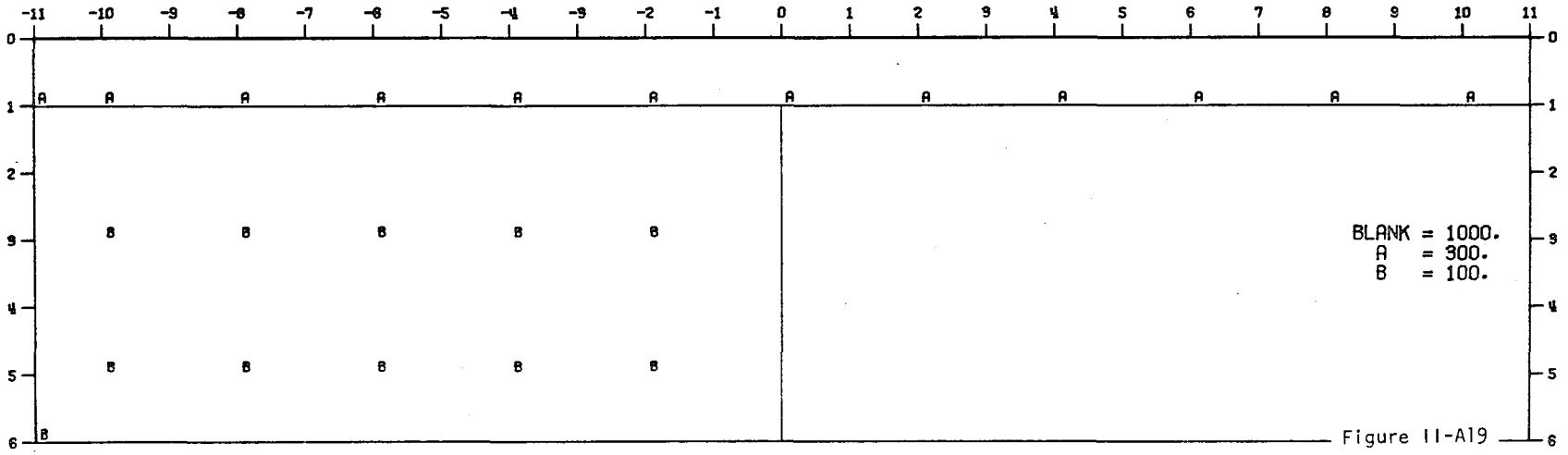

Figure II-A19

MODEL-- BURIED VERTICAL CONTACT 3
SCHLUMBERGER APPARENT RESISTIVITY PSEUDO-SECTION
PROFILE LINE IS INCLINED AT 90.0 DEGREES TO STRIKE

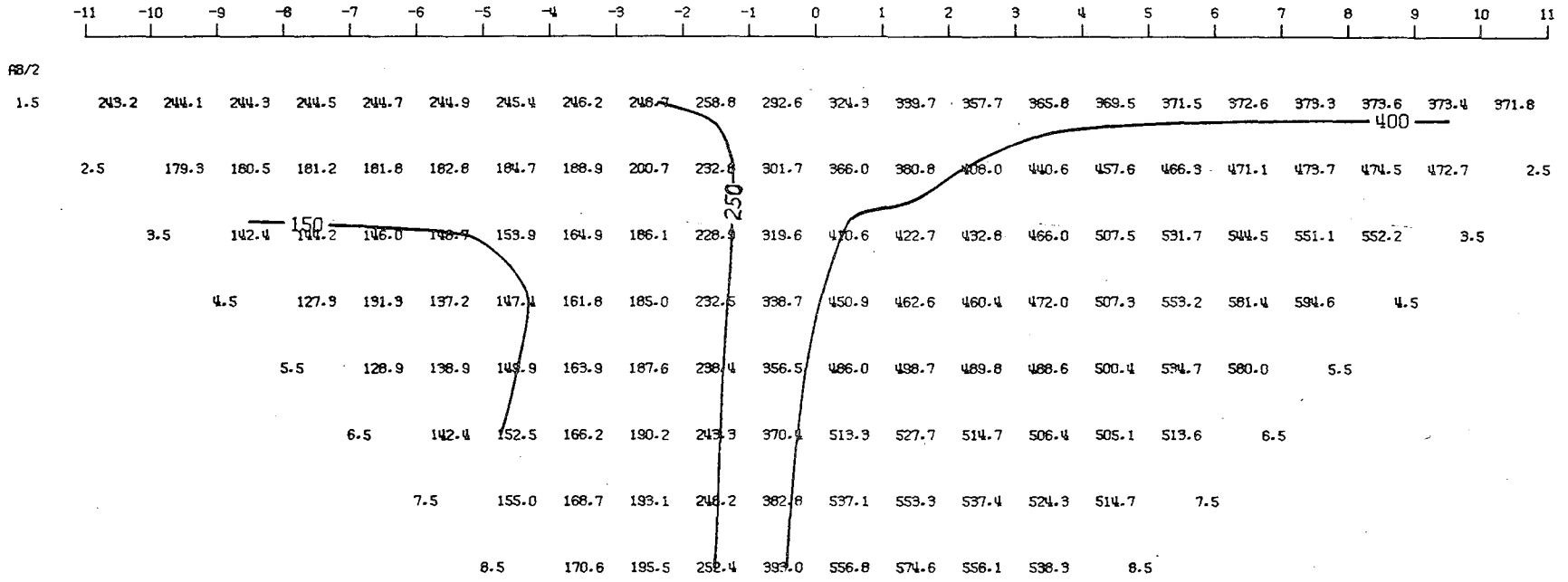

2-D RESISTIVITY MODEL -- BURIED VERTICAL CONTACT 3

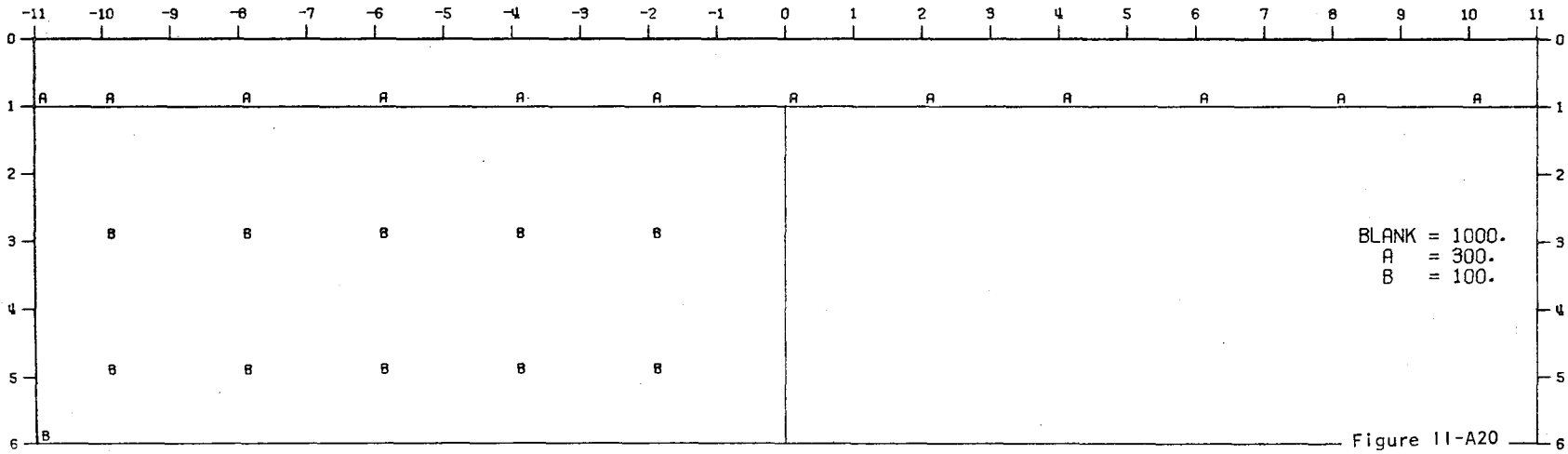

Figure II-A20

MODEL--14 DEGREE CONTACT
DIPOLE-DIPOLE APPARENT RESISTIVITY PSEUDO-SECTION
PROFILE LINE IS INCLINED AT 90.0 DEGREES TO STRIKE

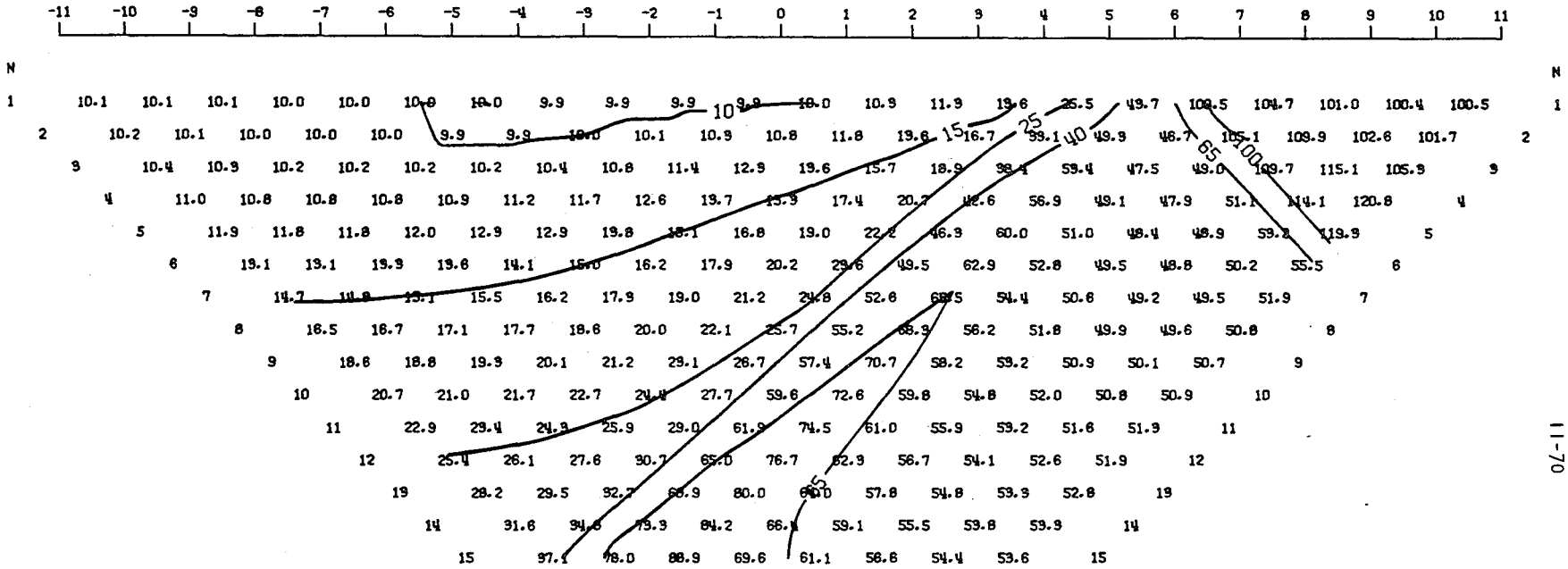

2-D RESISTIVITY MODEL -- 14 DEGREE CONTACT

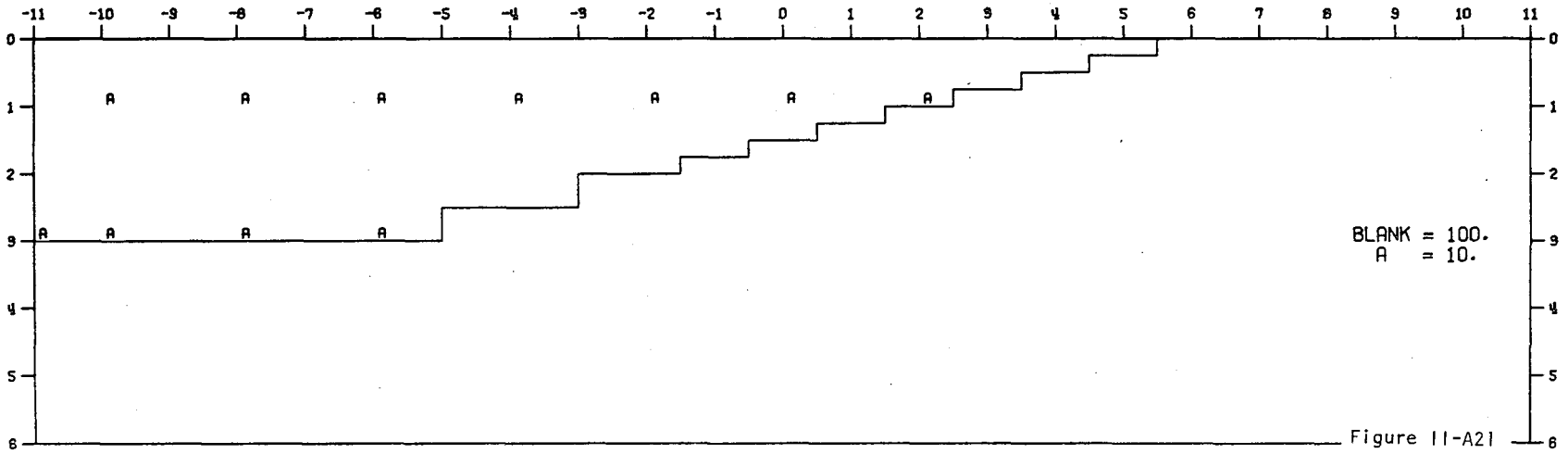

Figure II-A21

MODEL--14 DEGREE CONTACT
SCHLUMBERGER APPARENT RESISTIVITY PSEUDO-SECTION
PROFILE LINE IS INCLINED AT 90.0 DEGREES TO STRIKE

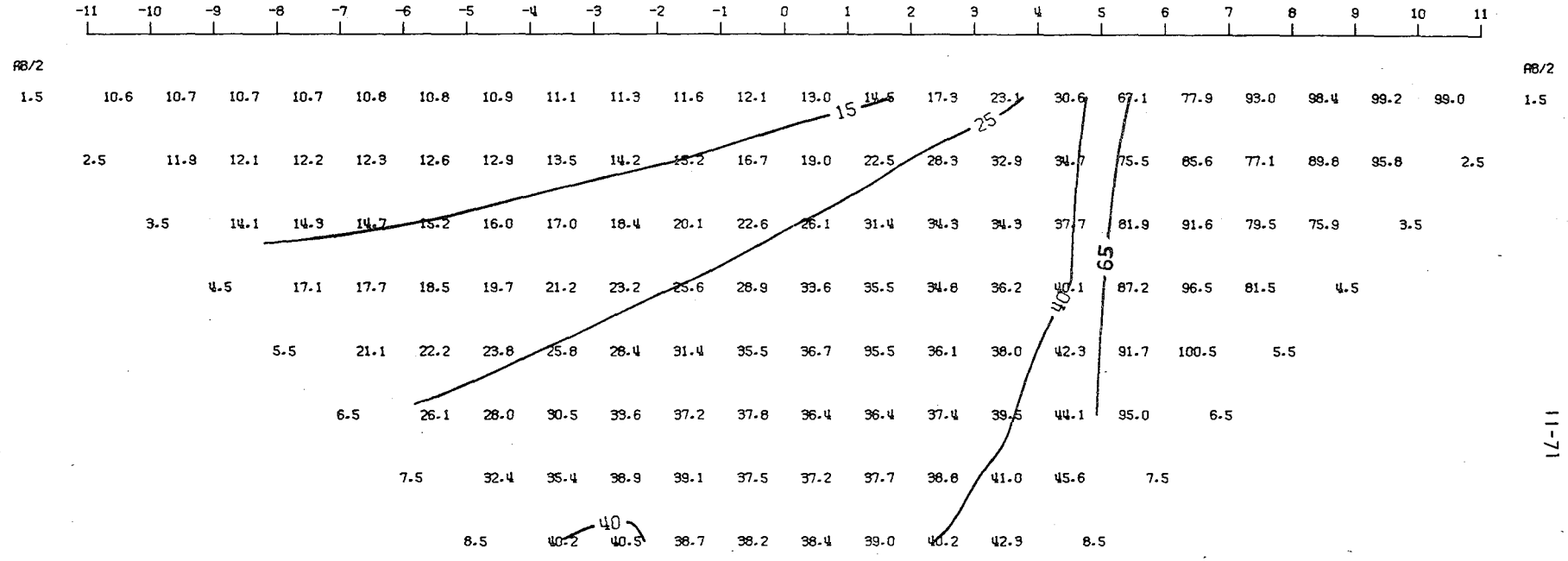

2-D RESISTIVITY MODEL -- 14 DEGREE CONTACT

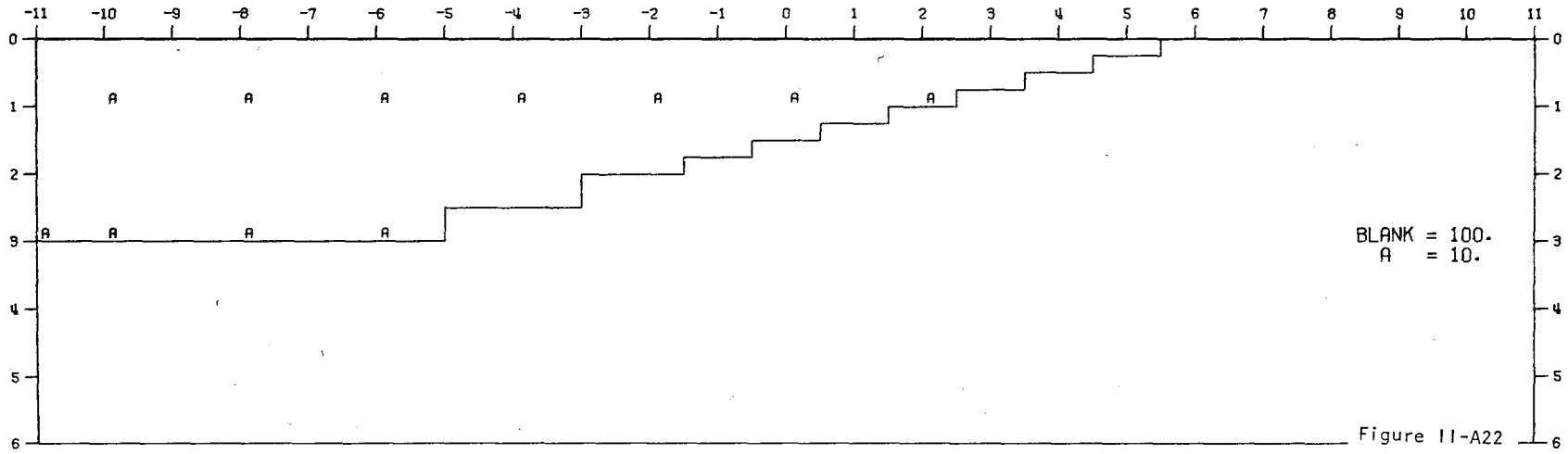

Figure 11-A22

MODEL-- BURIED VERTICAL CONTACT 4
DIPOLE-DIPOLE APPARENT RESISTIVITY PSEUDO-SECTION
PROFILE LINE IS INCLINED AT 90.0 DEGREES TO STRIKE

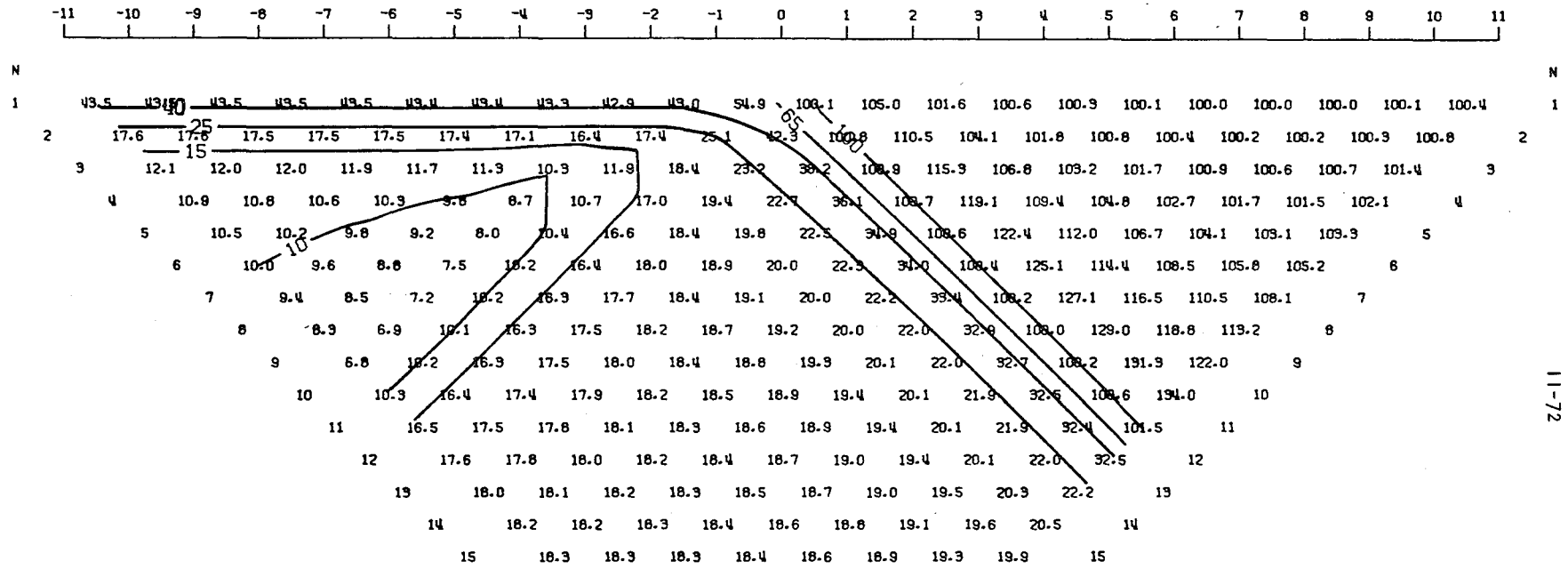

2-D RESISTIVITY MODEL -- BURIED VERTICAL CONTACT 4

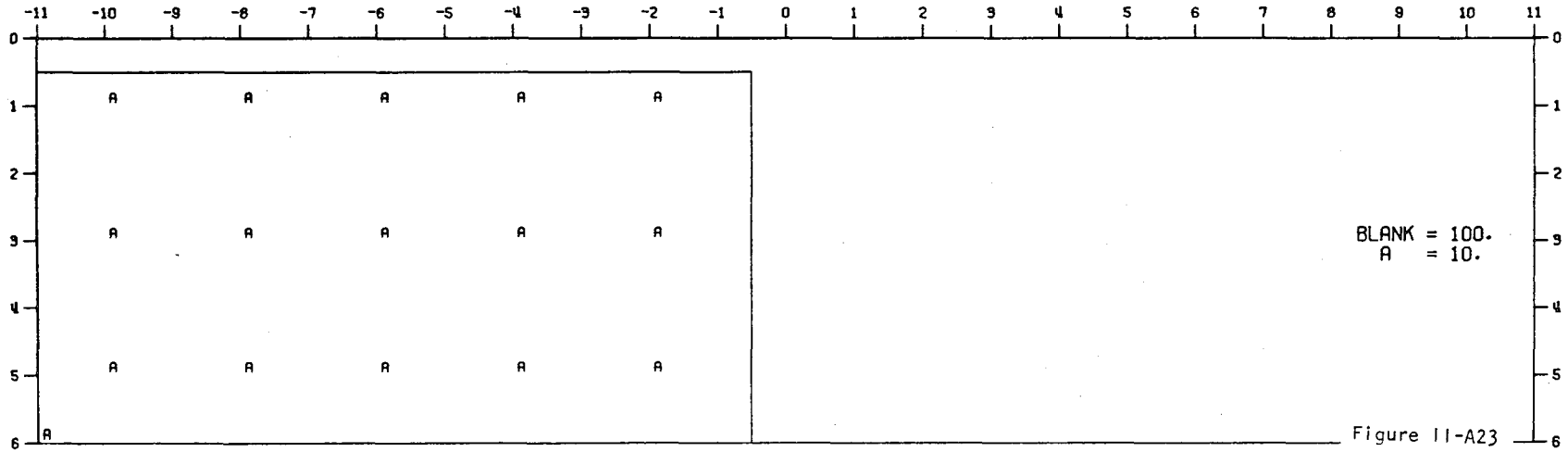

Figure II-A23

MODEL-- BURIED VERTICAL CONTACT 4
SCHLUMBERGER APPARENT RESISTIVITY PSEUDØ-SECTIØN
PROFILE LINE IS INCLINED AT 90.0 DEGREES TØ STRIKE

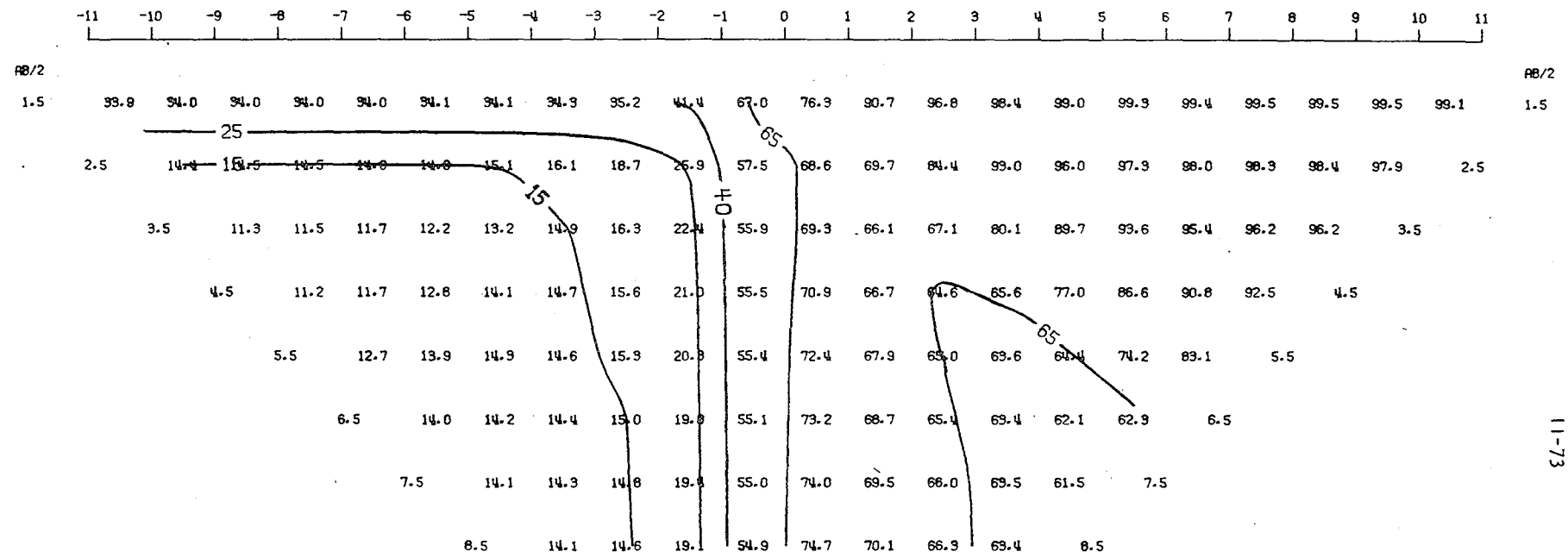

2-D RESISTIVITY MODEL -- BURIED VERTICAL CONTACT 4

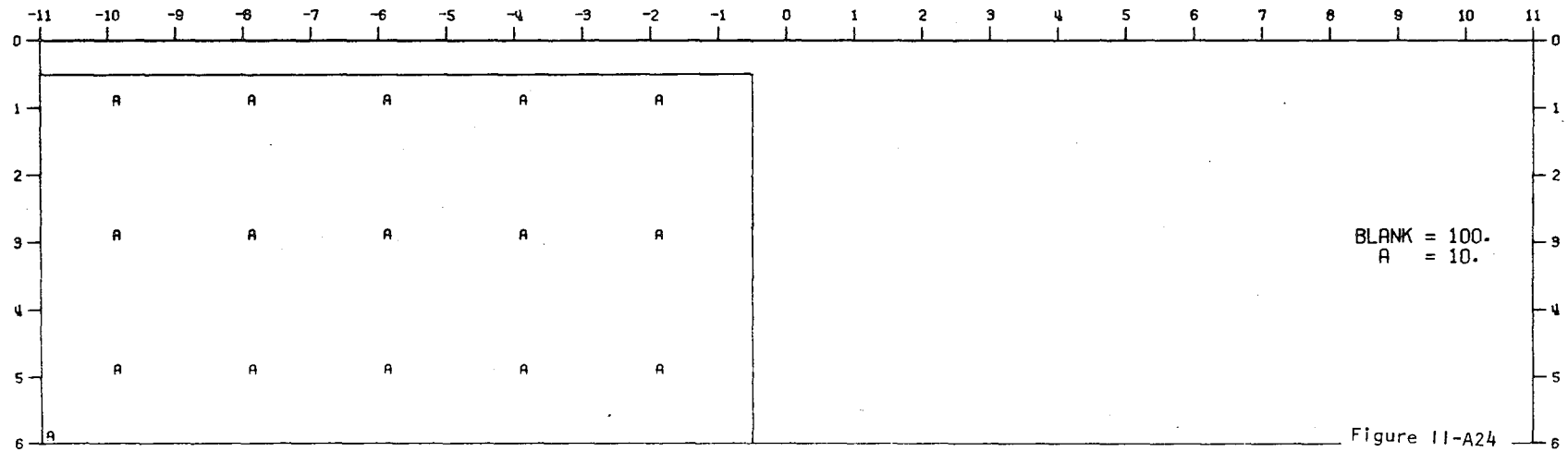

Figure II-A24

MODEL--FAULT 2

DIPOLE-DIPOLE APPARENT RESISTIVITY PSEUDO-SECTION

PROFILE LINE IS INCLINED AT 90.0 DEGREES TO STRIKE

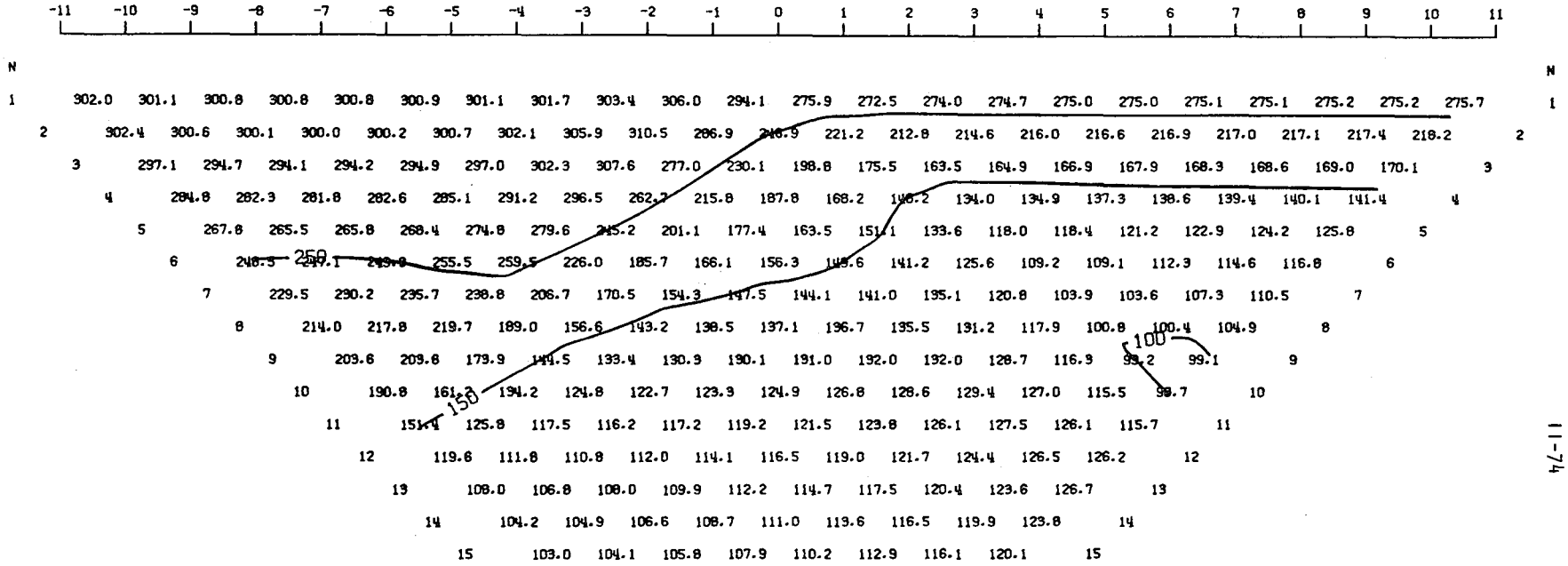

2-D RESISTIVITY MODEL -- FAULT 2

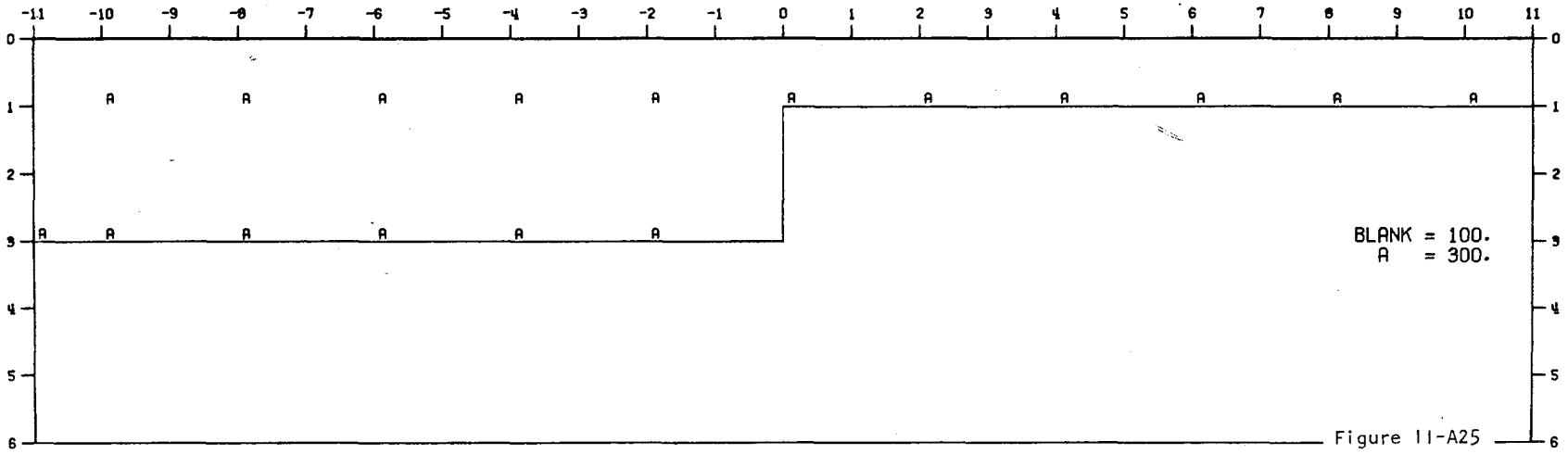

Figure II-A25

MODEL--FAULT 2
SCHLUMBERGER APPARENT RESISTIVITY PSEUDO-SECTION
PROFILE LINE IS INCLINED AT 90.0 DEGREES TO STRIKE

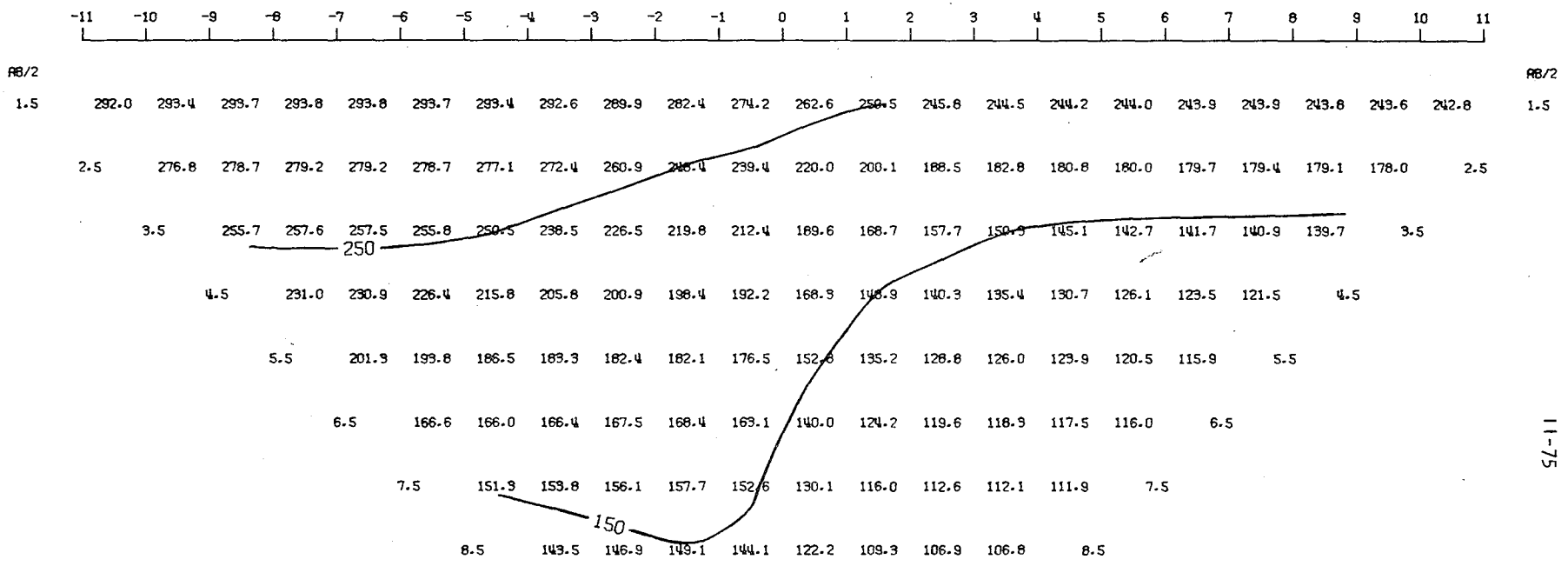

2-D RESISTIVITY MODEL -- FAULT 2

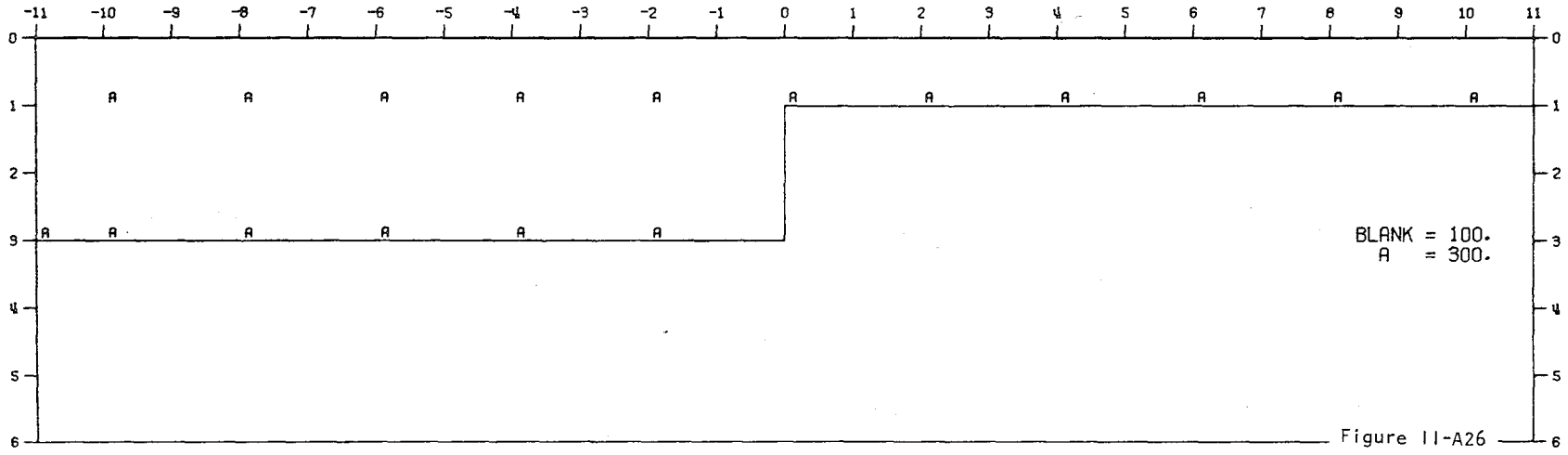

Figure II-A26

MODEL--THINNING CONDUCTIVE LAYER
DIPOLE-DIPOLE APPARENT RESISTIVITY PSEUDO-SECTION
PROFILE LINE IS INCLINED AT 90.0 DEGREES TO STRIKE

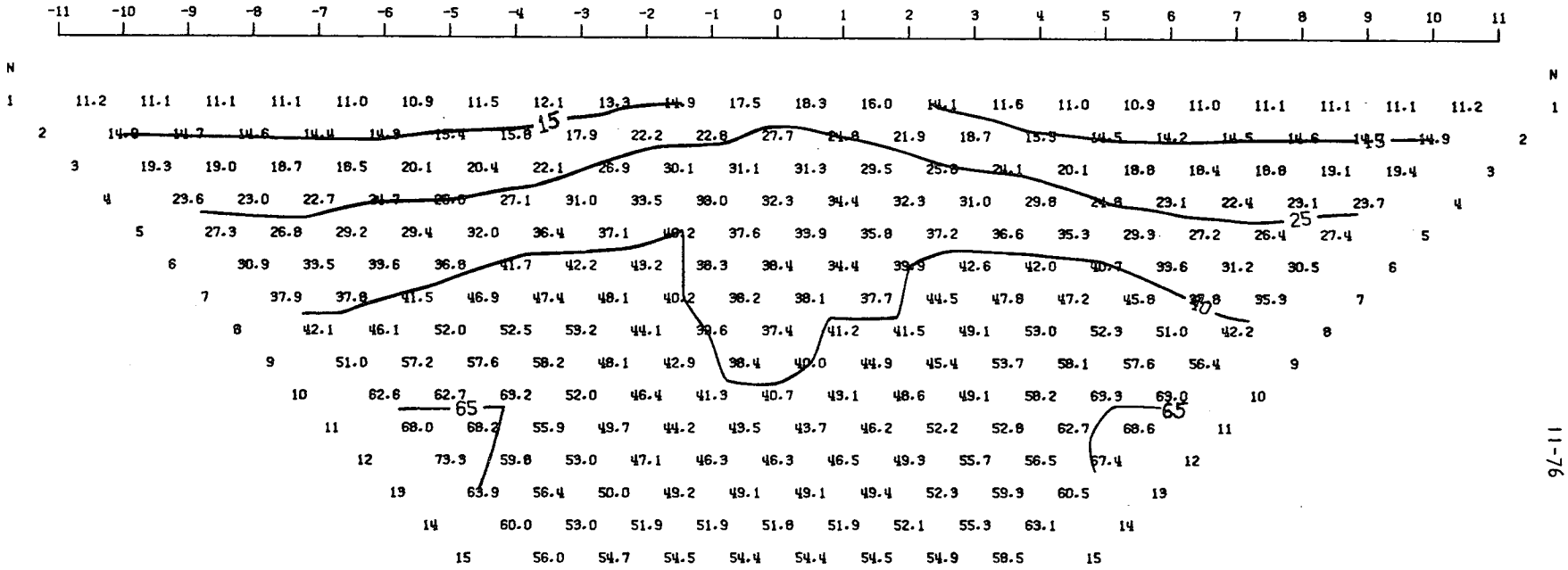

2-D RESISTIVITY MODEL -- THINNING LAYER

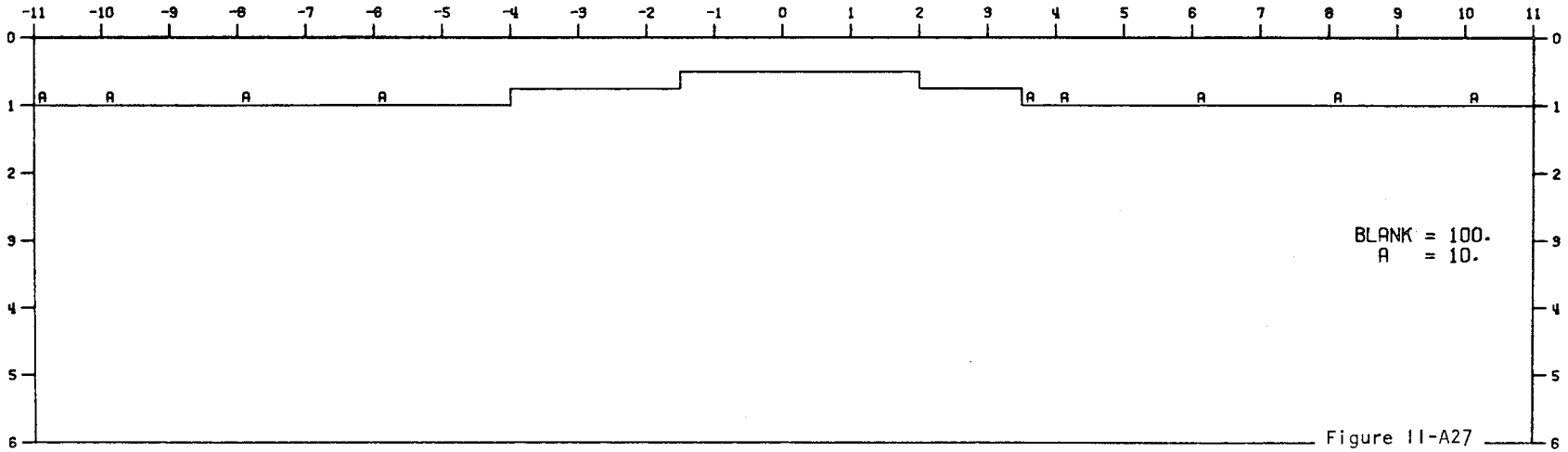

Figure II-A27

MODEL--THINNING CONDUCTIVE LAYER
SCHLUMBERGER APPARENT RESISTIVITY PSEUDO-SECTION
PROFILE LINE IS INCLINED AT 90.0 DEGREES TO STRIKE

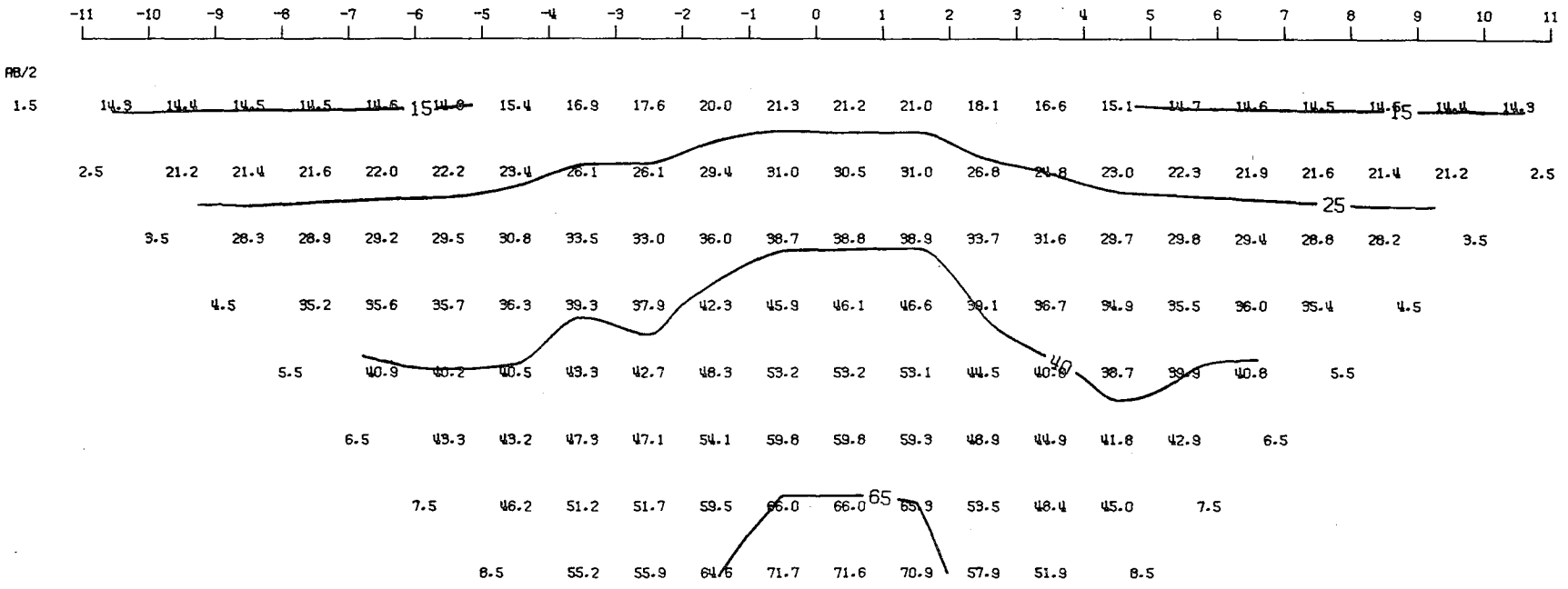

2-D RESISTIVITY MODEL -- THINNING LAYER

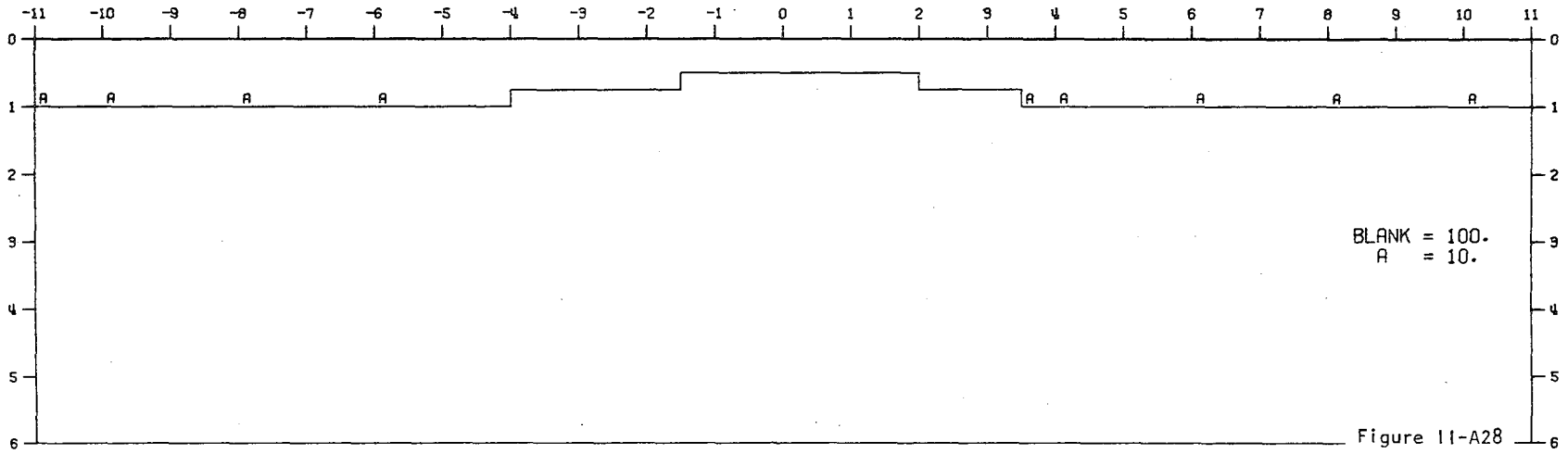

Figure 11-A28

MODEL--THICKENING CONDUCTIVE LAYER
DIPOLE-DIPOLE APPARENT RESISTIVITY PSEUDO-SECTION
PROFILE LINE IS INCLINED AT 90.0 DEGREES TO STRIKE

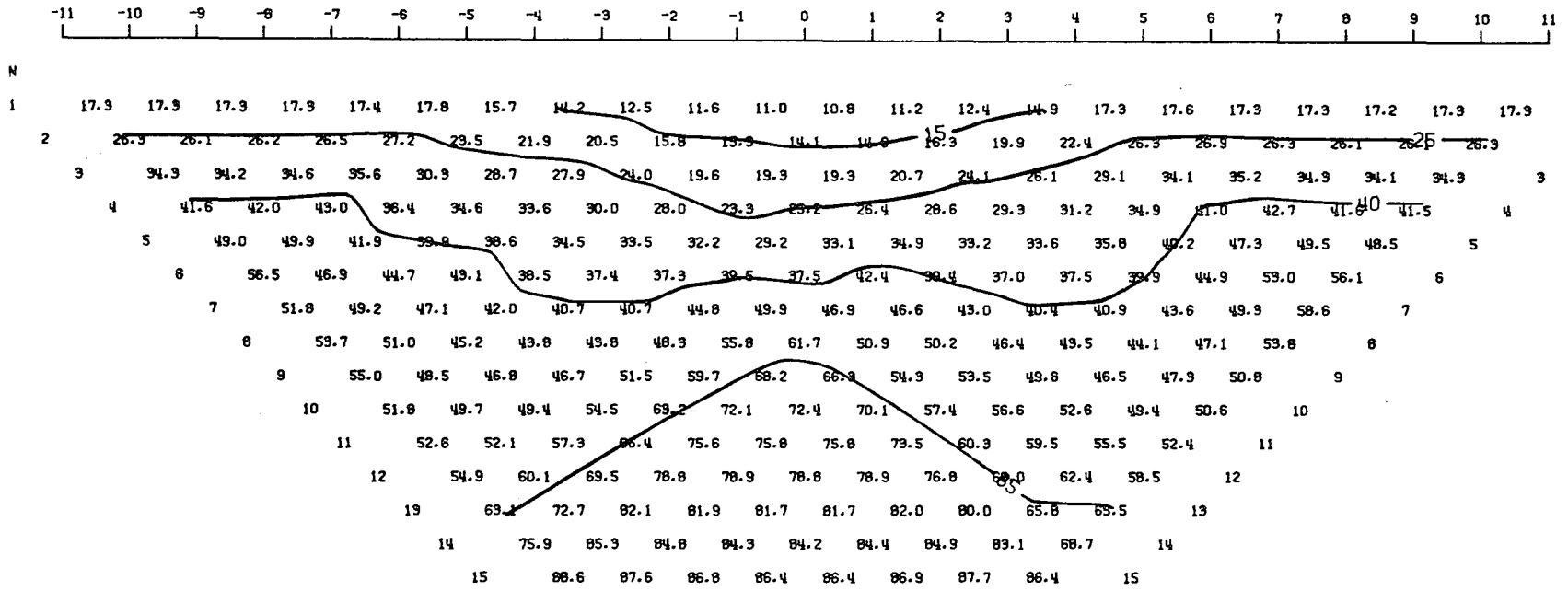

2-D RESISTIVITY MODEL -- THICKENING LAYER

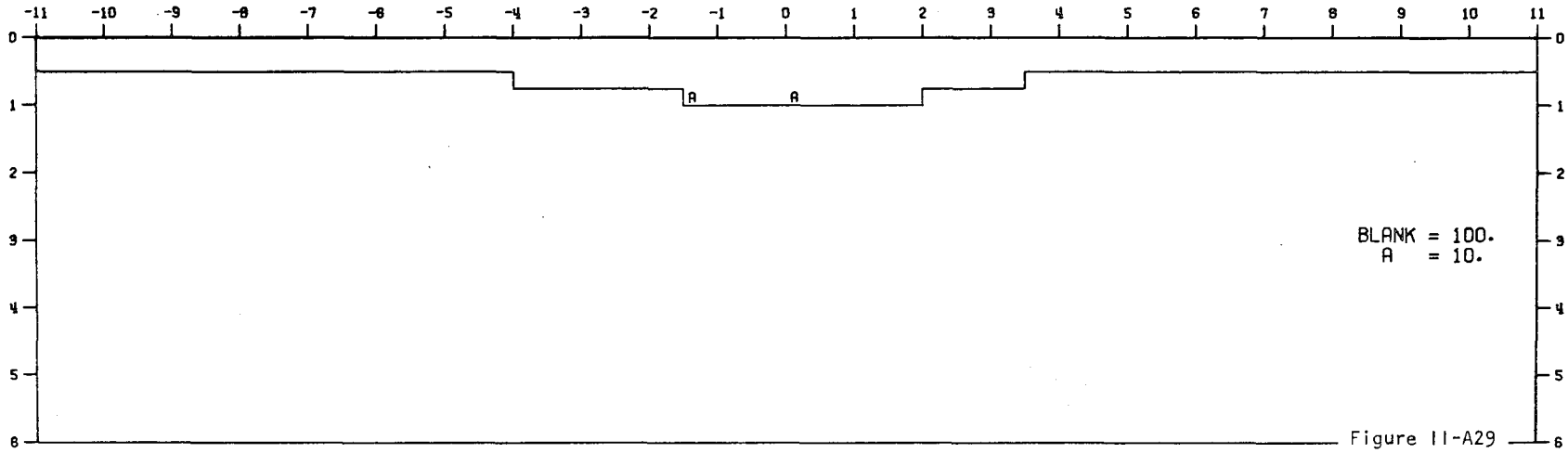

Figure II-A29

MODEL--THICKENING CONDUCTIVE LAYER
SCHLUMBERGER APPARENT RESISTIVITY PSEUDO-SECTION
PROFILE LINE IS INCLINED AT 90.0 DEGREES TO STRIKE

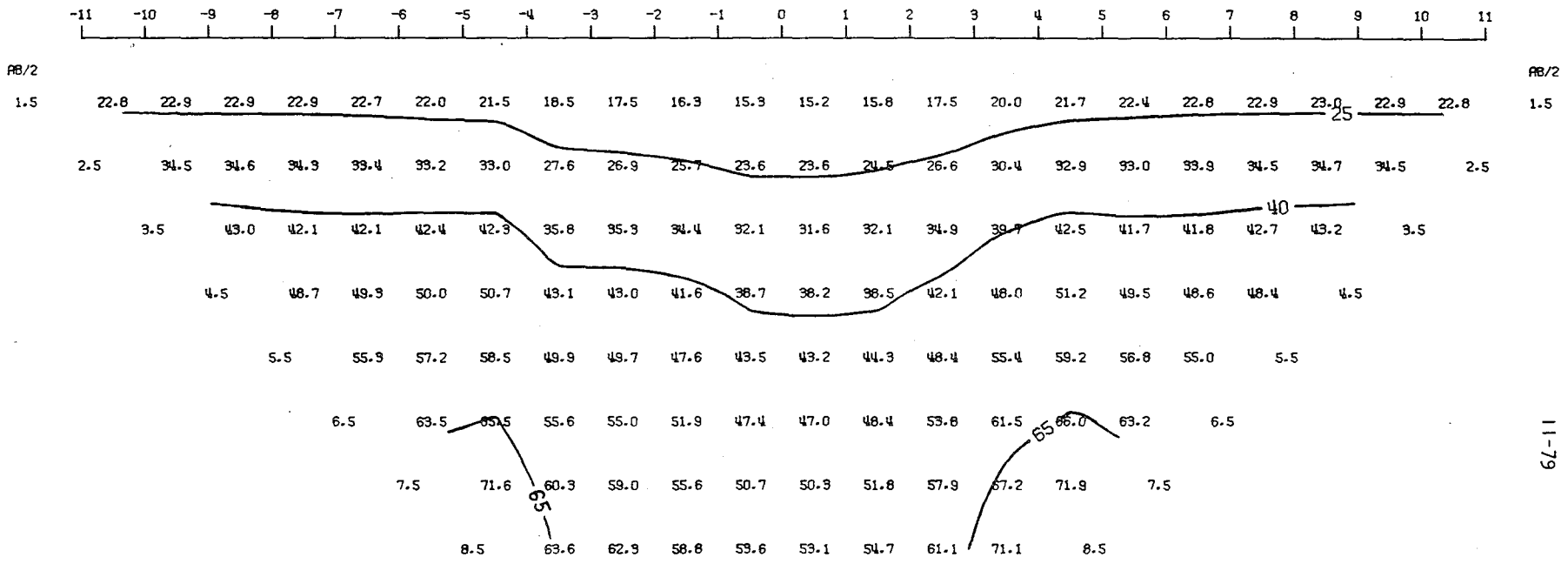

2-D RESISTIVITY MODEL -- THICKENING LAYER

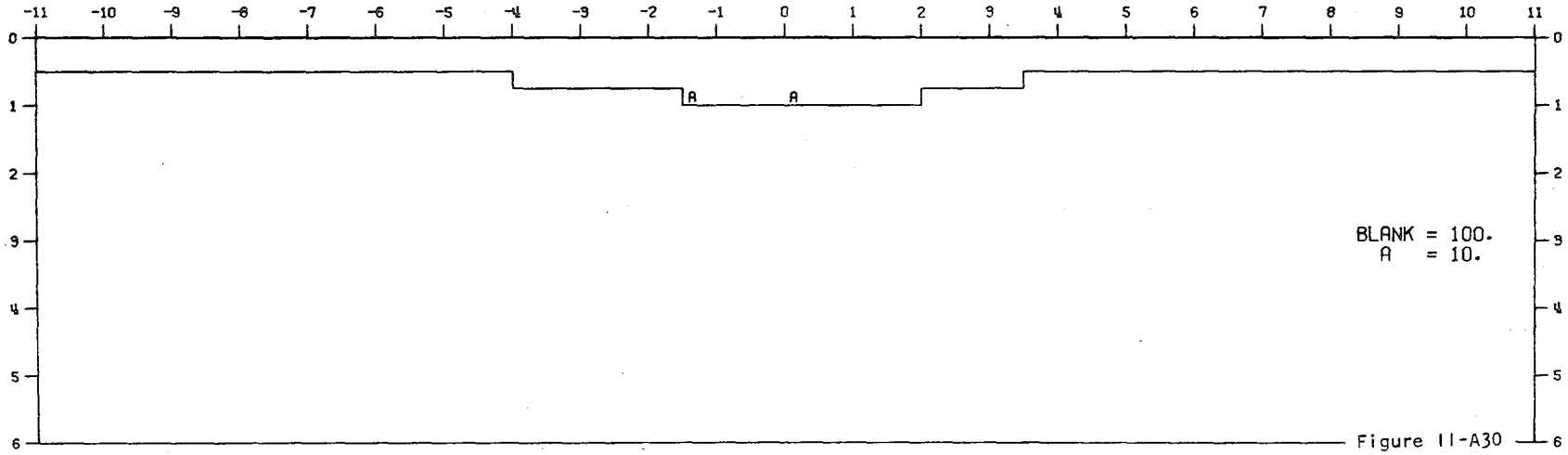

Figure II-A30

MODEL--THINNING RESISTIVE LAYER
DIPOLE-DIPOLE APPARENT RESISTIVITY PSEUDO-SECTION
PROFILE LINE IS INCLINED AT 90.0 DEGREES TO STRIKE

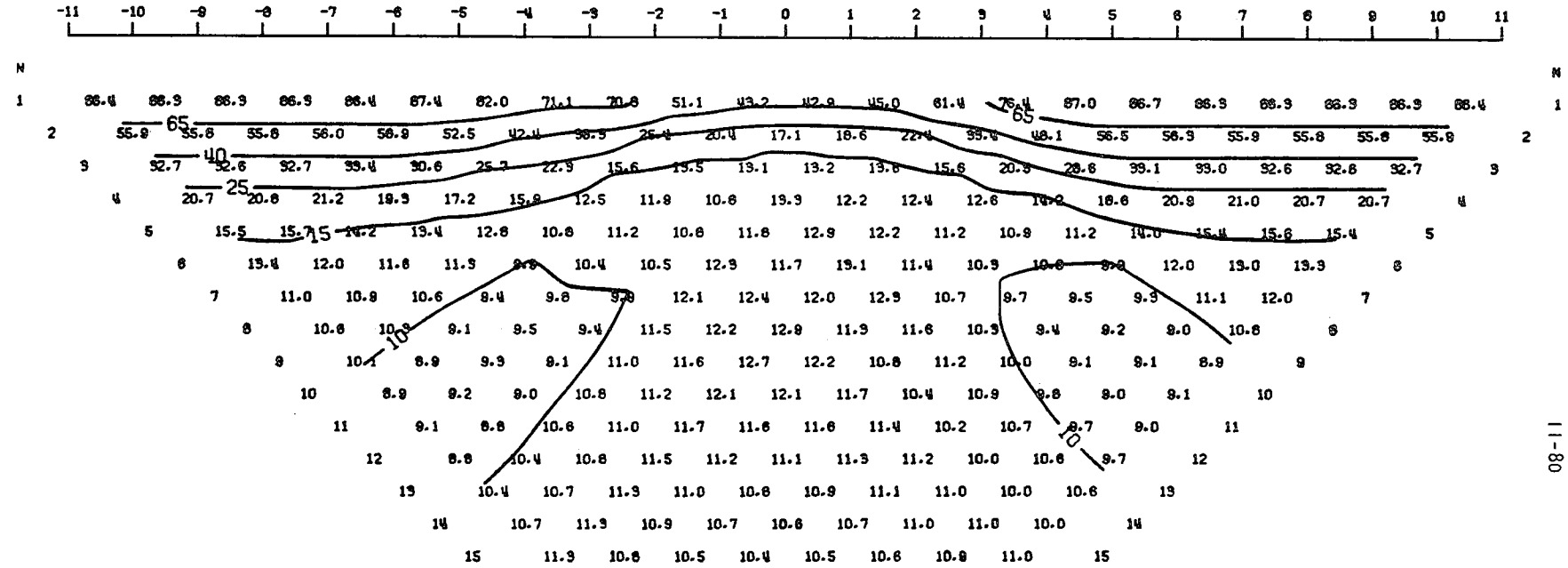

2-D RESISTIVITY MODEL -- THINNING RESISTIVE LAYER

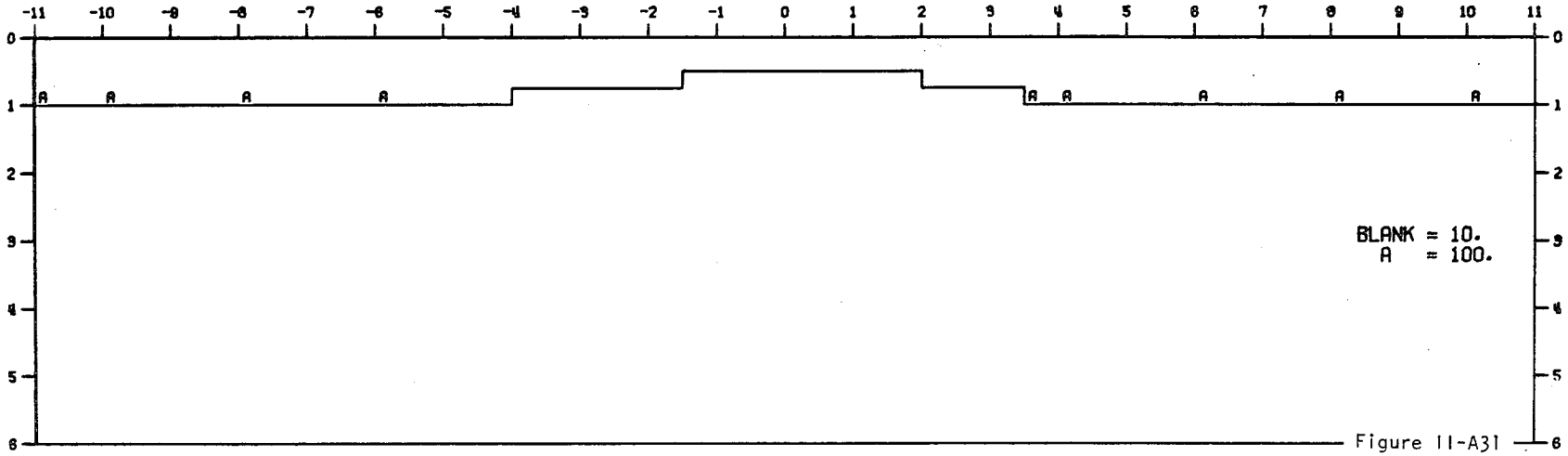

Figure II-A31

MODEL--THINNING RESISTIVE LAYER
SCHLUMBERGER APPARENT RESISTIVITY PSEUDO-SECTION
PROFILE LINE IS INCLINED AT 90.0 DEGREES TO STRIKE

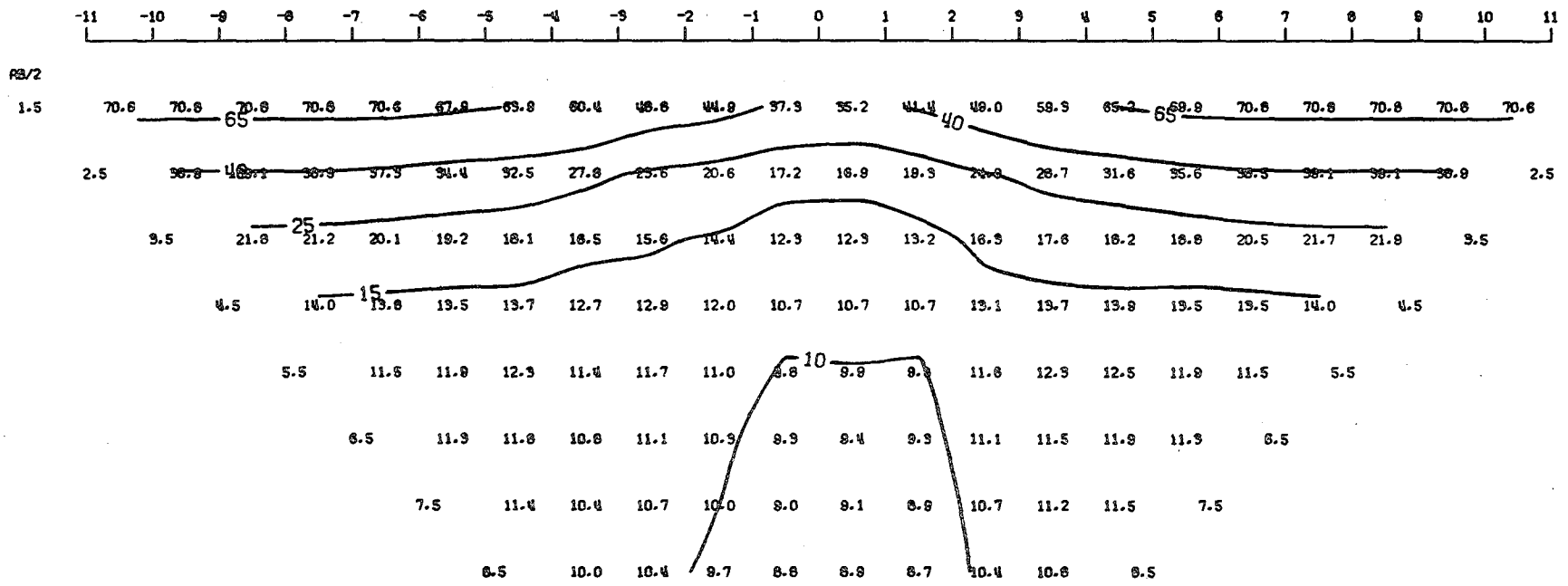

2-D RESISTIVITY MODEL -- THINNING RESISTIVE LAYER

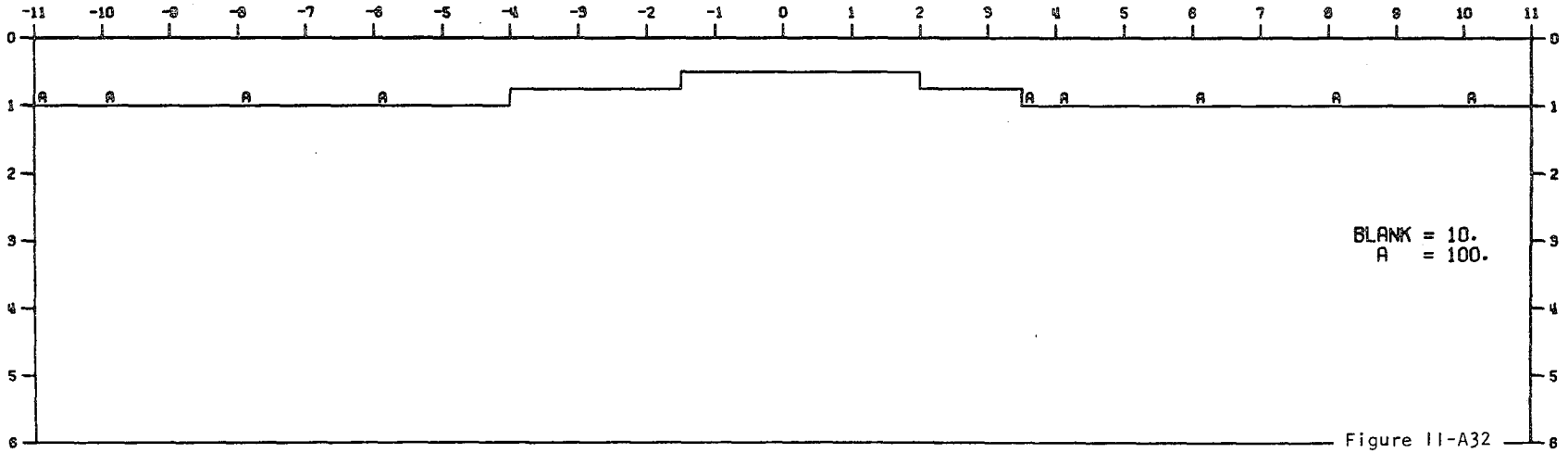

Figure II-A32

MODEL-- THICKENING RESISTIVE LAYER
DIPOLE-DIPOLE APPARENT RESISTIVITY PSEUDO-SECTION
PROFILE LINE IS INCLINED AT 90.0 DEGREES TO STRIKE

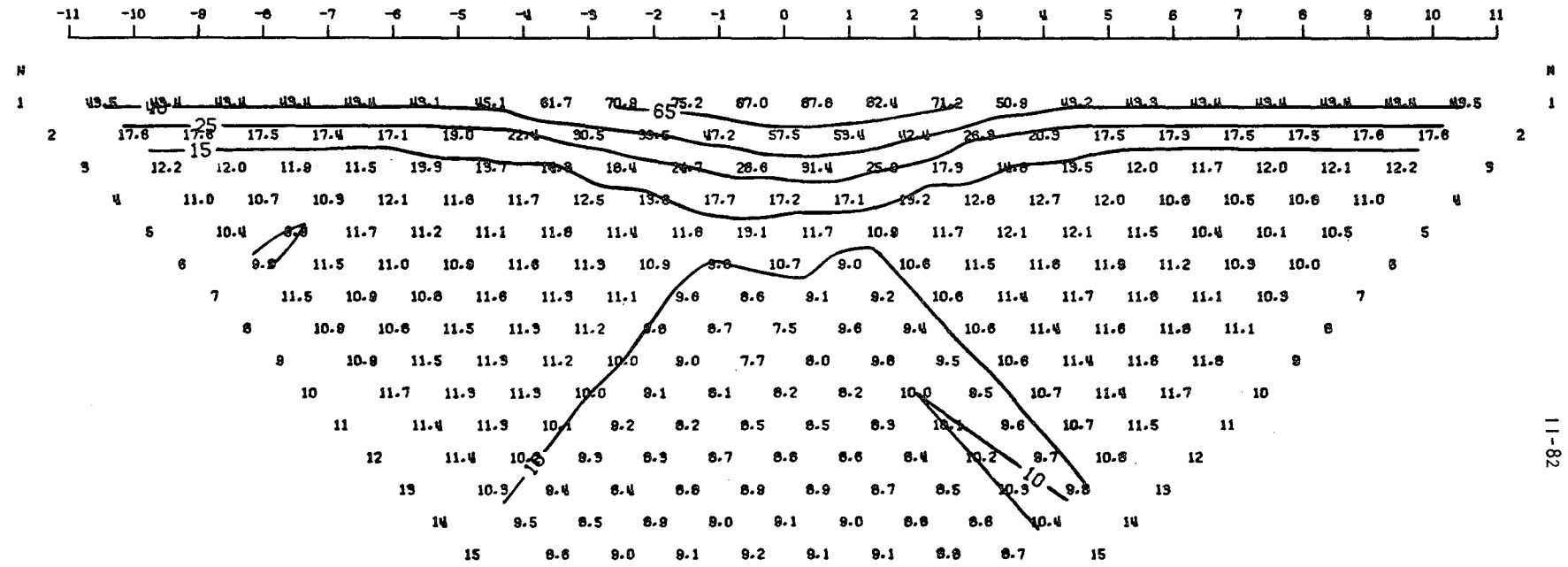

2-D RESISTIVITY MODEL -- THICKENING RESISTIVE LAYER

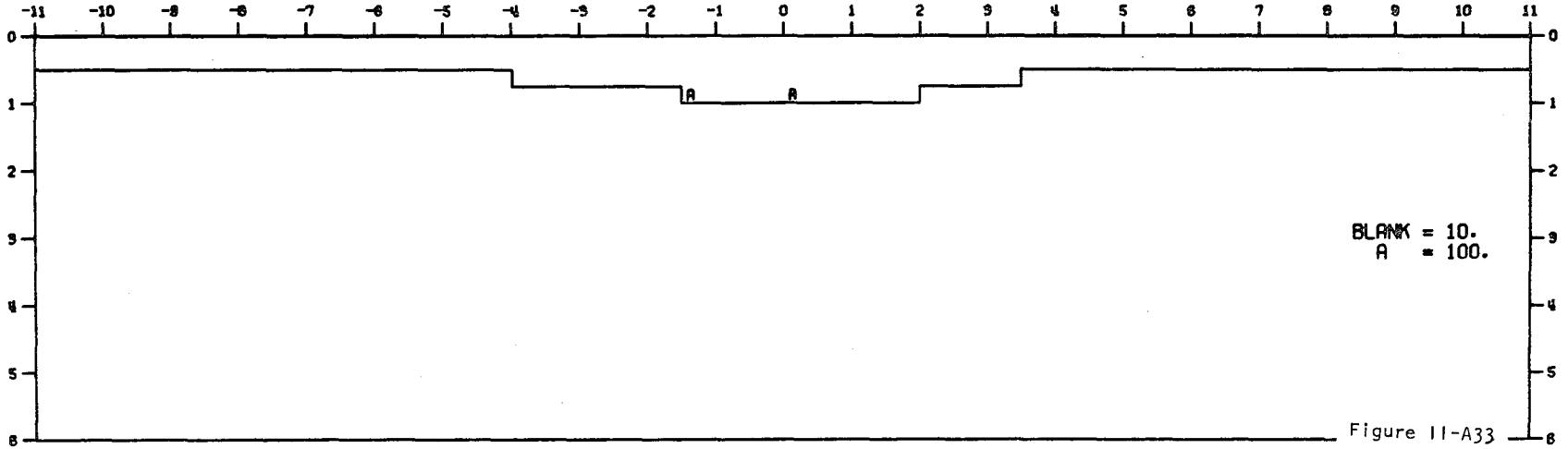

Figure II-A33

MODEL-- THICKENING RESISTIVE LAYER
SCHLUMBERGER APPARENT RESISTIVITY PSEUDO-SECTION
PROFILE LINE IS INCLINED AT 90.0 DEGREES TO STRIKE

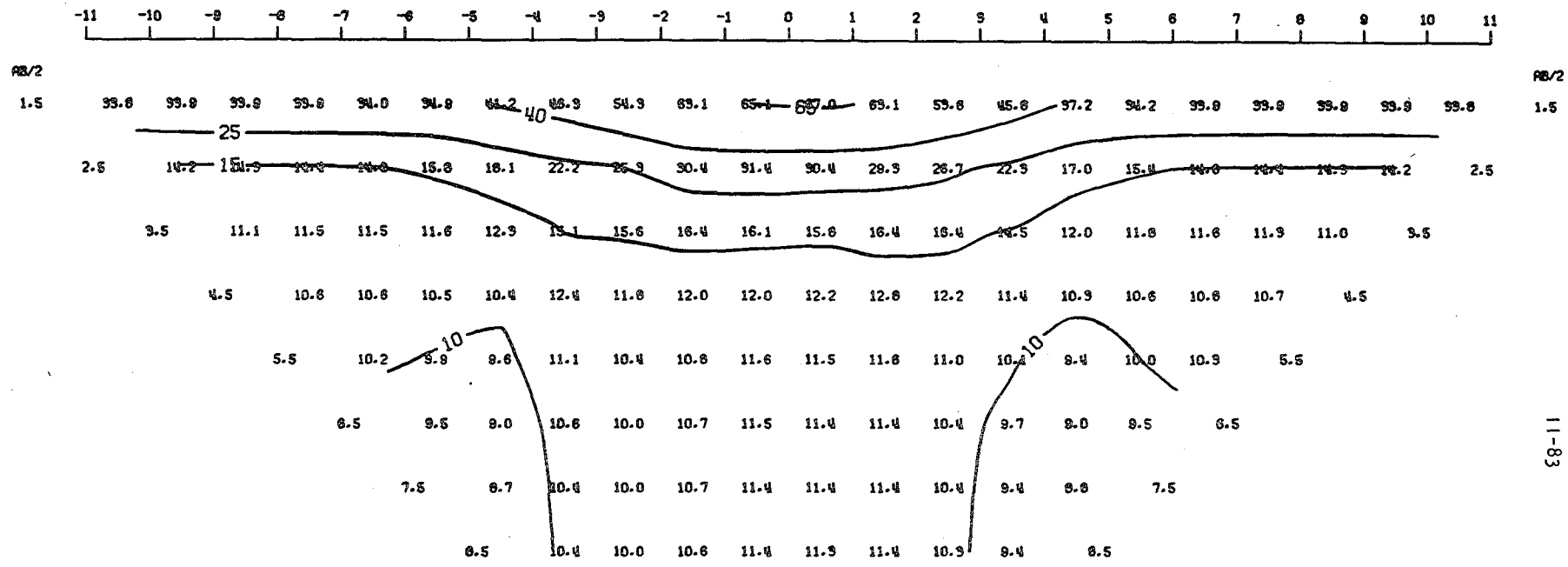

2-D RESISTIVITY MODEL -- THICKENING RESISTIVE LAYER

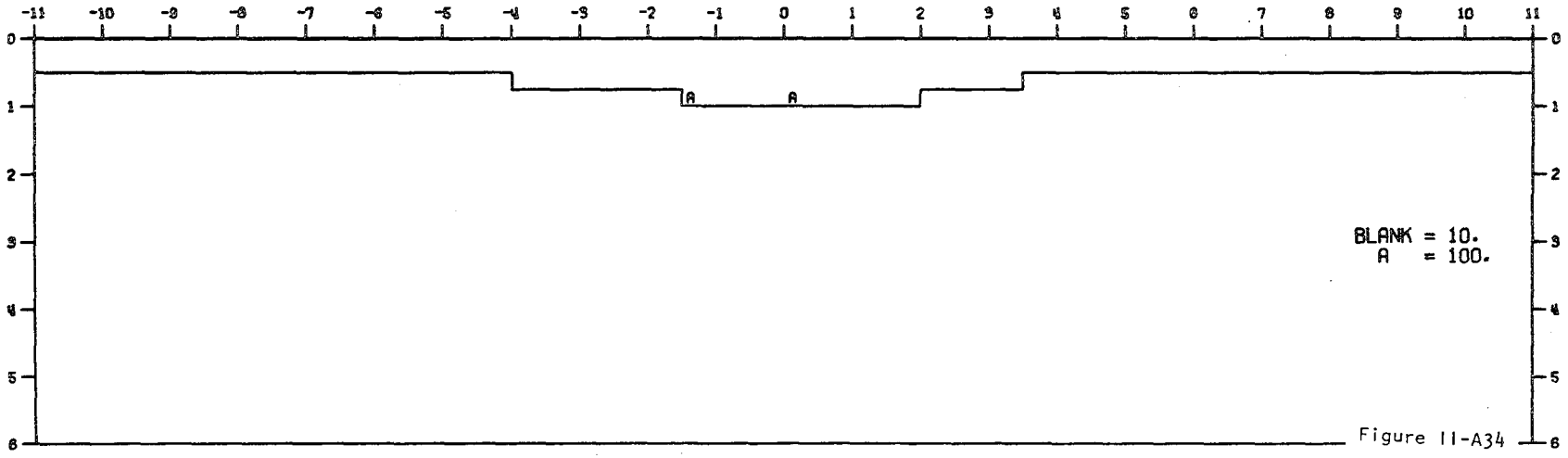

Figure II-A34

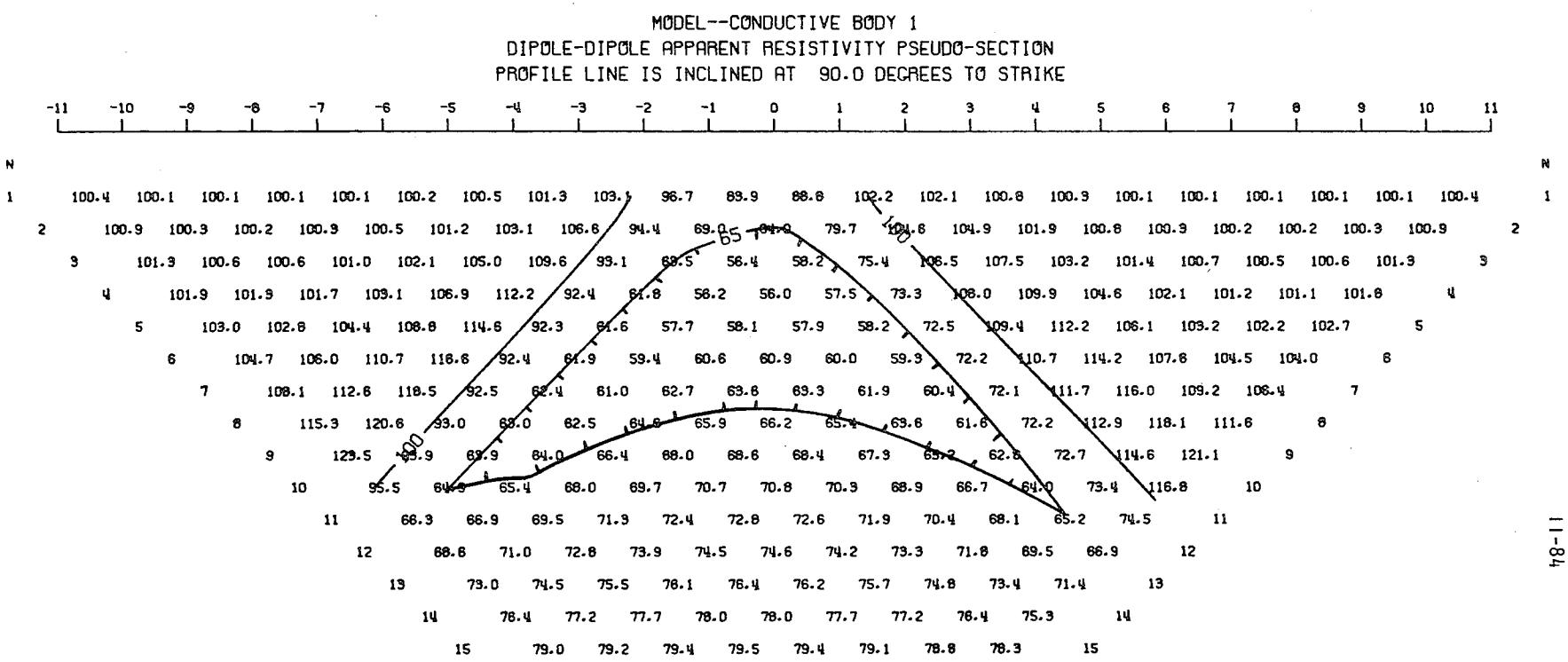

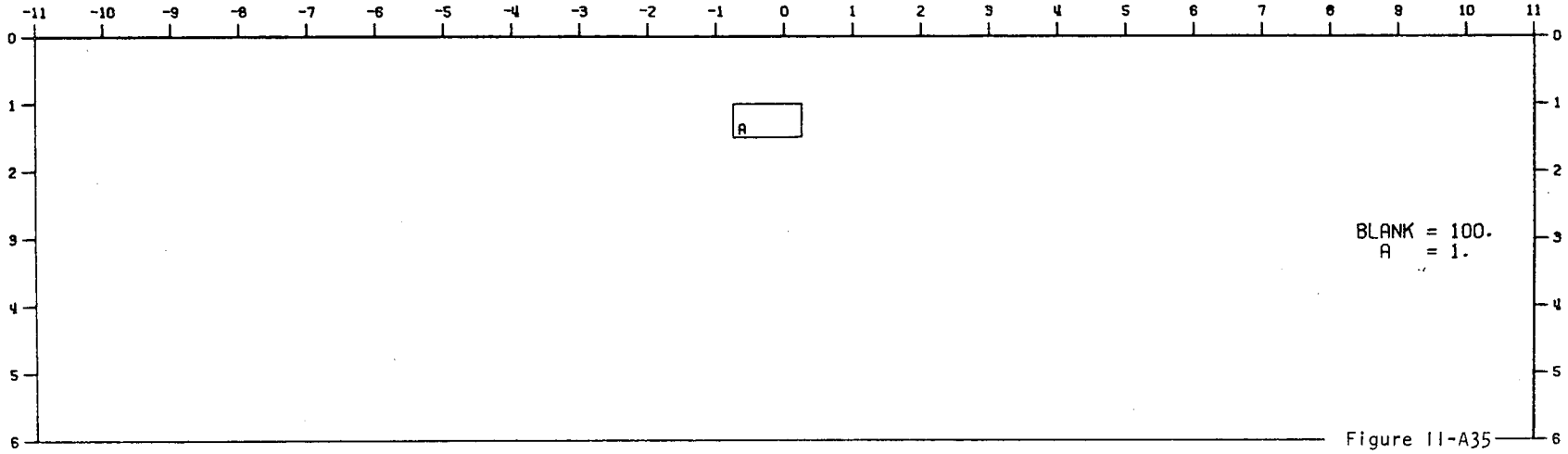

Figure II-A35

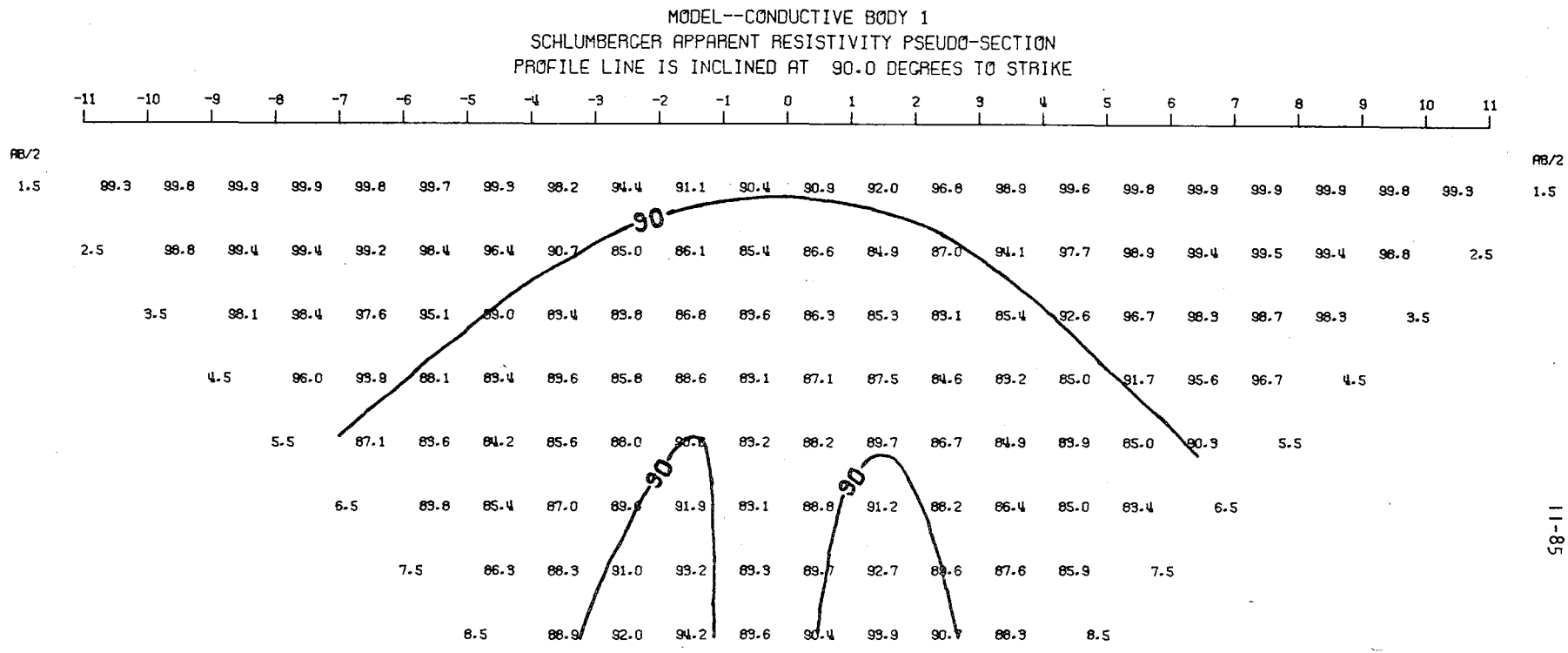

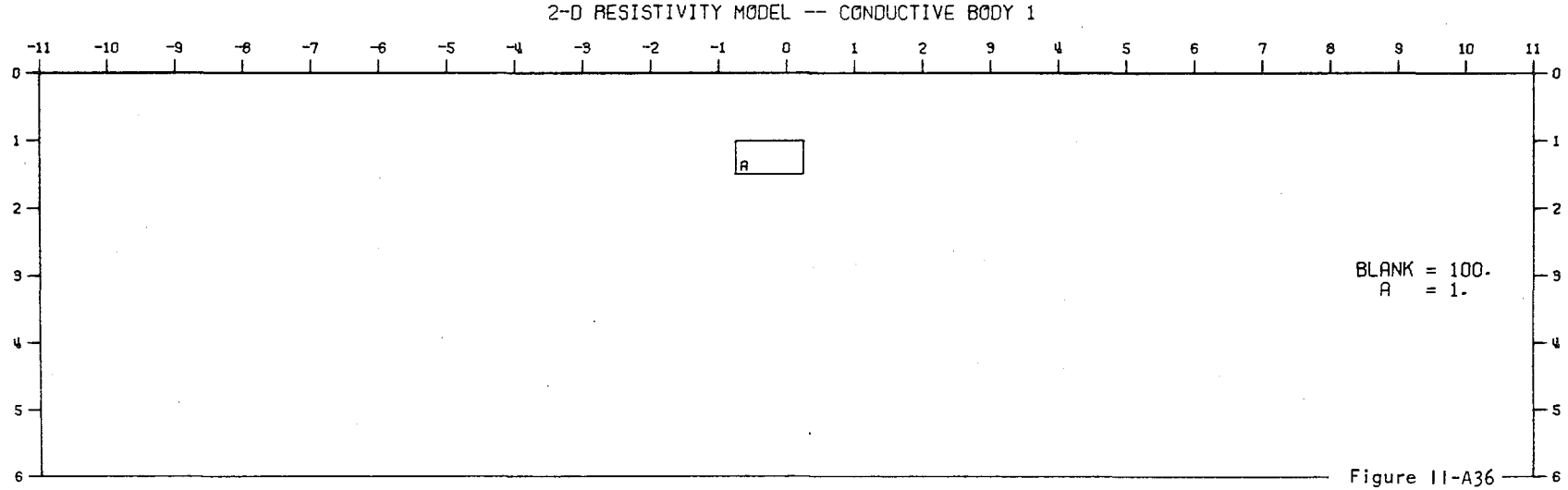

Figure II-A36

MODEL--CONDUCTIVE BODY 2
DIPOLE-DIPOLE APPARENT RESISTIVITY PSEUDO-SECTION
PROFILE LINE IS INCLINED AT 90.0 DEGREES TO STRIKE

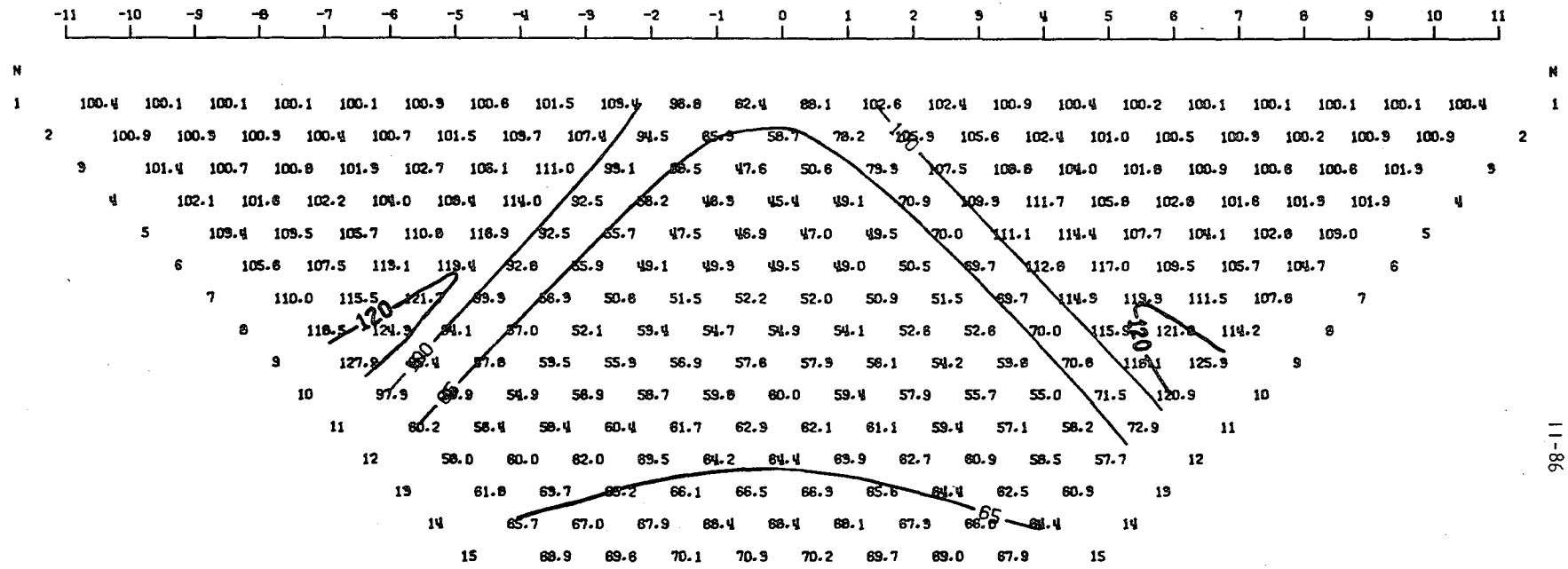

2-D RESISTIVITY MODEL -- CONDUCTIVE BODY 2

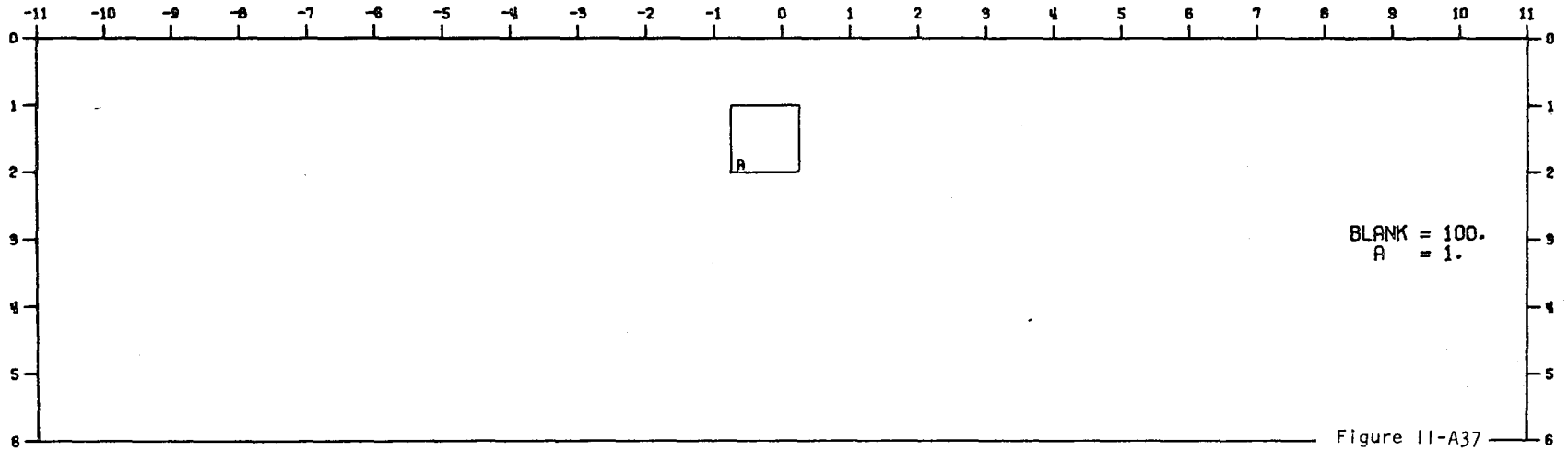

Figure II-A37

MODEL--CONDUCTIVE BODY 2
SCHLUMBERGER APPARENT RESISTIVITY PSEUDO-SECTION
PROFILE LINE IS INCLINED AT 90.0 DEGREES TO STRIKE

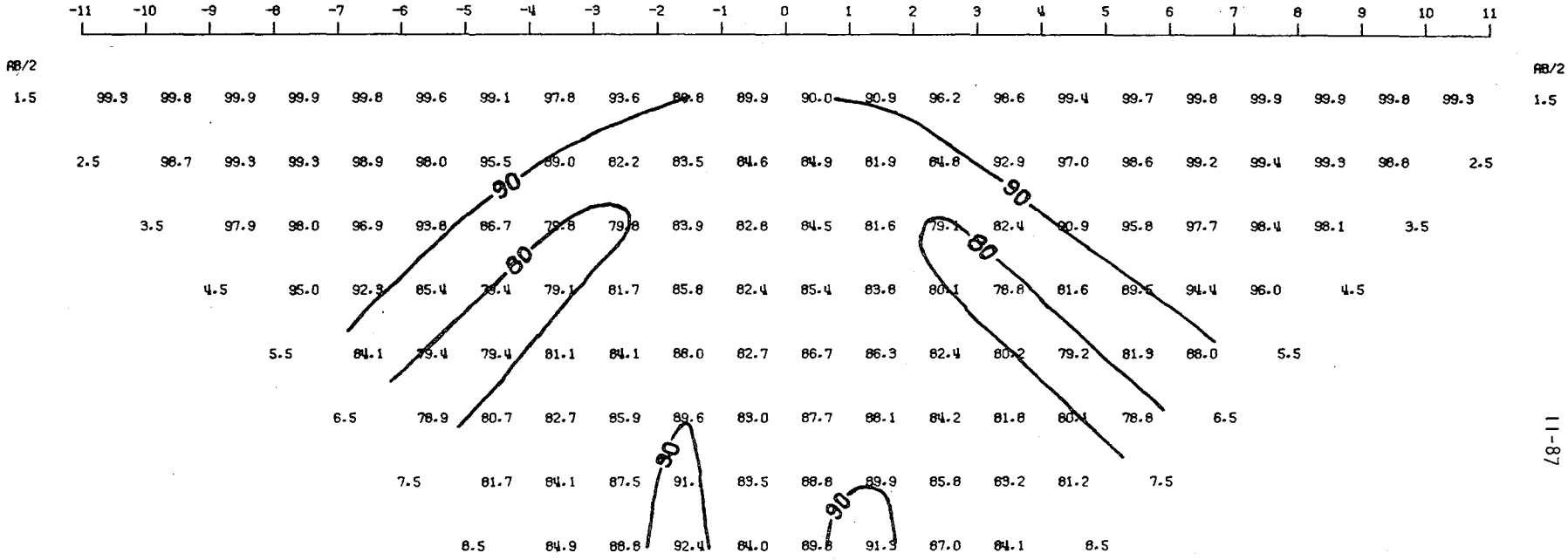

2-D RESISTIVITY MODEL -- CONDUCTIVE BODY 2

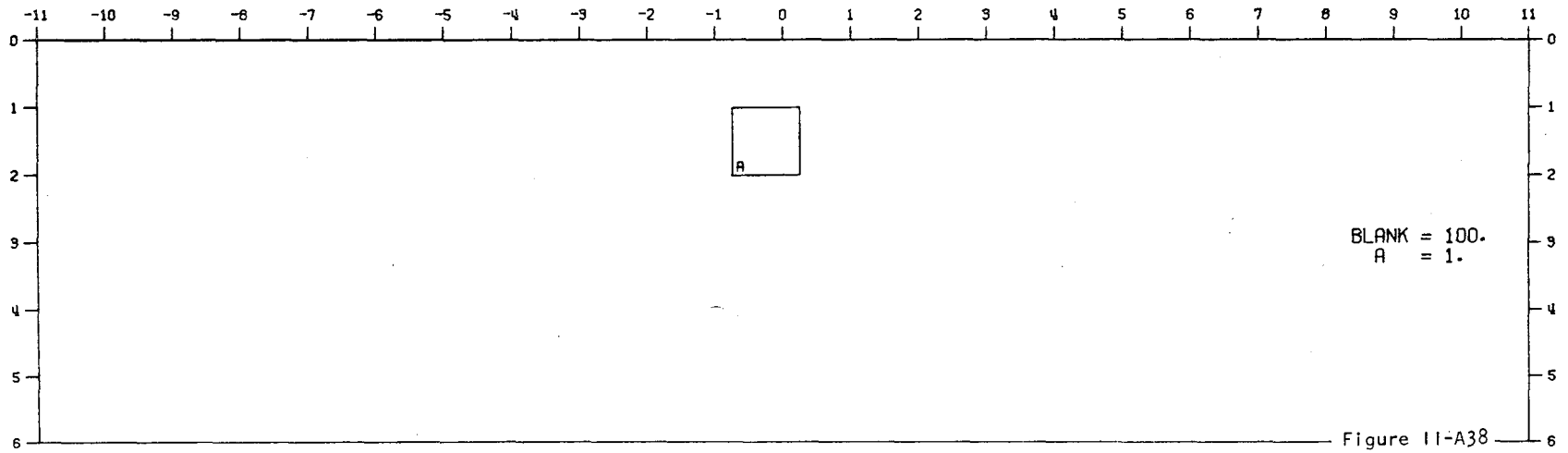

Figure II-A38

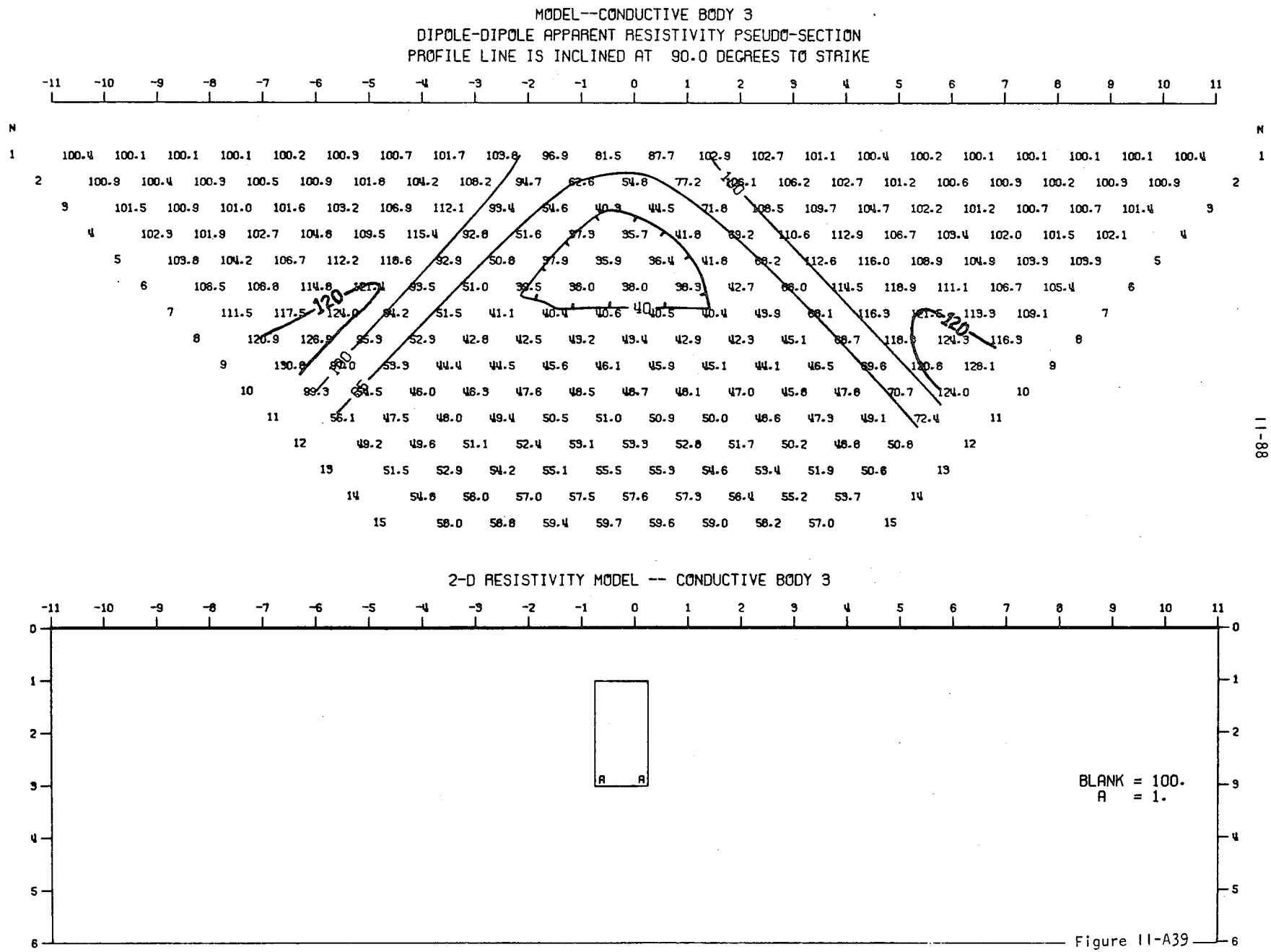

Figure II-A39

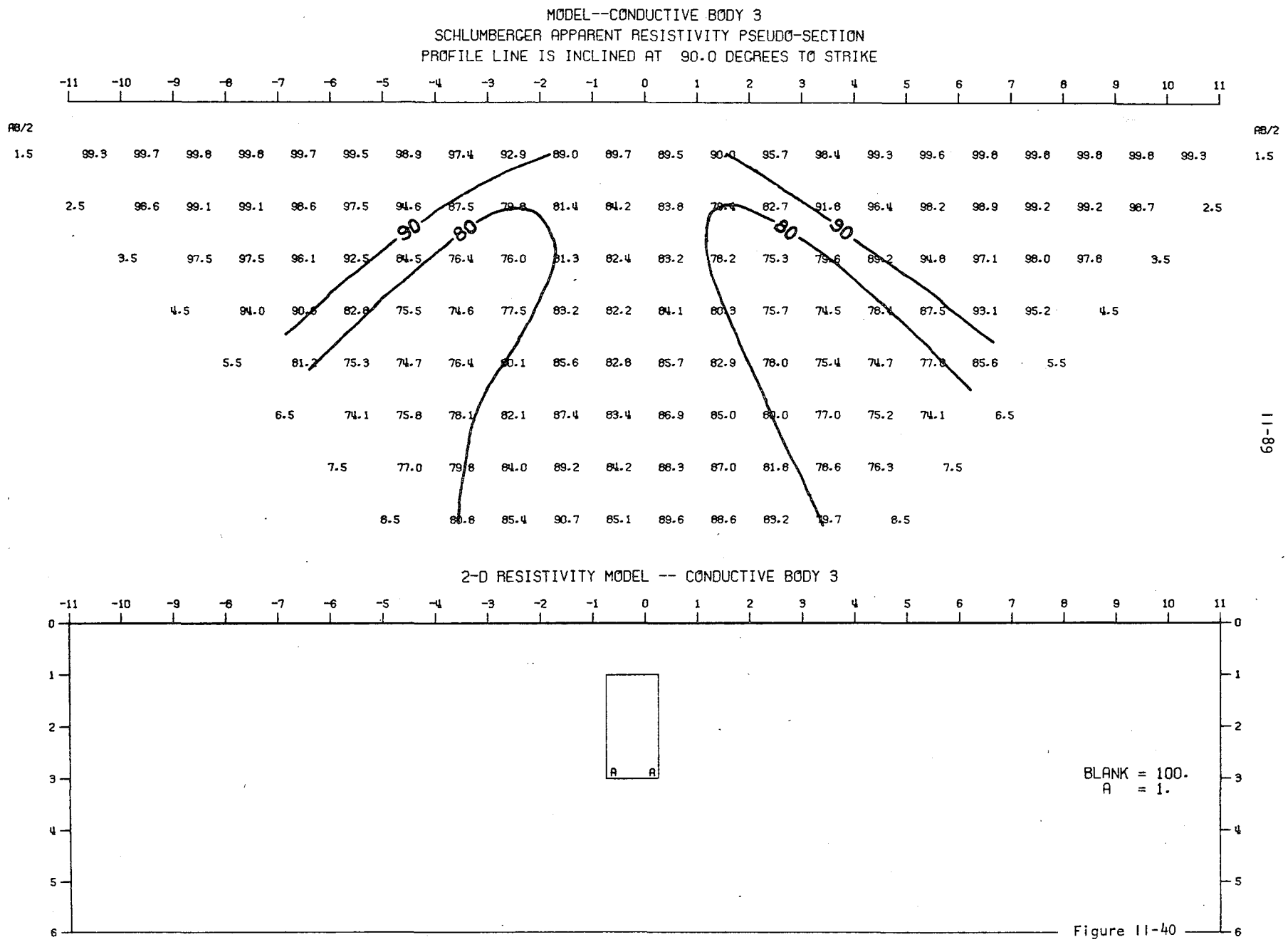
MODEL--CONDUCTIVE BODY 3
SCHLUMBERGER APPARENT RESISTIVITY PSEUDO-SECTION
PROFILE LINE IS INCLINED AT 90.0 DEGREES TO STRIKE
AB/2
90
80
2-D RESISTIVITY MODEL -- CONDUCTIVE BODY 3
A A
BLANK = 100.
A = 1.

Figure II-40

MODEL--CONDUCTIVE BODY 6
DIPOLE-DIPOLE APPARENT RESISTIVITY PSEUDO-SECTION
PROFILE LINE IS INCLINED AT 90.0 DEGREES TO STRIKE

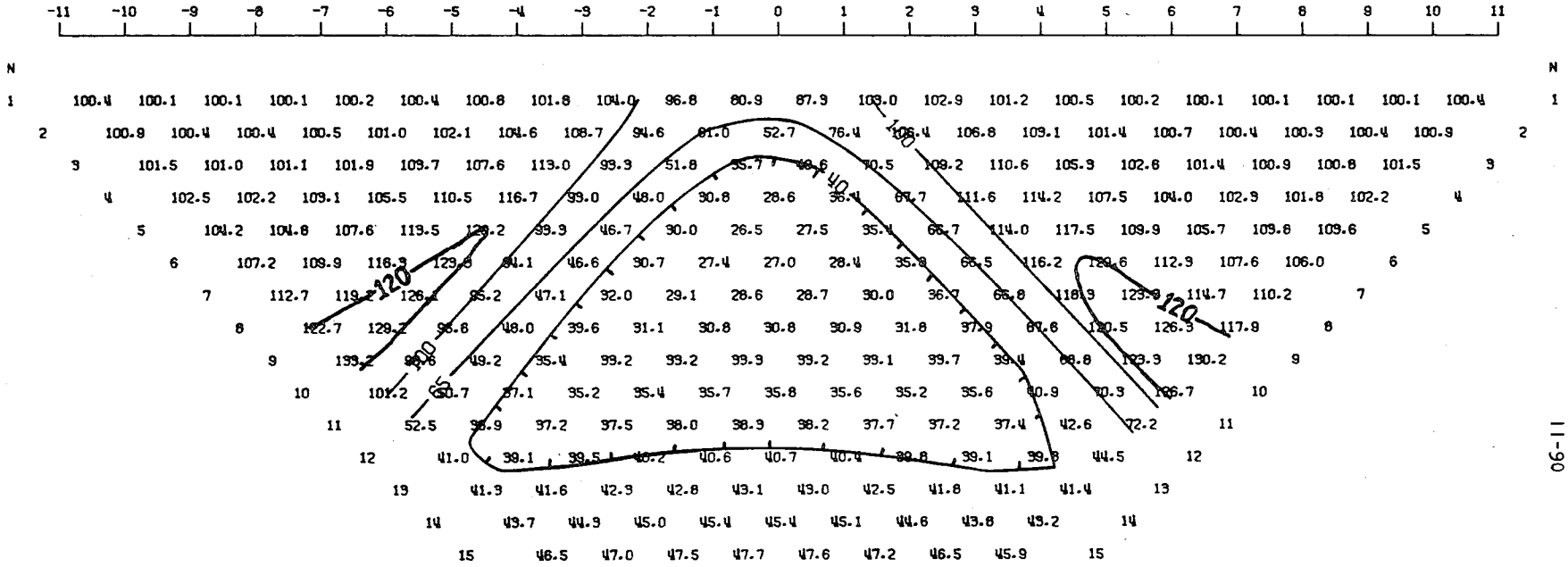

2-D RESISTIVITY MODEL -- CONDUCTIVE BODY 6

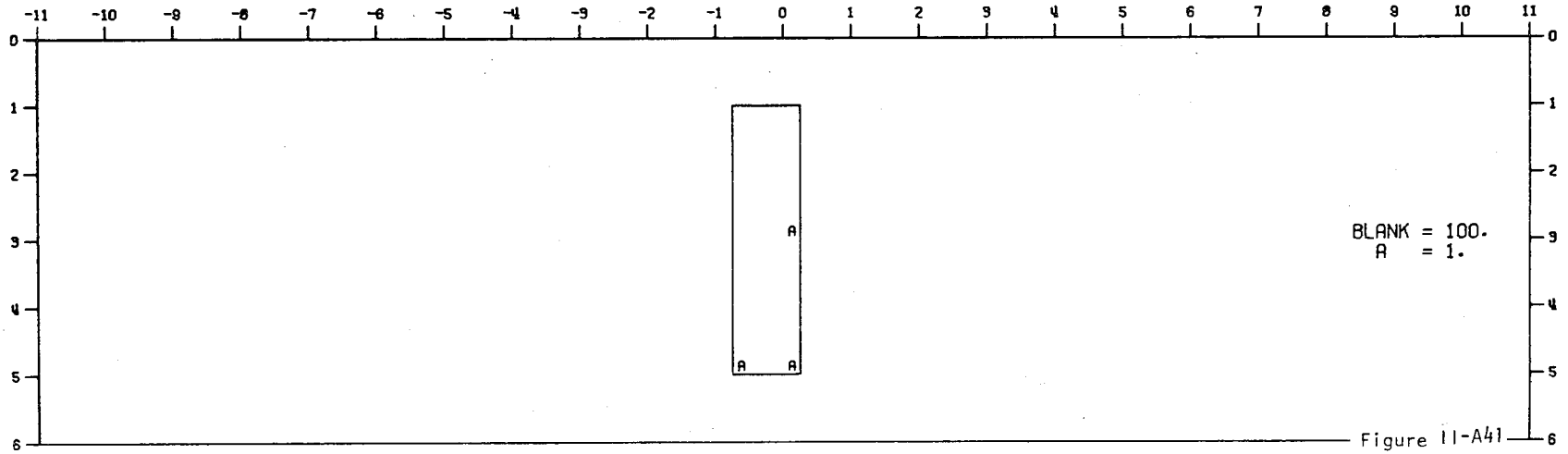

Figure II-A41

MODEL--CONDUCTIVE BODY 6
SCHLUMBERGER APPARENT RESISTIVITY PSEUDO-SECTION
PROFILE LINE IS INCLINED AT 90.0 DEGREES TO STRIKE

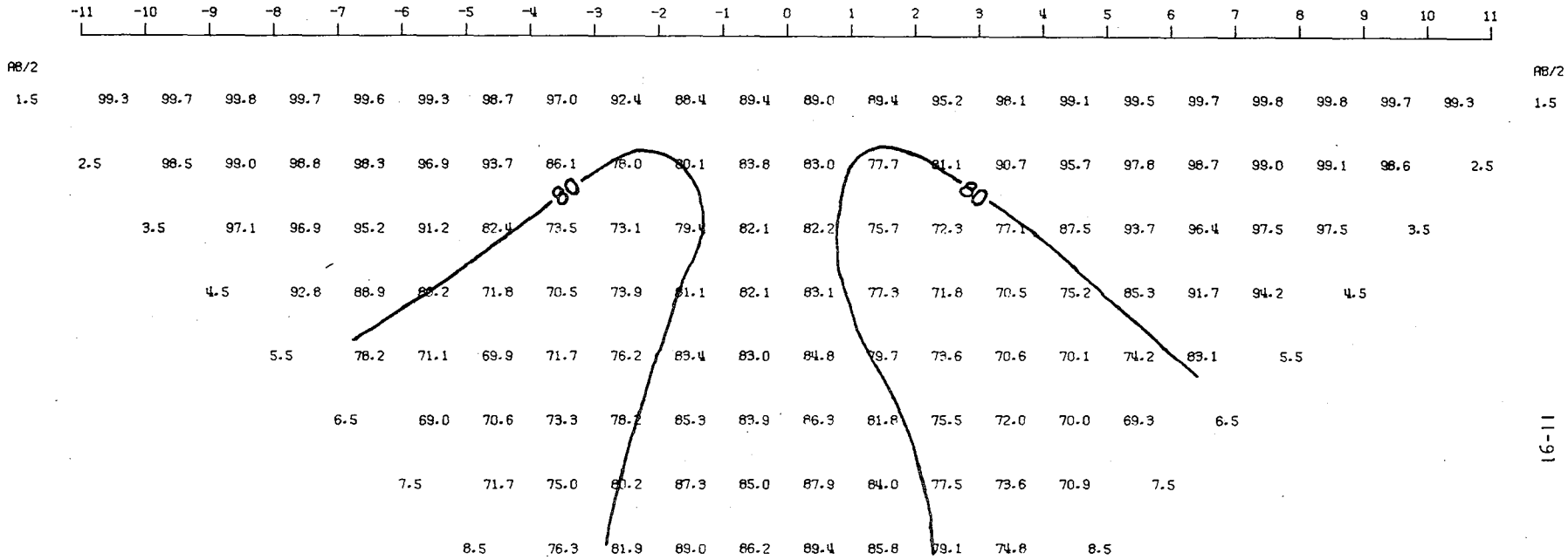

2-D RESISTIVITY MODEL -- CONDUCTIVE BODY 6

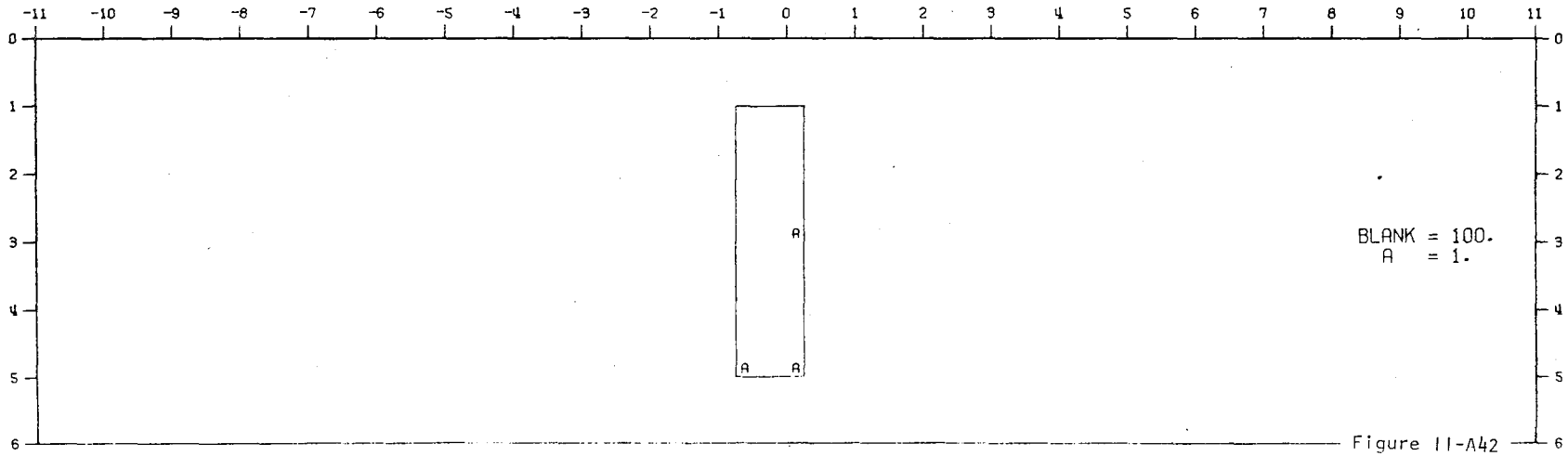

Figure II-A42

MODEL--CONDUCTIVE BODY 7
DIPOLE-DIPOLE APPARENT RESISTIVITY PSEUDO-SECTION
PROFILE LINE IS INCLINED AT 90.0 DEGREES TO STRIKE

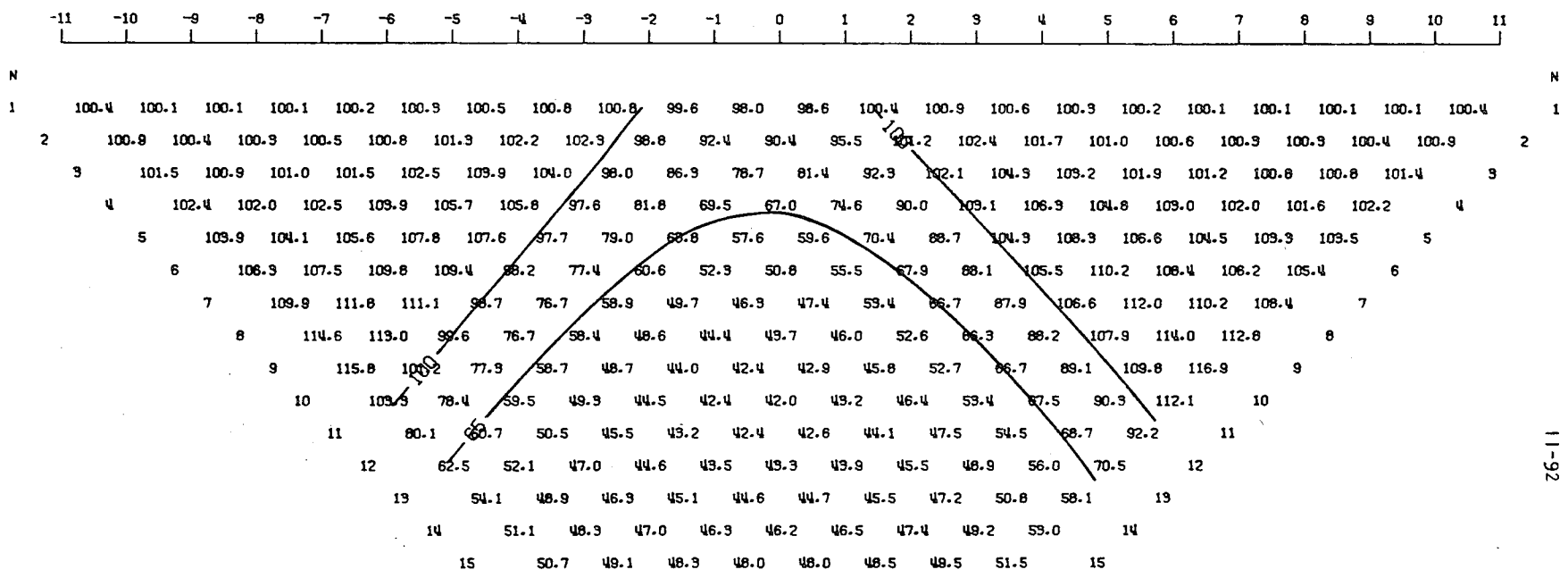

2-D RESISTIVITY MODEL -- CONDUCTIVE BODY 7

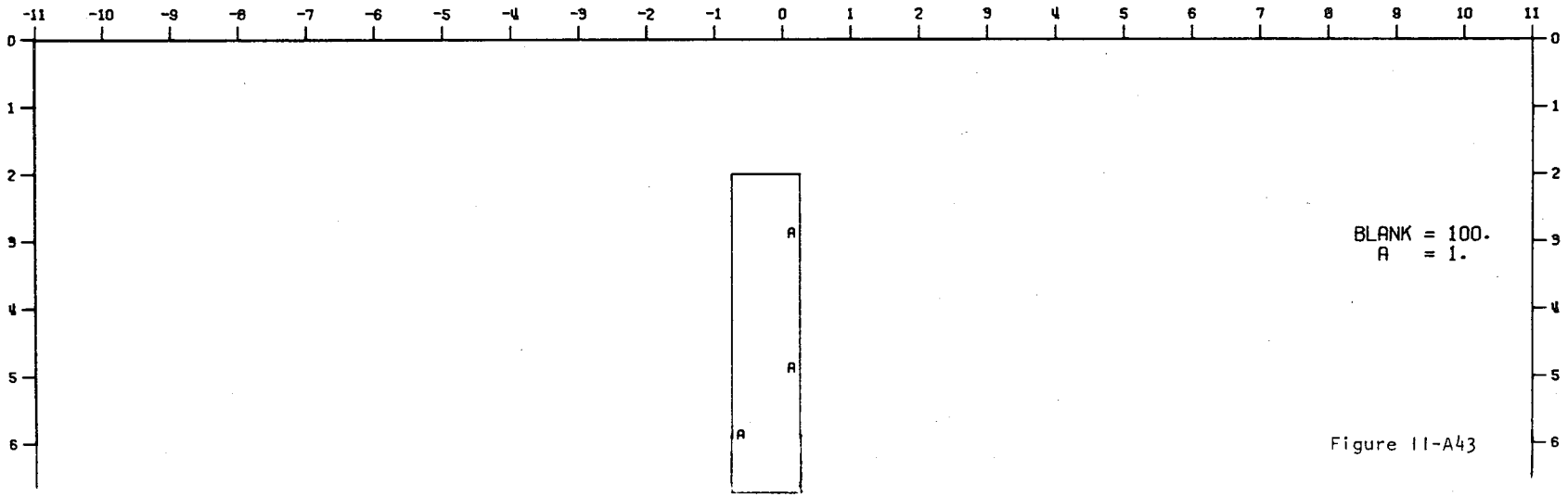

Figure II-A43

MODEL--CONDUCTIVE BODY 7
SCHLUMBERGER APPARENT RESISTIVITY PSEUDO-SECTION
PROFILE LINE IS INCLINED AT 90.0 DEGREES TO STRIKE

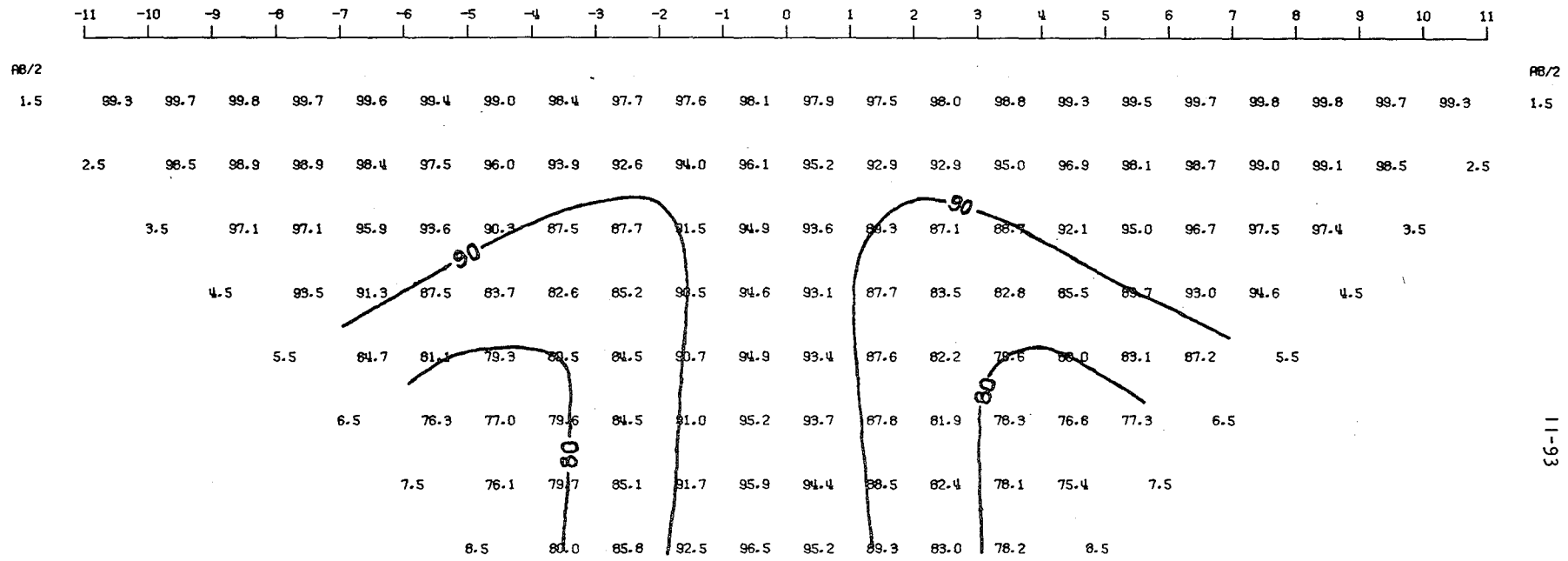

2-D RESISTIVITY MODEL -- CONDUCTIVE BODY 7

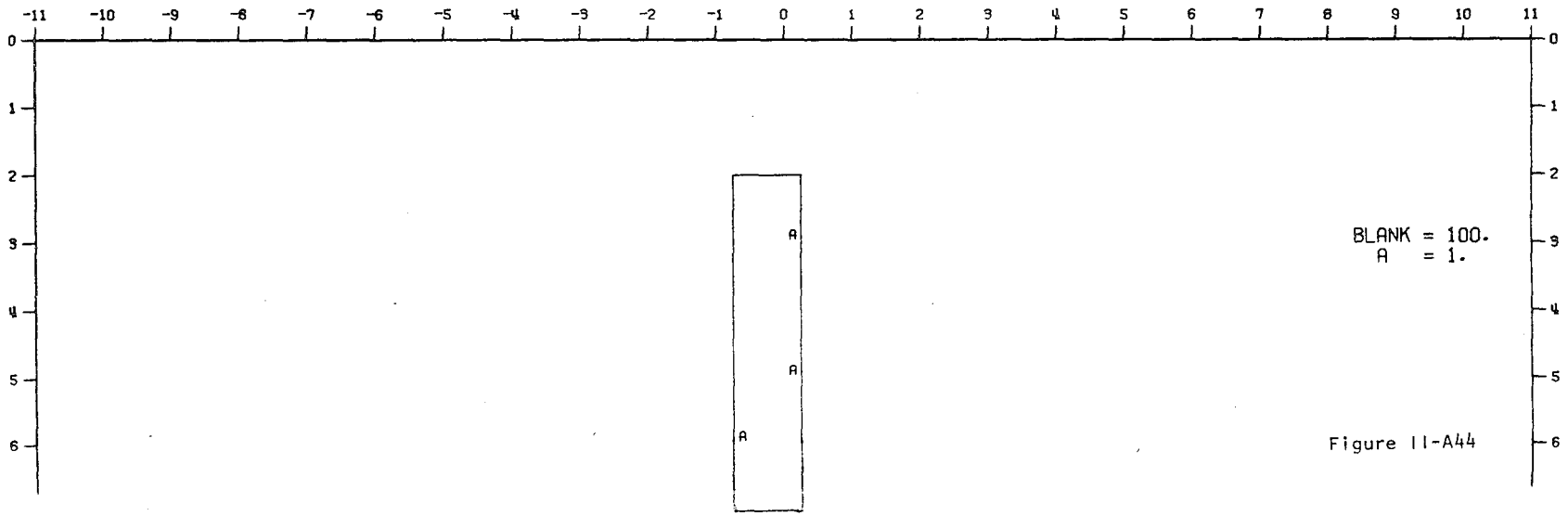

Figure II-A44

MODEL--CONDUCTIVE BODY 5
DIPOLE-DIPOLE APPARENT RESISTIVITY PSEUDO-SECTION
PROFILE LINE IS INCLINED AT 90.0 DEGREES TO STRIKE

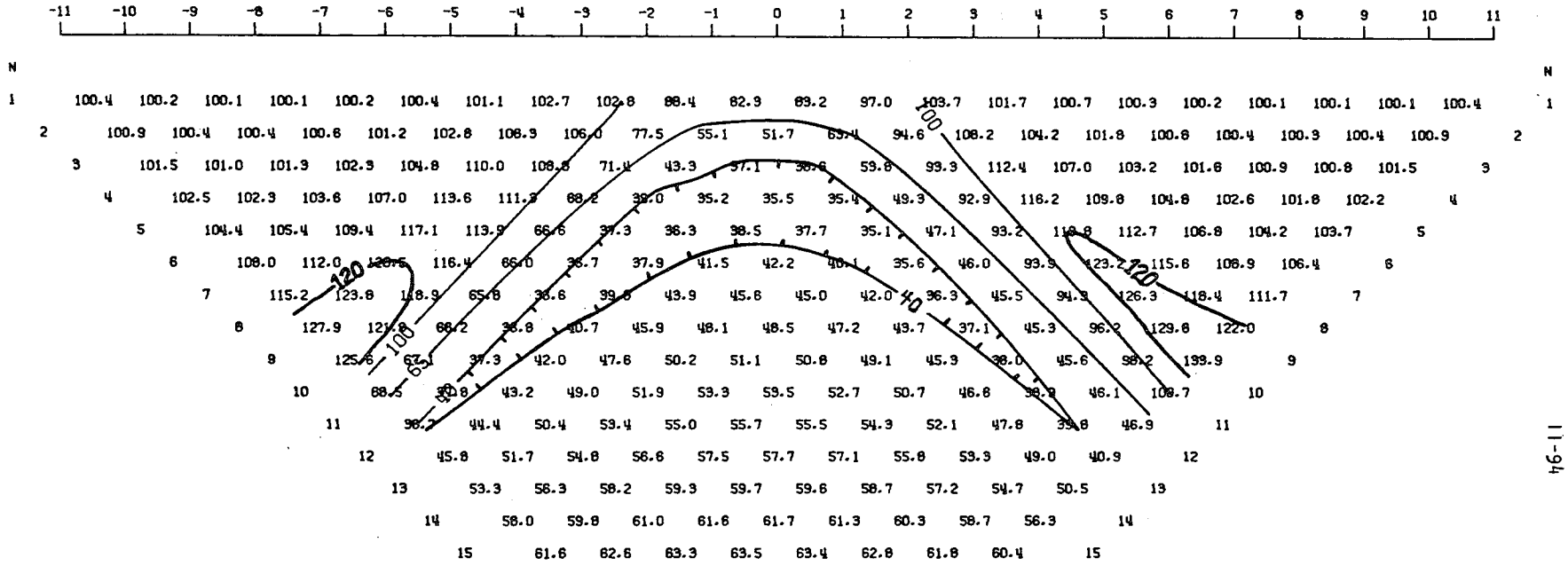

2-D RESISTIVITY MODEL -- CONDUCTIVE BODY 5

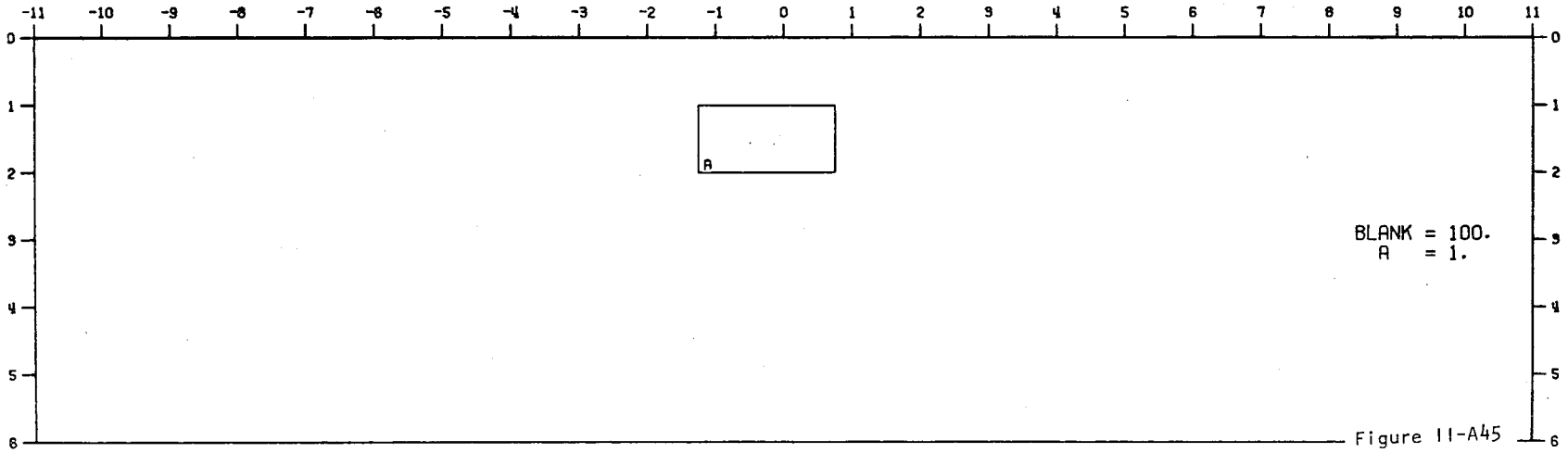

Figure II-A45

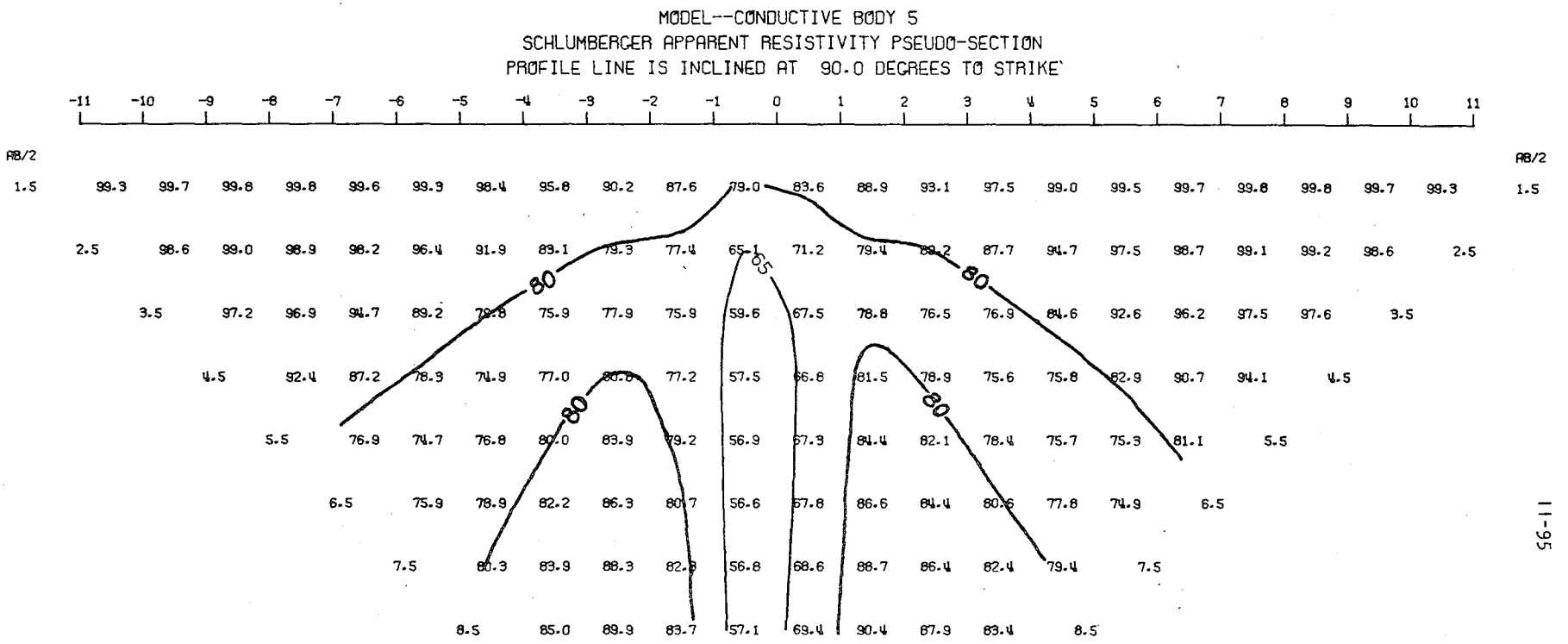

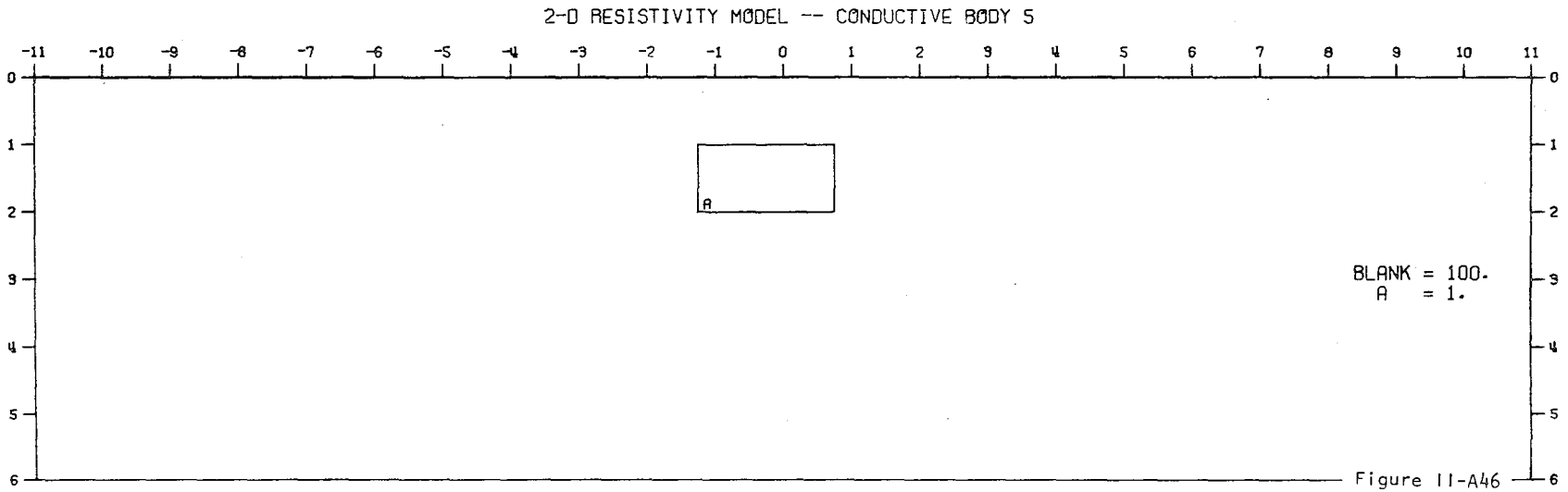

Figure II-A46

MODEL--CONDUCTIVE BODY 11
DIPOLE-DIPOLE APPARENT RESISTIVITY PSEUDO-SECTION
PROFILE LINE IS INCLINED AT 90.0 DEGREES TO STRIKE

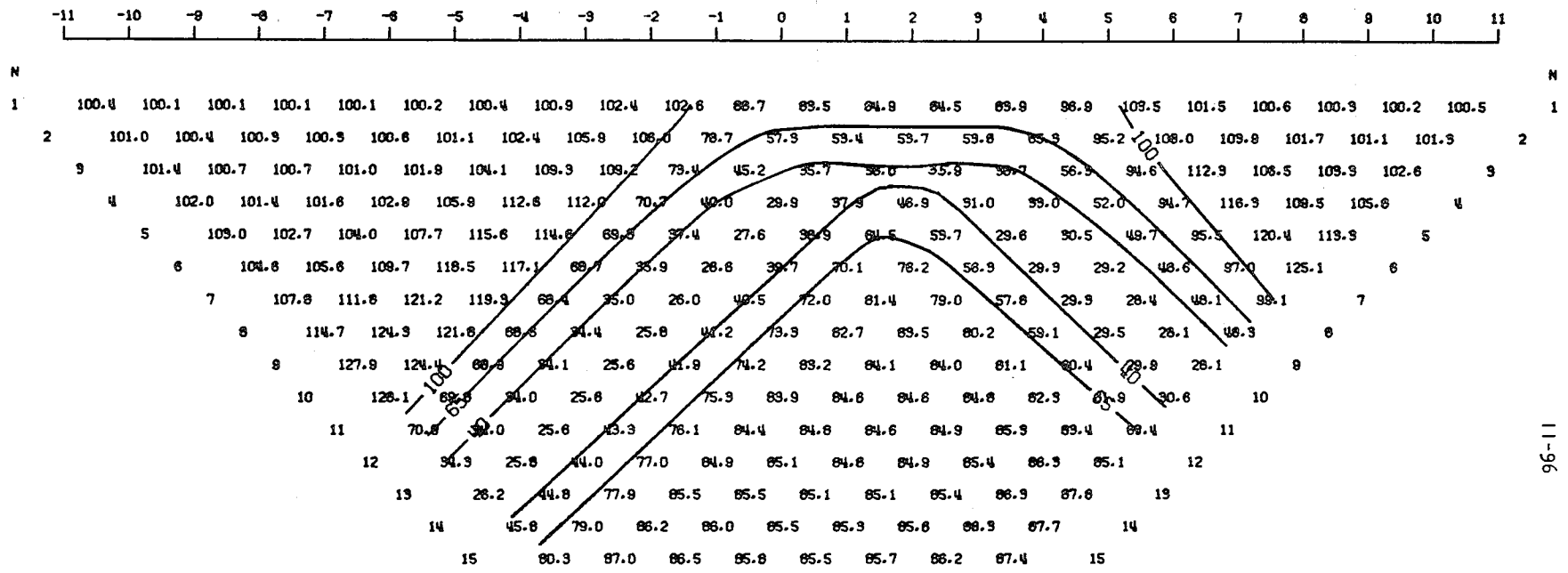

11-96

2-D RESISTIVITY MODEL -- CONDUCTIVE BODY 11

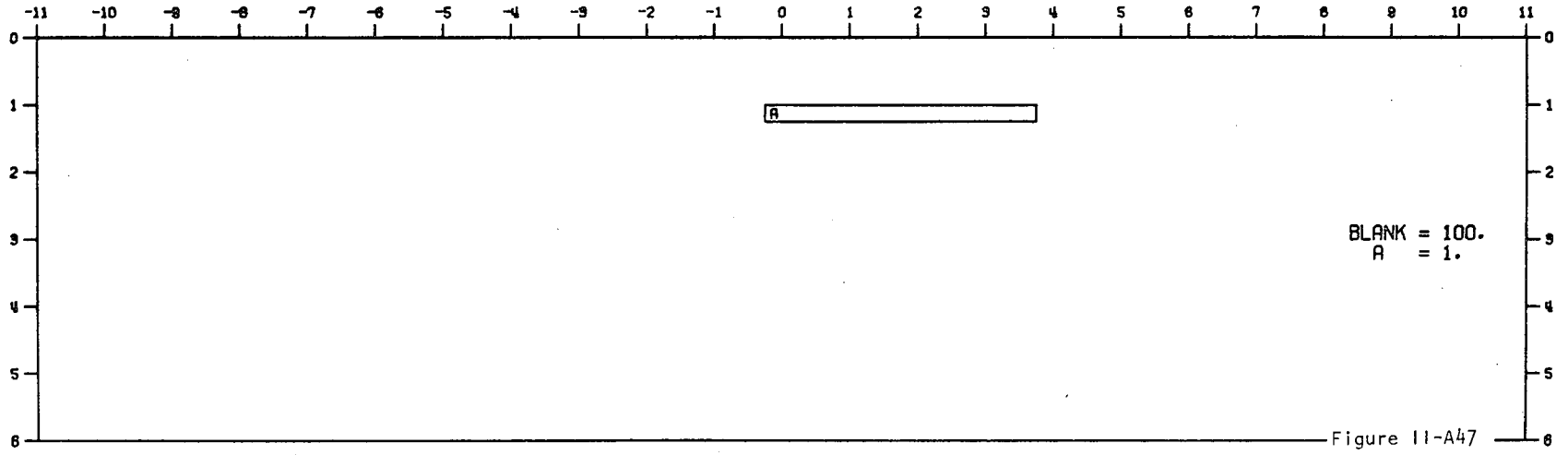

Figure II-A47

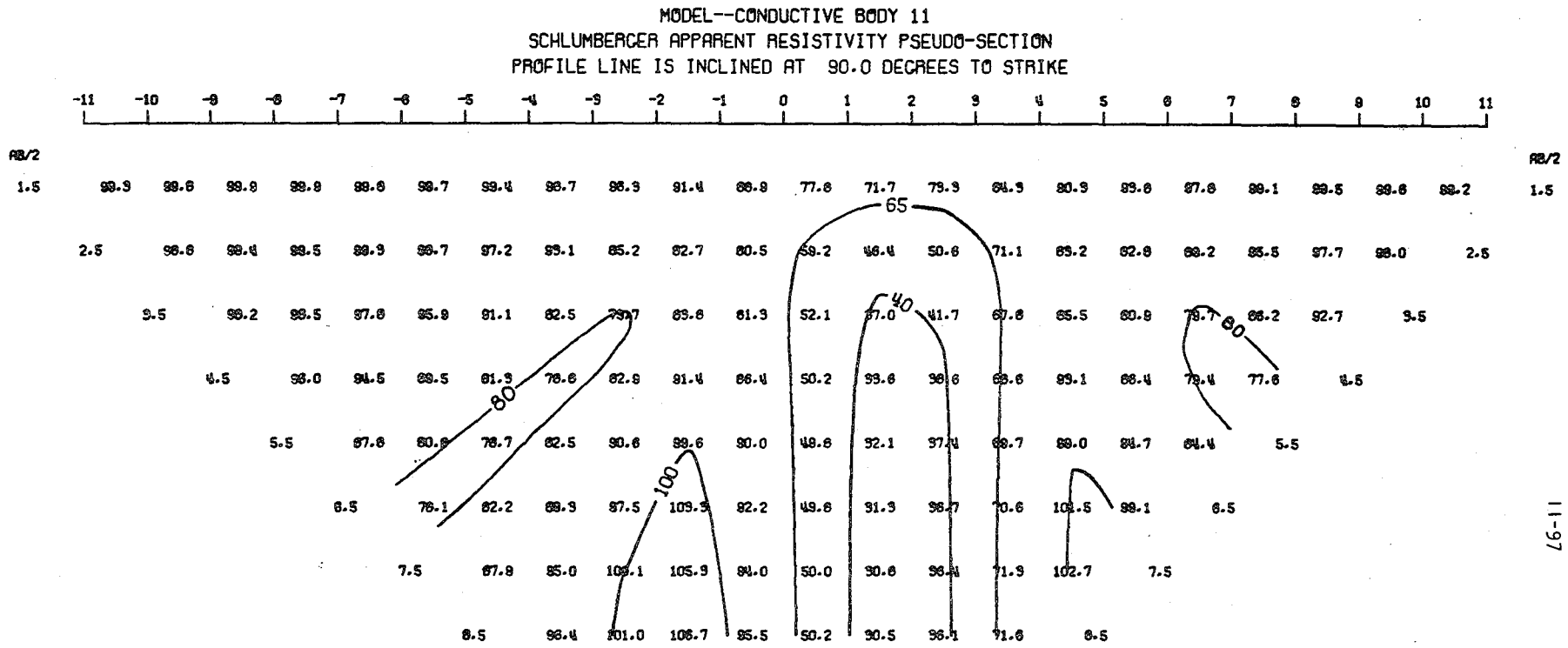

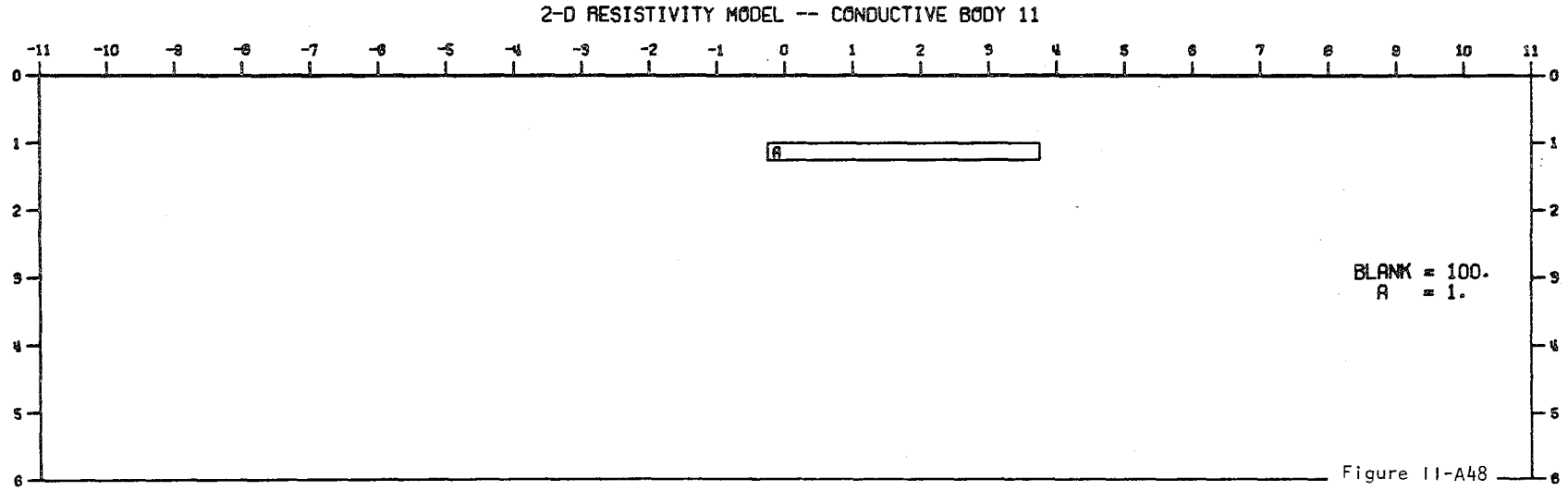

Figure II-A48

MODEL--CONDUCTIVE BODY 4
DIPOLE-DIPOLE APPARENT RESISTIVITY PSEUDO-SECTION
PROFILE LINE IS INCLINED AT 90.0 DEGREES TO STRIKE

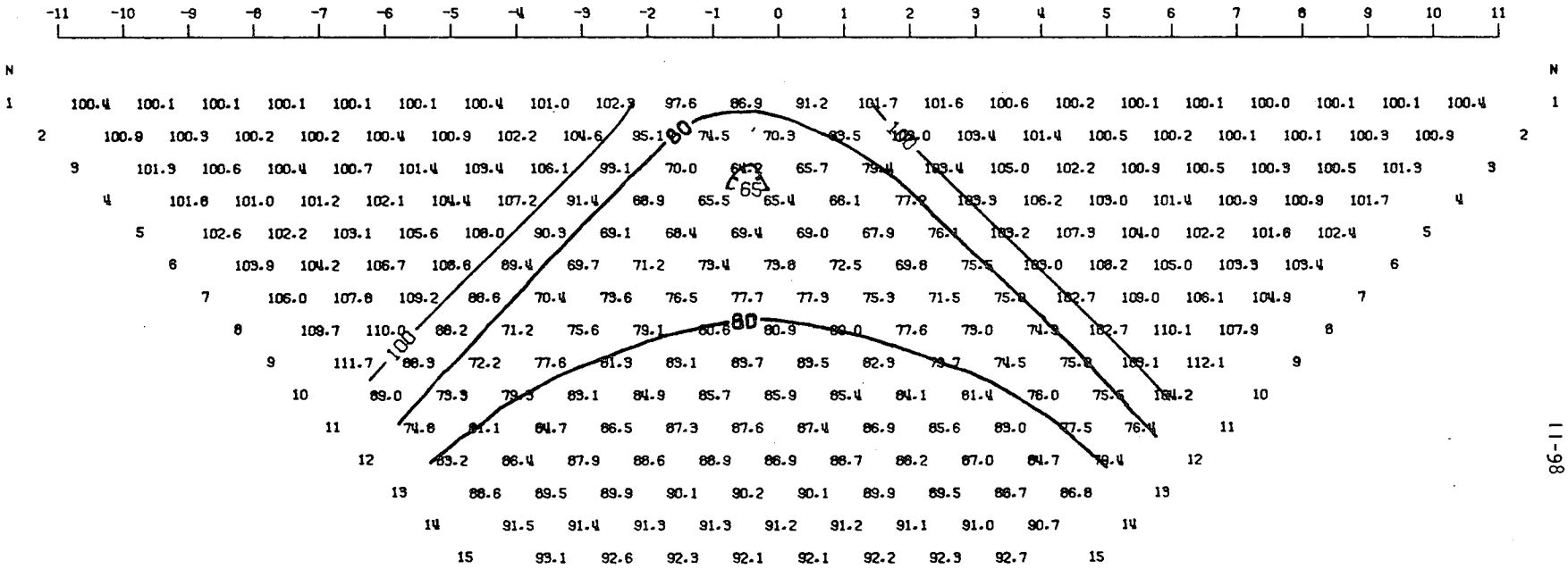

11-98

2-D RESISTIVITY MODEL -- CONDUCTIVE BODY 4

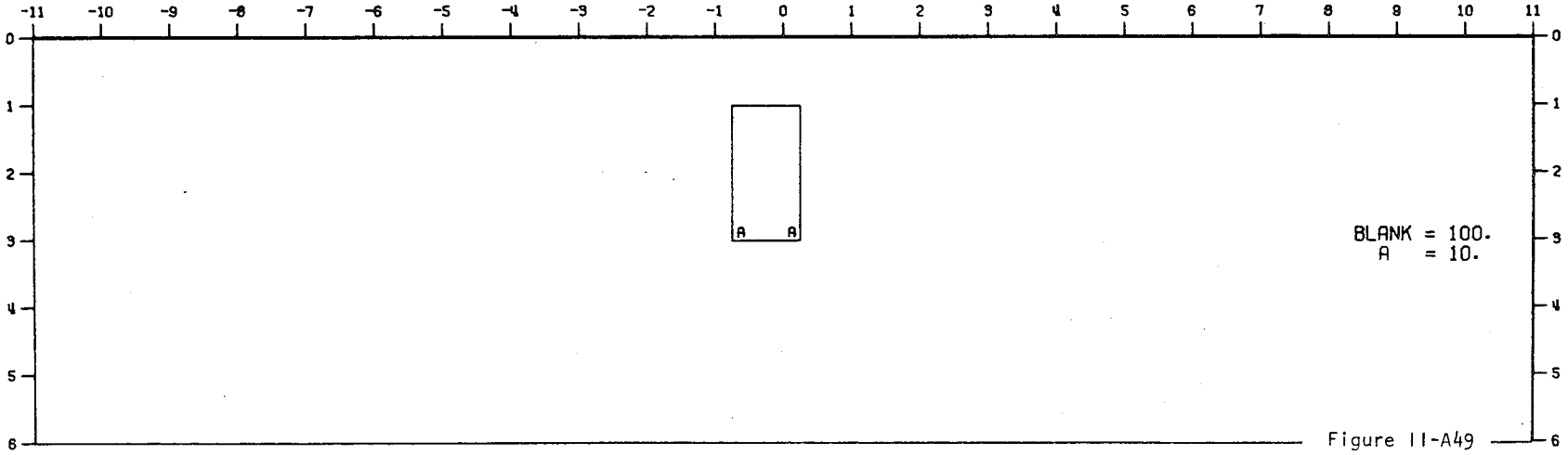

Figure II-A49

MODEL--CONDUCTIVE BODY 4
SCHLUMBERGER APPARENT RESISTIVITY PSEUDO-SECTION
PROFILE LINE IS INCLINED AT 90.0 DEGREES TO STRIKE

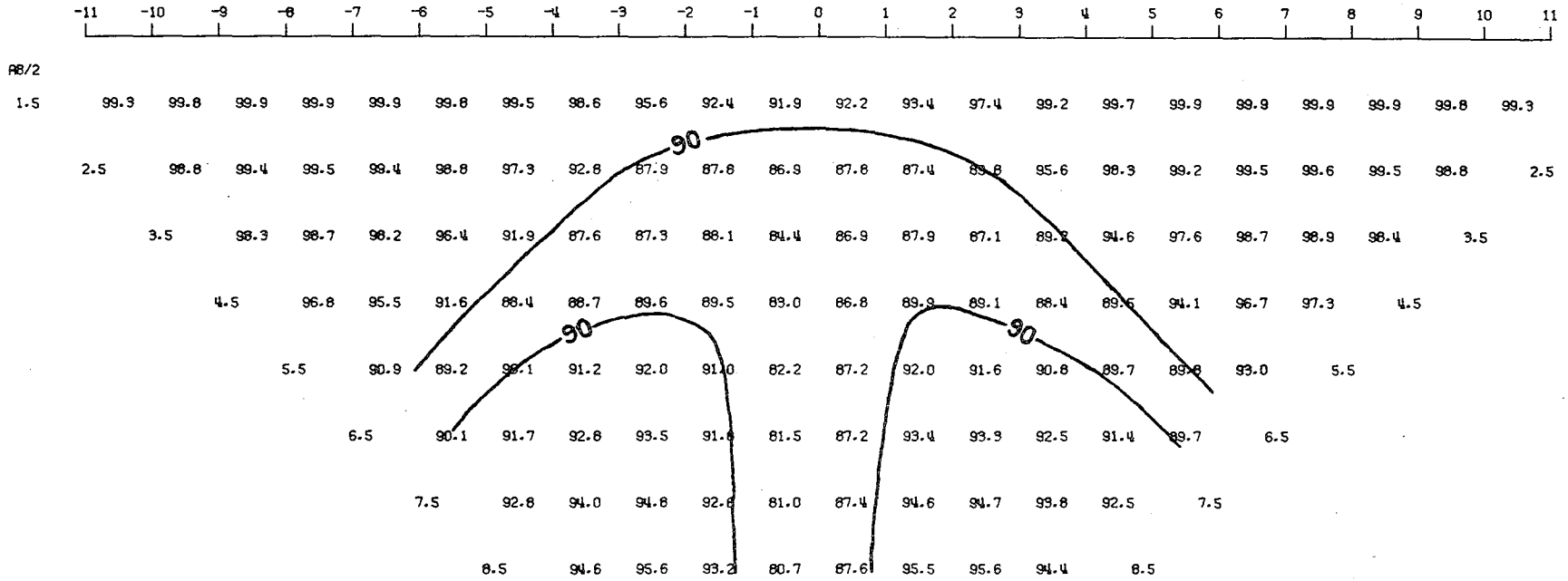

2-D RESISTIVITY MODEL -- CONDUCTIVE BODY 4

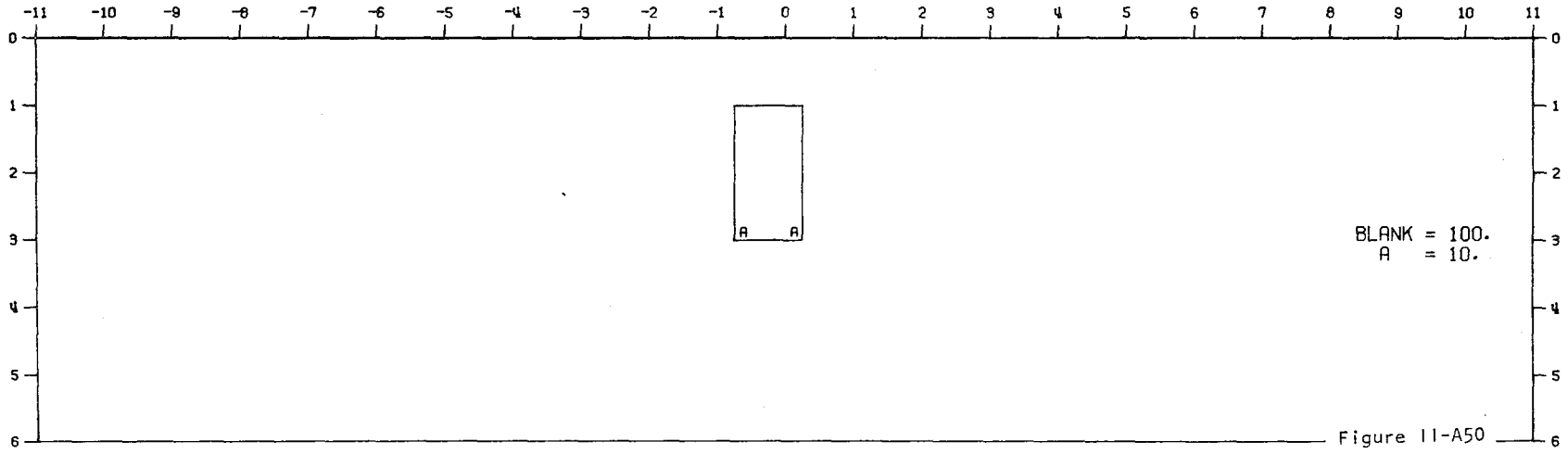

Figure 11-A50

MODEL--CONDUCTIVE BODY 11
DIPOLE-DIPOLE APPARENT RESISTIVITY PSEUDO-SECTION
PROFILE LINE IS INCLINED AT 90.0 DEGREES TO STRIKE

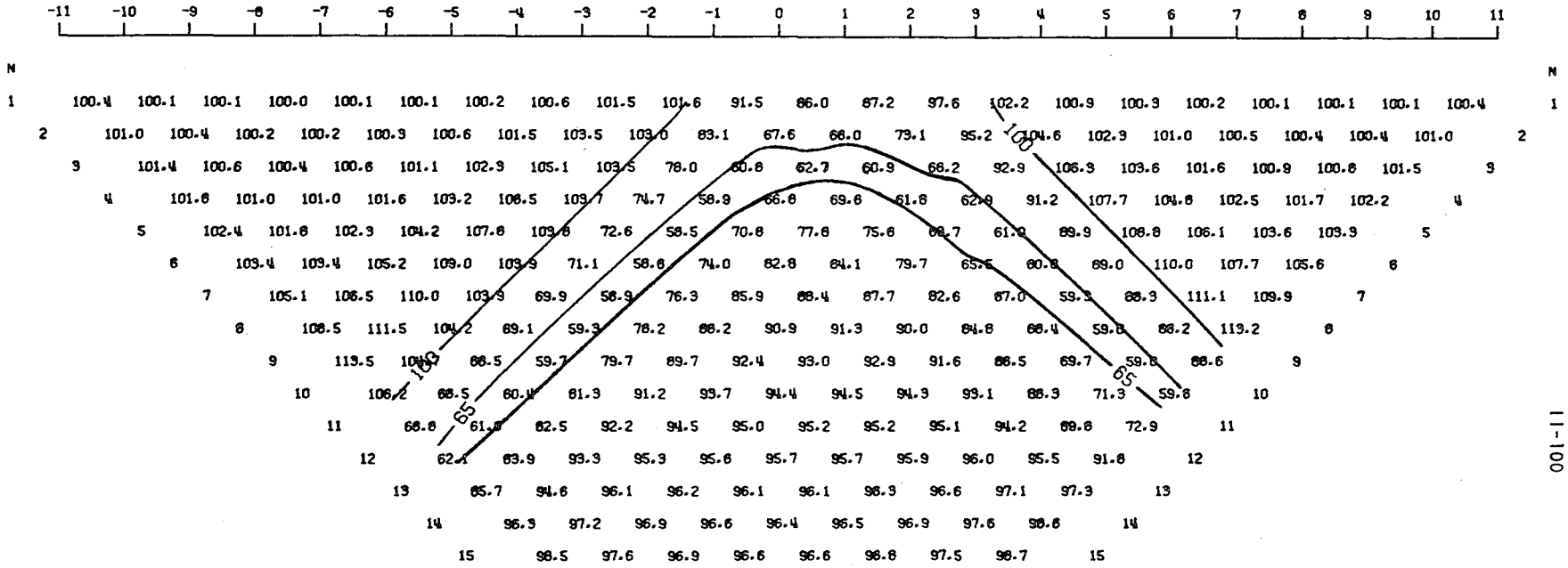

2-D RESISTIVITY MODEL -- CONDUCTIVE BODY 11

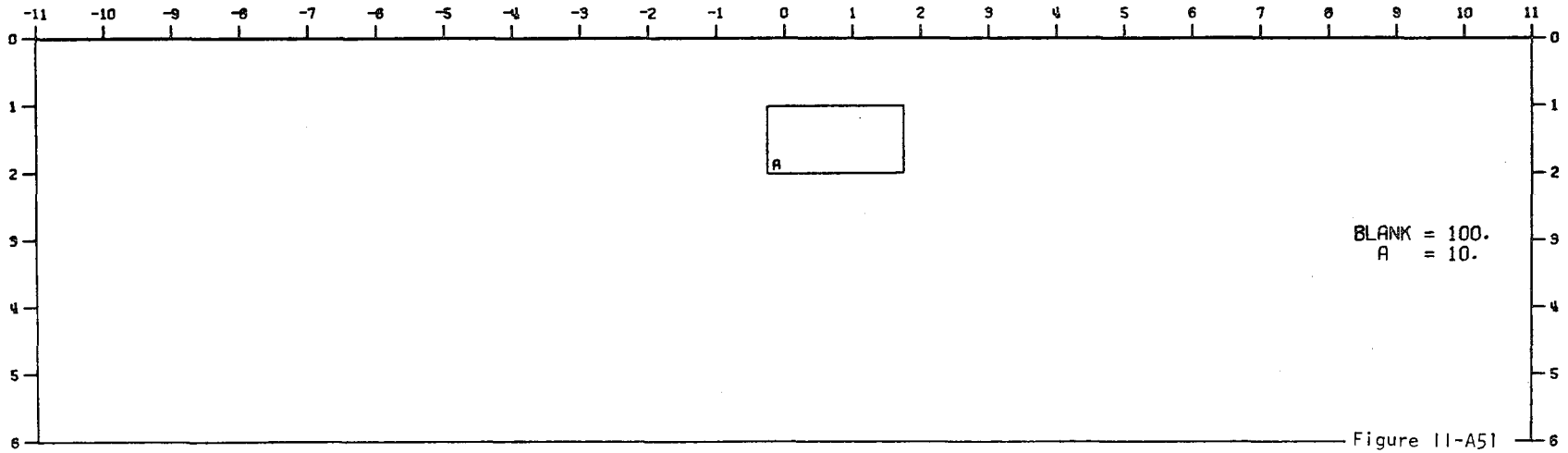

Figure II-A51

MODEL--CONDUCTIVE BODY 11
SCHLUMBERGER APPARENT RESISTIVITY PSEUDO-SECTION
PROFILE LINE IS INCLINED AT 90.0 DEGREES TO STRIKE

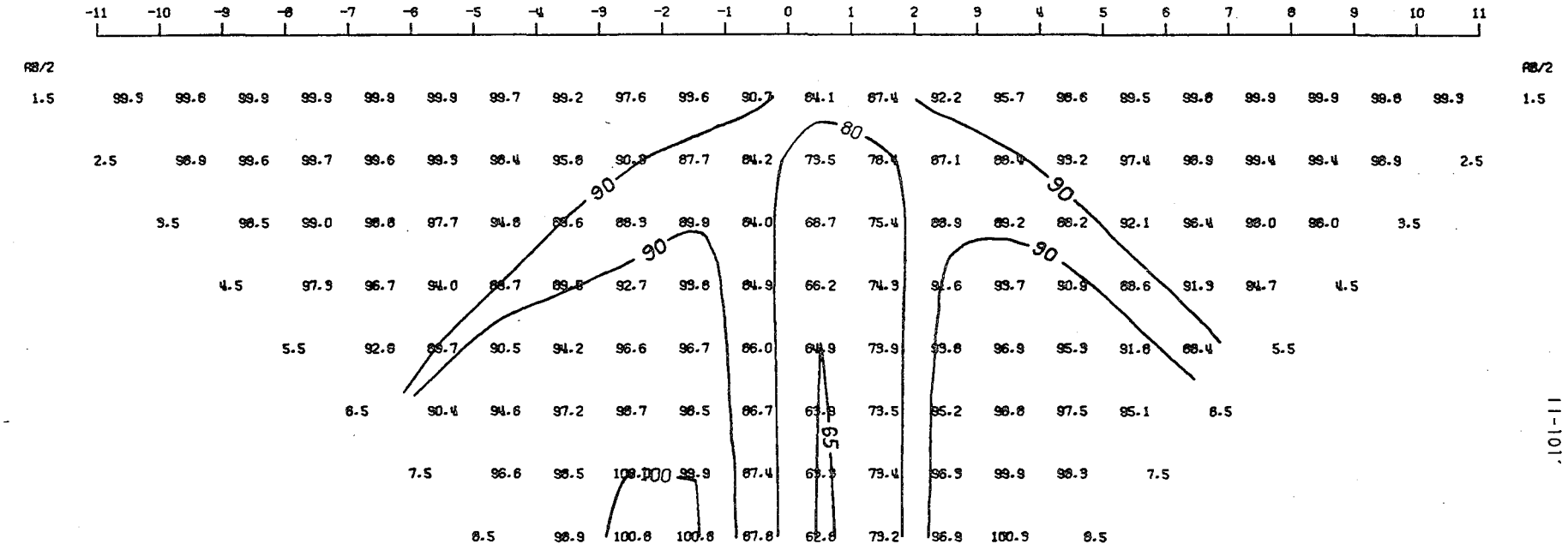

2-D RESISTIVITY MODEL -- CONDUCTIVE BODY 11

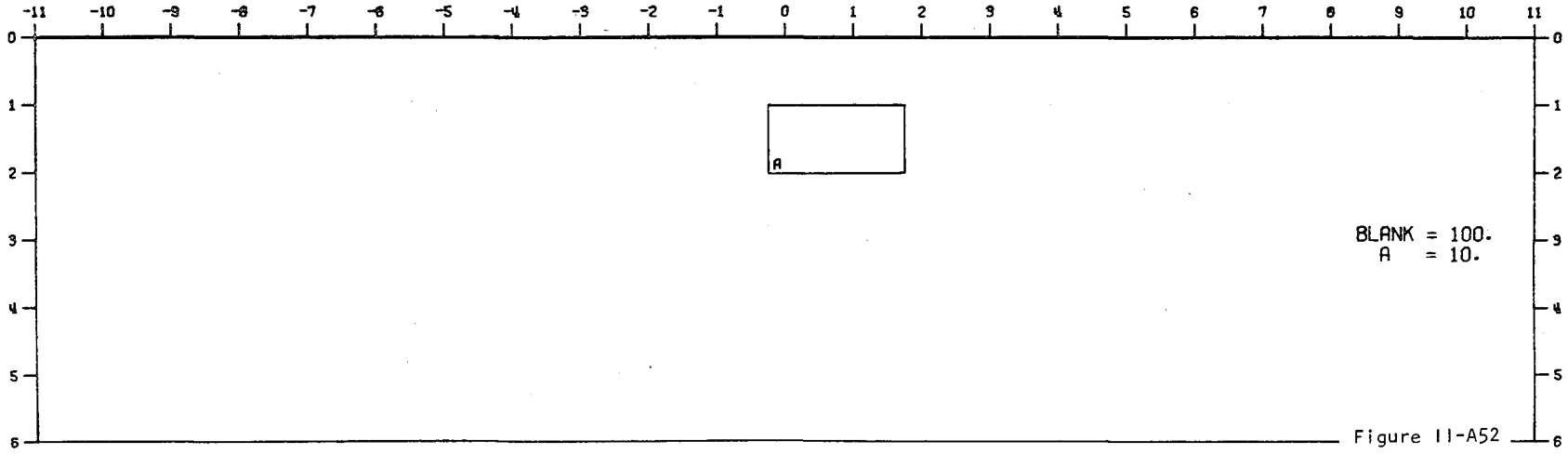

Figure 11-A52

MODEL--CONDUCTIVE BODY 12
DIPOLE-DIPOLE APPARENT RESISTIVITY PSEUDO-SECTION
PROFILE LINE IS INCLINED AT 90.0 DEGREES TO STRIKE

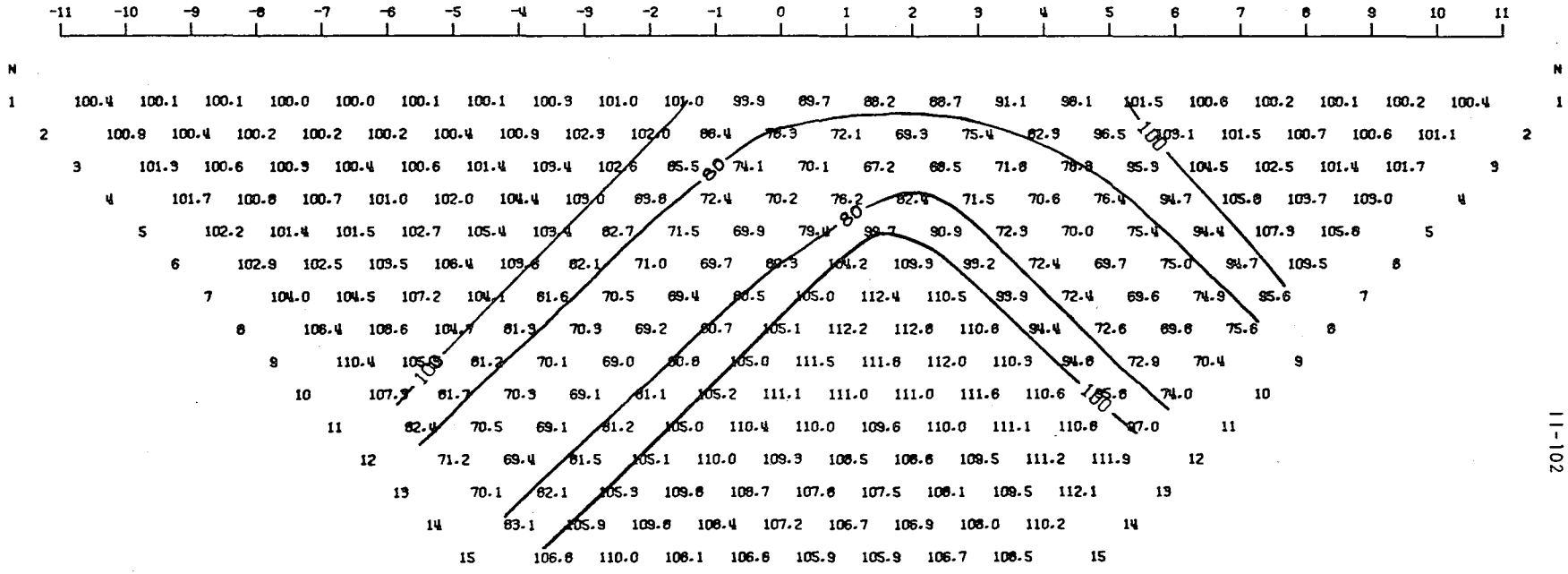

2-D RESISTIVITY MODEL -- CONDUCTIVE BODY 12

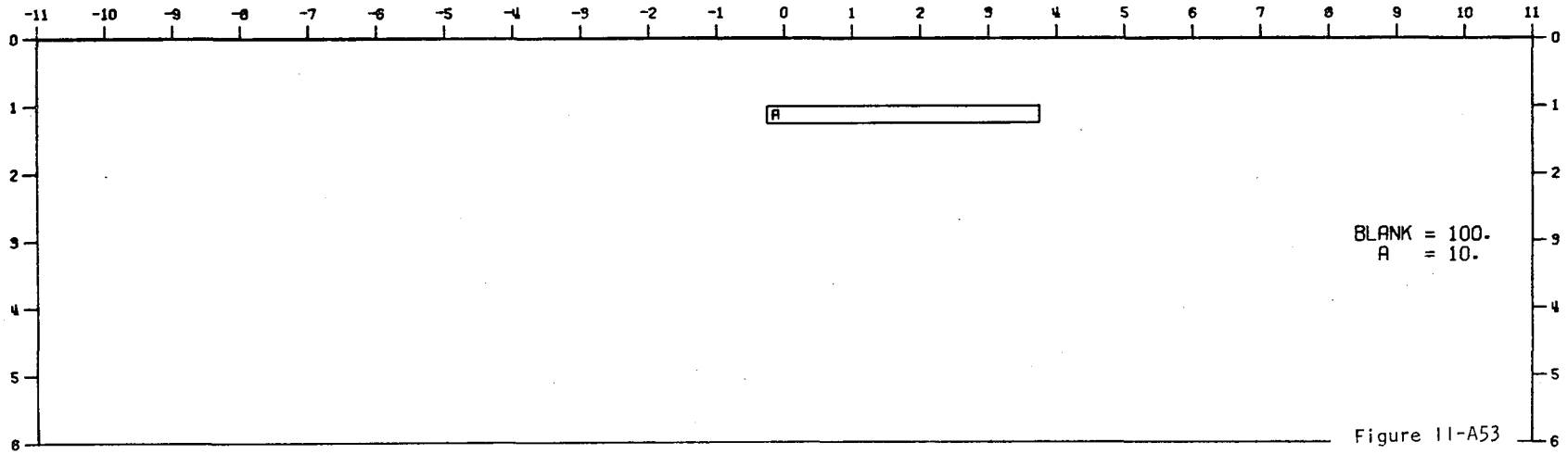

Figure II-A53

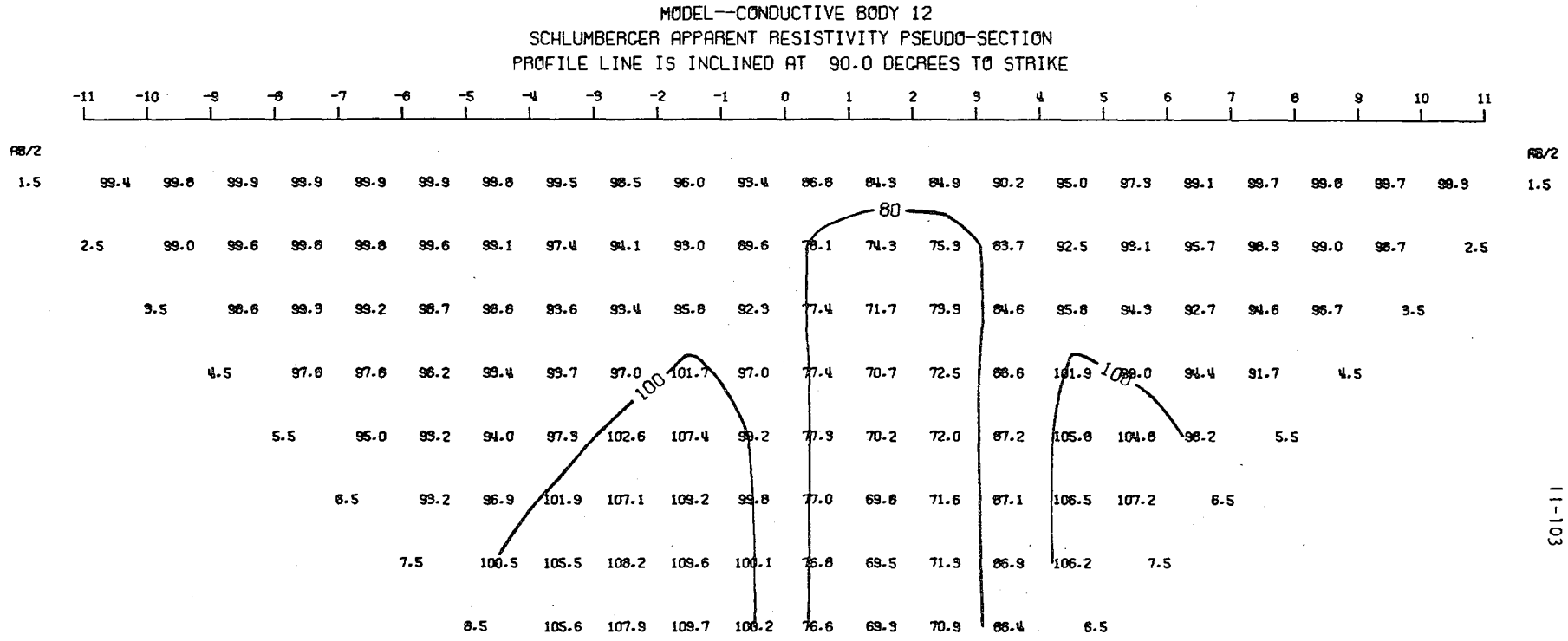

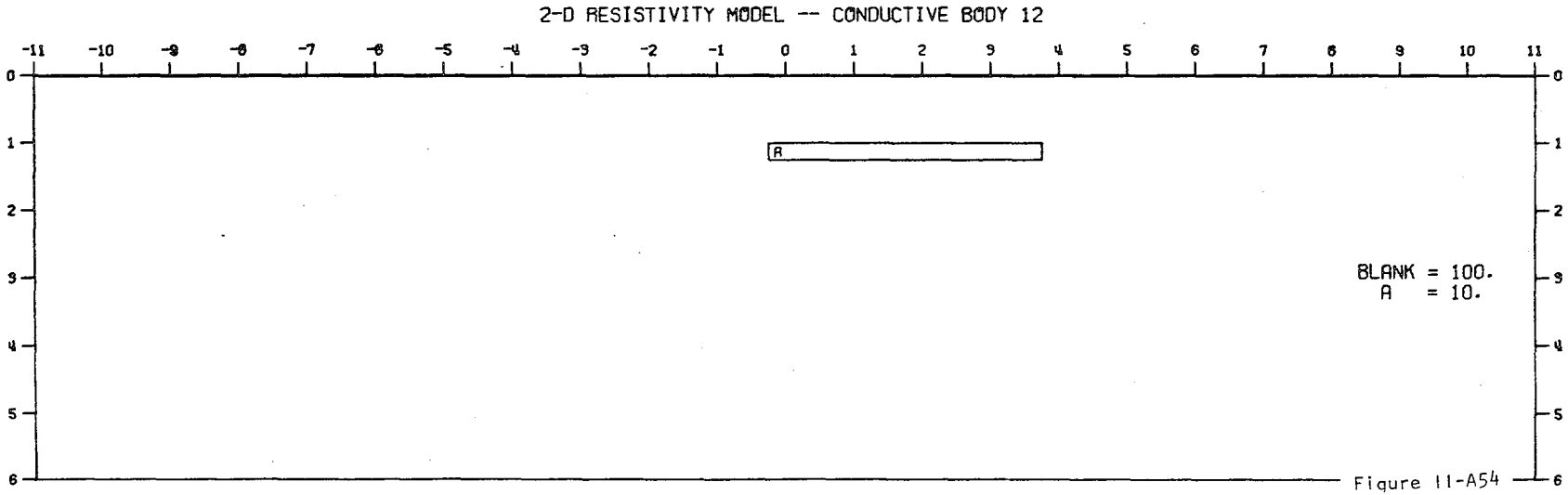

Figure 11-A54

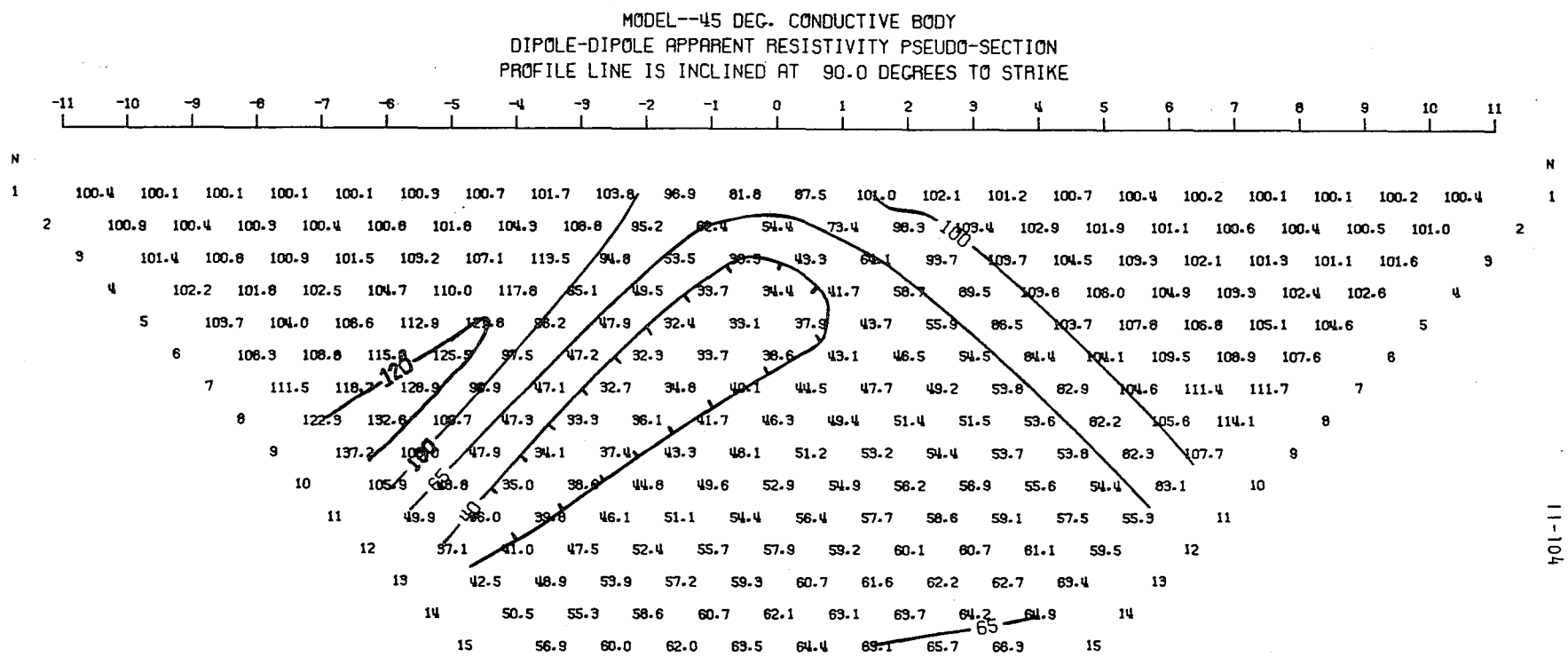

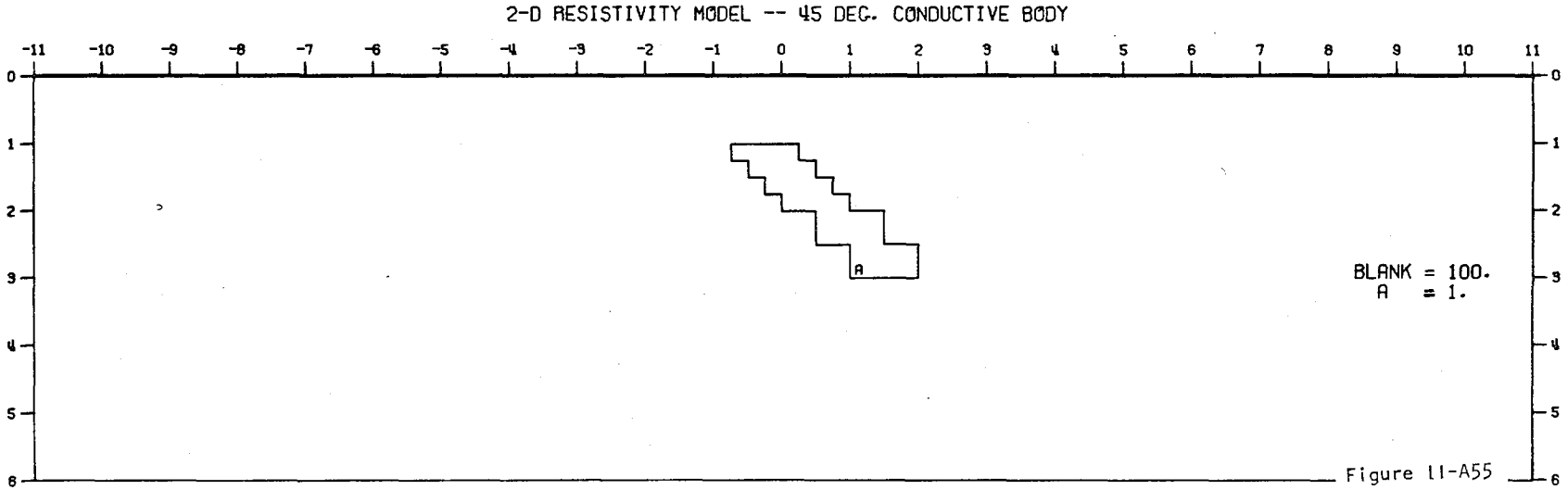

Figure 11-A55

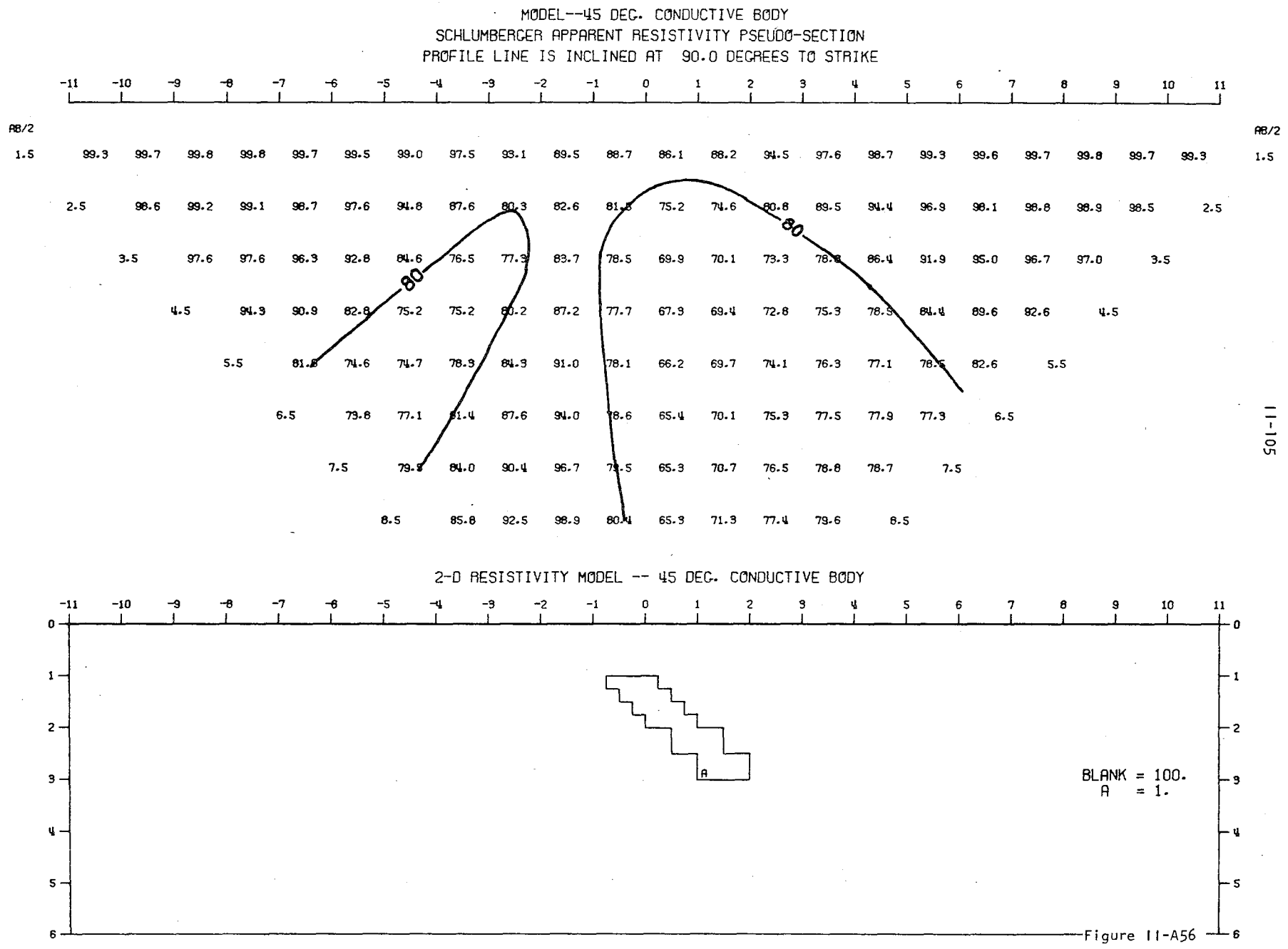

Figure II-A56

MODEL--27 DEG. CONDUCTIVE BODY
DIPOLE-DIPOLE APPARENT RESISTIVITY PSEUDO-SECTION
PROFILE LINE IS INCLINED AT 90.0 DEGREES TO STRIKE

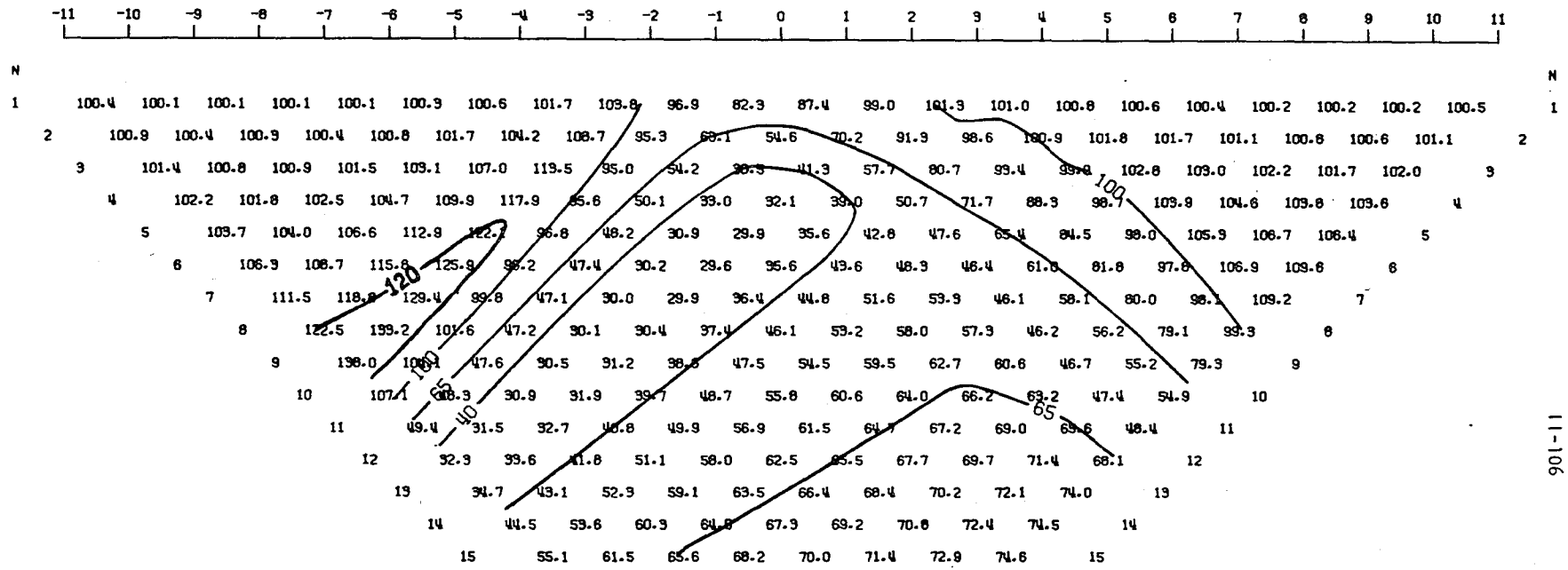

2-D RESISTIVITY MODEL -- 27 DEG. CONDUCTIVE BODY

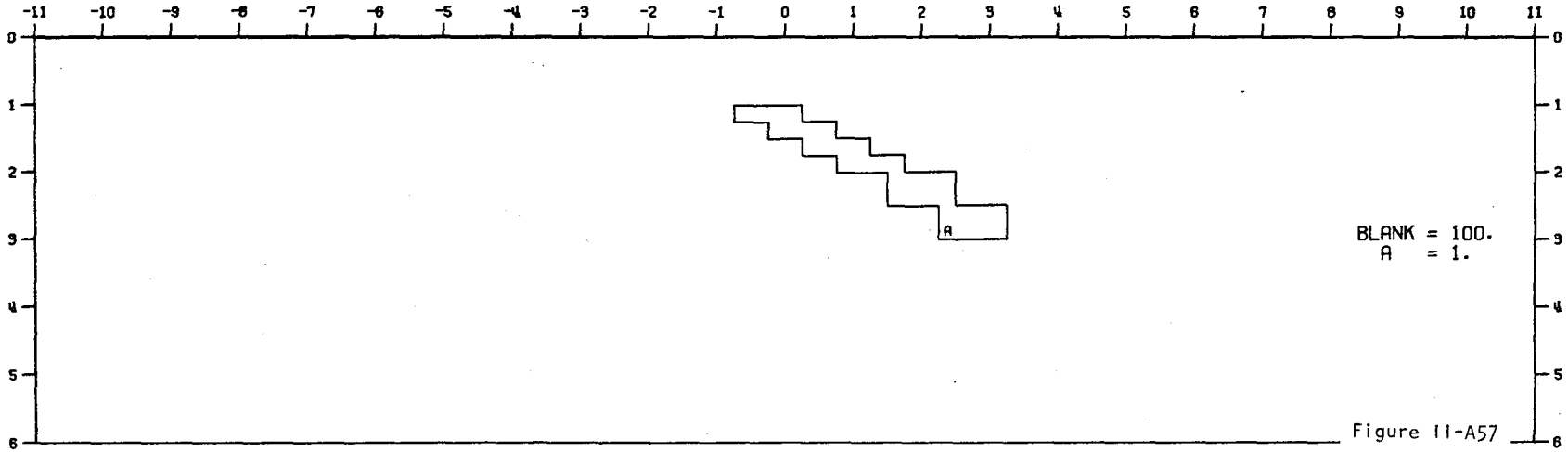

Figure II-A57

MODEL--27 DEC. CONDUCTIVE BODY
SCHLUMBERGER APPARENT RESISTIVITY PSEUDO-SECTION
PROFILE LINE IS INCLINED AT 90.0 DEGREES TO STRIKE

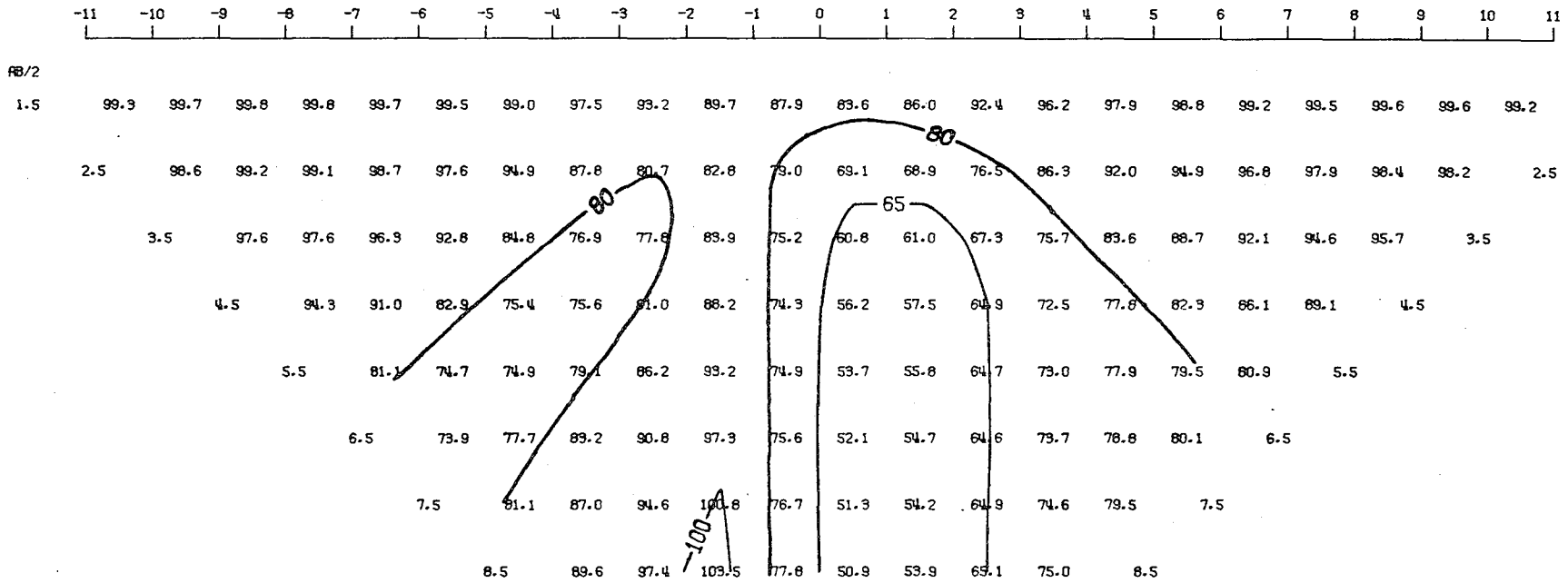

2-D RESISTIVITY MODEL -- 27 DEG. CONDUCTIVE BODY

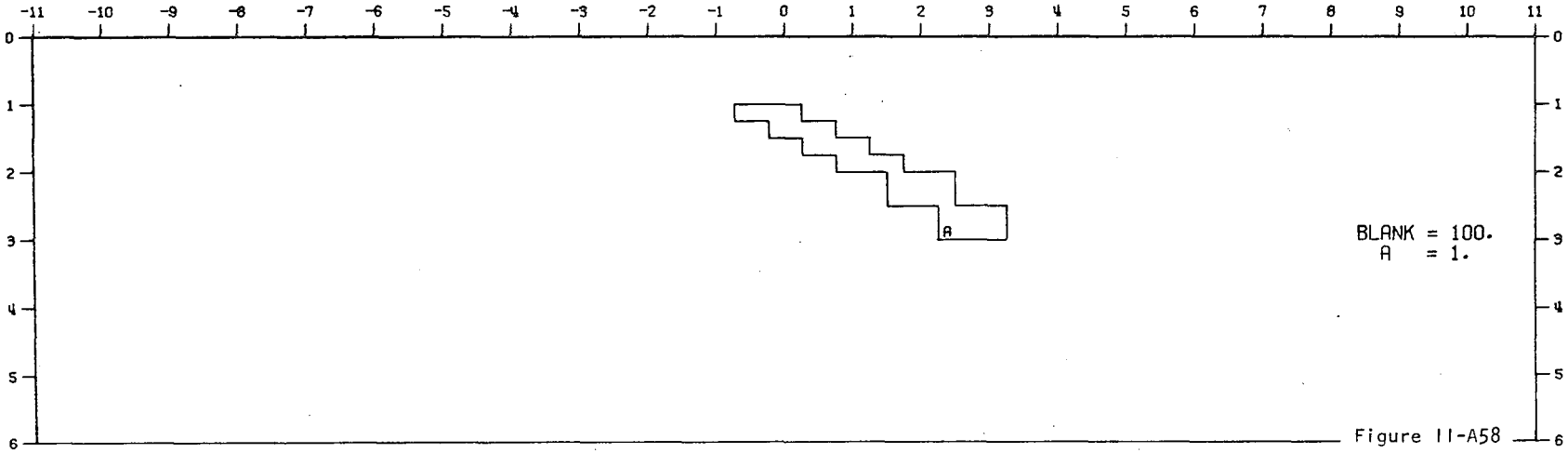

Figure II-A58

MODEL--CONDUCTIVE BODY 8
DIPOLE-DIPOLE APPARENT RESISTIVITY PSEUDO-SECTION
PROFILE LINE IS INCLINED AT 90.0 DEGREES TO STRIKE

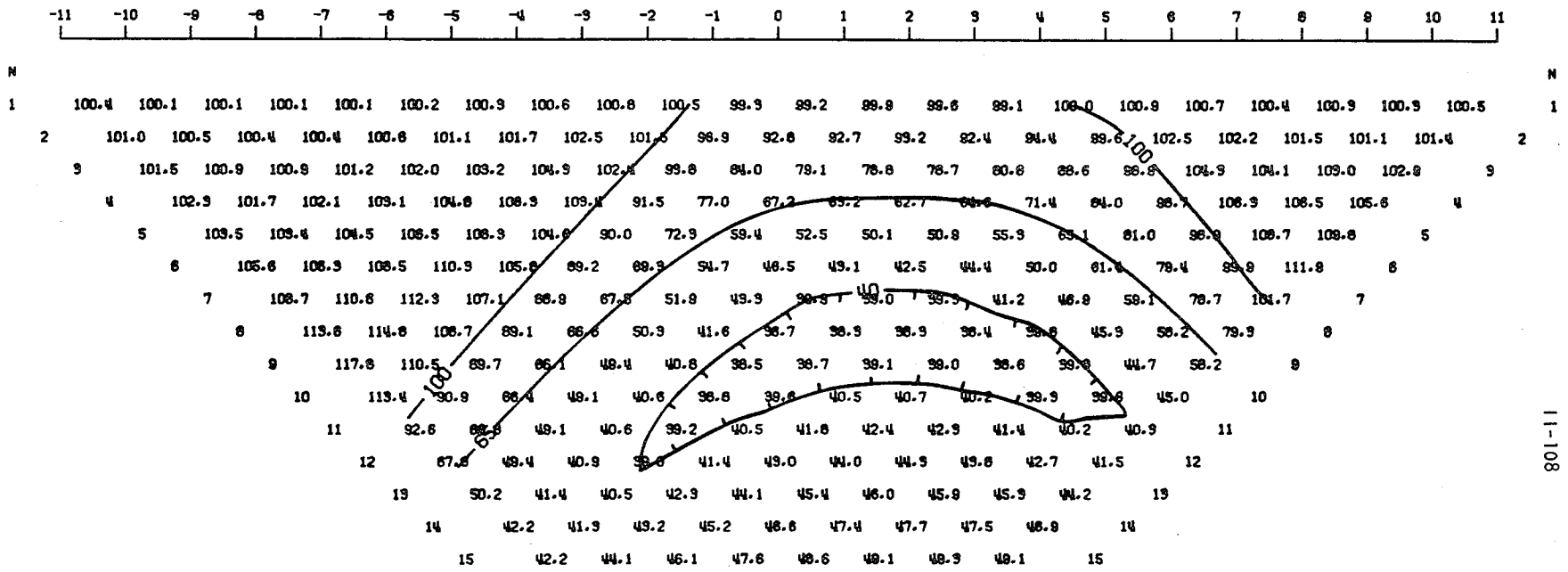

2-D RESISTIVITY MODEL -- CONDUCTIVE BODY 8

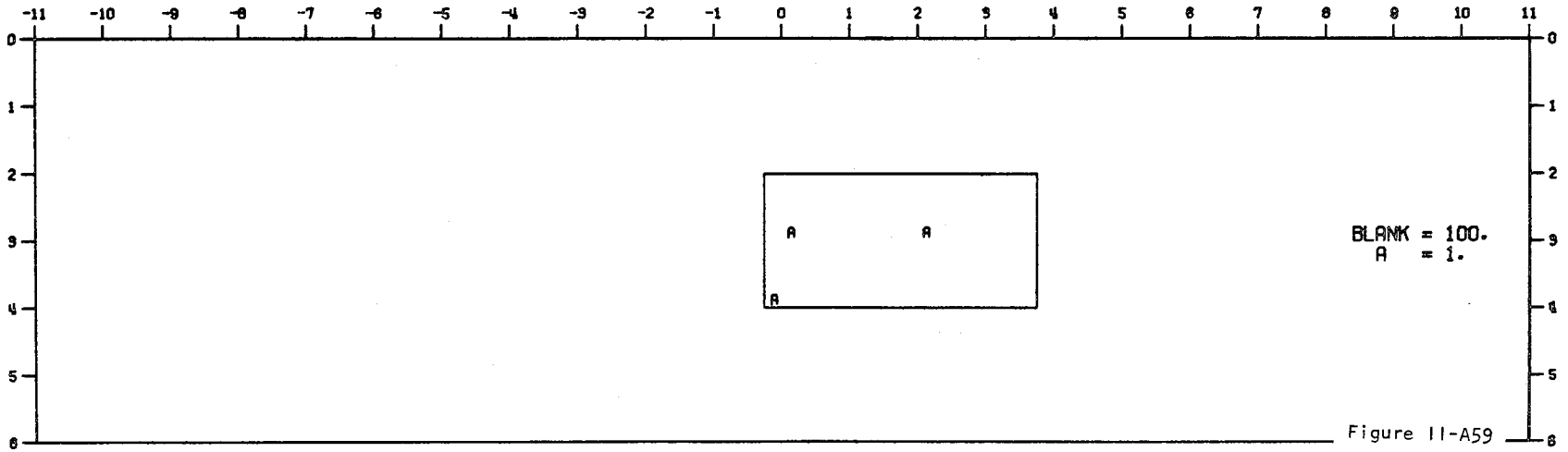

Figure II-A59

MODEL--CONDUCTIVE BODY 8
SCHLUMBERGER APPARENT RESISTIVITY PSEUDO-SECTION
PROFILE LINE IS INCLINED AT 90.0 DEGREES TO STRIKE

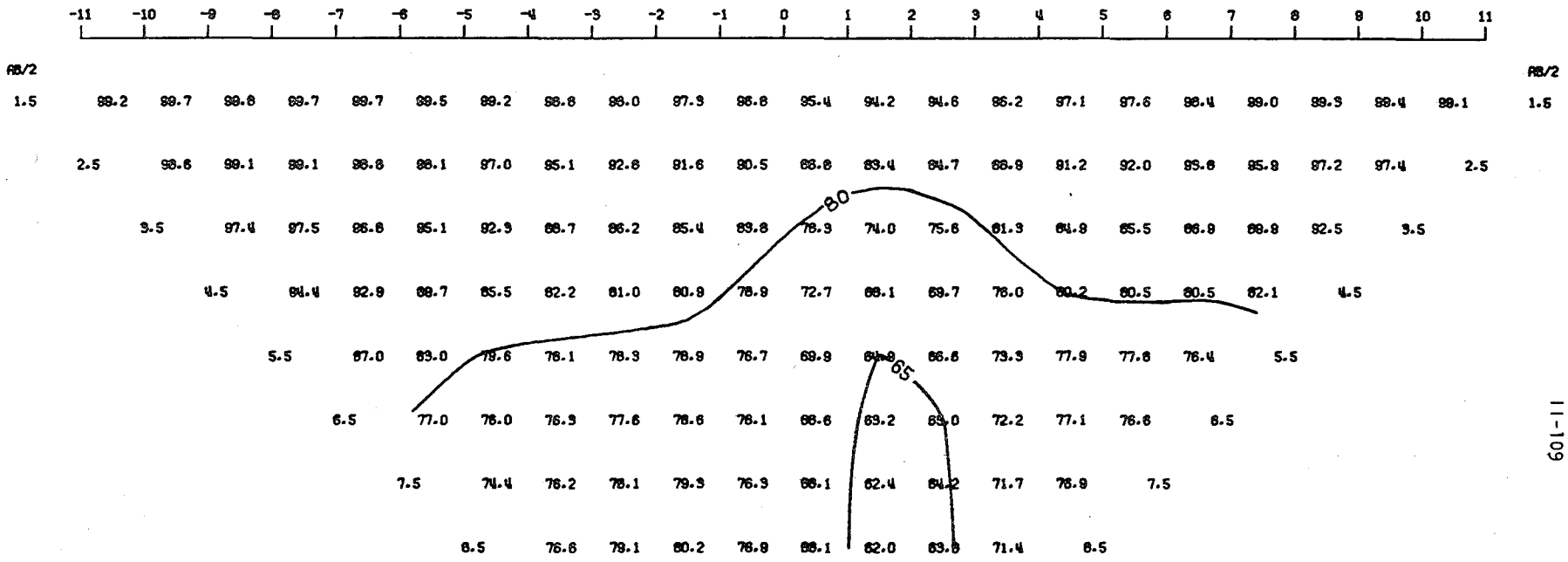

2-D RESISTIVITY MODEL -- CONDUCTIVE BODY 8

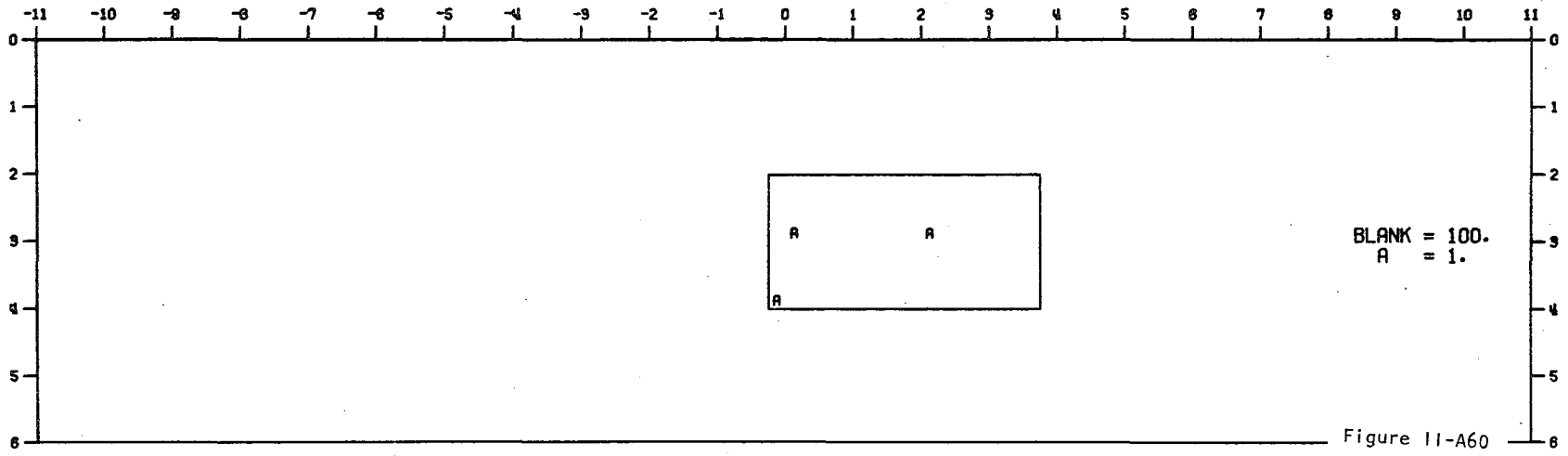

Figure II-A60

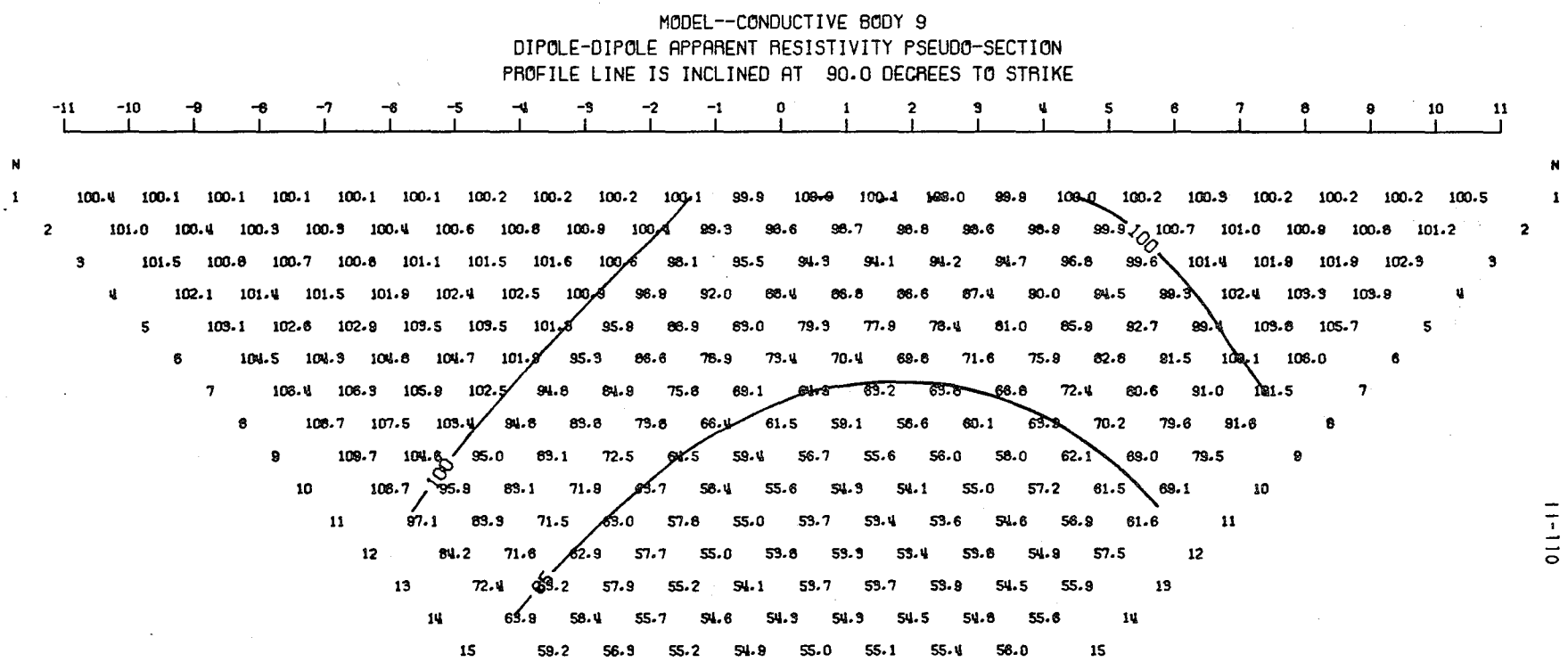

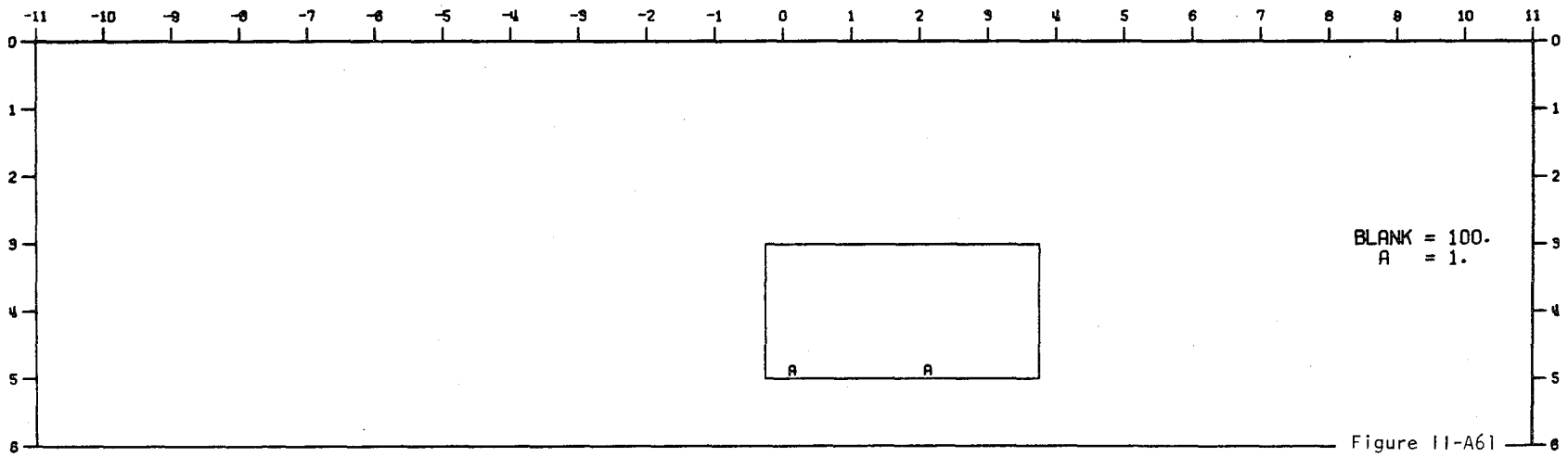

Figure II-A61

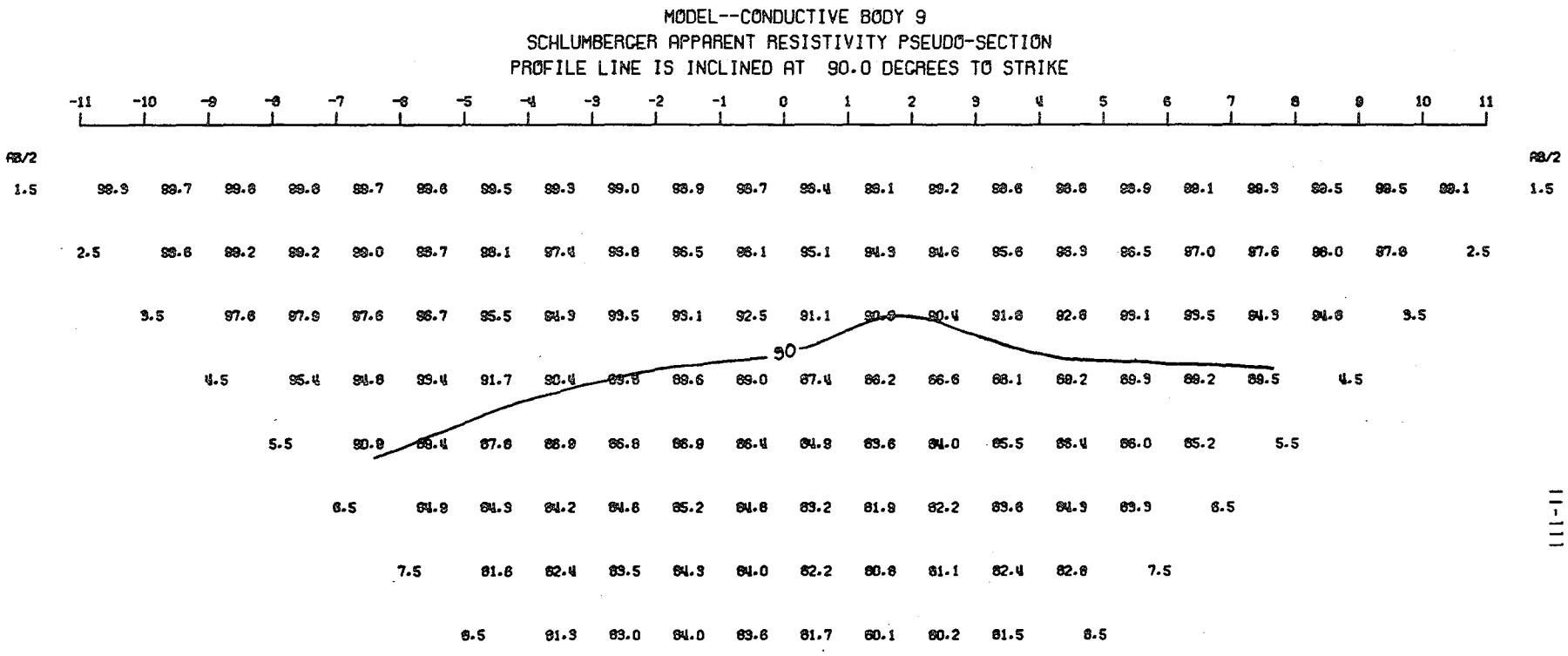

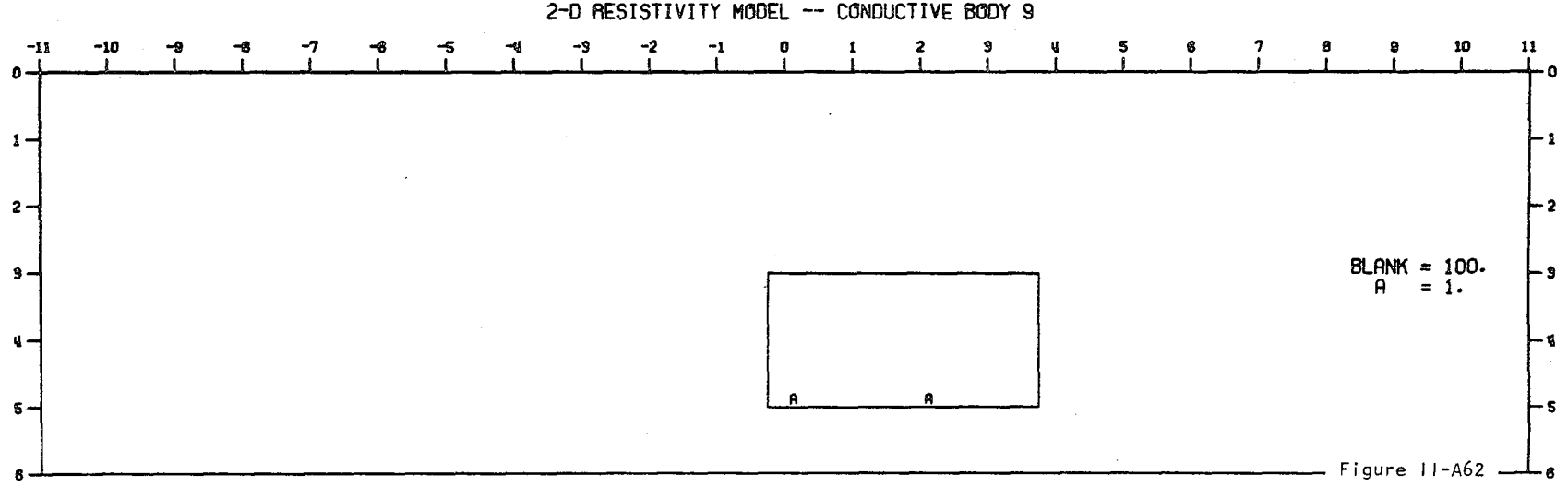

Figure II-A62

MODEL--CONDUCTIVE BODY 10
DIPOLE-DIPOLE APPARENT RESISTIVITY PSEUDO-SECTION
PROFILE LINE IS INCLINED AT 90.0 DEGREES TO STRIKE

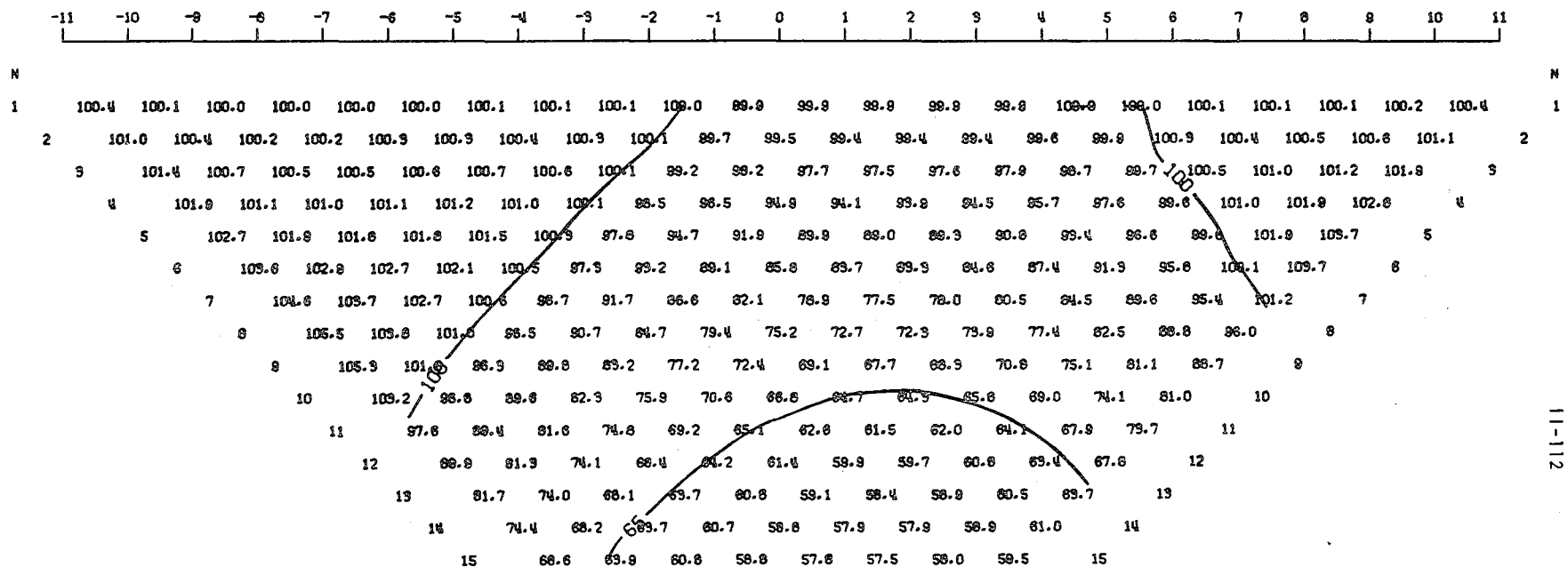

2-D RESISTIVITY MODEL -- CONDUCTIVE BODY 10

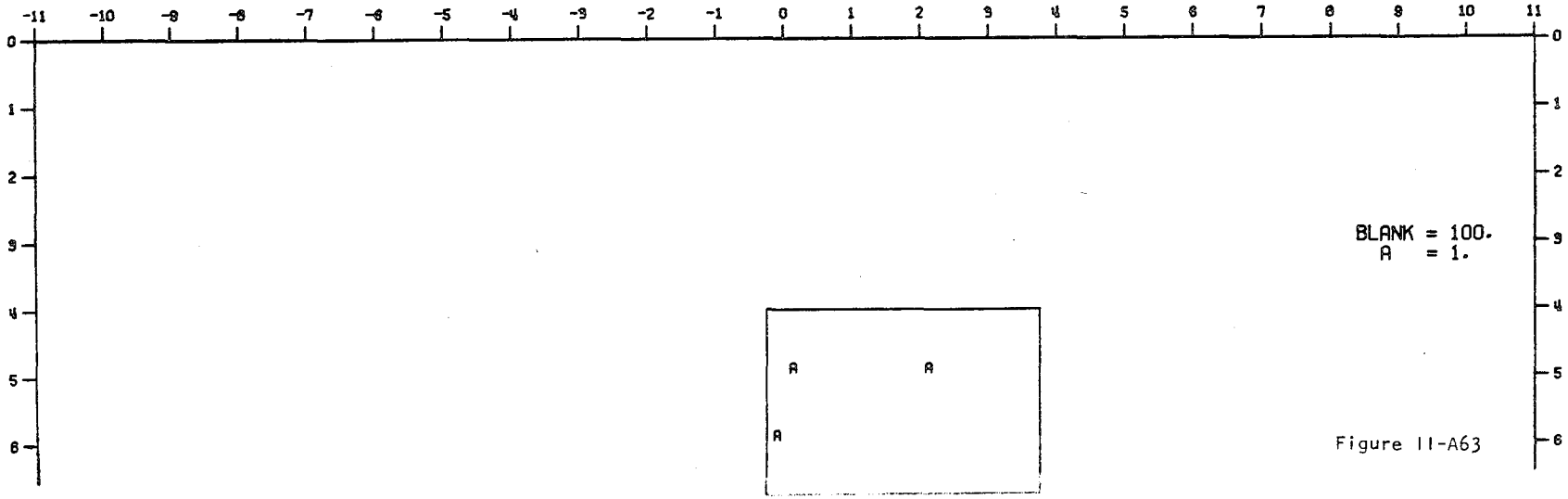

Figure II-A63

MODEL--CONDUCTIVE BODY 10
SCHLUMBERGER APPARENT RESISTIVITY PSEUDO-SECTION
PROFILE LINE IS INCLINED AT 90.0 DEGREES TO STRIKE

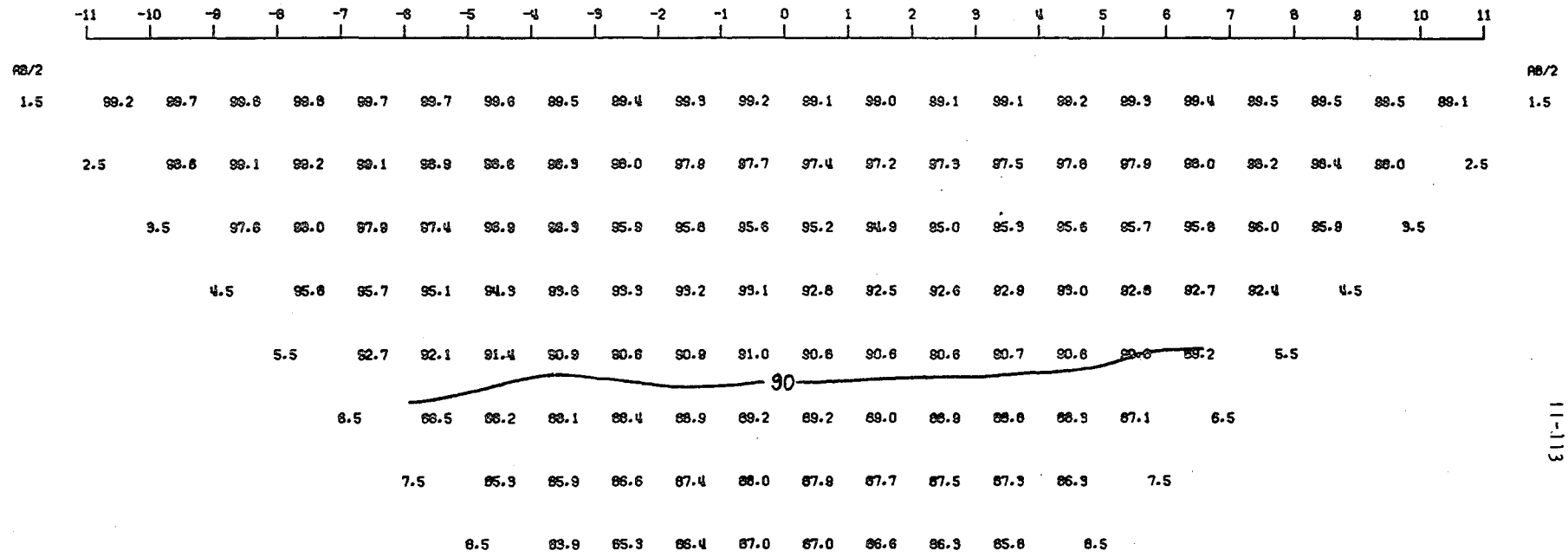

2-D RESISTIVITY MODEL -- CONDUCTIVE BODY 10

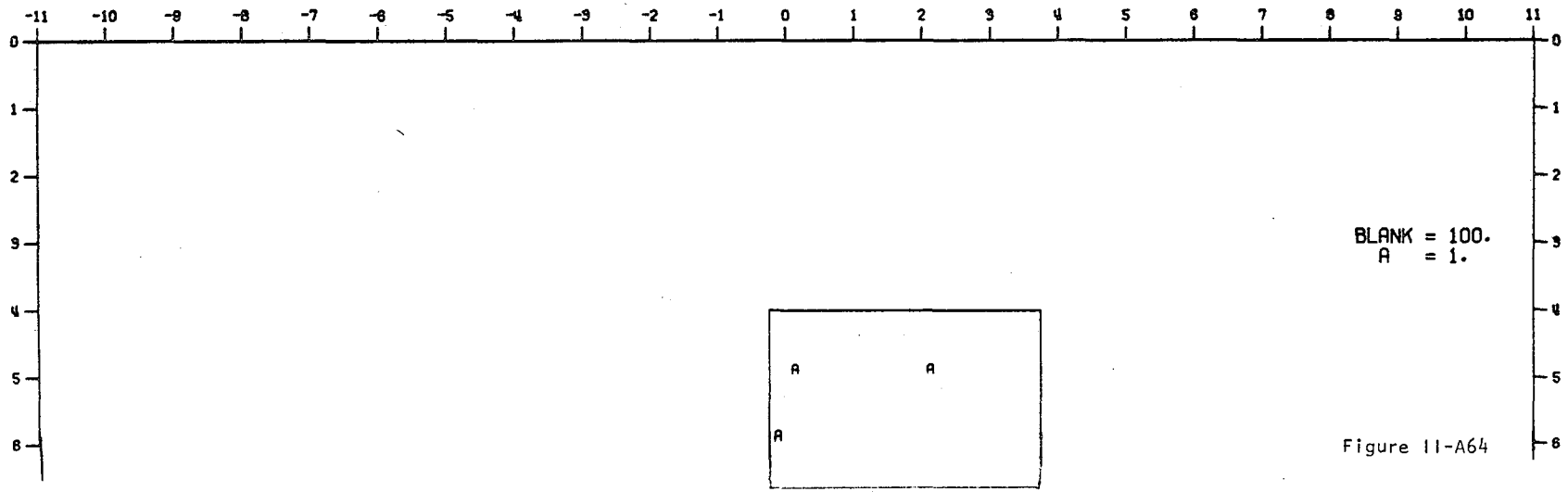

Figure II-A64

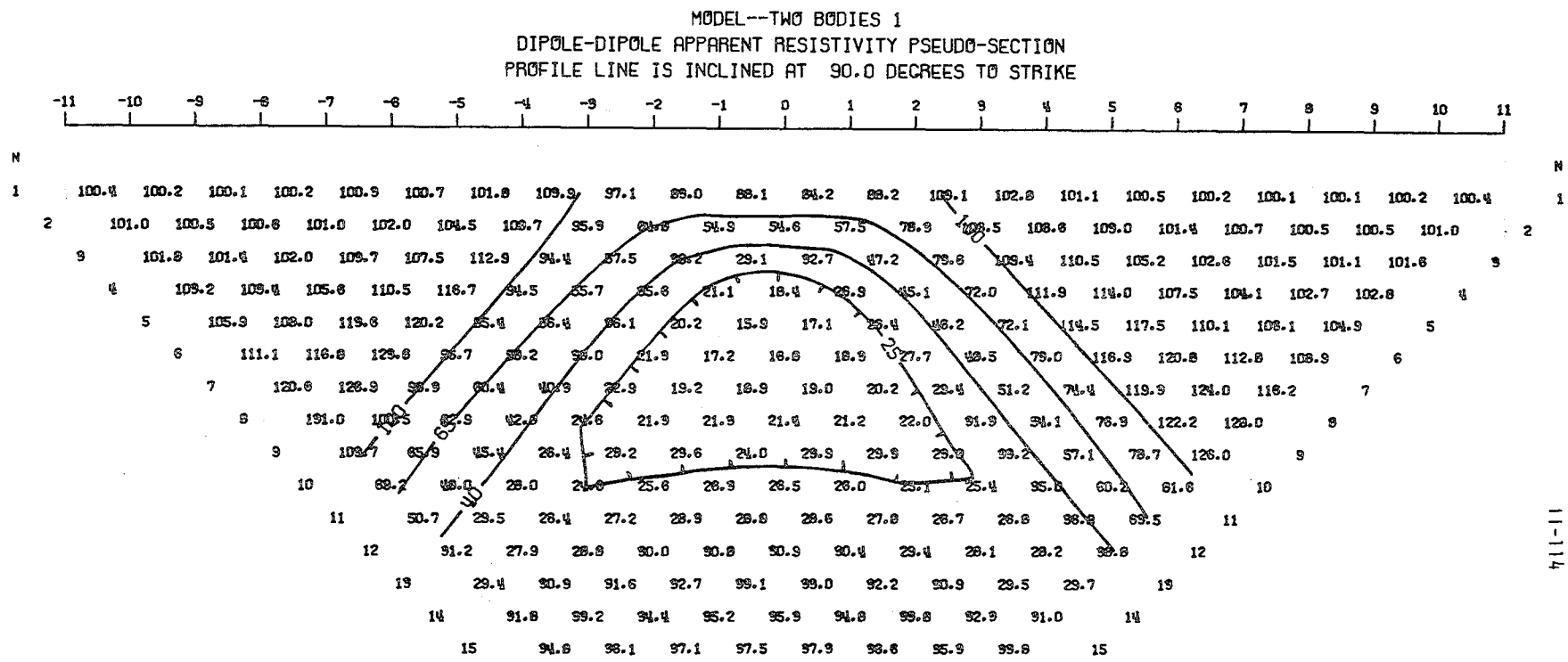

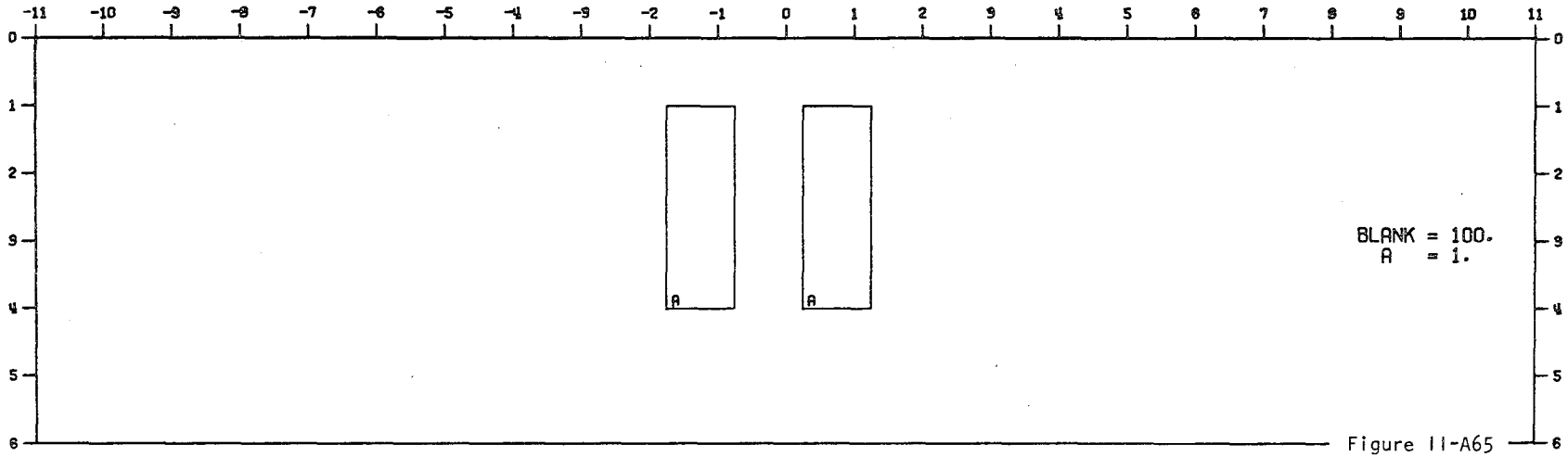

Figure II-A65

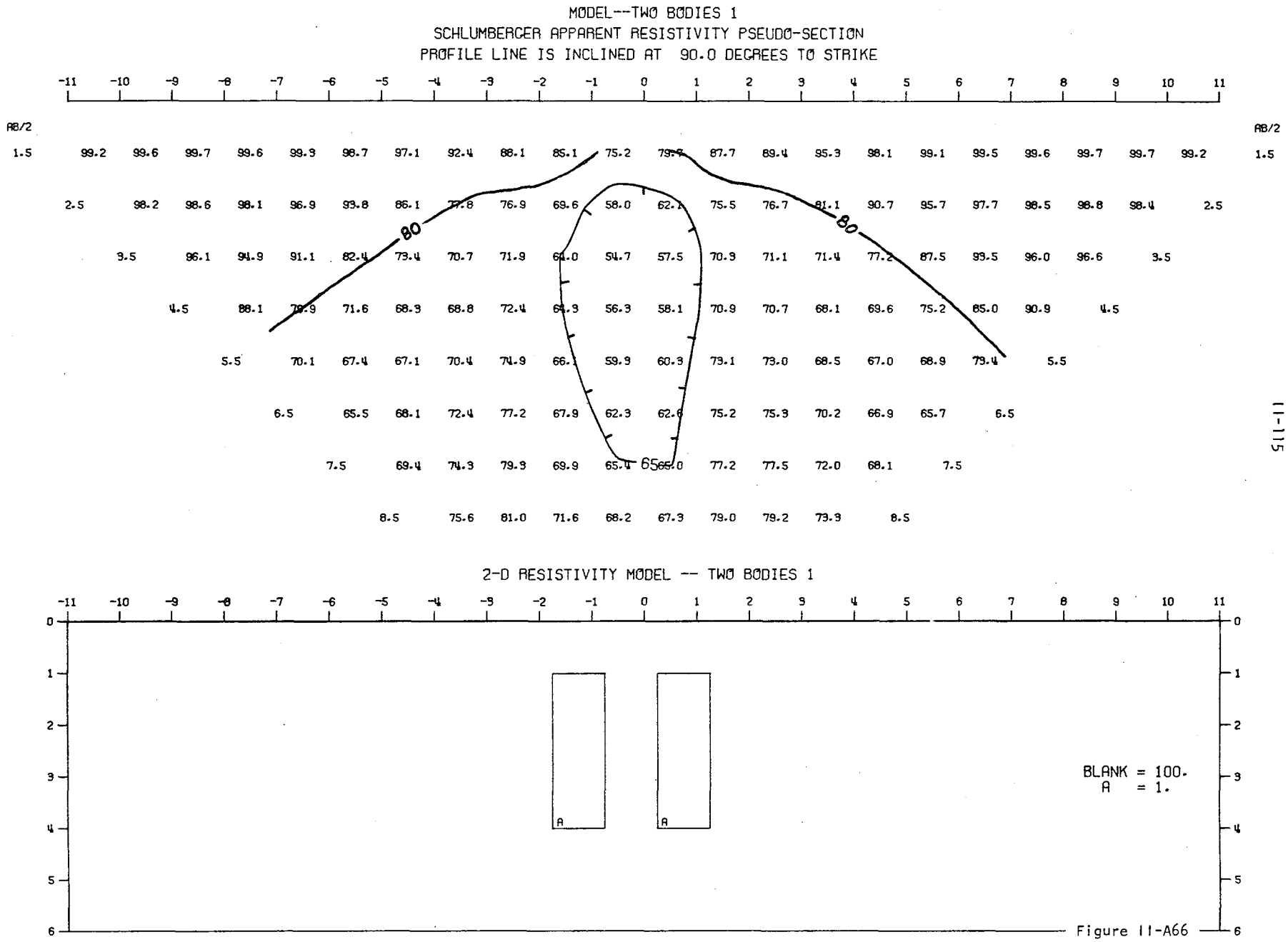

Figure II-A66

MODEL--TWO BODIES 2
DIPOLE-DIPOLE APPARENT RESISTIVITY PSEUDO-SECTION
PROFILE LINE IS INCLINED AT 90.0 DEGREES TO STRIKE

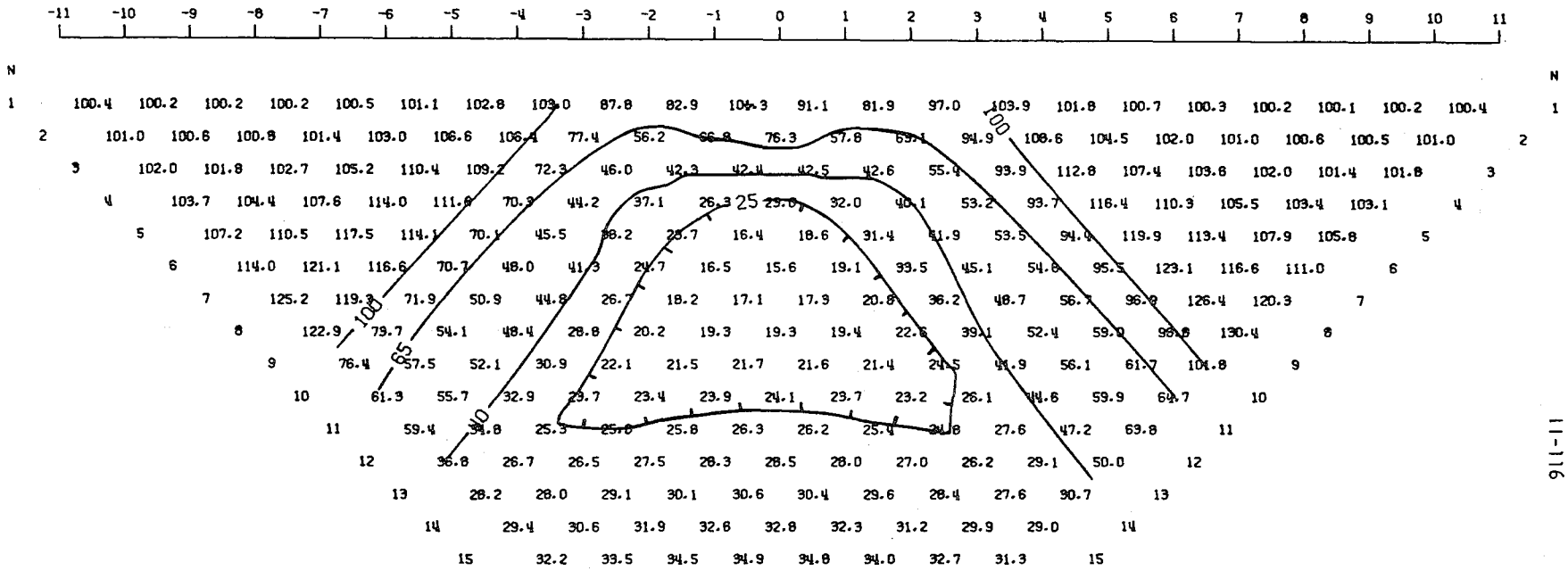

2-D RESISTIVITY MODEL -- TWO BODIES 2

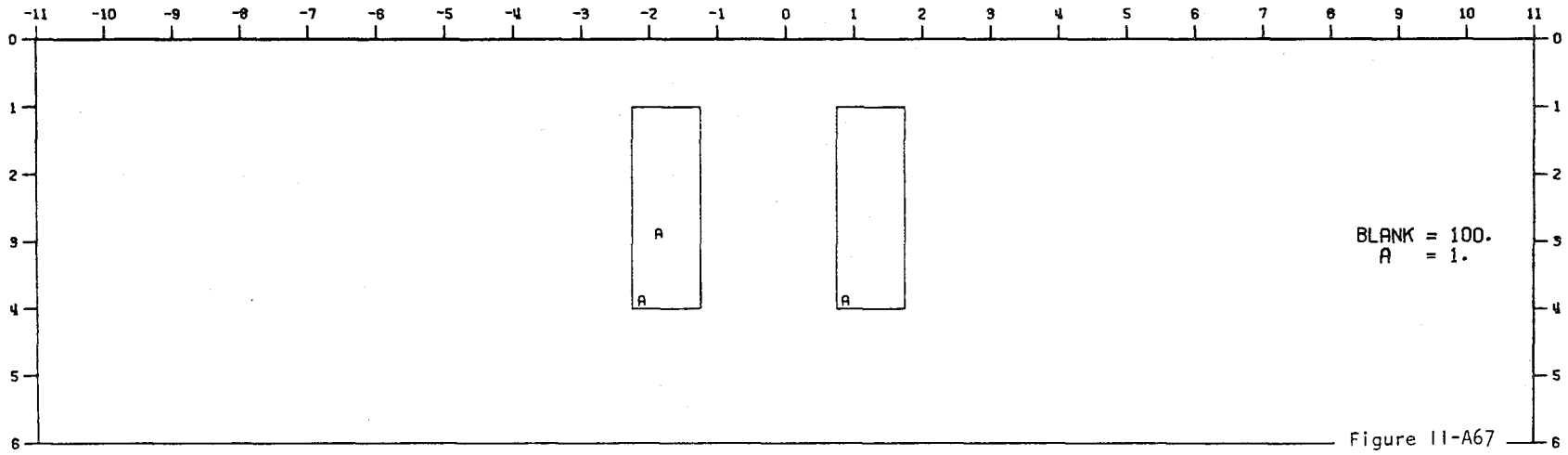

Figure II-A67

MODEL--TWO BODIES 2
SCHLUMBERGER APPARENT RESISTIVITY PSEUDO-SECTION
PROFILE LINE IS INCLINED AT 90.0 DEGREES TO STRIKE

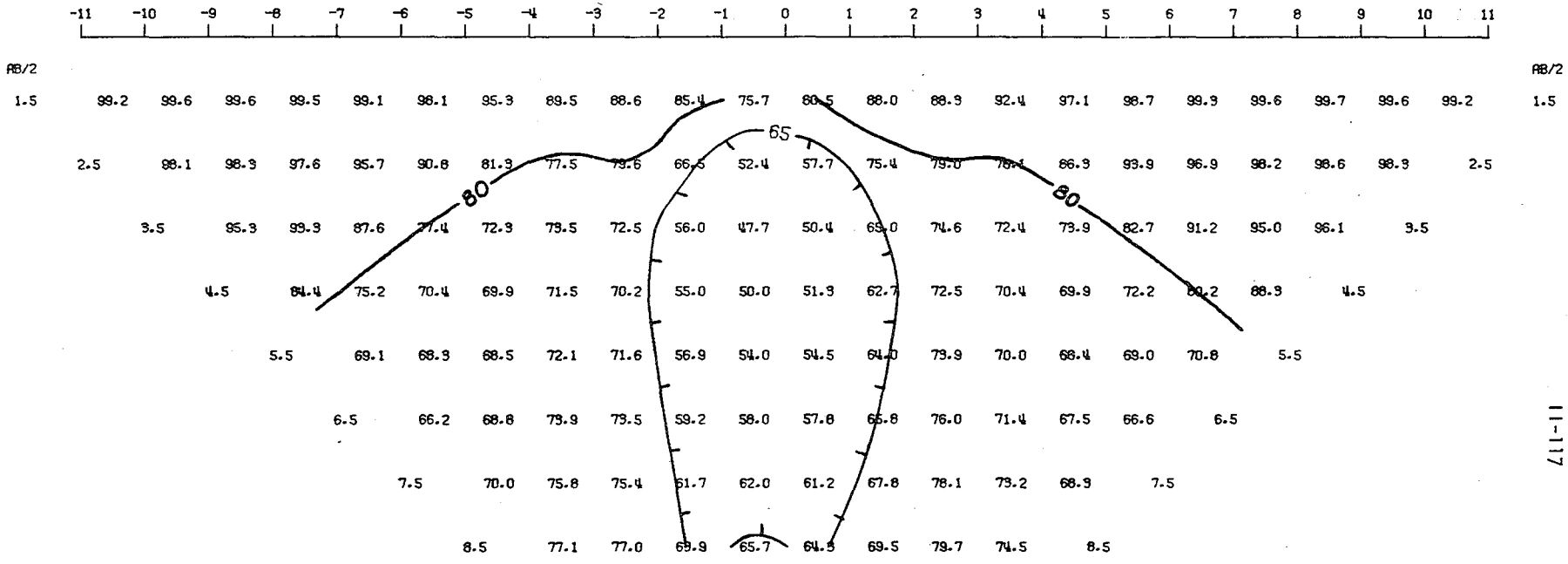

2-D RESISTIVITY MODEL -- TWO BODIES 2

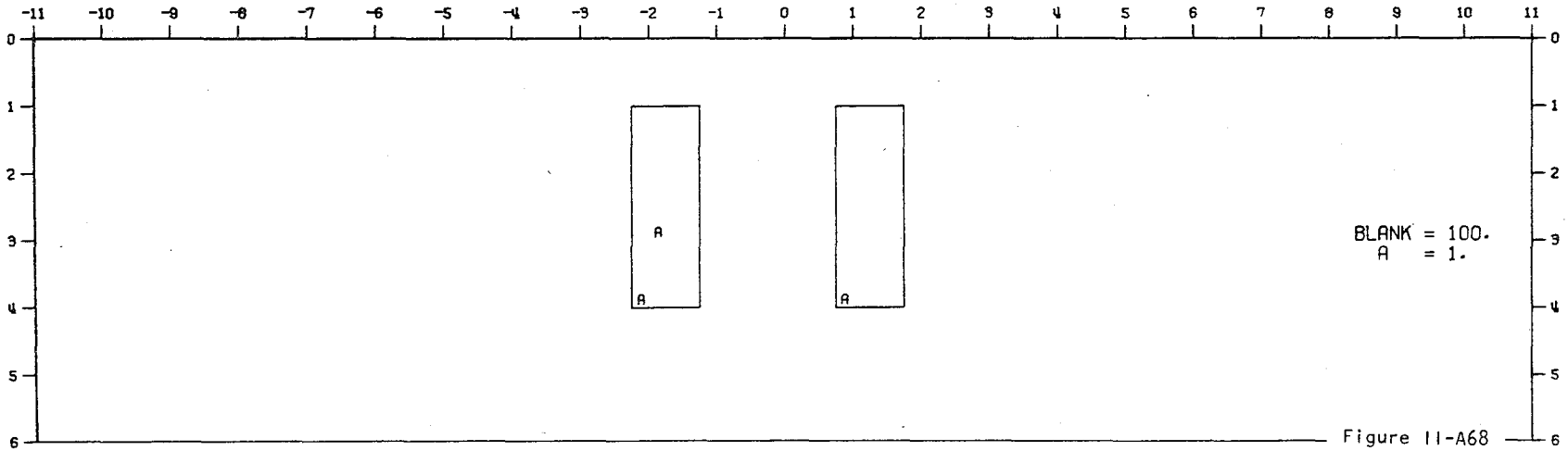

Figure II-A68

MODEL--TWO BODIES 3
DIPOLE-DIPOLE APPARENT RESISTIVITY PSEUDO-SECTION
PROFILE LINE IS INCLINED AT 90.0 DEGREES TO STRIKE

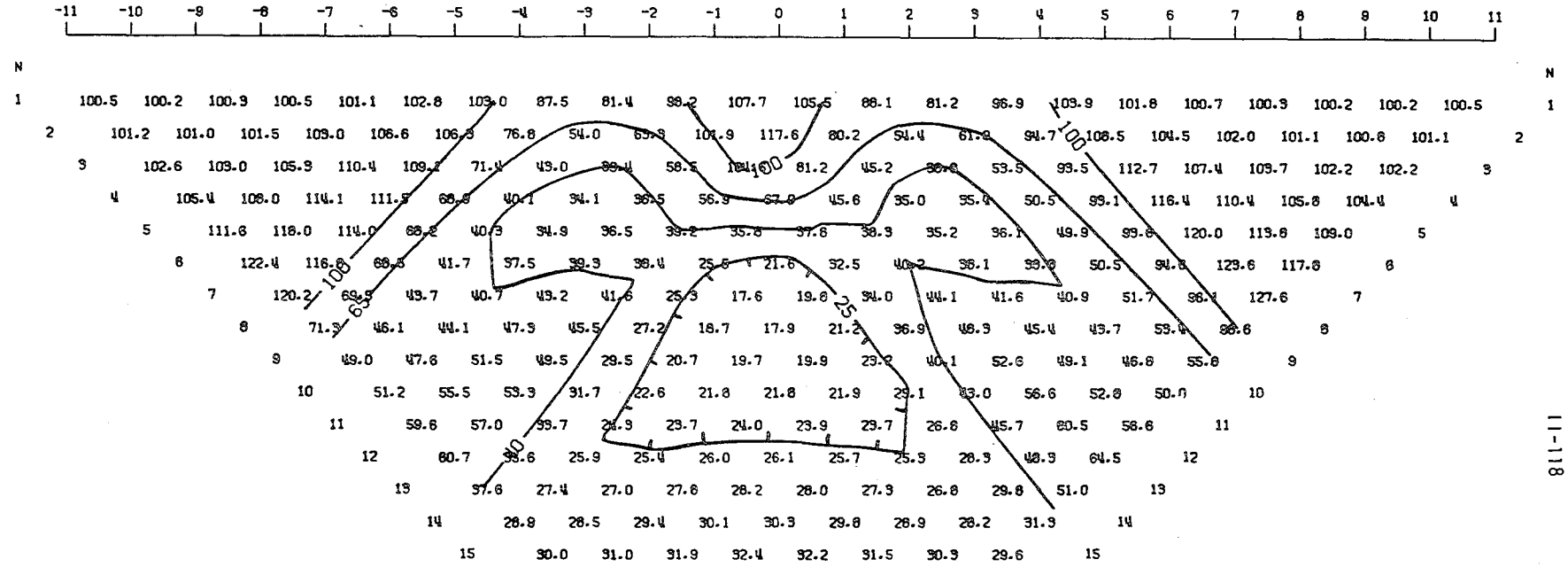

2-D RESISTIVITY MODEL -- TWO BODIES 3

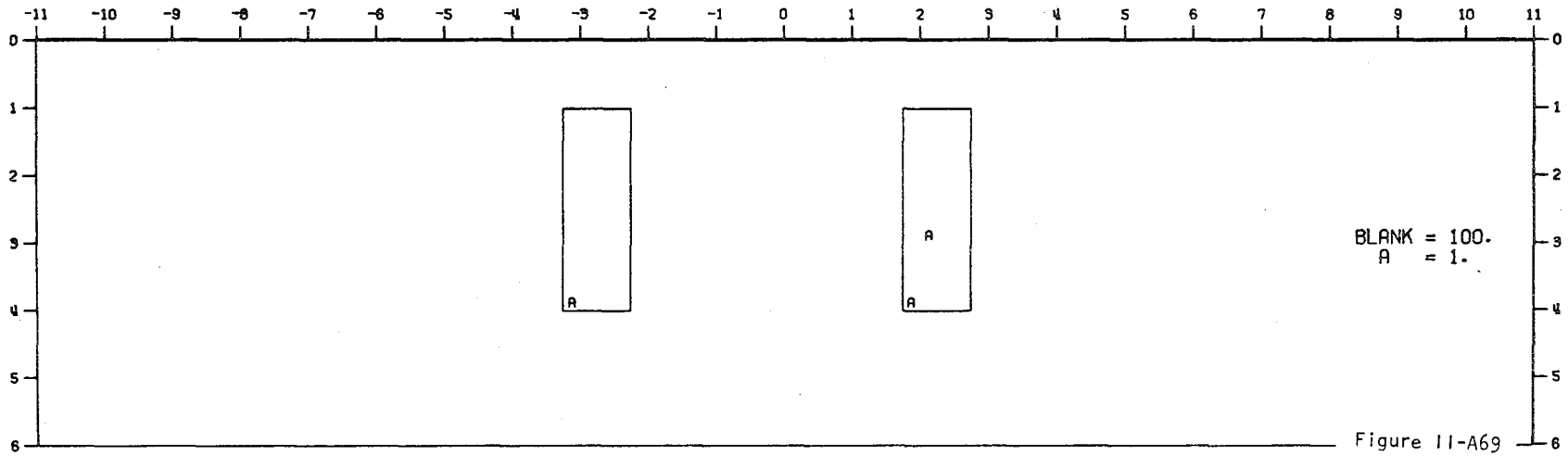

Figure II-A69

MODEL--TWO BODIES 3
SCHLUMBERGER APPARENT RESISTIVITY PSEUDO-SECTION
PROFILE LINE IS INCLINED AT 90.0 DEGREES TO STRIKE

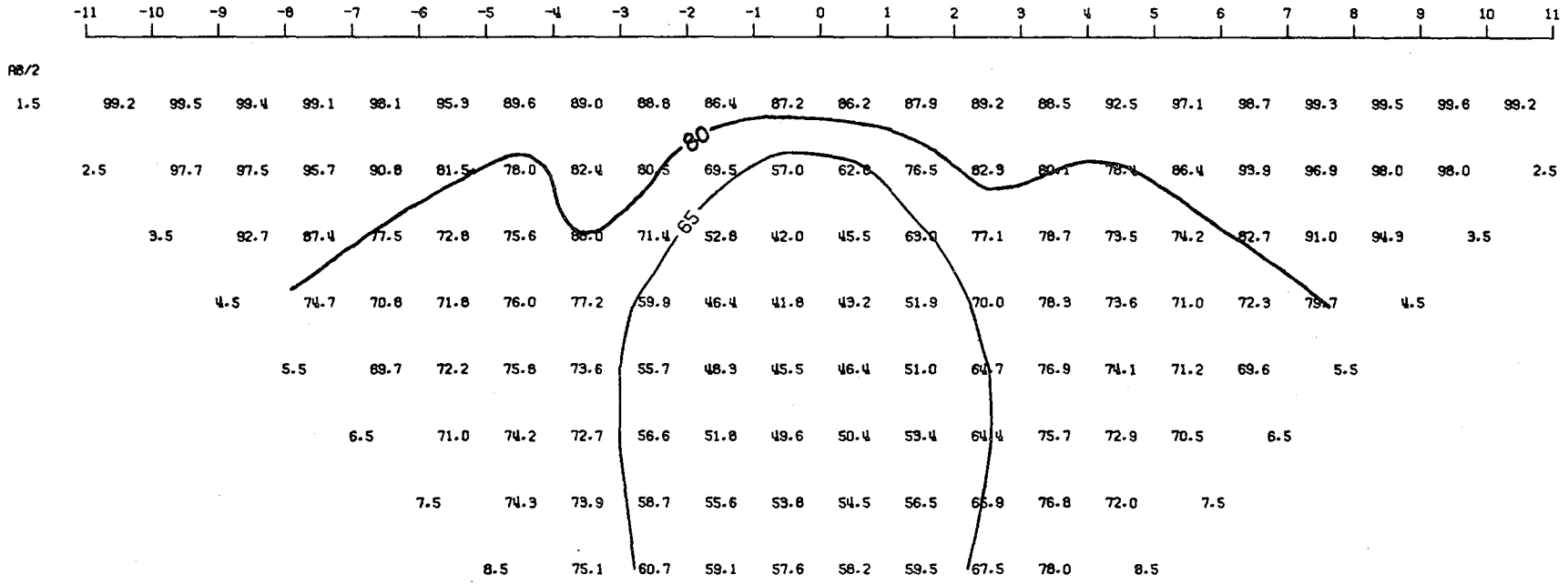

2-D RESISTIVITY MODEL -- TWO BODIES 3

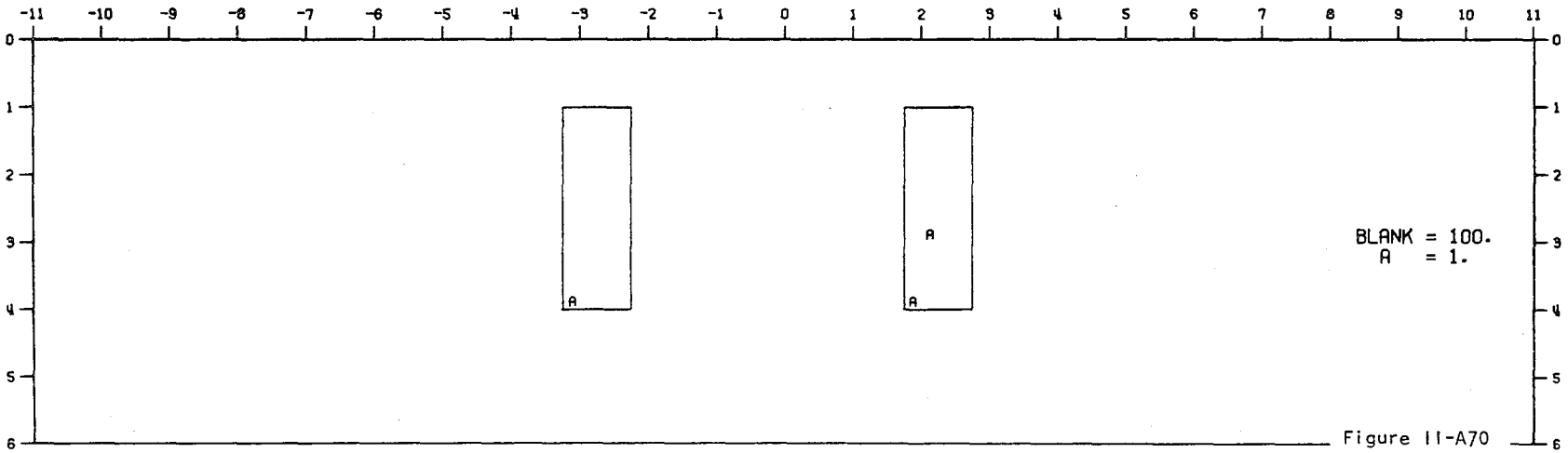

Figure II-A70

MODEL--RESISTIVE BODY
DIPOLE-DIPOLE APPARENT RESISTIVITY PSEUDO-SECTION
PROFILE LINE IS INCLINED AT 90.0 DECREES TO STRIKE

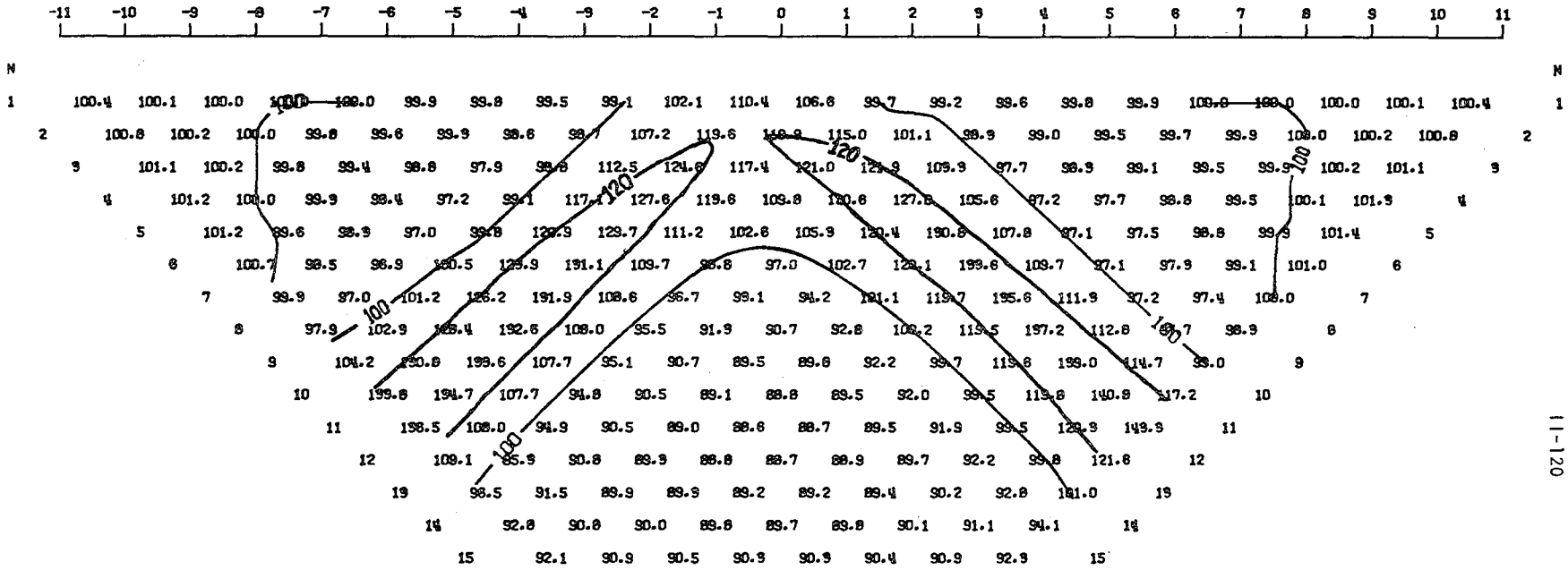

2-D RESISTIVITY MODEL -- RESISTIVE BODY

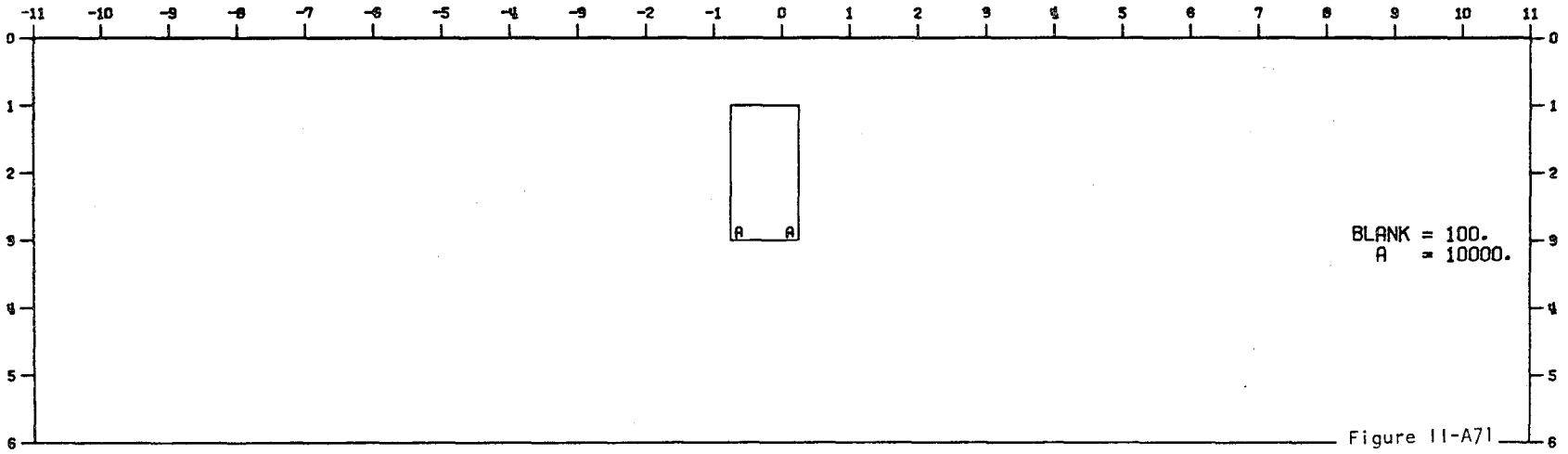

Figure II-A71

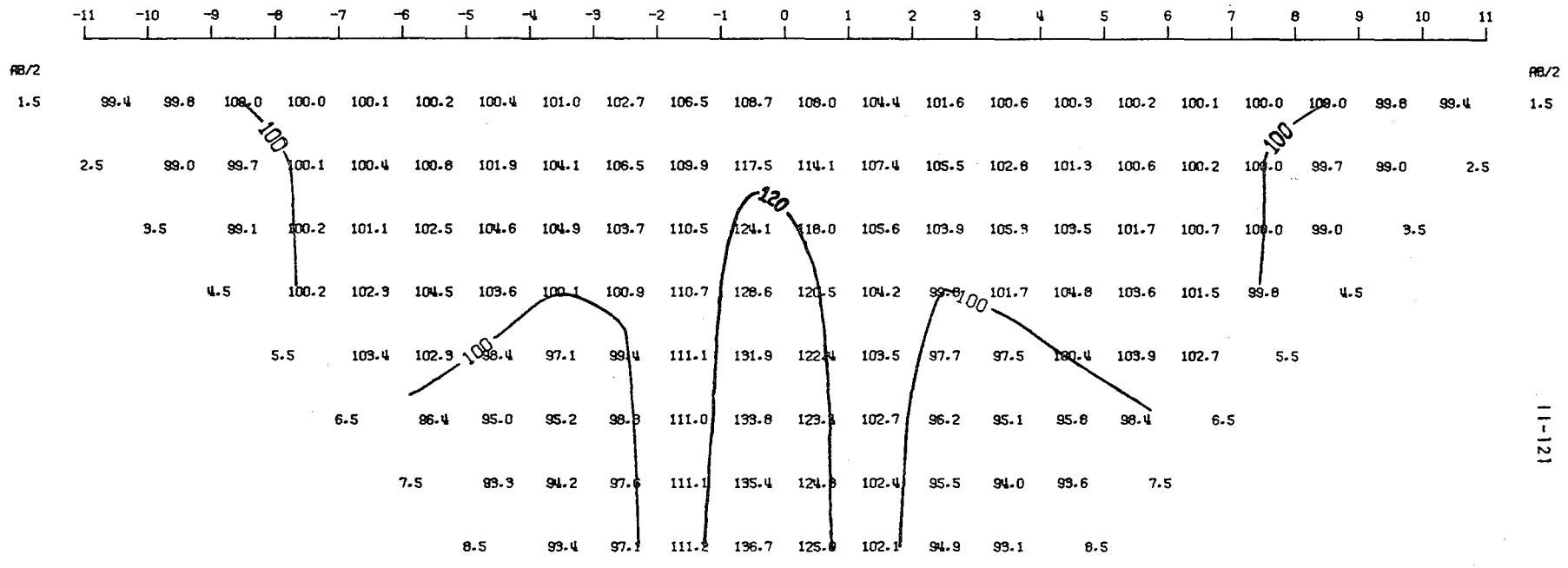

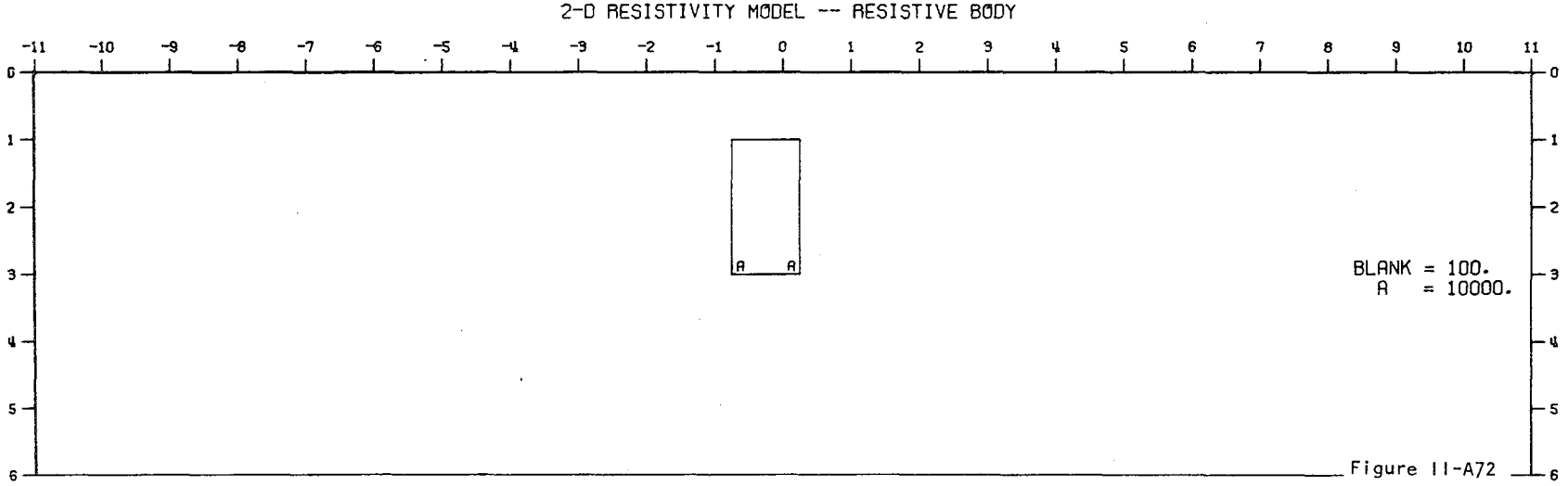

Figure 11-A72

MODEL--CONDUCTIVE BODY WITH OVERBURDEN 2
DIPOLE-DIPOLE APPARENT RESISTIVITY PSEUDO-SECTION
PROFILE LINE IS INCLINED AT 90.0 DEGREES TO STRIKE

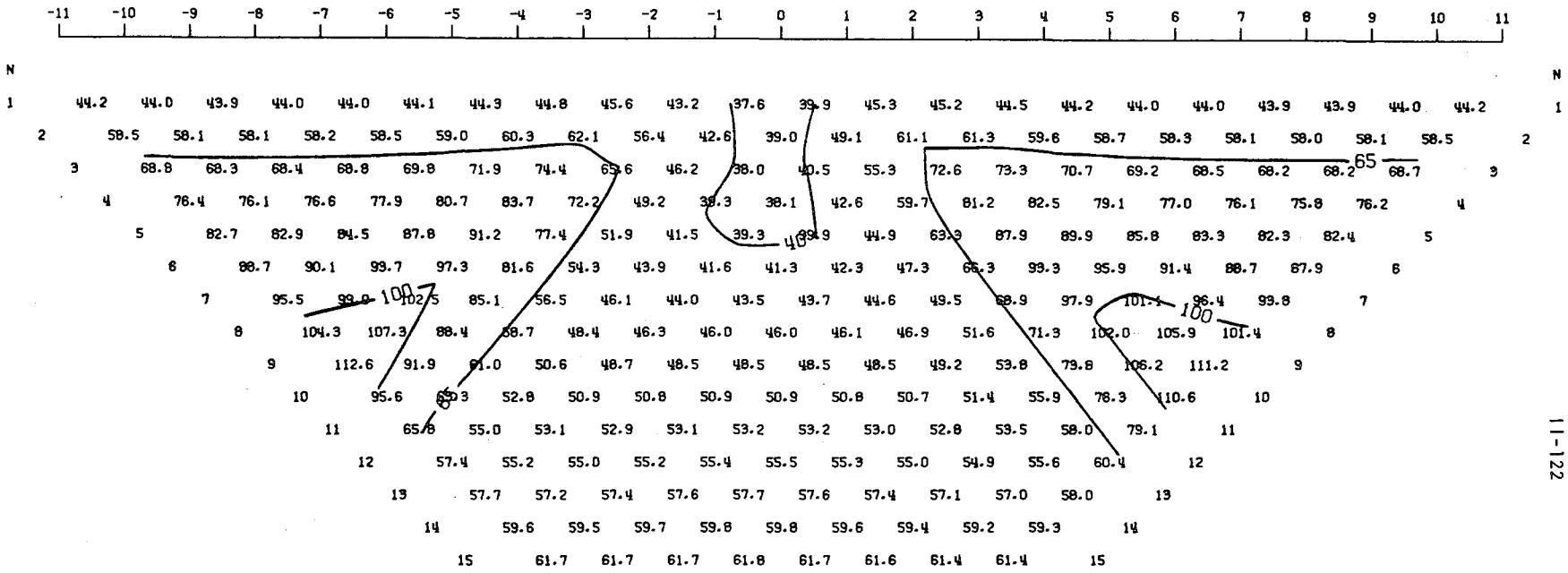

2-D RESISTIVITY MODEL -- CONDUCTIVE BODY WITH OVERBURDEN 2

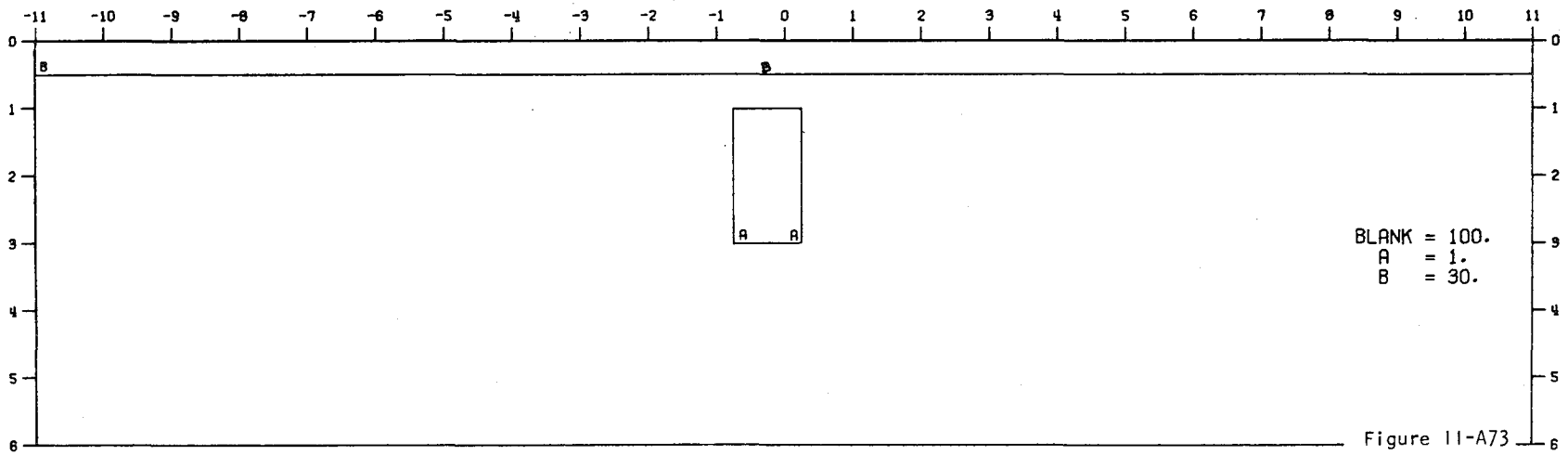

Figure 11-A73

MODEL--CONDUCTIVE BODY WITH OVERBURDEN 2
SCHLUMBERGER APPARENT RESISTIVITY PSEUDO-SECTION
PROFILE LINE IS INCLINED AT 90.0 DEGREES TO STRIKE

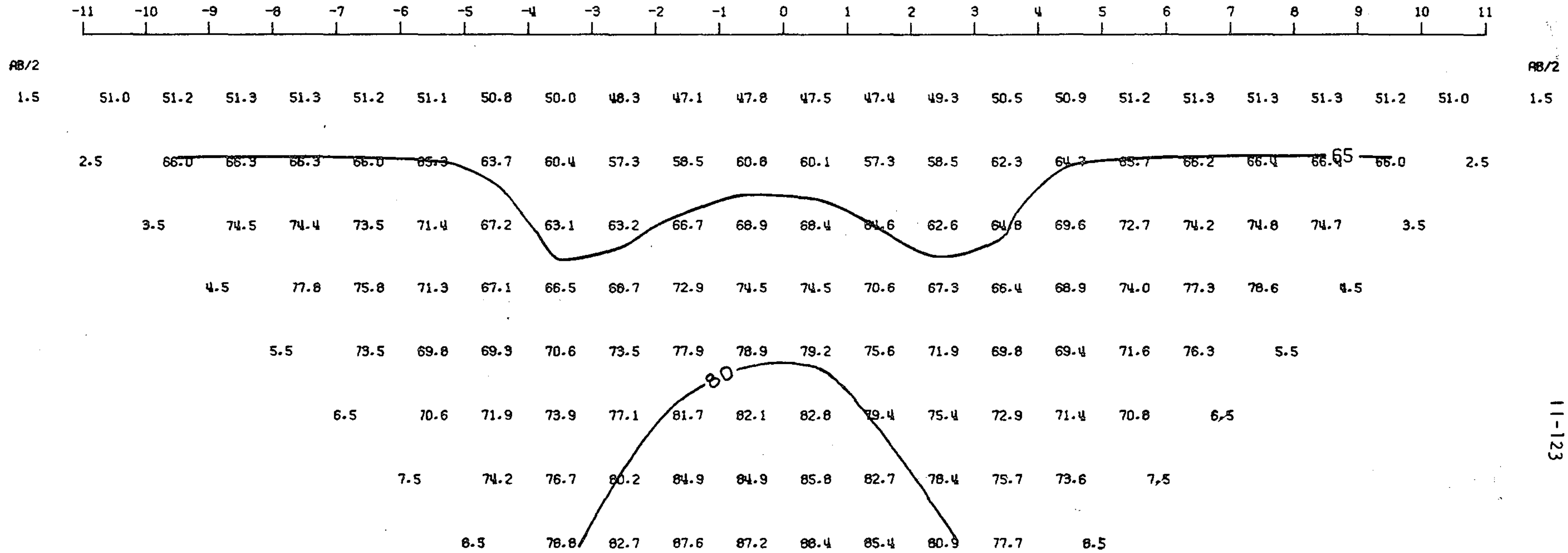

2-D RESISTIVITY MODEL -- CONDUCTIVE BODY WITH OVERBURDEN 2

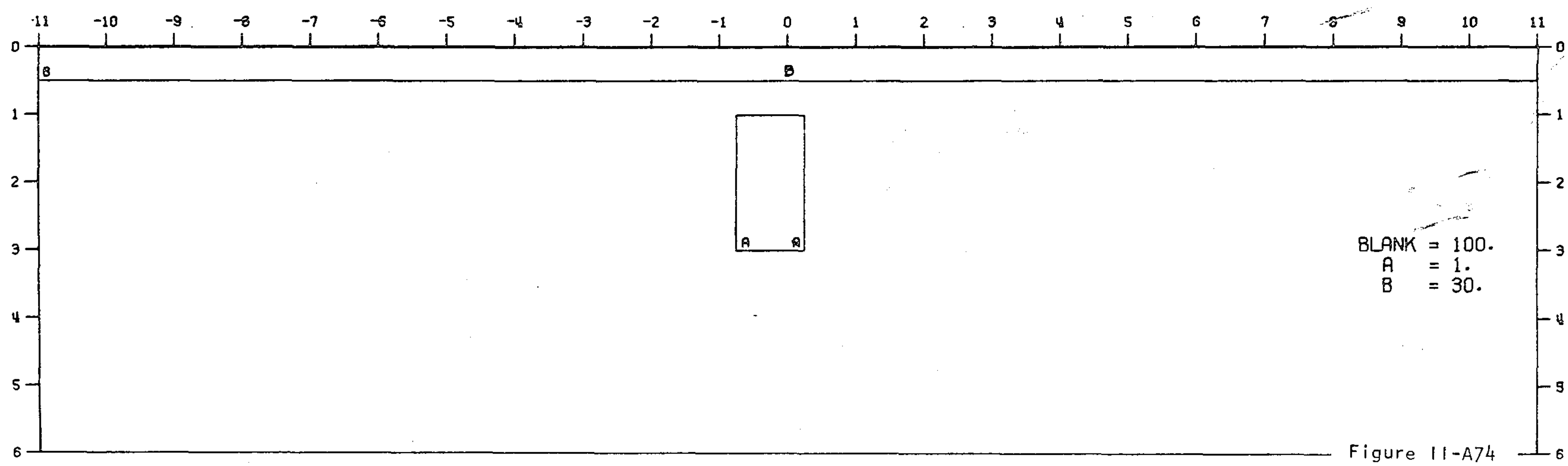

Figure II-A74

MODEL--CONDUCTIVE BODY WITH OVERBURDEN 1
DIPOLE-DIPOLE APPARENT RESISTIVITY PSEUDO-SECTION
PROFILE LINE IS INCLINED AT 90.0 DEGREES TO STRIKE

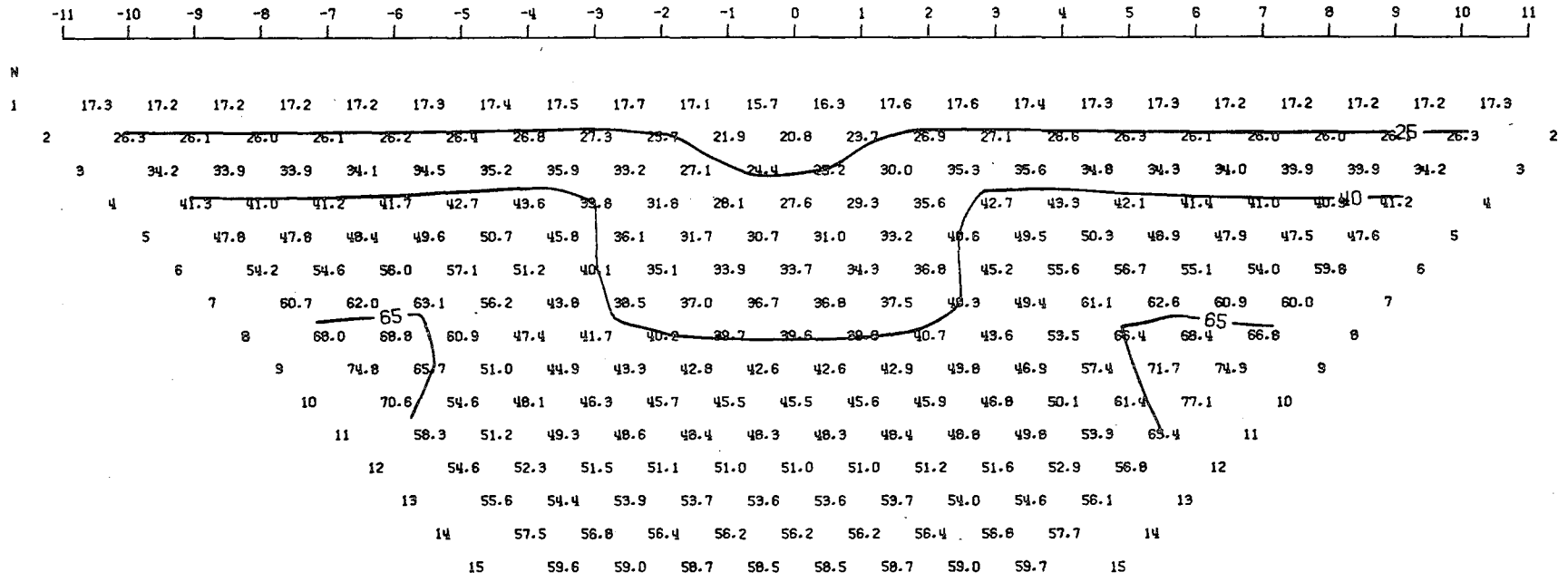

2-D RESISTIVITY MODEL -- CONDUCTIVE BODY WITH OVERBURDEN 1

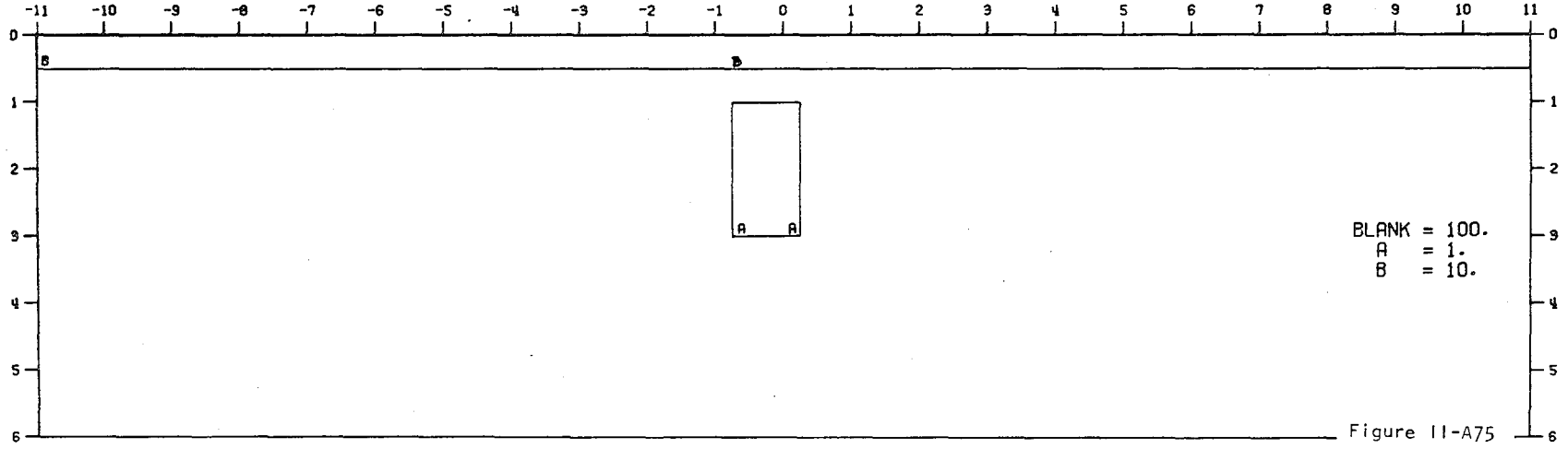

Figure II-A75

MODEL--CONDUCTIVE BODY WITH OVERBURDEN 1
SCHLUMBERGER APPARENT RESISTIVITY PSEUDO-SECTION
PROFILE LINE IS INCLINED AT 90.0 DEGREES TO STRIKE

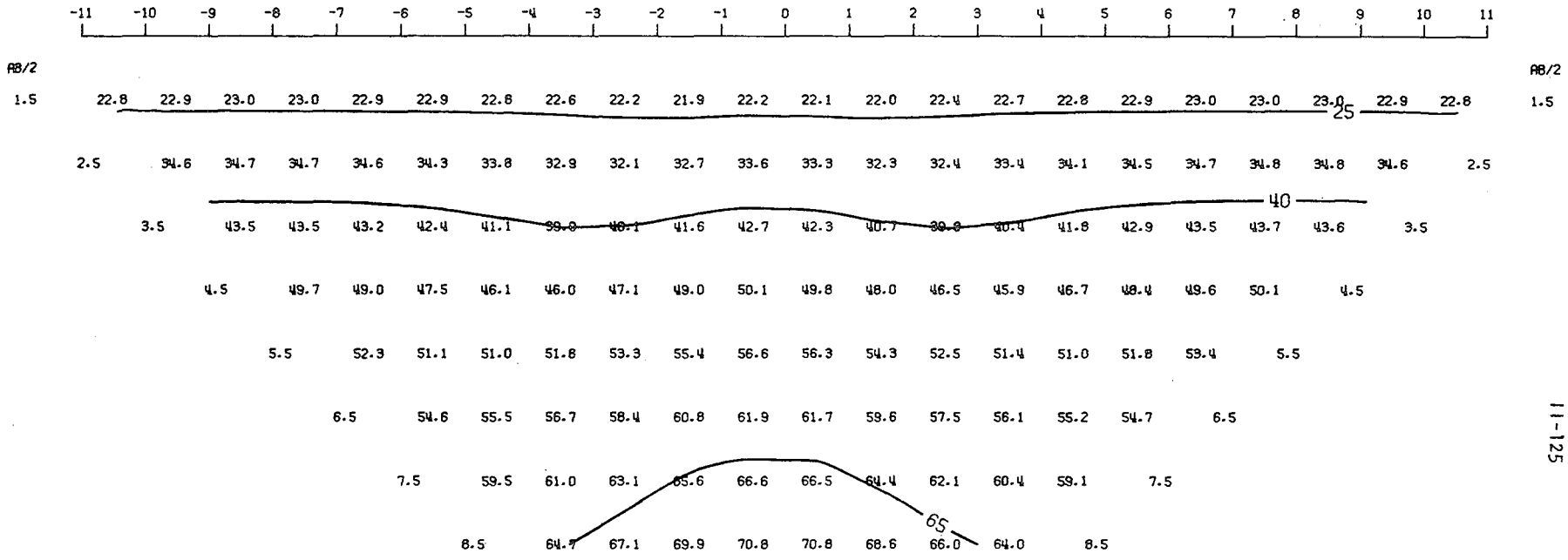

2-D RESISTIVITY MODEL -- CONDUCTIVE BODY WITH OVERBURDEN 1

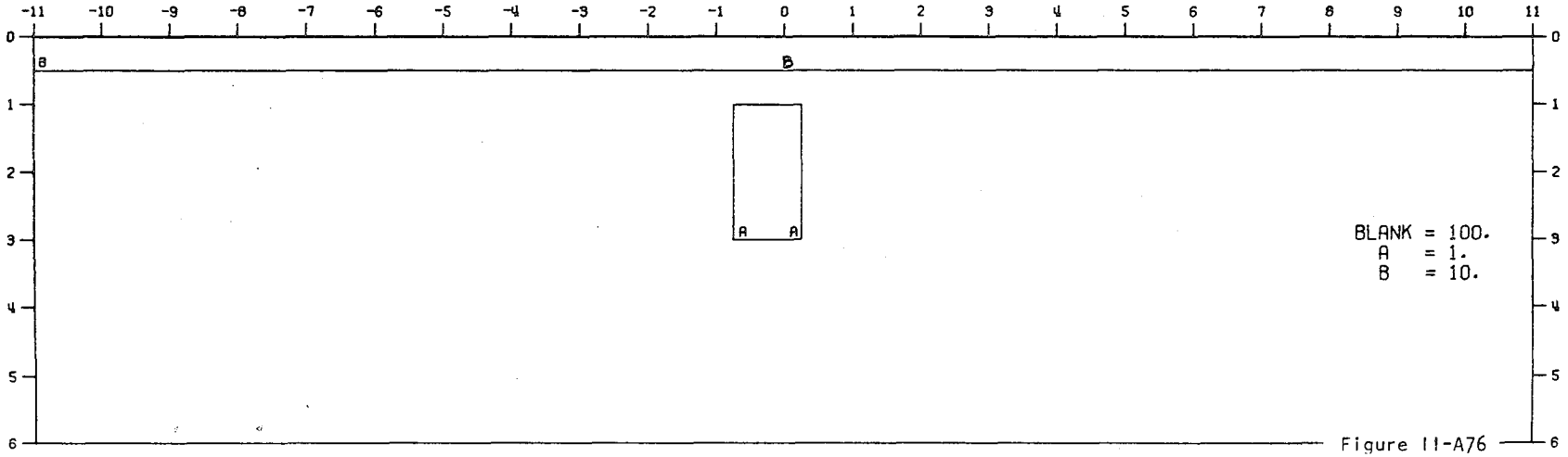

Figure 11-A76

MODEL--CONDUCTIVE BODY WITH OVERBURDEN 4
DIPOLE-DIPOLE APPARENT RESISTIVITY PSEUDO-SECTION
PROFILE LINE IS INCLINED AT 90.0 DEGREES TO STRIKE

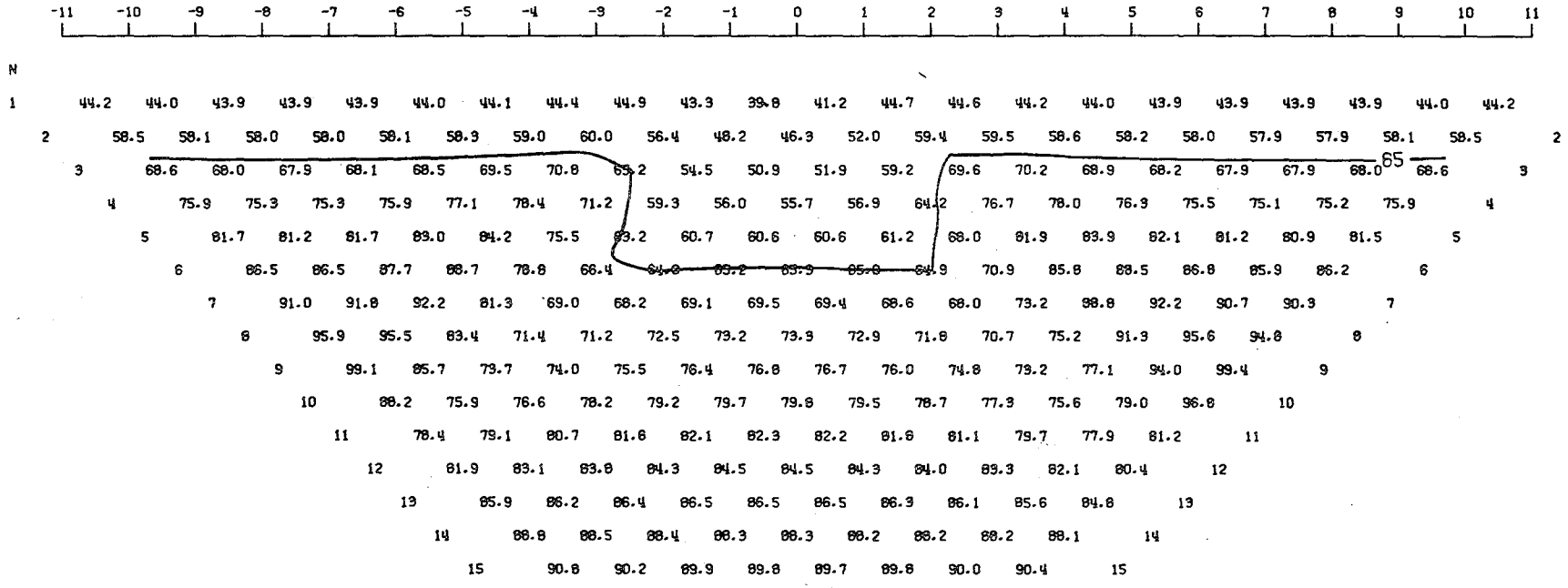

2-D RESISTIVITY MODEL -- CONDUCTIVE BODY WITH OVERBURDEN 4

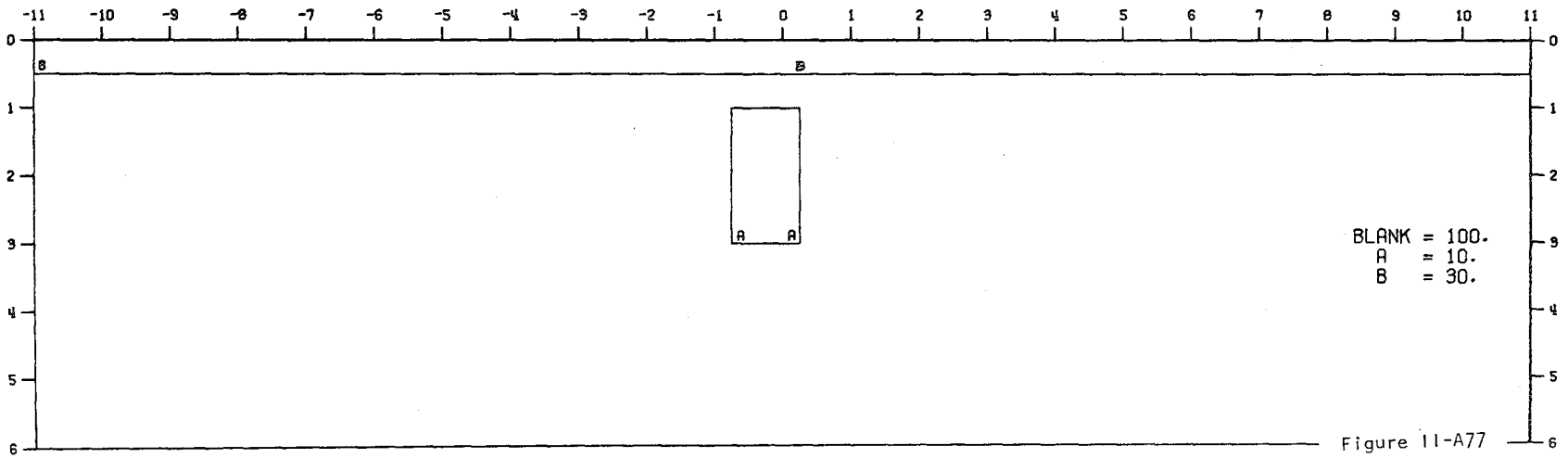

Figure 11-A77

MODEL--CONDUCTIVE BODY WITH OVERBURDEN 4
SCHLUMBERGER APPARENT RESISTIVITY PSEUDO-SECTION
PROFILE LINE IS INCLINED AT 90.0 DEGREES TO STRIKE

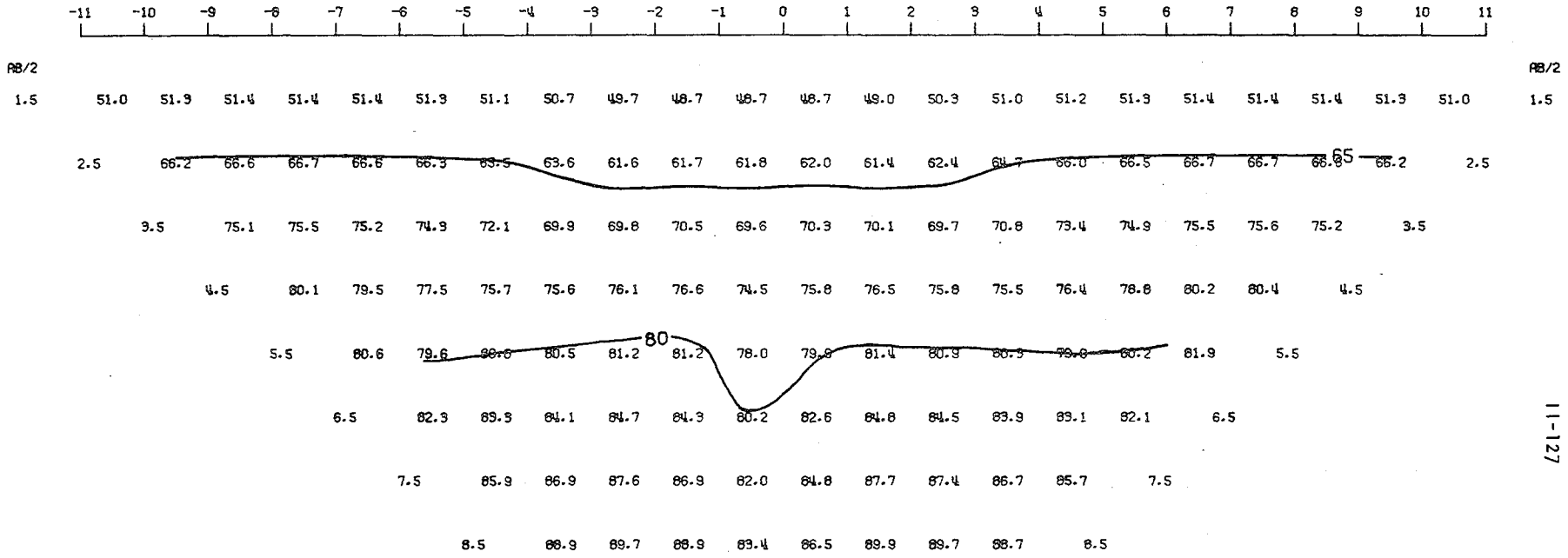

2-D RESISTIVITY MODEL -- CONDUCTIVE BODY WITH OVERBURDEN 4

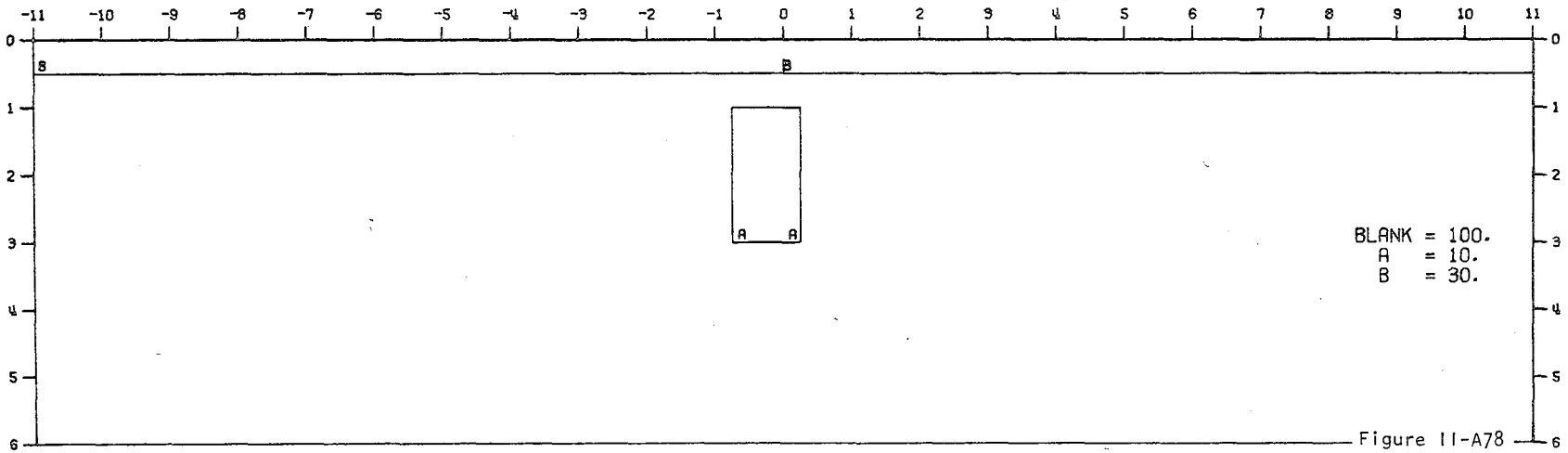

Figure II-A78

MODEL--CONDUCTIVE BODY WITH OVERBURDEN 3
DIPOLE-DIPOLE APPARENT RESISTIVITY PSEUDO-SECTION
PROFILE LINE IS INCLINED AT 90.0 DEGREES TO STRIKE

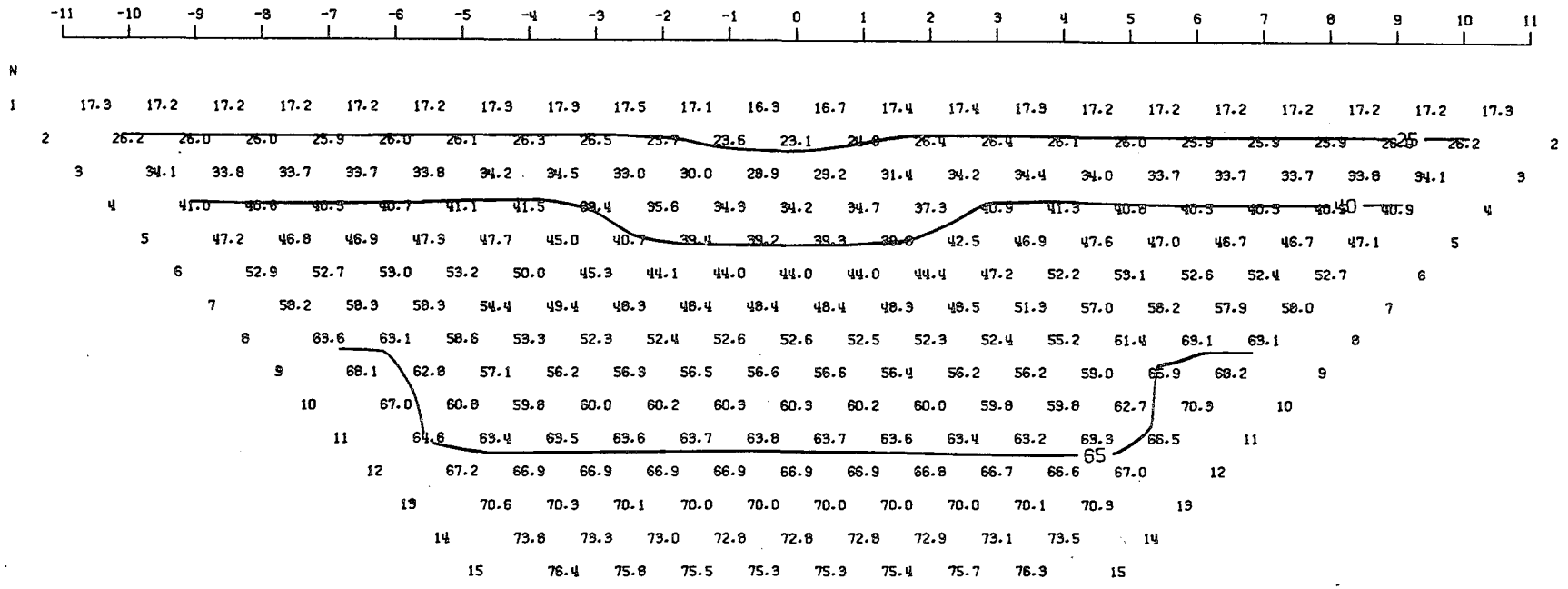

2-D RESISTIVITY MODEL -- CONDUCTIVE BODY WITH OVERBURDEN 3

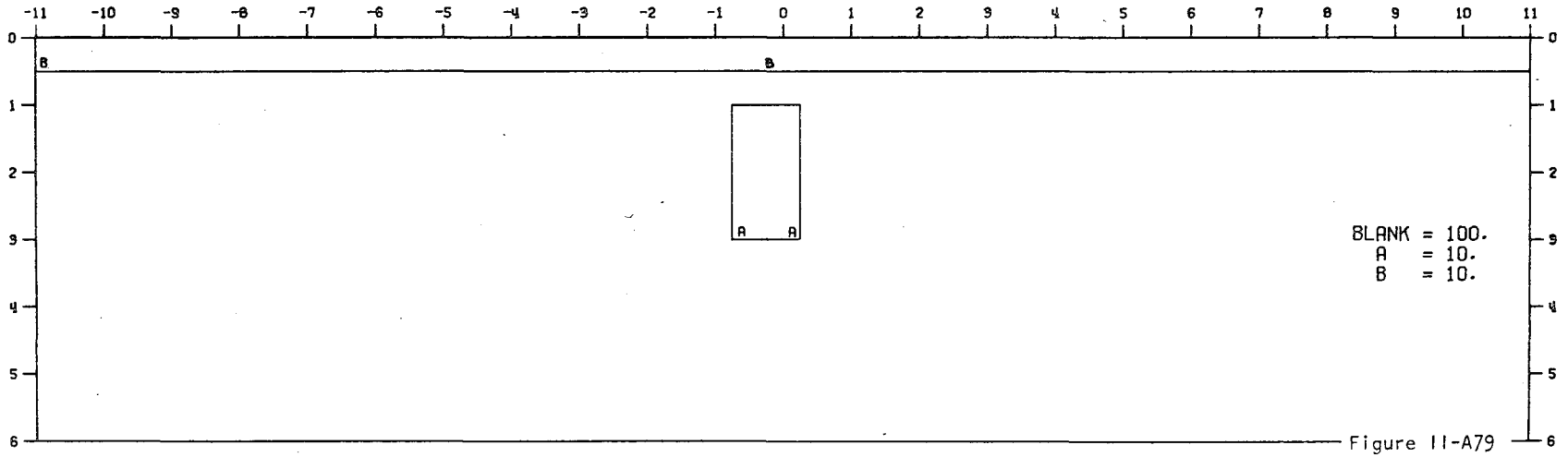

Figure II-A79

MODEL--CONDUCTIVE BODY WITH OVERBURDEN 3
SCHLUMBERGER APPARENT RESISTIVITY PSEUDO-SECTION
PROFILE LINE IS INCLINED AT 90.0 DEGREES TO STRIKE

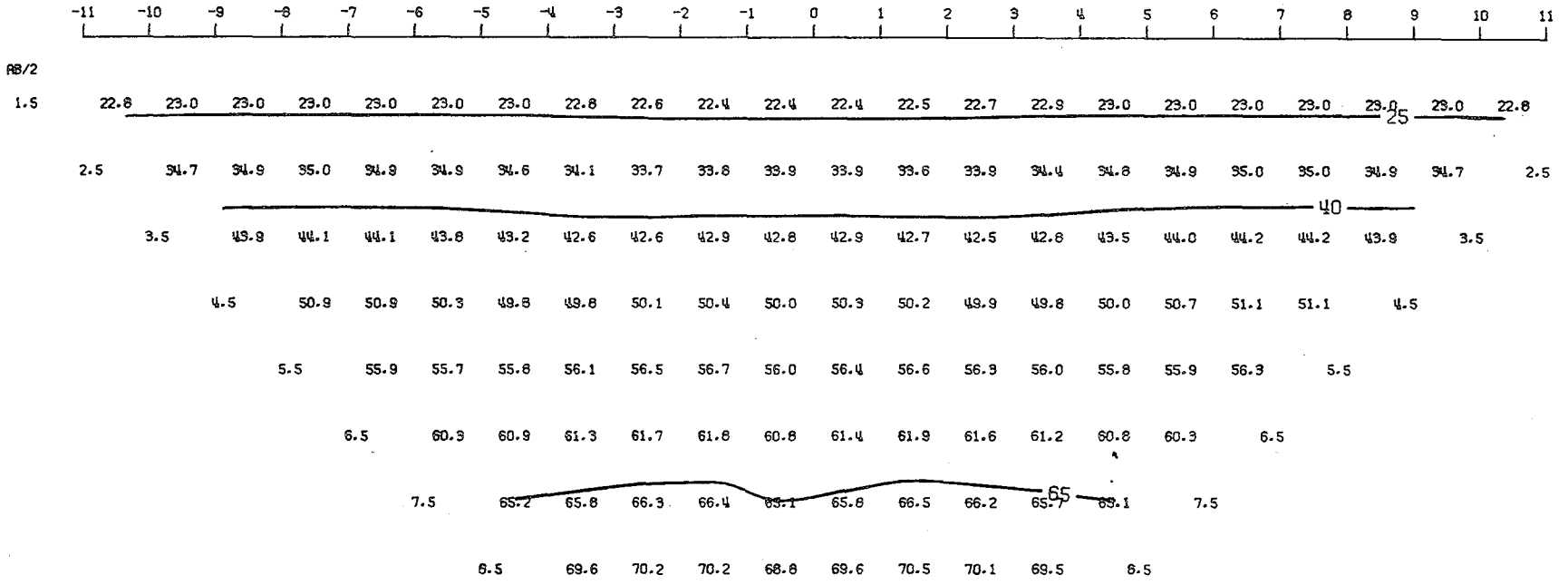

2-D RESISTIVITY MODEL -- CONDUCTIVE BODY WITH OVERBURDEN 3

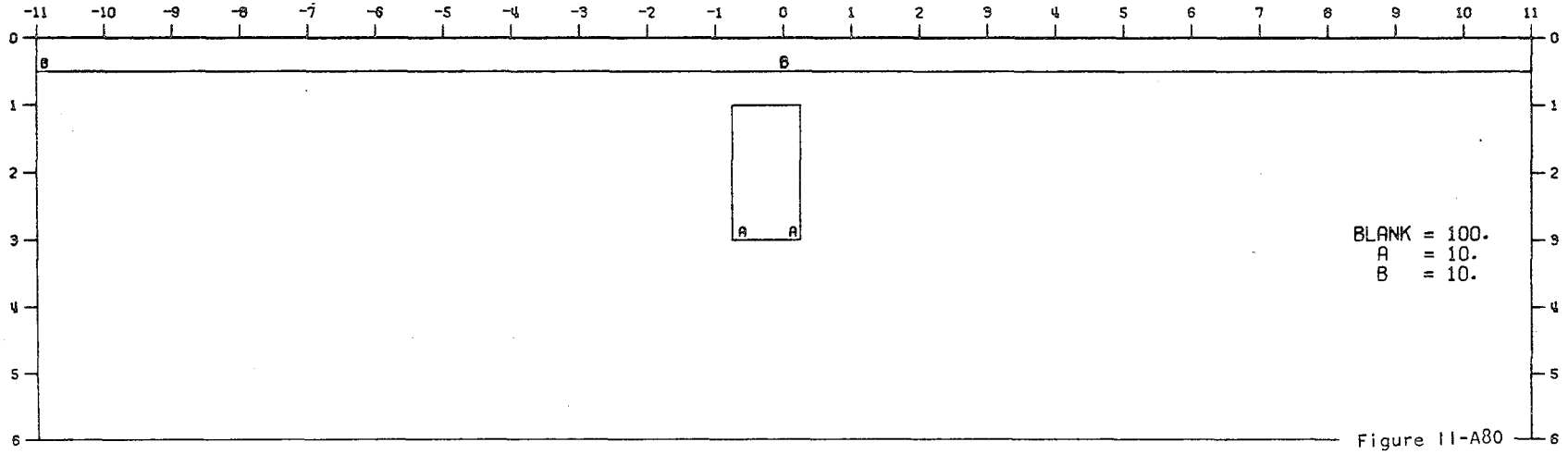

Figure II-A80

MODEL--CONDUCTIVE BODY WITH OVERBURDEN 5
DIPOLE-DIPOLE APPARENT RESISTIVITY PSEUDO-SECTION
PROFILE LINE IS INCLINED AT 90.0 DEGREES TO STRIKE

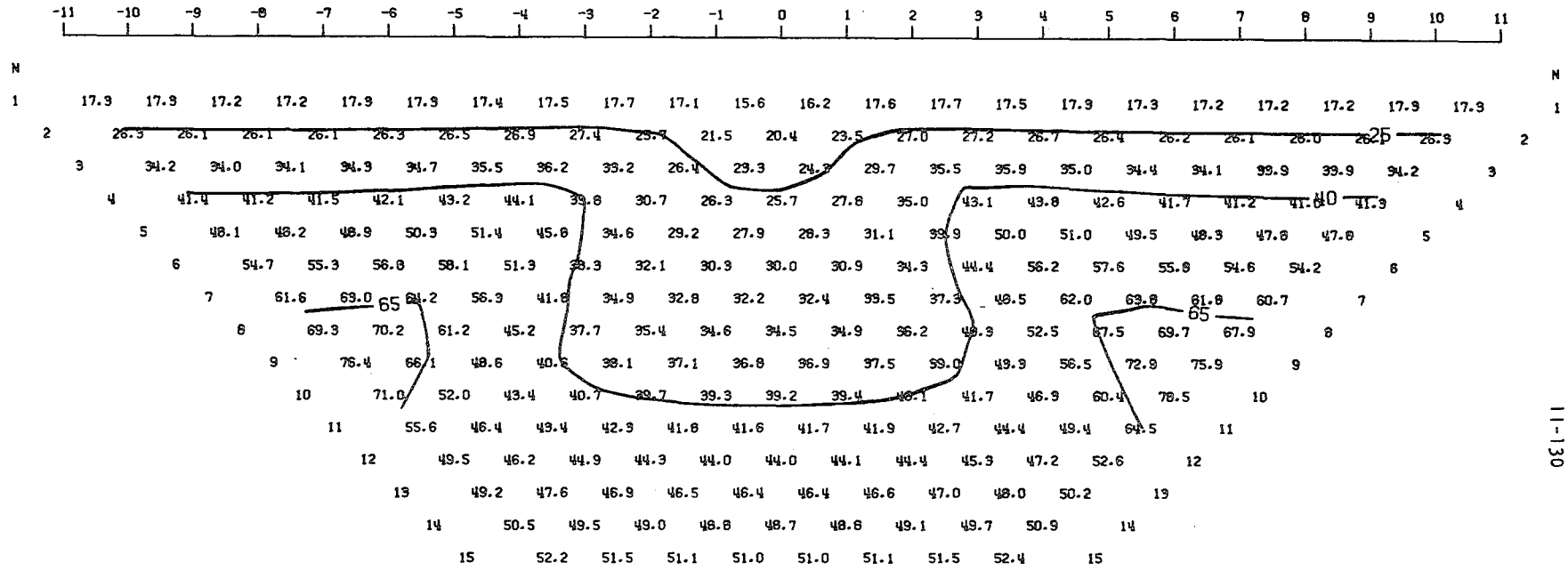

2-D RESISTIVITY MODEL -- CONDUCTIVE BODY WITH OVERBURDEN 5

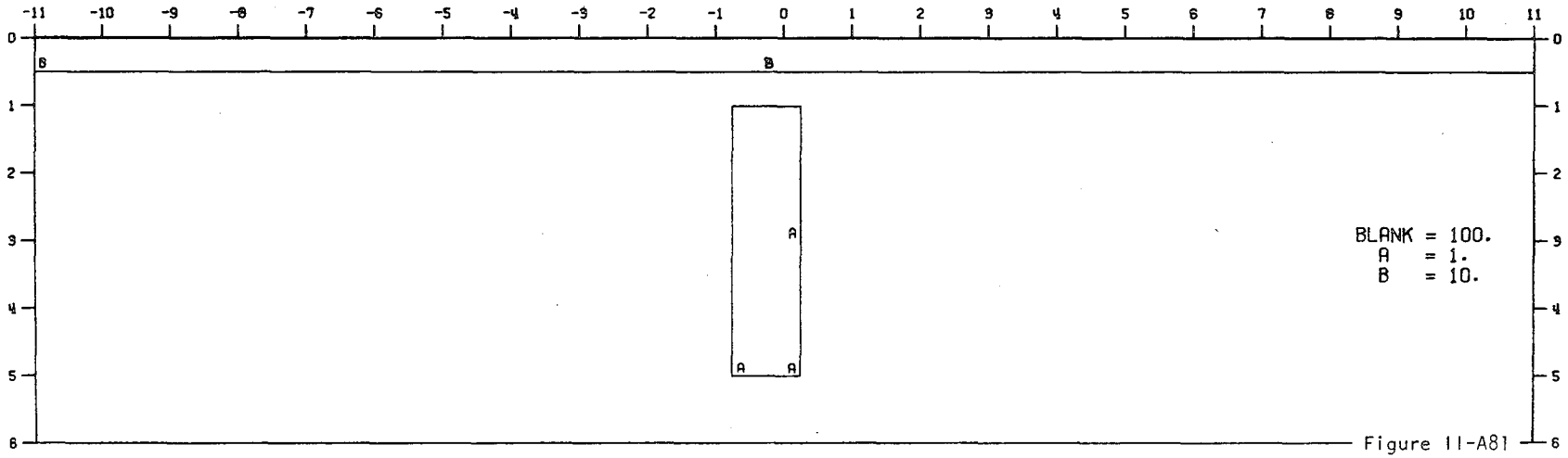

Figure II-A81

MODEL--CONDUCTIVE BODY WITH OVERBURDEN 5
SCHLUMBERGER APPARENT RESISTIVITY PSEUDO-SECTION
PROFILE LINE IS INCLINED AT 90.0 DEGREES TO STRIKE

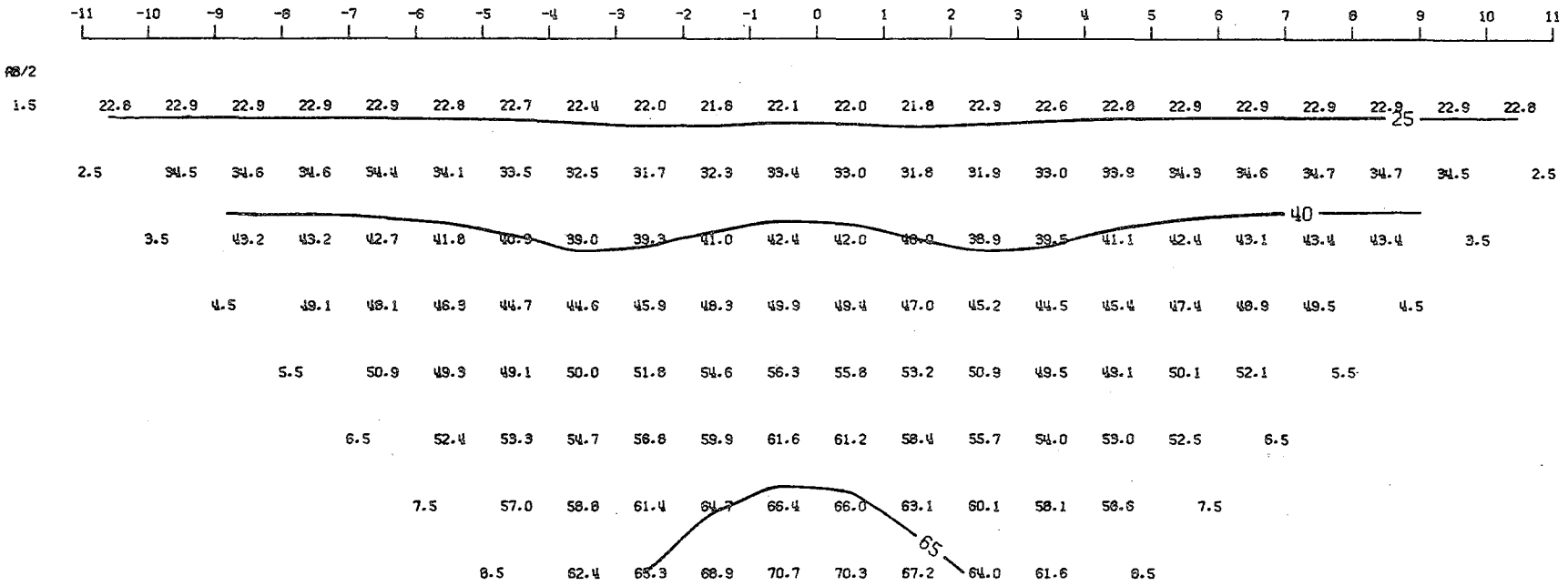

2-D RESISTIVITY MODEL -- CONDUCTIVE BODY WITH OVERBURDEN 5

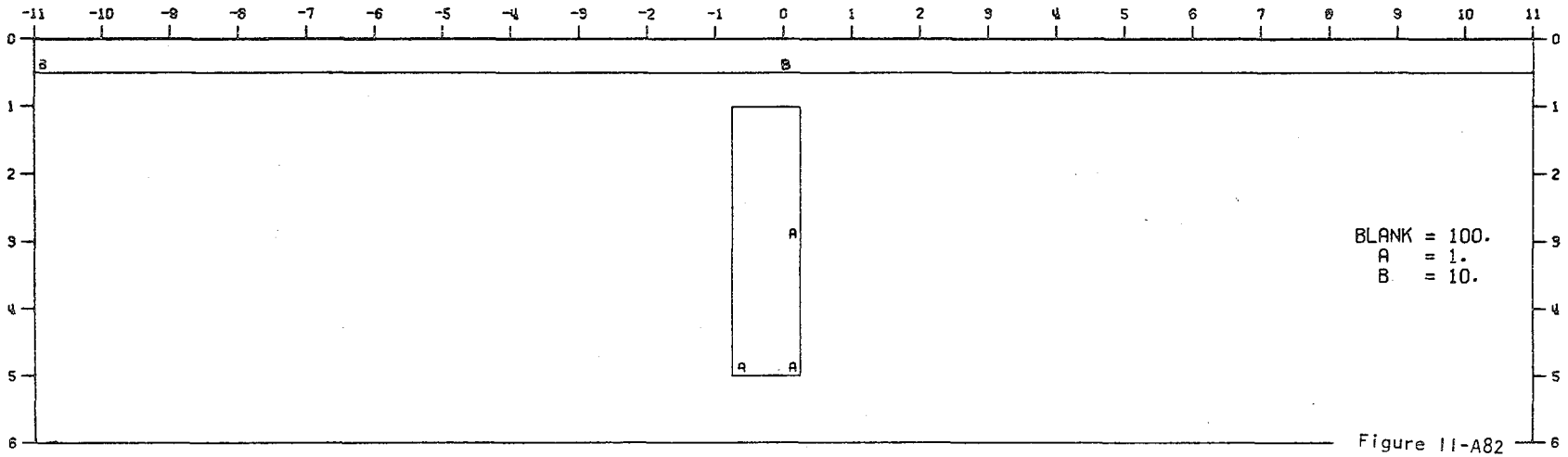

Figure II-A82

MODEL--CONDUCTIVE BODY WITH OVERBURDEN 6
DIPOLE-DIPOLE APPARENT RESISTIVITY PSEUDO-SECTION
PROFILE LINE IS INCLINED AT 90.0 DEGREES TO STRIKE

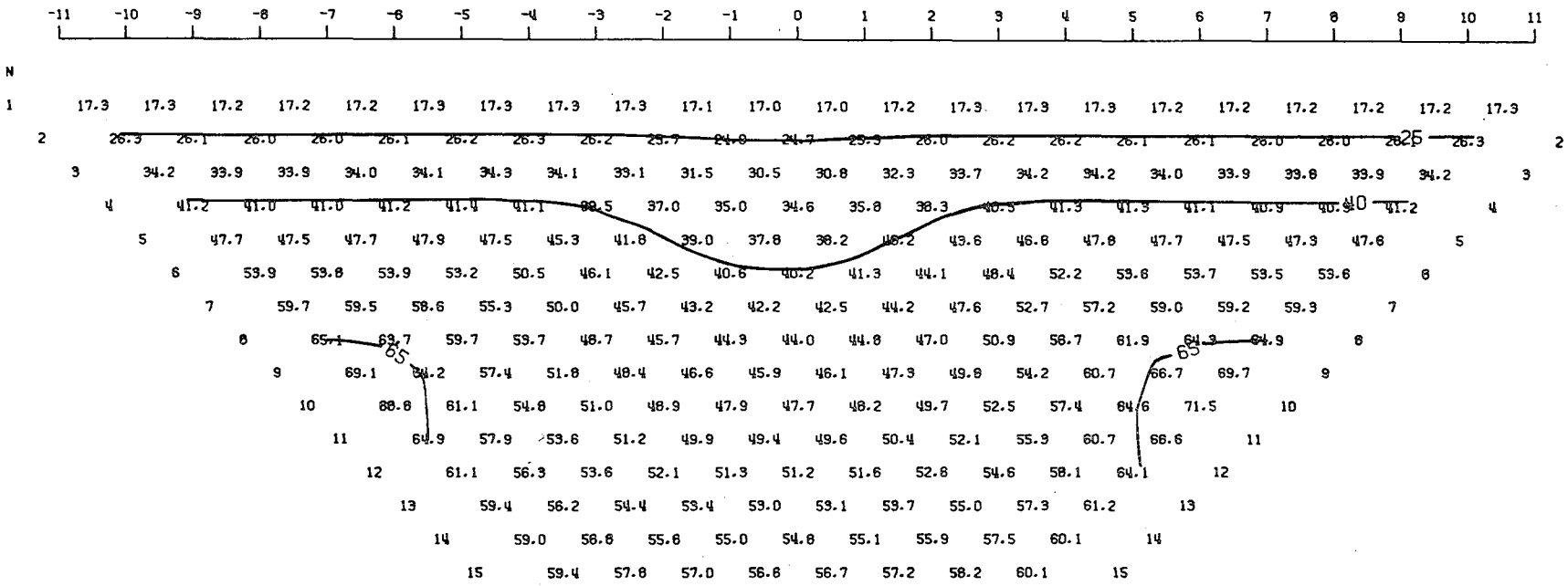

2-D RESISTIVITY MODEL -- CONDUCTIVE BODY WITH OVERBURDEN 6

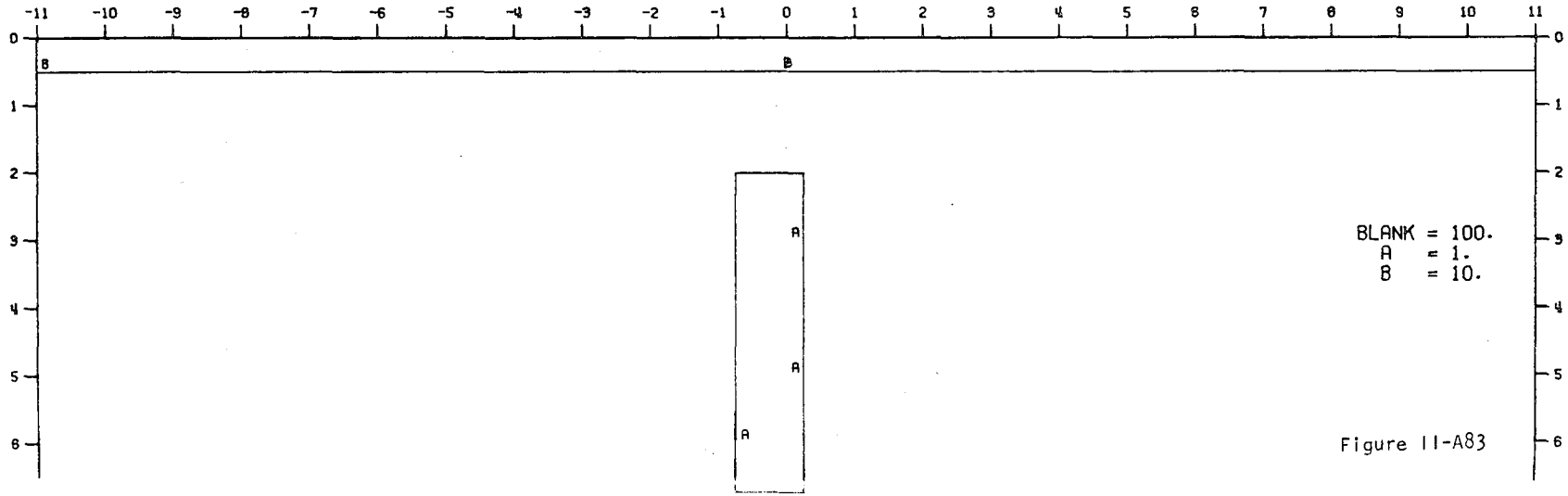

Figure II-A83

MODEL--CONDUCTIVE BODY WITH OVERBURDEN 6
SCHLUMBERGER APPARENT RESISTIVITY PSEUDO-SECTION
PROFILE LINE IS INCLINED AT 90.0 DEGREES TO STRIKE

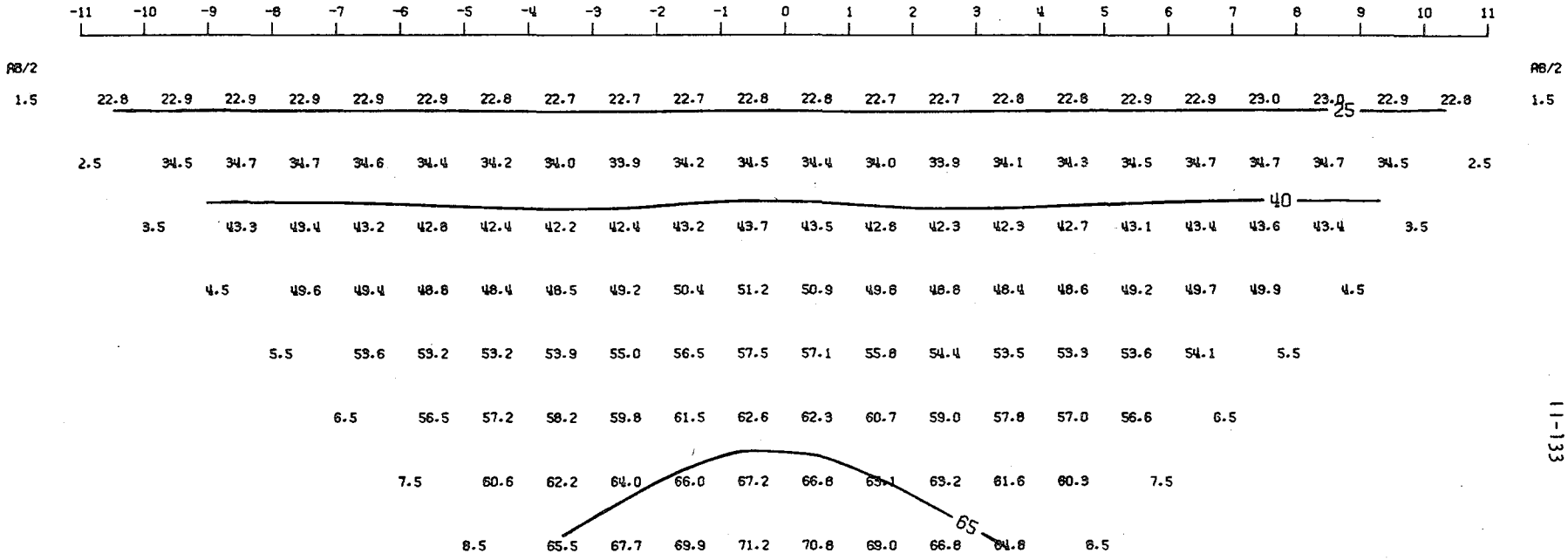

2-D RESISTIVITY MODEL -- CONDUCTIVE BODY WITH OVERBURDEN 6

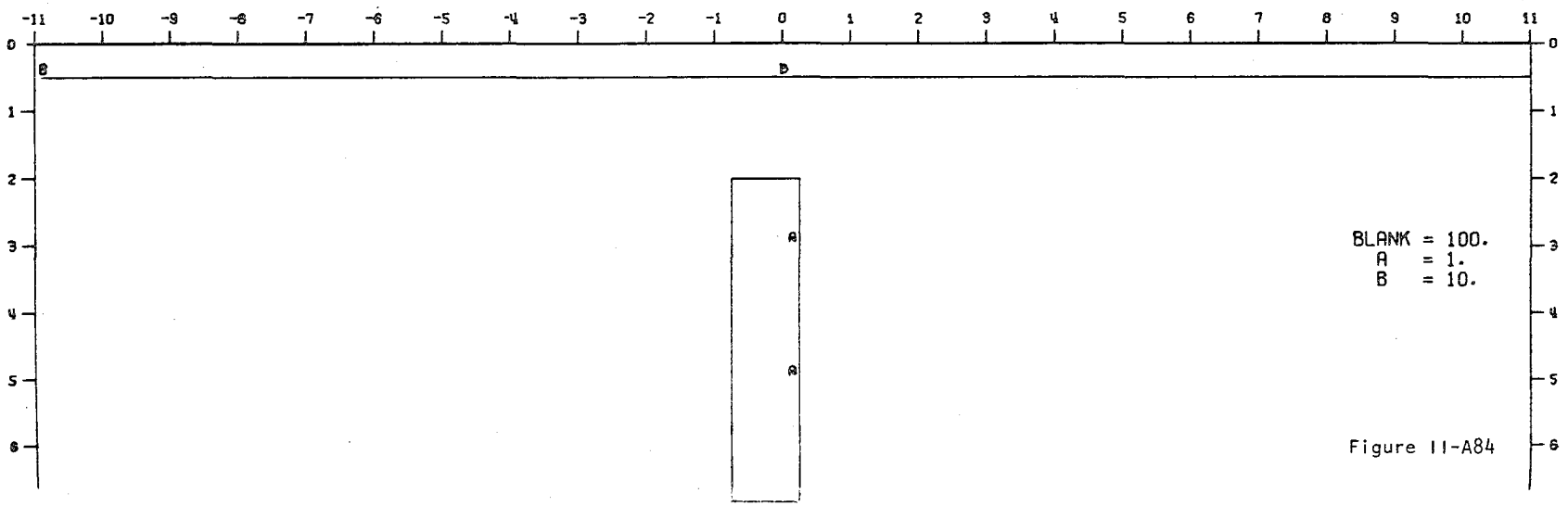

Figure II-A84

MODEL--CONDUCTIVE BODY WITH OVERBURDEN 7
DIPOLE-DIPOLE APPARENT RESISTIVITY PSEUDO-SECTION
PROFILE LINE IS INCLINED AT 90.0 DECREES TO STRIKE

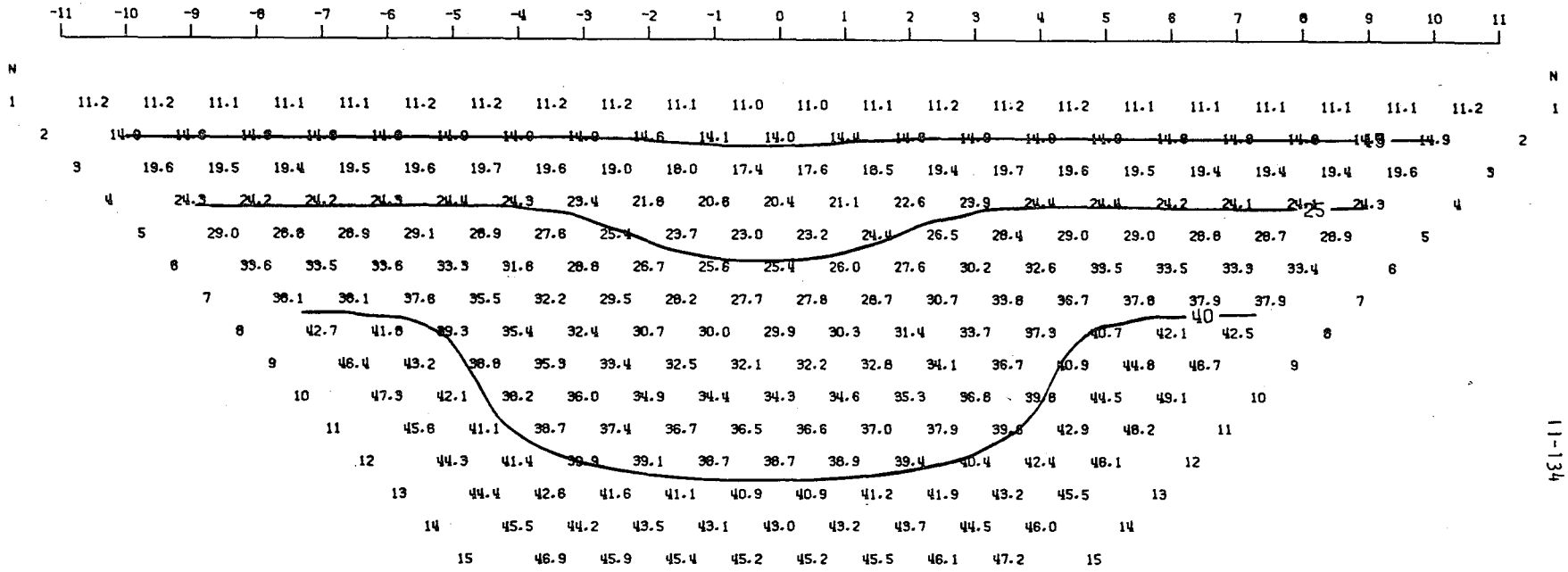

2-D RESISTIVITY MODEL -- CONDUCTIVE BODY WITH OVERBURDEN 7

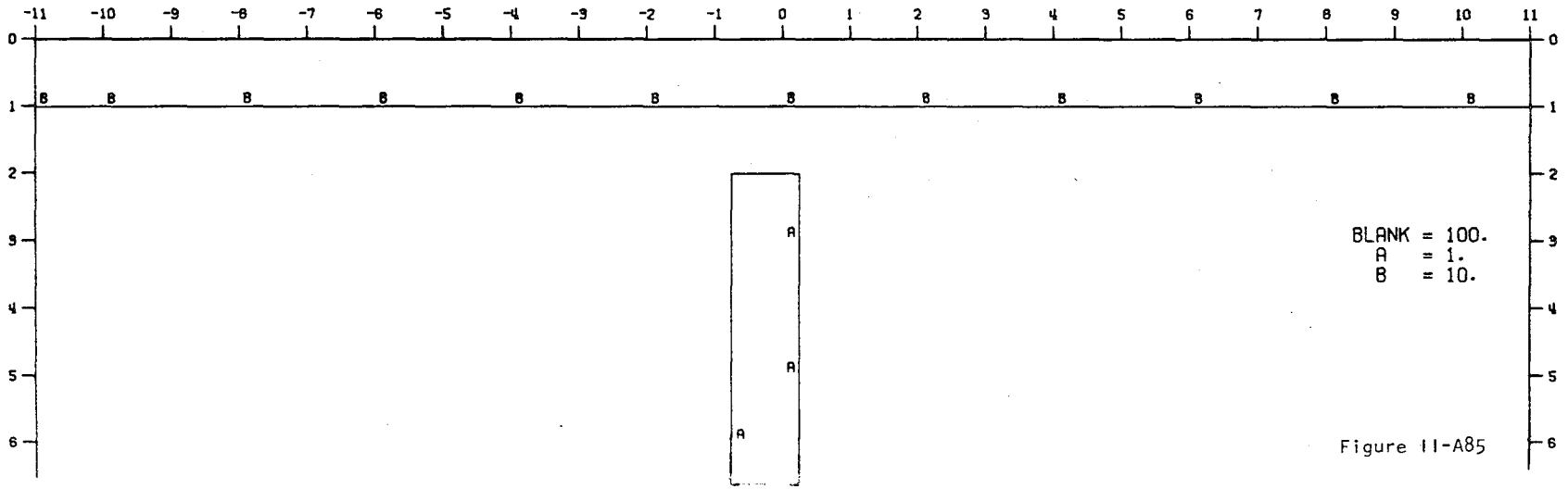

Figure II-A85

MODEL--CONDUCTIVE BODY WITH OVERBURDEN 7
SCHLUMBERGER APPARENT RESISTIVITY PSEUDO-SECTION
PROFILE LINE IS INCLINED AT 90.0 DEGREES TO STRIKE

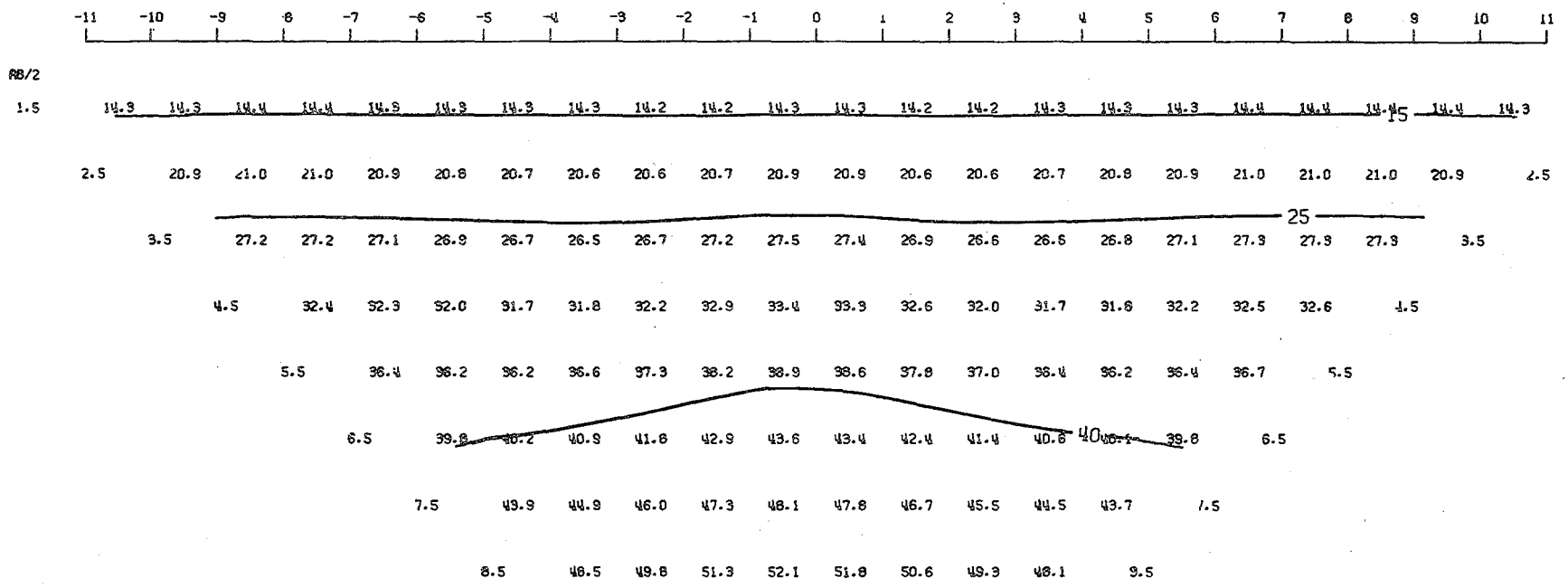

2-D RESISTIVITY MODEL -- CONDUCTIVE BODY WITH OVERBURDEN 7

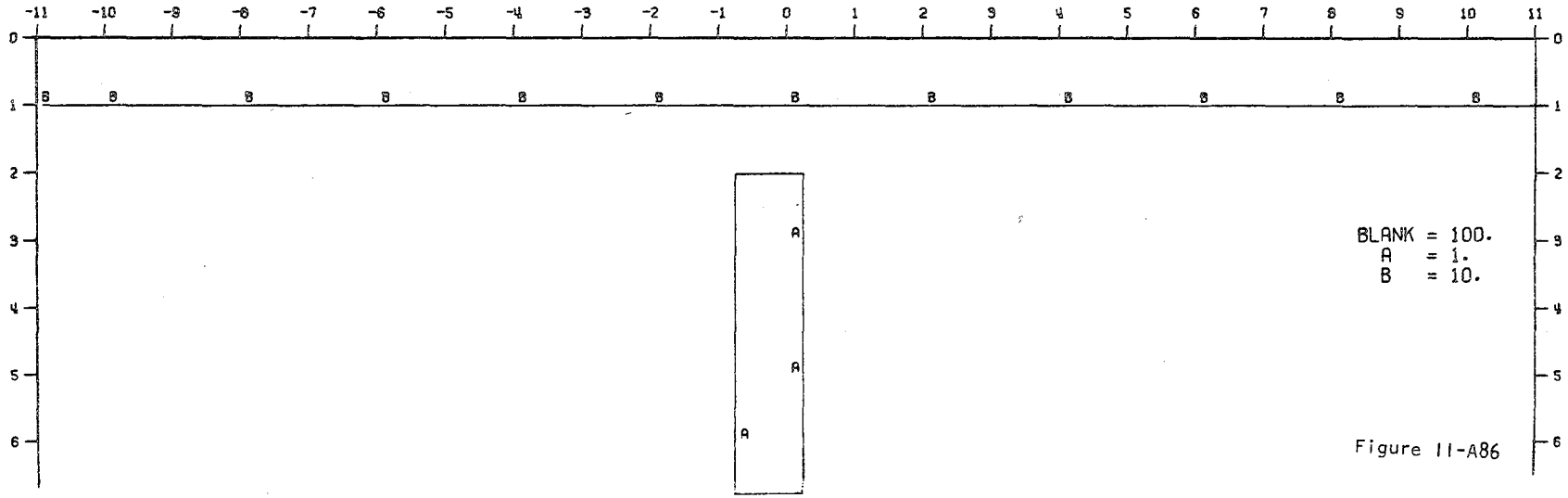

Figure 11-A86

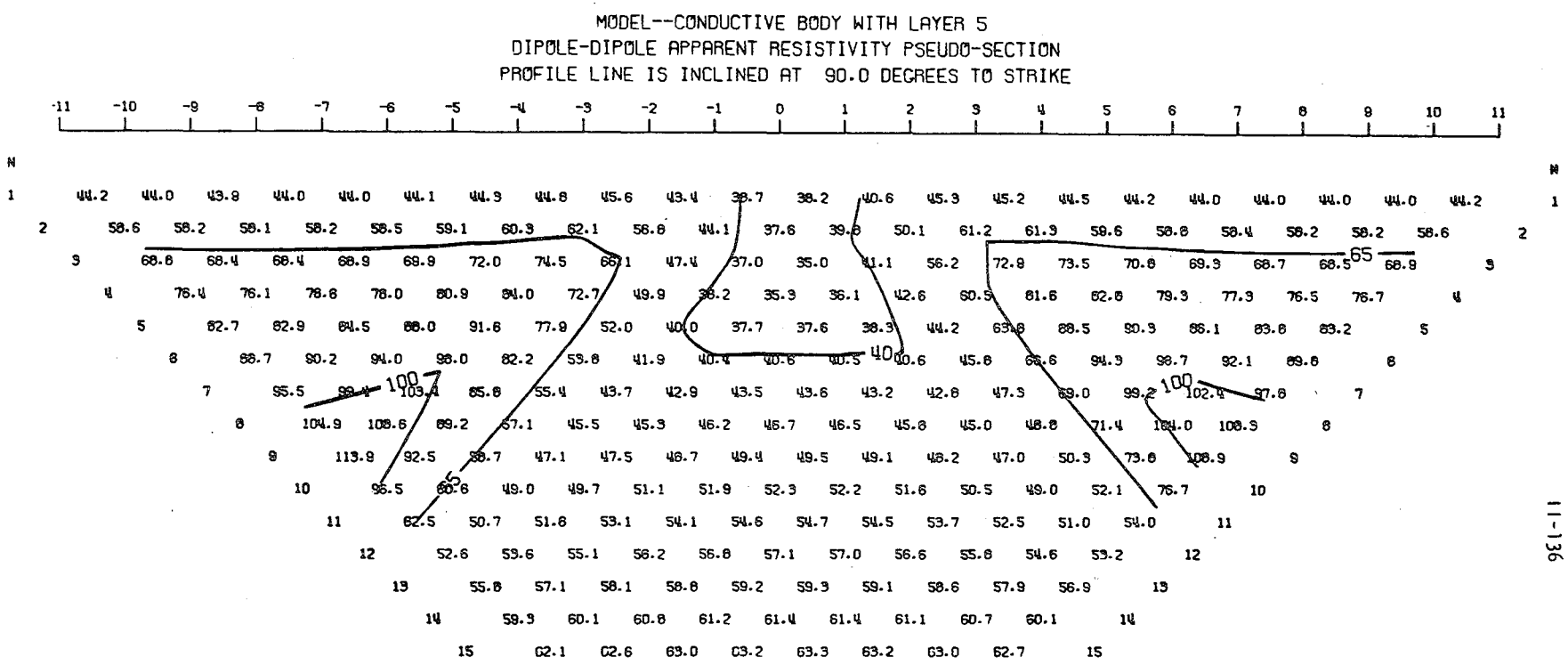

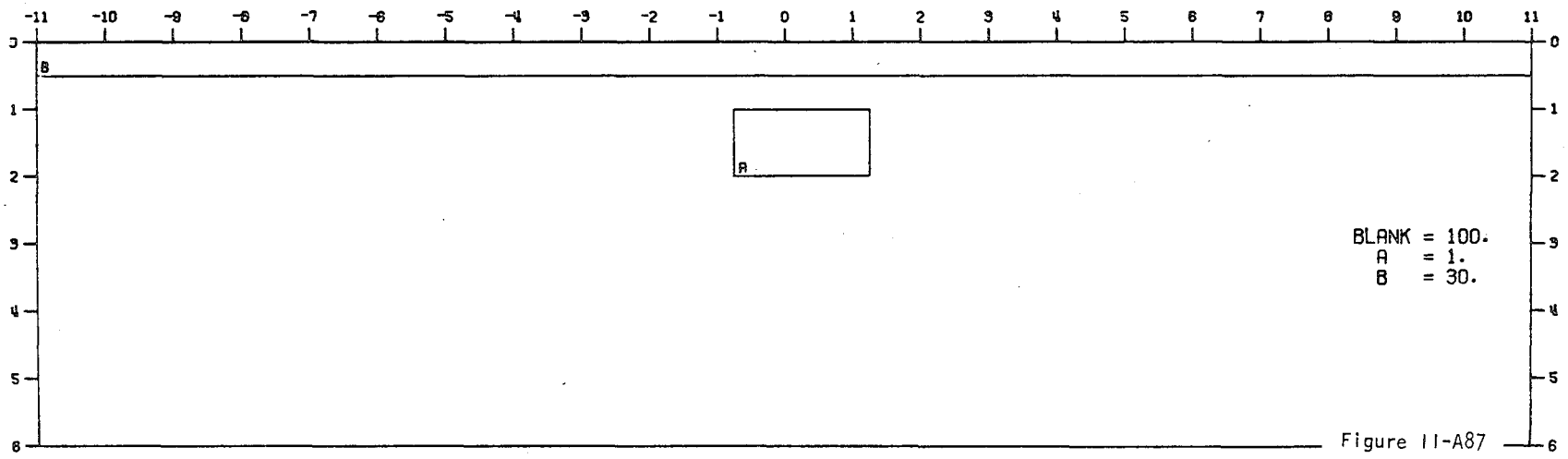

Figure II-A87

MODEL--CONDUCTIVE BODY WITH LAYER 5
SCHLUMBERGER APPARENT RESISTIVITY PSEUDO-SECTION
PROFILE LINE IS INCLINED AT 90.0 DEGREES TO STRIKE

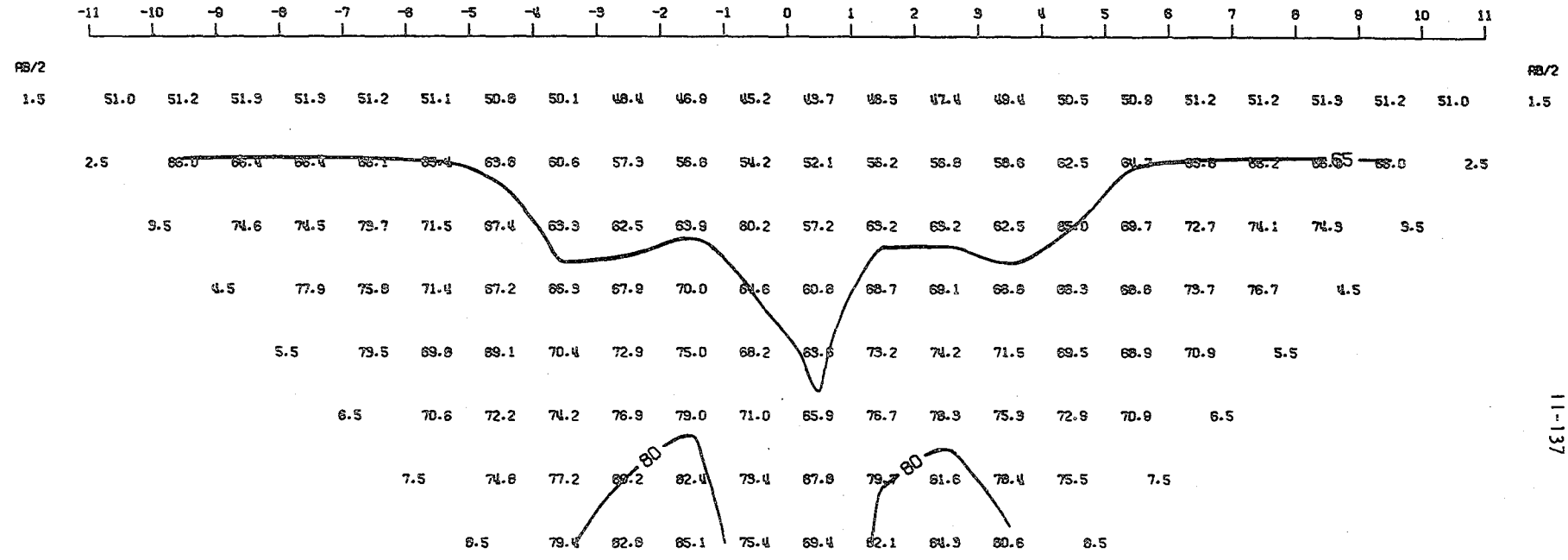

2-D RESISTIVITY MODEL -- CONDUCTIVE BODY WITH LAYER 5

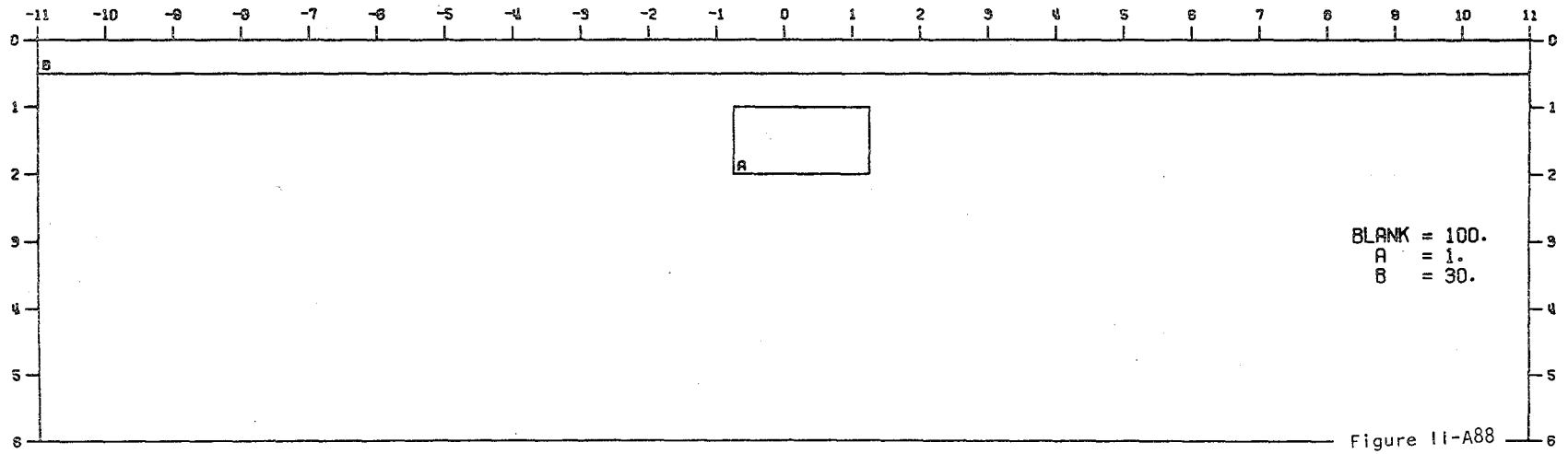

Figure II-A88

MODEL--CONDUCTIVE BODY WITH LAYER 6
DIPOLE-DIPOLE APPARENT RESISTIVITY PSEUDO-SECTION
PROFILE LINE IS INCLINED AT 90.0 DEGREES TO STRIKE

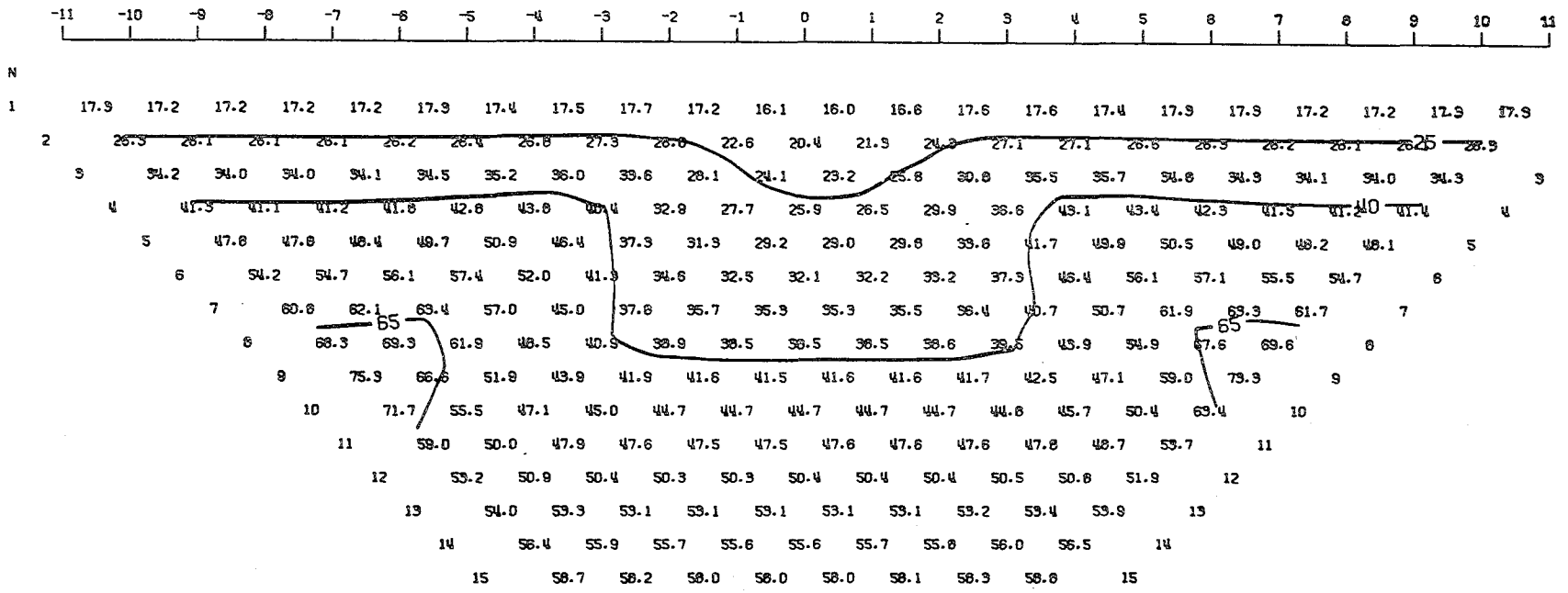

2-D RESISTIVITY MODEL -- CONDUCTIVE BODY WITH LAYER 6

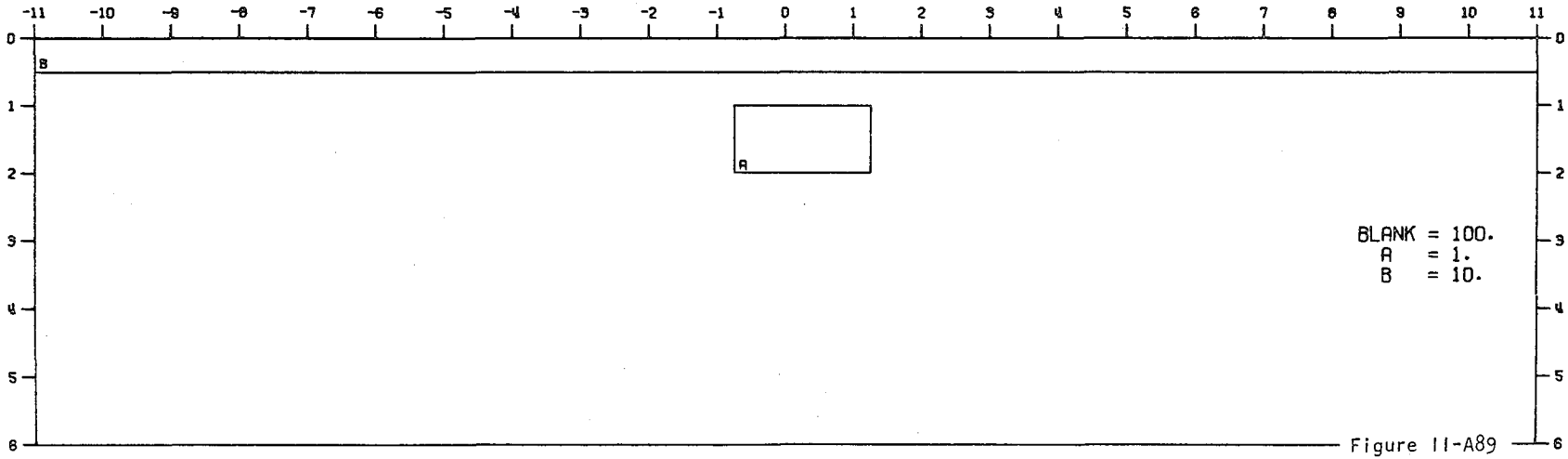

Figure II-A89

MODEL--CONDUCTIVE BODY WITH LAYER 6
SCHLUMBERGER APPARENT RESISTIVITY PSEUDO-SECTION
PROFILE LINE IS INCLINED AT 90.0 DEGREES TO STRIKE

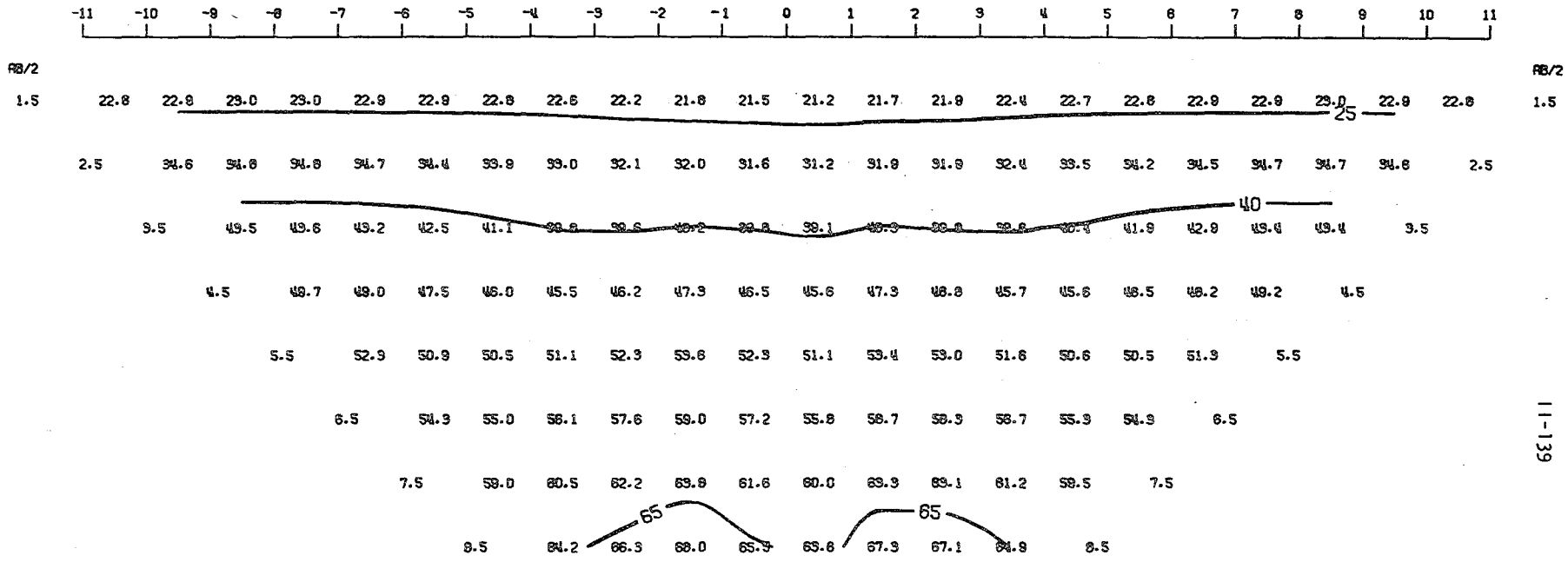

2-D RESISTIVITY MODEL -- CONDUCTIVE BODY WITH LAYER 6

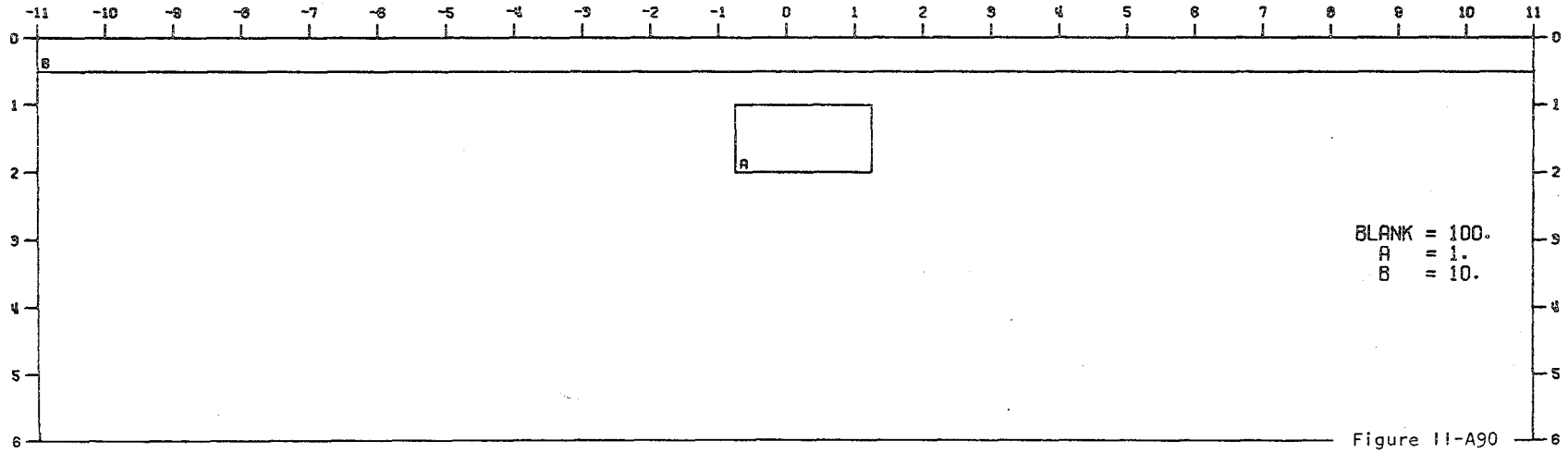

Figure II-A90

MODEL--CONDUCTIVE BODY WITH LAYER 7
DIPOLE-DIPOLE APPARENT RESISTIVITY PSEUDO-SECTION
PROFILE LINE IS INCLINED AT 90.0 DEGREES TO STRIKE

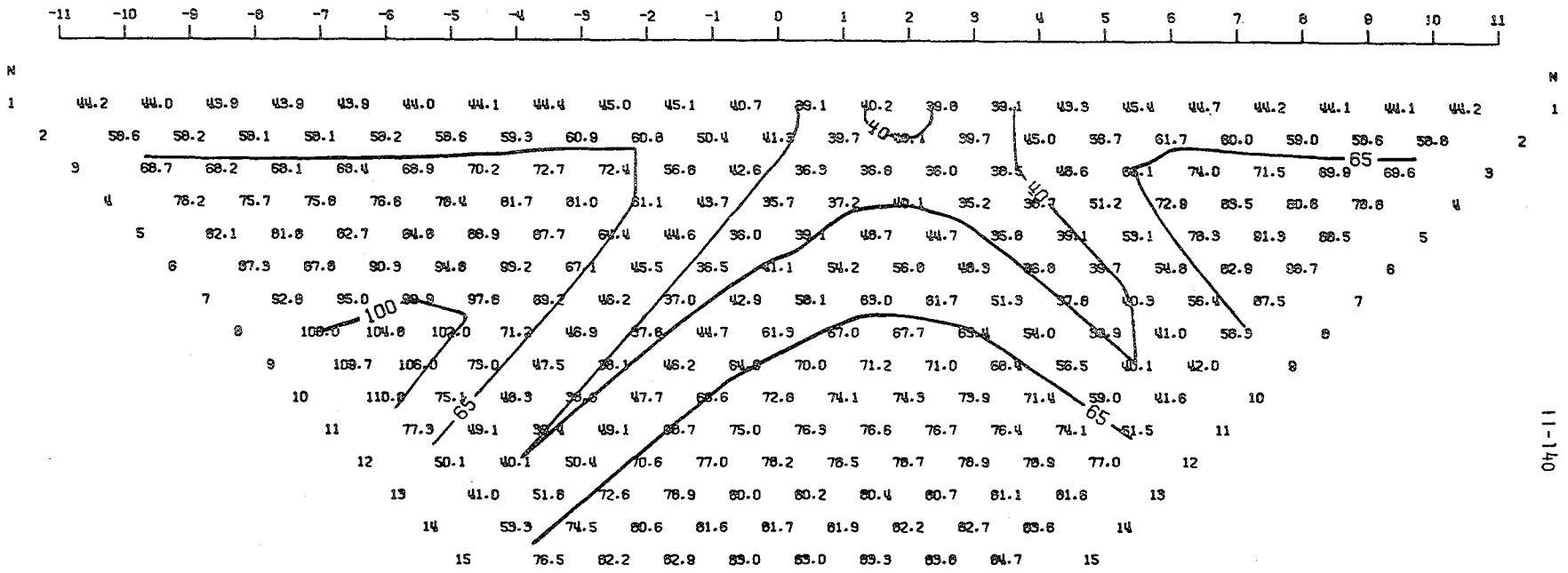

2-D RESISTIVITY MODEL -- CONDUCTIVE BODY WITH LAYER 7

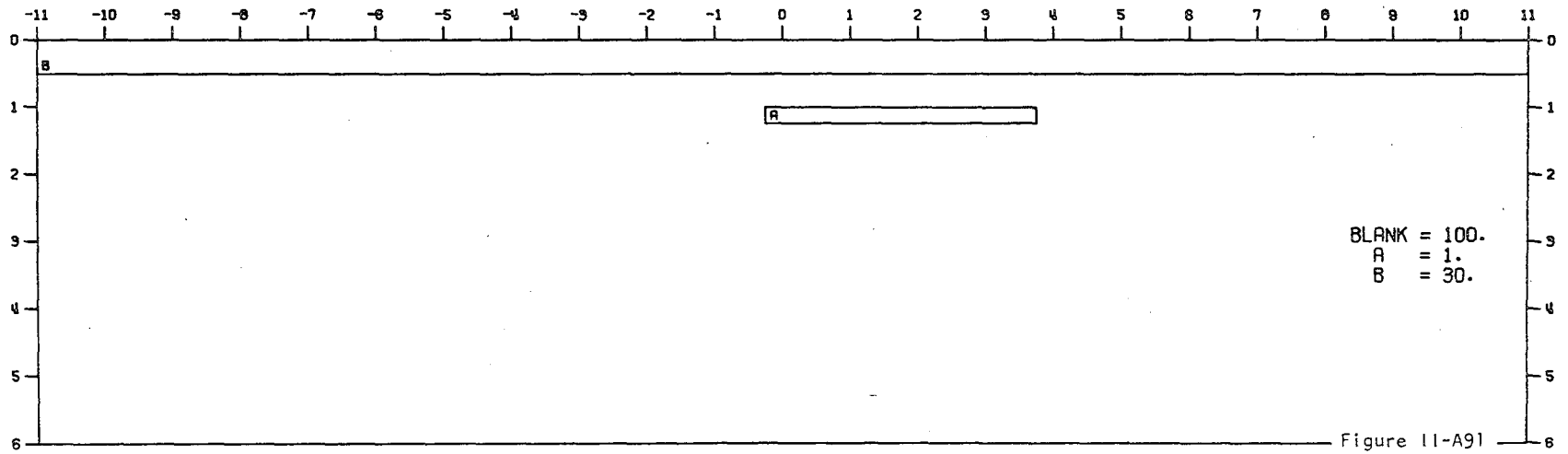

Figure II-A91

MODEL--CONDUCTIVE BODY WITH LAYER 7
SCHLUMBERGER APPARENT RESISTIVITY PSEUDO-SECTION
PROFILE LINE IS INCLINED AT 90.0 DEGREES TO STRIKE

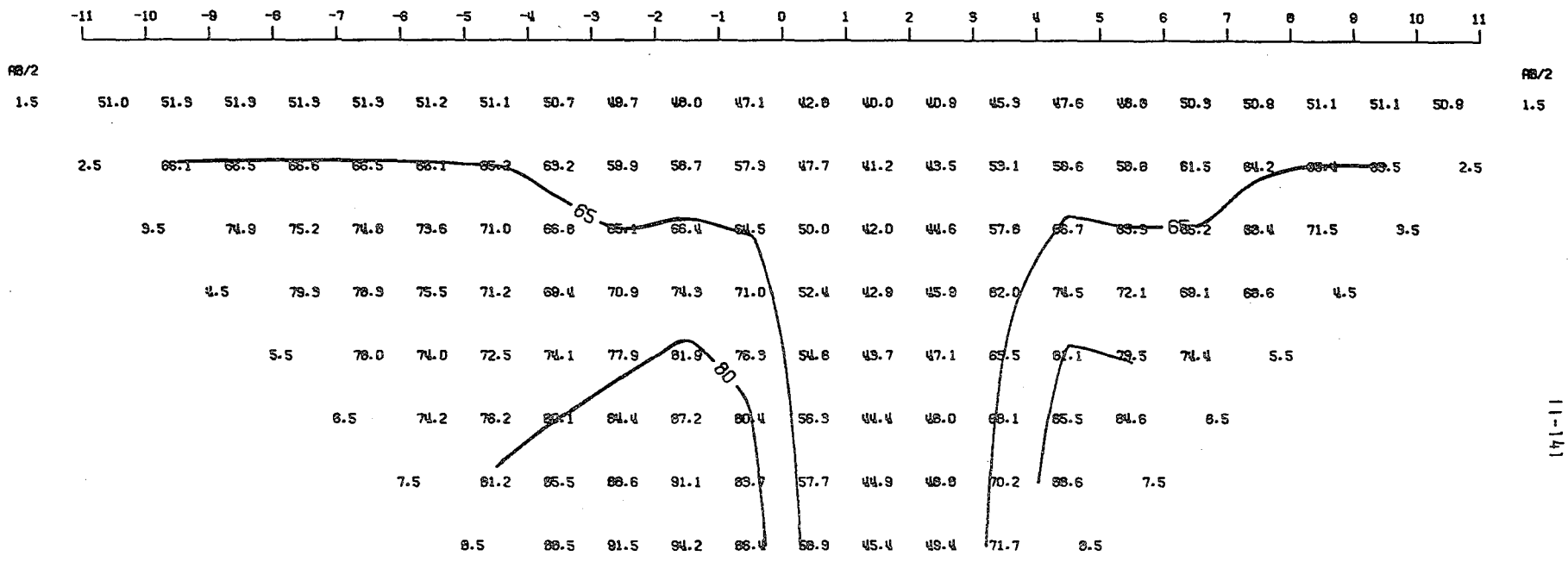

2-D RESISTIVITY MODEL -- CONDUCTIVE BODY WITH LAYER 7

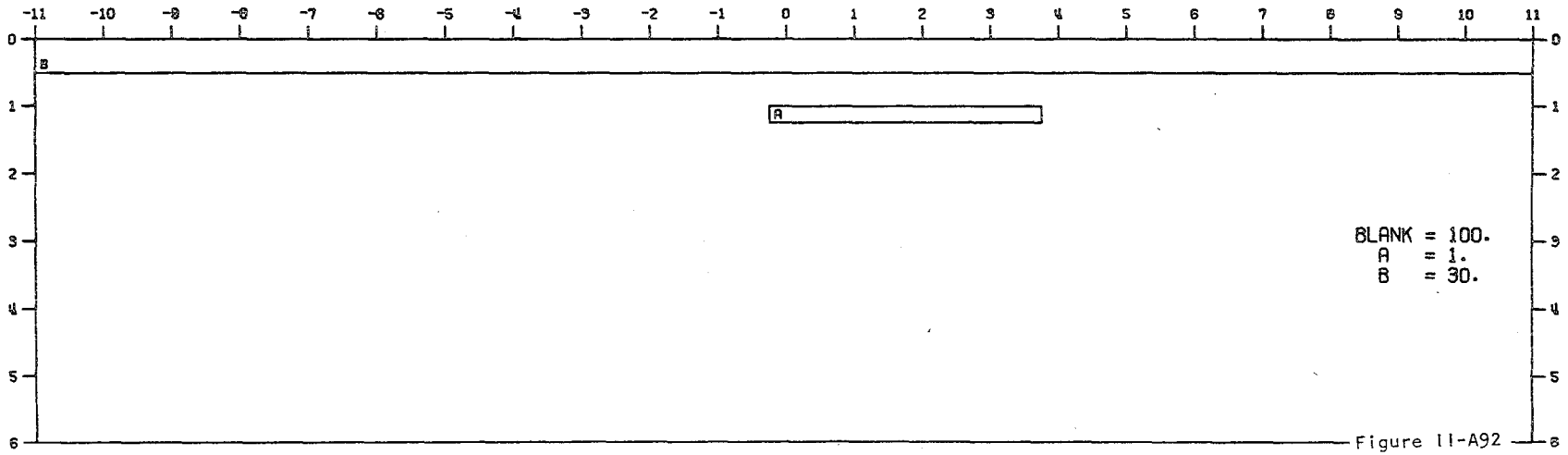

Figure II-A92

MODEL--CONDUCTIVE BODY WITH LAYER 8
DIPOLE-DIPOLE APPARENT RESISTIVITY PSEUDO-SECTION
PROFILE LINE IS INCLINED AT 90.0 DEGREES TO STRIKE

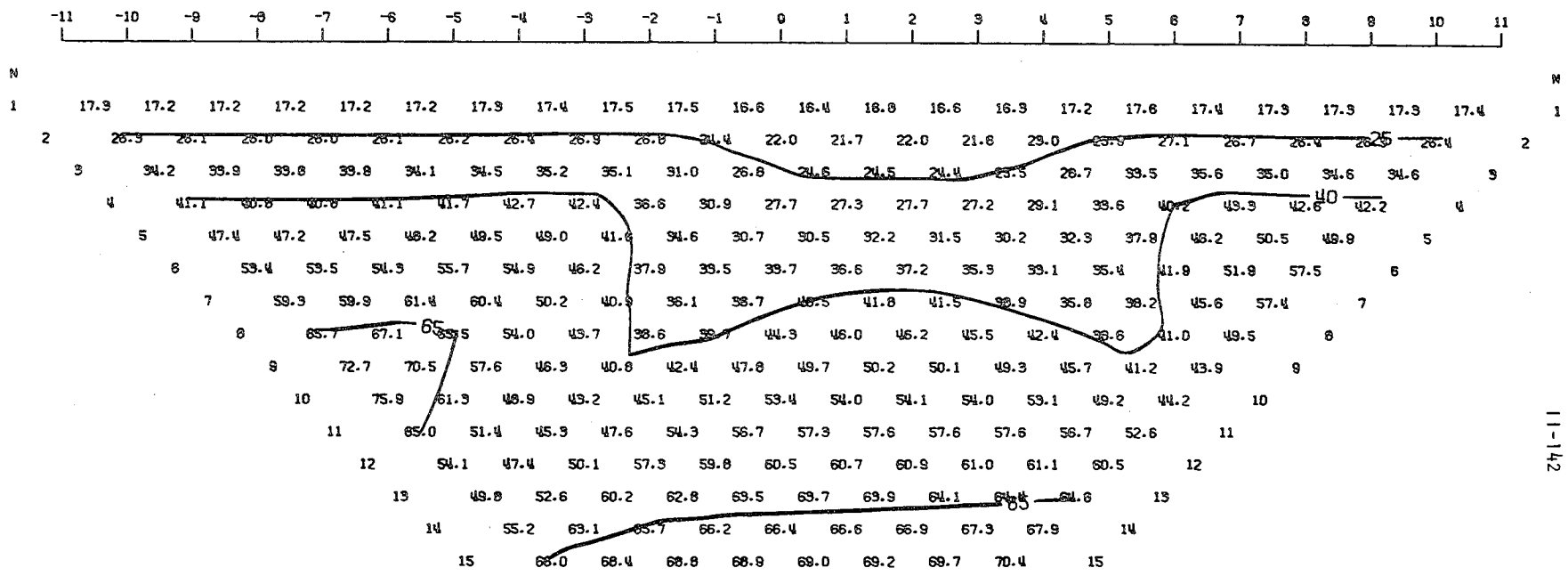

2-D RESISTIVITY MODEL -- CONDUCTIVE BODY WITH LAYER 8

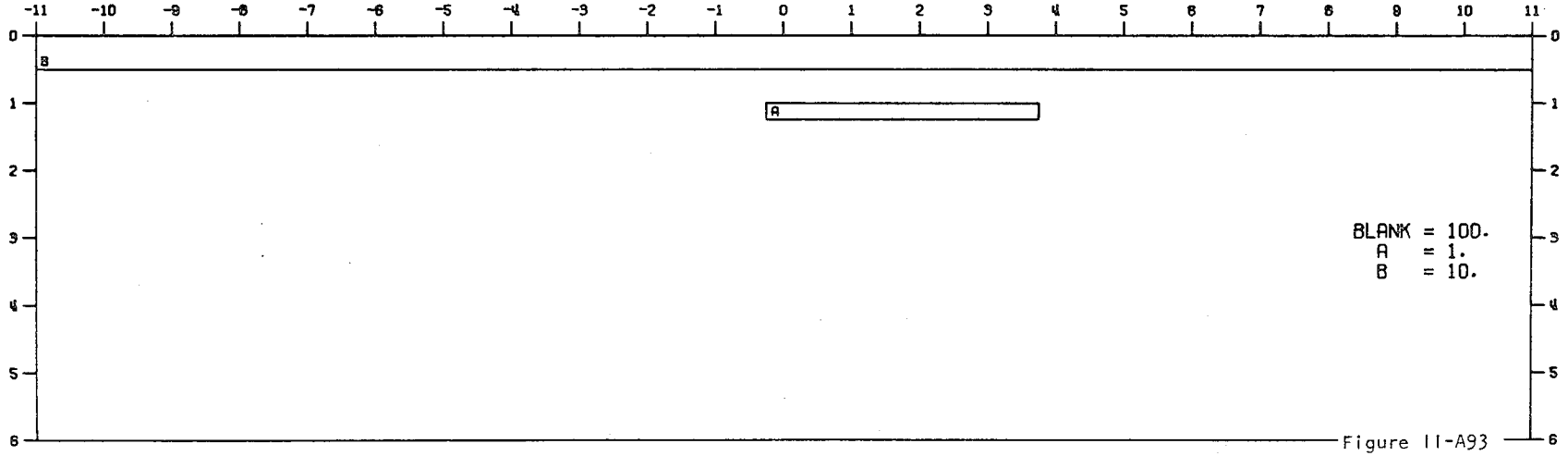

Figure II-A93

MODEL--CONDUCTIVE BODY WITH LAYER 8
SCHLUMBERGER APPARENT RESISTIVITY PSEUDO-SECTION
PROFILE LINE IS INCLINED AT 90.0 DEGREES TO STRIKE

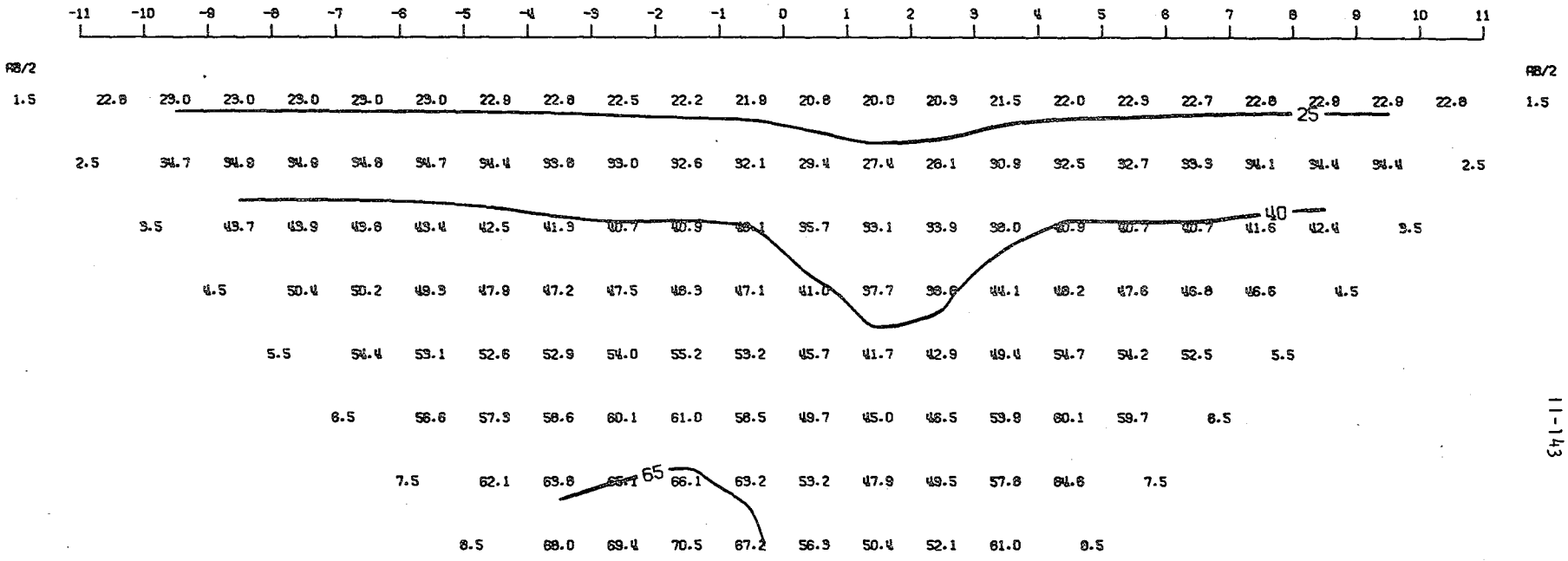

2-D RESISTIVITY MODEL -- CONDUCTIVE BODY WITH LAYER 8

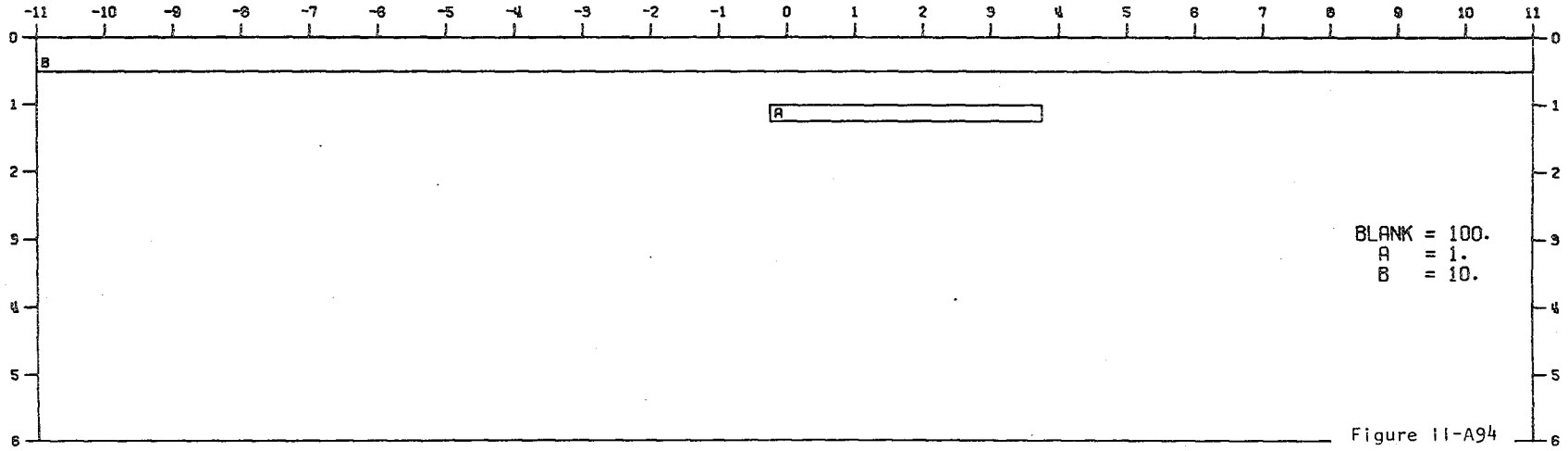

Figure II-A94

MODEL--CONDUCTIVE BODY WITH OVERBURDEN 9
DIPOLE-DIPOLE APPARENT RESISTIVITY PSEUDO-SECTION
PROFILE LINE IS INCLINED AT 90.0 DEGREES TO STRIKE

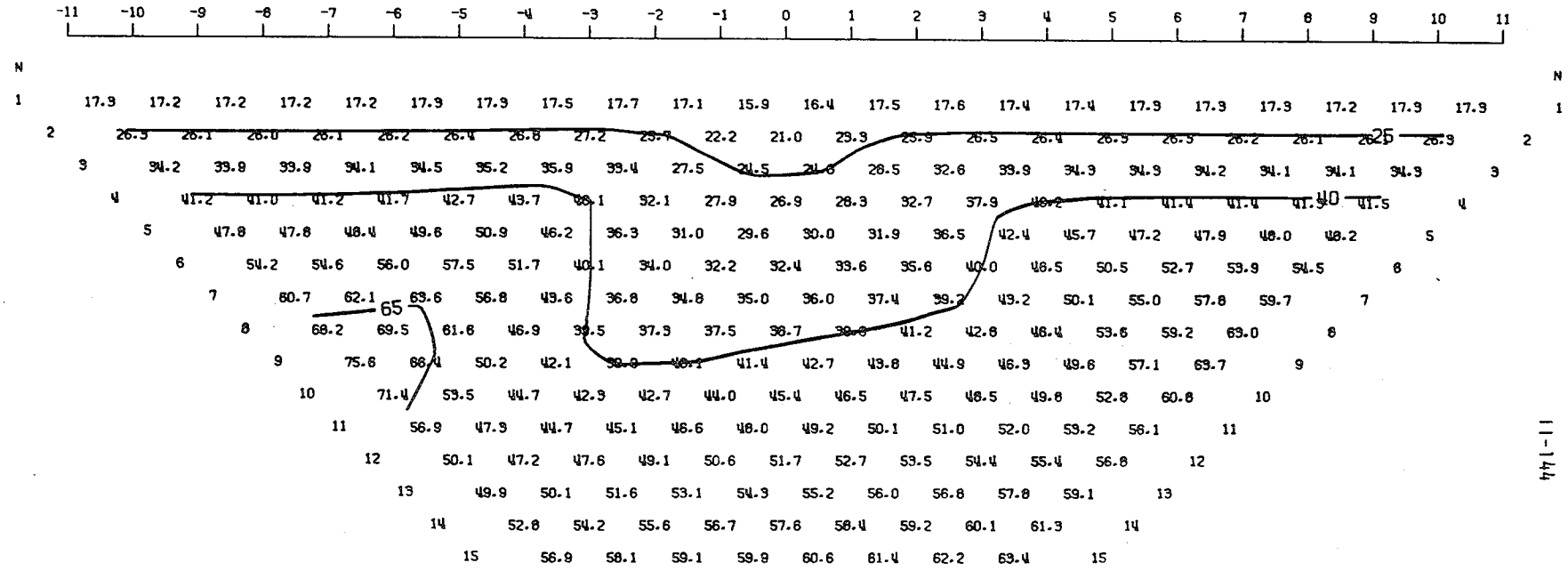

2-D RESISTIVITY MODEL -- CONDUCTIVE BODY WITH OVERBURDEN 8

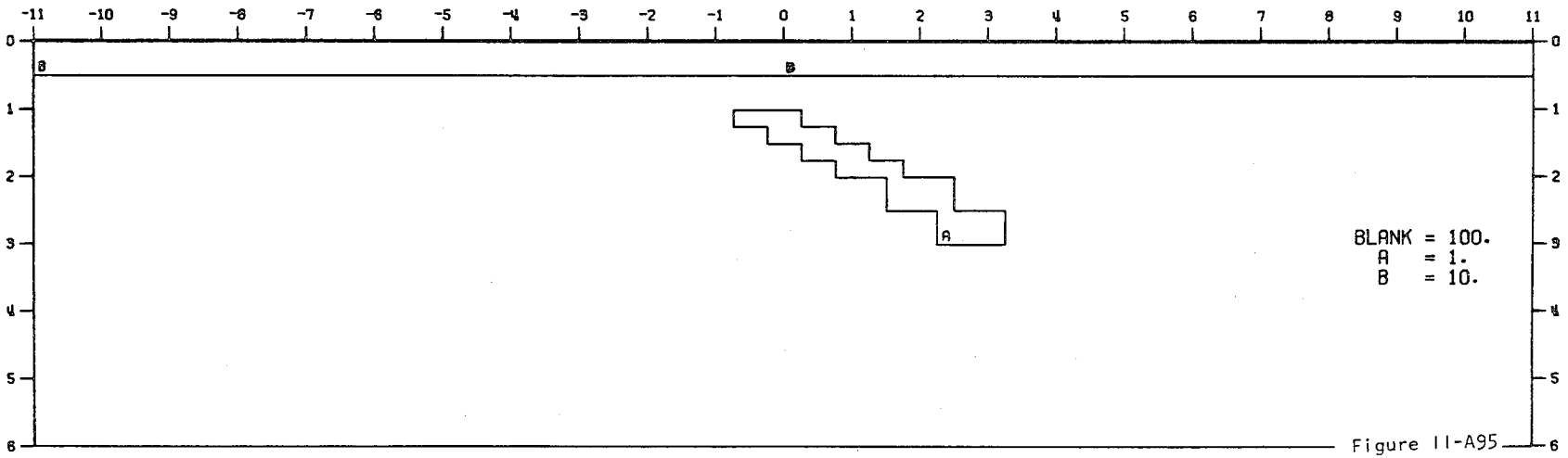

Figure II-A95

MODEL--CONDUCTIVE BODY WITH OVERBURDEN 9
SCHLUMBERGER APPARENT RESISTIVITY PSEUDO-SECTION
PROFILE LINE IS INCLINED AT 90.0 DEGREES TO STRIKE

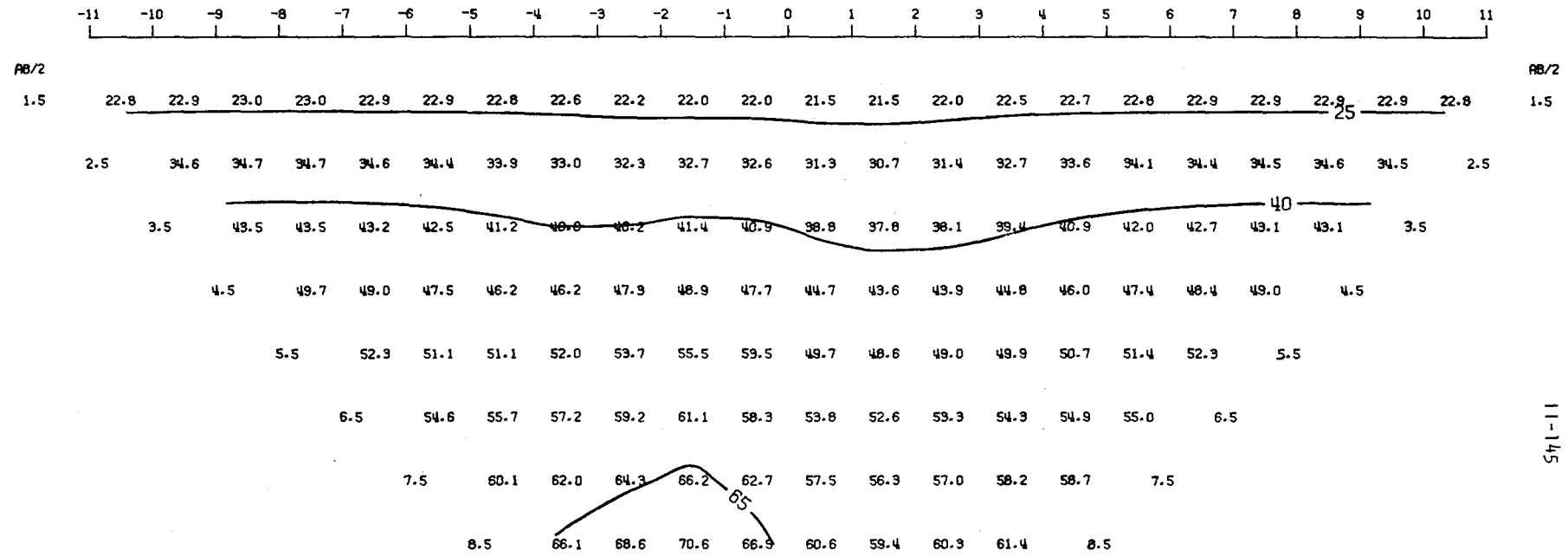

2-D RESISTIVITY MODEL -- CONDUCTIVE BODY WITH OVERBURDEN 8

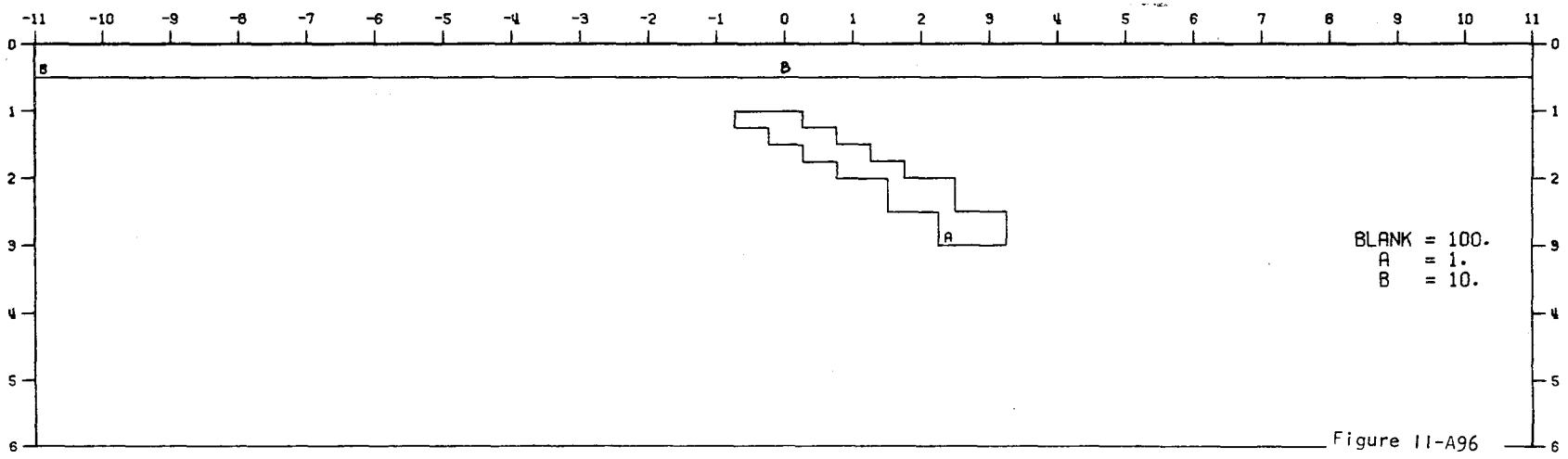

Figure II-A96

MODEL--TWO BODIES WITH OVERBURDEN 1
DIPOLE-DIPOLE APPARENT RESISTIVITY PSEUDO-SECTION
PROFILE LINE IS INCLINED AT 90.0 DEGREES TO STRIKE

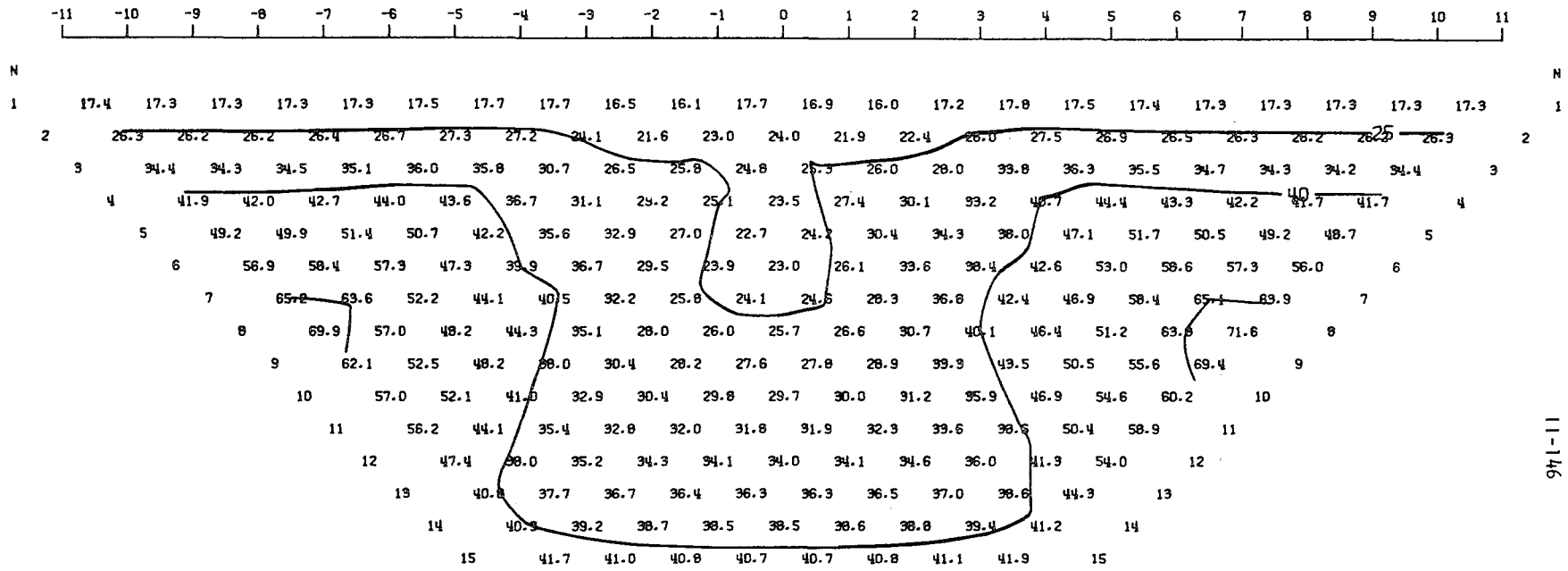

2-D RESISTIVITY MODEL -- TWO BODIES WITH OVERBURDEN 1

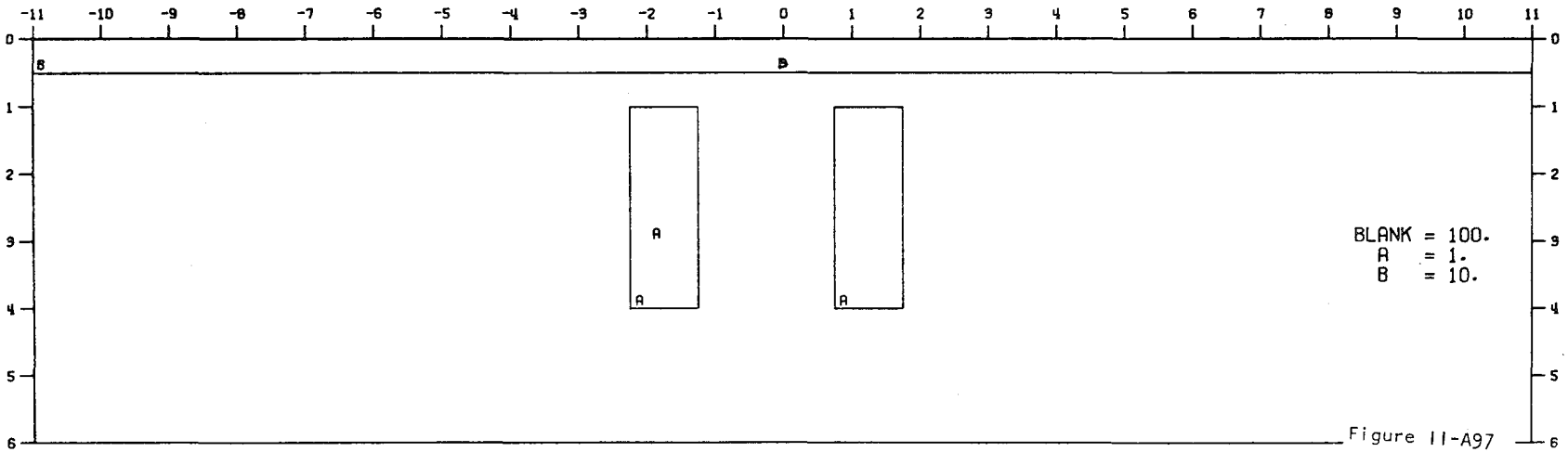

Figure II-A97

MODEL--TWO BODIES WITH OVERBURDEN 1
SCHLUMBERGER APPARENT RESISTIVITY PSEUDO-SECTION
PROFILE LINE IS INCLINED AT 90.0 DEGREES TO STRIKE

AB/2	-11	-10	-9	-8	-7	-6	-5	-4	-3	-2	-1	0	1	2	3	4	5	6	7	8	9	10	11	AB/2
1.5	22.8	22.9	22.9	22.8	22.7	22.6	22.2	21.8	21.8	21.5	20.5	20.9	21.7	21.7	22.0	22.4	22.7	22.8	22.9	22.9	22.9	22.8		1.5
2.5		34.3	34.4	34.2	33.8	33.0	31.8	31.4	31.8	30.4	28.6	29.3	31.4	31.6	31.4	32.4	33.4	34.0	34.4	34.5	34.4			2.5
3.5		42.6	42.1	41.0	39.3	38.3	38.5	38.6	36.9	35.6	36.1	37.9	38.7	38.3	38.7	40.2	41.7	42.5	42.8					3.5
4.5		46.7	44.9	43.7	43.4	43.6	44.2	43.0	41.9	42.3	43.7	44.0	43.5	43.5	44.2	46.0	47.7							4.5
5.5			47.8	47.4	47.2	48.9	49.7	48.6	47.7	48.1	49.9	49.2	47.7	47.4	47.8	48.5								5.5
6.5				49.8	50.7	52.8	54.6	53.5	52.8	53.1	54.2	54.0	51.7	50.3	50.1									6.5
7.5					54.3	57.0	59.0	58.1	57.6	57.8	58.8	58.5	55.8	53.5										7.5
8.5						60.6	63.0	62.2	61.9	62.1	62.8	62.4	59.3											8.5

25

40

2-D RESISTIVITY MODEL -- TWO BODIES WITH OVERBURDEN 1

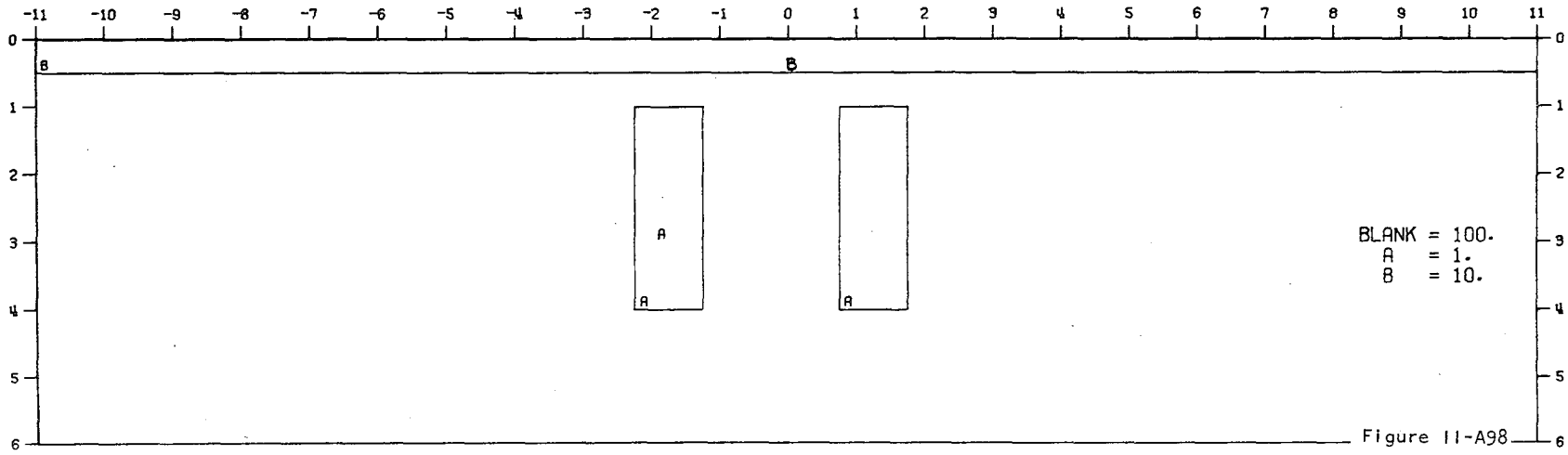

Figure 11-A98

MODEL--TWO BODIES WITH OVERBURDEN 2
DIPOLE-DIPOLE APPARENT RESISTIVITY PSEUDO-SECTION
PROFILE LINE IS INCLINED AT 90.0 DEGREES TO STRIKE

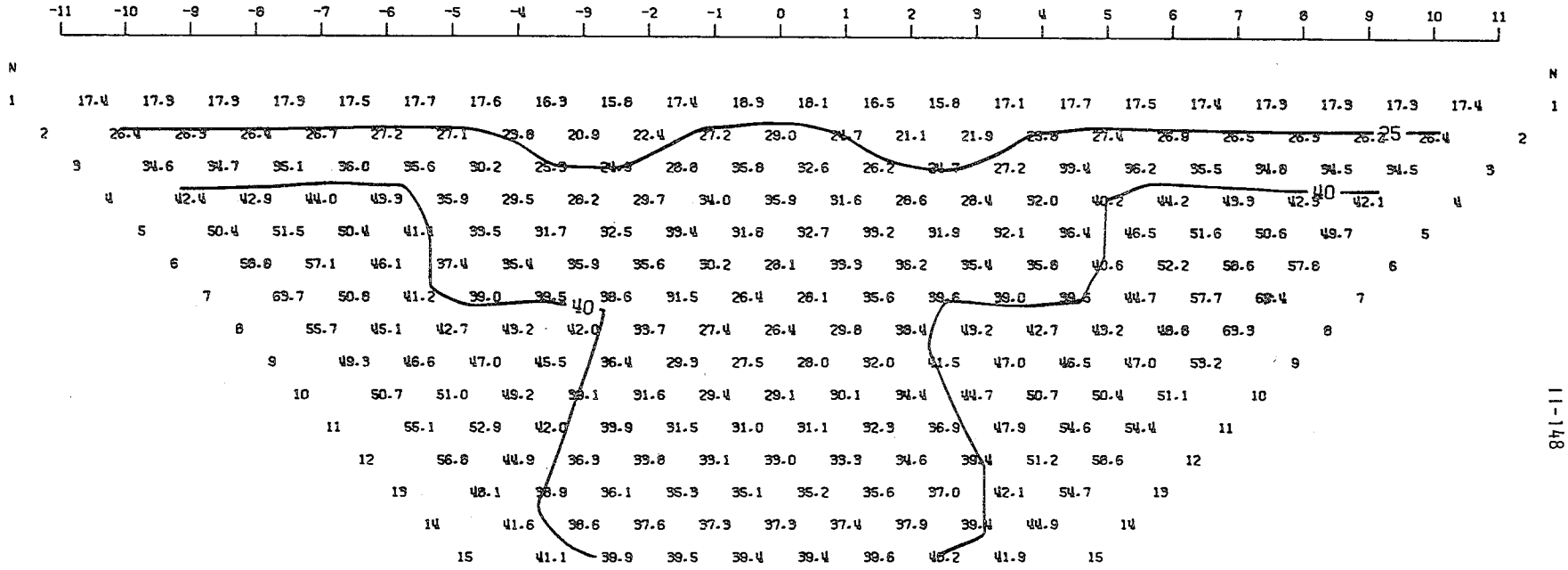

2-D RESISTIVITY MODEL -- TWO BODIES WITH OVERBURDEN 2

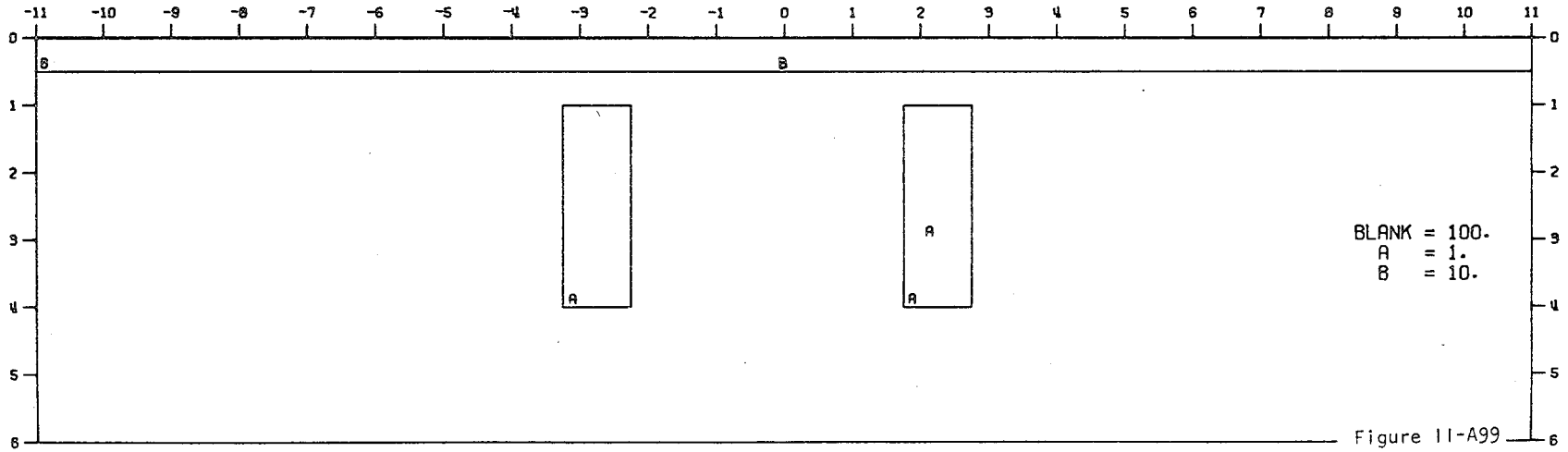

Figure II-A99

MODEL--TWO BODIES WITH OVERBURDEN 2
SCHLUMBERGER APPARENT RESISTIVITY PSEUDO-SECTION
PROFILE LINE IS INCLINED AT 90.0 DEGREES TO STRIKE

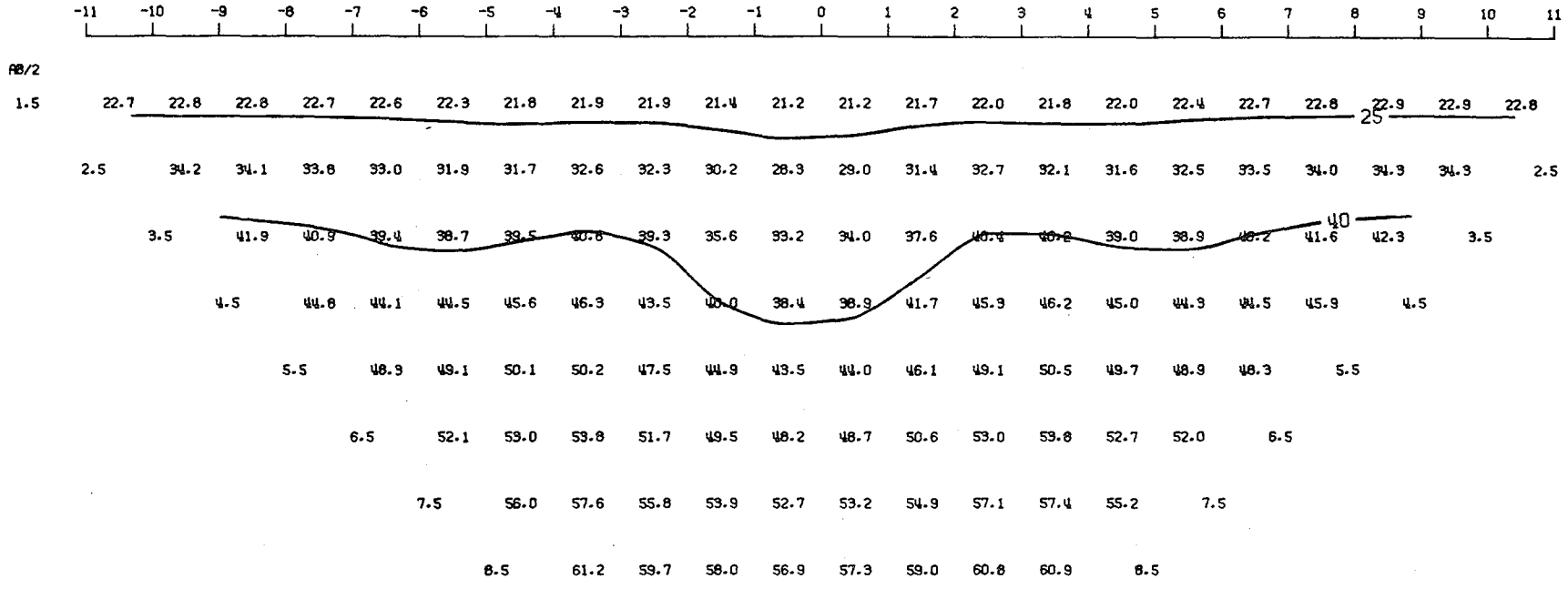

2-D RESISTIVITY MODEL -- TWO BODIES WITH OVERBURDEN 2

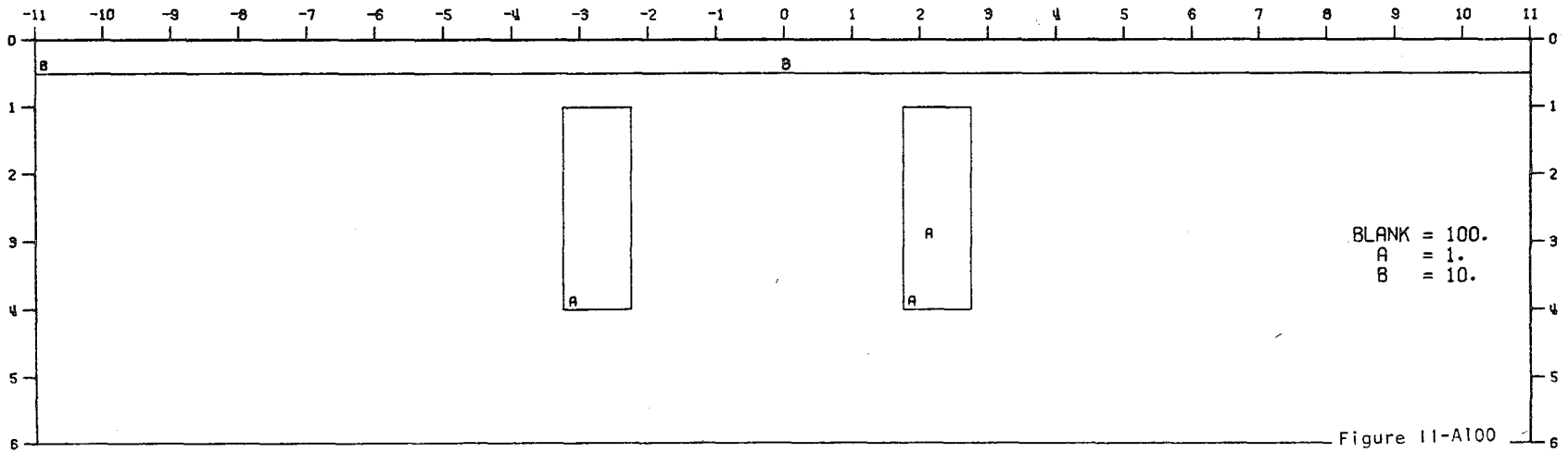

Figure 11-A100

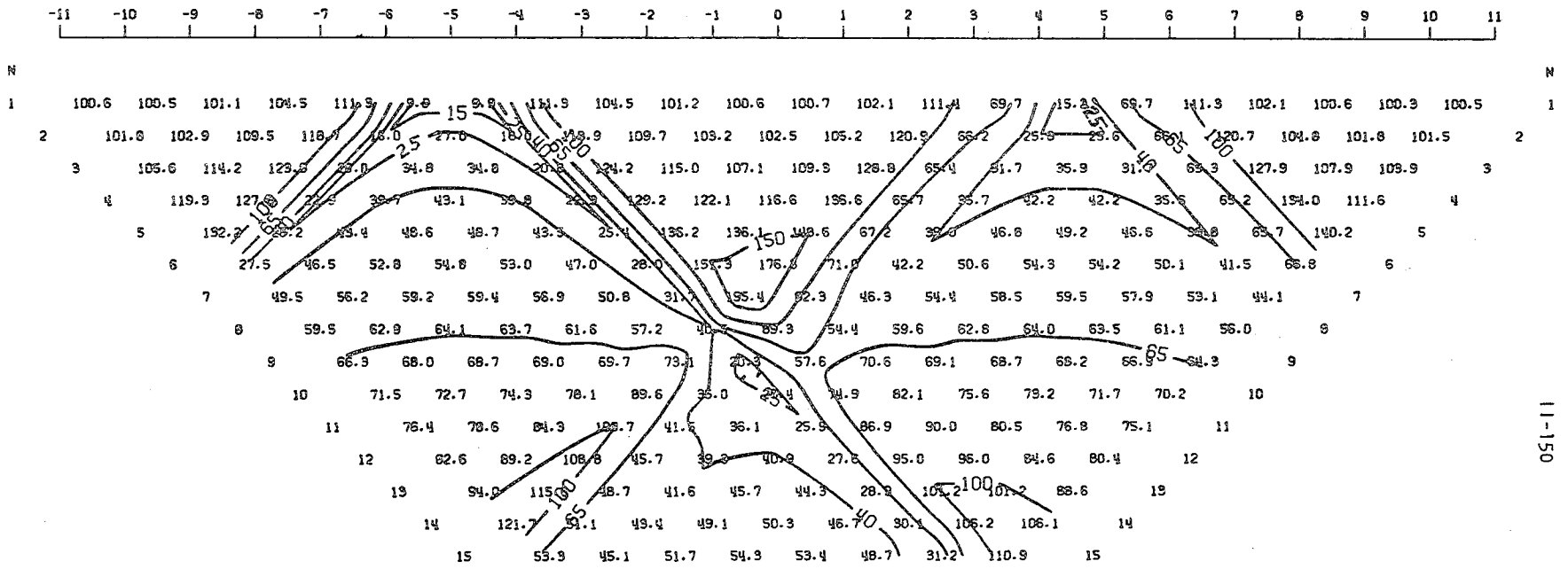

2-D RESISTIVITY MODEL -- CONDUCTIVE BODIES AT SURFACE

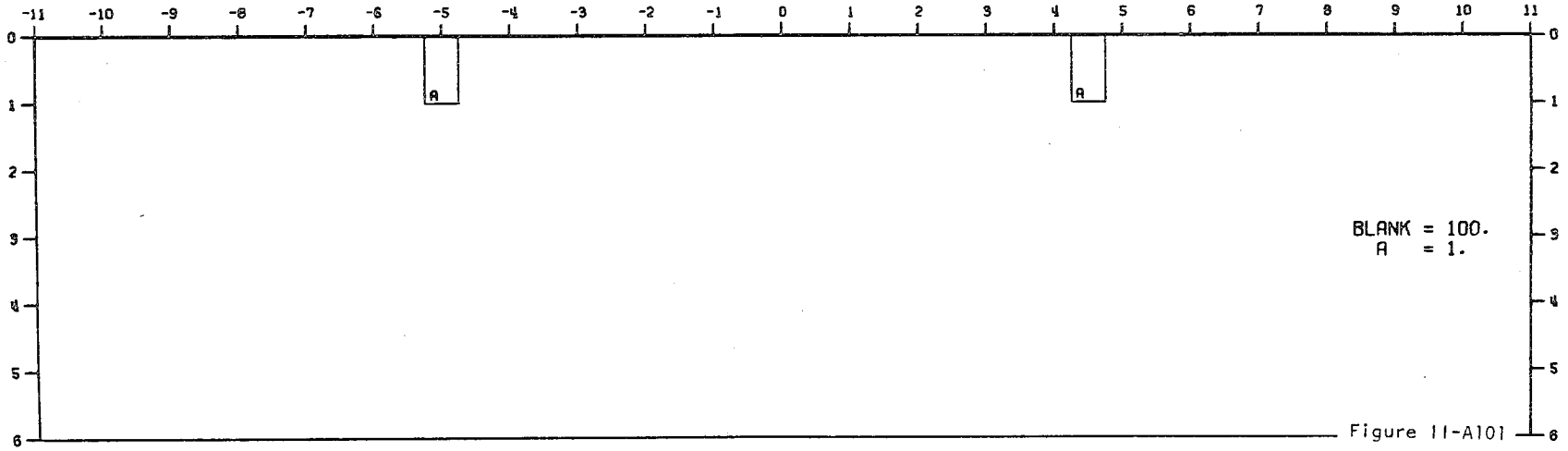

Figure 11-A101

MODEL--CONDUCTIVE BODIES AT SURFACE
SCHLUMBERGER APPARENT RESISTIVITY PSEUDO-SECTION
PROFILE LINE IS INCLINED AT 90.0 DEGREES TO STRIKE

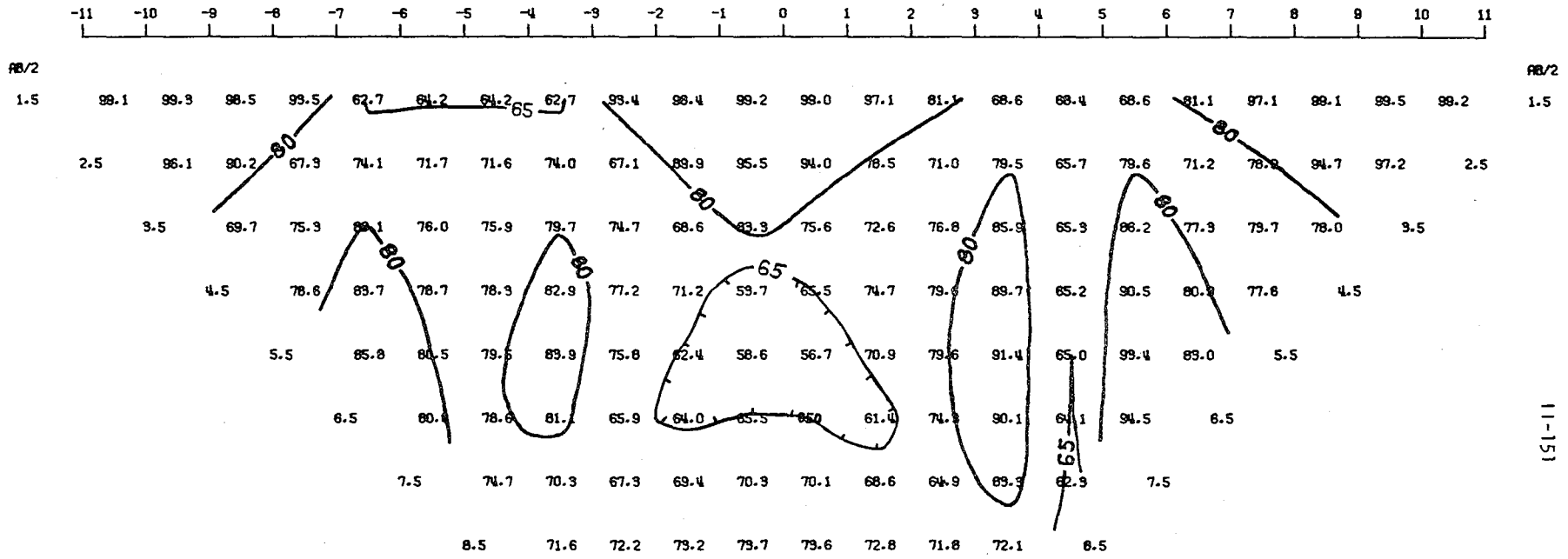

2-D RESISTIVITY MODEL -- CONDUCTIVE BODIES AT SURFACE

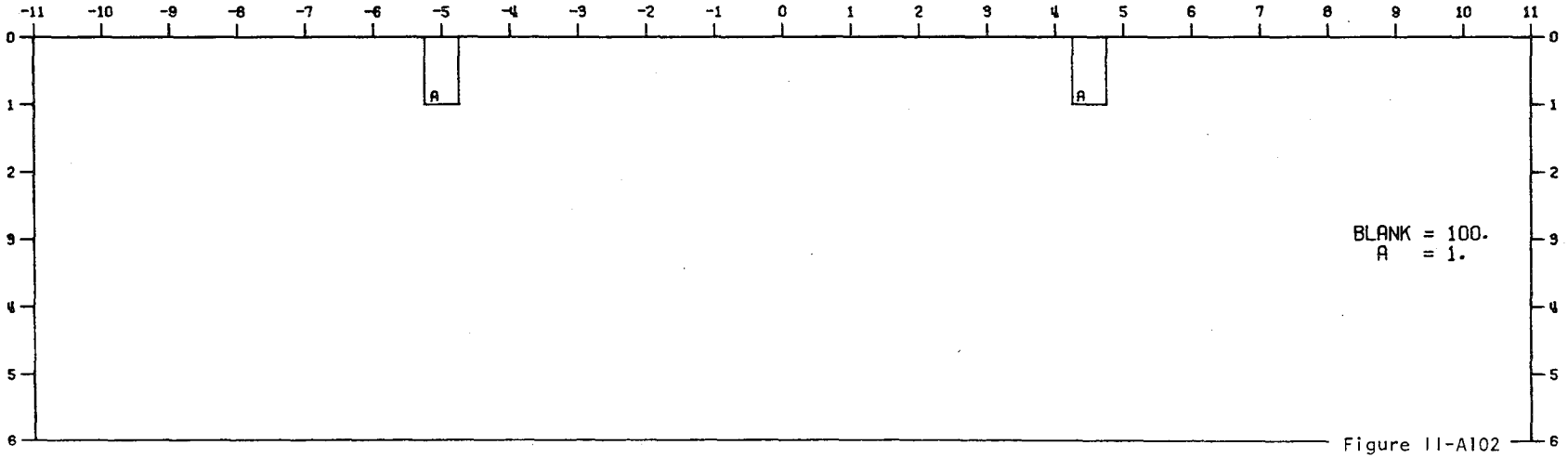

Figure II-A102

MODEL--CONDUCTIVE BODIES AT SURFACE 1
DIPOLE-DIPOLE APPARENT RESISTIVITY PSEUDO-SECTION
PROFILE LINE IS INCLINED AT 90.0 DEGREES TO STRIKE

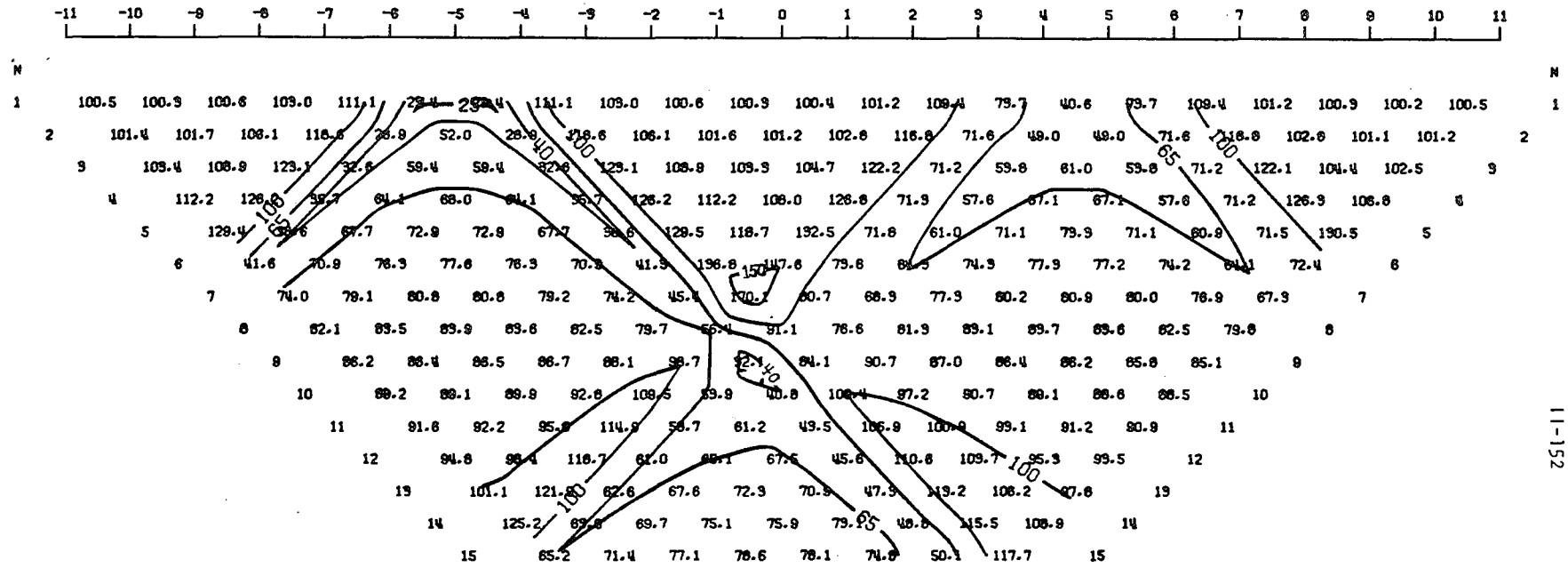

2-D RESISTIVITY MODEL -- CONDUCTIVE BODIES AT SURFACE 1

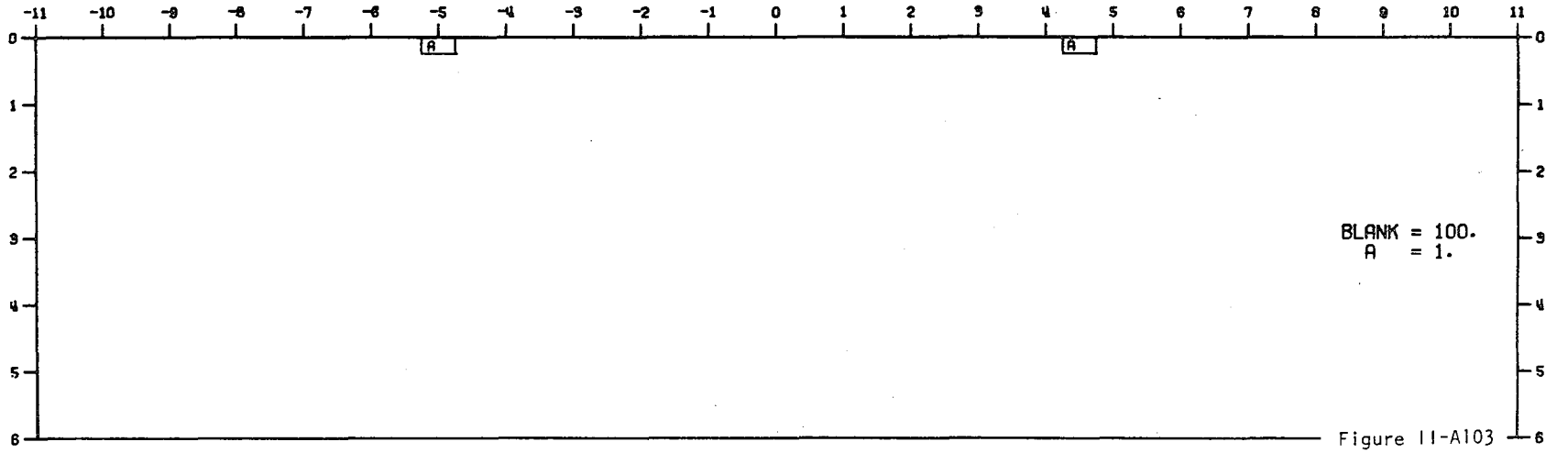

Figure II-A103

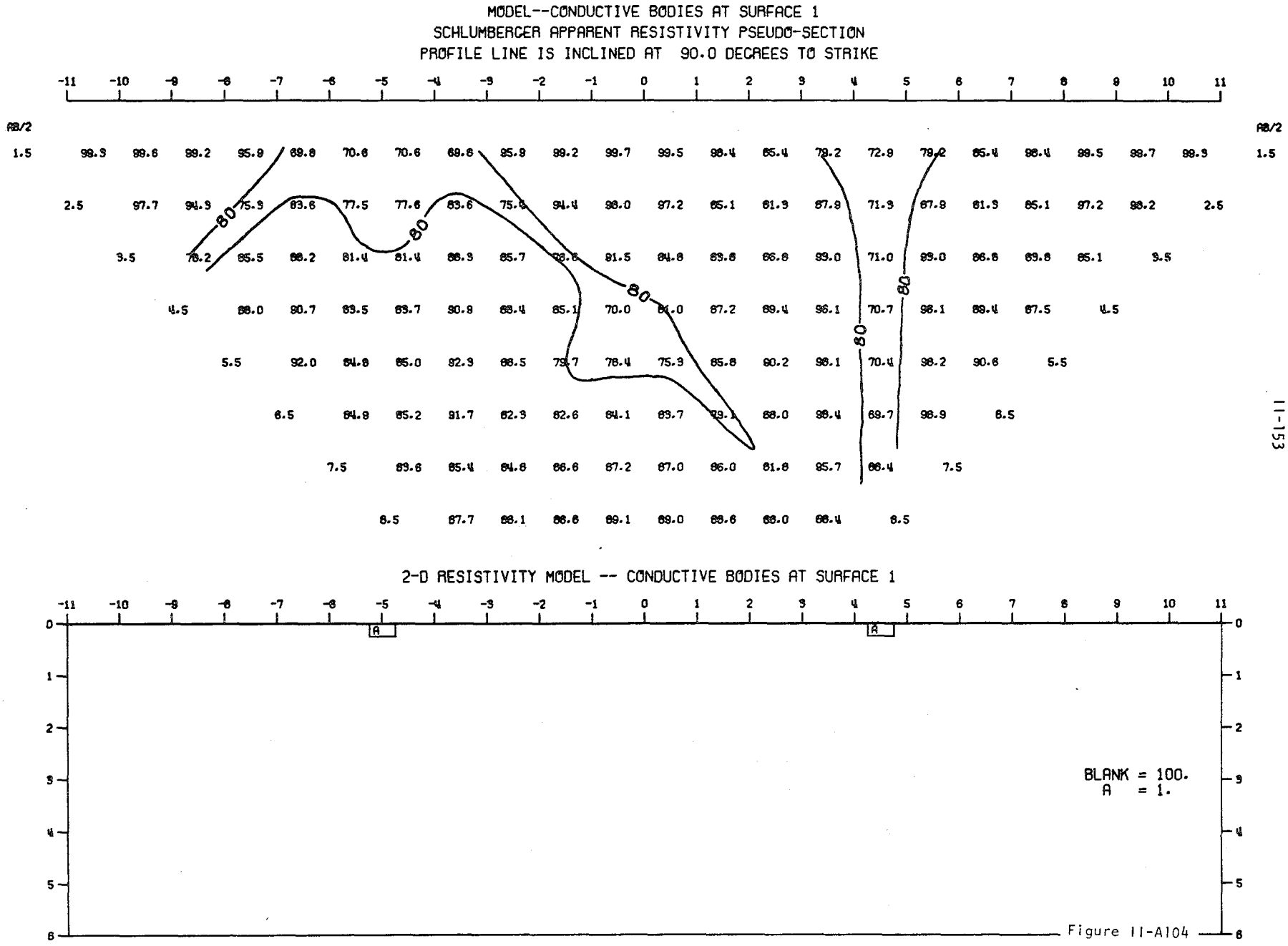

Figure II-A104

MODEL--CONDUCTIVE BODIES AT SURFACE 2
DIPOLE-DIPOLE APPARENT RESISTIVITY PSEUDO-SECTION
PROFILE LINE IS INCLINED AT 90.0 DEGREES TO STRIKE

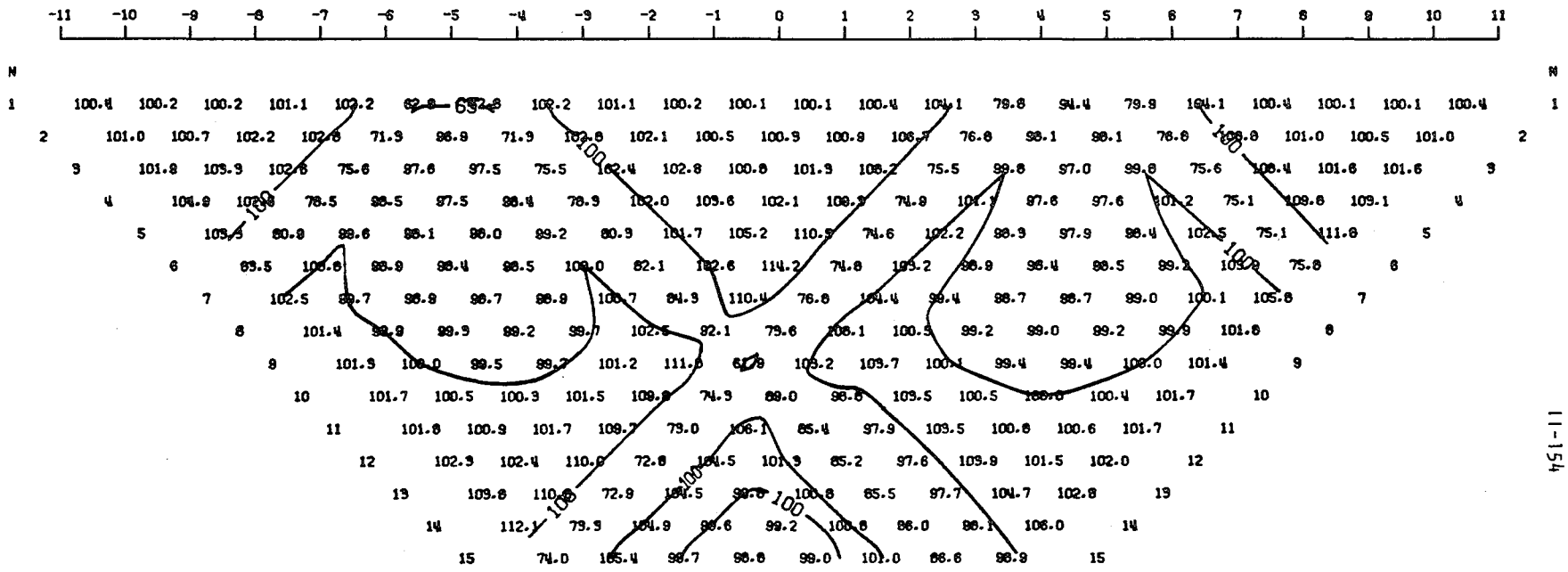

2-D RESISTIVITY MODEL -- CONDUCTIVE BODIES AT SURFACE 2

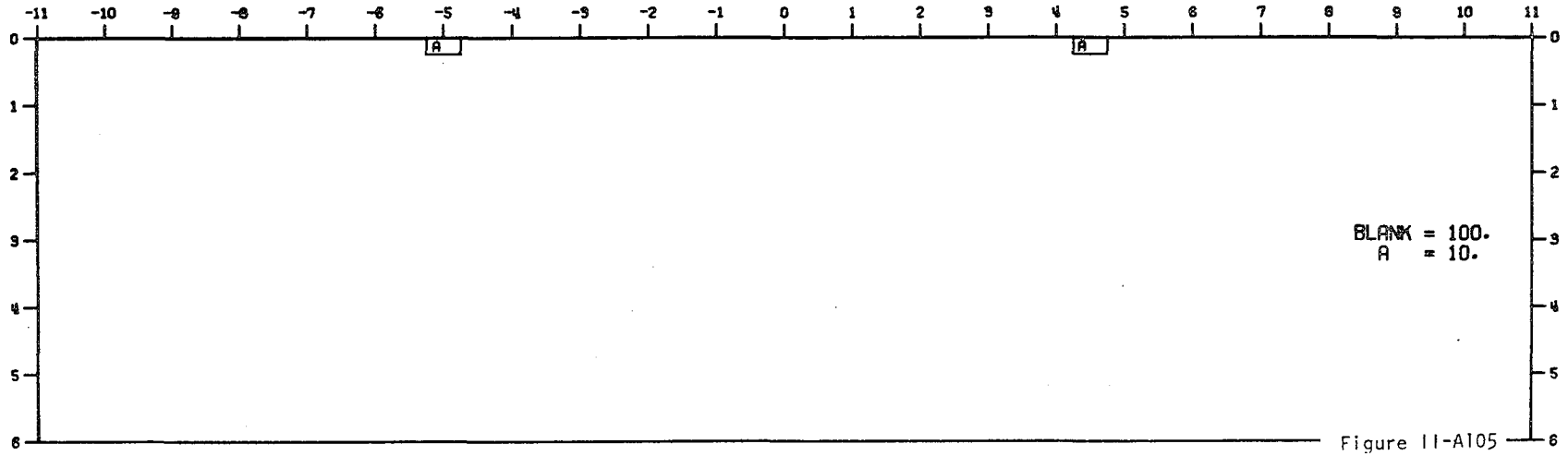

Figure II-A105

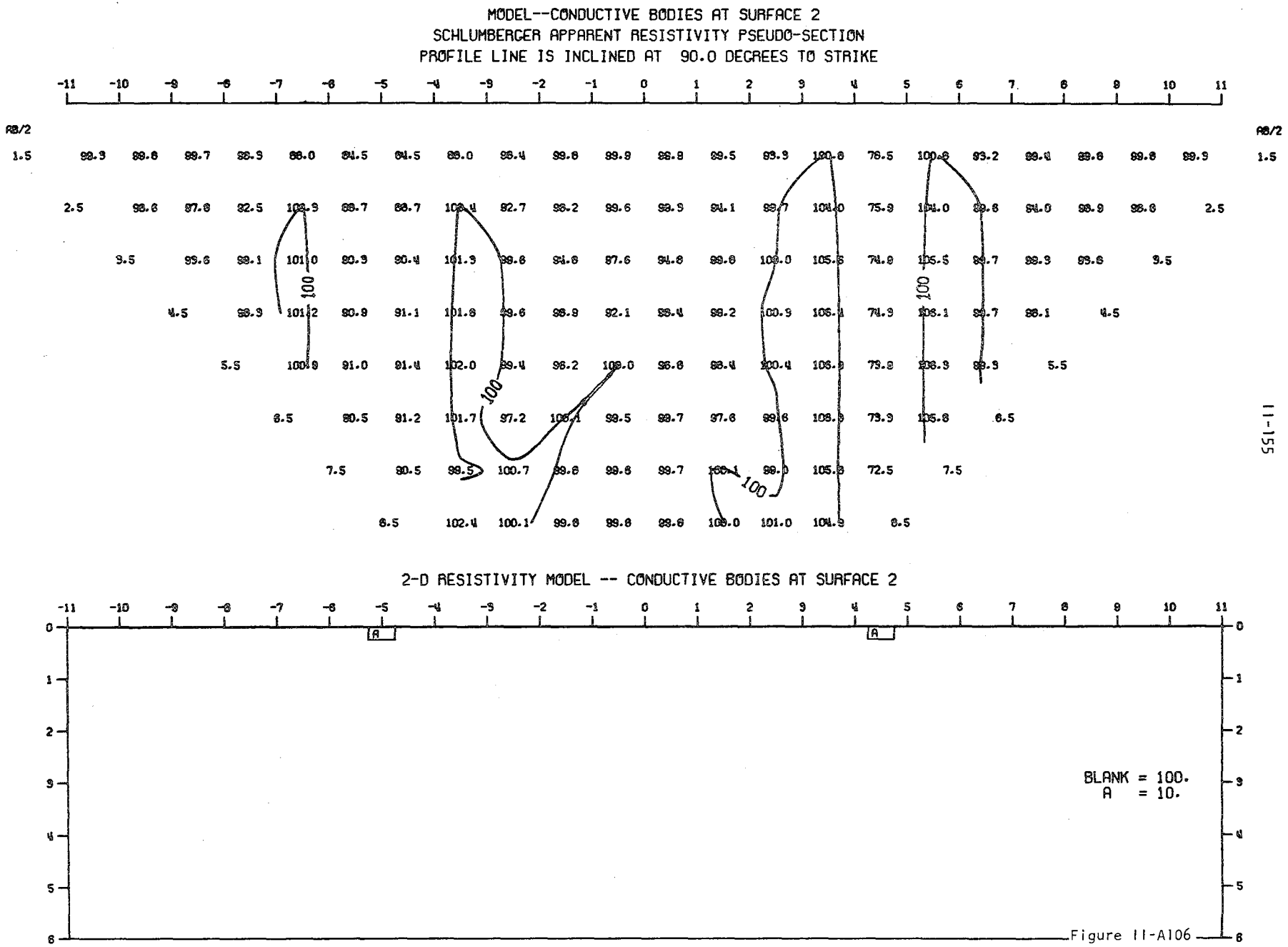

Figure 11-A106

MODEL--CONDUCTIVE BODIES AT SURFACE 3
DIPOLE-DIPOLE APPARENT RESISTIVITY PSEUDO-SECTION
PROFILE LINE IS INCLINED AT 90.0 DEGREES TO STRIKE

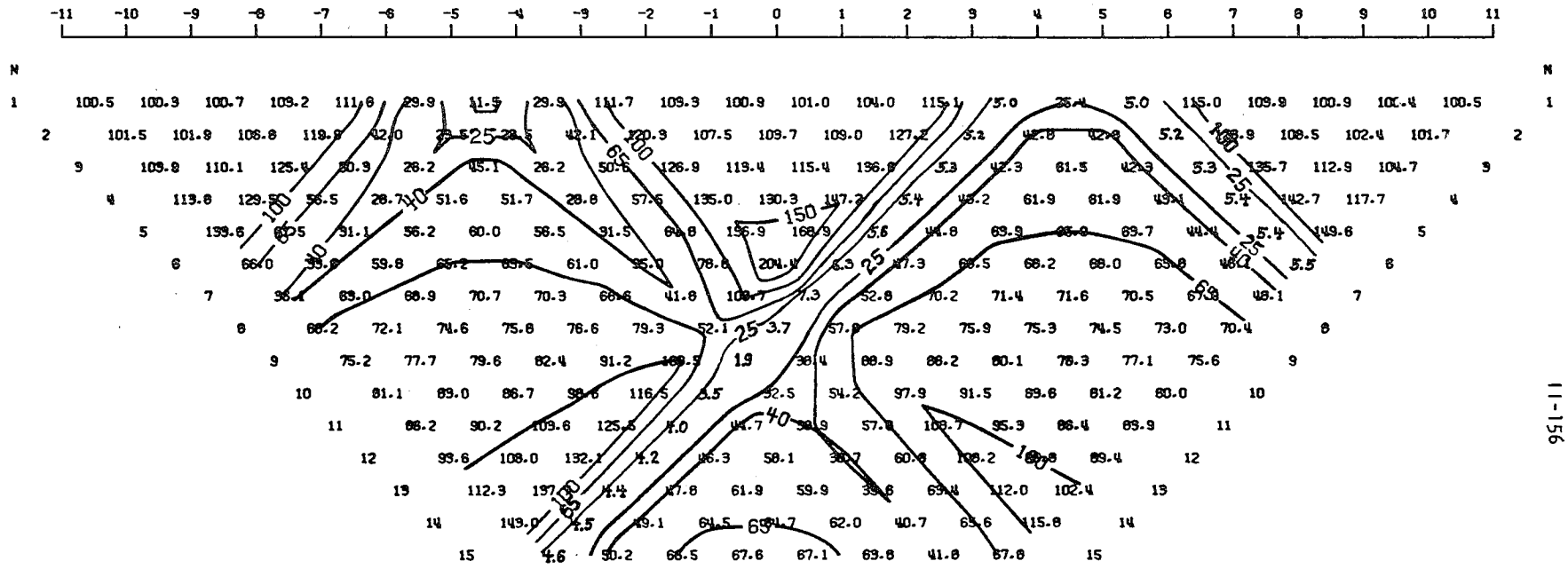

2-D RESISTIVITY MODEL -- CONDUCTIVE BODIES AT SURFACE 3

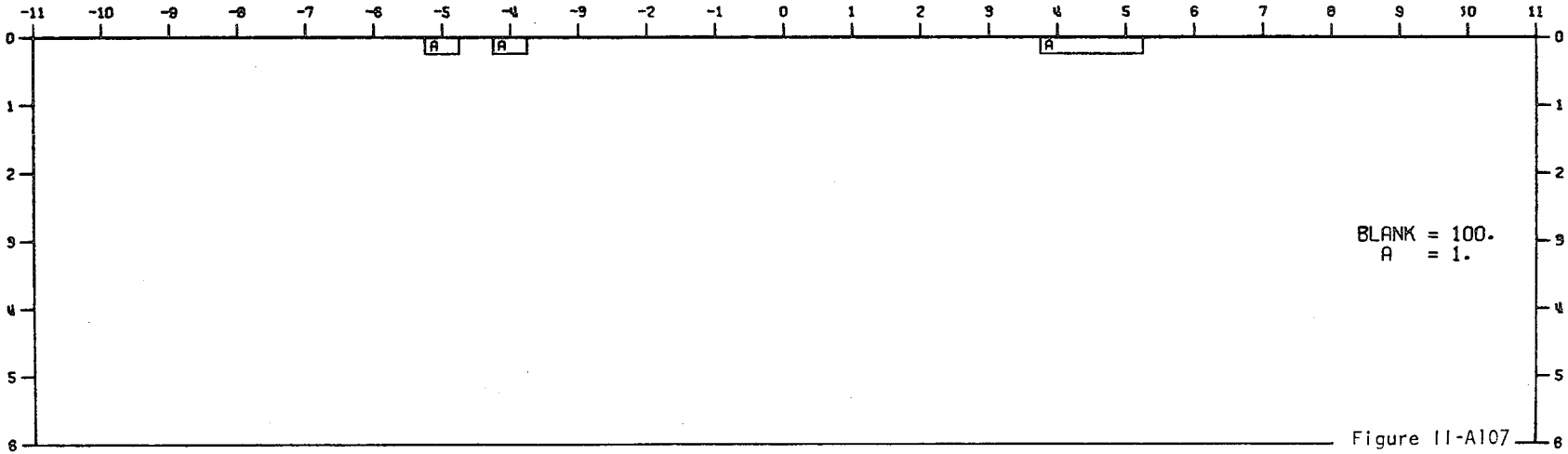

Figure II-A107

MODEL--CONDUCTIVE BODIES AT SURFACE 3
SCHLUMBERGER APPARENT RESISTIVITY PSEUDO-SECTION
PROFILE LINE IS INCLINED AT 90.0 DEGREES TO STRIKE

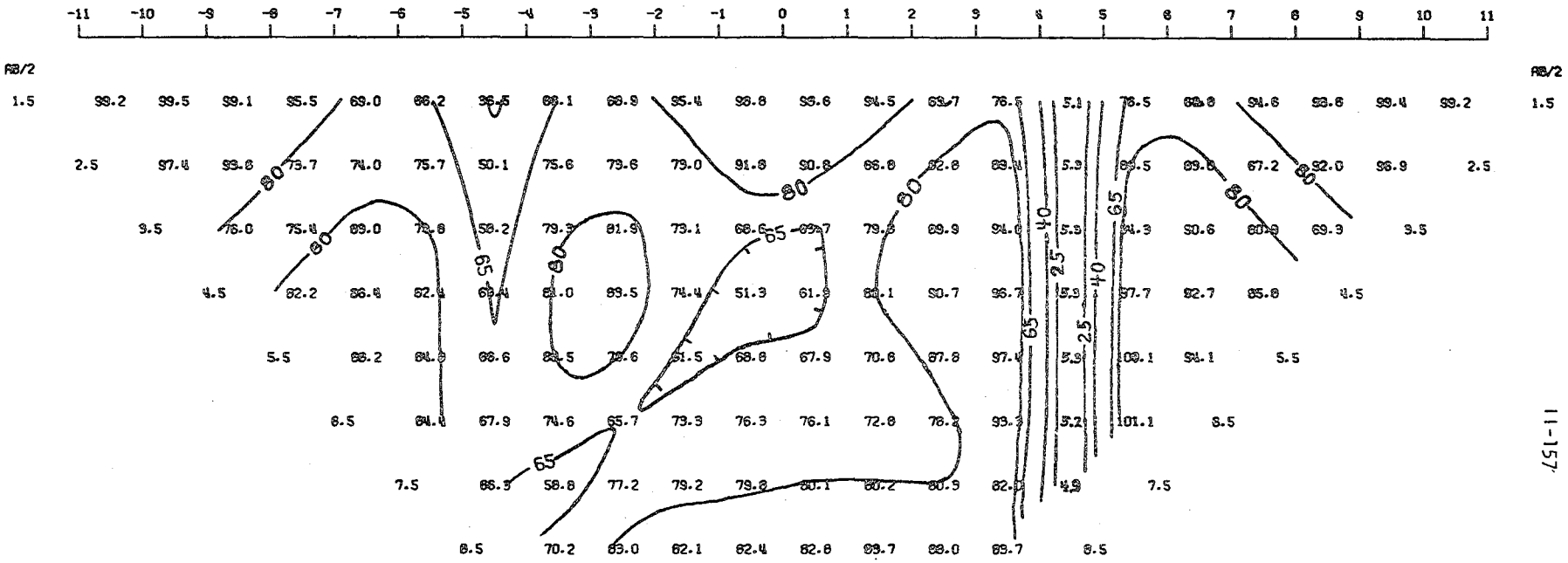

2-D RESISTIVITY MODEL -- CONDUCTIVE BODIES AT SURFACE 3

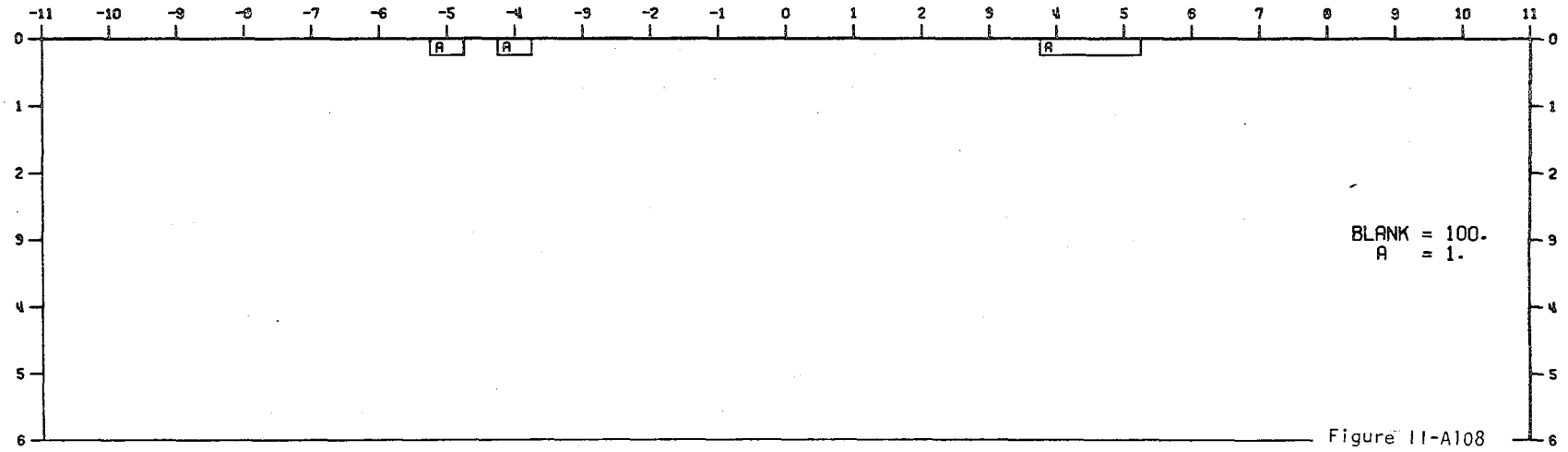

Figure II-A108

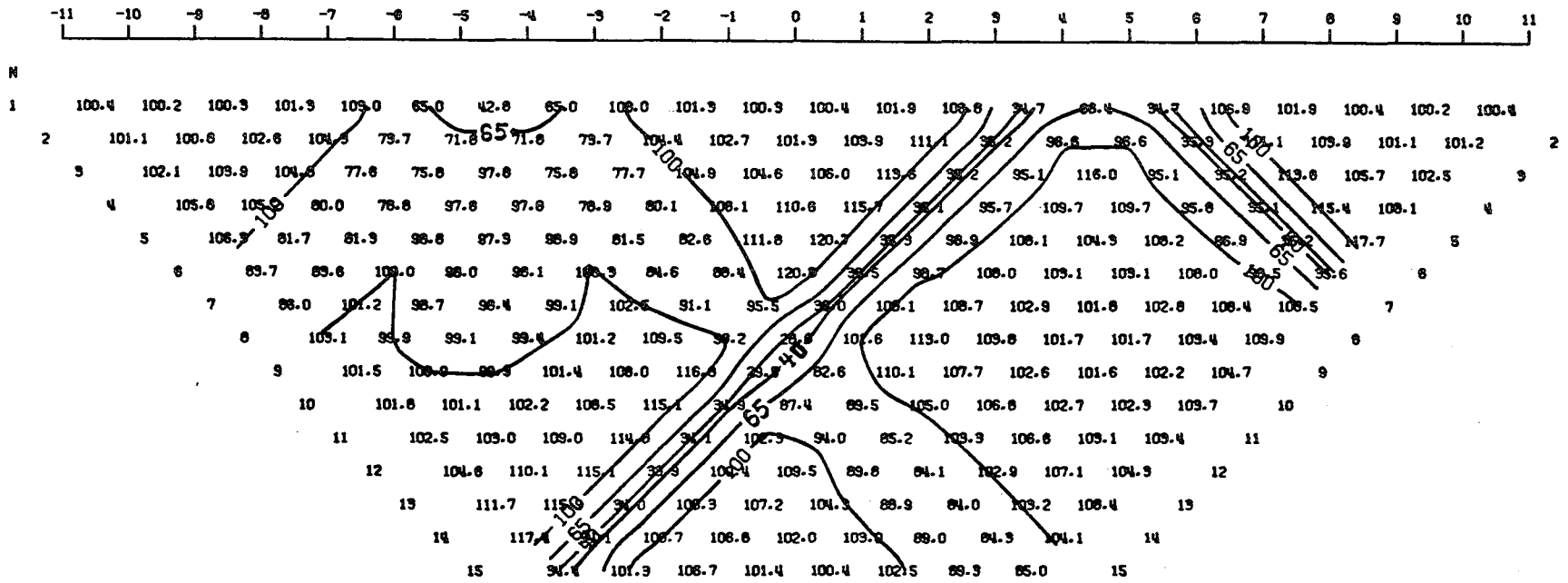

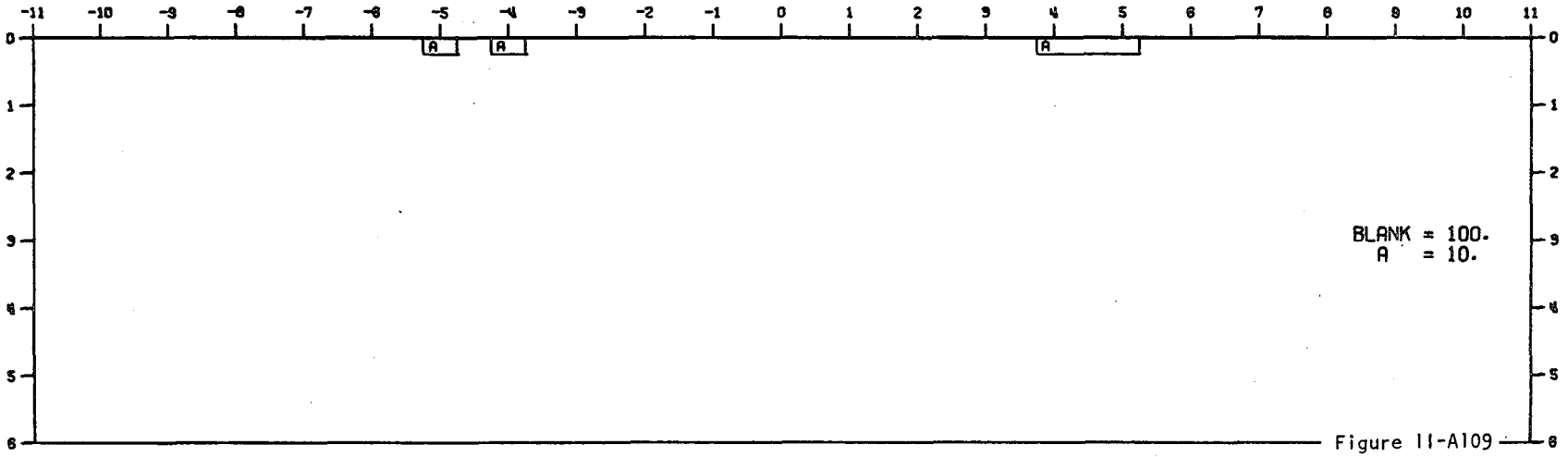

Figure II-A109

MODEL--CONDUCTIVE BODIES AT SURFACE 4
SCHLUMBERGER APPARENT RESISTIVITY PSEUDO-SECTION
PROFILE LINE IS INCLINED AT 90.0 DEGREES TO STRIKE

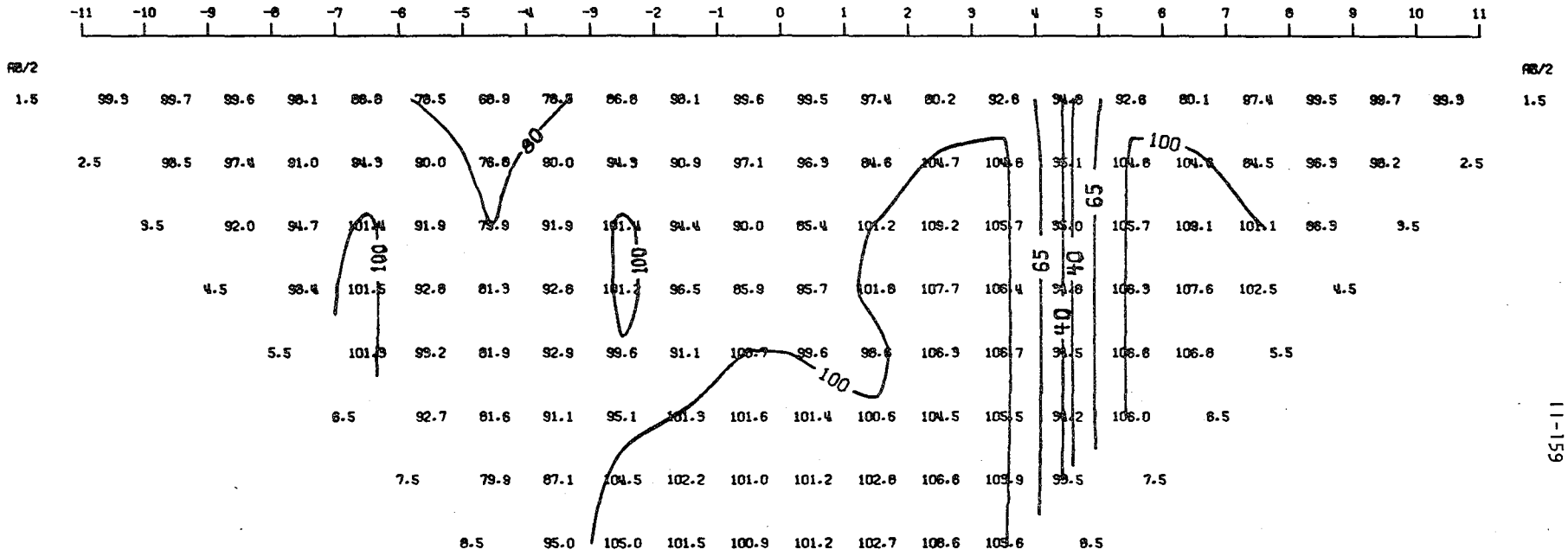

2-D RESISTIVITY MODEL -- CONDUCTIVE BODIES AT SURFACE 4

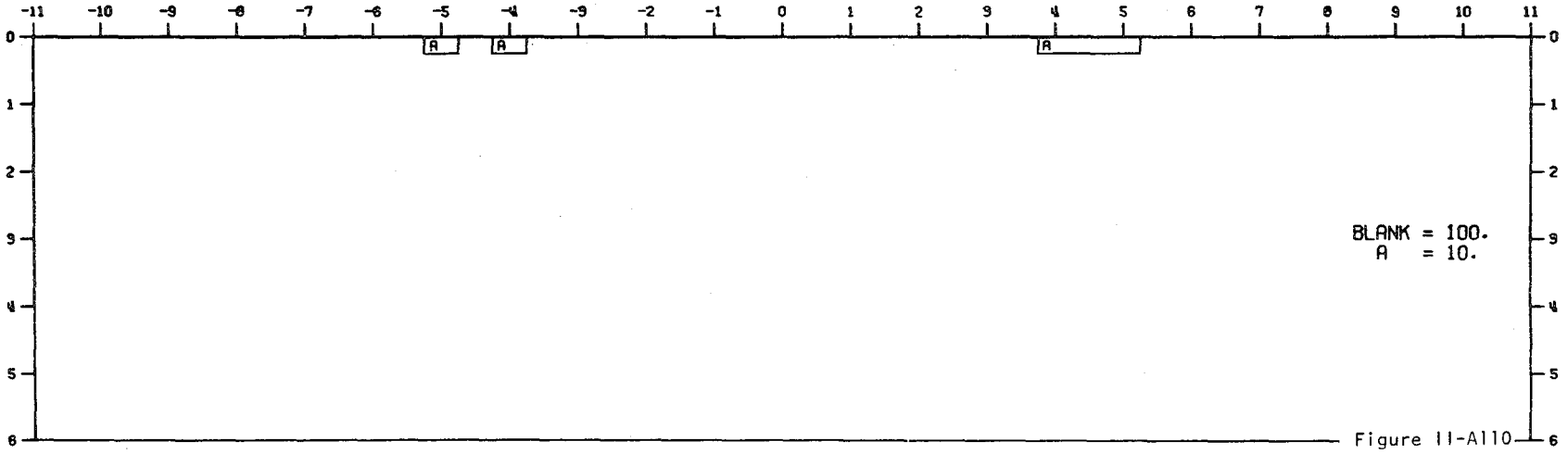

Figure II-A110

MODEL--RESISTIVE BODIES AT SURFACE
DIPOLE-DIPOLE APPARENT RESISTIVITY PSEUDO-SECTION
PROFILE LINE IS INCLINED AT 90.0 DEGREES TO STRIKE

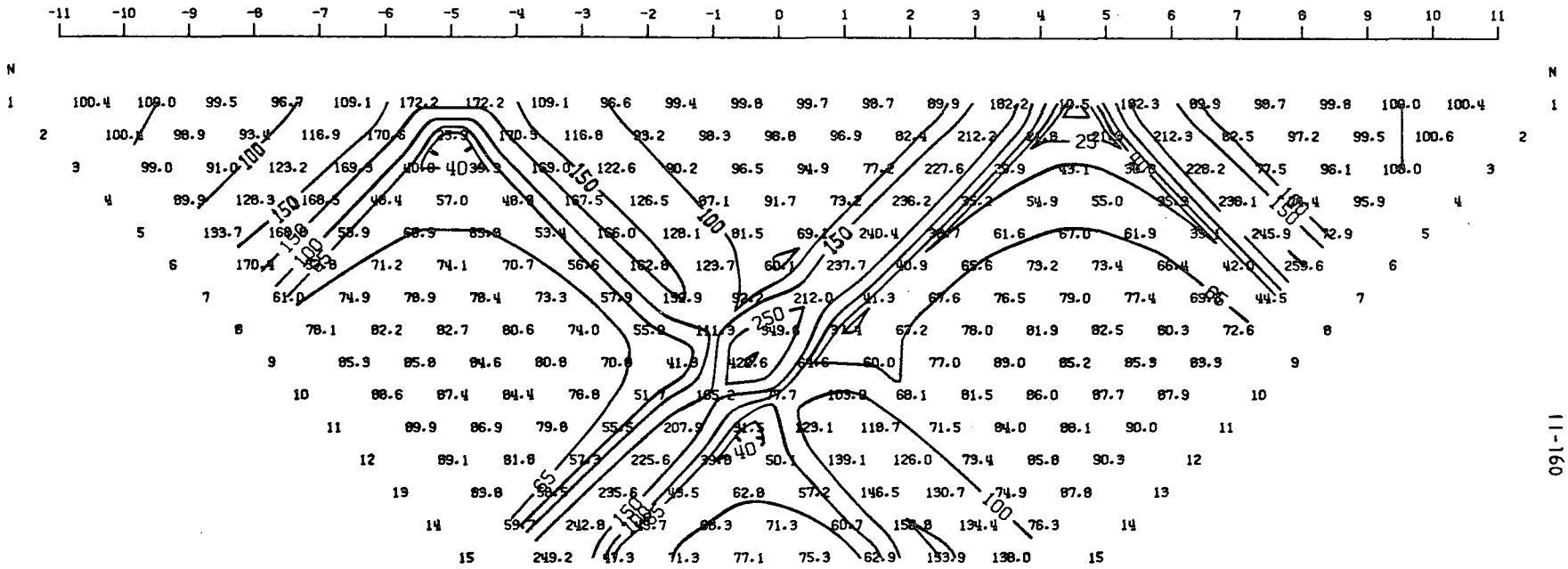

2-D RESISTIVITY MODEL -- RESISTIVE BODIES AT SURFACE 1

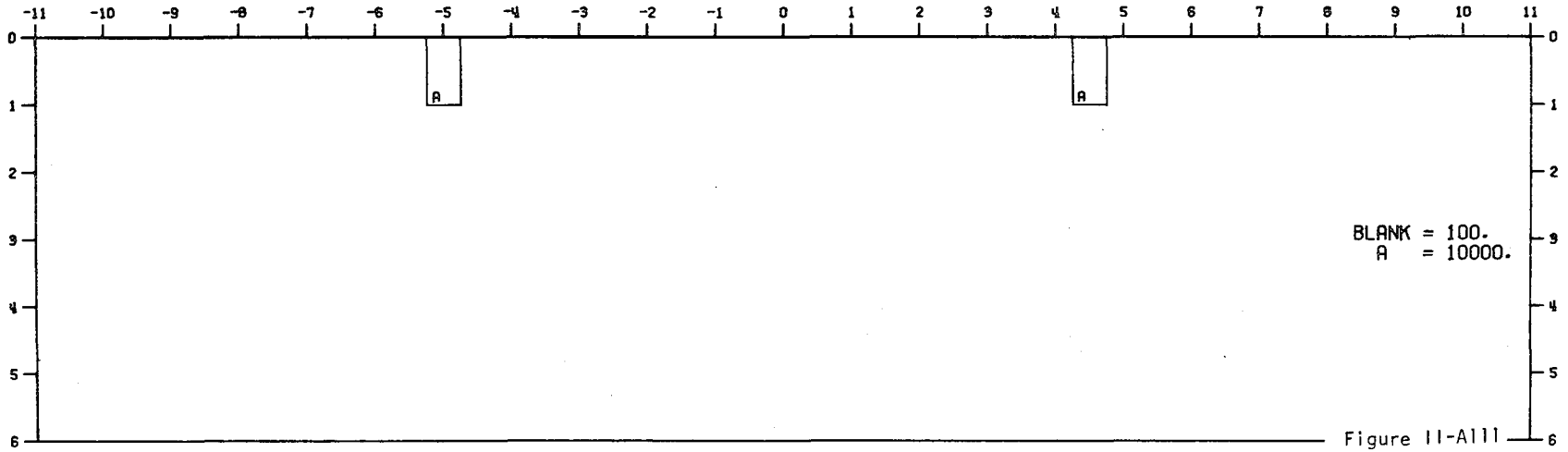

Figure II-A111

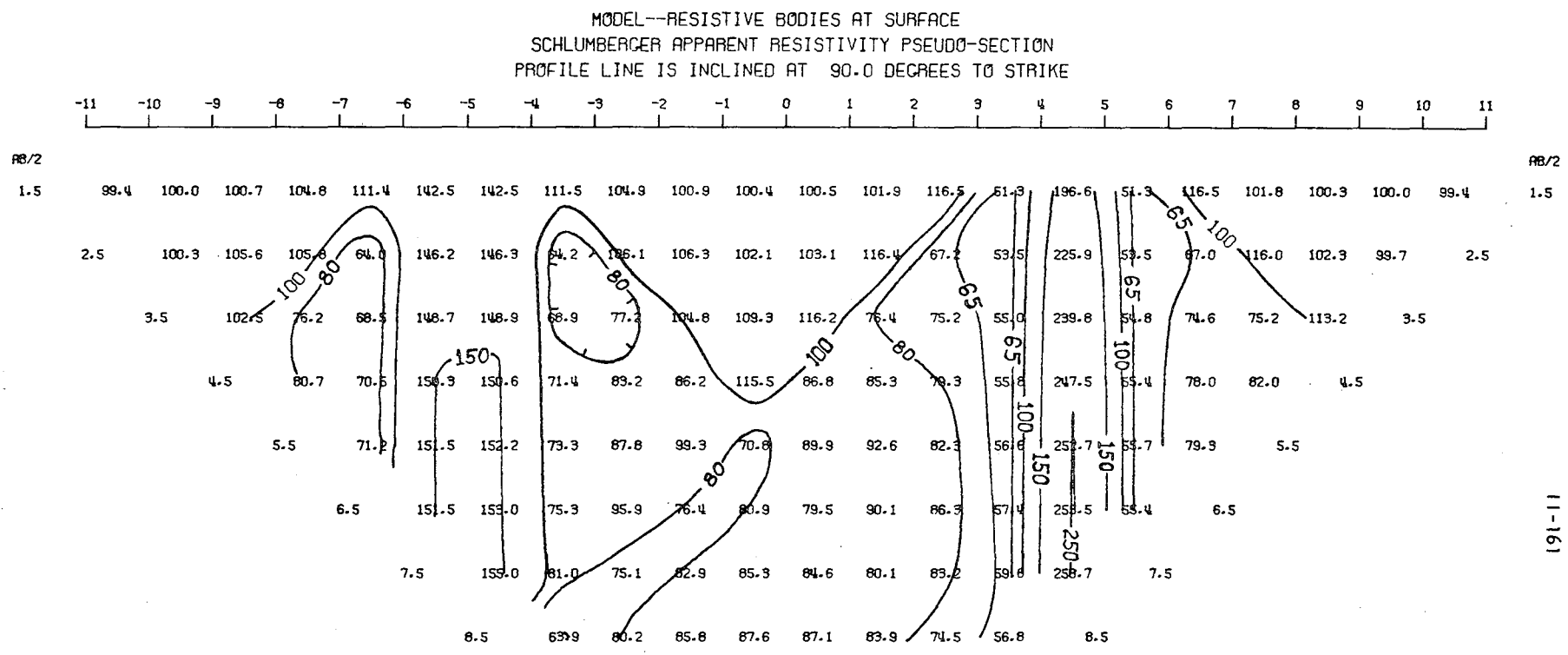

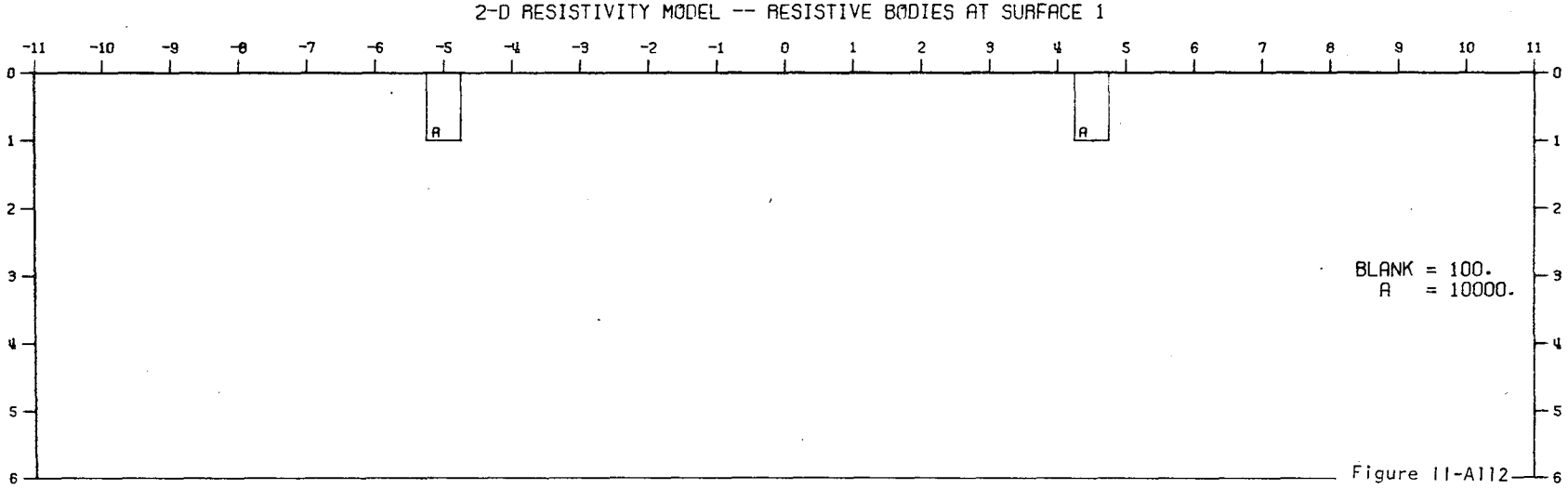

Figure II-A112

MODEL--RESISTIVE BODIES AT SURFACE 1
DIPOLE-DIPOLE APPARENT RESISTIVITY PSEUDO-SECTION
PROFILE LINE IS INCLINED AT 90.0 DEGREES TO STRIKE

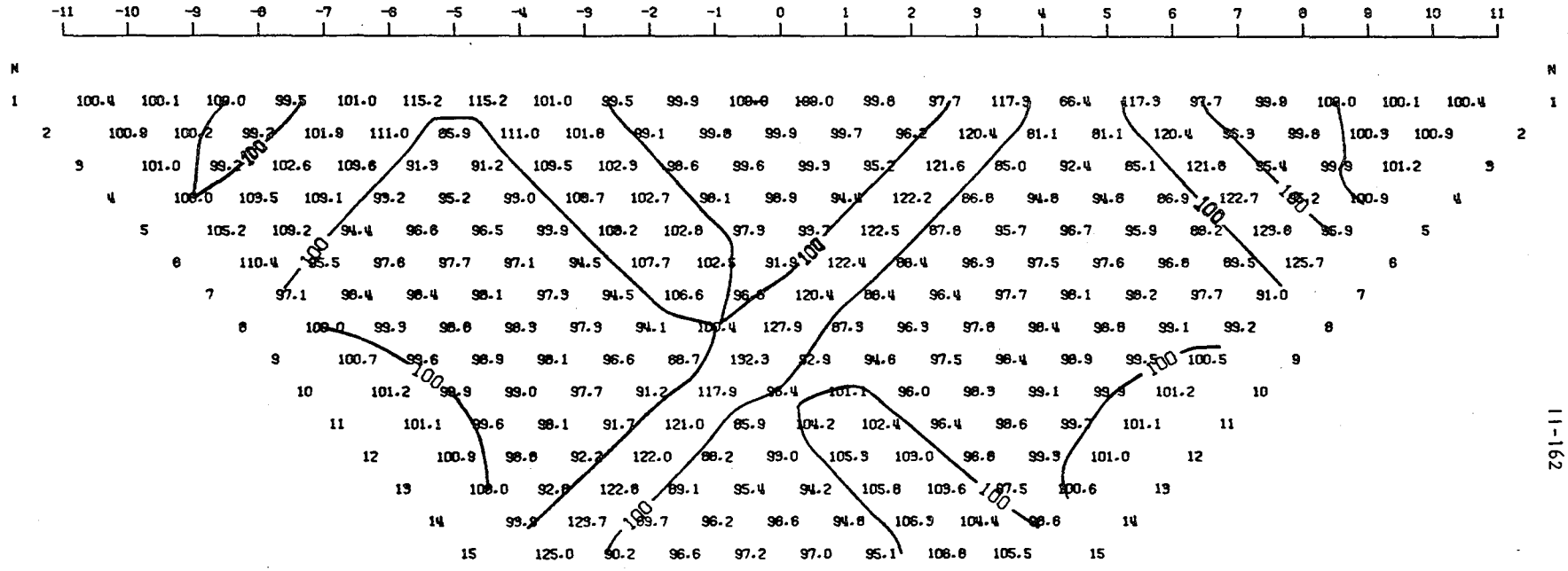

2-D RESISTIVITY MODEL -- RESISTIVE BODIES AT SURFACE 1

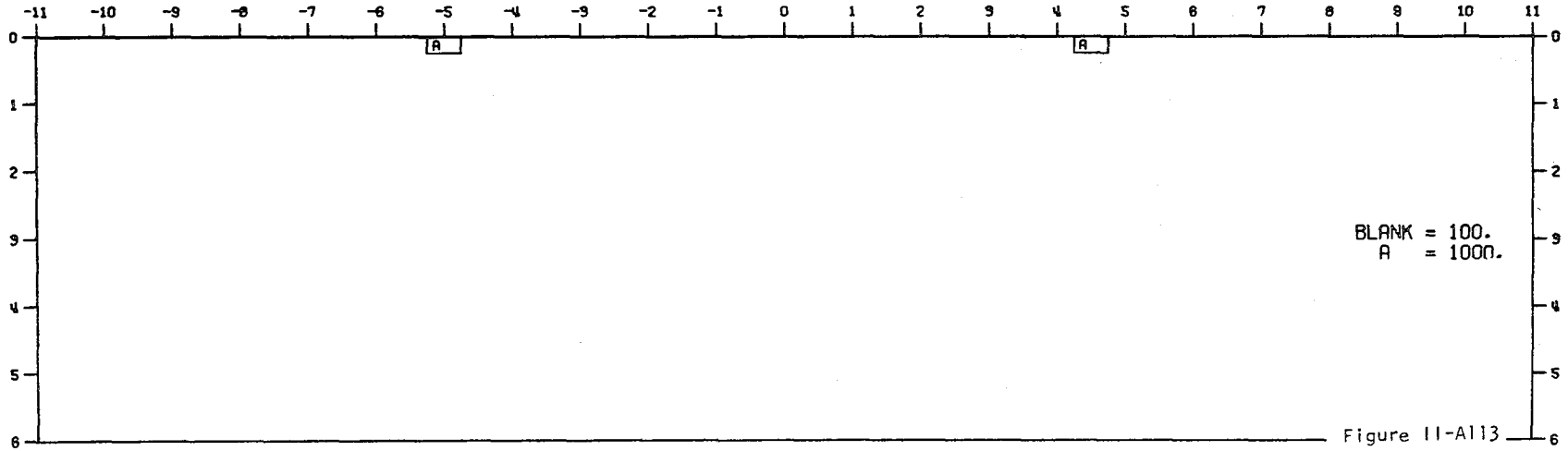

Figure II-A113

MODEL--RESISTIVE BODIES AT SURFACE 1
SCHLUMBERGER APPARENT RESISTIVITY PSEUDO-SECTION
PROFILE LINE IS INCLINED AT 90.0 DEGREES TO STRIKE

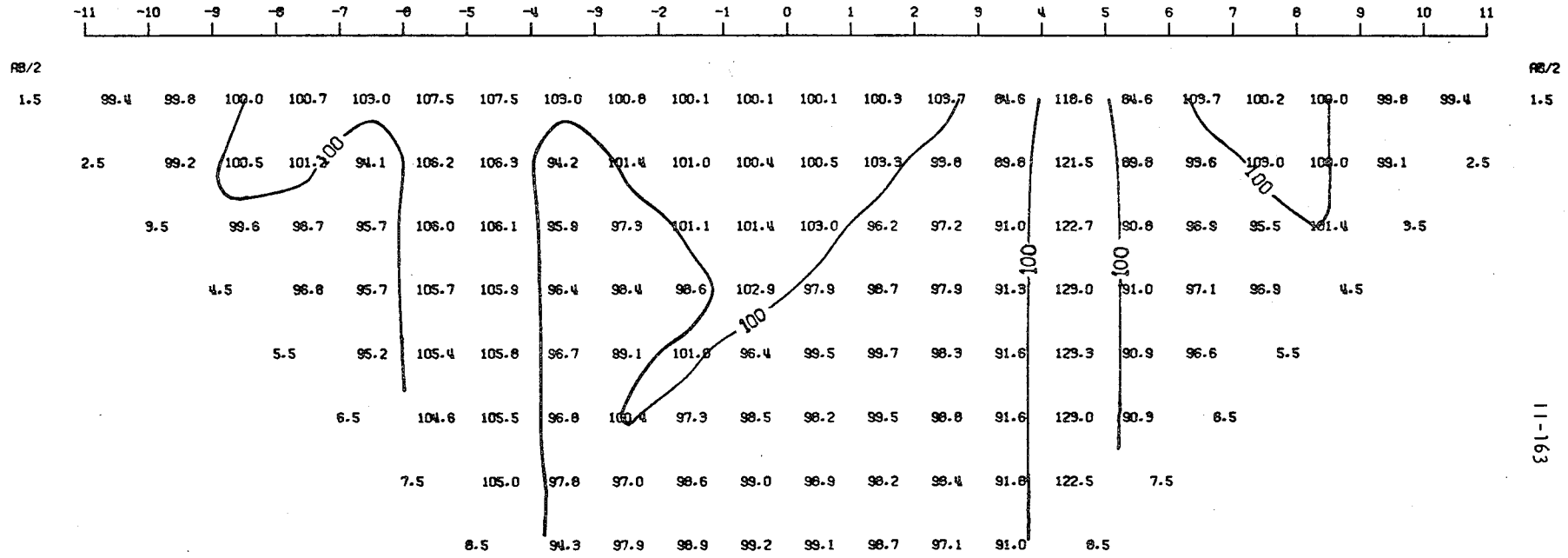

2-D RESISTIVITY MODEL -- RESISTIVE BODIES AT SURFACE 1

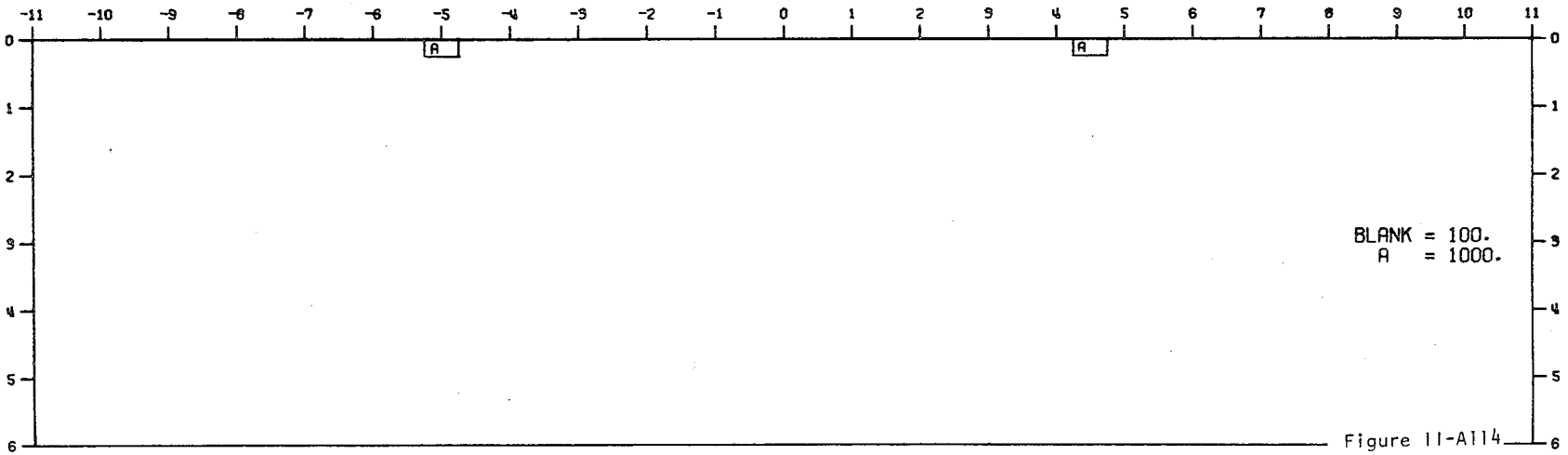

Figure II-A114

MODEL--RESISTIVE BODIES AT SURFACE 2
DIPOLE-DIPOLE APPARENT RESISTIVITY PSEUDO-SECTION
PROFILE LINE IS INCLINED AT 90.0 DEGREES TO STRIKE

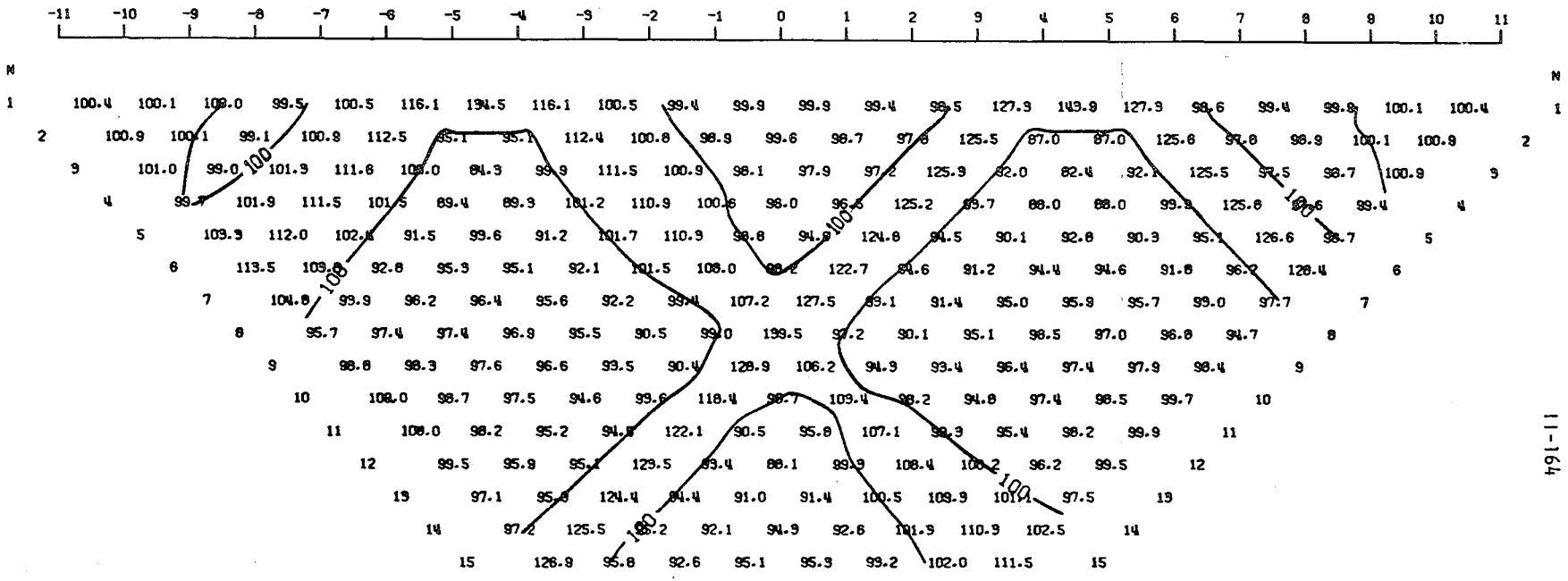

11-164

2-D RESISTIVITY MODEL -- RESISTIVE BODIES AT SURFACE 2

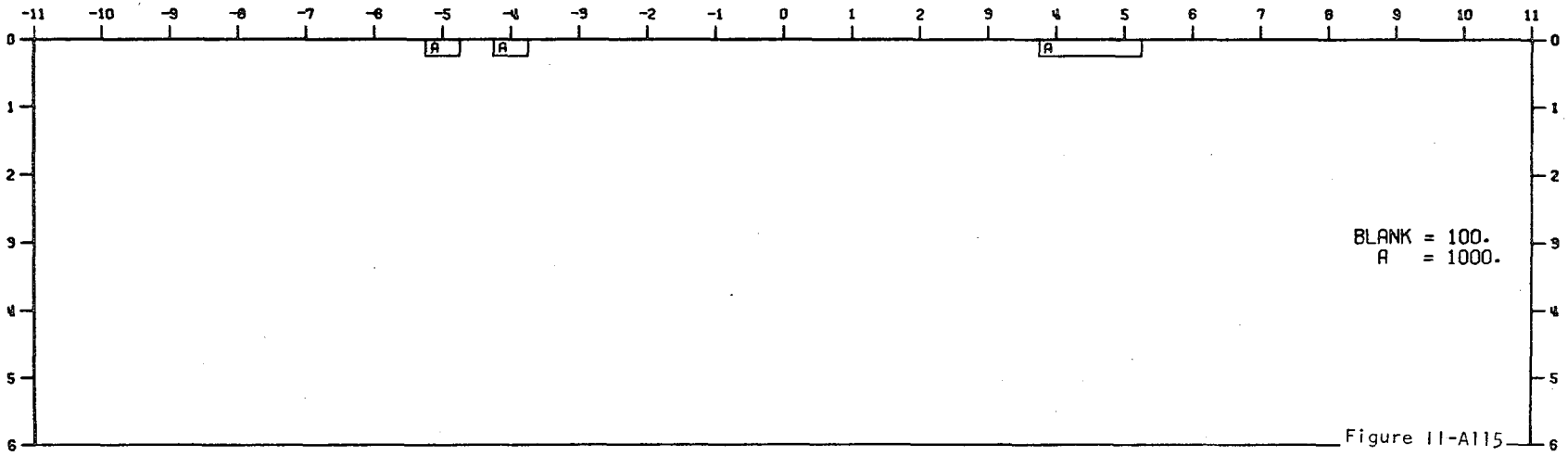

Figure 11-A115

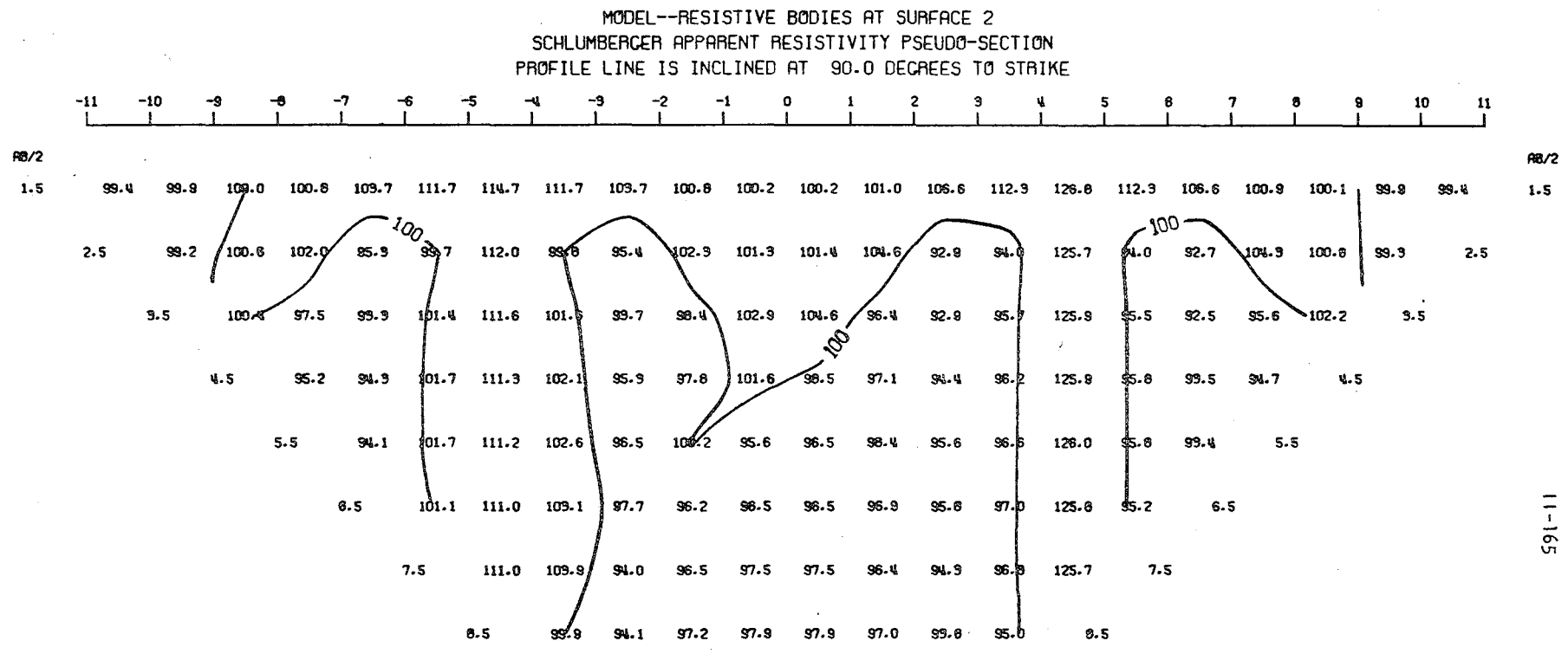

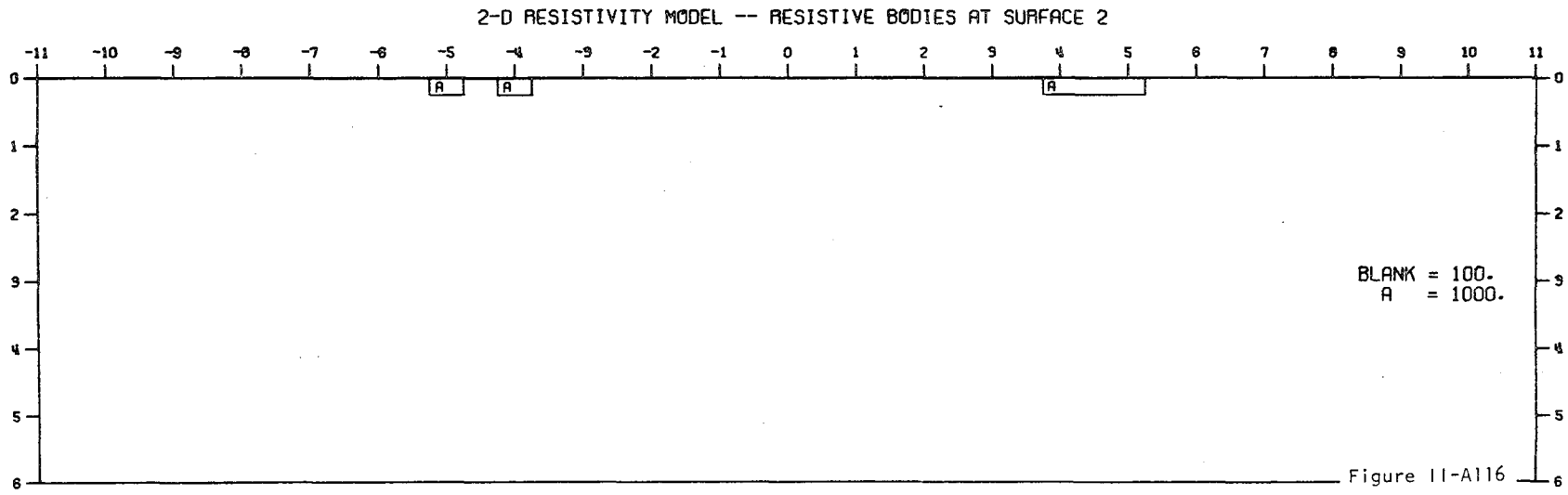

Figure II-A116

MODEL--RESISTIVE BODIES AT SURFACE 3
DIPOLE-DIPOLE APPARENT RESISTIVITY PSEUDO-SECTION
PROFILE LINE IS INCLINED AT 90.0 DEGREES TO STRIKE

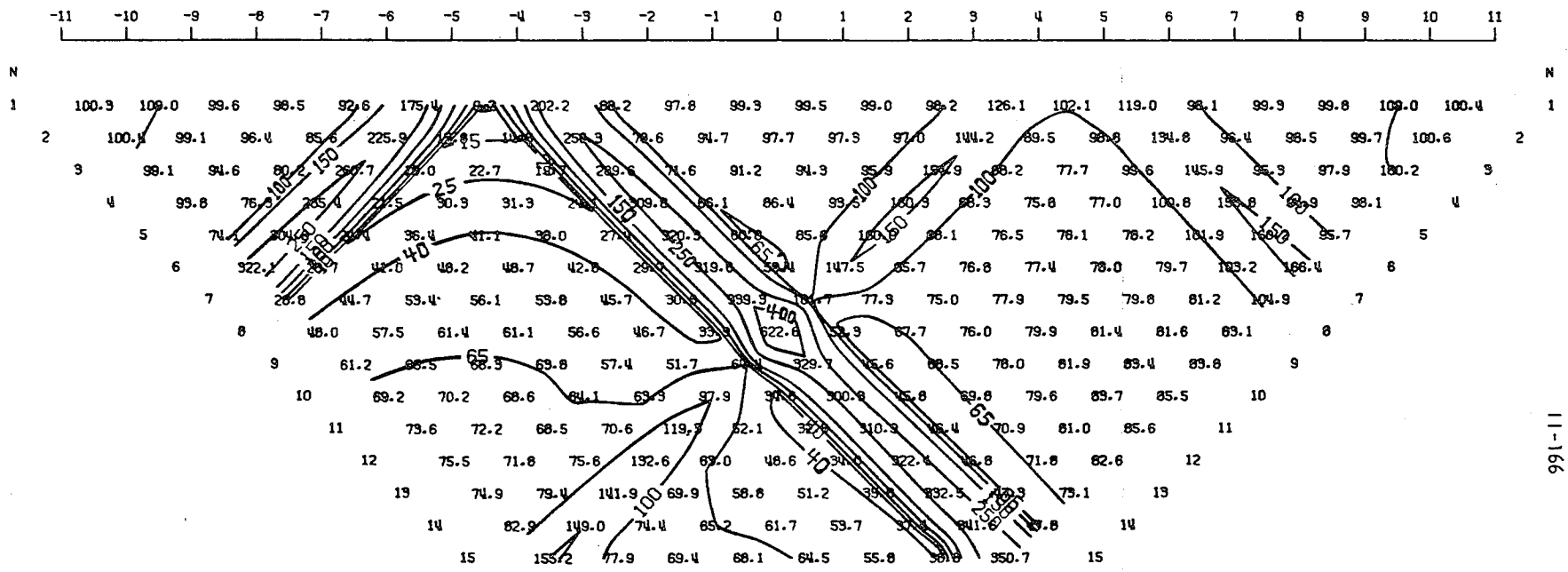

2-D RESISTIVITY MODEL -- RESISTIVE BODIES AT SURFACE 2

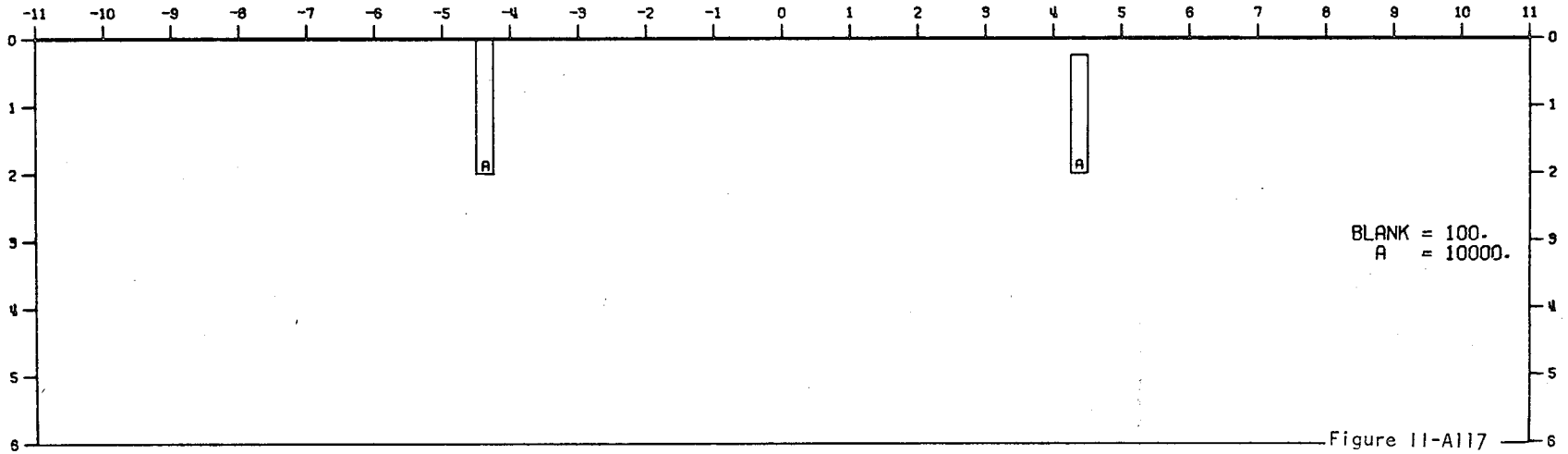

Figure II-A117

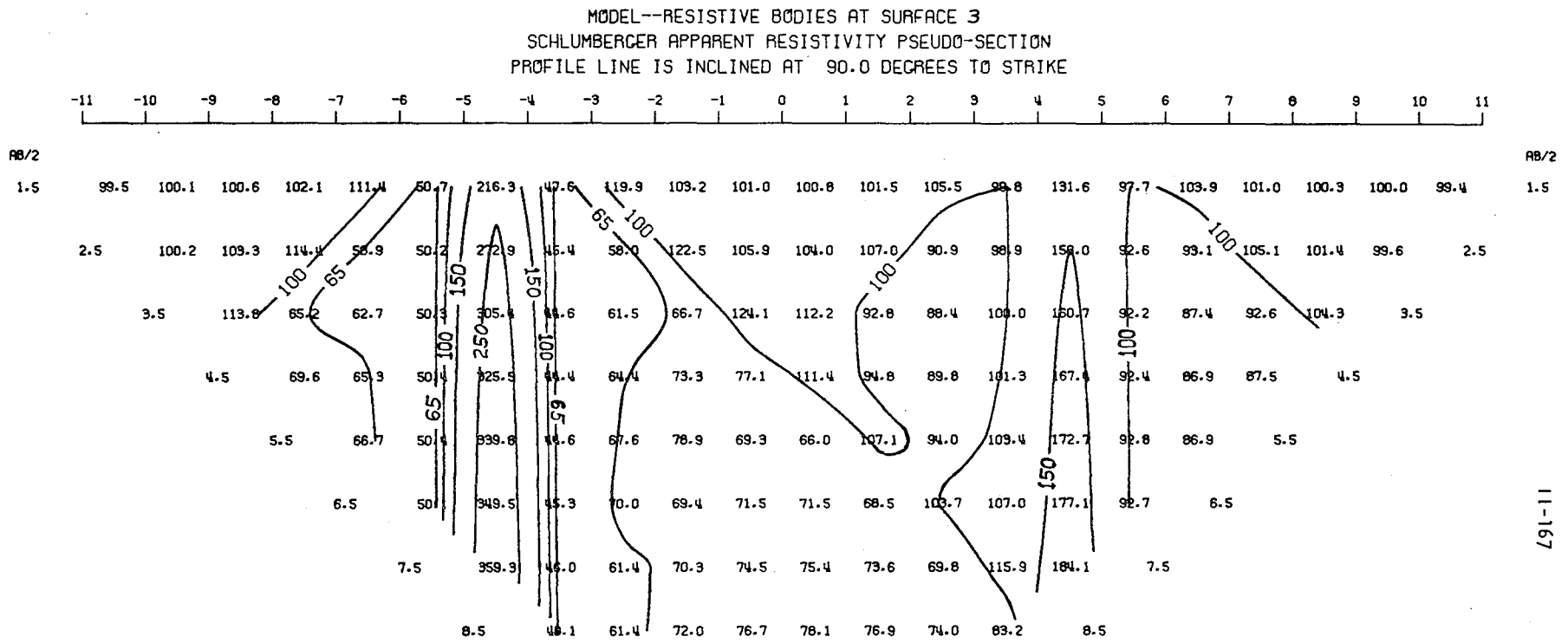

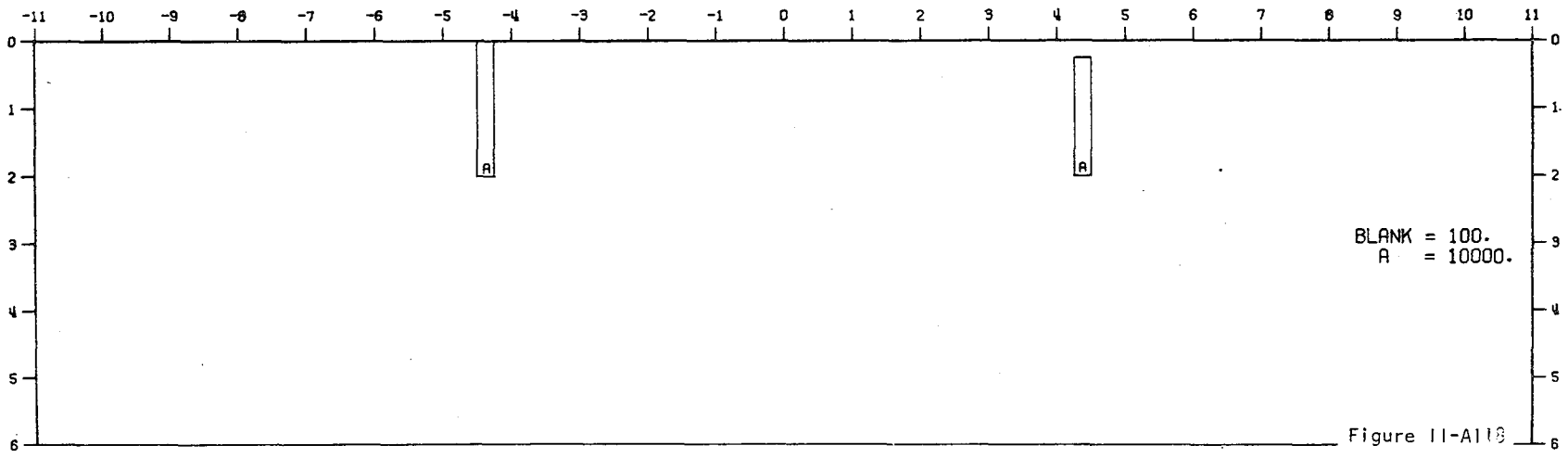

Figure II-A11

MODEL--VERTICAL CONTACT
DIPOLE-DIPOLE APPARENT RESISTIVITY PSEUDO-SECTION
PROFILE LINE IS INCLINED AT 45.0 DEGREES TO STRIKE

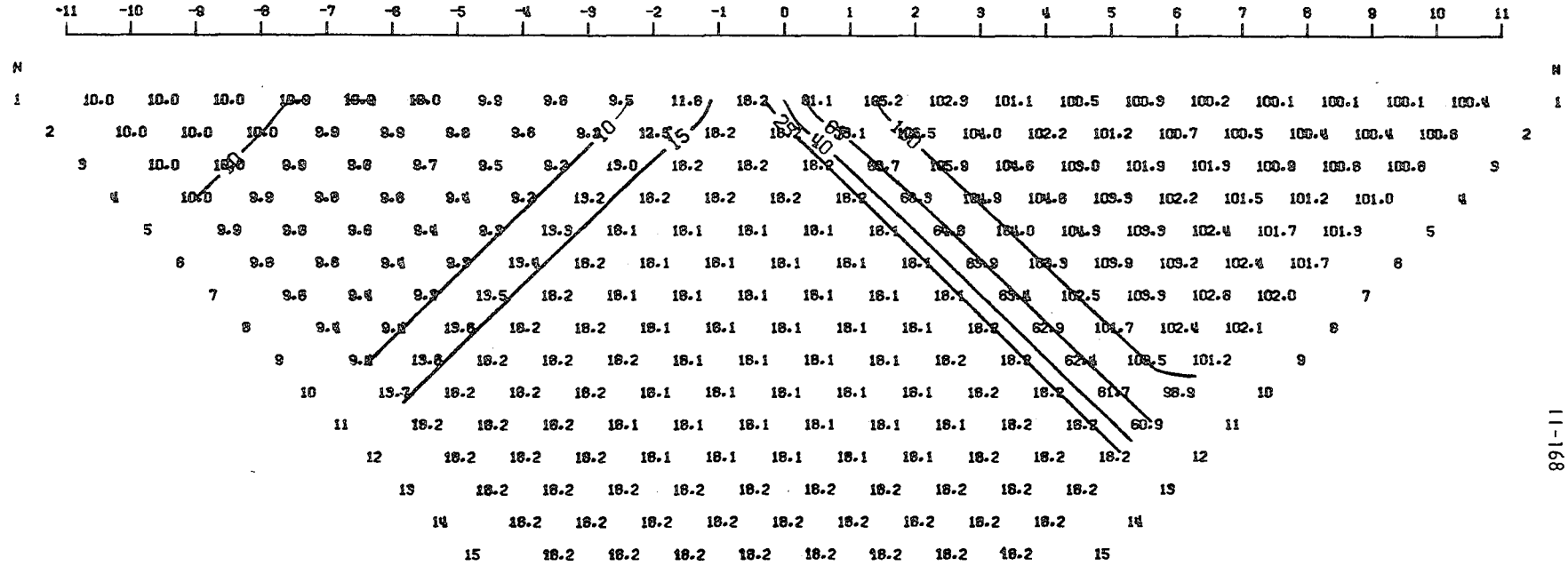

2-D RESISTIVITY MODEL. 45. DEG. PROJECTION--VERTICAL CONTACT

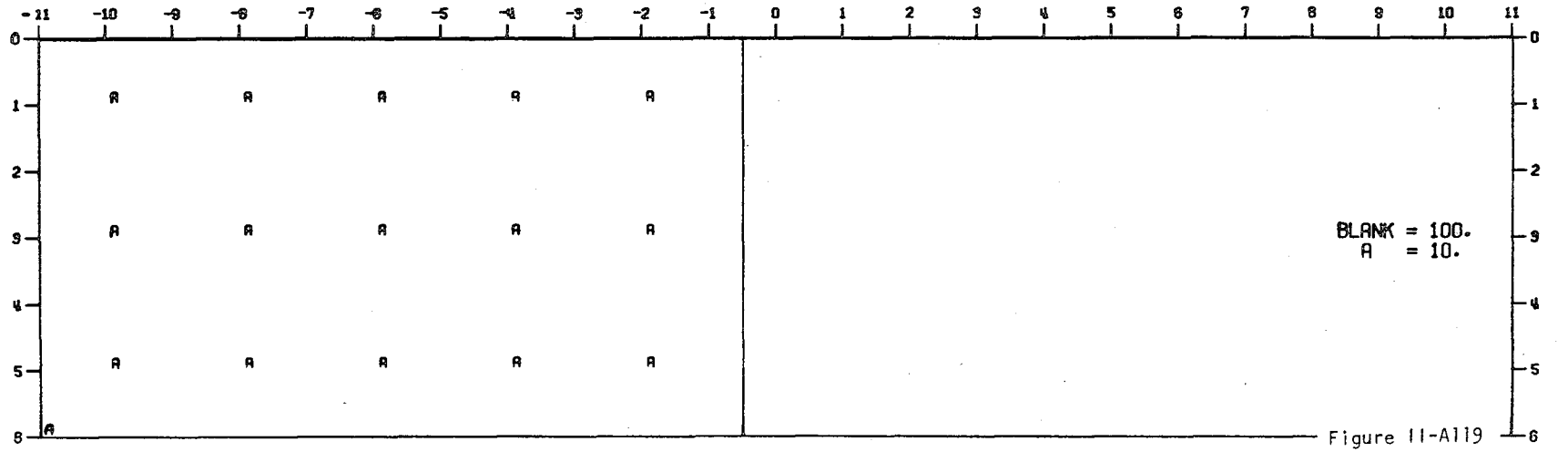

Figure II-A119

MODEL--VERTICAL CONTACT
SCHLUMBERGER APPARENT RESISTIVITY PSEUDO-SECTION
PROFILE LINE IS INCLINED AT 45.0 DEGREES TO STRIKE

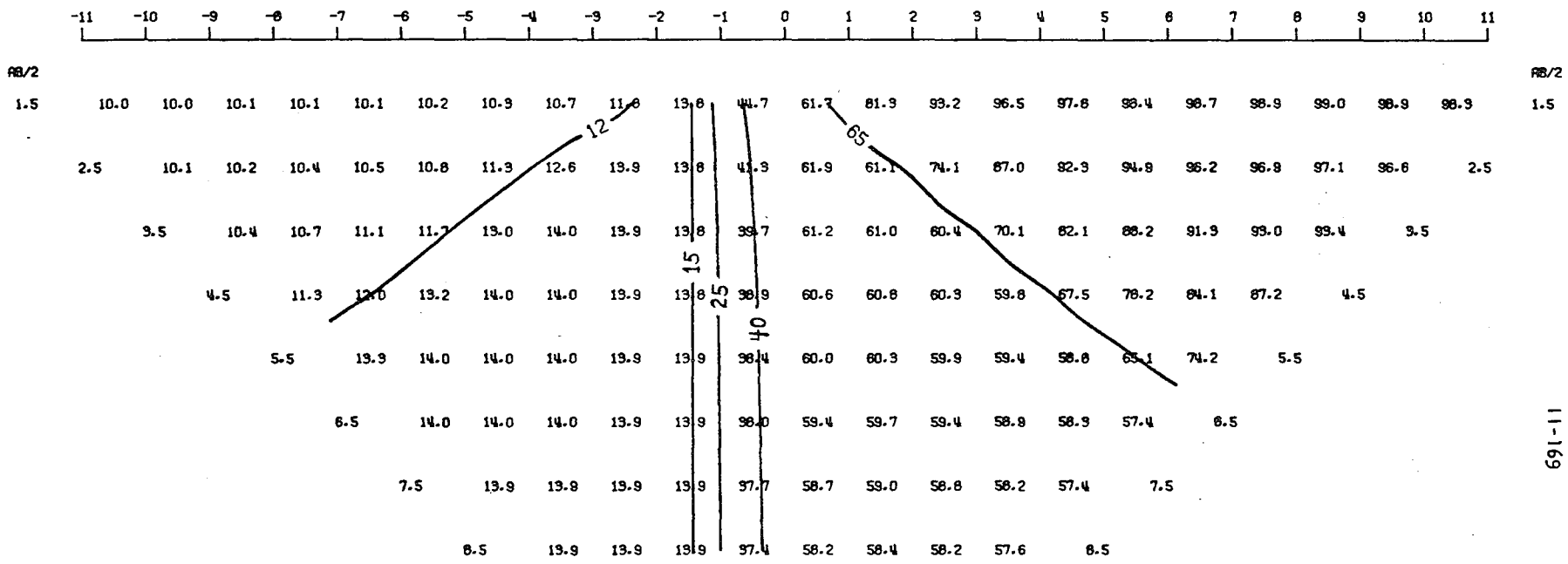

2-D RESISTIVITY MODEL, 45. DEG. PROJECTION--VERTICAL CONTACT

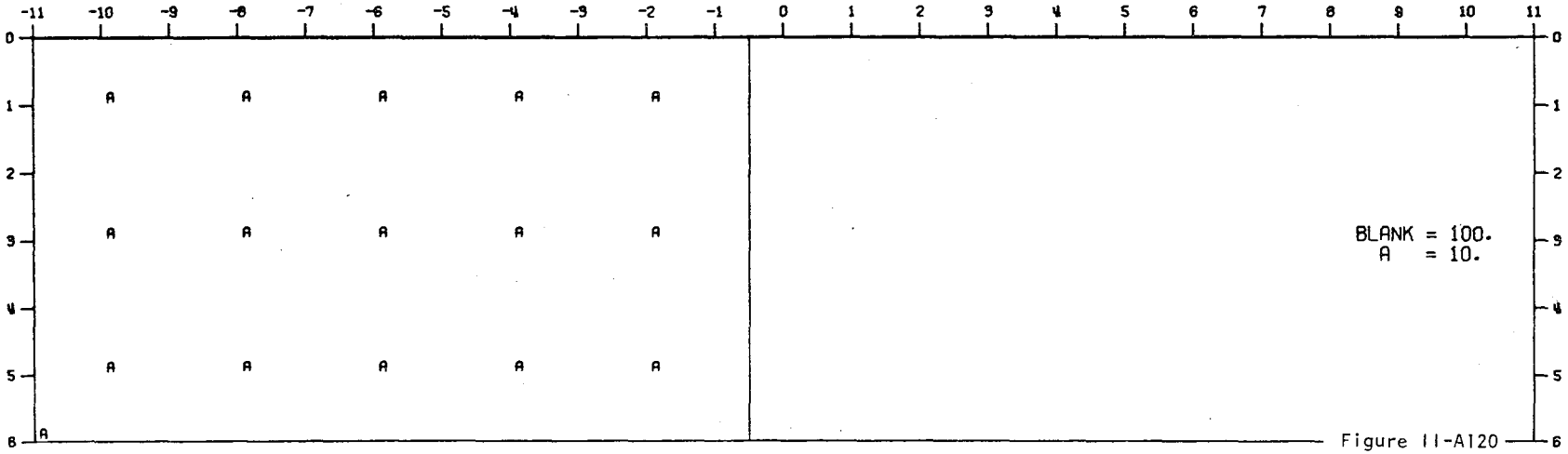

Figure 11-A120

MODEL--SHALLOW VALLEY A
DIPOLE-DIPOLE APPARENT RESISTIVITY PSEUDO-SECTION
PROFILE LINE IS INCLINED AT 45.0 DEGREES TO STRIKE

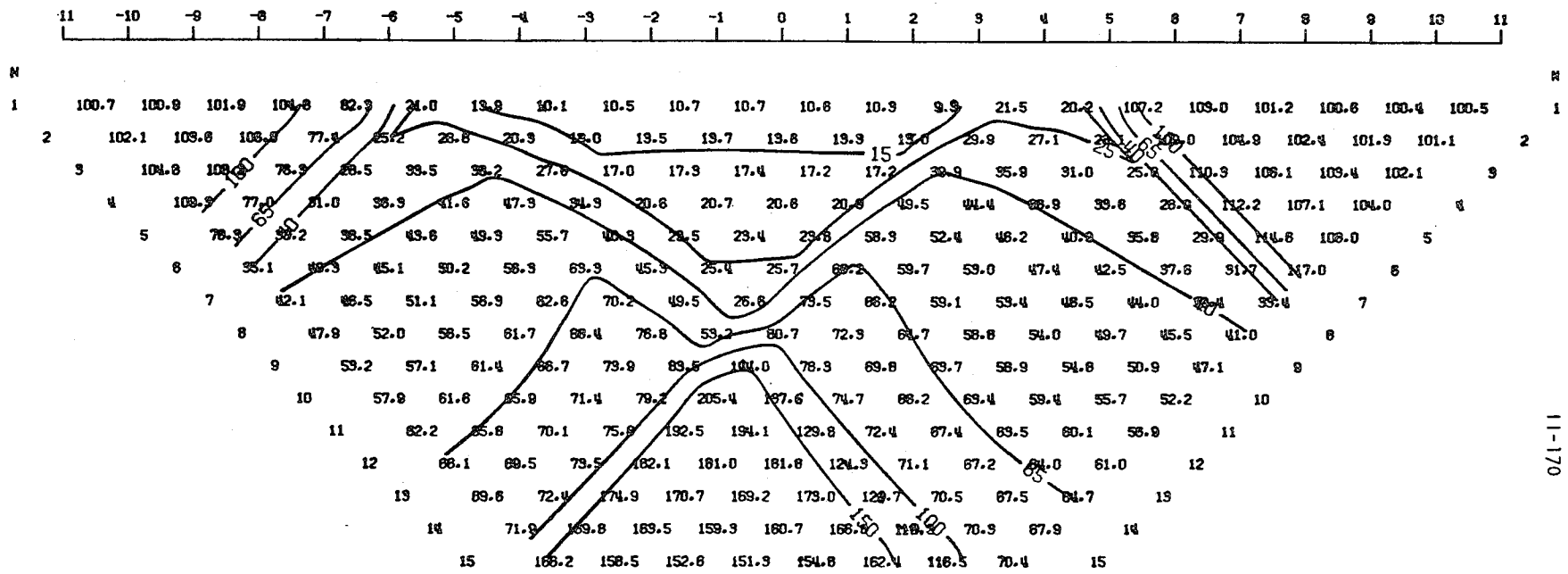

2-D RESISTIVITY MODEL. 45. DEG. PROJECTION--SHALLOW VALLEY

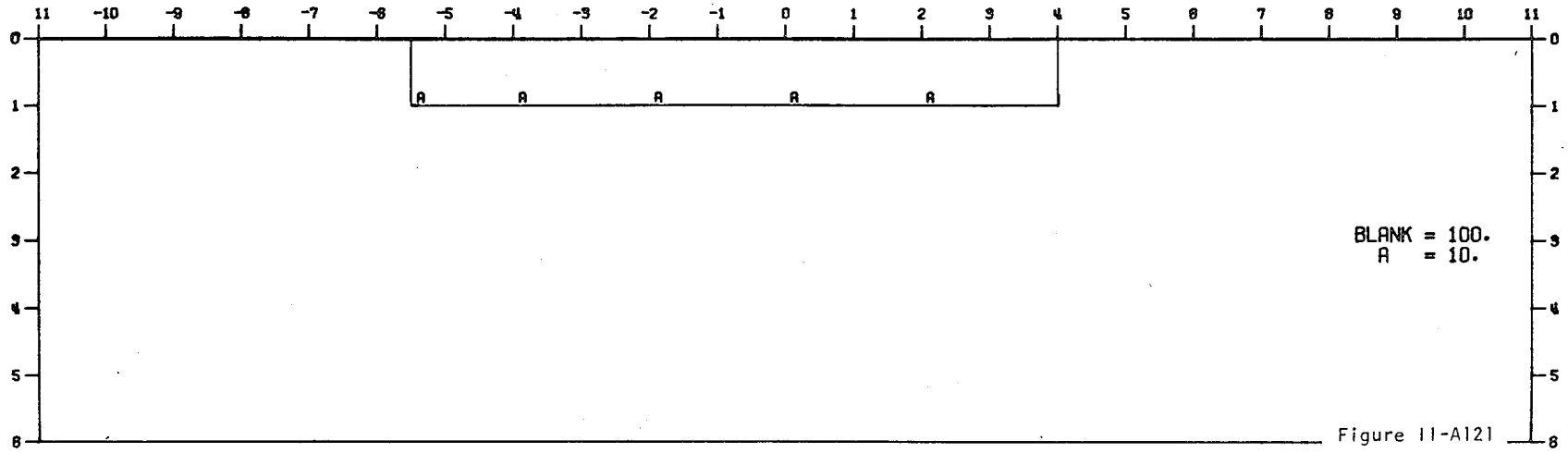

Figure 11-A121

MODEL--SHALLOW VALLEY A
SCHLUMBERGER APPARENT RESISTIVITY PSEUDO-SECTION
PROFILE LINE IS INCLINED AT 45.0 DEGREES TO STRIKE

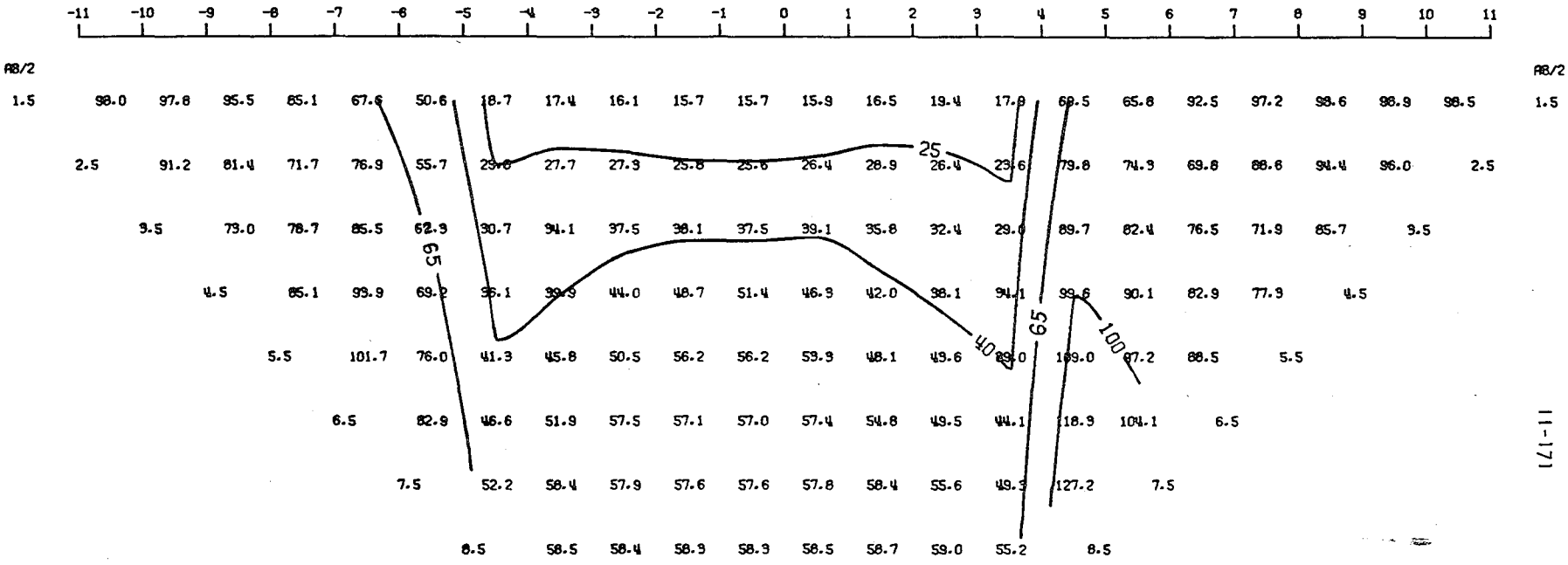

2-D RESISTIVITY MODEL, 45. DEG. PROJECTION--SHALLOW VALLEY

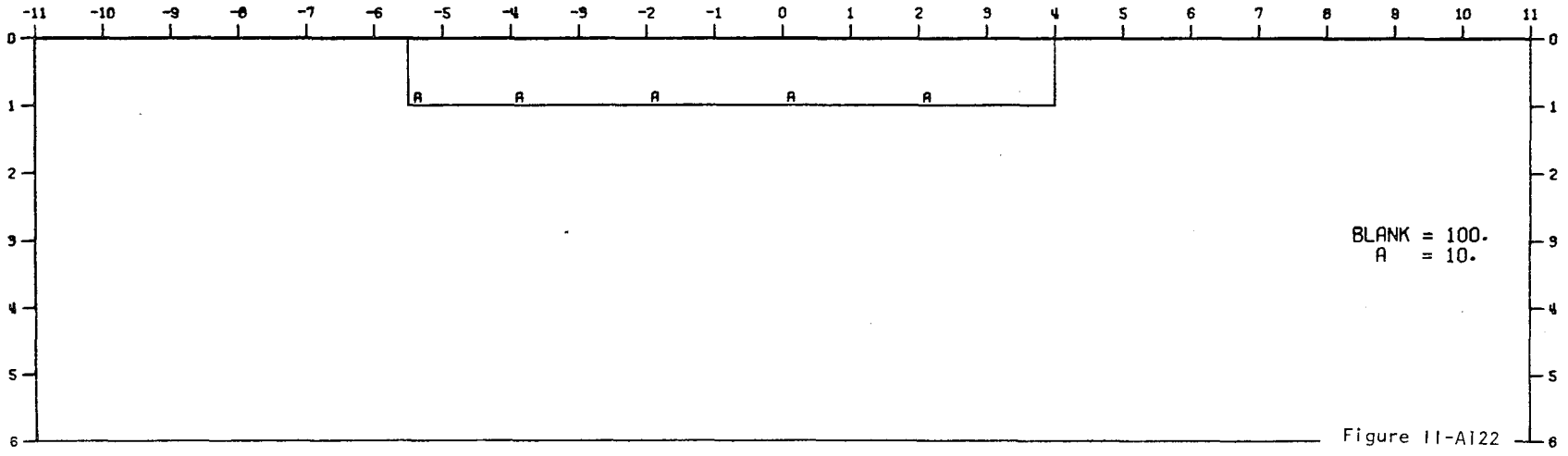

Figure II-A122

MODEL--BURIED VERTICAL CONTACT 1
DIPOLE-DIPOLE APPARENT RESISTIVITY PSEUDO-SECTION
PROFILE LINE IS INCLINED AT 45.0 DEGREES TO STRIKE

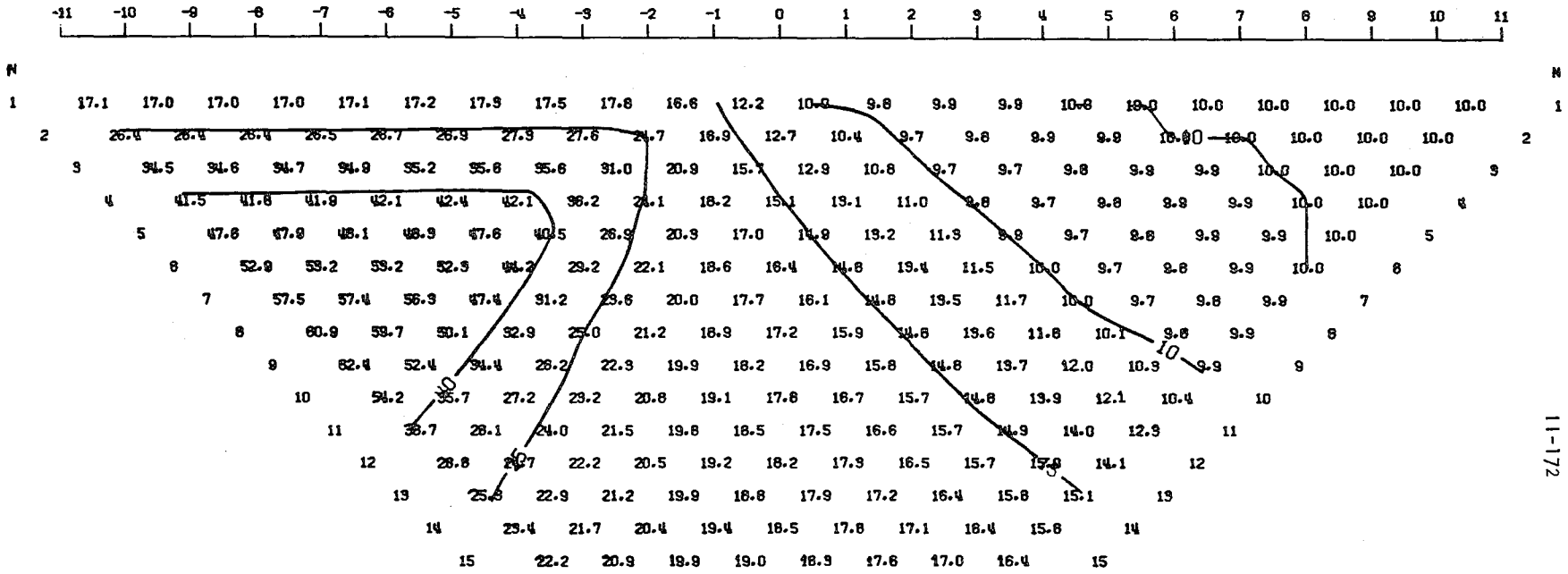

2-D RESISTIVITY MODEL, 45. DEG. PROJECTION--BURIED VERTICAL CONTACT 1

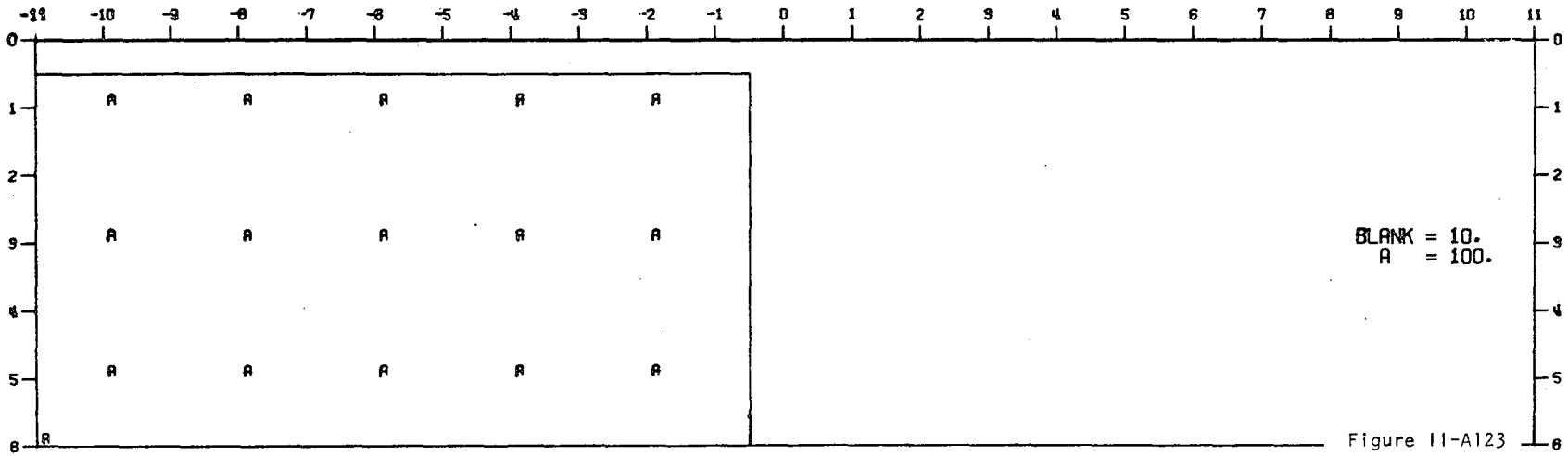

Figure II-A123

MODEL--BURIED VERTICAL CONTACT 1
SCHLUMBERGER APPARENT RESISTIVITY PSEUDO-SECTION
PROFILE LINE IS INCLINED AT 45.0 DEGREES TO STRIKE

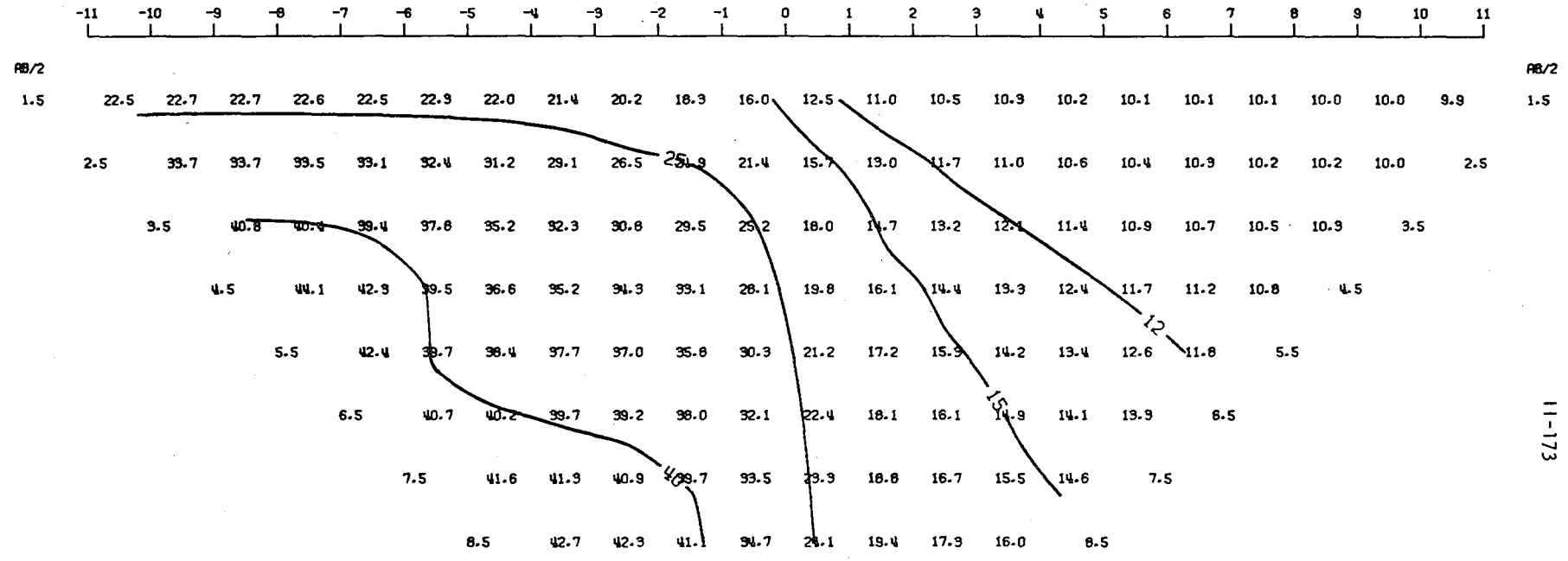

2-D RESISTIVITY MODEL, 45. DEG. PROJECTION--BURIED VERTICAL CONTACT 1

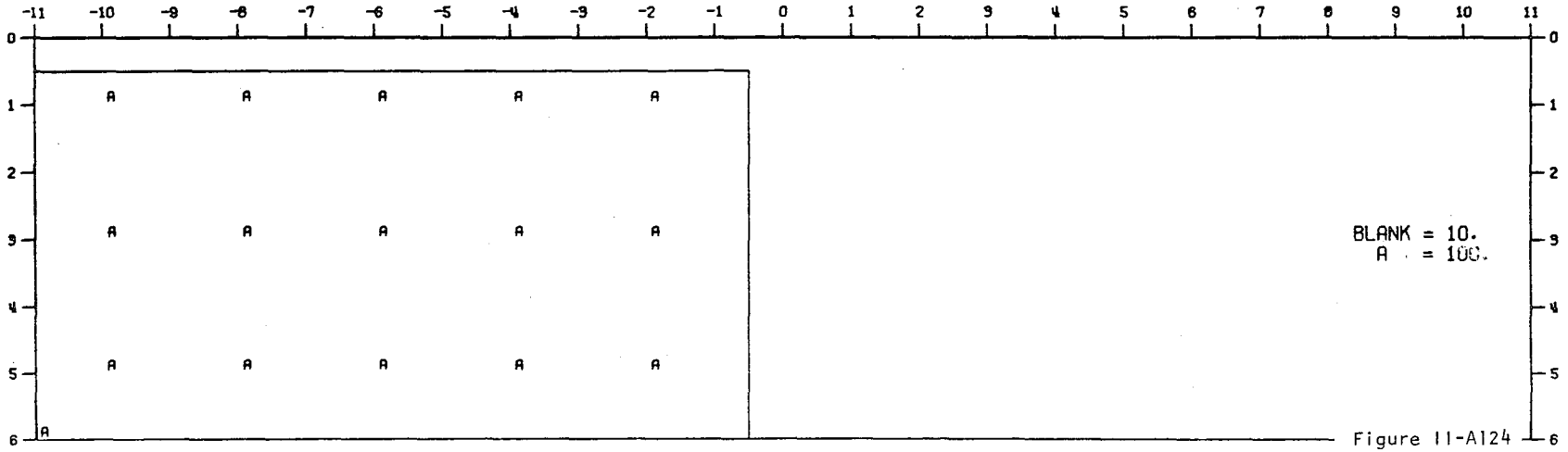

Figure II-A124

MODEL--FAULT 1
DIPOLE-DIPOLE APPARENT RESISTIVITY PSEUDO-SECTION
PROFILE LINE IS INCLINED AT 45.0 DEGREES TO STRIKE

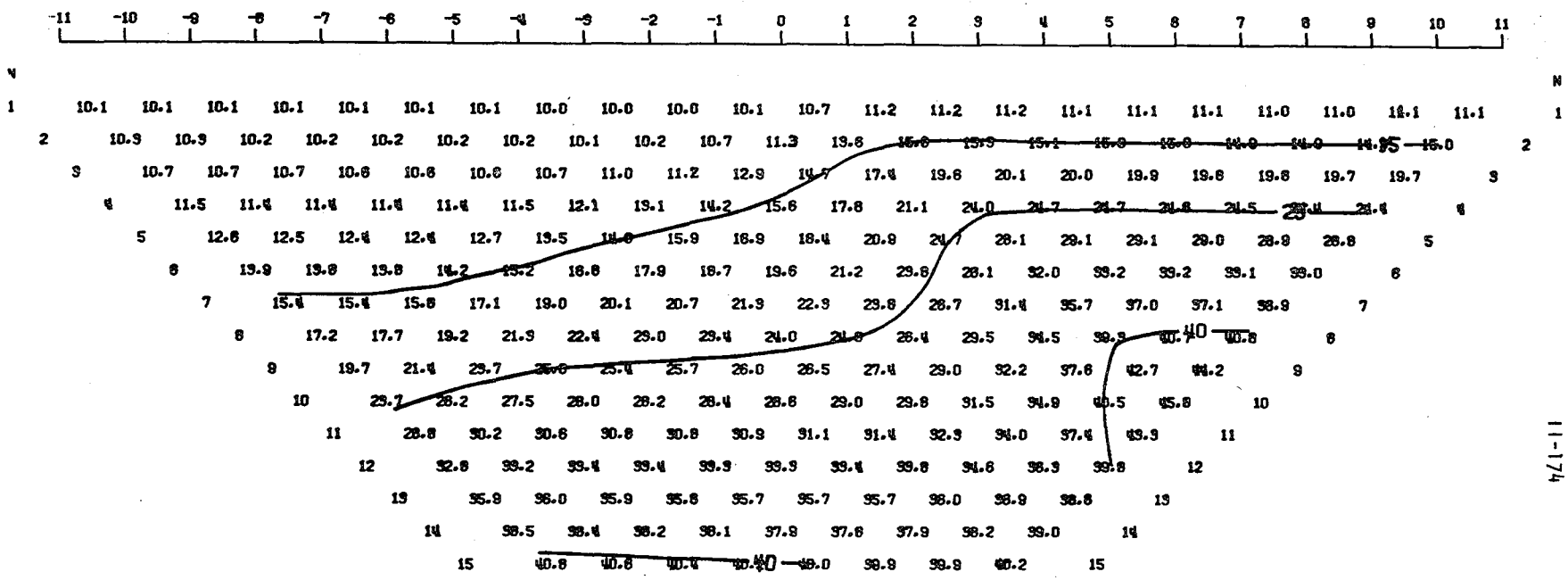

2-D RESISTIVITY MODEL, 45. DEG. PROJECTION--FAULT 1

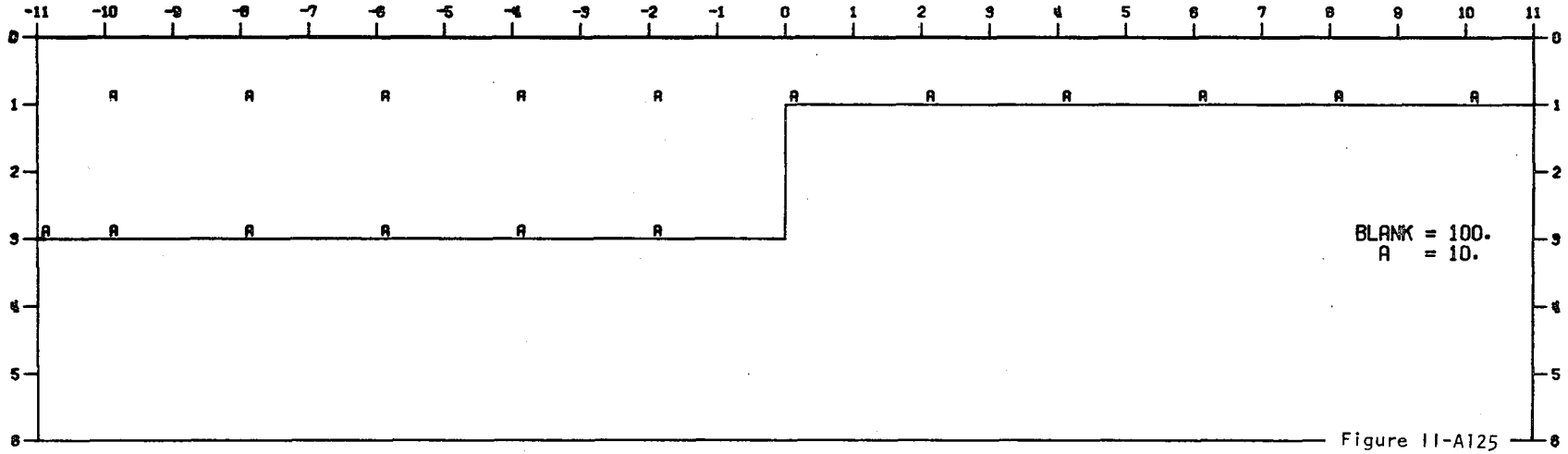

Figure II-A125

MODEL--FAULT 1
SCHLUMBERGER APPARENT RESISTIVITY PSEUDO-SECTION
PROFILE LINE IS INCLINED AT 45.0 DEGREES TO STRIKE

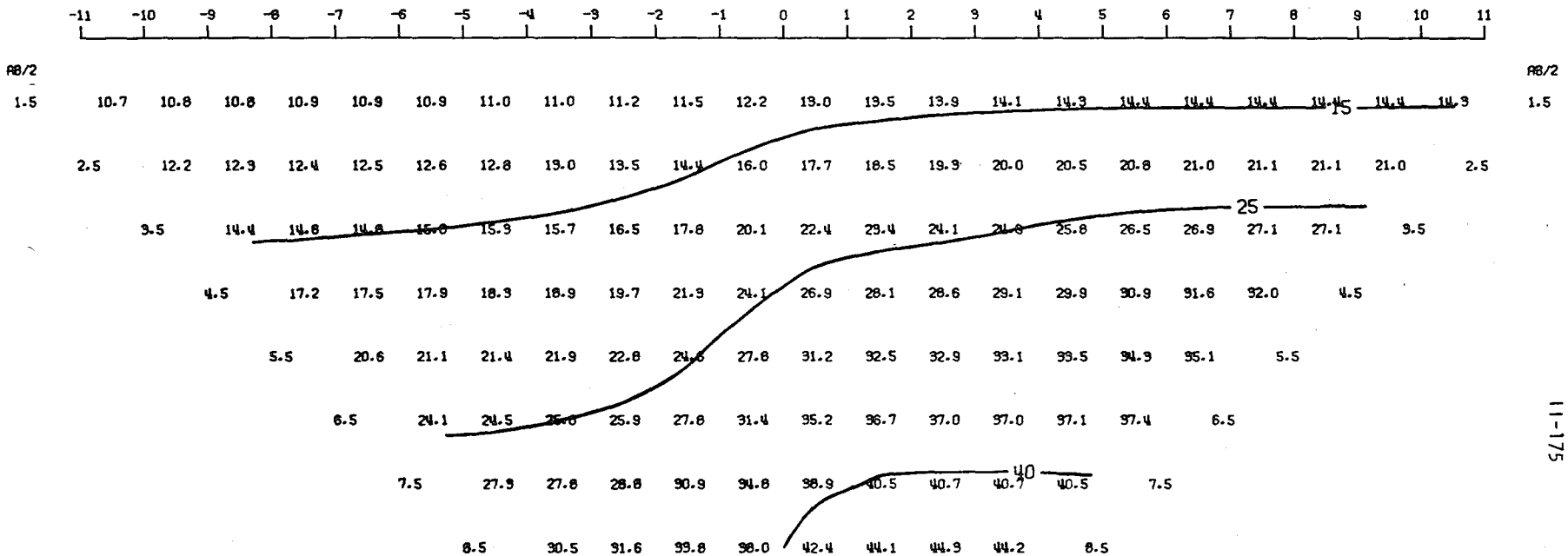

2-D RESISTIVITY MODEL, 45. DEG. PROJECTION--FAULT 1

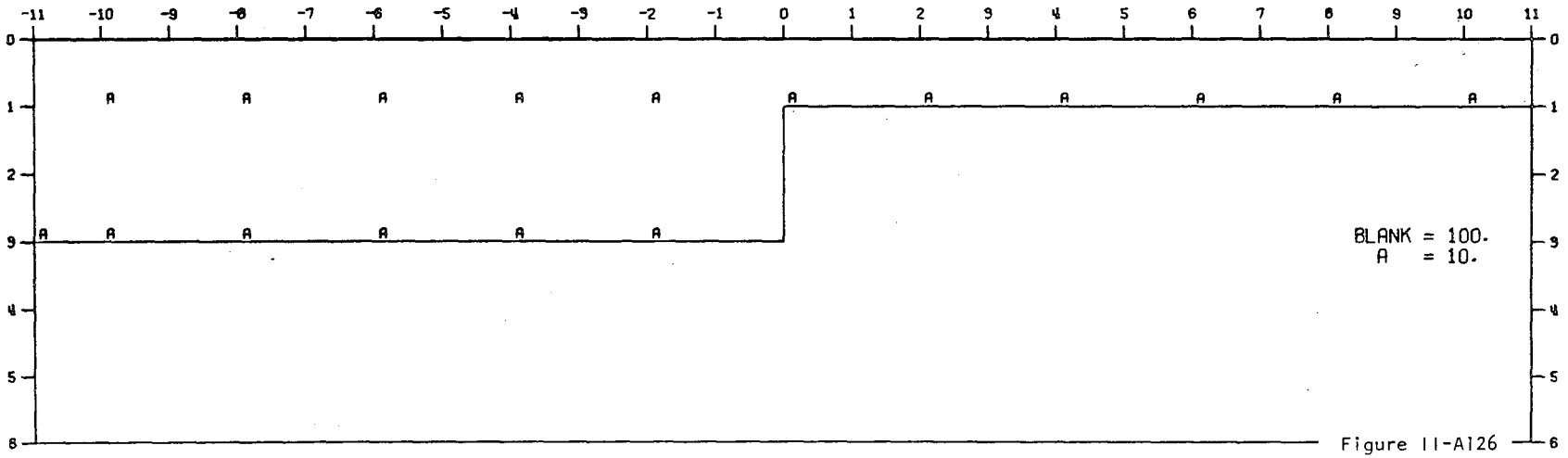

Figure II-A126

MODEL--BURIED VERTICAL CONTACT 2
DIPOLE-DIPOLE APPARENT RESISTIVITY PSEUDO-SECTION
PROFILE LINE IS INCLINED AT 45.0 DEGREES TO STRIKE

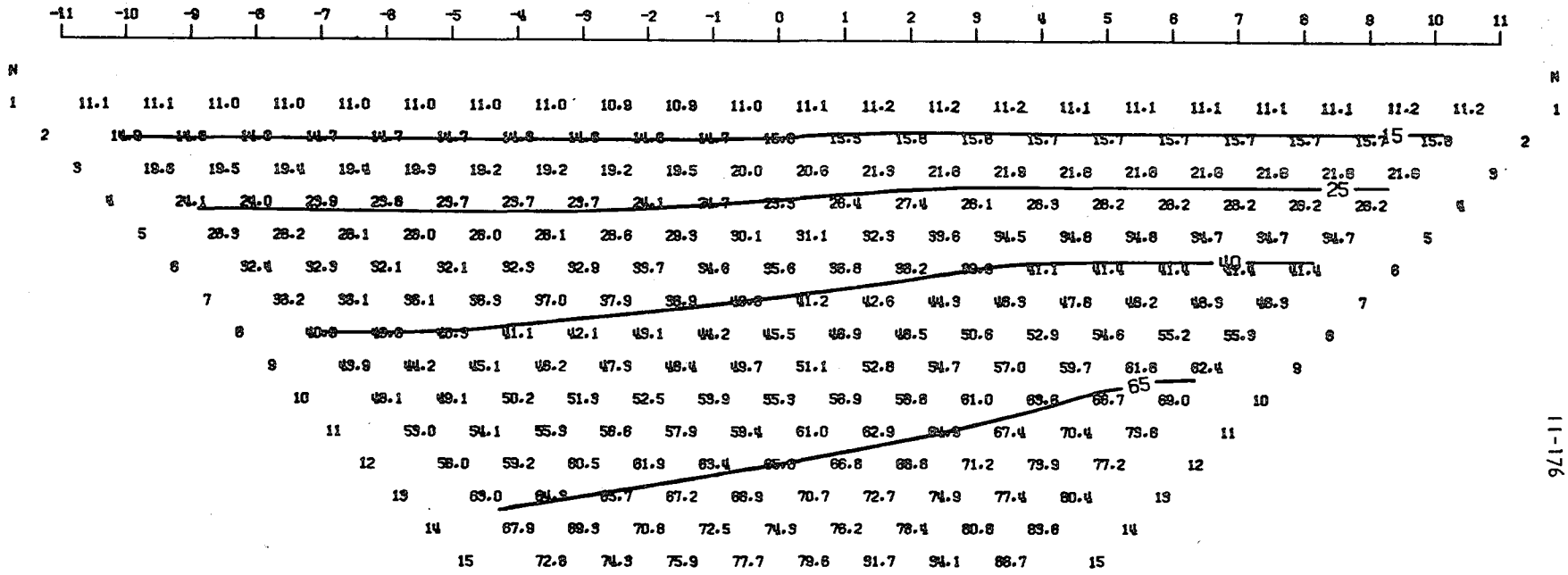

11-176

2-D RESISTIVITY MODEL, 45. DEG. PROJECTION--BURIED VERTICAL CONTACT 2

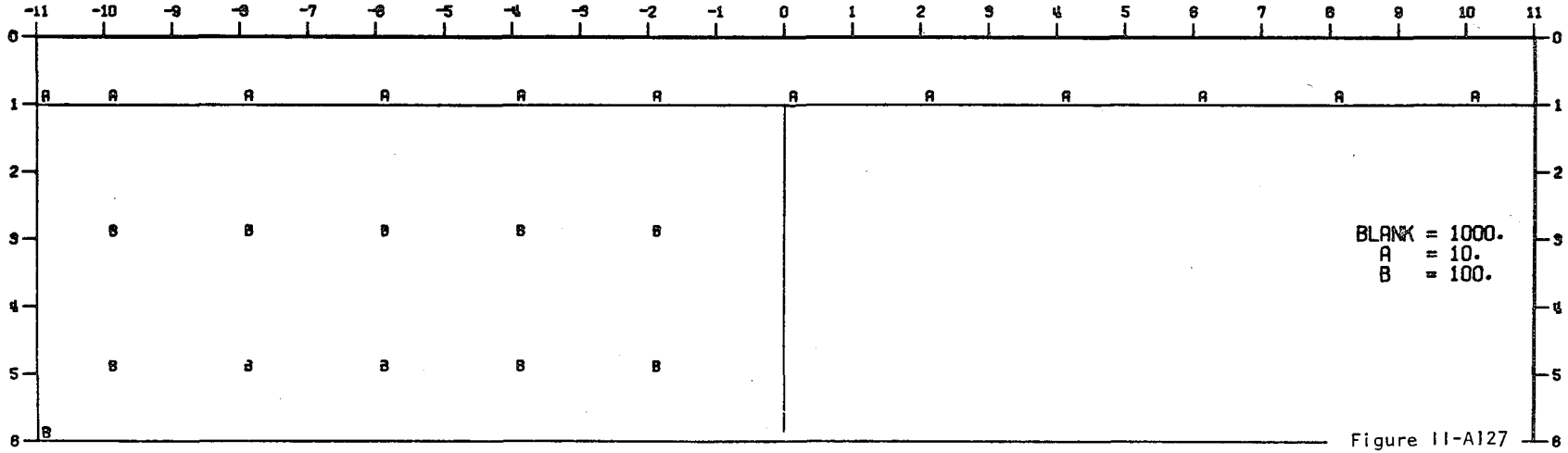

Figure II-A127

MODEL--BURIED VERTICAL CONTACT 2
SCHLUMBERGER APPARENT RESISTIVITY PSEUDO-SECTION
PROFILE LINE IS INCLINED AT 45.0 DEGREES TO STRIKE

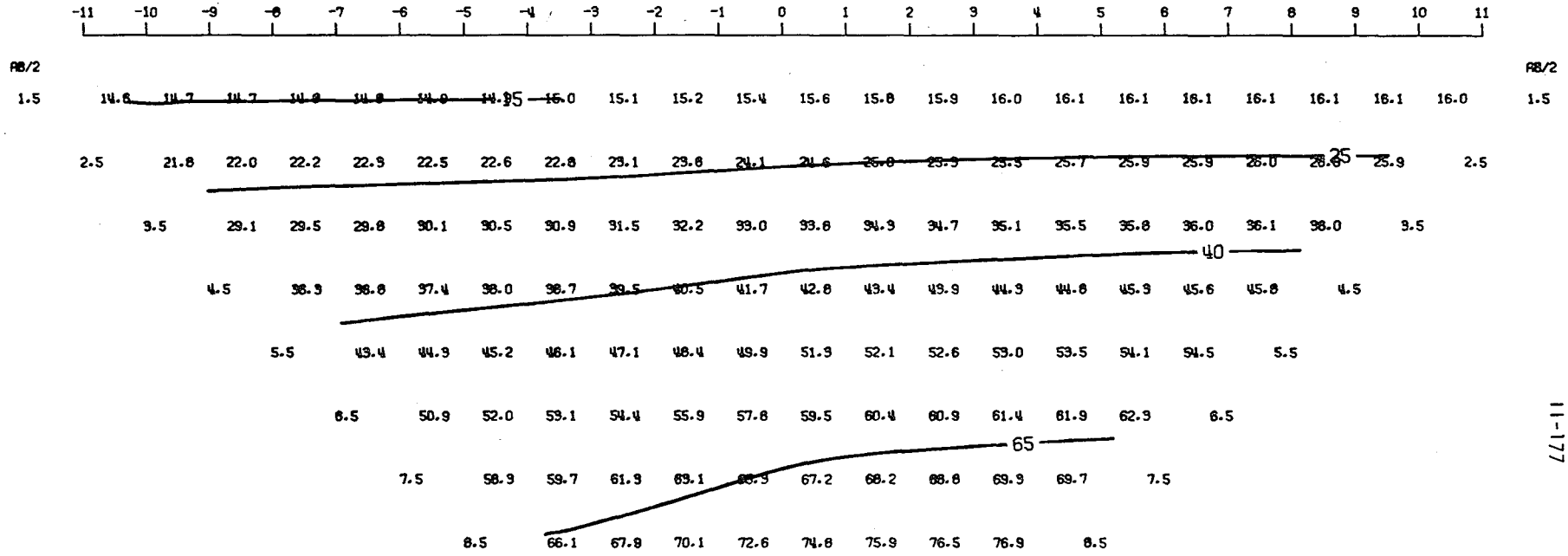

2-D RESISTIVITY MODEL, 45. DEG. PROJECTION--BURIED VERTICAL CONTACT 2

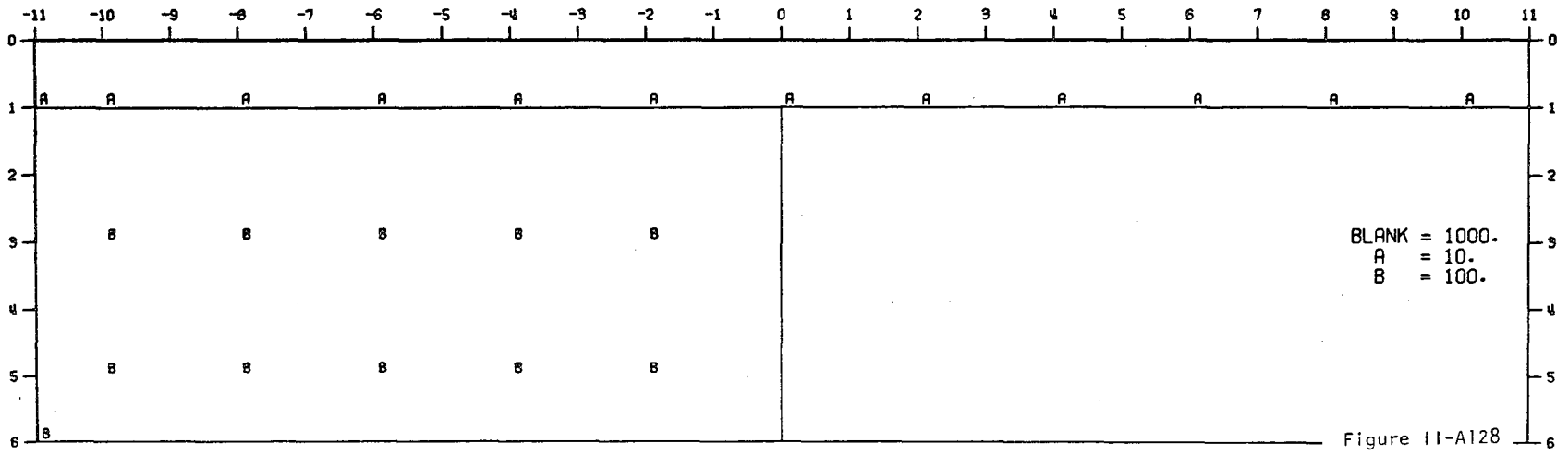

Figure II-A128

MODEL--CONDUCTIVE BODY 1A
DIPOLE-DIPOLE APPARENT RESISTIVITY PSEUDO-SECTION
PROFILE LINE IS INCLINED AT 45.0 DEGREES TO STRIKE

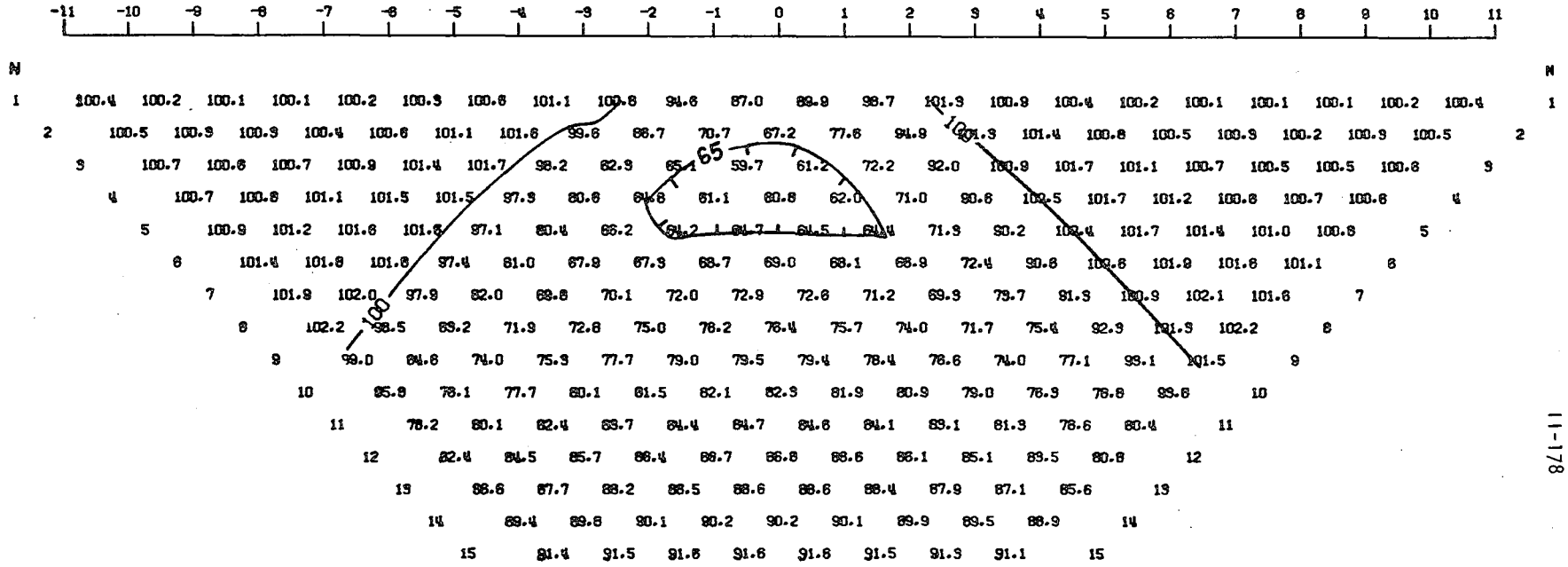

2-D RESISTIVITY MODEL. 45. DEG. PROJECTION--CONDUCTIVE BODY 1A

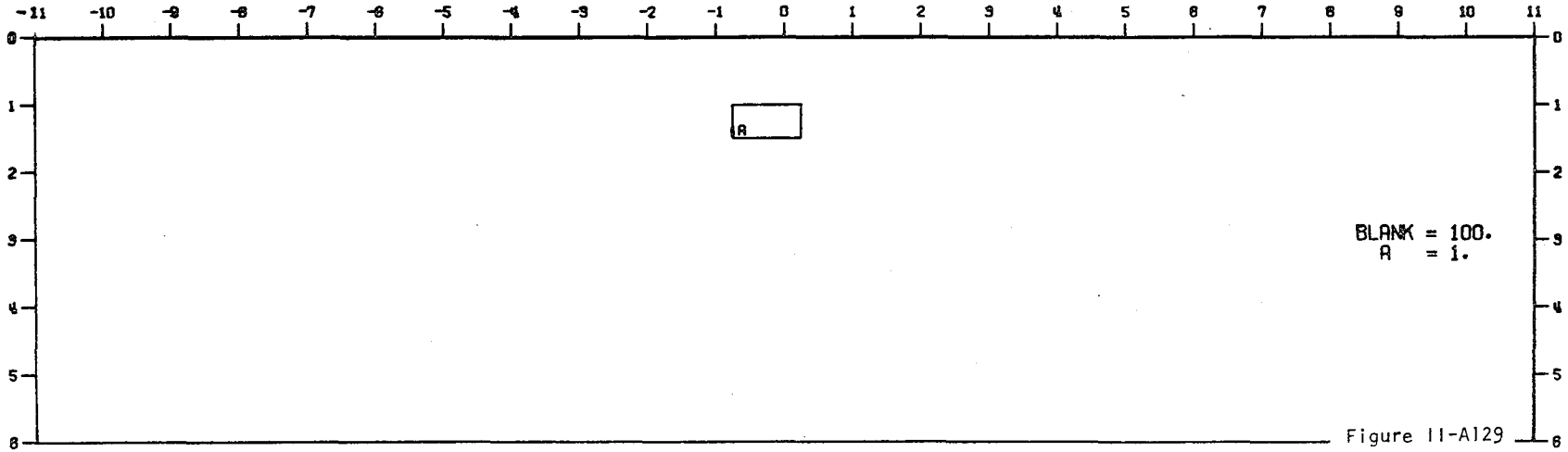

Figure II-A129

MODEL--CONDUCTIVE BODY 1A
SCHLUMBERGER APPARENT RESISTIVITY PSEUDO-SECTION
PROFILE LINE IS INCLINED AT 45.0 DEGREES TO STRIKE

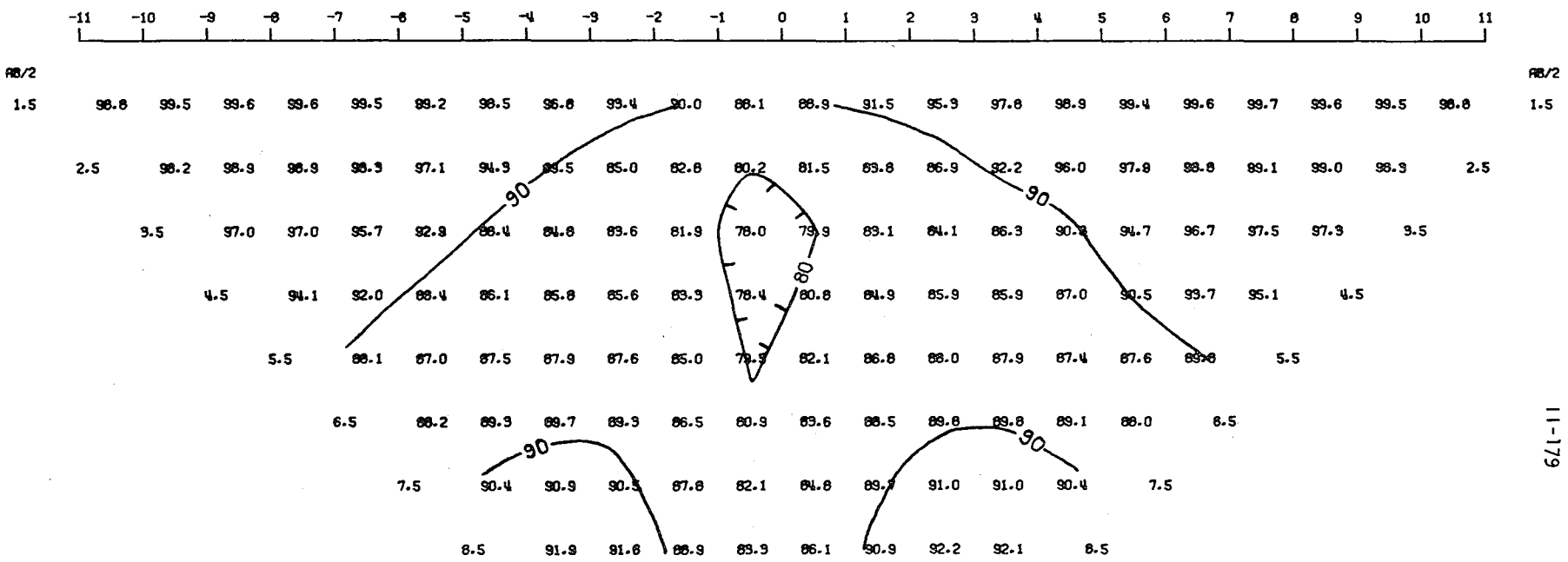

2-D RESISTIVITY MODEL, 45. DEG. PROJECTION--CONDUCTIVE BODY 1A

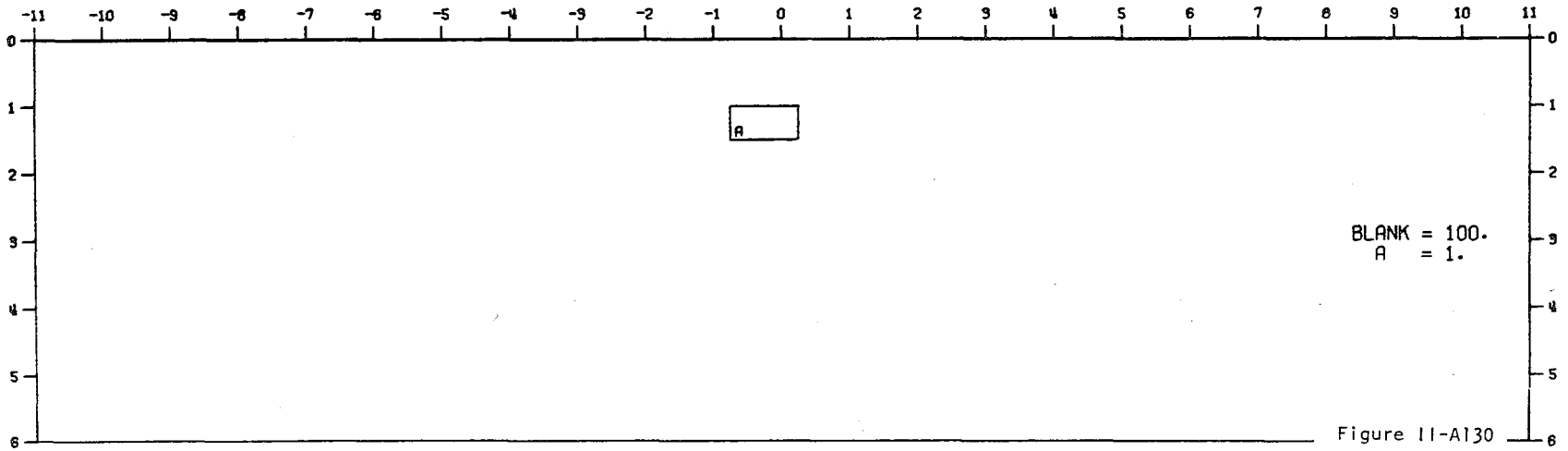

Figure II-A130

MODEL--CONDUCTIVE BODY 1B
DIPOLE-DIPOLE APPARENT RESISTIVITY PSEUDO-SECTION
PROFILE LINE IS INCLINED AT 45.0 DEGREES TO STRIKE

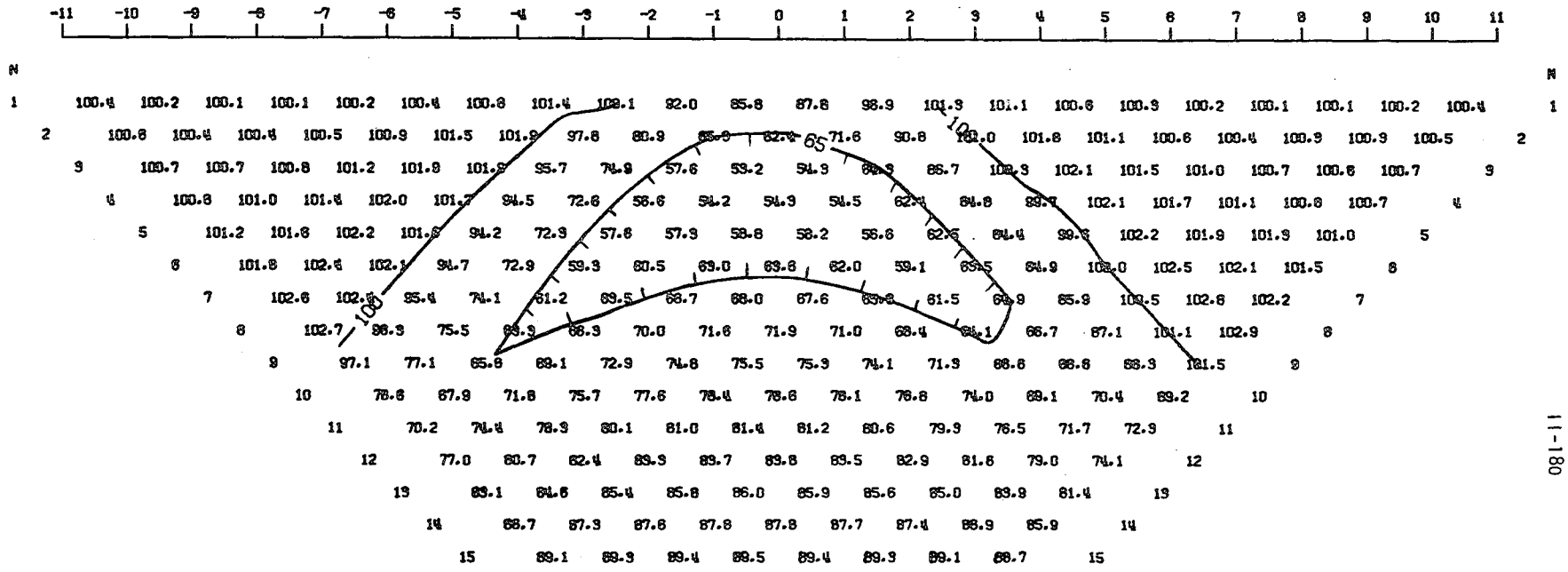

2-D RESISTIVITY MODEL, 45. DEC. PROJECTION--CONDUCTIVE BODY 1B

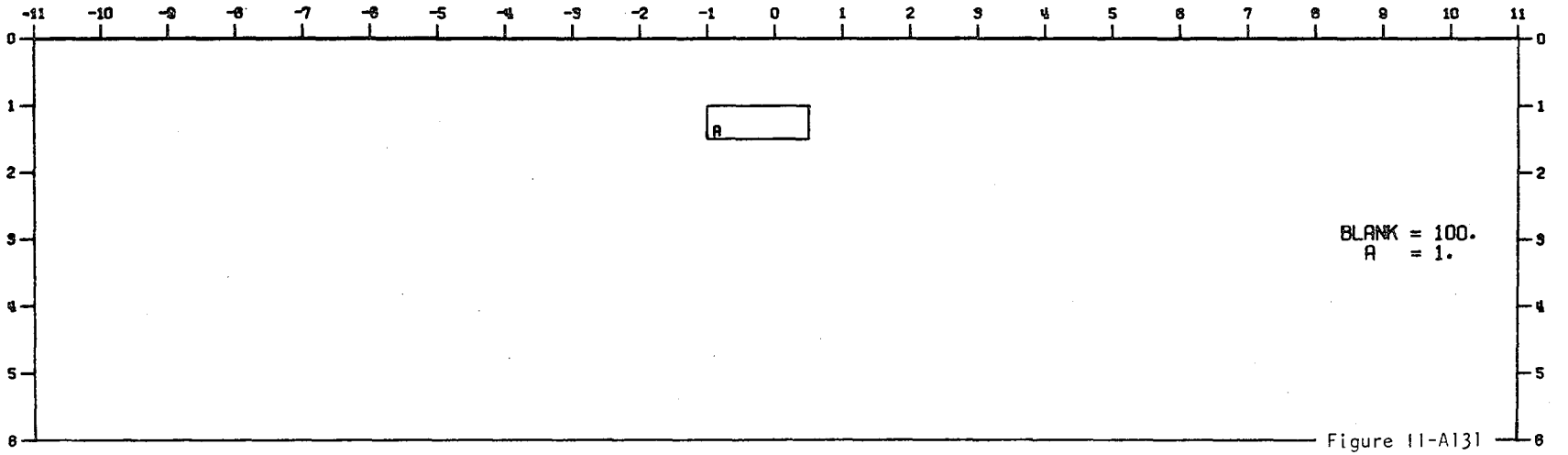

Figure II-A131

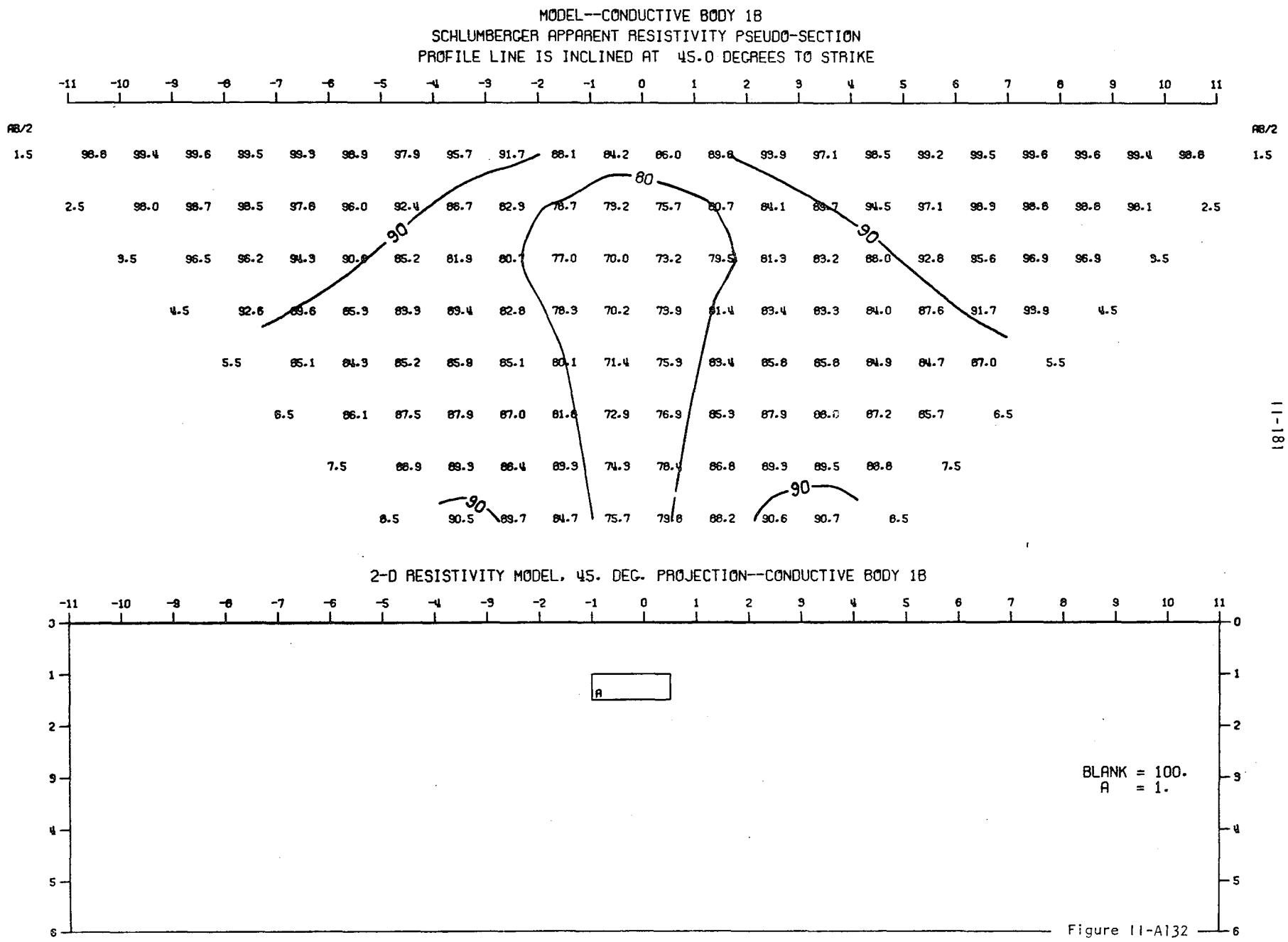

Figure II-A132

MODEL--CONDUCTIVE BODY 3A
DIPOLE-DIPOLE APPARENT RESISTIVITY PSEUDO-SECTION
PROFILE LINE IS INCLINED AT 45.0 DEGREES TO STRIKE

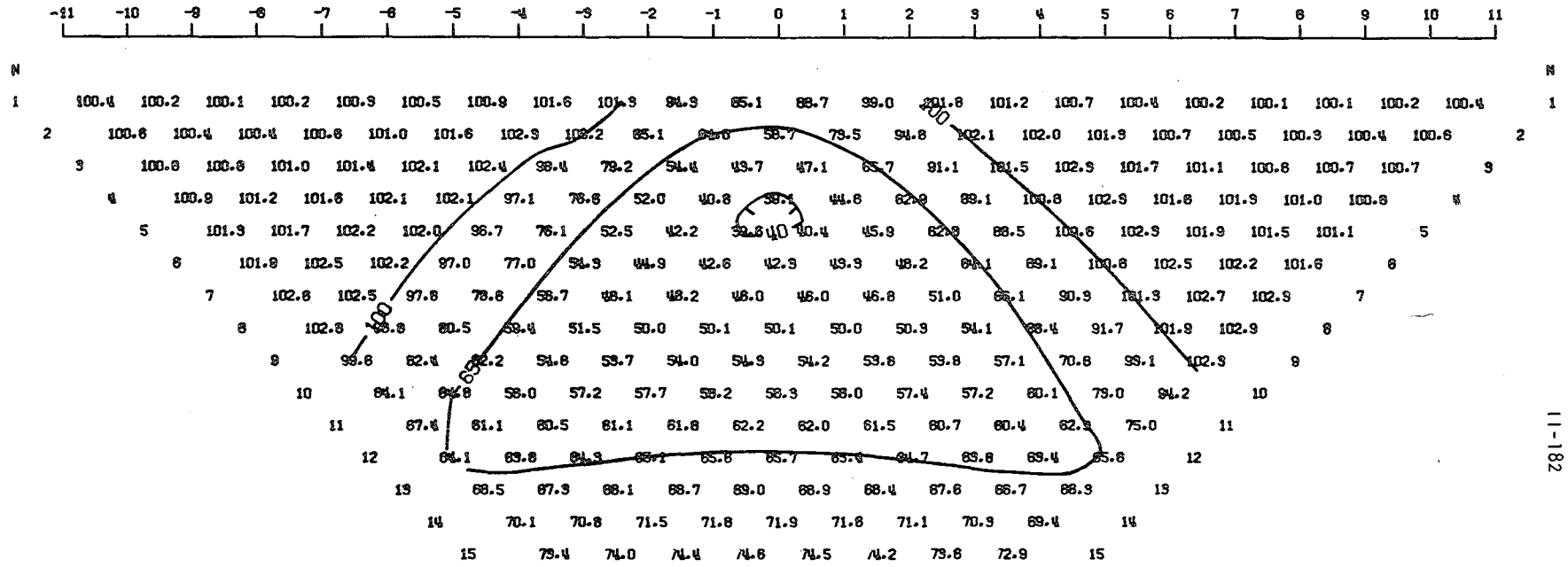

2-D RESISTIVITY MODEL, 45. DEG. PROJECTION--CONDUCTIVE BODY 3A

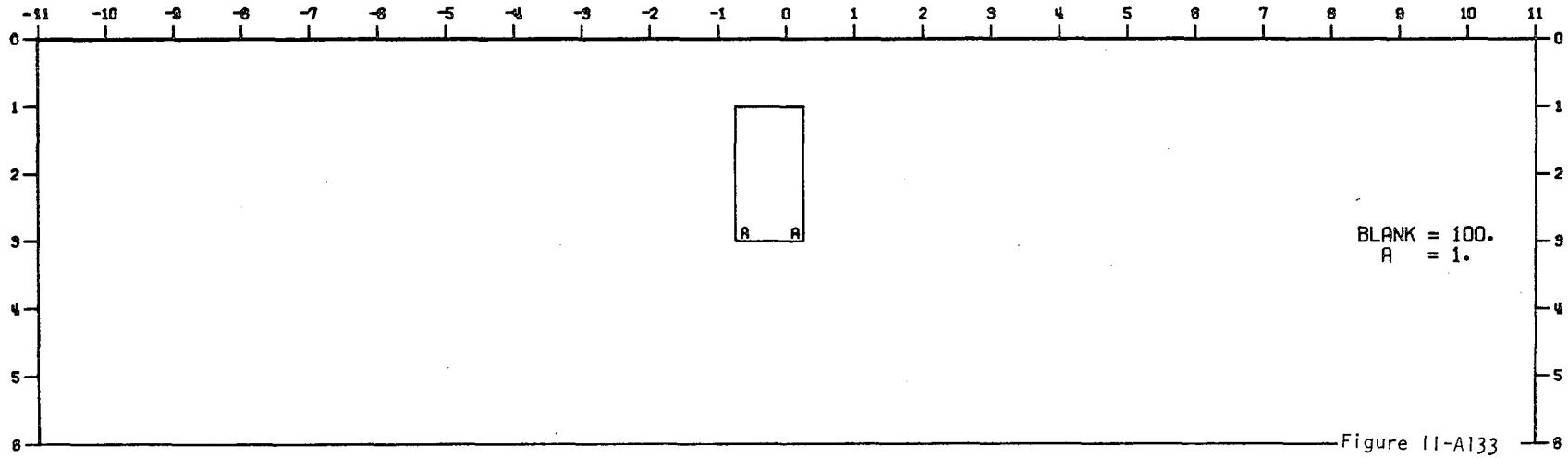

Figure 11-A133

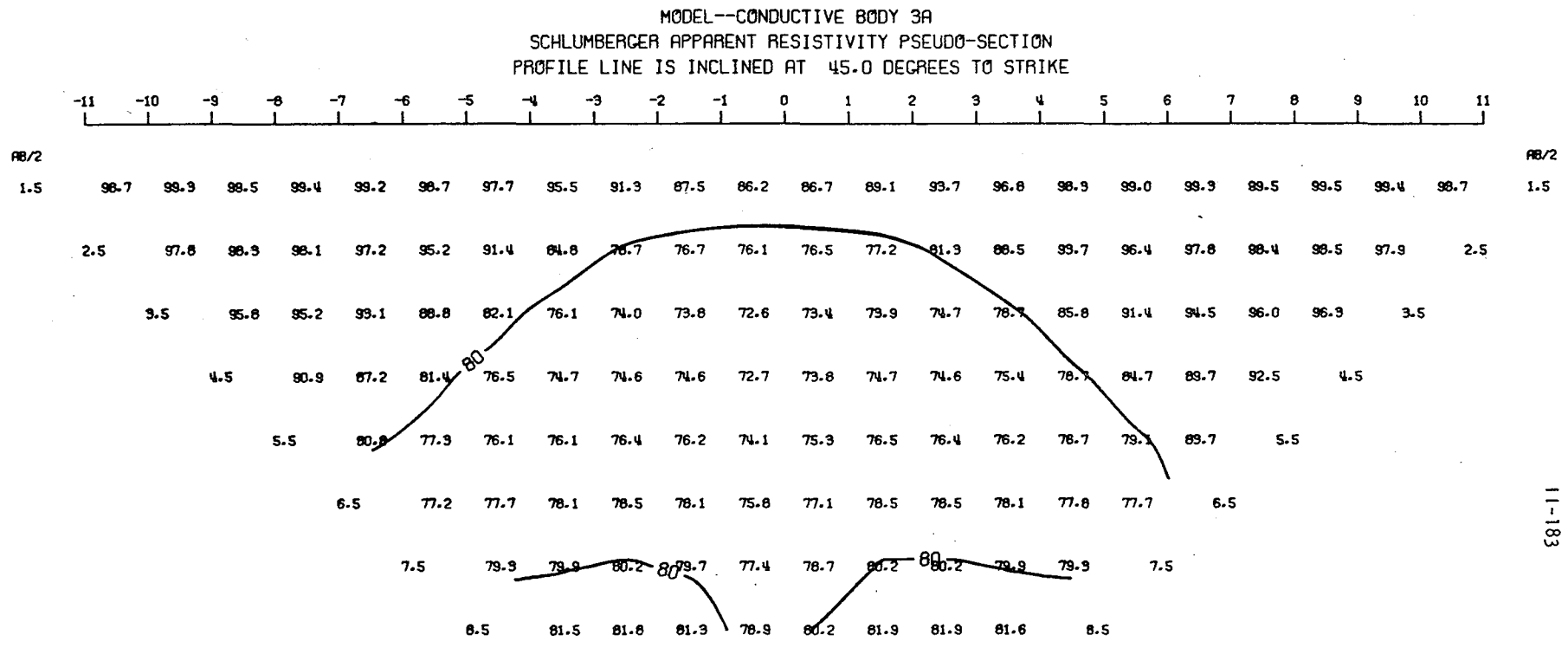

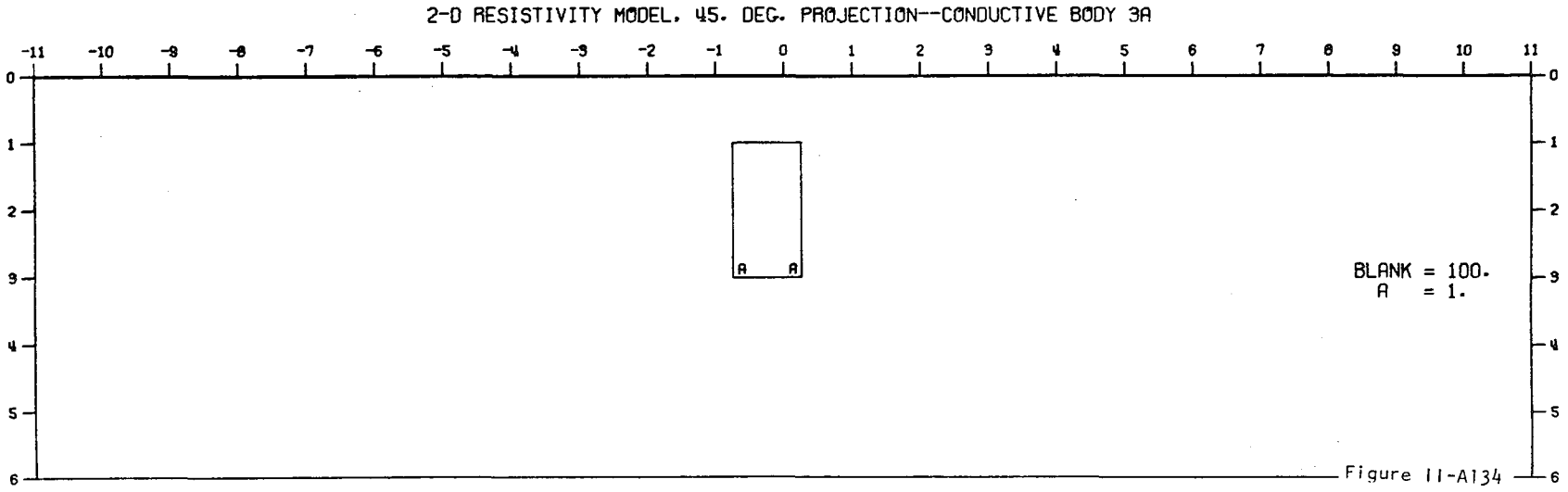

Figure II-A134

MODEL--CONDUCTIVE BODY 3B
DIPOLE-DIPOLE APPARENT RESISTIVITY PSEUDO-SECTION
PROFILE LINE IS INCLINED AT 45.0 DEGREES TO STRIKE

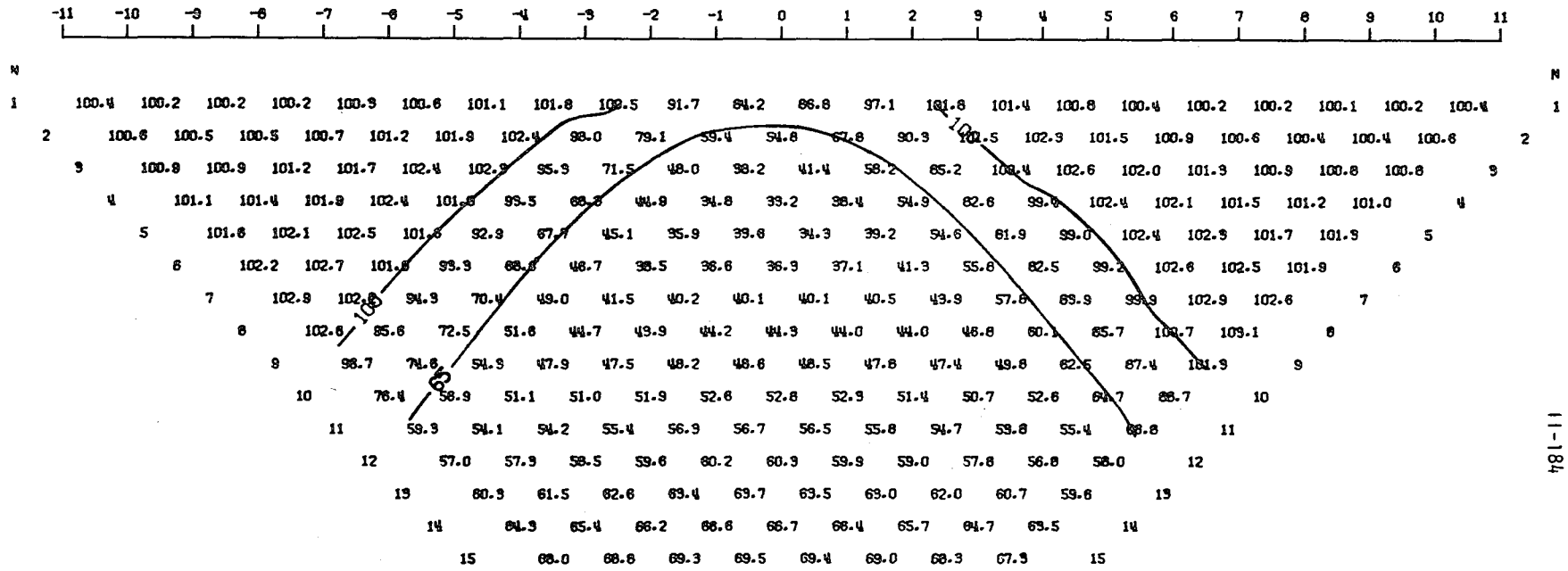

2-D RESISTIVITY MODEL, 45. DEG. PROJECTION--CONDUCTIVE BODY 3B

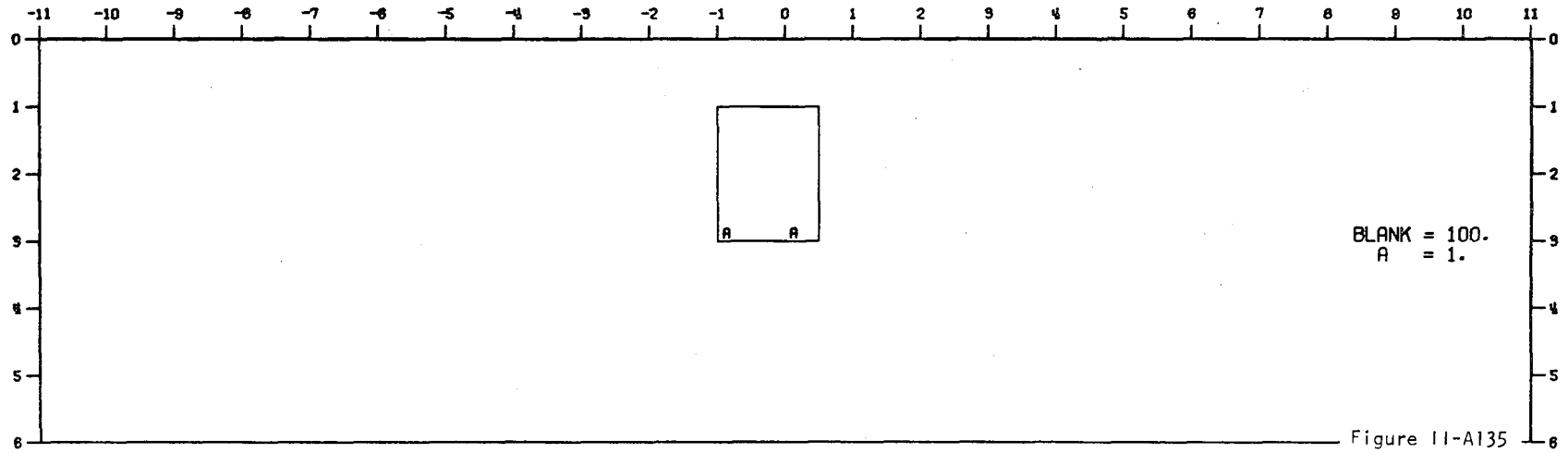

Figure 11-A135

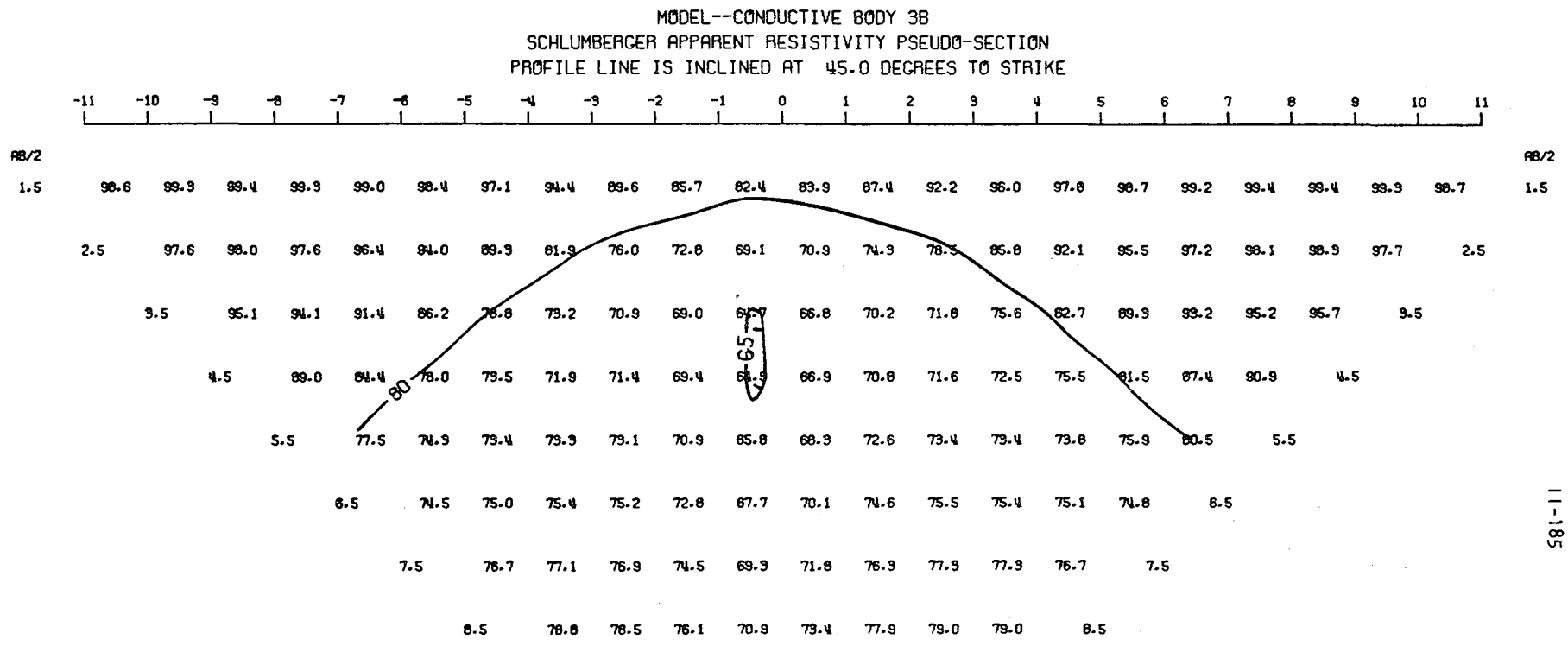

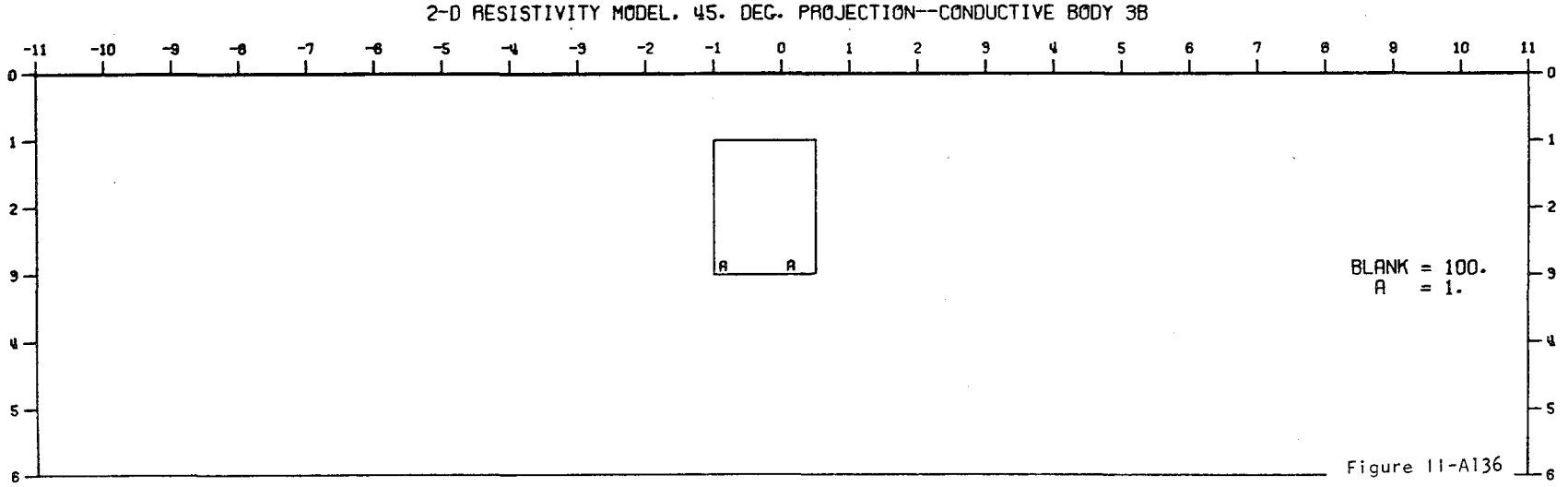

Figure II-A136

MODEL--CONDUCTIVE BODY 7A
DIPOLE-DIPOLE APPARENT RESISTIVITY PSEUDO-SECTION
PROFILE LINE IS INCLINED AT 45.0 DEGREES TO STRIKE

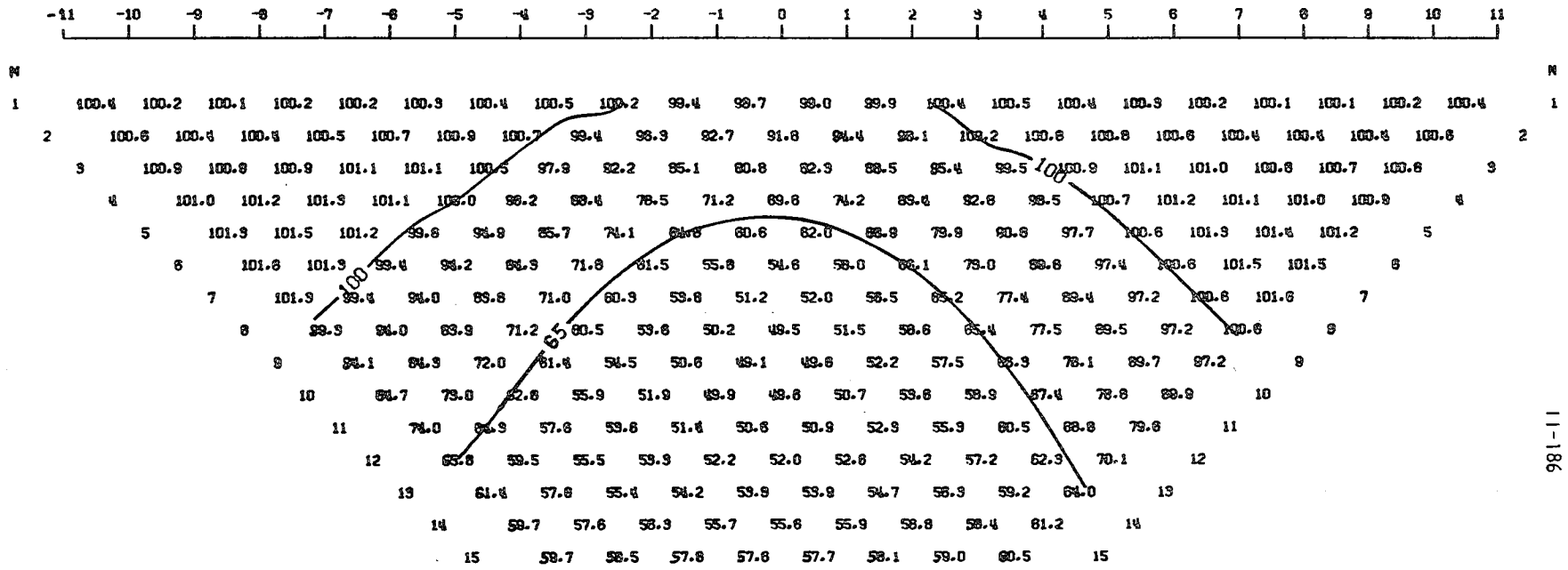

2-D RESISTIVITY MODEL. 45. DEG. PROJECTION--CONDUCTIVE BODY 7A

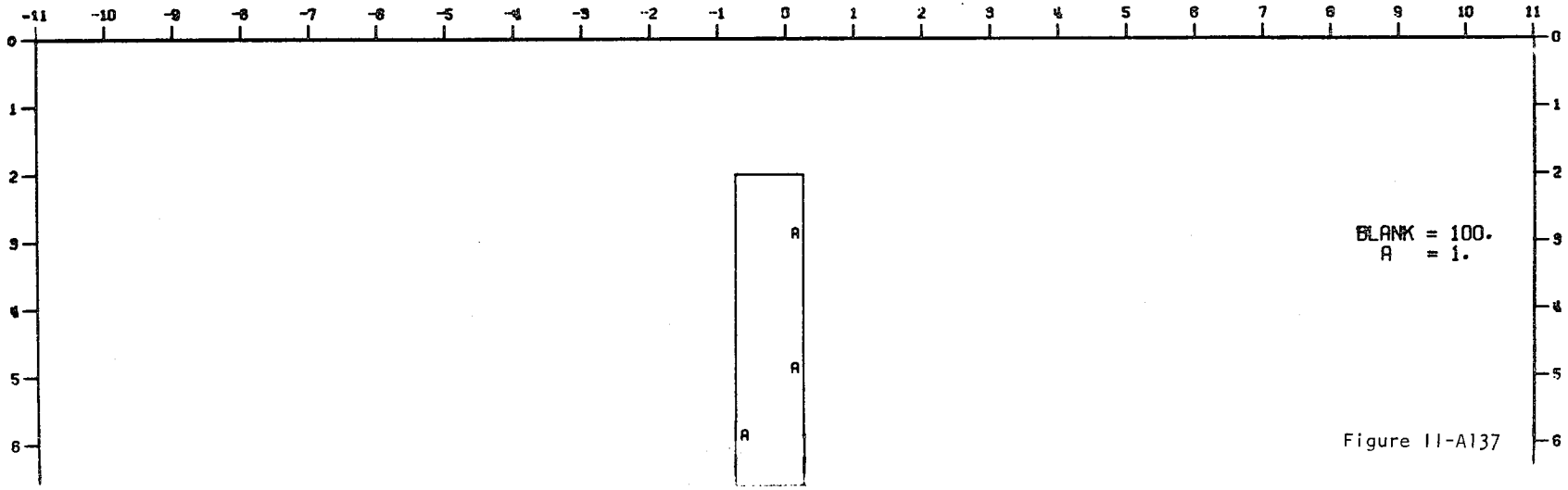

Figure II-A137

MODEL--CONDUCTIVE BODY 7A
SCHLUMBERGER APPARENT RESISTIVITY PSEUDO-SECTION
PROFILE LINE IS INCLINED AT 45.0 DEGREES TO STRIKE

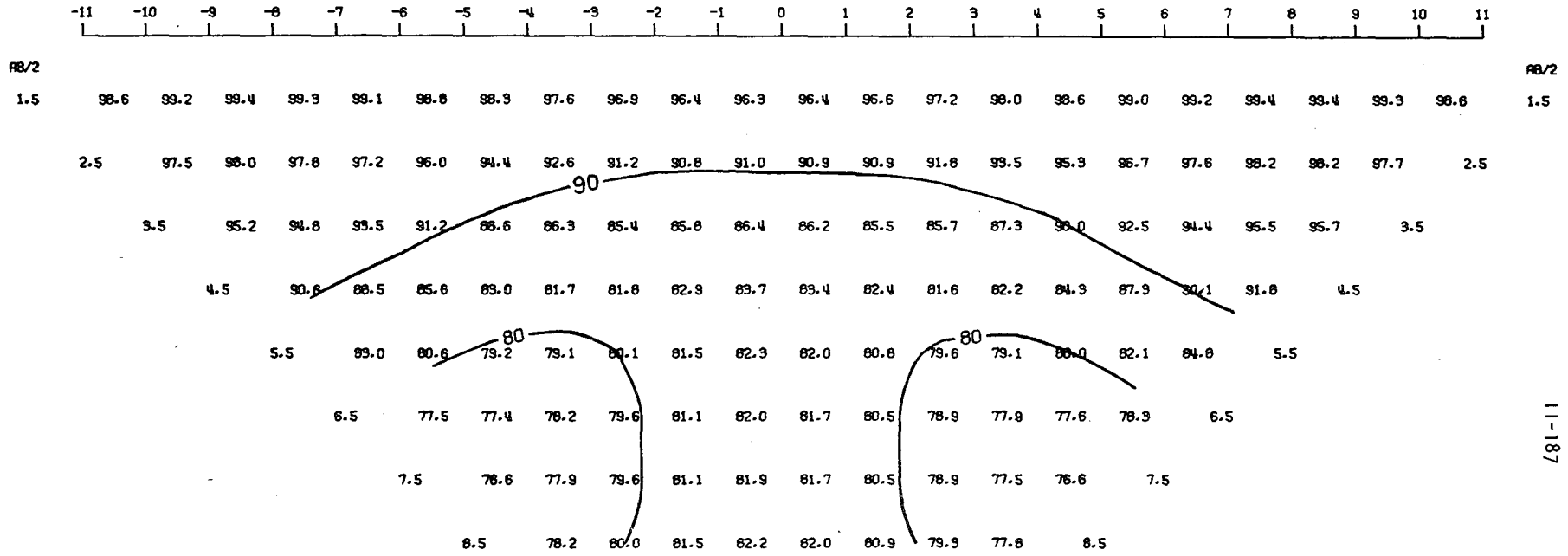

2-D RESISTIVITY MODEL, 45. DEG. PROJECTION--CONDUCTIVE BODY 7A

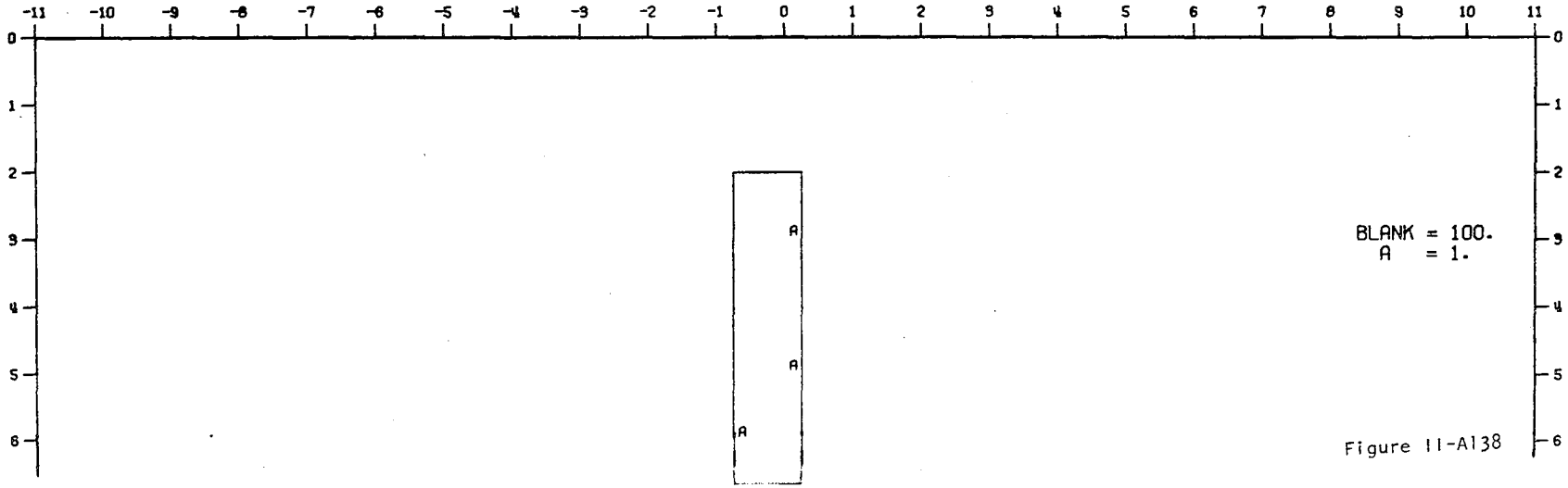

Figure II-A138

MODEL--CONDUCTIVE BODY 5A
DIPOLE-DIPOLE APPARENT RESISTIVITY PSEUDO-SECTION
PROFILE LINE IS INCLINED AT 45.0 DEGREES TO STRIKE

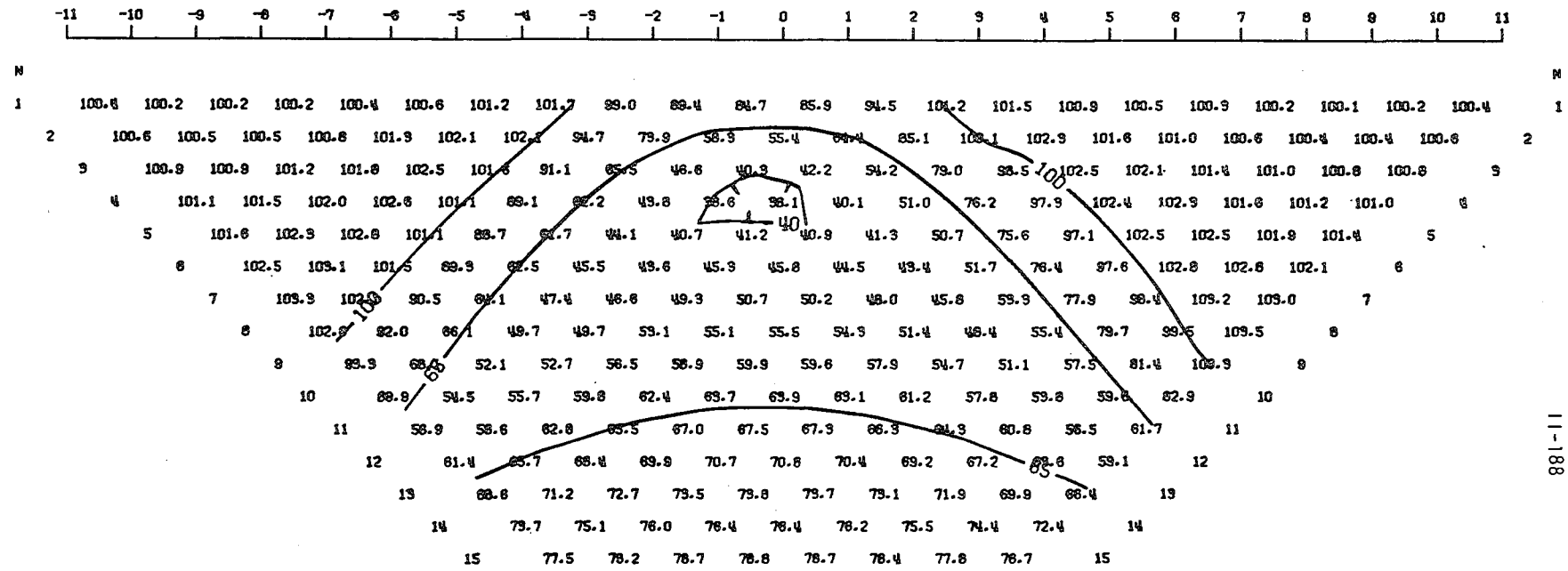

2-D RESISTIVITY MODEL. 45. DEG. PROJECTION--CONDUCTIVE BODY 5A

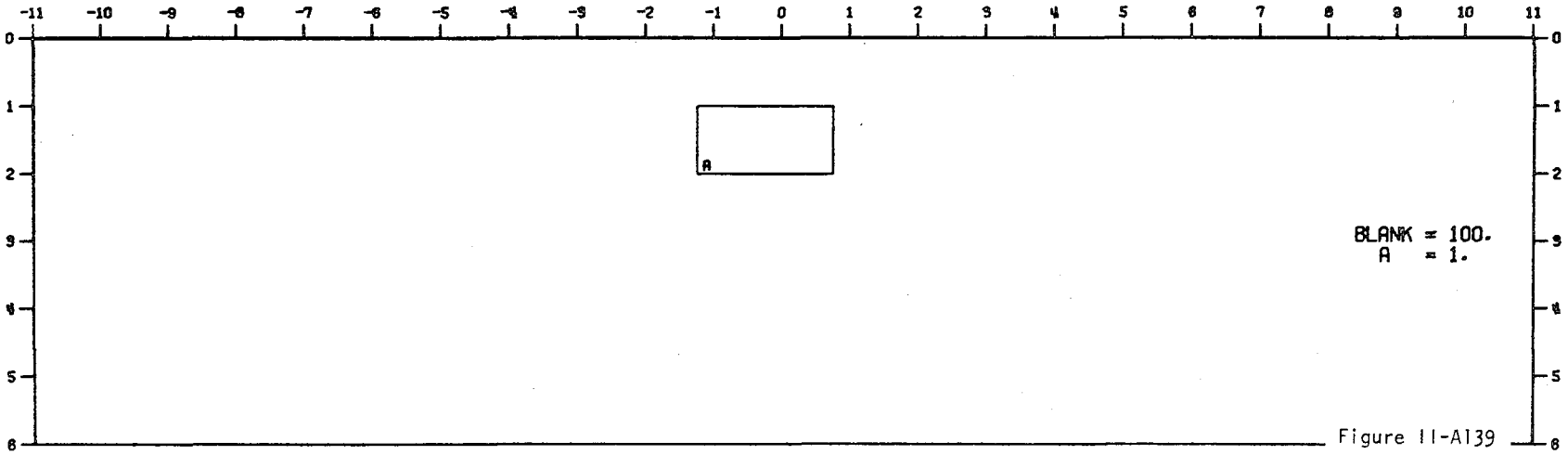

Figure II-A139

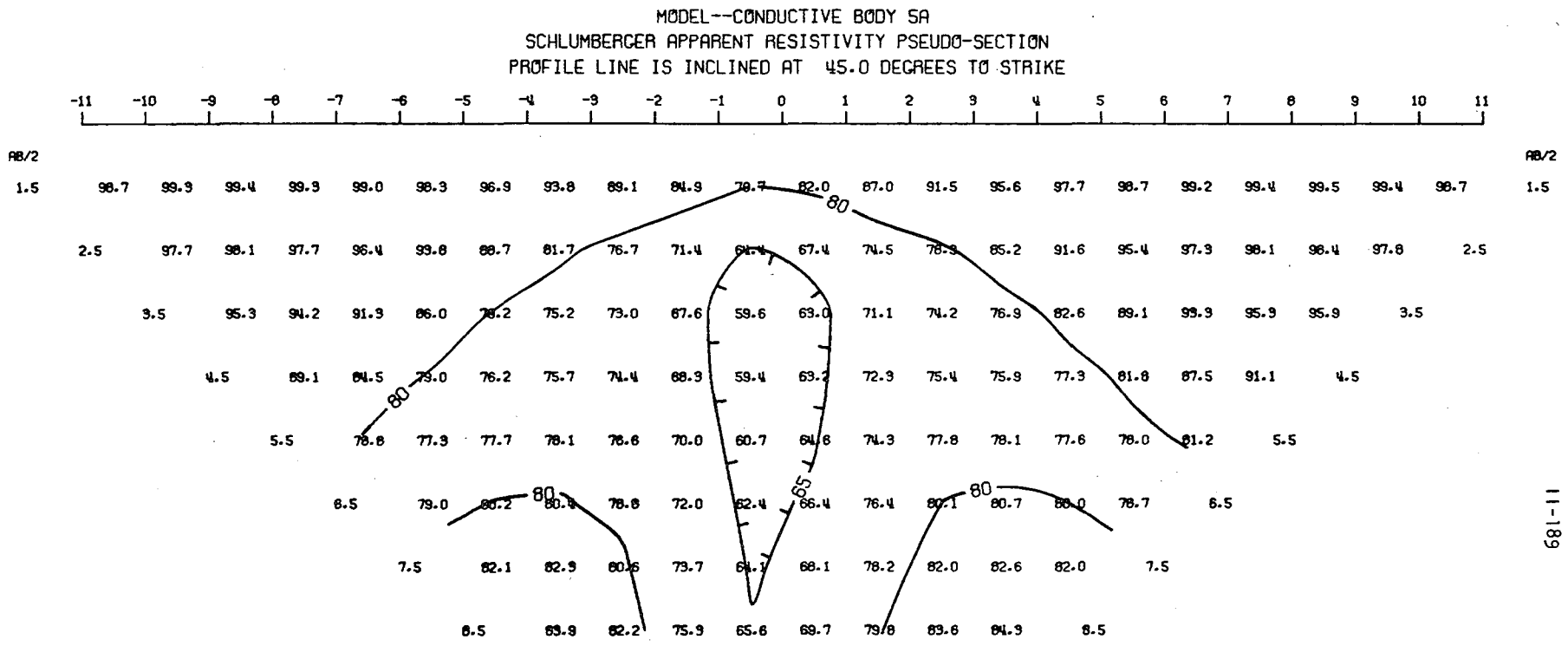

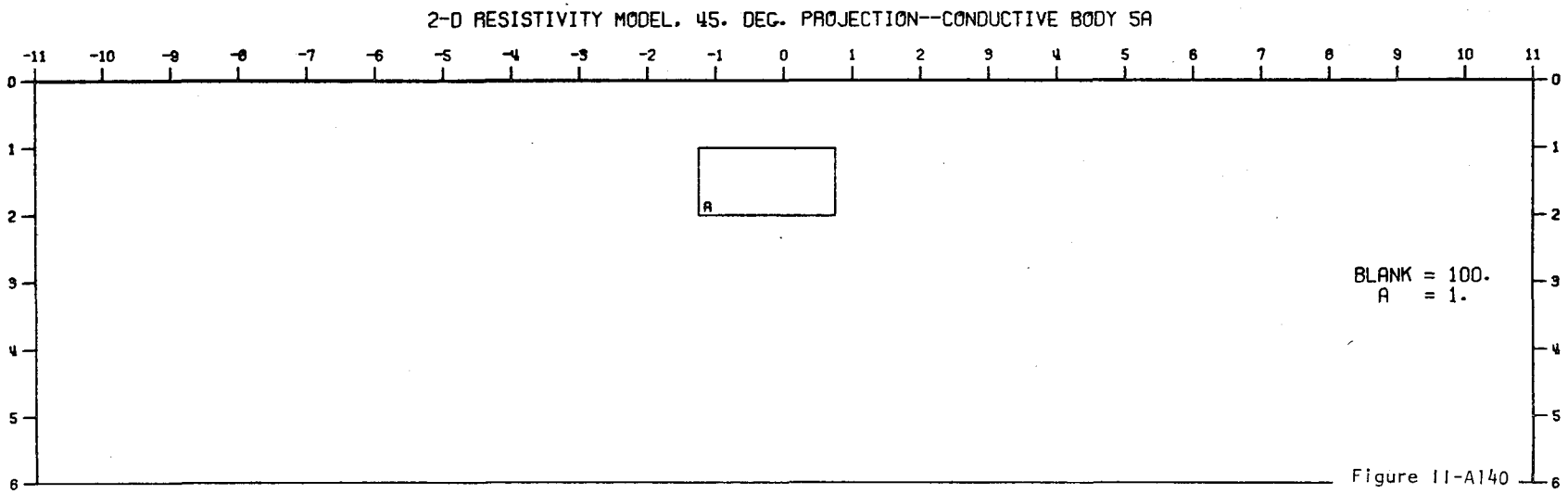

Figure II-A140

MODEL--CONDUCTIVE BODY 5B
DIPOLE-DIPOLE APPARENT RESISTIVITY PSEUDO-SECTION
PROFILE LINE IS INCLINED AT 45.0 DEGREES TO STRIKE

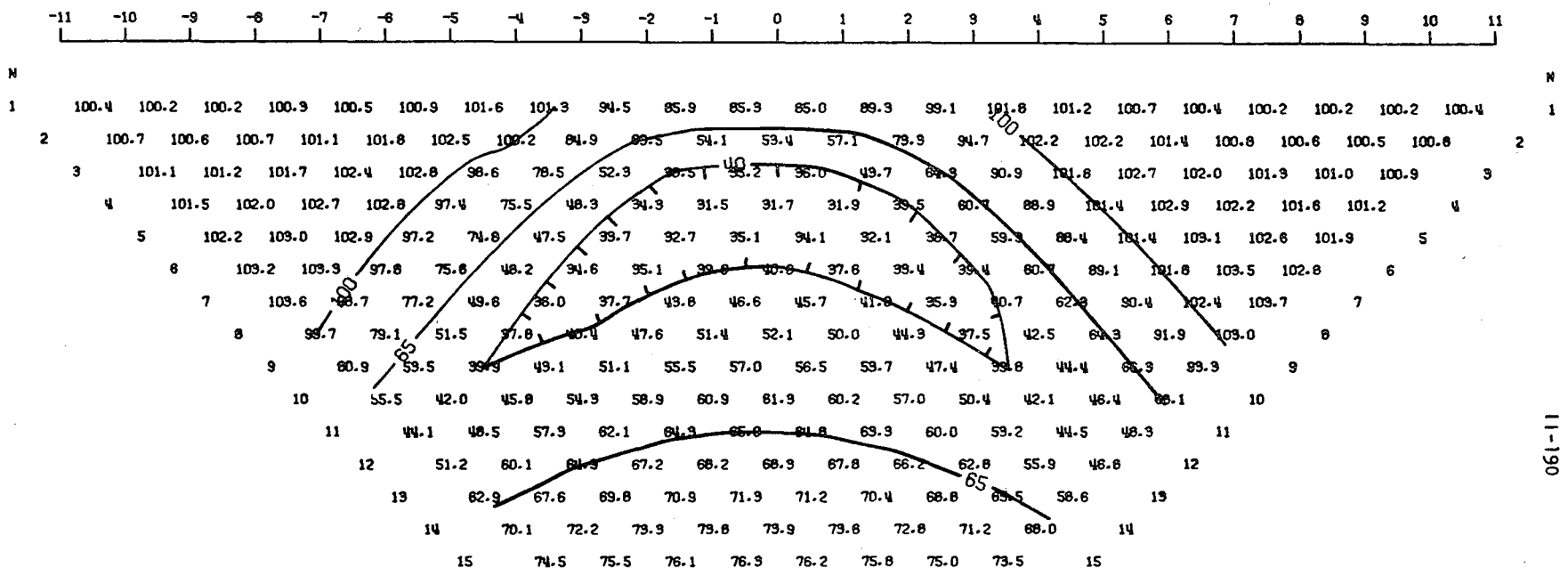

2-D RESISTIVITY MODEL, 45. DEC. PROJECTION--CONDUCTIVE BODY 5B

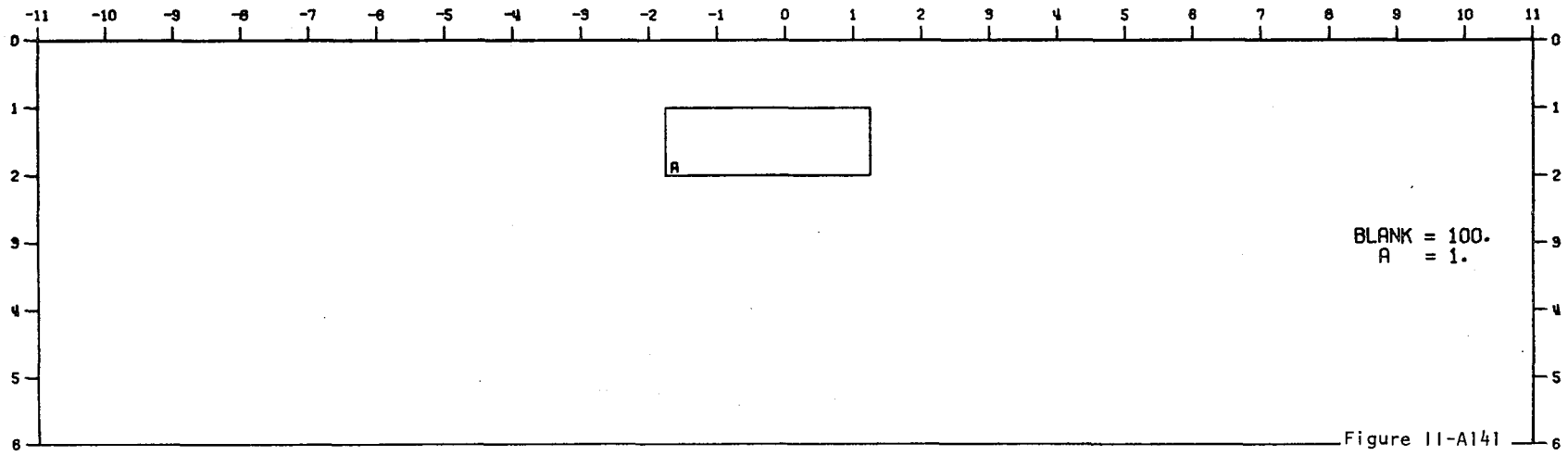

Figure II-A141

MODEL--CONDUCTIVE BODY 5B
SCHLUMBERGER APPARENT RESISTIVITY PSEUDO-SECTION
PROFILE LINE IS INCLINED AT 45.0 DEGREES TO STRIKE

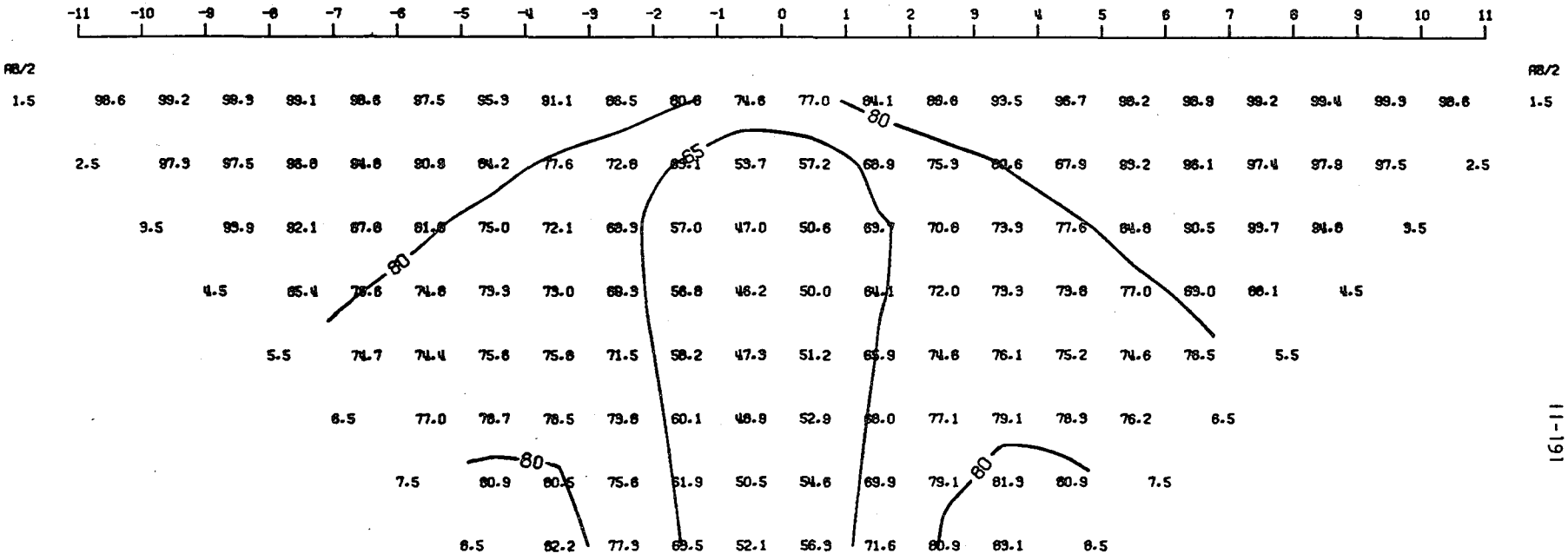

2-D RESISTIVITY MODEL, 45. DEG. PROJECTION--CONDUCTIVE BODY 5B

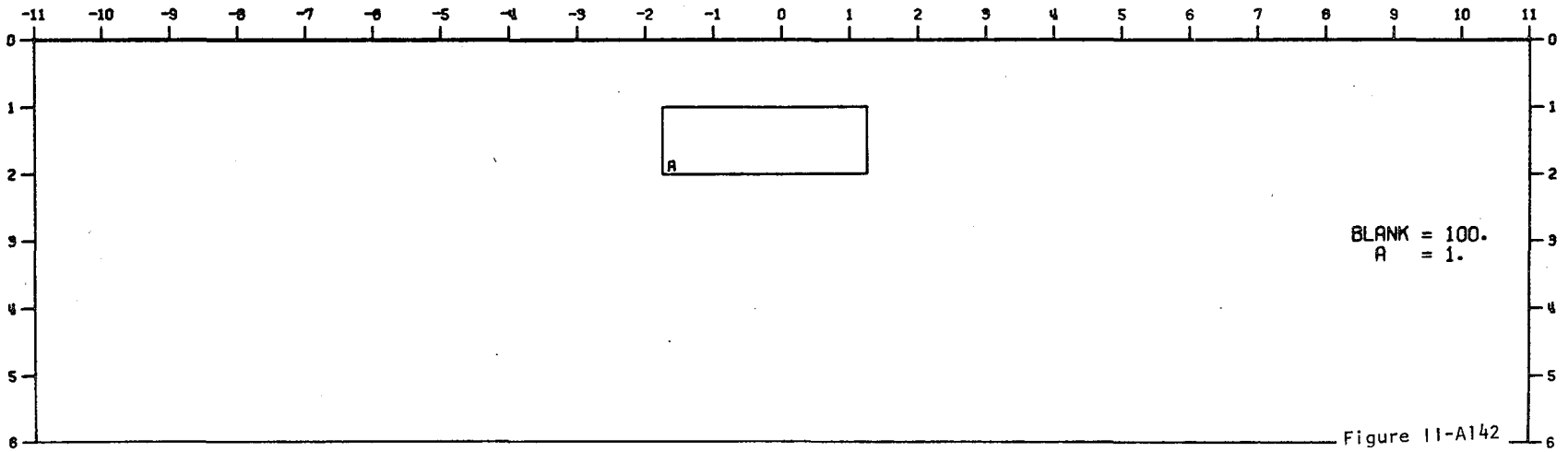

Figure II-A142

MODEL--CONDUCTIVE BODY 4B
DIPOLE-DIPOLE APPARENT RESISTIVITY PSEUDO-SECTION
PROFILE LINE IS INCLINED AT 45.0 DEGREES TO STRIKE

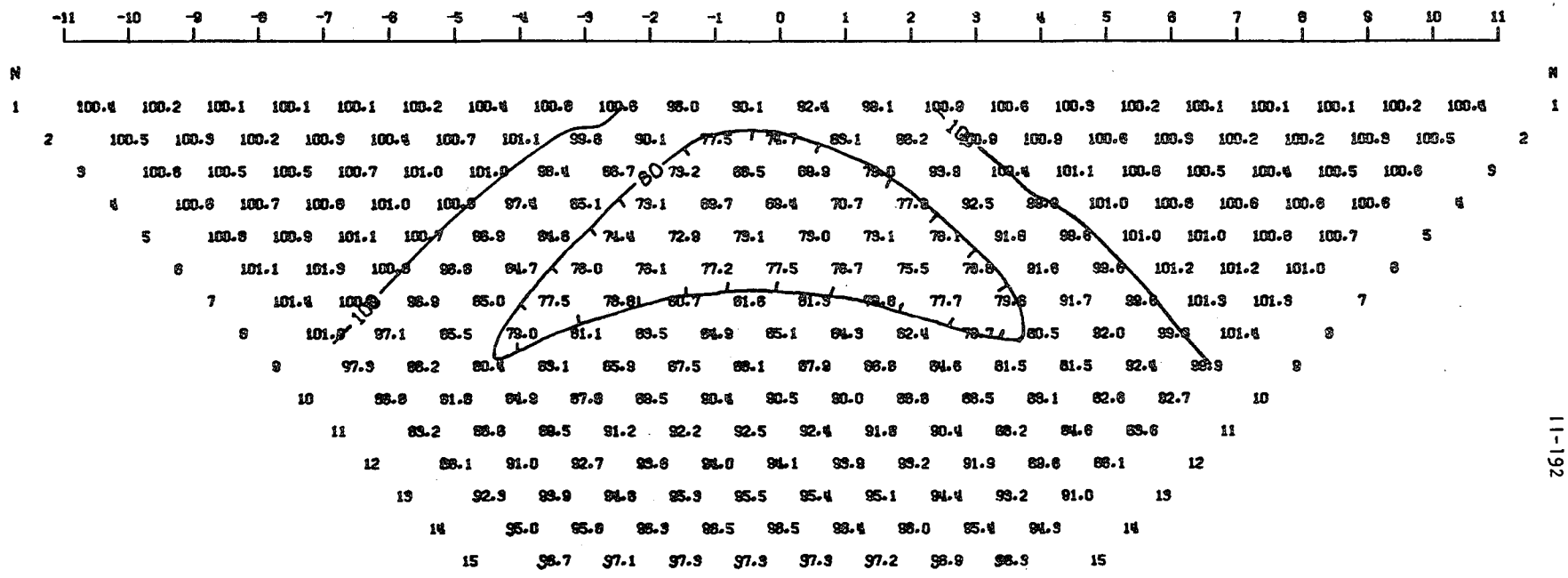

2-D RESISTIVITY MODEL, 45. DEG. PROJECTION--CONDUCTIVE BODY 4B

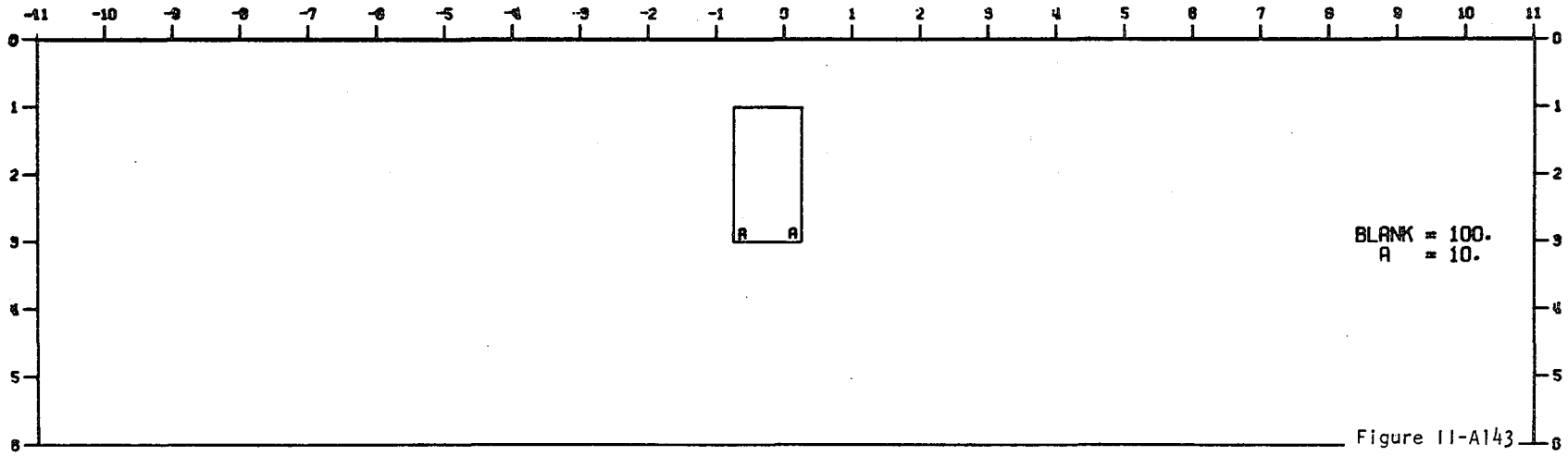

Figure II-A143

MODEL--CONDUCTIVE BODY 4B
SCHLUMBERGER APPARENT RESISTIVITY PSEUDO-SECTION
PROFILE LINE IS INCLINED AT 45.0 DEGREES TO STRIKE

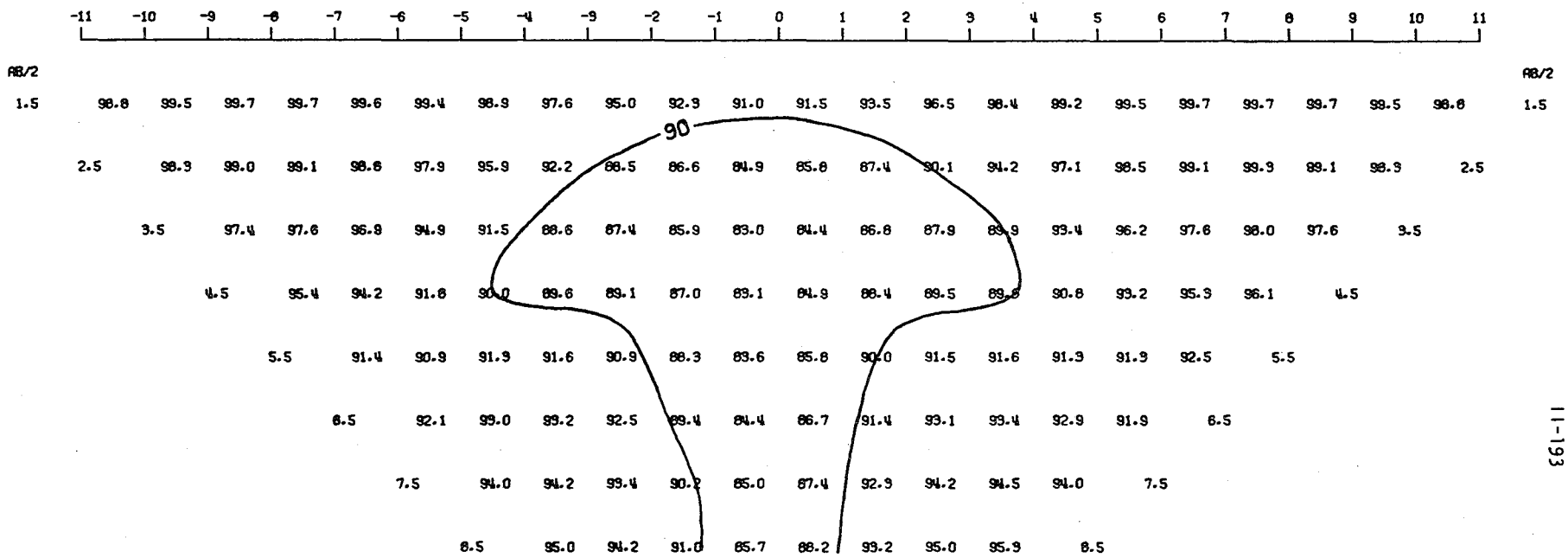

2-D RESISTIVITY MODEL, 45. DEG. PROJECTION--CONDUCTIVE BODY 4B

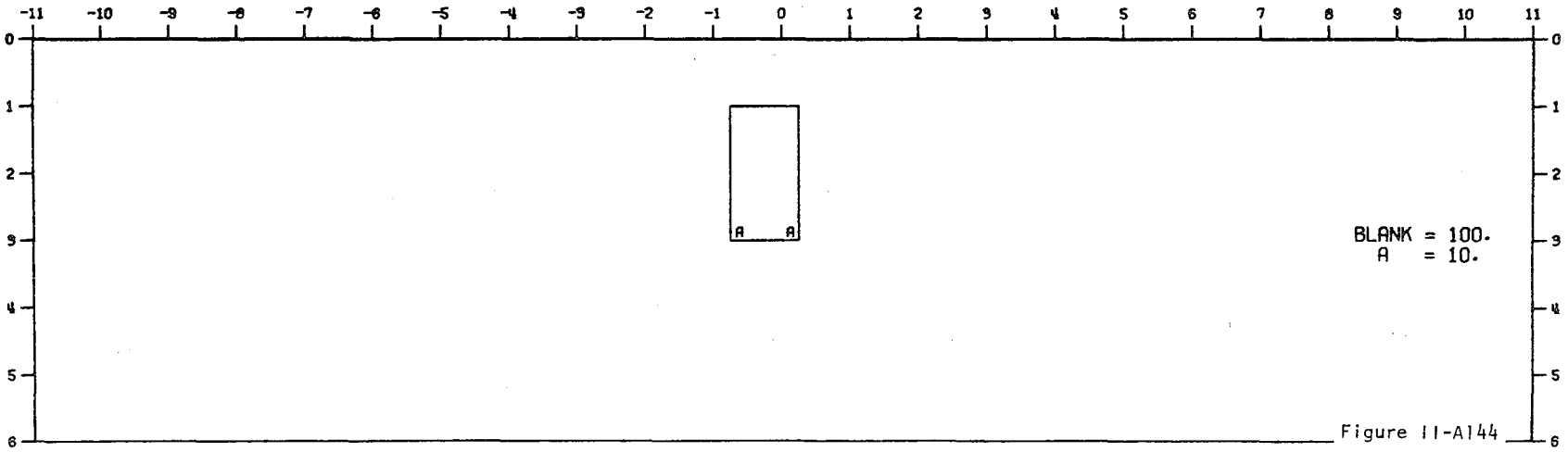

Figure II-A144

MODEL--27 DEC. CONDUCTIVE BODY A
DIPOLE-DIPOLE APPARENT RESISTIVITY PSEUDO-SECTION
PROFILE LINE IS INCLINED AT 45.0 DEGREES TO STRIKE

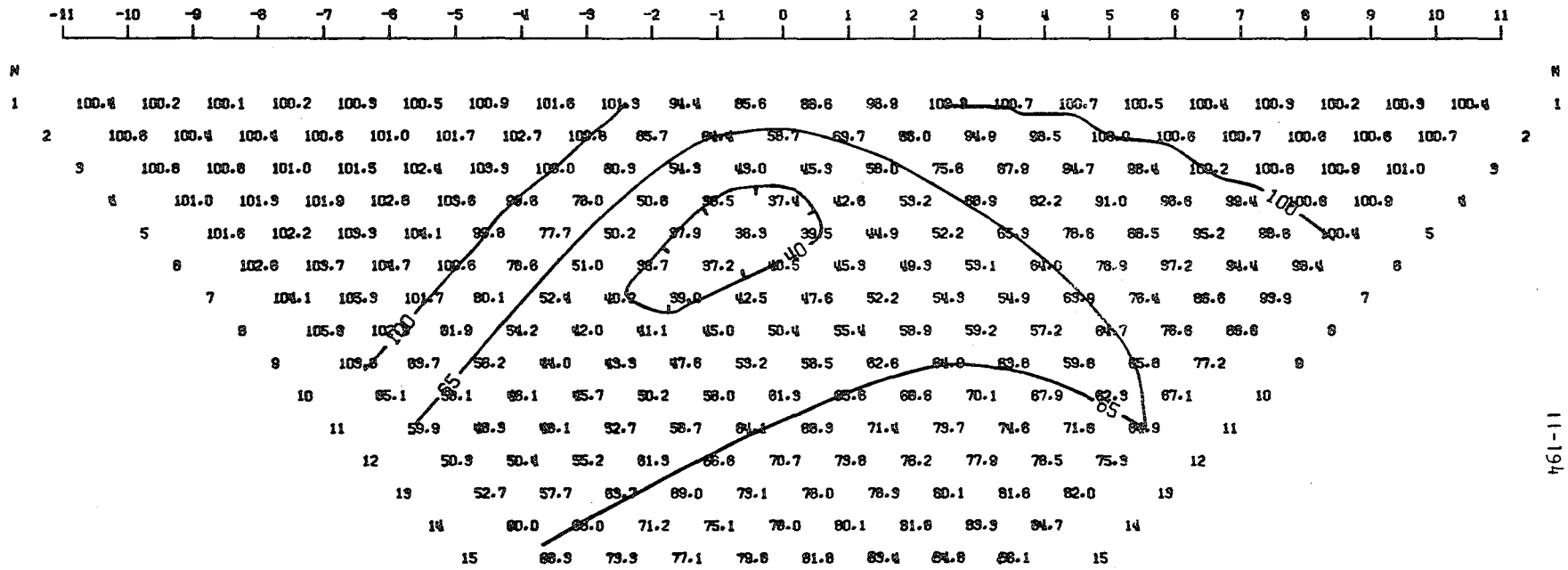

2-D RESISTIVITY MODEL. 45. DEG. PROJECTION--27 DEG. CONDUCTIVE BODY A

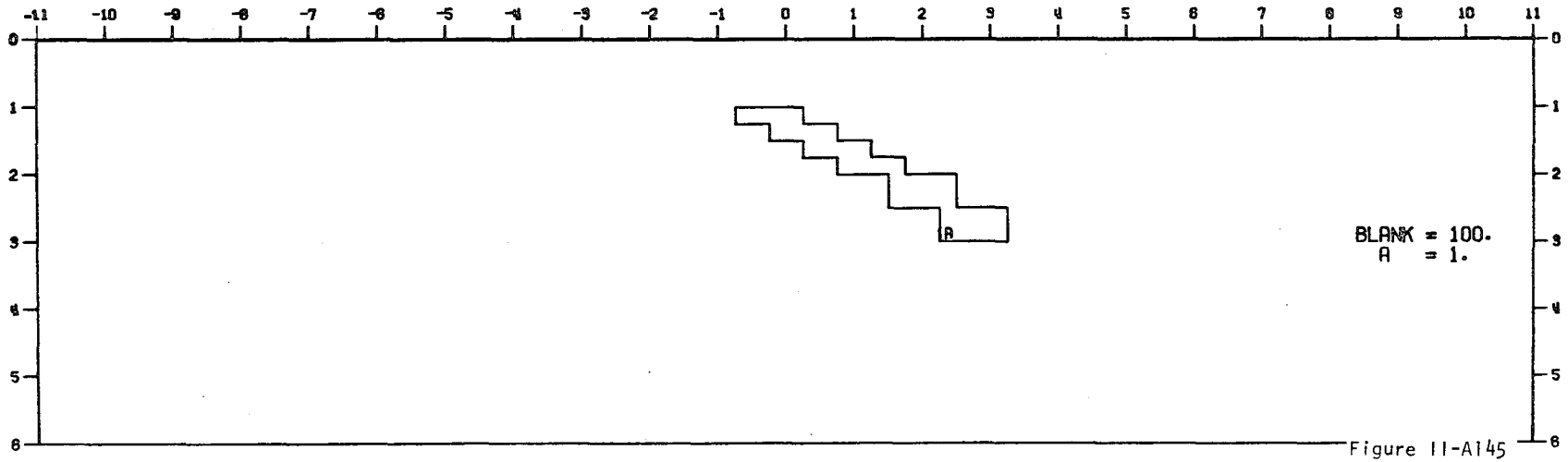

Figure II-A145

MODEL--27 DEG. CONDUCTIVE BODY A
SCHLUMBERGER APPARENT RESISTIVITY PSEUDO-SECTION
PROFILE LINE IS INCLINED AT 45.0 DEGREES TO STRIKE

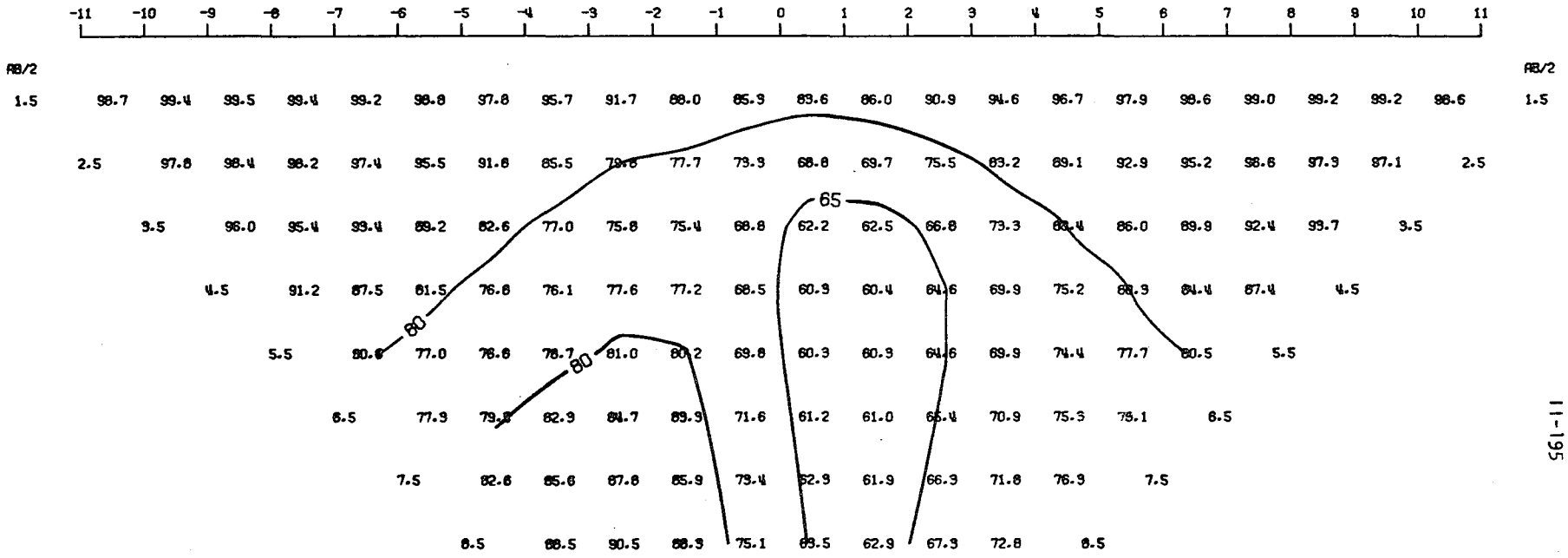

2-D RESISTIVITY MODEL, 45. DEG. PROJECTION--27 DEG. CONDUCTIVE BODY A

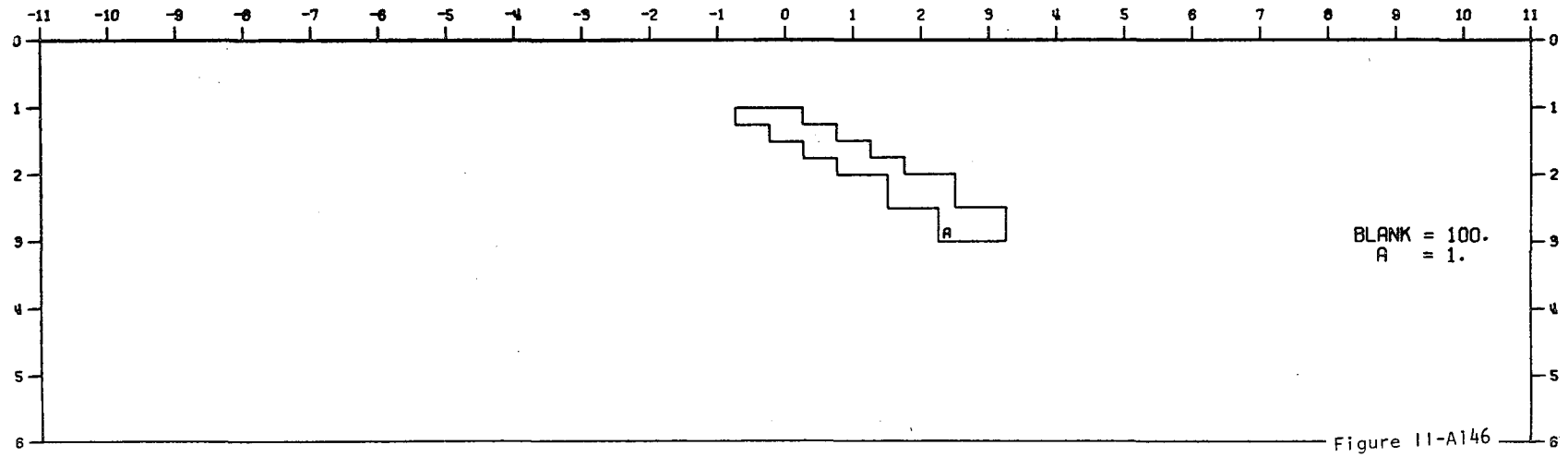

Figure II-A146

MODEL--TWO BODIES 2A
DIPOLE-DIPOLE APPARENT RESISTIVITY PSEUDO-SECTION
PROFILE LINE IS INCLINED AT 45.0 DEGREES TO STRIKE

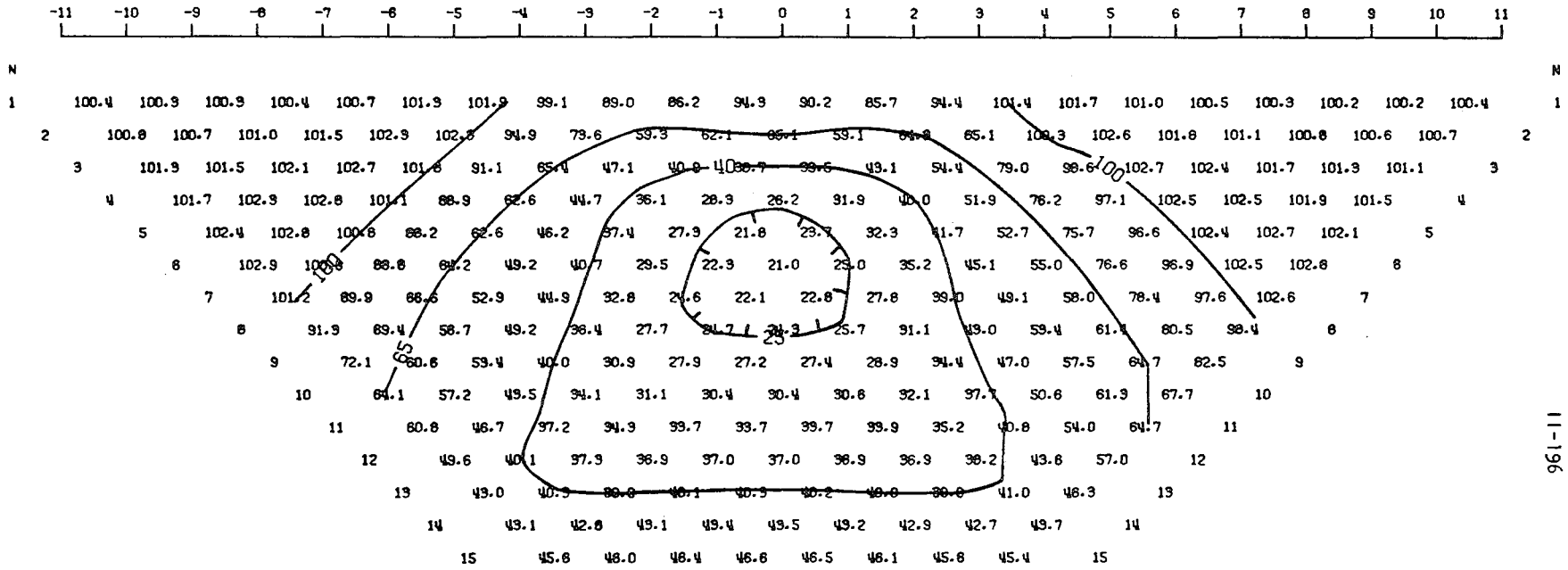

2-D RESISTIVITY MODEL. 45. DEG. PROJECTION--TWO BODIES 2A

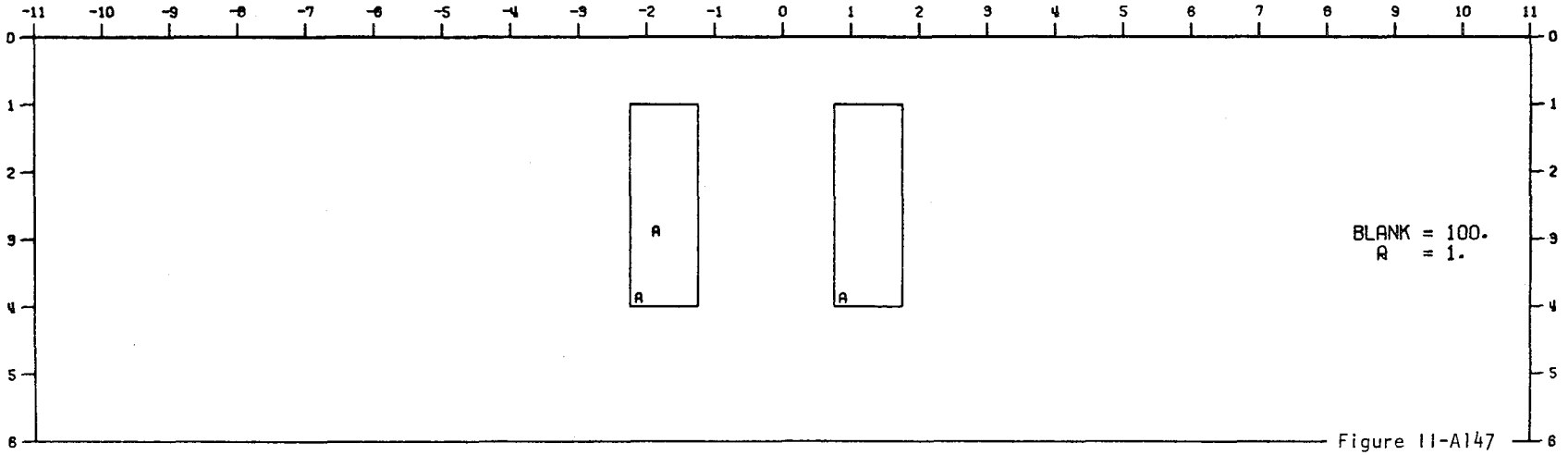

Figure II-A147

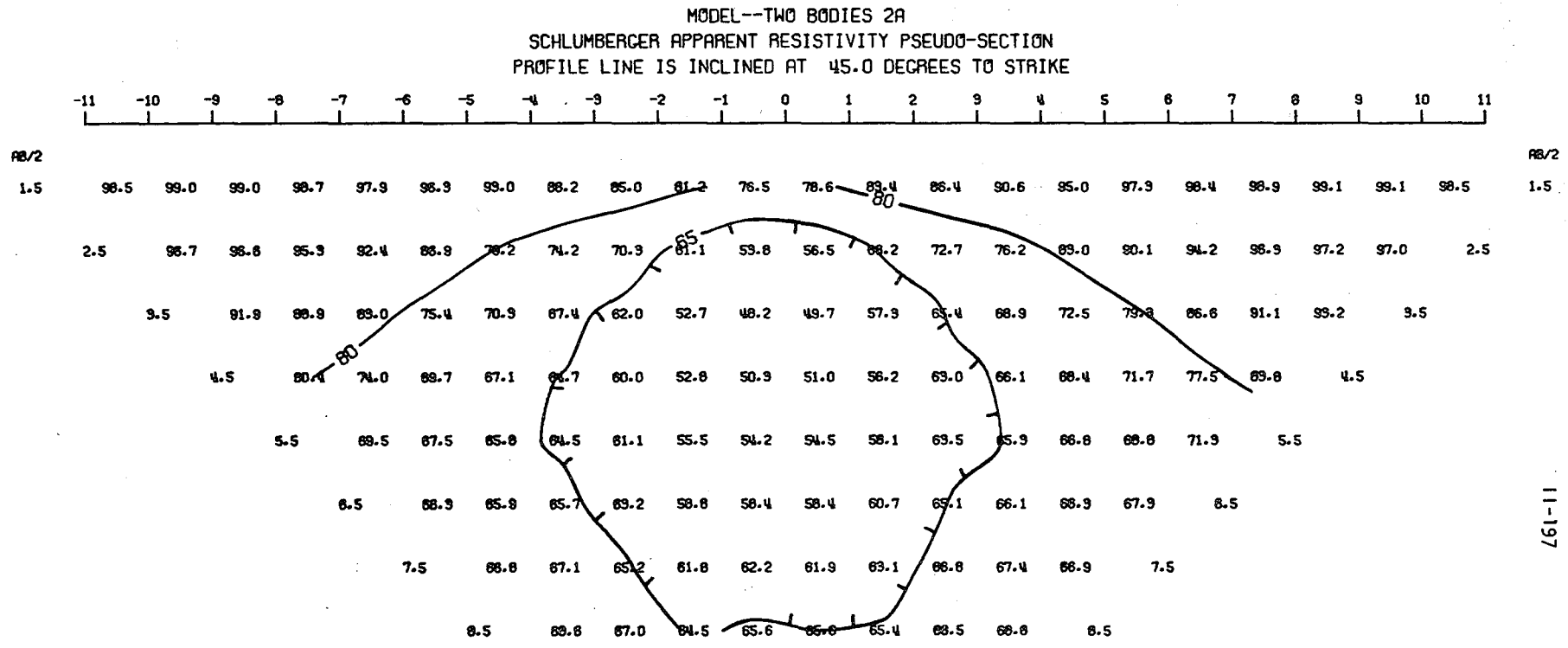

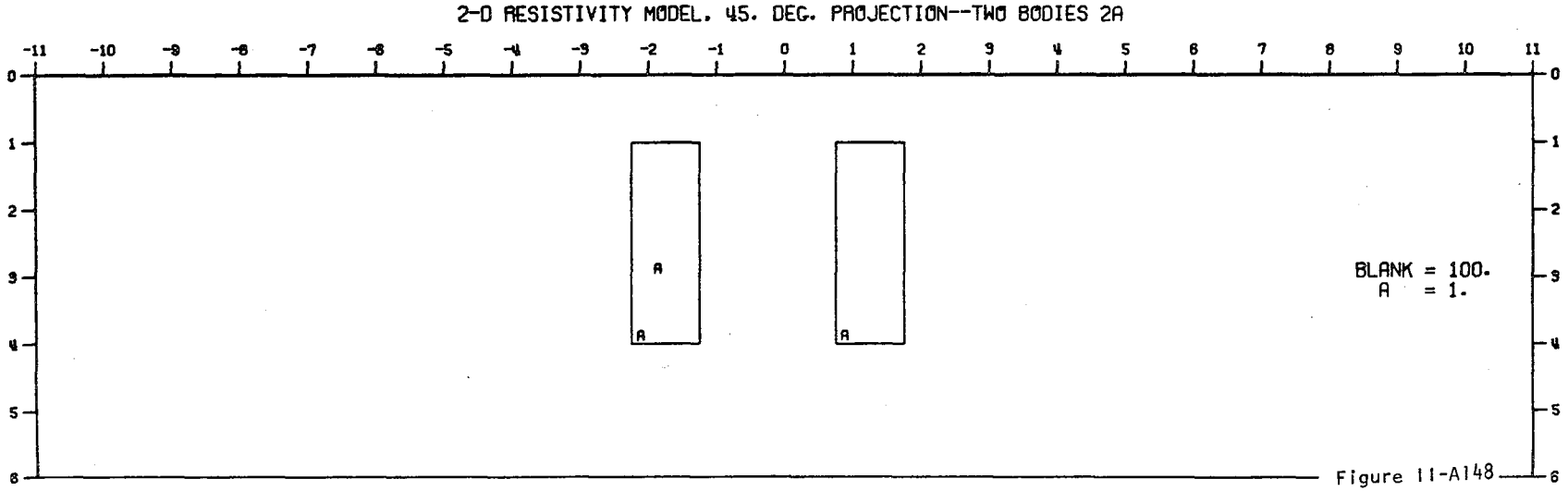

Figure 11-A148

MODEL--TWO BODIES 2B
DIPOLE-DIPOLE APPARENT RESISTIVITY PSEUDO-SECTION
PROFILE LINE IS INCLINED AT 45.0 DEGREES TO STRIKE

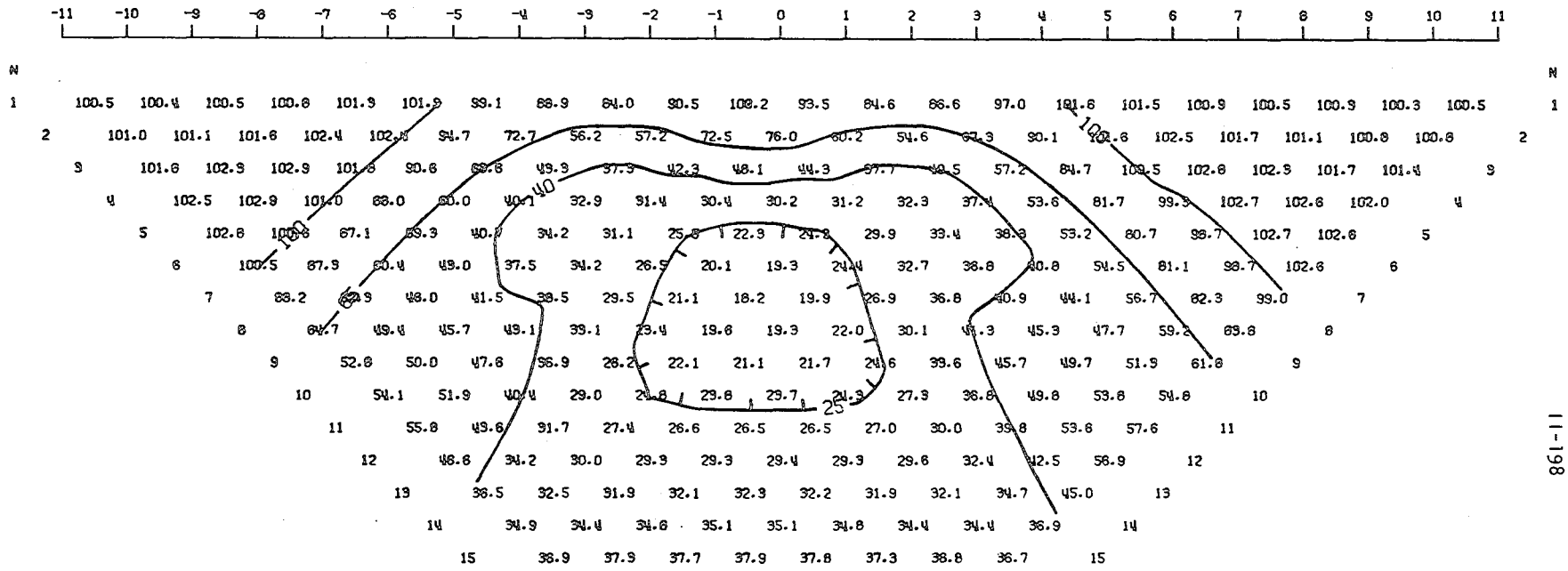

2-D RESISTIVITY MODEL. 45. DEG. PROJECTION--TWO BODIES 2B

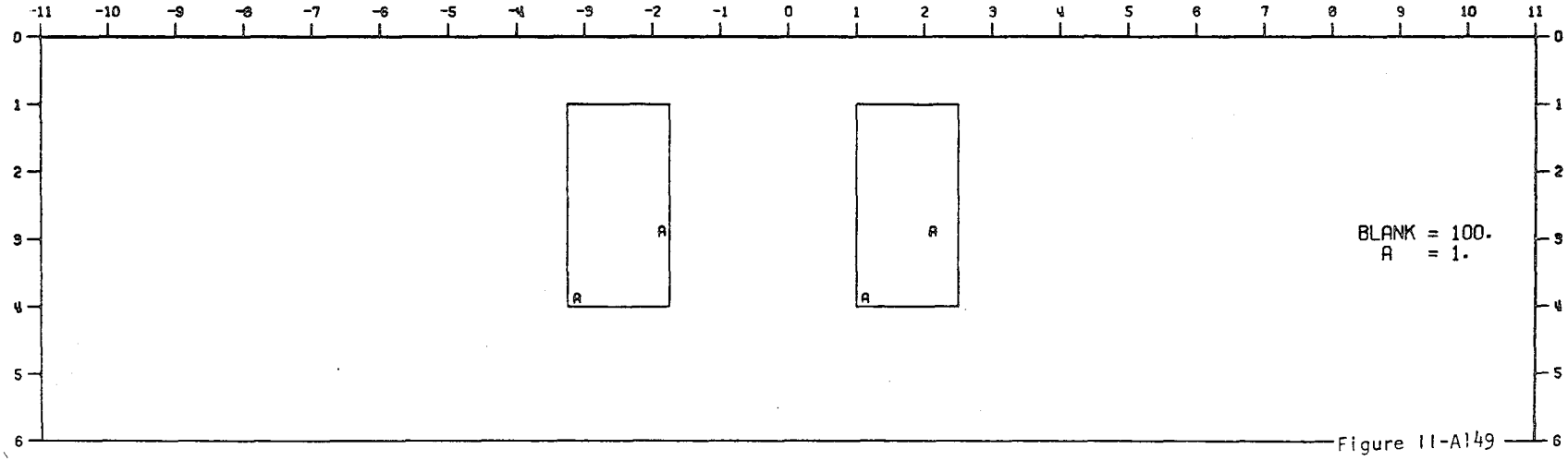

Figure II-A149

MODEL--TWO BODIES 2B
SCHLUMBERGER APPARENT RESISTIVITY PSEUDO-SECTION
PROFILE LINE IS INCLINED AT 45.0 DEGREES TO STRIKE

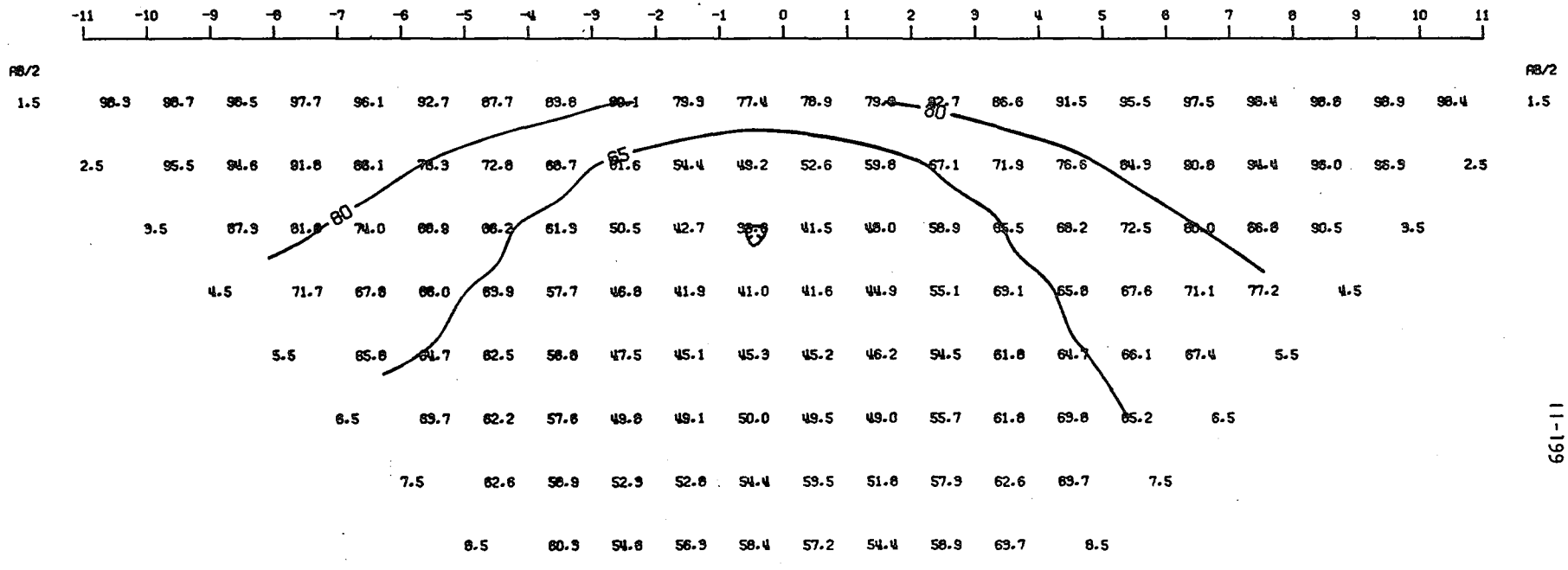

2-D RESISTIVITY MODEL, 45. DEG. PROJECTION--TWO BODIES 2B

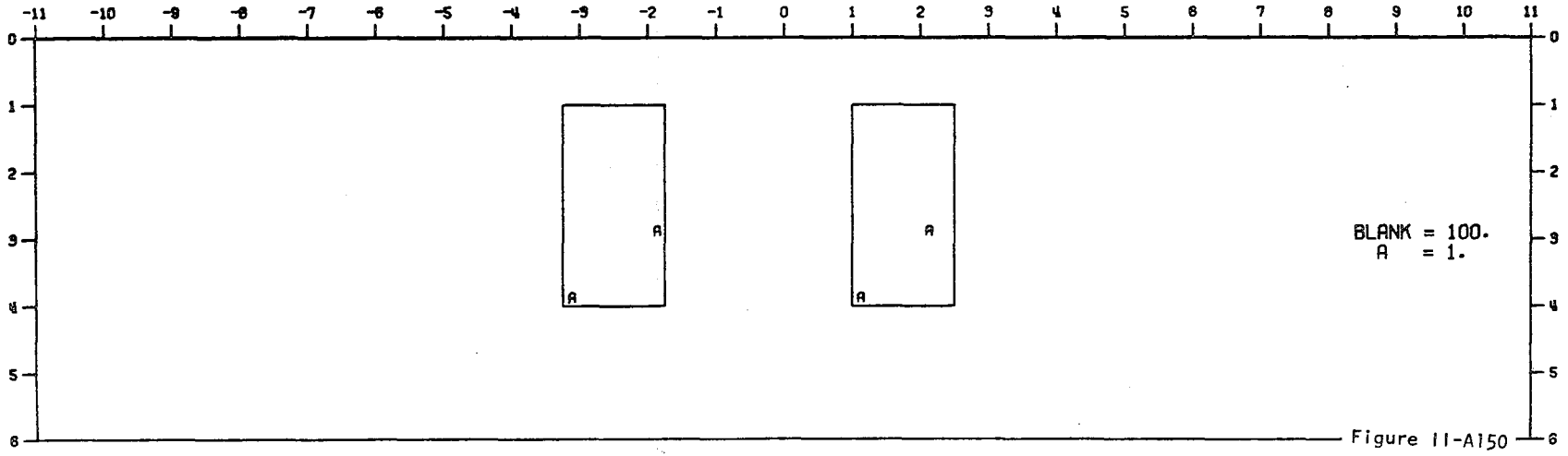

Figure II-A150

MODEL--RESISTIVE BODY A
DIPOLE-DIPOLE APPARENT RESISTIVITY PSEUDO-SECTION
PROFILE LINE IS INCLINED AT 45.0 DEGREES TO STRIKE

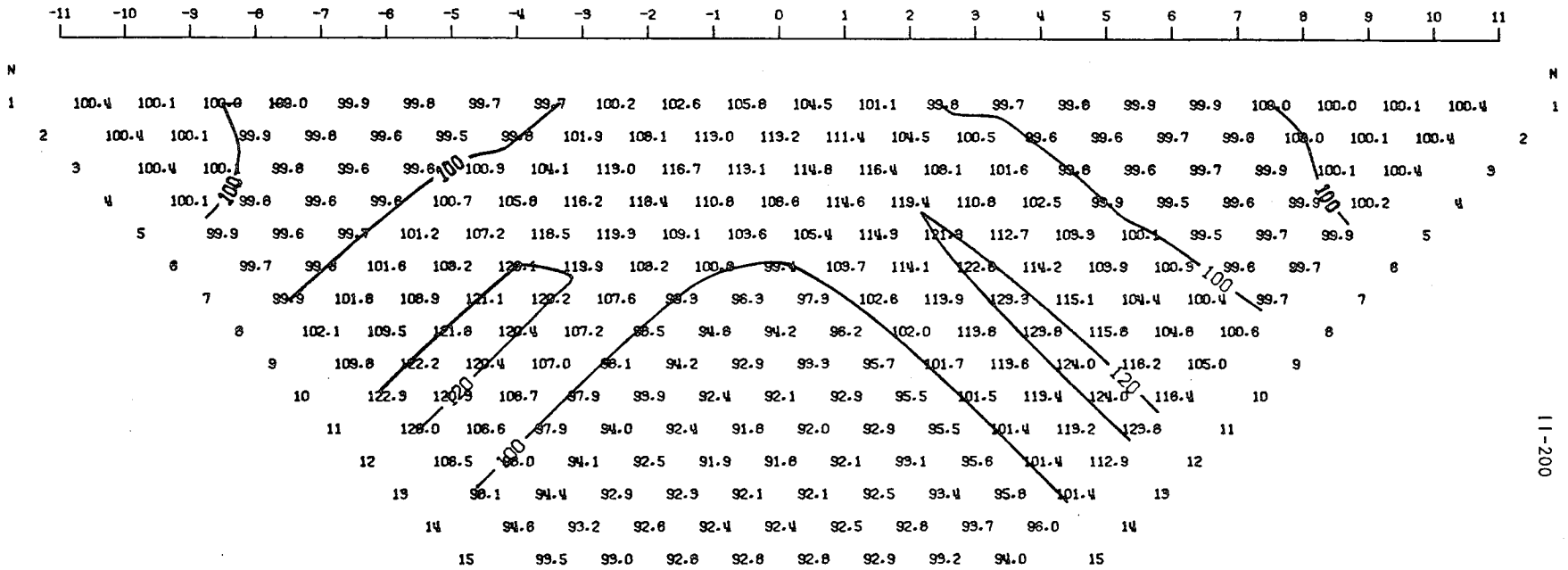

2-D RESISTIVITY MODEL, 45. DEG. PROJECTION--RESISTIVE BODY A

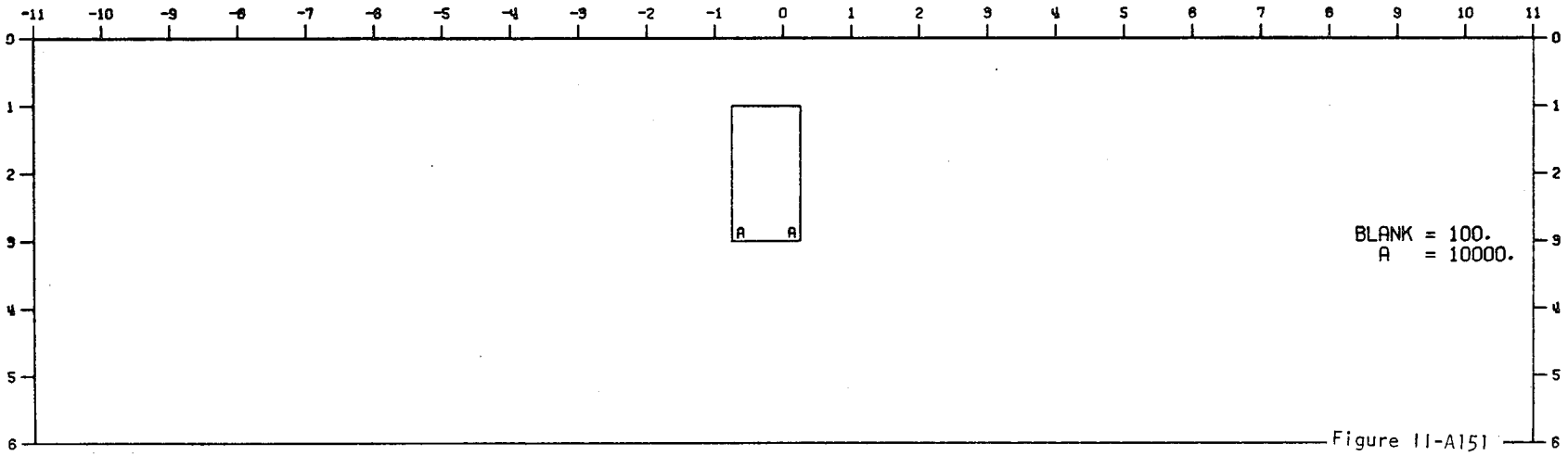

Figure II-A151

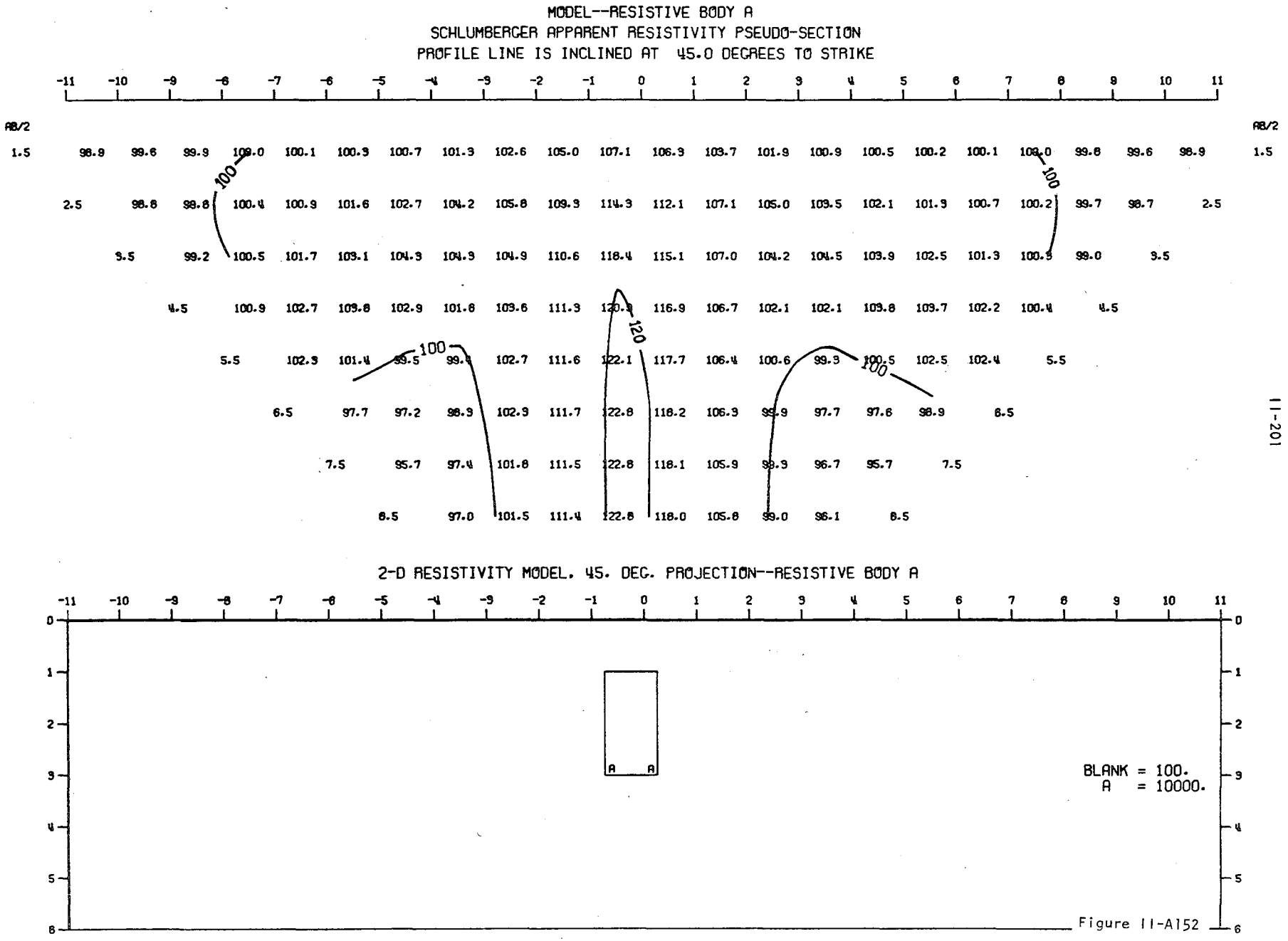

Figure II-A152

MODEL--RESISTIVE BODY B
DIPOLE-DIPOLE APPARENT RESISTIVITY PSEUDO-SECTION
PROFILE LINE IS INCLINED AT 45.0 DEGREES TO STRIKE

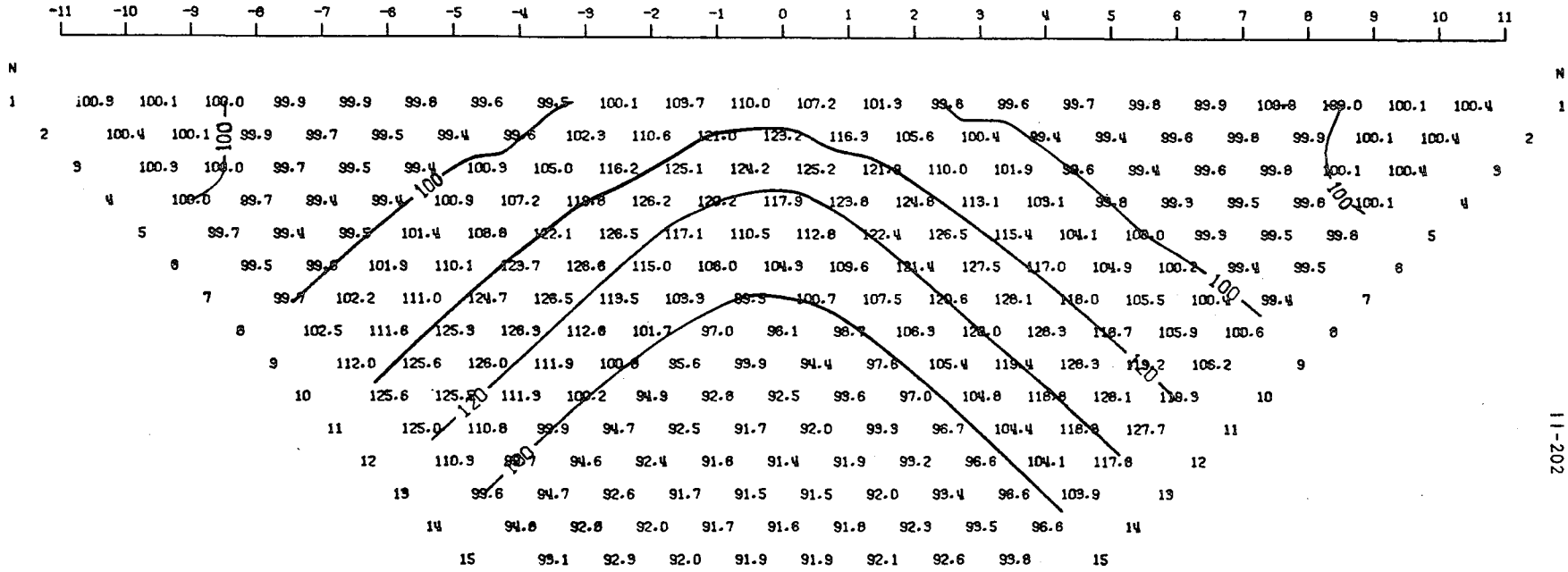

2-D RESISTIVITY MODEL, 45. DEG. PROJECTION--RESISTIVE BODY B

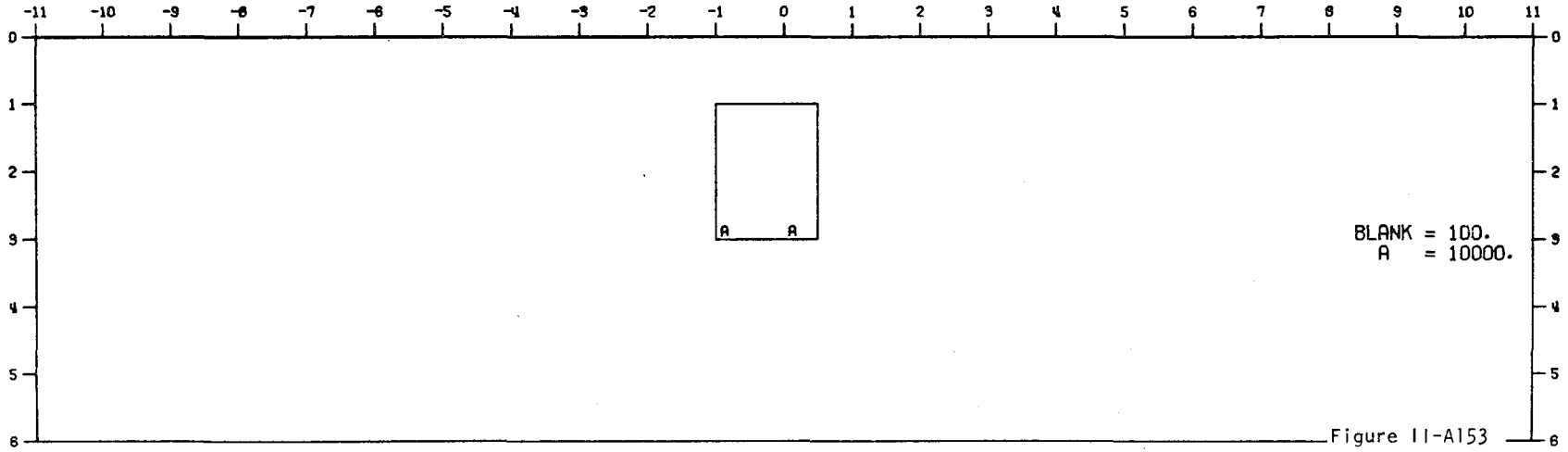

Figure II-A153

MODEL--RESISTIVE BODY B
SCHLUMBERGER APPARENT RESISTIVITY PSEUDO-SECTION
PROFILE LINE IS INCLINED AT 45.0 DEGREES TO STRIKE

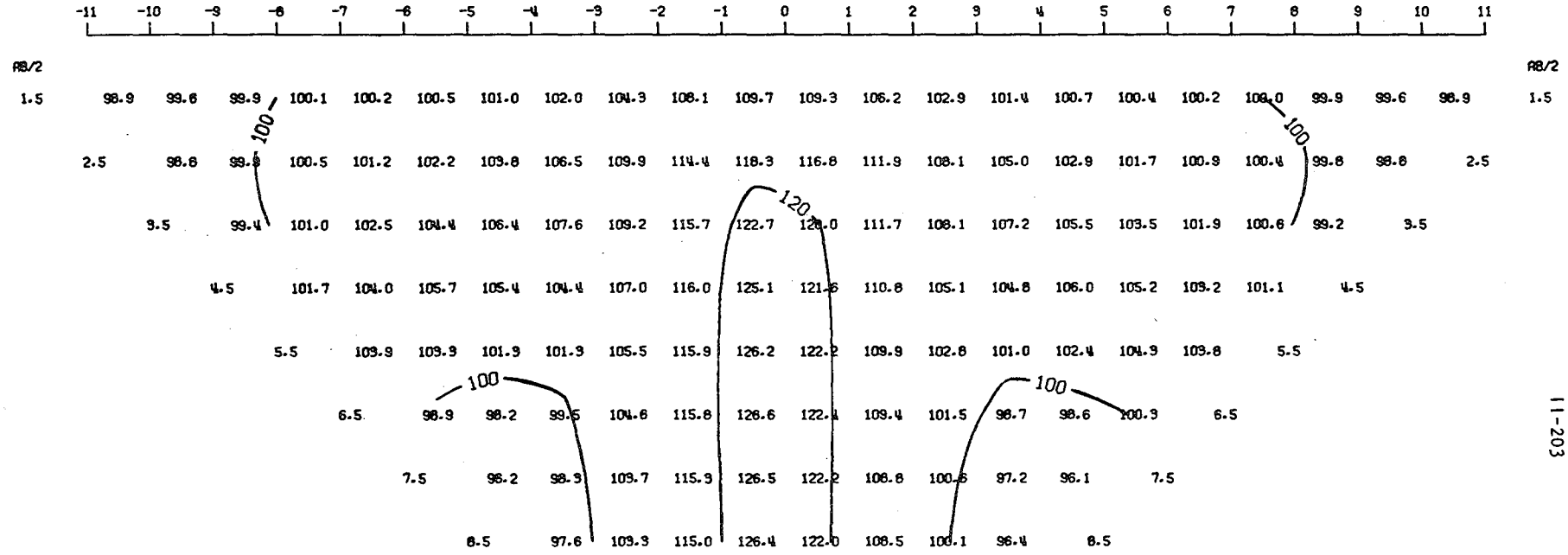

2-D RESISTIVITY MODEL, 45. DEG. PROJECTION--RESISTIVE BODY B

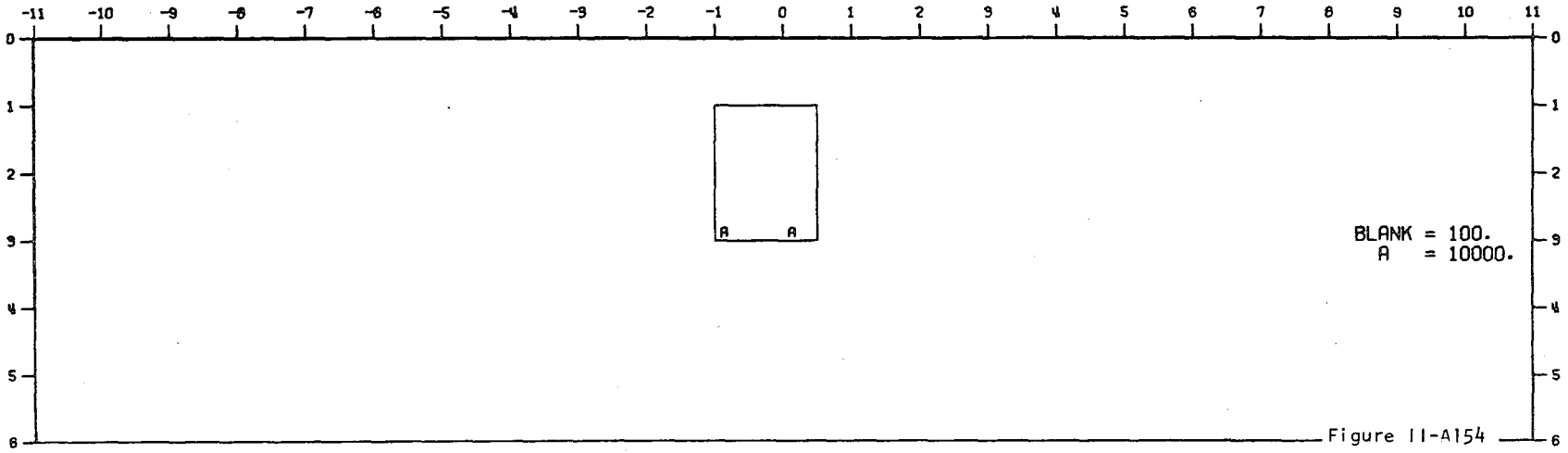

Figure II-A154

MODEL--CONDUCTIVE BODY WITH OVERBURDEN 1A
DIPOLE-DIPOLE APPARENT RESISTIVITY PSEUDO-SECTION
PROFILE LINE IS INCLINED AT 45.0 DEGREES TO STRIKE

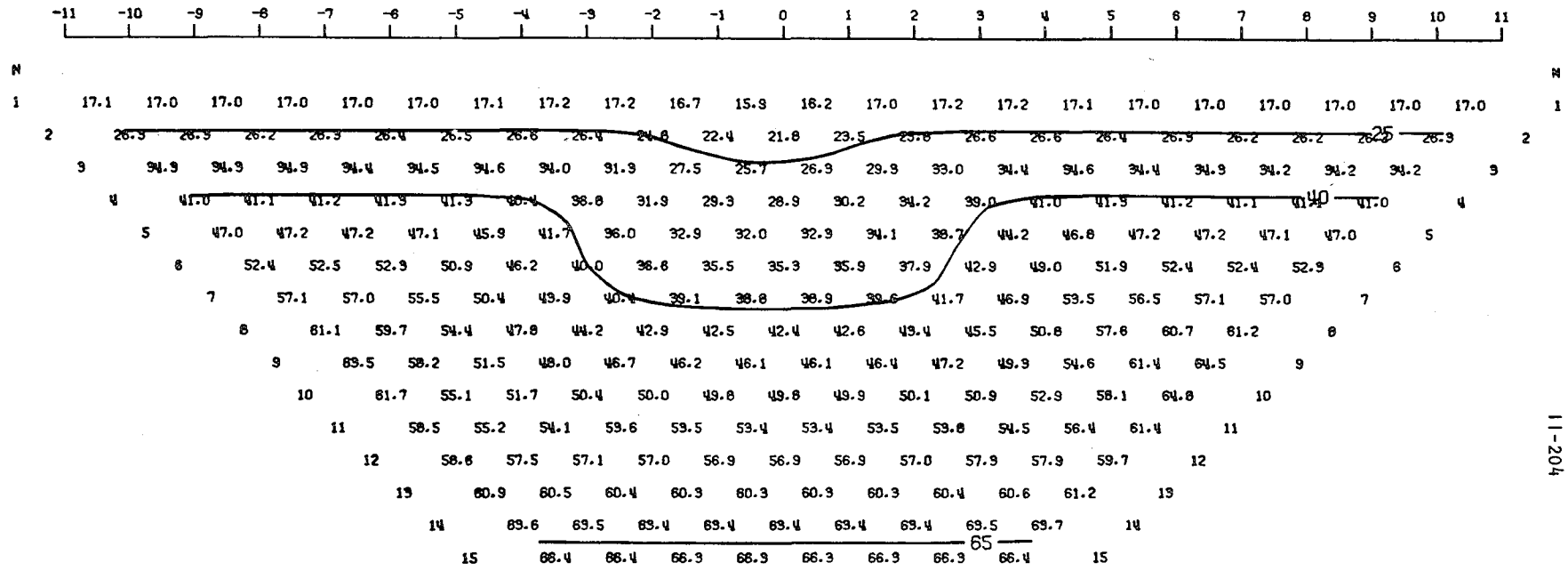

2-D RESISTIVITY MODEL, 45. DEG. PROJECTION--CONDUCTIVE BODY WITH OVERBURDEN 1A

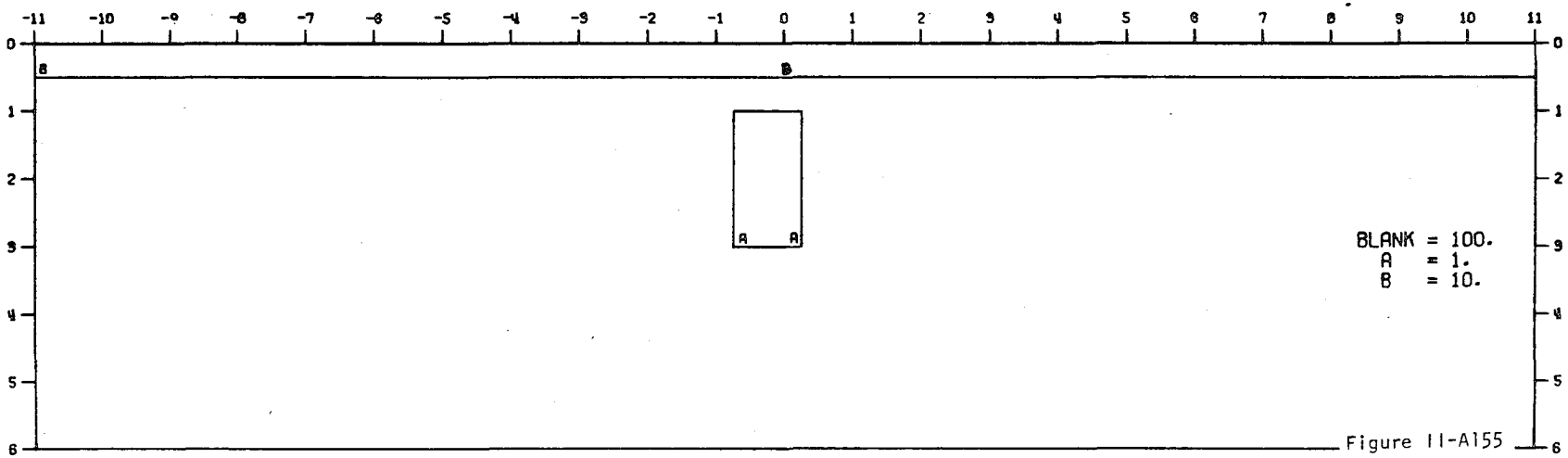

Figure II-A155

MODEL--CONDUCTIVE BODY WITH OVERBURDEN 1A
SCHLUMBERGER APPARENT RESISTIVITY PSEUDO-SECTION
PROFILE LINE IS INCLINED AT 45.0 DEGREES TO STRIKE

AB/2	-11	-10	-9	-8	-7	-6	-5	-4	-3	-2	-1	0	1	2	3	4	5	6	7	8	9	10	11	AB/2
1.5	22.8	29.0	29.0	29.0	29.0	22.9	22.7	22.5	22.1	21.8	21.7	21.7	21.9	22.3	22.6	22.8	22.9	29.0	29.0	29.0	29.0	22.8		1.5
2.5	34.7	34.9	34.9	34.7	34.4	33.8	32.9	32.2	32.0	32.1	32.1	32.0	32.5	33.4	34.1	34.6	34.9	35.0	35.0	34.8				2.5
3.5		43.3	43.3	42.9	42.1	40.9	40.0	39.7	39.8	40.0	39.8	39.7	39.8	40.4	41.6	42.6	43.2	43.5	43.5					3.5
4.5			49.3	48.6	47.4	48.4	48.1	46.1	46.4	46.5	46.5	46.3	46.1	46.2	46.9	48.1	49.2	49.7						4.5
5.5				52.5	51.7	51.4	51.5	51.8	52.0	52.0	52.1	51.9	51.7	51.5	51.8	52.2	53.2			5.5				
6.5					55.8	56.1	56.4	56.7	57.0	56.9	57.0	56.9	56.6	56.3	56.1	56.0			6.5					
7.5						60.1	60.6	61.0	61.2	61.1	61.2	61.2	60.9	60.5	60.1			7.5						
8.5							64.4	64.8	65.0	64.8	65.0	65.0	64.7	64.3			8.5							

25

40

2-D RESISTIVITY MODEL. 45. DEG. PROJECTION--CONDUCTIVE BODY WITH OVERBURDEN 1A

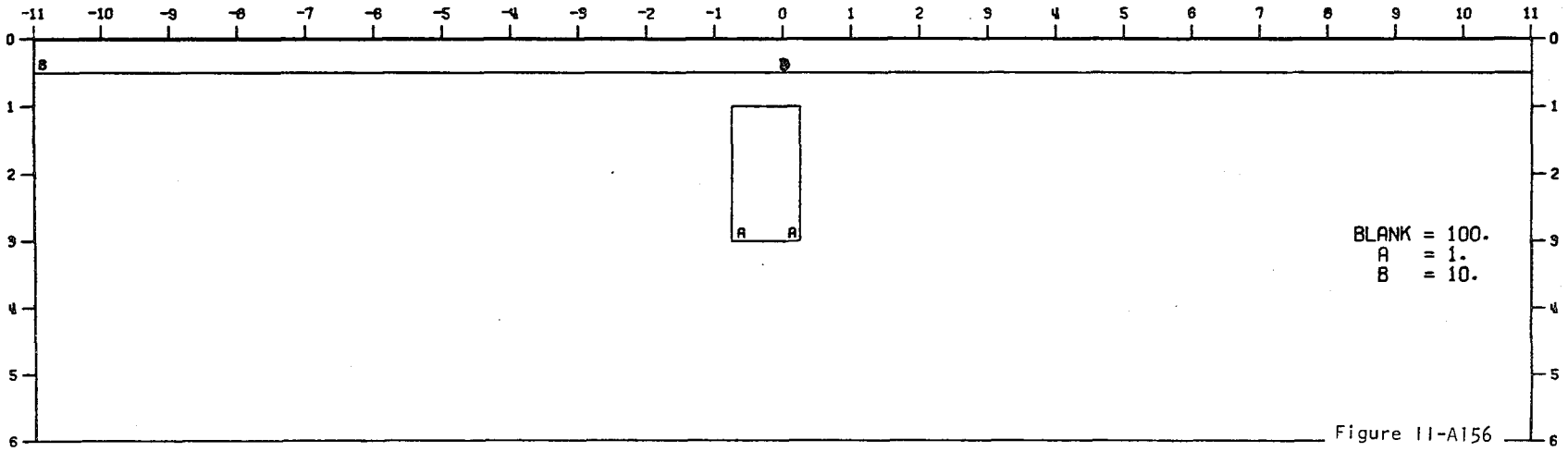

Figure II-A156

MODEL--CONDUCTIVE BODY WITH OVERBURDEN 1B
DIPOLE-DIPOLE APPARENT RESISTIVITY PSEUDO-SECTION
PROFILE LINE IS INCLINED AT 45.0 DEGREES TO STRIKE

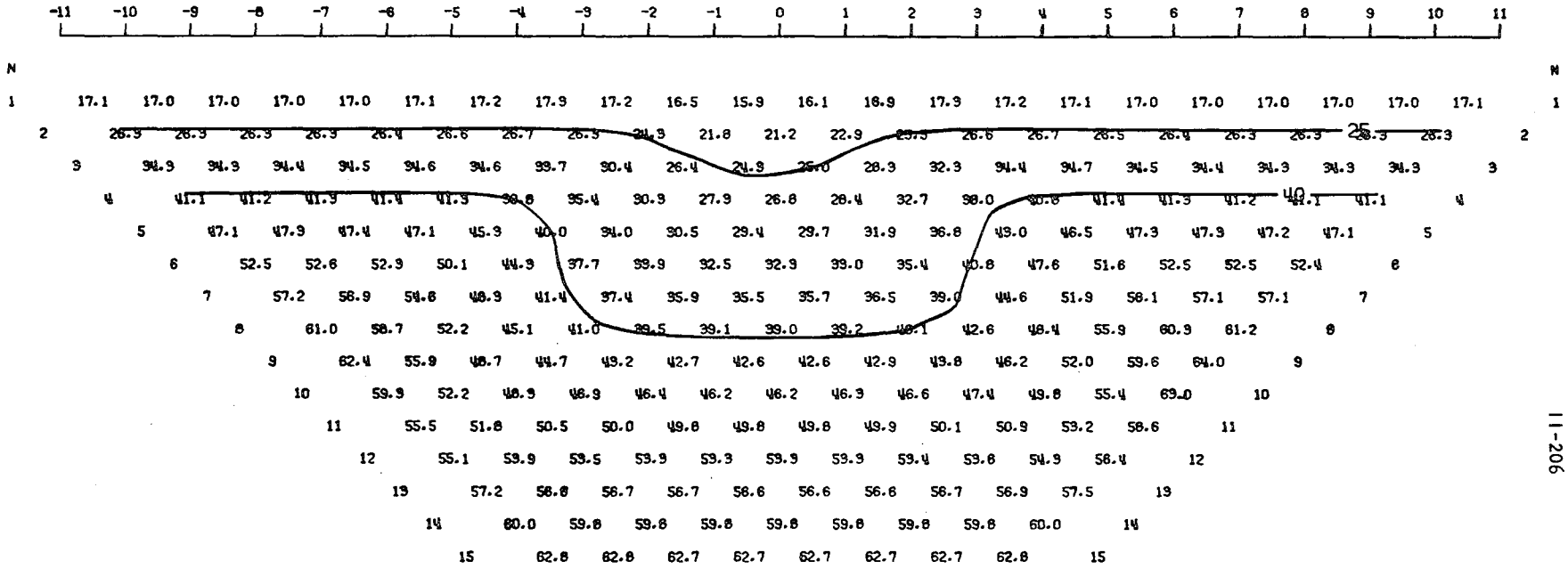

2-D RESISTIVITY MODEL, 45. DEG. PROJECTION--CONDUCTIVE BODY WITH OVERBURDEN 1B

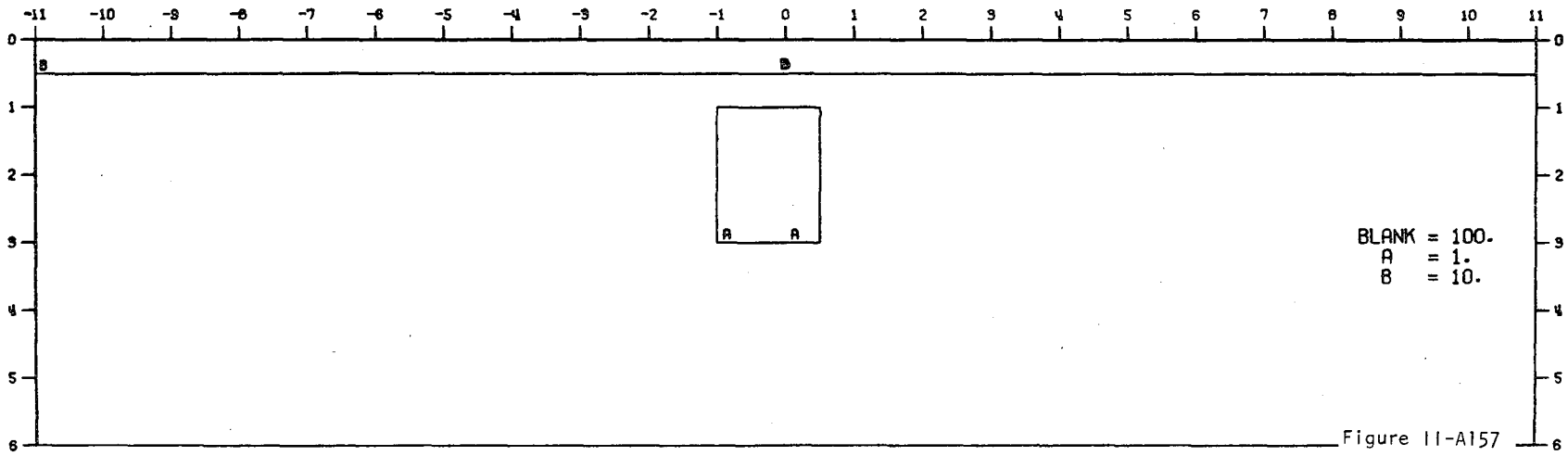

Figure II-A157

MODEL--CONDUCTIVE BODY WITH OVERBURDEN 1B
SCHLUMBERGER APPARENT RESISTIVITY PSEUDO-SECTION
PROFILE LINE IS INCLINED AT 45.0 DEGREES TO STRIKE

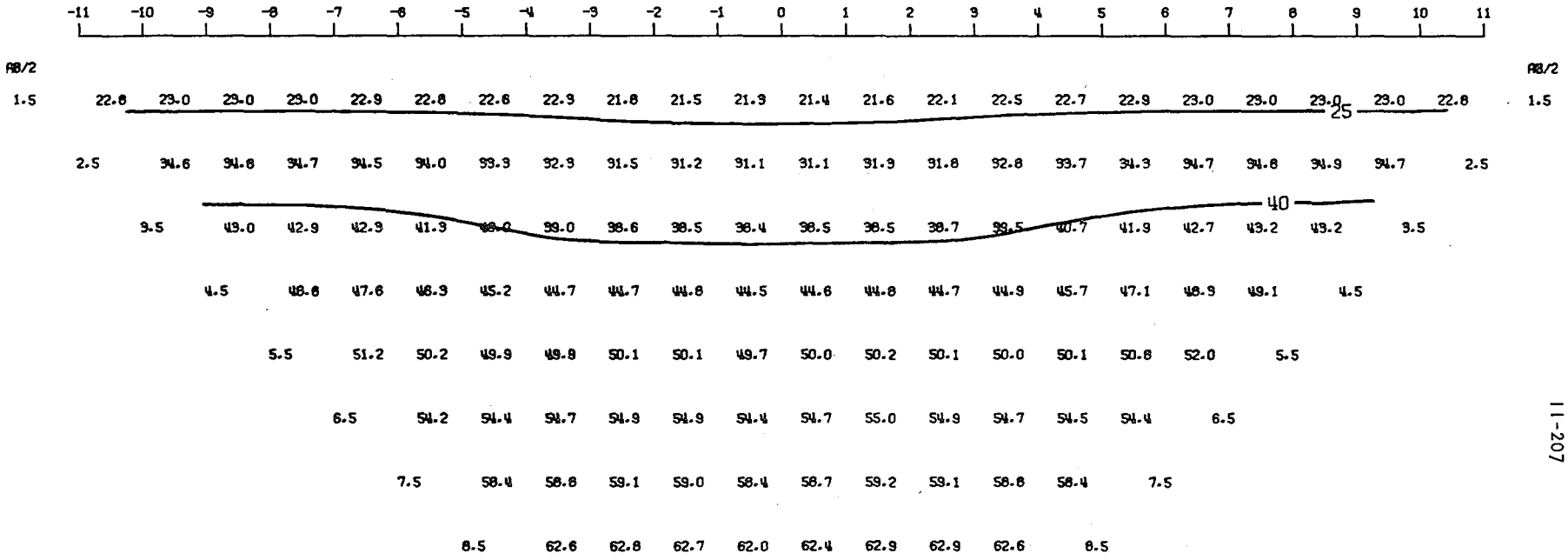

2-D RESISTIVITY MODEL, 45. DEG. PROJECTION--CONDUCTIVE BODY WITH OVERBURDEN 1B

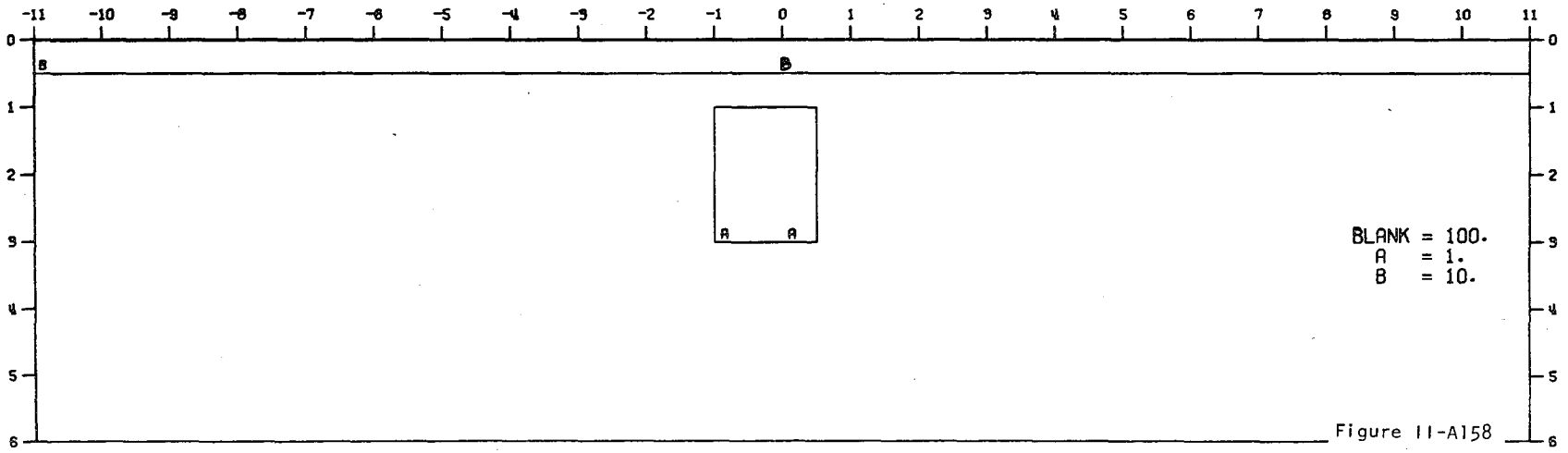

Figure 11-A158

MODEL--TWO BODIES W/ OVERBURDEN 1A
DIPOLE-DIPOLE APPARENT RESISTIVITY PSEUDO-SECTION
PROFILE LINE IS INCLINED AT 45.0 DEGREES TO STRIKE

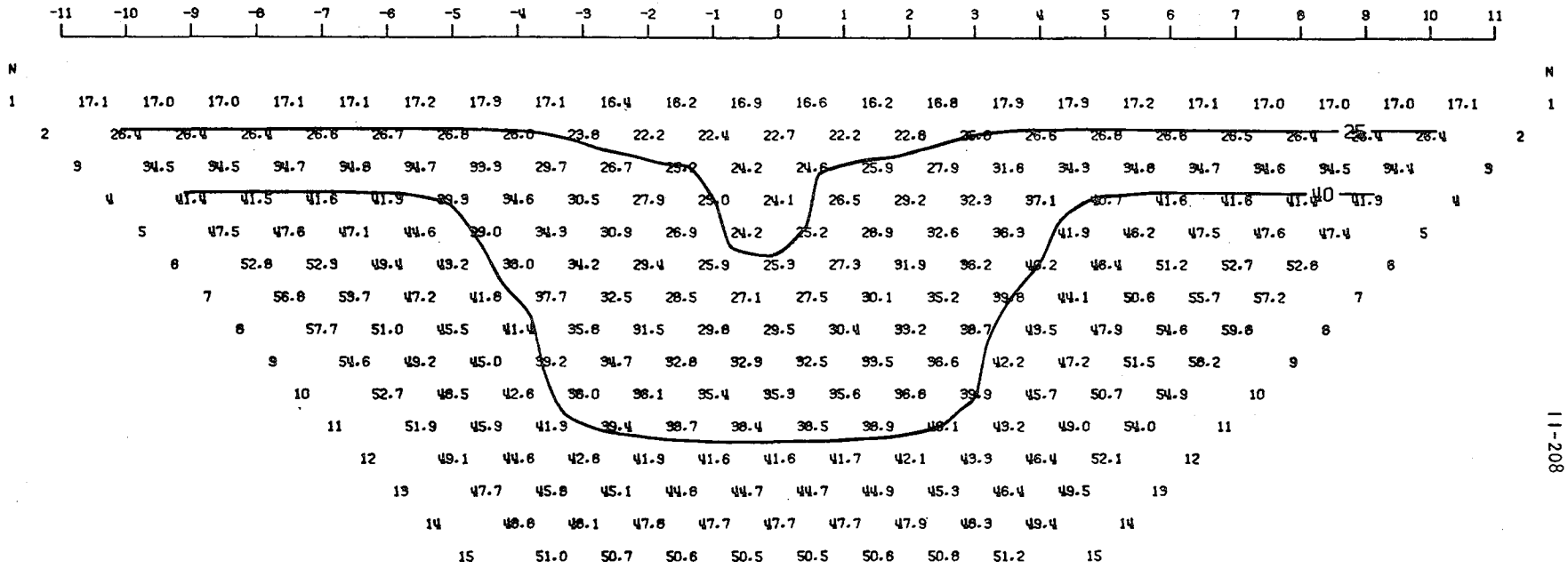

2-D RESISTIVITY MODEL. 45. DEG. PROJECTION--TWO BODIES W/ OVERBURDEN 1A

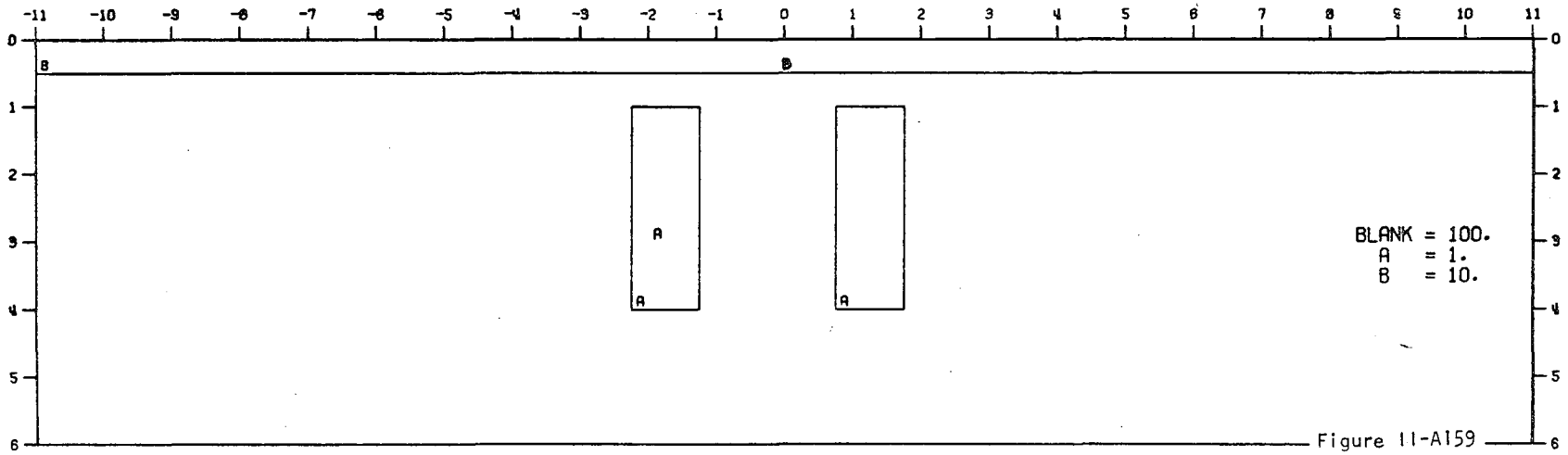

Figure 11-A159

MODEL--TWO BODIES W/ OVERBURDEN 1A
SCHLUMBERGER APPARENT RESISTIVITY PSEUDO-SECTION
PROFILE LINE IS INCLINED AT 45.0 DEGREES TO STRIKE

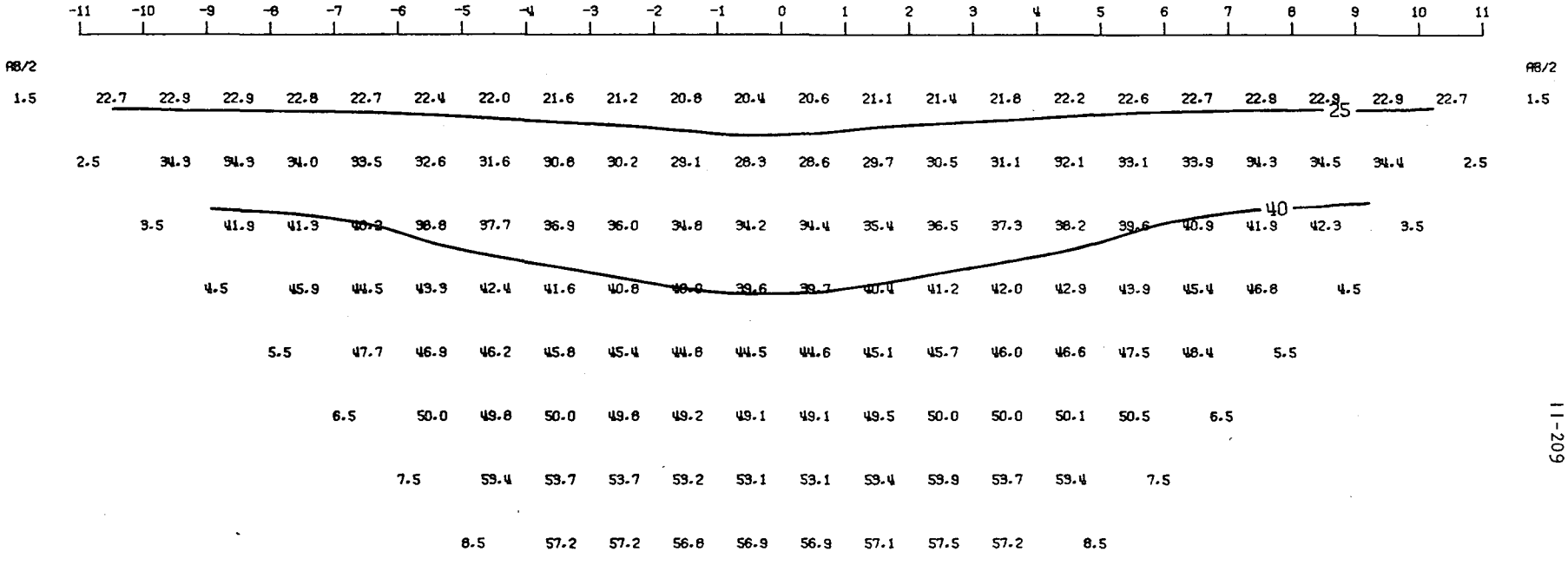

2-D RESISTIVITY MODEL, 45. DEG. PROJECTION--TWO BODIES W/ OVERBURDEN 1A

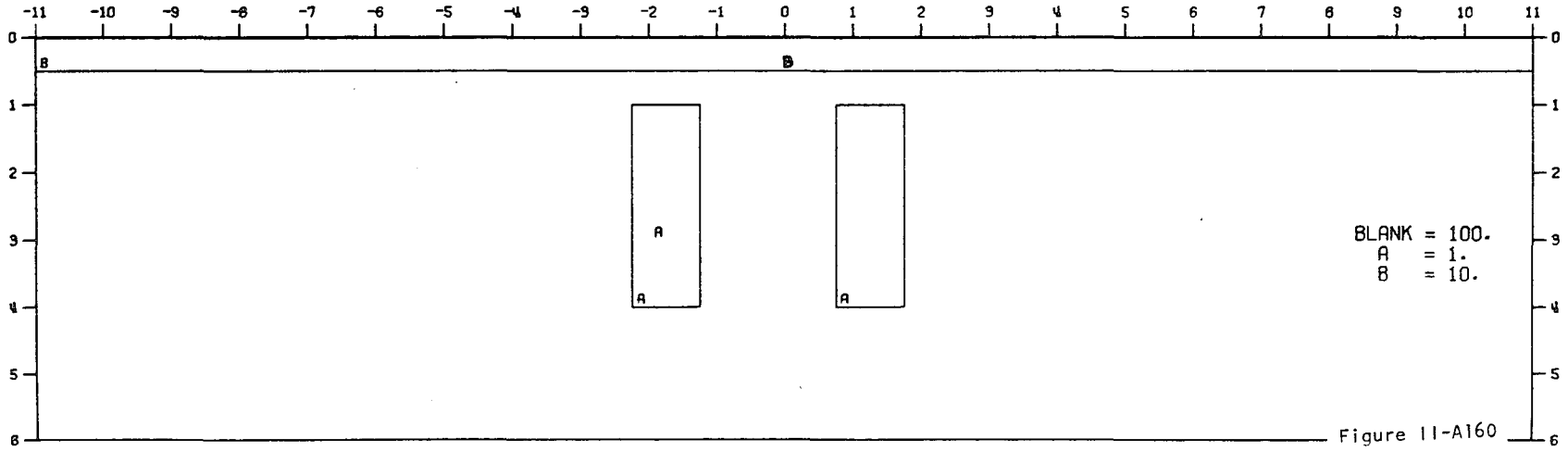

Figure II-A160

MODEL--TWO BODIES W/ OVERBURDEN 18
DIPOLE-DIPOLE APPARENT RESISTIVITY PSEUDO-SECTION
PROFILE LINE IS INCLINED AT 45.0 DEGREES TO STRIKE

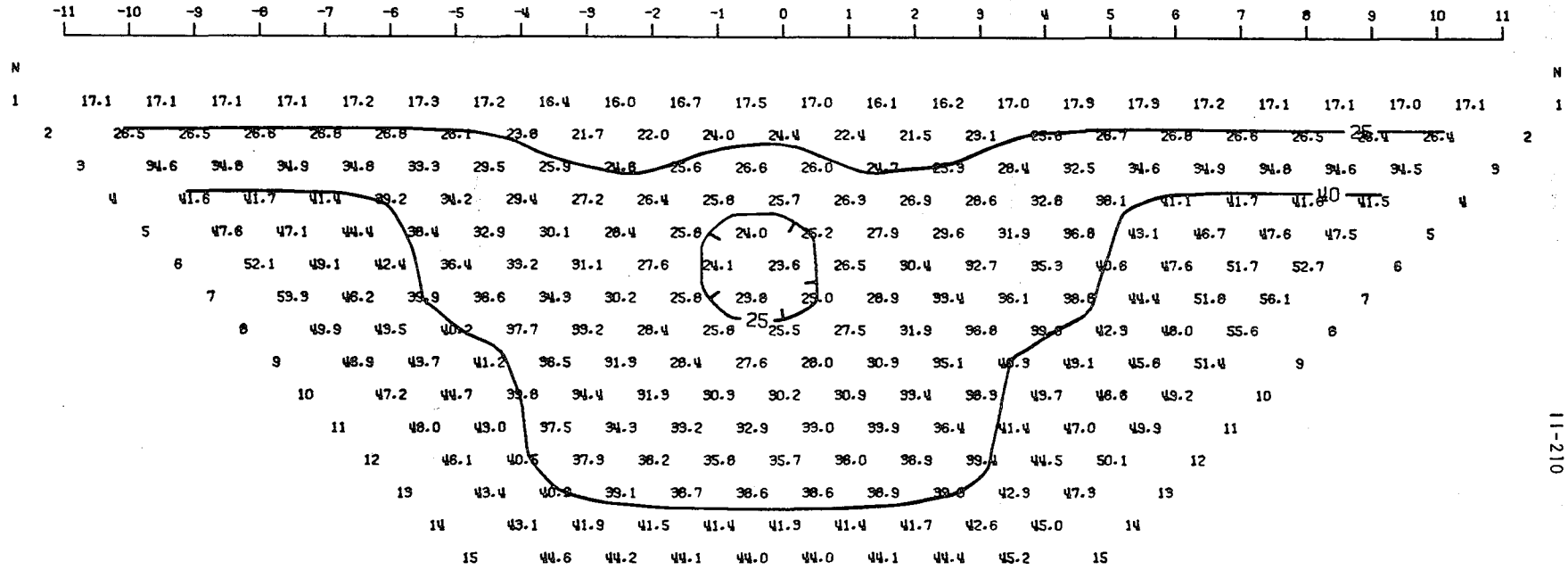

2-D RESISTIVITY MODEL, 45. DEG. PROJECTION--TWO BODIES W/ OVERBURDEN 18

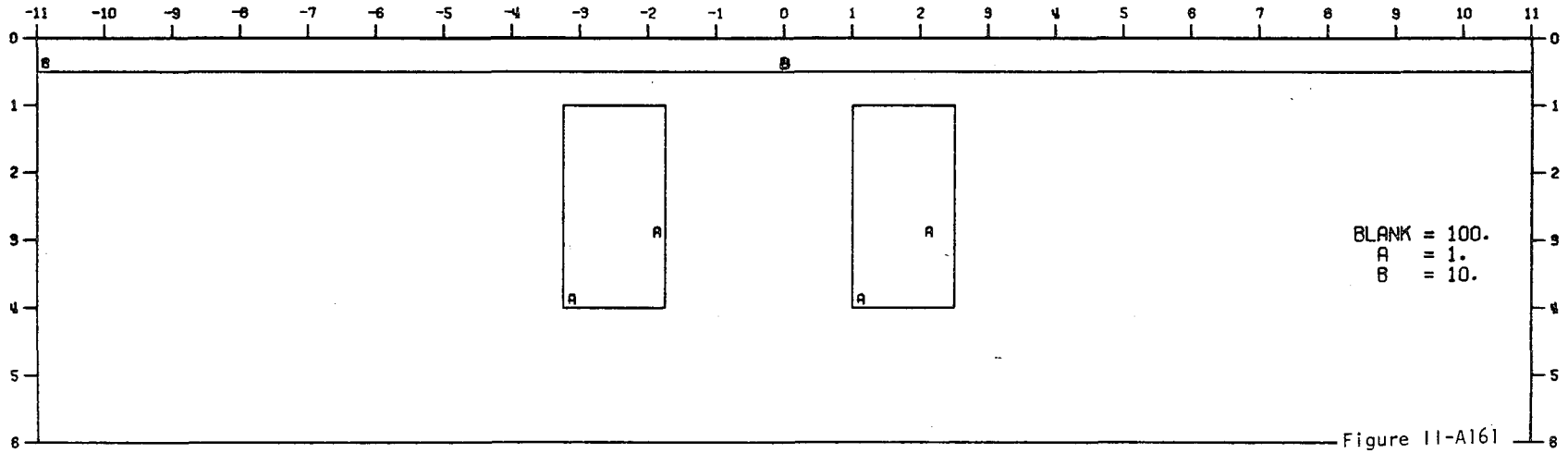

Figure II-A161

MODEL--TWO BODIES W/ OVERBURDEN 1B
SCHLUMBERGER APPARENT RESISTIVITY PSEUDO-SECTION
PROFILE LINE IS INCLINED AT 45.0 DEGREES TO STRIKE

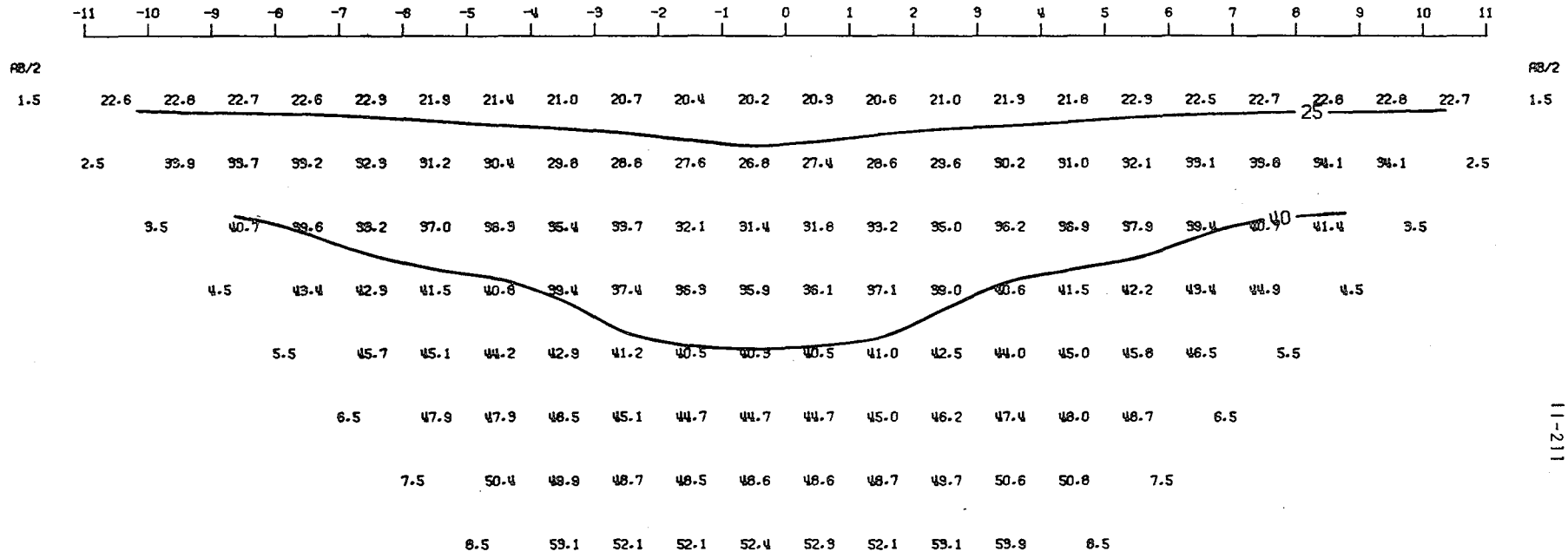

2-D RESISTIVITY MODEL, 45. DEG. PROJECTION--TWO BODIES W/ OVERBURDEN 1B

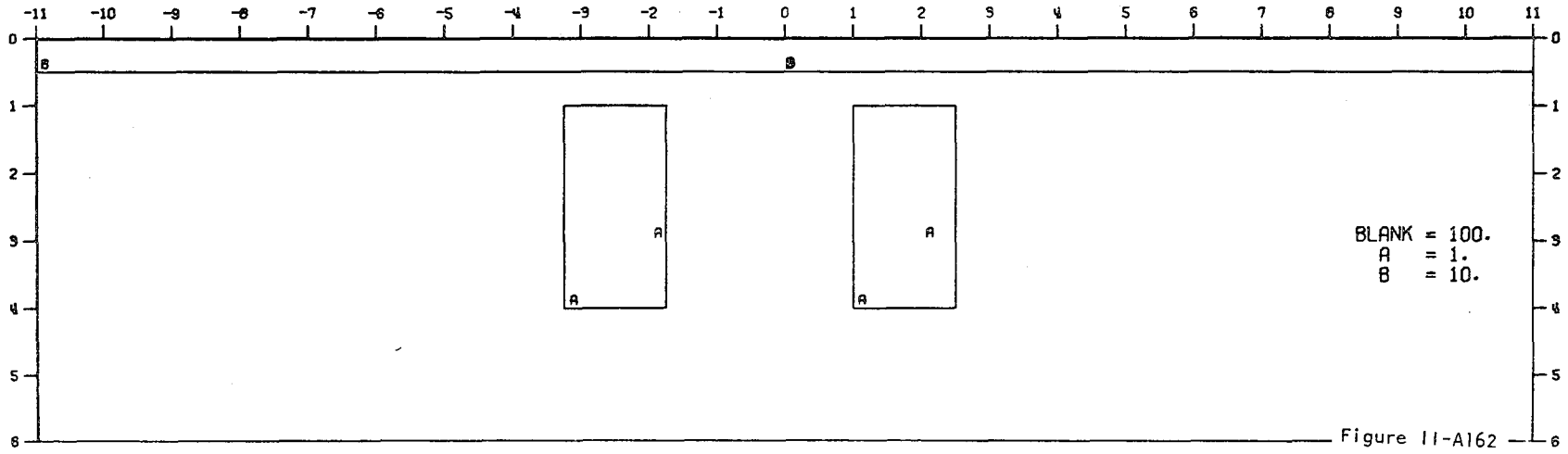

Figure 11-A162

This report was done with support from the United States Energy Research and Development Administration. Any conclusions or opinions expressed in this report represent solely those of the author(s) and not necessarily those of The Regents of the University of California, the Lawrence Berkeley Laboratory or the United States Energy Research and Development Administration.